


Methods in
Molecular Biology 683

Springer Protocols

Ulo Langel
Editor

Cell-Penetrating Peptides

Methods and Protocols

 Humana Press

METHODS IN MOLECULAR BIOLOGY™

Series Editor
John M. Walker
School of Life Sciences
University of Hertfordshire
Hatfield, Hertfordshire, AL10 9AB, UK

For other titles published in this series, go to
www.springer.com/series/7651

Cell-Penetrating Peptides

Methods and Protocols

Edited by

ÜLO LANGEL

*Department of Neurochemistry, Stockholm University,
Stockholm, Sweden*

 Humana Press

Editor

Ülo Langel, Ph.D.
Department of Neurochemistry
Stockholm University
S. Arrheniusv. 21A
SE-106 91 Stockholm
Sweden
ulo@neurochem.su.se

ISSN 1064-3745 e-ISSN 1940-6029
ISBN 978-1-60761-918-5 e-ISBN 978-1-60761-919-2
DOI 10.1007/978-1-60761-919-2
Springer New York Dordrecht Heidelberg London

Library of Congress Control Number: 2010938786

© Springer Science+Business Media, LLC 2011

All rights reserved. This work may not be translated or copied in whole or in part without the written permission of the publisher (Humana Press, c/o Springer Science+Business Media, LLC, 233 Spring Street, New York, NY 10013, USA), except for brief excerpts in connection with reviews or scholarly analysis. Use in connection with any form of information storage and retrieval, electronic adaptation, computer software, or by similar or dissimilar methodology now known or hereafter developed is forbidden.

The use in this publication of trade names, trademarks, service marks, and similar terms, even if they are not identified as such, is not to be taken as an expression of opinion as to whether or not they are subject to proprietary rights.

While the advice and information in this book are believed to be true and accurate at the date of going to press, neither the authors nor the editors nor the publisher can accept any legal responsibility for any errors or omissions that may be made. The publisher makes no warranty, express or implied, with respect to the material contained herein.

Printed on acid-free paper

Humana Press is part of Springer Science+Business Media (www.springer.com)

Preface

In the late 1980s and early 1990s, it became evident that the old dogma concerning the permeability properties of the cell membrane to proteins and peptides was not valid in several new and important cases. First, in 1988, two independent research groups demonstrated the shuttling properties for an HIV tat trans-activator protein (1, 2). Secondly, in 1991, the group of Alain Prochiantz reported (3) on cellular internalization of the homeodomain of Antennapedia (a *Drosophila* homeoprotein), followed in 1994 by the discovery of a short peptide, pAntp(43–58) or penetratin, which was necessary and sufficient for this translocation (4). Today, hundreds of such short peptides are known, and they are defined as cell-penetrating peptides (CPPs) (5) though a few research groups call them as protein transduction domains (PTDs, reflecting their protein origin sometimes), Trojan peptides, model amphipathic peptides (MAPs), or membrane translocating sequences (MTS).

In general, CPPs are still difficult to define exactly due to some uncertainties in characterizing their translocating mechanisms. However, today's understanding is that CPPs *are relatively short peptides, 5–40 aa, with the ability to gain access to the cell interior by means of different mechanisms, mainly including endocytosis, and with the capacity to promote the intracellular delivery of covalently or noncovalently conjugated bioactive cargoes* (6).

This handbook is divided into five parts, summarizing the most important areas of CPP research. Introductory Part I briefly presents the historical background of CPP studies, the classifications of the available CPPs, and summarizes the possibilities to predict them. An overview of penetratin studies is also included due to the importance of this CPP for the whole field.

Since this handbook is mainly the update of existing CPP methods, in the situation where the mechanisms of CPP uptake are still not totally clarified, the Part II deals with the methods for testing CPP mechanisms. The structure of CPPs and their interactions with phospholipid membranes are important factors in their functioning and, hence, the methods to study these are an essential part of this handbook. Manipulations of the kinetics and thermodynamics of CPP uptake are one set of important tools to study CPP mechanisms. Approaches for the testing of endocytotic pathways of CPP uptake are also described, among these fluorescent and electron microscopy together with functional splice correction assay and toxicity methods. Different CPP uptake experiments are compared and it is becoming clear that it is often best to apply several methods in a complementary manner in order to most comprehensively evaluate CPP uptake mechanisms due to the complexity of these processes.

Part III presents a representative and brief summary of methods that attempt to use the unique properties of CPPs to study biochemical intracellular mechanisms of interaction and signal transduction. Of special interest is the mimicry of proteins by short peptides in their sequences. Several examples of such protein mimicry are available and the methods for these are presented here, starting with an overview chapter of the field. I believe that this is one of the most exciting CPP applications, possibly becoming an

important therapeutic approach for interfering with intracellular protein–protein interactions. This goal is certainly achievable only when we will learn to unite the CPP and protein mimicking properties of these peptides. I hope the selected chapters will serve to stimulate work toward this goal.

Part IV summarizes the quickly growing field that applies CPPs to improve the delivery of the oligonucleotides involved in gene modulation, particularly for gene silencing by antisense or siRNA oligonucleotides. The application of splice correcting oligonucleotides is the modern antisense strategy where several different chemically modified oligonucleotides serve as efficient splice redirectors. It is hoped that this approach may lead to novel gene therapies, I am especially pleased to present some siRNA delivery strategies using CPPs. It seems that we are not far from siRNA therapies that harness CPPs to improve and precisely target delivery in vivo based upon the efficient in vitro applications already available today. In parallel, the methods for transfection of plasmids by CPPs or their chemically modified analogs are developing efficiently and quickly.

Part V is another important part of this handbook, discussing ideas for turning CPP-based strategies into drugs. Tumor-selective targeting with flexible CPP technologies has been fueling the CPP research for years, and now the first fruits of these studies have become available. Additional organ-selective delivery strategies are also described, demonstrating that the combination of CPPs with novel nanoparticles and polymer systems is an efficient method for drug delivery. This point is underscored by the contributions of authors based at pharma companies that have contributed their ideas about CPP applications in drug development to this handbook.

In summary, the short history of research of CPPs has clearly demonstrated that CPPs have helped us to expand beyond several long held dogmas. This presents us with superb opportunities to study many intracellular mechanisms in new ways and promote the future development of novel drug

Stockholm, Sweden

Ülo Langel

References

1. Frankel, A. D., and Pabo, C. O. (1988) Cellular uptake of the tat protein from human immunodeficiency virus, *Cell* 55, 1189–1193.
2. Green, M., and Loewenstein, P. M. (1988) Autonomous functional domains of chemically synthesized human immunodeficiency virus tat trans-activator protein, *Cell* 55, 1179–1188.
3. Joliot, A., Pernelle, C., Deagostini-Bazin, H., and Prochiantz, A. (1991) Antennapedia homeobox peptide regulates neural morphogenesis, *Proc. Natl Acad. Sci. USA* 88, 1864–1868.
4. Derossi, D., Joliot, A. H., Chassaing, G., and Prochiantz, A. (1994) The third helix of the Antennapedia homeodomain translocates through biological membranes, *J. Biol. Chem.* 269, 10444–10450.
5. Hansen, M., Kilk, K., and Langel, U. (2008) Predicting cell-penetrating peptides, *Adv Drug Deliv Rev* 60, 572–579.
6. Langel, Ü. (2006) Preface, in : *Handbook of Cell-Penetrating Peptides, 2nd Edition*, CRC Press/Taylor & Francis, Ed. Langel, Ü., Boca Raton, London, New York.

Contents

<i>Preface</i>	<i>v</i>
<i>Contributors</i>	<i>xi</i>
PART I INTRODUCTION	
1. Classes and Prediction of Cell-Penetrating Peptides.	3
<i>Maria Lindgren and Ülo Langel</i>	
2. Penetratin Story: An Overview	21
<i>Edmond Dupont, Alain Prochiantz, and Alain Joliot</i>	
PART II METHODS TO TEST MECHANISMS OF CELL-PENETRATING PEPTIDES	
3. Testing Membrane Interactions of CPPs	33
<i>Astrid Gröslund and Lena Mäler</i>	
4. Interactions of Amphipathic CPPs with Model Membranes	41
<i>Sébastien Deshayes, Karidia Konate, Gudrun Aldrian, Frédéric Heitz, and Gilles Divita</i>	
5. NMR Studies of Three-Dimensional Structure and Positioning of CPPs in Membrane Model Systems	57
<i>Lena Mäler and Astrid Gröslund</i>	
6. Measurements of the Intracellular Stability of CPPs.	69
<i>Ivo R. Ruttekkolk, Wouter P.R. Verdurmen, Yi-Da Chung, and Roland Brock</i>	
7. Tools for Predicting Binding and Insertion of CPPs Into Lipid Bilayers.	81
<i>Paulo F. Almeida</i>	
8. Studies of Proteoglycan Involvement in CPP-Mediated Delivery	99
<i>Anders Wittrup, Si-He Zhang, and Mattias Belting</i>	
9. Uptake Kinetics of Cell-Penetrating Peptides	117
<i>Anders Florén, Imre Mäger, and Ülo Langel</i>	
10. Thermodynamics of Lipid Interactions with Cell-Penetrating Peptides	129
<i>Reto Sauder, Joachim Seelig, and André Ziegler</i>	
11. Calcium and Membrane Repair	157
<i>Caroline Palm-Apergi and Mattias Hällbrink</i>	
12. Mapping of Protein Transduction Pathways with Fluorescent Microscopy	165
<i>Helin Räägel, Pille Säälük, Ülo Langel, and Margus Pooga</i>	
13. Insight into Cell-Entry Mechanisms of CPPs by Electron Microscopy	181
<i>Kärt Padari, Anneli Lorents, Eija Jokitalo, and Margus Pooga</i>	
14. Toxicity Methods for CPPs	195
<i>Per Lundin, Samir EL Andaloussi, and Ülo Langel</i>	
15. Comparison of CPP Uptake Methods	207
<i>Tina Holm, Samir EL Andaloussi, and Ülo Langel</i>	

16. Characterization of Cellular Internalization Pathways for CPP-Mediated Oligonucleotide Delivery	219
<i>Peter Guterstam, Samir EL Andaloussi, and Ülo Langel</i>	
PART III FUNCTIONALITY AND CELL-PENETRATING PEPTIDES	
17. Mimicry of Protein Function with Cell-Penetrating Peptides	233
<i>Henrik J. Johansson, Samir EL Andaloussi, and Ülo Langel</i>	
18. Homeoprotein Intercellular Transfer, the Hidden Face of Cell-Penetrating Peptides	249
<i>Alain Prochiantz</i>	
19. Pharmacology, Biodistribution, and Efficacy of GPCR-Based Pepducins in Disease Models	259
<i>Sarah L. Tressel, Georgios Koukos, Boris Tchernychev, Suzanne L. Jacques, Lidija Covic, and Athan Kuliopulos</i>	
20. Identification and Characterization of Tissue-Specific Protein Transduction Domains Using Peptide Phage Display	277
<i>Maliba Zahid and Paul D. Robbins</i>	
21. Applications of Cell-Penetrating Peptides as Signal Transduction Modulators for the Selective Induction of Apoptosis	291
<i>Sarah Jones and John Howl</i>	
PART IV APPLICATIONS OF CPPs IN GENE MODULATION	
22. Splice Redirection as a Convenient Assay to Monitor CPP-ON Efficiency and Mechanism	307
<i>Rachida Abes, Andrey A. Arzumanov, Amer F. Saleh, Fatouma Said Hassane, Michael J. Gait, and Bernard Lebleu</i>	
23. CPP-Directed Oligonucleotide Exon Skipping in Animal Models of Duchenne Muscular Dystrophy	321
<i>HaiFang Yin, Hong Moulton, Corinne Betts, and Matthew Wood</i>	
24. PTD-DRBD siRNA Delivery	339
<i>Caroline Palm-Apergi, Akiko Eguchi, and Steven F. Dowdy</i>	
25. A Non-Covalent Peptide-Based Strategy for siRNA Delivery	349
<i>Laurence Crombez and Gilles Divita</i>	
26. Application of PepFect Peptides for the Delivery of Splice-Correcting Oligonucleotides	361
<i>Samir EL Andaloussi, Taavi Lehto, Per Lundin, and Ülo Langel</i>	
27. Internalization of Nucleoside Phosphates into Live Cells by Complex Formation with Different CPPs and JBS-Nucleoducin	375
<i>Franziska Mussbach, Regina Pietrucha, Buerk Schaefer, and Siegmund Reissmann</i>	
28. Enhanced Cellular Delivery of Cell-Penetrating Peptide–Peptide Nucleic Acid Conjugates by Photochemical Internalization	391
<i>Takehiko Shiraishi and Peter E. Nielsen</i>	

PART V CPP IN VIVO AND AS FUTURE DRUGS

29. Identification of Homing Peptides Using the In Vivo Phage Display Technology	401
<i>Antti Rivinoja and Pirjo Laakkonen</i>	
30. Measuring the Action of CPP-siRNA Conjugates in the Lung.	417
<i>Sterghios A. Moschos, Karen G. Spink, and Mark A. Lindsay</i>	
31. Intracellular Delivery of Nanoparticles with CPPs	431
<i>Rupa Sawant and Vladimir Torchilin</i>	
32. Multifunctional CPP Polymer System for Tumor-Targeted pDNA and siRNA Delivery	453
<i>Christian Dohmen and Ernst Wagner</i>	
33. Cell-Penetrating Penta-Peptides and Bax-Inhibiting Peptides: Protocol for Their Application	465
<i>Jose Gomez and Shigemi Matsuyama</i>	
34. PAIR Technology: Exon-Specific RNA-Binding Protein Isolation in Live Cells . . .	473
<i>Thomas J. Bell, Emelía Eiríksdóttir, Ülo Langel, and James Eberwine</i>	
35. Quantitation of Cellular and Topical Uptake of Luciferin–Oligoarginine Conjugates	487
<i>Jonathan B. Rothbard and Lisa R. Jones</i>	
36. Industrial-Scale Manufacturing of a Possible Oligonucleotide Cargo CPP-Based Drug	505
<i>Ulf Tedebark, Anthony Scozzari, Oleg Werbitzky, Daniel Capaldi, and Lars Holmberg</i>	
37. Application of a Fusiogenic Peptide GALA for Intracellular Delivery	525
<i>Ikubiko Nakase, Kentaro Kogure, Hideyoshi Harashima, and Shiroh Futaki</i>	
38. Therapeutic Applications of Cell-Penetrating Peptides.	535
<i>Randolph M. Johnson, Stephen D. Harrison, and Derek Maclean</i>	
39. Nonclinical and Clinical Experiences with CPP-Based Self-Assembling Peptide Systems in Topical Drug Development	553
<i>Jacob M. Waugh, Jane Lee, Michael D. Dake, and Dan Browne</i>	
<i>Index</i>	573

Contributors

- RACHIDA ABES • *Université Montpellier, Montpellier, France*
- GUDRUN ALDRIAN • *Centre de Recherches de Biochimie Macromoléculaire, Peptide Chemistry and Synthesis core Facility, Montpellier, France*
- PAULO F. ALMEIDA • *Department of Chemistry and Biochemistry, University of North Carolina Wilmington, Wilmington, NC, USA*
- ANDREY A. ARZUMANOV • *Laboratory of Molecular Biology, Medical Research Council, Hills Road, Cambridge, UK*
- THOMAS J. BELL • *Department of Pharmacology and Psychiatry, University of Pennsylvania Medical Center, Philadelphia, PA, USA*
- MATTIAS BELTING • *Department of Clinical Sciences, Section of Oncology, Lund University, Lund, Sweden*
- CORINNE BETTS • *Department of Physiology, Anatomy and Genetics, University of Oxford, South Parks Road, Oxford, UK*
- ROLAND BROCK • *Department of Biochemistry, Nijmegen Centre for Molecular Life Sciences, Radboud University Nijmegen Medical Centre, Nijmegen, The Netherlands*
- DAN BROWNE • *Revance Therapeutics, Inc, Newark, CA, USA*
- DANIEL CAPALDI • *Analytical and Process Development, Isis Pharmaceuticals Inc, Carlsbad, CA, USA*
- YI-DA CHUNG • *Department of Biochemistry, Nijmegen Centre for Molecular Life Sciences, Radboud University Nijmegen Medical Centre, Nijmegen, The Netherlands*
- LIDIJA COVIC • *Tufts Medical Center, and Departments of Biochemistry and Medicine, Tufts University School of Medicine, Molecular Oncology Research Institute, Boston, MA, USA*
- LAURENCE CROMBEZ • *Department of Molecular Biophysics and Therapeutics, Centre de Recherches de Biochimie Macromoléculaire, Montpellier, France*
- MICHAEL D. DAKE • *Cardiothoracic Surgery Department, Falk Cardiovascular Research Center, Stanford University School of Medicine, Stanford, CA, USA*
- SÉBASTIEN DESHAYES • *Department of Molecular Biophysics and Therapeutics, Centre de Recherches de Biochimie Macromoléculaire, Montpellier, France*
- GILLES DIVITA • *Biophysics Department, Centre de Recherches de Biochimie Macromoléculaire, Montpellier University, Montpellier, France*
- CHRISTIAN DOHMEN • *Department of Pharmacy, Pharmaceutical Biotechnology, Centre for Drug Research, Ludwig-Maximilians-Universität, Munich, Germany*
- STEVEN F. DOWDY • *Investigator, Howard Hughes Medical Institute, Professor, Department of Cellular and Molecular Medicine UCSD School of Medicine, La Jolla, CA, USA*
- EDMOND DUPONT • *Homeoprotein Cell Biology, Ecole normale supérieure and Collège de France, Paris, France*

- JAMES EBERWINE • *Department of Pharmacology and Psychiatry, University of Pennsylvania Medical Center, Philadelphia, PA, USA*
- AKIKO EGUCHI • *Department of Cellular and Molecular Medicine, UCSD School of Medicine, Howard Hughes Medical Institute, La Jolla, CA, USA*
- EMELÍA EIRÍKSDÓTTIR • *Department of Neurochemistry, Stockholm University, Stockholm, Sweden*
- SAMIR EL ANDALOUSSI • *Department of Neurochemistry, Stockholm University, Stockholm, Sweden*
- ANDERS FLORÉN • *Laboratory of Molecular Biotechnology, Institute of Technology, Tartu University, Tartu, Estonia*
- SHIROH FUTAKI • *Kyoto University, Institute for Chemical Research, Uji, Kyoto, Japan*
- MICHAEL J. GAIT • *Laboratory of Molecular Biology, Medical Research Council, Hills Road, Cambridge, England*
- JOSE GOMEZ • *Department of Pharmacology, School of Medicine, Case Western Reserve University, Cleveland, OH, USA*
- ASTRID GRÄSLUND • *Department of Biochemistry and Biophysics, Stockholm University, Stockholm, Sweden*
- PETER GUTERSTAM • *Department of Neurochemistry, Stockholm University, Stockholm, Sweden*
- HIDEYOSHI HARASHIMA • *Faculty of Pharmaceutical Sciences, Hokkaido University, Sapporo, Hokkaido, Japan*
- STEPHEN D. HARRISON • *KAI Pharmaceuticals, Inc, San Francisco, CA, USA*
- FRÉDÉRIC HEITZ • *Biophysics Department, Centre de Recherches de Biochimie Macromoléculaire, Montpellier University, Montpellier, France*
- TINA HOLM • *Department of Neurochemistry, Stockholm University, Stockholm, Sweden*
- LARS HOLMBERG • *GE Healthcare Bio-Sciences, Uppsala, Sweden*
- JOHN HOWL • *School of Applied Sciences, Research Institute in Healthcare Science, University of Wolverhampton, Wolverhampton, UK*
- MATTIAS HÄLLBRINK • *Department Neurochemistry, Stockholm University, Stockholm, Sweden*
- SUZANNE L. JACQUES • *Tufts Medical Center, Molecular Oncology Research Institute, Boston, MA, USA*
- HENRIK J. JOHANSSON • *Department of Oncology-Pathology, Karolinska Biomics Center, Karolinska Institutet, Stockholm, Sweden*
- RANDOLPH M. • *Johnson Vice President and Chief of Technology Development KAI Pharmaceuticals, Inc, San Francisco, CA, 94080, USA*
- EIJA JOKITALO • *Electron Microscopy Unit, Institute of Biotechnology, University of Helsinki, Viikinkaari, Finland*
- ALAIN JOLIOT • *Ecole Normale Supérieure, Paris, France*
- LISA RENEE JONES • *Department of Chemistry, Stanford University, Stanford, CA, USA*
- SARAH JONES • *Research Institute in Healthcare Science, School of Applied Sciences, University of Wolverhampton, Wolverhampton, UK*
- KENTARO KOGURE • *Department of Biophysical Chemistry, Kyoto Pharmaceutical University, Yamashinaku, Kyoto, Japan*

- KARIDIA KONATE • *Department of Molecular Biophysics and Therapeutics, Centre de Recherches de Biochimie Macromoléculaire, Montpellier, France*
- GEORGIOS KOUKOS • *Tufts Medical Center, Molecular Oncology Research Institute, Boston, MA, USA*
- ATHAN KULIOPULOS • *Tufts Medical Center, and Departments of Biochemistry and Medicine, Tufts University School of Medicine, Molecular Oncology Research Institute, Boston, MA, USA*
- PIRJO LAAKKONEN • *Molecular Cancer Biology Research Program and Institute of Biomedicine, Biomedicum Helsinki, University of Helsinki, Helsinki, Finland; Department of Biotechnology and Molecular Medicine, A.I. Virtanen Institute for Molecular Sciences, University of Kuopio, Kuopio, Finland*
- ÜLO LANGEL • *Department of Neurochemistry, Stockholm University, Stockholm, Sweden; Laboratory of Molecular Biotechnology, Institute of Technology, Tartu University, Tartu, Estonia*
- BERNARD LEBLEU • *Université Montpellier, Montpellier, France*
- JANE LEE • *Revance Therapeutics, Inc, Newark, CA, USA*
- TAAVI LEHTO • *Laboratory of Molecular Biotechnology, Institute of Technology, Tartu University, Tartu, Estonia*
- MARIA LINDGREN • *Cepep II AB, Stockholm, Sweden*
- MARK A. LINDSAY • *NIHR Translational Research Facility in Respiratory Medicine, Wythenshawe Hospital, University of Manchester Education and Research Centre, Southmoor Road, Manchester, UK*
- ANNELY LORENTS • *Institute of Molecular and Cell Biology, University of Tartu, Tartu, Estonia*
- PER LUNDIN • *Department of Neurochemistry, Stockholm University, Stockholm, Sweden*
- DEREK MACLEAN • *KAI Pharmaceuticals, Inc, San Francisco, CA, USA*
- SHIGEMI MATSUYAMA • *Departments of Medicine, Pharmacology, and Pathology, School of Medicine, Case Western Reserve University, Cleveland, OH, USA*
- STERGHIOS A. MOSCHOS • *Biotherapeutics, Pfizer Global Research and Development, Pfizer Inc, Sandwich, Kent, UK*
- HONG MOULTON • *Oregon State University, Corvallis, OR, USA*
- FRANZISKA MUSSBACH • *Faculty of Biology and Pharmacy, Friedrich-Schiller-University, Jena, Germany*
- IMRE MÄGER • *Laboratory of Molecular Biotechnology, Institute of Technology, Tartu University, Tartu, Estonia*
- LENA MÄLER • *Department of Biochemistry and Biophysics, Stockholm University, Stockholm, Sweden*
- IKUHIKO NAKASE • *Institute for Chemical Research, Kyoto University, Uji, Kyoto, Japan*
- PETER E. NIELSEN • *Department of Cellular and Molecular Medicine, Faculty of Health, Sciences, The Panum Institute, University of Copenhagen, Copenhagen N, Denmark*
- KÄRT PADARI • *Institute of Molecular and Cell Biology, University of Tartu, Tartu, Estonia*
- CAROLINE PALM-APERGI • *Department of Cellular and Molecular Medicine, UCSD School of Medicine, Howard Hughes Medical Institute, La Jolla, CA, USA*

- REGINA PIETRUCHA • *Jena Bioscience, Jena, Germany*
- MARGUS POOGA • *Institute of Molecular and Cell Biology, University of Tartu, Tartu, Estonia*
- ALAIN PROCHIANTZ • *Chaire des processus morphogénétiques, Ecole normale supérieure and Collège de France, Paris, France*
- SIEGMUND REISSMANN • *Faculty of Biology and Pharmacy, Institute of Biochemistry and Biophysics, Friedrich-Schiller-University, Jena, Germany*
- ANTTI RIVINOJA • *Molecular Cancer Biology Research Program and Institute of Biomedicine, Biomedicum Helsinki, University of Helsinki, Helsinki, Finland*
- PAUL D. ROBBINS • *Professor of Microbiology and Molecular Genetics and Orthopaedic Surgery University of Pittsburgh School of Medicine, Pittsburgh, PA, USA*
- JONATHAN B. ROTHBARD • *Division of Rheumatology, Department of Medicine, Stanford University School of Medicine, Stanford, CA, USA*
- IVO R. RUTTEKOLK • *Department of Biochemistry, Nijmegen Centre for Molecular Life Sciences, Radboud University Nijmegen Medical Centre, Nijmegen, The Netherlands*
- HELIN RÄÄGEL • *Institute of Molecular and Cell Biology, University of Tartu, Tartu, Estonia*
- FATOUMA SAID HASSANE • *Université Montpellier, Montpellier, France*
- AMER F. SALEH • *Laboratory of Molecular Biology, Medical Research Council, Hills Road, Cambridge, UK*
- RETO SAUDER • *Department of Biophysical Chemistry, Biozentrum of the University of Basel, Basel, Switzerland*
- RUPA SAWANT • *Research Associate Center for Pharmaceutical Biotechnology and Nanomedicine, Northeastern University, Boston, MA, USA*
- BUERK SCHAEFER • *Jena Bioscience, Jena, Germany*
- ANTHONY SCOZZARI • *Development Chemistry and Manufacturing, Isis Pharmaceuticals, Inc, Carlsbad, CA, USA*
- JOACHIM SEELIG • *Department of Biophysical Chemistry, Biozentrum of the University of Basel, Klingelbergstrasse, Basel, Switzerland*
- TAKEHIKO SHIRAISHI • *Department of Cellular and Molecular Medicine, Faculty of Health Sciences, The Panum Institute, University of Copenhagen, Copenhagen, Denmark*
- KAREN G. SPINK • *Biotherapeutics, Pfizer Global Research and Development Pfizer Inc, Kent, UK*
- PILLE SÄÄLIK • *Institute of Molecular and Cell Biology, University of Tartu, 23A Riia Street, Tartu, Estonia*
- BORIS TCHERNYCHEV • *Tufts Medical Center, Molecular Oncology Research Institute, Boston, MA, USA*
- ULF TEDEBARK • *GE Healthcare Bio-Sciences, Uppsala, Sweden*
- VLADIMIR P. TORCHILIN • *Center for Pharmaceutical, Biotechnology and Nanomedicine, Northeastern University, Mugar Building, Boston, MA, USA*
- SARAH L. TRESSEL • *Tufts Medical Center, Molecular Oncology Research Institute, Boston, MA, USA*

- WOUTER P.R. VERDURMEN • *Department of Biochemistry, Nijmegen
Centre for Molecular Life Sciences, Radboud University Nijmegen Medical Centre,
Nijmegen, The Netherlands*
- ERNST WAGNER • *Chair, Pharmaceutical Biotechnology Department of Pharmacy,
Centre for Drug Research, Ludwig-Maximilians-Universität, Munich, Germany*
- JACOB M. WAUGH • *Revance Therapeutics Inc, Newark, CA, USA*
- OLEG WERBITZKY • *Director Innovation LONZA AG, Basel, Switzerland*
- ANDERS WITTRUP • *Department of Clinical Sciences, Section of Oncology,
Lund University, Lund, Sweden*
- MATTHEW WOOD • *Anatomy and Genetics, Department of Physiology,
University of Oxford, South Parks Road, Oxford, UK*
- HAIFANG YIN • *Anatomy and Genetics, Department of Physiology,
University of Oxford, South Parks Road, Oxford, UK*
- MALIHA ZAHID • *Department of Microbiology and Molecular Genetics,
University of Pittsburgh School of Medicine, Biomedical Science Tower,
Pittsburgh, PA, USA*
- SI-HE ZHANG • *Department of Clinical Sciences, Section of Oncology,
Lund University, Lund, Sweden*
- ANDRÉ ZIEGLER • *Department of Biophysical Chemistry, Biozentrum
of the University of Basel, Klingelbergstrasse, Basel, Switzerland*

Part I

Introduction

Chapter 1

Classes and Prediction of Cell-Penetrating Peptides

Maria Lindgren and Ülo Langel

Abstract

The classical view on how peptides enter cells has been changed due to the development in the research field of cell-penetrating peptides (CPPs). During the last 15 years, more than 100 peptide sequences have been published to enter cells and also to bring different biological cargoes with them. Here, we present an overview of CPPs, mainly trying to analyze their common properties yielding the prediction of their cell-penetrating properties. Furthermore, examples of recent research, ideas on classification and uptake mechanisms, as well as a summary of the therapeutic potential of CPPs are presented.

Key words: Cell-penetrating peptide, Cellular uptake, Intracellular delivery, Drug delivery, siRNA, Selective delivery

1. Cell-Penetrating Peptides

The research field of cell-penetrating peptides (CPPs), or alternatively called protein transduction domains (PTDs), has increased rapidly in the last years. CPPs constitute one of the most promising tools for the delivery of biologically active molecules into cells and therefore play a key role in future development of therapeutics (1–3). CPPs have been shown to efficiently improve intracellular delivery of various biomolecules, including plasmid DNA, oligonucleotides, siRNA (short interfering RNA), PNA (peptide nucleic acid), proteins and peptides, as well as liposome nanoparticles, into cells and tissues both *in vitro* and *in vivo*.

The first CPPs found were the parts of naturally occurring proteins that have the ability to enter cells; pAnt and Tat. Furthermore, there are also “unnatural” CPPs such as model amphipathic peptide (MAP) and transportan which do not have any natural parent proteins. Even though the CPP’s primary sequence differ, there are certain features that tie them together. The essential feature being that the peptides have the ability to

transport other molecules. The classical definition is presented in the “Preface” of this book.

In the class of CPPs, there are several subgroups, as defined by their origin or sequence characteristics (Table 1). The classification is a way to comprehend the mechanisms of how CPPs function as well as their connection, and to elucidate whether other peptides are part of the CPP family.

Table 1
Families of cell-penetrating peptides with a few examples

Family	Name and sequence	Origin	References
Protein derived	Penetratin RQIKIWFQNRRMKWKK-NH ₂	<i>Drosophila</i> homeoprotein Antennapedia	(7)
	Tat (48–60) GRKKRRQRRRPPQ	Human immunodeficiency virus type 1 (HIV-1) Tat	(16)
	pVEC LLIILRRRIRKQAHAHSK-amide	VE-cadherin	(58)
	VP22 peptide NAKTRRHERRRKLAIER	Herpes simplex virus	(14)
	Chimeric	MPG GALFLGFLGAAGSTMGA-cya	A hydrophobic domain from the fusion sequence of HIV gp41 and NLS of SV40 T-antigen
Pep-1 KETWWETWWTEWSQPKKKRKV-cya		NLS from Simian Virus 40 large antigen T and reverse transcriptase of HIV	(23)
Transportan/TP10 GWTLNS-/ AGYLLGK*INLKALAALAKKIL-NH ₂		Galanin and mastoparan	(6, 25)
M918 MVTVLFRRRLRIRACGPPRVRV-NH ₂		The tumor suppressor protein p14ARF, amino acids 1–22 with positions 3–8 inverted	(63)
YTA2,4 YTAIAWVKAFIRKL RK-NH ₂ IAWVKAFIRKLKRGPLG-NH ₂		MMP cleavage site as seeding sequence	(35)
Synthetic		MAP KLALKLALKALKAALKLA	Amphipathic model peptide
	Octa/NonaArginine RRRRRRRR/R	Positively charged sequence	(40, 50)
	CADY GLWRALWRLRLSLWRLWRA-cya	Derived from PPTG1 peptide, W and charged amino acids	(32)
	POD GGG[ARKKAACA]4	Peptide for ocular delivery	(86)

-NH₂ N-terminal amide, -cya N-terminal cysteamide

*For side chain conjugation

As mentioned above, there are naturally occurring PTDs, a subgroup of CPPs. For instance, the CPP pAnt or penetratin is derived from a homeoprotein (2), as described by Prochiantz and Joliot (Table 1). They suggest that the CPPs or PTDs contain a code (4), a specific signal for secretion that the cell machinery recognizes and that is then necessary for transcellular delivery. However, there are several publications that instead suggest an equilibrium across the cell membrane (5, 6) where no special signal for exiting the cell is necessary. Another possible natural role for CPPs, based on their structural similarities with membrane active peptides, such as perforin or gramicidin, may suggest similar functions; entering unwanted cells and lyse lysosomes as part of our innate immune response (7).

2. Families of CPPs

The CPPs can be divided into families or subgroups: protein derived (P), chimeric (C), and designed/synthetic (S). The difference between chimeric and designed is that the parental sequences in C are partly naturally occurring.

The largest family, and perhaps the most well known, is the protein-derived CPPs. Among them, pAnt or penetratin, a homeodomain-derived peptide, is of special importance (see Chapter 2). Homeoproteins define a class of transcription factors that bind DNA through a structure of 60 amino acids in length, called the homeodomain. The initial clue that transcription factors can traverse from cell to cell and thus be secreted and internalized by live cells was the internalization of the homeodomain of Antennapedia (a *Drosophila* homeoprotein) (8). In an attempt to further understand its mechanism of internalization, the homeodomain was modified by site-directed mutagenesis; its third helix (amino acids 43–58) was necessary and sufficient for translocation (9) (for review see ref. 10). This led to the development of penetratin (Table 1), which has emerged as the most abundantly applied CPP in the literature. Structure–function relationship studies of penetratin yielded several active and inactive analogs that allowed formulation of the inverted micelle internalization model for their cellular internalization (11).

Tat-derived peptides are parts of the Tat protein, which is a transcription-activating factor of 86–102 amino acids in length, depending on the viral strain, and is involved in the replication of HIV. It is organized in three different functional domains (12, 13): (1) an acidic N-terminal region important for transactivation; (2) a cysteine-rich DNA-binding region (22–37 amino acids) with a zinc-finger motif; and (3) a basic region (49–58 amino acids)

responsible for nuclear import. Like some homeoproteins and the herpes simplex virus type 1 protein VP22 (14), Tat is secreted from, and then reinternalized by, live cells (13, 15). Tat uptake is time- and concentration-dependent and can be partially inhibited by lowering temperature. The most efficient fragment is Tat48–60 (Table 1), which encompasses the whole basic region of the protein (16) and its nuclear localization signal (NLS). However, this NLS is not sufficient for translocation in itself because Tat37–53, which encompasses only the NLS, is not taken up. Furthermore, the N-terminus of Tat48–60, which contains the whole basic region but carries deletions in the helical domain, is sufficient for translocation and shows cellular and nuclear localization (16). Today, there are several research groups that have simplified the Tat48–60 sequence to a short stretch of six to nine arginines (Table 1) which also works well as a CPP, especially as a PTD on recombinantly expressed proteins (17, 18).

The next family of CPPs is the chimeric peptides; these are the CPPs that are partly derived from naturally occurring peptides or protein. One example is signal sequences of proteins, which are recognized by acceptor proteins that aid in addressing the preprotein from the translation machinery into the membrane of the appropriate intracellular organelles. Signal sequences that direct proteins to the same intracellular compartment, e.g., endoplasmic reticulum or mitochondria, share structural traits. Signal sequences coupled to NLS have been shown to enter several cell types and to accumulate in their nucleus. For example, this has been demonstrated for a sequence derived from the hydrophobic regions of the signal sequences from Kaposi's sarcoma fibroblast growth factor 1 (K-FGF) (19), the fusion sequence of HIV-1 gp41 (20), and the signal sequence of the variable immunoglobulin light chain Ig(v) (21) conjugated to NLS peptides originating from nuclear transcription factor κ B (NF- κ B) (22) or Simian virus 40 (SV40) T-antigen (23).

The peptide introduced by our group, transportan, is derived from galparan (24), a fusion between the neuropeptide galanin-1–13 and the wasp venom peptide mastoparan. It was developed under a program that was aimed at creating galanin receptor antagonists by using a chimerical strategy. Because it was known that analogs with a substitution of Pro13 to N ϵ -biotinyl-Lys retained affinity for the galanin receptor, a similar substitution of Pro13 was made on galparan. Strikingly, although cells incubated with labeled galanin showed almost no intracellular labeling, those incubated with the biotinylated galparan analog were heavily labeled in both the cytoplasm and the nucleus. Thus, the new peptide was named transportan (Table 1) (25). We have published a number of analogs of transportan; however, transportan 10 (TP10) is the most efficient of them and has thus been extensively applied (26, 27).

Another early peptide defined as a CPP is the “model amphipathic peptide” (MAP) which is part of the final group of synthetic CPPs that may be the most homogeneous of the presented families, because many of them are designed to form amphipathic α helices. This peptide was found when investigating the proposed direct contact between several peptides and G proteins, as suggested for the poly-cationic peptides mastoparan and substance P. Oehlke et al. (28) designed an 18-mer amphipathic model peptide (Table 1). This peptide crosses the plasma membranes of, for instance, mast cells and endothelial cells by both energy-dependent and energy-independent mechanisms (29), and can act as an efficient transporter for different peptide cargoes. The model peptide shows perforations of the plasma membrane at $\geq 4 \mu\text{M}$; however, several analogs showing less toxicity, and higher uptake have been synthesized (30).

The group of Divita has developed several CPPs for noncovalent ON delivery and siRNA (reviewed in ref. 31). One of their latest publications describe a new peptide called CADY (32), which was developed to bind siRNA originating from an amphipathic peptide with plasmid condensing properties (33). CADY is also part of the synthetic CPP family (Table 1).

Additional examples of the synthetic or designed CPPs are the two closely related peptides designed in our laboratory called YTA-2 and YTA-4 (Table 1). When designing these two peptides, we started out with a short amino acid sequence corresponding to a rather unspecific matrix metallo protease cleavage site, as a seeding sequence. The prediction program by Hällbrink et al. (34) added a random sequence to make them cell-penetrating. They have been shown to transport both a fluorophore and the cytosstatic methotrexate into drug-resistant breast cancer cells (35).

As mentioned earlier, there are over 100 peptide sequences known to be cell-penetrating today. Here, we have presented just a few examples of both the most abundantly applied CPPs and newly published ones, to give an idea on how the members of the CPP family have been found. For more examples see Table 1.

3. Translocation Mechanisms

The main body of publications is on successful applications of CPPs as delivery vectors; in addition, the investigations of the CPPs mechanism of entering cells are second in number. For a visual summary, see Fig. 1.

When comparing the primary sequence of CPPs, it is easy to detect the similarities with lytic peptides such as melittin, magainin, perforin, and others. Cytolytic peptides accumulate on the

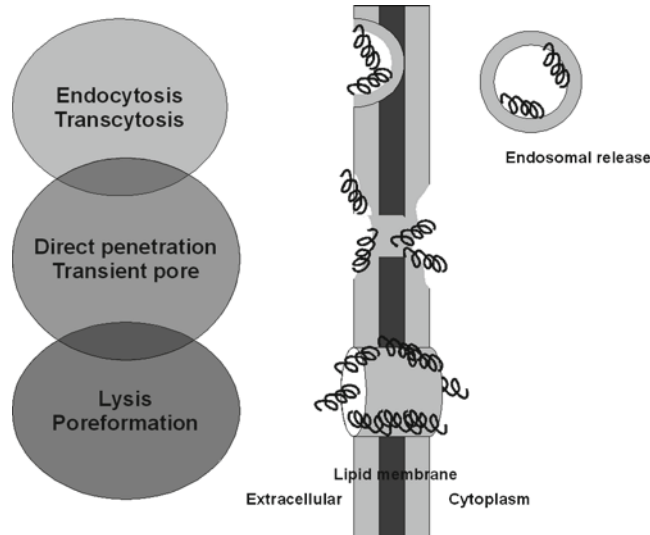


Fig. 1. Illustration of suggested mechanisms of entry into cells by cell-penetrating peptides. The *circles* are an attempt to visualize the ongoing discussion and research in the field.

membrane and eventually form a pore, through which they can enter. As a result the cell membrane is destroyed; this further may lead to cell death. At the other end of the spectra, membrane-receptor binding peptides such as insulin or galanin enter cells via receptor-mediated endocytosis, where a specific receptor is needed on the cell surface and the uptake is strictly regulated. By definition insulin and galanin are then ligands to their receptors and not CPPs per se. Neither of these classes of peptides has shown such potential in delivering cargoes across the bilayer of cell membranes as CPPs. One may speculate that CPPs have a position somewhere between the two, with the unique ability for nontoxic and en masse delivery.

It has now been established that different CPPs and also differently modified CPPs (or with different cargo) change the way they enter cells. This may be one of the reasons why it is still ongoing research to define their mechanism of entry and the fact that CPPs are a very divergent family of peptides and not defined by their way of entry.

There are at least two suggested cell entry mechanisms, endocytosis and direct penetration, maybe via a transient pore formation. Which of these mechanisms a CPP will utilize is dependent on several parameters such as size (with cargo), temperature, cell type, etc. (36, 37). It could be argued that peptides entering cells merely by endocytosis via interaction with an unspecific receptor, such as heparan sulfates, still are ligands and not CPPs.

As pointed out above, the entry mechanism of CPPs into cells is still a matter of discussion (for review (38)). It was first proposed that CPPs, especially Tat and penetratin, but also others such as poly-Arg (39–41), transportan (25), MPG (20) or Pep-1 (42),

could pass through the plasma membrane via an energy-independent pathway. For instance, the formations of micro-micelles at the membrane (11) or direct translocation through the lipid bilayer (43, 44) have been suggested. The hypothesis of a direct translocation through the plasma membrane became less popular when the entry mechanism for the Tat and the poly-arginine CPPs had to be re-evaluated following evidences of fixation artifacts during the preparation of samples for microscopic observation (45). Indeed, fixation has been described to interfere with the subcellular localization of constructs with a high content in cationic residues, such as histones and the VP22 protein (46). This redistribution upon fixation has been clearly demonstrated using fusion proteins made of penetratin, poly-Arg, or Tat peptides (47). As a consequence, the majority of the new microscopic studies on CPP cargo localization have been conducted in live cells.

A very interesting comparison of the CPP TP10, antimicrobial, and cytolytic peptides were recently published (42, 48). A hypothesis was presented that the peptide sequence only indirectly determines the mechanism; through the thermodynamics of the insertion of peptides in the lipid bilayer from the surface bound state. This would explain the Apparent lack of correlation between sequence and mechanism of entry. In addition, it is clear that the affinity for hydrophilic sequence increases when they bind the membrane in a helical formation. Hällbrink et al. (5, 34) have also performed comparative studies of the CPP uptake mechanism, and suggested that the extra- and intracellular stability is one parameter that determines the amount of peptide to enter cells (44). In addition, they propose a transient pore-formation mechanism for direct penetration (49). The cell is equipped to fix membrane damage by recruiting vesicles to the membrane and fuse them with the plasma membrane. It is well known that at low CPP concentrations, no membrane leakage can be detected, and the involvement of the membrane repair system seems to be responsible for this.

For short arginine-rich CPPs, transport has been shown to mainly follow a cellular endocytosis-mediated uptake (50–52). According to this mechanism, CPPs, particularly those with a high content in cationic residues, are first simply adsorbed at the cell surface thanks to the numerous anionic moieties, such as heparan sulfate, sialic, or phospholipidic acid (8, 53–55).

Later on, CPPs have been reported to apply different endocytosis routes: via caveolae (56) and macropinocytosis (57), through a clathrin-dependent pathway (58), and via a cholesterol-dependent clathrin-mediated pathway (59).

There are also publications that provide convincing arguments against one or the other of these cellular pathways, despite the use of rather similar experimental set-ups. It has been suggested that these controversies might be due to the use of different peptide concentrations as they can trigger different endocytotic

pathways (4). Higher CPP concentration (over 10 μM) could possibly lead to an energy-independent internalization (36, 52).

Even though the exact route into cells keeps escaping our investigations, it is clear that cargoes such as oligonucleotides are trapped in vesicular structures within the cell. Thus, increasing the escape rate from the endosome is the new strategy to improve intracellular delivery of CPP cargoes. There are several approaches; one possibility is to increase the hydrophobicity of CPPs to favor the destabilization of the endosomal membrane, whereby lipid moieties have been coupled to molecules to be delivered inside the cells. For example, such an improvement has been observed upon stearylation of an octa-arginine peptide (60) or following the introduction of a proline amino acid derivative with a higher hydrophobicity into a proline-rich CPP (61).

4. Can a CPP be Predicted to Enter Cells?

Due to the complex parameters that determine the way of uptake of a CPP, all peptides need to be tested at least by three different assays, before it can be defined as a CPP (see refs. 62, 63). However, the ability for a certain sequence to enter across a lipid bilayer can be predicted. The ability is determined by the properties of the amino acids in the primary sequence of the CPP.

Hällbrink et al. set out to predict the ability for a peptide sequence to be able to translocate a lipid membrane (34). The starting point was a library of cell-penetrating sequences which was compared with their reported inactive analogs. The sequences were converted to a sum of their bulk properties with already published (see references in Hällbrink et al.) descriptors such as partition coefficients, pK_a , molecular weight, number of heavy atoms, as well as donated and accepted hydrogen bonds. Putting these descriptors to the CPP sequences in the list showed that almost all fall in the “highly likely to translocate” category, except the Tat peptide. The criteria can be used to screen known or random protein sequences, thus this method can be used for de novo design of CPPs.

Using an evolutionary approach, Hansen et al. showed that by making a phylogenetic lineage of the classic CPP sequences, the protein derived and the synthetic and chimeric CPPs formed closer relations, or clusters, within their respective groups rather than between the groups (64).

Another similar approach was made already in the late 1990s; Duguid et al. published a physiochemical approach to predict the efficacy of plasmid-delivering peptides (33). This study is also based on the “bulk” properties of the peptides rather than the simple primary sequence.

So, yes the probability that a certain sequence will be able to enter a cell can be predicted with about 80% certainties. The YTA peptides are examples of the application possible with the method described, where a seeding sequence has been used (35), as mentioned above.

5. Applications

Historically, CPPs have been used for the delivery of drugs and biologically active peptides and proteins within the research fields of neurobiology and cancer. Already from the start, the delivery of gene-modulating agents has been an obvious field of application for these versatile peptides, this has lately been the main, if almost the only, application. For an overview of CPP-aided delivery, see Fig. 2.

In the field of cancer research, CPPs have been effectively used to increase the efficiency of cancer drugs commonly used in chemotherapy. Doxorubicin–Tat peptide conjugates have been shown to increase apoptosis on drug-resistant MCF-7/ADR breast cancer cell line by Liang and Yang (65). Lindgren et al. (35) used the CPPs YTA2 and YTA4 to increase the effects of a cytostatic agent methotrexate (MTX) on 100-fold MTX-resistant breast cancer cells MDA-MB-231. Estimated EC₅₀s for MTX, MTX–YTA2, and YTA2 were determined to be 18.5, 3.8, and 20 μ M, respectively, which proved the potency of already well-characterized therapeutic molecules into drug-resistant tumor cells. In addition, there are also several apoptosis inducing peptides of which their potency has been increased by conjugating them to CPPs.

When using CPPs in conjunction with either conventional cancer drugs or antimicrobial/proapoptotic peptides, there can be

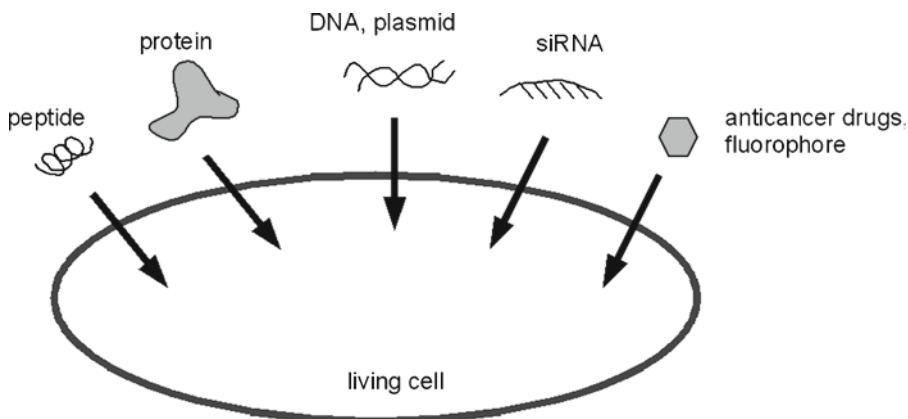


Fig. 2. Schematic overview of possible applications where cell-penetrating peptides have been shown to function well as delivery vehicles, both in vitro and in vivo.

side effects since CPPs themselves are not cell specific enough. One way of increasing the specificity is by adding homing sequences to the CPP. Homing peptides for tumor blood and lymph vasculature have been identified by using *in vivo* screening of phage-displayed peptide libraries (66, 67). PEGA peptide (a peptide that has been shown to accumulate in breast cancer cells in mice) has recently been conjugated to pVEC retaining its homing properties to blood vessels in breast cancer *in vivo*; also the efficiency of chlorambucil when conjugated to aforementioned PEGA-pVEC chimeric peptide was shown to increase its potency by a factor of 4 (68).

For neuroscientists, CPPs have shown to be an appreciated tool for neuronal rescue in several models of neurodegenerative diseases (69, 70). CPPs have been used to examine β -amyloid function and toxicity (71, 72), apoptotic processes (73), axon studies (71, 74), and nerve trauma (75), just to mention a few. In neuroscience, there is another aspect of barrier delivery to consider; delivery to the central nervous system, which means crossing the blood–brain barrier. Here, the CPPs are of particular interest (4, 6), especially when current gene vectors or proteins do not cross the BBB, and only a few brain diseases respond well to small-molecule drugs.

The poor permeability of the plasma membrane of eukaryotic cells to DNA, together with the low efficiency of DNA or oligonucleotides to reach their target within cells, constitutes the major barriers for the development of oligonucleotide-based therapeutic molecules. The development of gene delivery has been directly correlated with the dramatic acceleration in the production of new therapeutic molecules. A number of nonviral strategies have been proposed, including lipid-, poly-cationic-, nanoparticle-, and peptide-based methods (76) (reviewed in ref. 77), but only a few of these technologies have been efficiently applied *in vivo* at either preclinical or clinical levels.

Within the field of delivery, there are different schools on how to “conjugate” the cargo. Divita and colleagues have developed CPPs that noncovalently forms complexes with ONs (78) while Gait and others (79) applies the linkage via a disulfide bond. It is partly dependent on which ON is used. Although conjugation methods offer several advantages for *in vivo* applications, including rationalization and control of the CPP – cargo, they remain limited from the chemical point of view, as they might risk altering the biological activity of the cargoes. The CPPs MPG and Pep have been described to form stable nanoparticles with cargoes without the need for cross-linking or chemical modifications. MPG have been shown to deliver nucleic acids (plasmid DNA, oligonucleotides, and siRNA) and Pep for proteins and peptides into a variety of cell lines and *in vivo* (80, 81). This noncovalent strategy has been recently extended to other CPPs, including Tat (82) and transportan (83, 84).

6. Hot Spots in CPP Research

The hot spot is, as mentioned earlier, siRNA delivery by CPPs. In addition, the possibilities emerging for targeting CPPs to a certain tissue are also one of the main interests of today's research.

RNA interference constitutes a powerful tool for biological studies, but has also become one of the most challenging therapeutic strategies. Small interfering RNA (siRNA)-based strategies have the ability to specifically inhibit the expression of any protein; however, the strategy suffers from poor delivery and biodistribution; siRNA cannot enter into cells and end up in the liver or kidney upon systemic delivery. Among the new CPP-based delivery systems proposed that enable siRNA to cross cell membranes, only a few possess the properties of a therapeutic carrier including high-delivery efficiency and absence of cytotoxicity and immunogenicity. Efficient uptake allows to decrease the dose required to achieve a significant effect, thereby decreasing secondary side effects associated with a lack of specificity.

Gait and Lindsey delivered siRNA to lung tissue using disulfide conjugated to the CPPs Tat and penetratin, adding a cholesterol group to the conjugate increased the stability (3). Furthermore, mucosal (85) and ocular (86) delivery have been enhanced by adding CPPs.

Eguchi et al. (87) report a siRNA delivery approach using a peptide transduction domain–double-stranded RNA-binding fusion protein. They bind to siRNAs with high avidity, masking the siRNA's negative charge thereby allowing cellular uptake.

The literature on selective delivery using peptides, especially for cancer targeting (as reviewed in ref. 88), is steadily increasing. The approaches vary from adding a targeting ligand in order to have higher binding affinity for the intended tissue (68) to activating the penetration at the correct site (89, 90). Targeted cancer drugs which can specifically kill tumor cells will avoid side effects and lower doses. There are several publications on cancer drug delivery (91, 92). Another application is to use selective delivery for imaging purposes (93) to, for instance, increase the success rate after tumor surgery. As the view of peptides as drugs is changing, the use of peptide-based targeting strategies holds a certain place in drug development, for instance (94).

Finally, CPPs are now sold as tools for research. For example, penetratin in its commercial version has an activated group sensitive to nucleophilic attack by a sulfhydryl function conveniently allowing the spontaneous formation of a disulfide bridge between any cargo molecule and penetratin. It is noteworthy to consider that a stable covalent linkage has to be formed between CPP and cargo to allow translocation, although a couple of publications also reported a surprising efficacy upon simple mixing with the

cargo entities. Pep-1, which has been marketed as “Chariot” (42), can induce internalization of a cargo molecule just by being mixed with it (31).

7. Conclusions and Potential in Therapeutics

Due to their low biomembrane permeability and their relatively rapid degradation, polypeptides and oligonucleotides were generally considered to be of limited therapeutic value. However, there has been a drastic change of view on peptides as drugs; they are now considered “druggable.”

Delivering peptides across a lipid layer such as the cell membrane has probably been the major barrier in using peptides as drugs, however, when applying CPPs this is not a problem. Moreover, recent publications (95–98) show that peptides are stable enough for in vivo applications, and there are well-known modifications that can prolong their half-life, such as D-amino acids exchange or pegylation. Another aspect of CPPs as therapeutics, which is close to a solution, is their unspecific entry into cells. Today, there are several examples on targeted delivery by CPPs such as Tsien and colleagues (89) and Torchilin et al. (99), for review see ref. 88.

Peptides have many advantages over small organic molecules such as that they can be more potent, show higher specificity, and have fewer toxicology problems. They do not have drug–drug interaction challenges and so far no major activation of the immune system as CPPs have been suggested to deliver vaccines (100).

Here, we have presented an overview of the research field of CPPs today which also include several clinical trials ongoing, for example, phosphothioates conjugated to an arginine-rich CPP for splice correction (95, 101). In conclusion, even though the future is bright for CPPs as therapeutics, the applications are still far from the clinic so therefore applied research and more clinical trials in the field of CPPs are needed.

Acknowledgements

The work presented in this article was supported by Swedish Research Council (VR-NT); by Center for Biomembrane Research, Stockholm; and by Knut and Alice Wallenberg’s Foundation.

References

1. Järver, P., and Langel, Ü. (2004) The use of cell-penetrating peptides as a tool for gene regulation. *Drug Discov Today* **9**, 395–402.
2. Joliot, A. (2005) Transduction peptides within naturally occurring proteins. *Sci STKE* **2005**, pe54.
3. Moschos, S. A., Jones, S. W., Perry, M. M., Williams, A. E., Erjefalt, J. S., Turner, J. J., Barnes, P. J., Sproat, B. S., Gait, M. J., and Lindsay, M. A. (2007) Lung delivery studies using siRNA conjugated to TAT(48–60) and penetratin reveal peptide induced reduction in gene expression and induction of innate immunity. *Bioconjug Chem* **18**, 1450–9.
4. Dupont, E., Prochiantz, A., and Joliot, A. (2007) Identification of a signal peptide for unconventional secretion. *J Biol Chem* **282**, 8994–9000.
5. Hällbrink, M., Florén, A., Elmquist, A., Pooga, M., Bartfai, T., and Langel, Ü. (2001) Cargo delivery kinetics of cell-penetrating peptides. *Biochim Biophys Acta* **1515**, 101–9.
6. Lindgren, M. E., Hällbrink, M. M., Elmquist, A. M., and Langel, Ü. (2004) Passage of cell-penetrating peptides across a human epithelial cell layer in vitro. *Biochem J* **377**, 69–76.
7. Ma, H. L., Whitters, M. J., Konz, R. F., Senices, M., Young, D. A., Grusby, M. J., Collins, M., and Dunussi-Joannopoulos, K. (2003) IL-21 activates both innate and adaptive immunity to generate potent antitumor responses that require perforin but are independent of IFN-gamma. *J Immunol* **171**, 608–15.
8. Joliot, A., Pernelle, C., Deagostini-Bazin, H., and Prochiantz, A. (1991) Antennapedia homeobox peptide regulates neural morphogenesis. *Proc Natl Acad Sci U S A* **88**, 1864–8.
9. Derossi, D., Joliot, A. H., Chassaing, G., and Prochiantz, A. (1994) The third helix of the Antennapedia homeodomain translocates through biological membranes. *J Biol Chem* **269**, 10444–50.
10. Derossi, D., Chassaing, G., and Prochiantz, A. (1998) Trojan peptides: the penetratin system for intracellular delivery. *Trends Cell Biol* **8**, 84–7.
11. Derossi, D., Calvet, S., Trembleau, A., Brunissen, A., Chassaing, G., and Prochiantz, A. (1996) Cell internalization of the third helix of the Antennapedia homeodomain is receptor-independent. *J Biol Chem* **271**, 18188–93.
12. Ruben, S., Perkins, A., Purcell, R., Joung, K., Sia, R., Burghoff, R., Haseltine, W. A., and Rosen, C. A. (1989) Structural and functional characterization of human immunodeficiency virus tat protein. *J Virol* **63**, 1–8.
13. Vogel, B. E., Lee, S. J., Hildebrand, A., Craig, W., Pierschbacher, M. D., Wong-Staal, F., and Ruoslahti, E. (1993) A novel integrin specificity exemplified by binding of the alpha v beta 5 integrin to the basic domain of the HIV Tat protein and vitronectin. *J Cell Biol* **121**, 461–8.
14. Elliot, B. C., Wisniewski, A. V., Johnson, J., Fenwick-Smith, D., Wiest, P., Hamer, D., Kresina, T., and Flanigan, T. P. (1997) In vitro inhibition of *Cryptosporidium parvum* infection by human monoclonal antibodies. *Infect Immun* **65**, 3933–5.
15. Ensoli, B., Buonaguro, L., Barillari, G., Fiorelli, V., Gendelman, R., Morgan, R. A., Wingfield, P., and Gallo, R. C. (1993) Release, uptake, and effects of extracellular human immunodeficiency virus type 1 Tat protein on cell growth and viral transactivation. *J Virol* **67**, 277–87.
16. Vives, E., Brodin, P., and Lebleu, B. (1997) A truncated HIV-1 Tat protein basic domain rapidly translocates through the plasma membrane and accumulates in the cell nucleus. *J Biol Chem* **272**, 16010–7.
17. Schwarze, S. R., Ho, A., Vocero-Akbani, A., and Dowdy, S. F. (1999) In vivo protein transduction: delivery of a biologically active protein into the mouse. *Science* **285**, 1569–72.
18. Futaki, S., Nakase, I., Tadokoro, A., Takeuchi, T., and Jones, A. T. (2007) Arginine-rich peptides and their internalization mechanisms. *Biochem Soc Trans* **35**, 784–7.
19. Lin, M. L., and Bertics, P. J. (1995) Laminin responsiveness is associated with changes in fibroblast morphology, motility, and anchorage-independent growth: cell system for examining the interaction between laminin and EGF signaling pathways. *J Cell Physiol* **164**, 593–604.
20. Morris, M. C., Vidal, P., Chaloin, L., Heitz, F., and Divita, G. (1997) A new peptide vector for efficient delivery of oligonucleotides into mammalian cells. *Nucleic Acids Res* **25**, 2730–6.
21. Chaloin, L., Vidal, P., Heitz, A., Van Mau, N., Mery, J., Divita, G., and Heitz, F. (1997) Conformations of primary amphipathic carrier peptides in membrane mimicking environments. *Biochemistry* **36**, 11179–87.

22. Zhang, M. Y., Sun, S. C., Bell, L., and Miller, B. A. (1998) NF-kappaB transcription factors are involved in normal erythropoiesis. *Blood* **91**, 4136–44.
23. Chaloin, L., Vidal, P., Lory, P., Mery, J., Lautredou, N., Divita, G., and Heitz, F. (1998) Design of carrier peptide–oligonucleotide conjugates with rapid membrane translocation and nuclear localization properties. *Biochem Biophys Res Commun* **243**, 601–8.
24. Pooga, M., Lindgren, M., Hällbrink, M., Bräkenhielm, E., and Langel, Ü. (1998) Galanin-based peptides, galparan and transportan, with receptor-dependent and independent activities. *Ann N Y Acad Sci* **863**, 450–3.
25. Pooga, M., Hällbrink, M., Zorko, M., and Langel, Ü. (1998) Cell penetration by transportan. *FASEB J* **12**, 67–77.
26. Pooga, M., Soomets, U., Hällbrink, M., Valkna, A., Saar, K., Rezaei, K., Kahl, U., Hao, J. X., Xu, X. J., Wiesenfeld-Hallin, Z., Hökfelt, T., Bartfai, T., and Langel, Ü. (1998) Cell penetrating PNA constructs regulate galanin receptor levels and modify pain transmission in vivo. *Nat Biotechnol* **16**, 857–61.
27. Mäe, M., and Langel, Ü. (2006) Cell-penetrating peptides as vectors for peptide, protein and oligonucleotide delivery. *Curr Opin Pharmacol* **6**, 509–14.
28. Oehlke, J., Scheller, A., Wiesner, B., Krause, E., Beyermann, M., Klauschenz, E., Melzig, M., and Bienert, M. (1998) Cellular uptake of an alpha-helical amphipathic model peptide with the potential to deliver polar compounds into the cell interior non-endocytically. *Biochim Biophys Acta* **1414**, 127–39.
29. Oehlke, J., Krause, E., Wiesner, B., Beyermann, M., and Bienert, M. (1997) Extensive cellular uptake into endothelial cells of an amphipathic beta-sheet forming peptide. *FEBS Lett* **415**, 196–9.
30. Scheller, A., Oehlke, J., Wiesner, B., Dathe, M., Krause, E., Beyermann, M., Melzig, M., and Bienert, M. (1999) Structural requirements for cellular uptake of alpha-helical amphipathic peptides. *J Pept Sci* **5**, 185–94.
31. Deshayes, S., Simeoni, F., Morris, M. C., Divita, G., and Heitz, F. (2007) Peptide-mediated delivery of nucleic acids into mammalian cells. *Methods Mol Biol* **386**, 299–308.
32. Crombez, L., Aldrian-Herrada, G., Konate, K., Nguyen, Q. N., McMaster, G. K., Brasseur, R., Heitz, F., and Divita, G. (2009) A new potent secondary amphipathic cell-penetrating peptide for siRNA delivery into mammalian cells. *Mol Ther* **17**, 95–103.
33. Duguid, J. G., Li, C., Shi, M., Logan, M. J., Alila, H., Rolland, A., Tomlinson, E., Sparrow, J. T., and Smith, L. C. (1998) A physicochemical approach for predicting the effectiveness of peptide-based gene delivery systems for use in plasmid-based gene therapy. *Biophys J* **74**, 2802–14.
34. Hällbrink, M., Kilk, K., Elmquist, A., Lundberg, P., Lindgren, M., Jiang, Y., Pooga, M., Soomets, U., and Langel, Ü. (2005) Prediction of cell-penetrating peptides. *Int J Pept Res Ther* **11**, 249–59.
35. Lindgren, M., Rosenthal-Aizman, K., Saar, K., Eiriksdottir, E., Jiang, Y., Sassian, M., Östlund, P., Hällbrink, M., and Langel, Ü. (2006) Overcoming methotrexate resistance in breast cancer tumour cells by the use of a new cell-penetrating peptide. *Biochem Pharmacol* **71**, 416–25.
36. Tünnemann, G., Martin, R. M., Haupt, S., Patsch, C., Edenhofer, F., and Cardoso, M. C. (2006) Cargo-dependent mode of uptake and bioavailability of TAT-containing proteins and peptides in living cells. *FASEB J* **20**, 1775–84.
37. El-Andaloussi, S., Järver, P., Johansson, H. J., and Langel, Ü. (2007) Cargo-dependent cytotoxicity and delivery efficacy of cell-penetrating peptides: a comparative study. *Biochem J* **407**, 285–92.
38. Heitz, F., Morris, M. C., and Divita, G. (2009) Twenty years of cell-penetrating peptides: from molecular mechanisms to therapeutics. *Br J Pharmacol* **157**, 195–206.
39. Wender, P. A., Mitchell, D. J., Pattabiraman, K., Pelkey, E. T., Steinman, L., and Rothbard, J. B. (2000) The design, synthesis, and evaluation of molecules that enable or enhance cellular uptake: peptoid molecular transporters. *Proc Natl Acad Sci U S A* **97**, 13003–8.
40. Rothbard, J. B., Garlington, S., Lin, Q., Kirschberg, T., Kreider, E., McGrane, P. L., Wender, P. A., and Khavari, P. A. (2000) Conjugation of arginine oligomers to cyclosporin A facilitates topical delivery and inhibition of inflammation. *Nat Med* **6**, 1253–7.
41. Futaki, S. (2002) Arginine-rich peptides: potential for intracellular delivery of macromolecules and the mystery of the translocation mechanisms. *Int J Pharm* **245**, 1–7.
42. Morris, M. C., Depollier, J., Mery, J., Heitz, F., and Divita, G. (2001) A peptide carrier for the delivery of biologically active proteins into mammalian cells. *Nat Biotech* **19**, 1173–6.
43. Thorén, P. E., Persson, D., Lincoln, P., and Norden, B. (2005) Membrane destabilizing properties of cell-penetrating peptides. *Biophys Chem* **114**, 169–79.
44. Palm, C., Jayamanne, M., Kjellander, M., and Hällbrink, M. (2007) Peptide degradation

- is a critical determinant for cell-penetrating peptide uptake. *Biochim Biophys Acta* **1768**, 1769–76.
45. Richard, J. P., Melikov, K., Vives, E., Ramos, C., Verbeure, B., Gait, M. J., Chernomordik, L. V., and Lebleu, B. (2003) Cell-penetrating peptides. A reevaluation of the mechanism of cellular uptake. *J Biol Chem* **278**, 585–90.
 46. Lundberg, M., and Johansson, M. (2002) Positively charged DNA-binding proteins cause apparent cell membrane translocation. *Biochem Biophys Res Commun* **291**, 367–71.
 47. Vives, E., Richard, J. P., Rispal, C., and Lebleu, B. (2003) TAT peptide internalization: seeking the mechanism of entry. *Curr Protein Pept Sci* **4**, 125–32.
 48. Almeida, P. F., and Pokorny, A. (2009) Mechanisms of antimicrobial, cytolytic, and cell-penetrating peptides: from kinetics to thermodynamics. *Biochemistry* **48**, 8083–93.
 49. Palm-Apergi, C., Lorents, A., Padari, K., Pooga, M., and Hällbrink, M. (2009) The membrane repair response masks membrane disturbances caused by cell-penetrating peptide uptake. *FASEB J* **23**, 214–23.
 50. Futaki, S. (2006) Oligoarginine vectors for intracellular delivery: design and cellular-uptake mechanisms. *Biopolymers* **84**, 241–9.
 51. Jones, S. W., Christison, R., Bundell, K., Voyce, C. J., Brockbank, S. M., Newham, P., and Lindsay, M. A. (2005) Characterisation of cell-penetrating peptide-mediated peptide delivery. *Br J Pharmacol* **145**, 1093–102.
 52. Duchardt, F., Fotin-Mlecsek, M., Schwarz, H., Fischer, R., and Brock, R. (2007) A comprehensive model for the cellular uptake of cationic cell-penetrating peptides. *Traffic* **8**, 848–66.
 53. Vivés, E. (2003) Cellular uptake [correction of uptake] of the Tat peptide: an endocytosis mechanism following ionic interactions. *J Mol Recognit* **16**, 265–71.
 54. Brooks, H., Lebleu, B., and Vivés, E. (2005) Tat peptide-mediated cellular delivery: back to basics. *Adv Drug Deliv Rev* **57**, 559–77.
 55. Nakamura, T., Moriguchi, R., Kogure, K., Shastri, N., and Harashima, H. (2008) Efficient MHC class I presentation by controlled intracellular trafficking of antigens in octaarginine-modified liposomes. *Mol Ther* **16**, 1507–14.
 56. Fittipaldi, A., Ferrari, A., Zoppe, M., Arcangeli, C., Pellegrini, V., Beltram, F., and Giacca, M. (2003) Cell membrane lipid rafts mediate caveolar endocytosis of HIV-1 Tat fusion proteins. *J Biol Chem* **278**, 34141–9.
 57. Nakase, I., Niwa, M., Takeuchi, T., Sonomura, K., Kawabata, N., Koike, Y., Takehashi, M., Tanaka, S., Ueda, K., Simpson, J. C., Jones, A. T., Sugiura, Y., and Futaki, S. (2004) Cellular uptake of arginine-rich peptides: roles for macropinocytosis and actin rearrangement. *Mol Ther* **10**, 1011–22.
 58. Säälil, P., Elmquist, A., Hansen, M., Padari, K., Saar, K., Viht, K., Langel, Ü., and Pooga, M. (2004) Protein cargo delivery properties of cell-penetrating peptides. A comparative study. *Bioconjug Chem* **15**, 1246–53.
 59. Foerg, C., Ziegler, U., Fernandez-Carneado, J., Giralt, E., Rennert, R., Beck-Sickinger, A. G., and Merkle, H. P. (2005) Decoding the entry of two novel cell-penetrating peptides in HeLa cells: lipid raft-mediated endocytosis and endosomal escape. *Biochemistry* **44**, 72–81.
 60. Futaki, S., Ohashi, W., Suzuki, T., Niwa, M., Tanaka, S., Ueda, K., Harashima, H., and Sugiura, Y. (2001) Stearylated arginine-rich peptides: a new class of transfection systems. *Bioconjug Chem* **12**, 1005–11.
 61. Pujals, S., Fernandez-Carneado, J., Kogan, M. J., Martinez, J., Cavellier, F., and Giralt, E. (2006) Replacement of a proline with silyproline causes a 20-fold increase in the cellular uptake of a pro-rich peptide. *J Am Chem Soc* **128**, 8479–83.
 62. Holm, T., Johansson, H., Lundberg, P., Pooga, M., Lindgren, M., and Langel, Ü. (2006) Studying the uptake of cell-penetrating peptides. *Nat Protoc* **1**, 1001–5.
 63. El-Andaloussi, S., Johansson, H. J., Holm, T., and Langel, Ü. (2007) A novel cell-penetrating peptide, M918, for efficient delivery of proteins and peptide nucleic acids. *Mol Ther* **15**, 1820–6.
 64. Hansen, M., Kilk, K., and Langel, Ü. (2008) Predicting cell-penetrating peptides. *Adv Drug Deliv Rev* **60**, 572–9.
 65. Liang, J. F., and Yang, V. C. (2005) Synthesis of doxorubicin-peptide conjugate with multidrug resistant tumor cell killing activity. *Bioorg Med Chem Lett* **15**, 5071–5.
 66. Ruoslahti, E., Duza, T., and Zhang, L. (2005) Vascular homing peptides with cell-penetrating properties. *Curr Pharm Des* **11**, 3655–60.
 67. Laakkonen, P., Akerman, M. E., Biliran, H., Yang, M., Ferrer, F., Karpanen, T., Hoffman, R. M., and Ruoslahti, E. (2004) Antitumor activity of a homing peptide that targets tumor lymphatics and tumor cells. *Proc Natl Acad Sci U S A* **101**, 9381–6.
 68. Myrberg, H., Zhang, L., Mäe, M., and Langel, Ü. (2008) Design of a tumor-homing cell-penetrating peptide. *Bioconjug Chem* **19**, 70–5.
 69. Dietz, G. P., and Bahr, M. (2007) Synthesis of cell-penetrating peptides and their application

- in neurobiology. *Methods Mol Biol* **399**, 181–98.
70. Dietz, G. P., and Bahr, M. (2005) Peptide-enhanced cellular internalization of proteins in neuroscience. *Brain Res Bull* **68**, 103–14.
 71. Allinquant, B., Hantraye, P., Maillieux, P., Moya, K., Bouillot, C., and Prochiantz, A. (1995) Downregulation of amyloid precursor protein inhibits neurite outgrowth in vitro. *J Cell Biol* **128**, 919–27.
 72. Pizzi, M., Sarnico, I., Boroni, F., Benarese, M., Steimberg, N., Mazzoleni, G., Dietz, G. P., Bahr, M., Liou, H. C., and Spano, P. F. (2005) NF-kappaB factor c-Rel mediates neuroprotection elicited by mGlu5 receptor agonists against amyloid beta-peptide toxicity. *Cell Death Differ* **12**, 761–72.
 73. Dietz, G. P., Kilic, E., and Bahr, M. (2002) Inhibition of neuronal apoptosis in vitro and in vivo using TAT-mediated protein transduction. *Mol Cell Neurosci* **21**, 29–37.
 74. Theodore, L., Derossi, D., Chassaing, G., Llirbat, B., Kubes, M., Jordan, P., Chneiweiss, H., Godement, P., and Prochiantz, A. (1995) Intraneuronal delivery of protein kinase C pseudosubstrate leads to growth cone collapse. *J Neurosci* **15**, 7158–67.
 75. Kilic, U., Kilic, E., Dietz, G. P., and Bahr, M. (2004) The TAT protein transduction domain enhances the neuroprotective effect of glial-cell-line-derived neurotrophic factor after optic nerve transection. *Neurodegener Dis* **1**, 44–9.
 76. Morris, M. C., Chaloin, L., Heitz, F., and Divita, G. (2000) Translocating peptides and proteins and their use for gene delivery. *Curr Opin Biotechnol* **11**, 461–6.
 77. Abes, R., Arzumanov, A. A., Moulton, H. M., Abes, S., Ivanova, G. D., Iversen, P. L., Gait, M. J., and Lebleu, B. (2007) Cell-penetrating-peptide-based delivery of oligonucleotides: an overview. *Biochem Soc Trans* **35**, 775–9.
 78. Deshayes, S., Morris, M., Heitz, F., and Divita, G. (2008) Delivery of proteins and nucleic acids using a non-covalent peptide-based strategy. *Adv Drug Deliv Rev* **60**, 537–47.
 79. Turner, J. J., Ivanova, G. D., Verbeure, B., Williams, D., Arzumanov, A. A., Abes, S., Lebleu, B., and Gait, M. J. (2005) Cell-penetrating peptide conjugates of peptide nucleic acids (PNA) as inhibitors of HIV-1 Tat-dependent trans-activation in cells. *Nucleic Acids Res* **33**, 6837–49.
 80. Morris, M. C., Gros, E., Aldrian-Herrada, G., Choob, M., Archdeacon, J., Heitz, F., and Divita, G. (2007) A non-covalent peptide-based carrier for in vivo delivery of DNA mimics. *Nucleic Acids Res* **35**, e49.
 81. Simeoni, F., Morris, M. C., Heitz, F., and Divita, G. (2005) Peptide-based strategy for siRNA delivery into mammalian cells. *Methods Mol Biol* **309**, 251–60.
 82. Meade, B. R., and Dowdy, S. F. (2007) Exogenous siRNA delivery using peptide transduction domains/cell penetrating peptides. *Adv Drug Deliv Rev* **59**, 134–40.
 83. Lundberg, P., El-Andaloussi, S., Sutlu, T., Johansson, H., and Langel, Ü. (2007) Delivery of short interfering RNA using endosomolytic cell-penetrating peptides. *FASEB J* **21**, 2664–71.
 84. Mäe, M., El Andaloussi, S., Lundin, P., Oskolkov, N., Johansson, H. J., Guterstam, P., and Langel, Ü. (2009) A stearylated CPP for delivery of splice correcting oligonucleotides using a non-covalent co-incubation strategy. *J Control Release* **134**, 221–7.
 85. Khafagy El, S., Morishita, M., Isowa, K., Imai, J., and Takayama, K. (2009) Effect of cell-penetrating peptides on the nasal absorption of insulin. *J Control Release* **133**, 103–8.
 86. Johnson, L. N., Cashman, S. M., and Kumar-Singh, R. (2008) Cell-penetrating peptide for enhanced delivery of nucleic acids and drugs to ocular tissues including retina and cornea. *Mol Ther* **16**, 107–14.
 87. Eguchi, A., Meade, B. R., Chang, Y. C., Fredrickson, C. T., Willert, K., Puri, N., and Dowdy, S. F. (2009) Efficient siRNA delivery into primary cells by a peptide transduction domain-dsRNA binding domain fusion protein. *Nat Biotechnol* **27**, 567–71.
 88. Vivés, E., Schmidt, J., and Pelegrin, A. (2008) Cell-penetrating and cell-targeting peptides in drug delivery. *Biochim Biophys Acta* **1786**, 126–38.
 89. Jiang, T., Olson, E. S., Nguyen, Q. T., Roy, M., Jennings, P. A., and Tsien, R. Y. (2004) Tumor imaging by means of proteolytic activation of cell-penetrating peptides. *Proc Natl Acad Sci U S A* **101**, 17867–72.
 90. Pipkorn, R., Waldeck, W., Spring, H., Jenne, J. W., and Braun, K. (2006) Delivery of substances and their target-specific topical activation. *Biochim Biophys Acta* **1758**, 606–10.
 91. Sethuraman, V. A., and Bae, Y. H. (2007) TAT peptide-based micelle system for potential active targeting of anti-cancer agents to acidic solid tumors. *J Control Release* **118**, 216–24.
 92. Aroui, S., Brahim, S., Hamelin, J., De Waard, M., Breard, J., and Kenani, A. (2009) Conjugation

- of doxorubicin to cell-penetrating peptides sensitizes human breast MDA-MB 231 cancer cells to endogenous TRAIL-induced apoptosis. *Apoptosis* **14**, 1352–65.
93. Maxwell, D., Chang, Q., Zhang, X., Barnett, E. M., and Piwnica-Worms, D. (2009) An improved cell-penetrating, caspase-activatable, near-infrared fluorescent peptide for apoptosis imaging. *Bioconjug Chem* **20**, 702–9.
94. Orive, G., Hernandez, R. M., Rodriguez Gascon, A., Dominguez-Gil, A., and Pedraz, J. L. (2003) Drug delivery in biotechnology: present and future. *Curr Opin Biotechnol* **14**, 659–64.
95. Amantana, A., Moulton, H. M., Cate, M. L., Reddy, M. T., Whitehead, T., Hassinger, J. N., Youngblood, D. S., and Iversen, P. L. (2007) Pharmacokinetics, biodistribution, stability and toxicity of a cell-penetrating peptide-morpholino oligomer conjugate. *Bioconjug Chem* **18**, 1325–31.
96. Pujals, S., Fernandez-Carneado, J., Ludevid, M. D., and Giralt, E. (2008) D-SAP: a new, noncytotoxic, and fully protease resistant cell-penetrating peptide. *ChemMedChem* **3**, 296–301.
97. Neundorff, I., Rennert, R., Franke, J., Kozle, I., and Bergmann, R. (2008) Detailed analysis concerning the biodistribution and metabolism of human calcitonin-derived cell-penetrating peptides. *Bioconjug Chem* **19**, 1596–603.
98. Weiss, H. M., Wirz, B., Schweitzer, A., Amstutz, R., Rodriguez Perez, M. I., Andres, H., Metz, Y., Gardiner, J., and Seebach, D. (2007) ADME investigations of unnatural peptides: distribution of a ^{14}C -labeled beta 3-octaarginine in rats. *Chem Biodivers* **4**, 1413–37.
99. Torchilin, V. P. (2007) Targeted pharmaceutical nanocarriers for cancer therapy and imaging. *AAPS J* **9**, E128–47.
100. Brooks, N. A., Pouniotis, D. S., Tang, C. K., Apostolopoulos, V., and Pietersz, G. A. (2010) Cell penetrating peptides: application in vaccine delivery. *Biochim Biophys Acta* **1805**, 25–34.
101. Lebleu, B., Moulton, H. M., Abes, R., Ivanova, G. D., Abes, S., Stein, D. A., Iversen, P. L., Arzumanov, A. A., and Gait, M. J. (2008) Cell penetrating peptide conjugates of steric block oligonucleotides. *Adv Drug Deliv Rev* **60**, 517–29.

Chapter 2

Penetratin Story: An Overview

Edmond Dupont, Alain Prochiantz, and Alain Joliot

Abstract

Cell-penetrating peptides are short, often hydrophilic peptides that get access to the intracellular milieu. They have aroused great interest both in academic and applied research. First, cellular internalization of CPPs often involves the crossing of a biological membrane (plasma or vesicular), thus challenging the view of the nonpermeability of these structures to large hydrophilic molecules. Secondly, CPPs can drive the internalization of hydrophilic cargoes into cells, a rate-limiting step in the development of many therapeutic substances. Interestingly, the two mostly used CPPs, TAT and Penetratin peptides, are derived from natural proteins, HIV Tat and Antennapedia homeoprotein, respectively. The identification of the Penetratin peptide, summarized in this review, is intimately linked to the study of its parental natural protein.

Key words: Penetratin, Cell-penetrating peptide, Homeodomain, Homeoprotein

1. Introduction

It is extremely striking that the transgression of the dogma of membrane impermeability to hydrophilic molecules at the origin, 20 years ago, of the cell-permeable peptide field stems from the study of two unrelated transcriptional regulators, HIV Tat protein and Antennapedia homeoprotein. In both cases, the necessity to verify their pure intracellular activity had motivated the addition of these proteins in the extracellular medium. With unexpected results that suggested internalization by cultured cells leading to the development of first cell-permeable peptides, to expression strategies based on direct protein delivery – instead of classical nucleic acid transfection – and to the search for the underlying biological function of protein transduction.

2. The Origin of an Unexpected Observation

In 1988, the capture of HIV-TAT by cells and its transport to the nucleus was described (1, 2). At the same time, our laboratory was trying to correlate neuronal shape and position, and in this position/shape context, had started to investigate the function of homeoprotein transcription factors.

In the mid-1980s, we observed that brain neurons in culture adopt different polarity patterns depending on the origin of the astrocytes on which they were plated (3, 4). It was particularly striking that dendrites would only develop when neurons and astrocytes were derived from the same structure. This allowed us to establish a theoretical link between developmental morphogenetic programs and positional information. At the same time, the homeoprotein family of transcription factors that link organ shape to their positional information was discovered in *Drosophila*. We asked whether morphogenetic programs acting at the multicellular levels might also act at the single cell level on neuronal shape.

Homeoproteins are defined by the nature of their DNA-binding domain, the homeodomain. This domain is highly conserved across homeoproteins and species, and is composed of three α -helices, the third helix being more particularly dedicated to the recognition of the DNA target site (5). We wanted to test our hypothesis by injecting a homeodomain within live neurons. The logic was that the injected homeodomain would gain access to the nucleus and displace endogenous homeoproteins away from their cognate sites, thus revealing their morphological function at the single cell level. We used the homeodomain of Antennapedia for practical reasons and on the basis of the strong sequence conservation between homeodomains. Antagonizing transcriptional activity of endogenous homeoproteins was achieved through the mechanical internalization of FITC-labeled homeodomains into live postmitotic neurons (6–8). The addition of exogenous *Drosophila* Antennapedia homeodomain (AntpHD) induced strong neurite outgrowth as expected that was attributed to a competition between the homeodomain and endogenous homeoproteins for their binding sites (8). But the surprise was total when adding the homeodomain into the culture medium, for a control, we observed the same phenotype. This suggested either that the effect of the injected homeodomain was due to its leakage outside the cells – an artifact – or that the homeodomain was internalized. We verified the latter possibility and observed, much to our surprise, that the 60 amino acid long polypeptide was captured by the cells and addressed to their nuclei (8).

3. Homeodomain Translocation

In an attempt to analyze the neurite promoting function of the homeodomain and its mechanism of action, two different point mutations affecting the specificity of protein/DNA interactions (AntpHD 50A) or the structure of the homeodomain (AntpHD 48S) were introduced (9–11). The DNA-binding capacity of the two mutants is either decreased (AntpHD 50A) or completely abolished (AntpHD 48S), and the biological activity (neurite outgrowth stimulation) is lost in both cases (9–11). Most importantly, translocation into live cells is lost only in the AntpHD 48S mutant, in which a single serine residue replaces three amino acids (tryptophan 48, phenylalanine 49, and glutamine 50). Tryptophan 48 (Trp 48), and phenylalanine 49 (Phe 49) are conserved in almost all homeodomains, and important for the homeodomain structure (10).

This observation was so unexpected and disturbing that we decided to identify the mechanism involved in homeodomain capture. Interestingly, the intracellular distribution showing uniform cytoplasmic staining, and nuclear accumulation was at odd with endocytosis. Indeed, uptake was observed at 4°C, with the same uniform cytoplasmic staining. To preclude that this diffusion was due to AntpHD redistribution following fixation, the same experiments done with a FITC-tagged homeodomain on live cells and with the help of confocal microscopy gave identical results (8). Finally, it was verified that the AntpHD was retrieved, intact, from the cell nuclei at both temperature, demonstrating very limited degradation (12).

4. The Penetratin Peptide

The results with AntpHD 48S suggested the presence of a cell translocation sequence in the third helix. The 16 amino acids of the helix (amino acids 43–58 of the homeodomain) were synthesized, and internalization into live cells was followed thanks to a N-terminal biotin (13). Shorter versions of the same peptide, with N-ter or C-ter deletions, are not internalized suggesting that this sequence, thereafter Penetratin, is necessary and sufficient for internalization.

Similar to AntpHD, Penetratin can be internalized by an energy-independent mechanism at both 4 and 37°C, and has access to the cytoplasm and nucleus from which it is retrieved without apparent degradation (13). Penetratin high content in basic amino acids is reminding of TAT and oligoarginine peptides. In contrast, a unique feature of Penetratin is the presence of

hydrophobic residues, in particular tryptophanes, which are critical to the translocation process (13). Indeed, Penetratin and other basic PTDs differ in their cellular behaviors, even in the same experimental set-up (14–17). Although biophysical and biological studies have greatly help to our comprehension of Penetratin behavior, a full understanding of its mechanism of translocation is still in process.

4.1. Charge and Hydrophobicity: A Dual Mode of Interaction

Because Penetratin composed of D-amino acids (D-Penetratin) and an *inverso* form of the peptide are internalized as efficiently as Penetratin (18), it was concluded that a chiral membrane receptor (usually a protein) is not required for cellular translocation. On the other hand, the specific ability of Penetratin to form multimers in the presence of ionic detergents has led to a close examination of Penetratin/lipid interactions (13). Biophysical studies have established that Penetratin preferentially interacts with anionic phospholipids mainly through electrostatic interactions, followed by limited peptide insertion into the bilayer (19–21). Although the first studies strongly suggested that Penetratin binds to the lipid headgroups, a situation not in favor of direct translocation across pure lipid bilayers (22, 23), a more recent diversification of the experimental models and techniques have revealed a different picture. Penetratin actually crosses pure lipid bilayers, either in the presence of an applied transmembrane pH gradient (24, 25) or in response to a self-generated potential resulting from asymmetric peptide aggregation at one side of the bilayer (electroporation-like mechanism) (19). Recently, the spontaneous insertion of non-aggregated Penetratin in the inner leaflet of lipid bilayers was reported using a novel solid-state NMR technique (26). The absence of Penetratin translocation reported by other groups could reflect an unfavorable lipid composition (27–29).

It must be kept in mind that Penetratin/lipid interaction is a reciprocal process affecting both partners. Penetratin adopts a random coil structure in an aqueous environment but becomes structured in the presence of anionic phospholipids. At a low peptide/lipid ratio (1/325), the peptide adopts an α -helical conformation (13, 30–33). At a high peptide/lipid ratio (1/10), the peptide forms anti-parallel β -sheets (21, 33, 34). Conversely, Penetratin alters the organization of lipid bilayers, and the orientation of lipid acyl chains is modified upon the deep insertion of Penetratin into membrane bicelles (35). When applied on a brain lipid mixture preparation, Penetratin induces the formation of hexagonal phases (31). We have proposed that the transient remodeling of lipid organization induced by Penetratin places the peptide in a pseudo-hydrophilic environment and

allows its transfer from the extracellular medium to the cytoplasm of the cell.

4.2. Influence of Structural Parameters on Peptide Translocation

Mutation analysis has confirmed the contribution of both hydrophobic and electrostatic properties to Penetratin translocation. Mutation of basic residues favors peptide insertion in the acyl chains but destabilizes the bilayer (36). A similar situation is observed upon addition of fluorescent probes to Penetratin, which increases its hydrophobicity (37), and induces a transient destabilization of the plasma membrane in live cells, demonstrated by the uptake of a cell-impermeant DNA dye and the appearance of Phosphatidylserine at the cell surface (38). Taken together many arguments suggest that a subtle interplay between hydrophobic and electrostatic properties of Penetratin is required for its translocation. In fact, even minimal modifications, such as substitution of the two Trp residues by two Phe residues, modify peptide/lipid interactions and impair translocation in live cells (13, 35, 37, 39). By contrast neither peptide helicity nor amphipathicity seems to be required for peptide internalization (18). Indeed, increasing the amphipathicity of Penetratin by mutations increases the toxicity of the peptide rather than its translocation efficiency (40).

4.3. One or More Mechanisms of Penetratin Internalization

Recent studies on the mechanism of internalization of Penetratin in live cells have revealed a more complex picture than previously thought, and concluded to a predominant endocytic uptake and vesicular localization of the peptide (14, 15). This proposal is at odd with a direct translocation process demonstrated by several internalization protocols, in particular at 4°C, and biophysical studies. In fact there is no reason to exclude that Penetratin can be captured by endocytosis depending on cell type and tagging procedure. It remains that, in contrast to Tat, endocytosis is not a prerequisite for Penetratin transfer into the cytoplasm and nucleus. Among possible modifiers of Penetratin uptake are the highly negatively charged carbohydrates that surround most cells, in particular, glycosaminoglycans (GAGs). The complex sugars could restrict Penetratin access to the membrane, promote Penetratin aggregation (41), and induce endocytosis, with the possibility (or not) that the peptide crosses the bilayer latter, once within endosomes. Conversely, GAGs may increase peptide concentration near the membrane and favor its interaction with phospholipids and translocation.

This diversity of mechanisms has been illustrated by several studies (36, 42, 43). For example, the intracellular distribution of internalized Penetratin greatly differ between HeLa and MC57 cell lines, or the macropynocytosis inhibitor ethylisopropylamide (EIPA) decreases Penetratin uptake added at high (50 μM) but not at low (10 μM) concentration (17, 44).

5. The First Applications

Soon after the observation of homeodomain translocation, we have demonstrated the usefulness of this process for the efficient cell delivery, and biological activity of hydrophilic molecules. Both anti-sense oligonucleotides (against the β -amyloid precursor protein) and protein domains (C-terminus domain of rab3a) were efficiently internalized by cells in culture upon fusion to AntpHD (45, 46). The first in vivo application of AntpHD-mediated vectorization was the induction of T-cell responses by a peptide derived from the HLA-cw3 cytotoxic-T-cell epitope (47). It appeared very quickly that the 16 amino acid long peptide Penetratin could substitute advantageously for AntpHD, both for oligopeptide and oligonucleotide delivery (48, 49). Since this time, this vectorization strategy has expanded dramatically (50), and proven to be highly versatile toward the nature of the transported cargo (from small drugs to nanoparticles) and the biological context (both ex vivo and in vivo). Most importantly, a large panel of peptides has been characterized on the basis of their cell-penetrating behavior although only some of them have been validated with a biological cargo.

6. Conclusions

More than 10 years after the initial reports, one can ask whether CPP-based cellular delivery has reached maturity. The naïve view of a universal magic CPP bullet that delivers any hydrophilic molecule into the cell has been replaced by a more complex picture, where, for instance, the nature of the transported cargo, its mode of linkage to the CPP, or the targeted intracellular compartment have to be considered. Our knowledge in this field still remains largely empirical rather than predictive, and often relies on the setting up of dedicated experimental protocols, such as those described in this book.

References

1. Frankel, A. D., and Pabo, C. O. (1988) Cellular uptake of the Tat protein from human immunodeficiency virus, *Cell* **55**, 1189–1193.
2. Green, M., and Loewenstein, P. M. (1988) Autonomous functional domains of chemically synthesized human immunodeficiency virus tat trans-activator protein, *Cell* **55**, 1179–1188.
3. Denis-Donini, S., Glowinski, J., and Prochiantz, A. (1984) Glial heterogeneity may define the three-dimensional shape of mouse mesencephalic dopaminergic neurones, *Nature* **307**, 641–643.
4. Chamak, B., Fellous, A., Glowinski, J., and Prochiantz, A. (1987) MAP2 expression and neuritic outgrowth and branching are coregulated

- through region-specific neuro-astroglial interactions, *J Neurosci* **7**, 3163–3170.
5. Gehring, W. J., Qian, Y. Q., Billeter, M., Furukubo-Tokunaga, K., Schier, A. F., Resendez-Perez, D., Affolter, M., Otting, G., and Wuthrich, K. (1994) Homeodomain-DNA recognition, *Cell* **78**, 211–223.
 6. Ayala, J., Touchot, N., Zahraoui, A., Tavitian, A., and Prochiantz, A. (1990) The product of rab2, a small GTP binding protein, increases neuronal adhesion, and neurite growth in vitro, *Neuron* **4**, 797–805.
 7. Borasio, G. D., John, J., Wittinghofer, A., Barde, Y. A., Sendtner, M., and Heumann, R. (1989) ras p21 protein promotes survival and fiber outgrowth of cultured embryonic neurons, *Neuron* **2**, 1087–1096.
 8. Joliot, A., Pernelle, C., Deagostini-Bazin, H., and Prochiantz, A. (1991) Antennapedia homeobox peptide regulates neural morphogenesis, *Proc Natl Acad Sci U S A* **88**, 1864–1868.
 9. Bloch-Gallego, E., Le Roux, I., Joliot, A. H., Volovitch, M., Henderson, C. E., and Prochiantz, A. (1993) Antennapedia homeobox peptide enhances growth and branching of embryonic chicken motoneurons in vitro, *J Cell Biol* **120**, 485–492.
 10. Le Roux, I., Joliot, A. H., Bloch-Gallego, E., Prochiantz, A., and Volovitch, M. (1993) Neurotrophic activity of the Antennapedia homeodomain depends on its specific DNA-binding properties, *Proc Natl Acad Sci U S A* **90**, 9120–9124.
 11. Le Roux, I., Duharcourt, S., Volovitch, M., Prochiantz, A., and Ronchi, E. (1995) Promoter-specific regulation of gene expression by an exogenously added homeodomain that promotes neurite growth, *FEBS Lett* **368**, 311–314.
 12. Joliot, A. H., Triller, A., Volovitch, M., Pernelle, C., and Prochiantz, A. (1991) alpha-2,8-Polysialic acid is the neuronal surface receptor of antennapedia homeobox peptide, *New Biol* **3**, 1121–1134.
 13. Derossi, D., Joliot, A. H., Chassaing, G., and Prochiantz, A. (1994) The third helix of the Antennapedia homeodomain translocates through biological membranes, *J Biol Chem* **269**, 10444–10450.
 14. Duchardt, F., Fotin-Mlecsek, M., Schwarz, H., Fischer, R., and Brock, R. (2007) A comprehensive model for the cellular uptake of cationic cell-penetrating peptides, *Traffic* **8**, 848–866.
 15. Maiolo, J. R., Ferrer, M., and Ottinger, E. A. (2005) Effects of cargo molecules on the cellular uptake of arginine-rich cell-penetrating peptides, *Biochim Biophys Acta* **1712**, 161–172.
 16. Manceur, A., Wu, A., and Audet, J. (2007) Flow cytometric screening of cell-penetrating peptides for their uptake into embryonic and adult stem cells, *Anal Biochem* **364**, 51–59.
 17. Nakase, I., Niwa, M., Takeuchi, T., Sonomura, K., Kawabata, N., Koike, Y., Takehashi, M., Tanaka, S., Ueda, K., Simpson, J. C., Jones, A. T., Sugiura, Y., and Futaki, S. (2004) Cellular uptake of arginine-rich peptides: roles for macropinocytosis and actin rearrangement, *Mol Ther* **10**, 1011–1022.
 18. Derossi, D., Calvet, S., Trembleau, A., Brunissen, A., Chassaing, G., and Prochiantz, A. (1996) Cell internalization of the third helix of the Antennapedia homeodomain is receptor-independent, *J Biol Chem* **271**, 18188–18193.
 19. Binder, H., and Lindblom, G. (2003) Charge-dependent translocation of the Trojan peptide Penetratin across lipid membranes, *Biophys J* **85**, 982–995.
 20. Christiaens, B., Symoens, S., Verheyden, S., Engelborghs, Y., Joliot, A., Prochiantz, A., Vandekerckhove, J., Rosseneu, M., Vanloo, B., and Vanderheyden, S. (2002) Tryptophan fluorescence study of the interaction of penetratin peptides with model membranes, *Eur J Biochem* **269**, 2918–2926.
 21. Persson, D., Thorén, P. E. G., and Nordén, B. (2001) Penetratin-induced aggregation and subsequent dissociation of negatively charged phospholipid vesicles, *FEBS Lett* **25245**, 1–6.
 22. Fragneto, G., Bellet-Amalric, E., Charitat, T., Dubos, P., Graner, F., and Perino-Galice, L. (2000) Neutron and X-ray reflectivity studies at solid-liquid interfaces: the interactions of a peptide with model membranes, *Physica B* **276–278**, 501–502.
 23. Fragneto, G., Graner, F., Charitat, T., Dubos, P., and Bellet-Amalric, E. (2000) Interaction of the third helix of Antennapedia homeodomain with a deposited phospholipid bilayer: a neutron reflectivity structural study, *Langmuir* **16**, 4581–4588.
 24. Björklund, J., Biverstahl, H., Gräslund, A., Måler, L., and Brzezinski, P. (2006) Real-time transmembrane translocation of penetratin driven by light-generated proton pumping, *Biophys J* **91**, L29–L31.
 25. Magzoub, M., Pramanik, A., and Gräslund, A. (2005) Modeling the endosomal escape of cell-penetrating peptides: transmembrane pH gradient driven translocation across phospholipid bilayers, *Biochemistry* **44**, 14890–14897.

26. Su, Y., Mani, R., and Hong, M. (2008) Asymmetric insertion of membrane proteins in lipid bilayers by solid-state NMR paramagnetic relaxation enhancement: a cell-penetrating peptide example, *J Am Chem Soc* **130**, 8856–8864.
27. Barany-Wallje, E., Keller, S., Serowy, S., Geibel, S., Pohl, P., Bienert, M., and Dathe, M. (2005) A critical reassessment of penetratin translocation across lipid membranes, *Biophys J* **89**, 2513–2521.
28. Persson, D., Thorén, P. E., Esbjorner, E. K., Goksor, M., Lincoln, P., and Norden, B. (2004) Vesicle size-dependent translocation of penetratin analogs across lipid membranes, *Biochim Biophys Acta* **1665**, 142–155.
29. Terrone, D., Sang, S. L., Roudaia, L., and Silvius, J. R. (2003) Penetratin and related cell-penetrating cationic peptides can translocate across lipid bilayers in the presence of a transbilayer potential, *Biochemistry* **42**, 13787–13799.
30. Drin, G., Mazel, M., Clair, P., Mathieu, D., Kaczorek, M., and Temsamani, J. (2001) Physico-chemical requirements for cellular uptake of pAntp peptide. Role of lipid-binding affinity, *Eur J Biochem* **268**, 1304–1314.
31. Berlose, J. P., Convert, O., Derossi, D., Brunissen, A., and Chassaing, G. (1996) Conformational and associative behaviours of the third helix of antennapedia homeodomain in membrane-mimetic environments, *Eur J Biochem* **242**, 372–386.
32. Lindberg, M., and Gräslund, A. (2001) The position of the cell penetrating peptide penetratin in SDS micelles determined by NMR, *FEBS Lett* **497**, 39–44.
33. Magzoub, M., Kilk, K., Eriksson, L. E., Langel, Ü., and Gräslund, A. (2001) Interaction and structure induction of cell-penetrating peptides in the presence of phospholipid vesicles, *Biochim Biophys Acta* **1512**, 77–89.
34. Bellet-Amalric, E., Blaudez, D., Desbat, B., Graner, F., Gauthier, F., and Renault, A. (2000) Interaction of the third helix of Antennapedia homeodomain and a phospholipid monolayer, studied by ellipsometry and PM-IRRAS at the air–water interface, *Biochim Biophys Acta* **1467**, 131–143.
35. Zhang, W., and Smith, S. O. (2005) Mechanism of penetration of Antp(43–58) into membrane bilayers, *Biochemistry* **44**, 10110–10118.
36. Christiaens, B., Grooten, J., Reusens, M., Joliot, A., Goethals, M., Vandekerckhove, J., Prochiantz, A., and Rosseneu, M. (2004) Membrane interaction and cellular internalization of penetratin peptides, *Eur J Biochem* **271**, 1187–1197.
37. Esbjorner, E. K., Lincoln, P., and Norden, B. (2007) Counterion-mediated membrane penetration: cationic cell-penetrating peptides overcome born energy barrier by ion-pairing with phospholipids, *Biochim Biophys Acta* **1768**, 1550–1558.
38. Dupont, E., Prochiantz, A., and Joliot, A. (2007) Identification of a signal peptide for unconventional secretion, *J Biol Chem* **282**, 8994–9000.
39. Magzoub, M., Eriksson, L. E., and Gräslund, A. (2003) Comparison of the interaction, positioning, structure induction and membrane perturbation of cell-penetrating peptides and non-translocating variants with phospholipid vesicles, *Biophys Chem* **103**, 271–288.
40. Drin, G., Demene, H., Temsamani, J., and Bresseur, R. (2001) Translocation of the pAntp peptide and its amphipathic analogue AP-2AL, *Biochemistry* **40**, 1824–1834.
41. Ghibaudi, E., Boscolo, B., Insera, G., Laurenti, E., Traversa, S., Barbero, L., and Ferrari, R. P. (2005) The interaction of the cell-penetrating peptide penetratin with heparin, heparansulfates and phospholipid vesicles investigated by ESR spectroscopy, *J Pept Sci* **11**, 401–409.
42. Letoha, T., Gaal, S., Somlai, C., Czajlik, A., Perczel, A., and Penke, B. (2003) Membrane translocation of penetratin and its derivatives in different cell lines, *J Mol Recognit* **16**, 272–279.
43. Letoha, T., Gaal, S., Somlai, C., Venkei, Z., Glavinas, H., Kusz, E., Duda, E., Czajlik, A., Petak, F., and Penke, B. (2005) Investigation of penetratin peptides. Part 2. In vitro uptake of penetratin and two of its derivatives, *J Pept Sci* **11**, 805–811.
44. Fischer, R., Waizenegger, T., Kohler, K., and Brock, R. (2002) A quantitative validation of fluorophore-labelled cell-permeable peptide conjugates: fluorophore and cargo dependence of import, *Biochim Biophys Acta* **1564**, 365–374.
45. Allinquant, B., Hantraye, P., Mailleux, P., Moya, K., Bouillot, C., and Prochiantz, A. (1995) Downregulation of amyloid precursor protein inhibits neurite outgrowth in vitro, *J Cell Biol* **128**, 919–927.
46. Perez, F., Lledo, P. M., Karagogeos, D., Vincent, J. D., Prochiantz, A., and Ayala, J. (1994) Rab3A and Rab3B carboxy-terminal peptides are both potent and specific inhibitors of prolactin release by rat cultured anterior pituitary cells, *Mol Endocrinol* **8**, 1278–1287.

47. Schutze-Redelmeier, M. P., Gournier, H., Garcia-Pons, F., Moussa, M., Joliot, A. H., Volovitch, M., Prochiantz, A., and Lemonnier, F. A. (1996) Introduction of exogenous antigens into the MHC class I processing and presentation pathway by *Drosophila* antennapedia homeodomain primes cytotoxic T cells in vivo, *J Immunol* **157**, 650–655.
48. Theodore, L., Derossi, D., Chassaing, G., Llibat, B., Kubes, M., Jordan, P., Chneiweiss, H., Godement, P., and Prochiantz, A. (1995) Intraneuronal delivery of protein kinase C pseudosubstrate leads to growth cone collapse, *J Neurosci* **15**, 7158–7167.
49. Troy, C. M., Derossi, D., Prochiantz, A., Greene, L. A., and Shelanski, M. L. (1996) Downregulation of Cu/Zn superoxide dismutase leads to cell death via the nitric oxide-peroxynitrite pathway, *J Neurosci* **16**, 253–261.
50. Dupont, E., Prochiantz, A. and Joliot, A. (2005) Penetratins, in *Handbook of Cell-Penetrating Peptides*, pp. 5–28, CRC Press, Florida.

Part II

Methods to Test Mechanisms of Cell-Penetrating Peptides

Chapter 3

Testing Membrane Interactions of CPPs

Astrid Gräslund and Lena Mäler

Abstract

The chapter deals with some biophysical methods used for investigating CPP-induced changes in membrane properties by spectroscopy methods such as fluorescence or NMR and methods used for probing CPP-induced leakage in membranes. Some useful model systems for biomembranes are described. These include large unilamellar phospholipid vesicles (LUVs) of well-defined size (diameter typically 100 nm). A protocol for the preparation of such vesicles is included. The leakage studies make use of LUVs with entrapped dye molecules. The NMR studies make use of mixed micelles (bicelles) as a membrane mimetic system, which can be oriented in the magnetic field of the spectrometer.

Key words: Fluorescence, NMR, Large unilamellar vesicles, Bicelles, Membrane leakage, Membrane fluidity, Membrane dynamics

1. Introduction

The mechanistic aspect of CPPs is still a debated question. There is some consensus that different CPPs may employ different pathways to enter the cell, and that the presence of cargo may also change the dominating pathway, also depending on the cell type in question and other conditions. For most CPPs, the endocytotic pathways dominate, particularly in the presence of a large cargo. For translocation of large ONs, macropinocytosis initiated by interaction of the CPP complex with proteoglycans on the cell surface seems to be the major pathway (1–4). However, both direct translocation through the plasma membrane or endosomal escape following endosomal entry into the cell should involve interactions of the CPP with the biological membranes.

For a better mechanistic understanding of CPP activities, it is important to probe the interaction of the CPP with model membranes by biophysical methods. Typical methods involve

studying the membrane properties in the absence or presence of peptide by the use of fluorescence or other probes or by investigating peptide-induced leakage through the membrane. Whereas potent antimicrobial peptides can be seen to cause formation of stable pores in a phospholipid membrane or artificial bilayers, which can even be seen with microscopy, the CPPs are considered to cause formation of transient pores, which cannot be observed directly (5). In this chapter, we will discuss some methods used for investigating peptide-induced changes in membrane properties by spectroscopy methods such as fluorescence or NMR and methods used for probing peptide-induced leakage in membranes.

In the fluorescence studies, a suitable fluorescence probe is dissolved into the membrane preparation, whereupon fluorescence polarization anisotropy studies report on the dynamic behavior of the probe, which reflects on the membrane fluidity and dynamics (6). The NMR studies typically do not need an external probe, but a lipid where protons are exchanged to deuterons at specific locations which can directly give information about the dynamics of the bilayer. In these studies, ^2H NMR is used for analysis of magnetically aligned lipid mixtures (bicelles), which gives information about the quadrupolar splittings for different positions in the lipid acyl chains. For a bicelle aligned with its normal perpendicular to the static magnetic field, this relation is given by $\Delta = 3/2(e^2qQ/h)S_{\text{CD}}(1/2)$, where Δ is the quadrupolar splitting and S_{CD} is the segmental order parameter, carrying direct information about the lipid order. In favorable cases, it is possible to determine the effect that peptides have on different parts of the lipid acyl chain (7).

In a simple case, the leakage studies concern leakage of a fluorescent dye entrapped inside vesicles when the CPP is added from the outside (8, 9). More elaborate studies concern vesicle-entrapped fluorescence-labeled CPPs and their translocation through the bilayer under varying conditions (10, 11).

For these biophysical studies, model membranes of well-defined composition in terms of phospholipid content must be used. Under favorable conditions, when amphiphilic lipids are mixed with an aqueous solution, they will form bilayers, which can close and form particles, liposomes. Depending on the further treatment, the particles will develop into different kinds of vesicles, with different sizes and lamellarity. By simple agitation, the lipids form multilamellar structures (Large Multilamellar Vesicles, LMVs).

More well-defined structures can be formed from the LMV dispersions after freeze–thawing, followed by e.g., suspension through a microfilter, which results in Large Unilamellar Vesicles (LUVs, diameter typically 100–200 nm) or by sonication (ultrasound treatment), which results in Small Unilamellar Vesicles

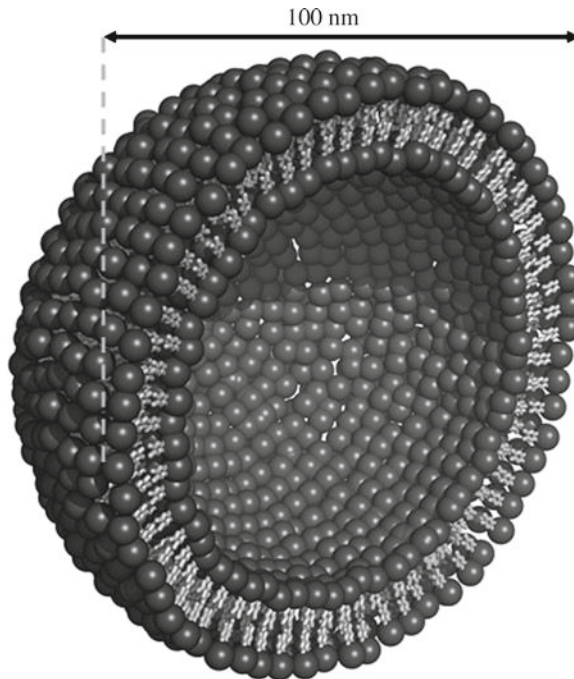


Fig. 1. Model of a large unilamellar phospholipid vesicle (LUV) with 100 nm diameter.

(SUVs, diameter typically 20–50 nm). These unilamellar vesicles can be considered as small spheres filled with water entrapped by a phospholipid bilayer (Fig. 1). The phospholipid bilayer has a thickness of about 5 nm, which implies that the SUVs have a strong curvature. The LUVs are considered as good cell mimetics, with less curvature and a relatively large inner volume. They can be used successfully in various optical spectroscopic studies, although light scattering may sometimes cause serious problems for these studies. A third category of unilamellar vesicles is Giant Unilamellar Vesicles (GUVs, diameter 10–100 μm). Below, we will describe in detail how to prepare SUVs and LUVs (see also the CPP Handbook, the chapter by Eriksson and Gräslund (12) for a more detailed discussion of the different kinds of unilamellar vesicles and their uses).

For solution NMR studies of magnetically aligned lipid mixtures, certain concentration ratios of the phospholipids DMPC and DHPC can be used. Typically, the concentration ratio between the two, $q = [\text{DMPC}]/[\text{DHPC}]$, is around 3.5, which produces mixtures (so-called mixed micelles or bicelles) that align spontaneously in a magnetic field (13–15). These mixtures have been carefully investigated, and it has been observed that they form continuous phases in the presence of a magnetic field and at temperatures well above the gel – liquid crystal transition temperature (16).

2. Materials

2.1. Vesicle Preparation

1. Phospholipids, typically 1-palmitoyl-2-oleoyl-phosphatidylcholine (POPC) with zwitterionic headgroups and 1-palmityl-2-oleoyl-phosphatidylglycerol (POPG) with negatively charged headgroups; Avanti Polar Lipids, Alabaster (AL, USA). Alternatively, dioleoyl-phosphatidylcholine (DOPC) and dioleoyl-phosphatidylglycerol (DOPG) may be used.
2. Phosphate buffer, pH around 7 (around 50 mM).
3. Lyophilizer.
4. Ultrasound bath (sonicator).
5. Polycarbonate filter with 100 nm pores; Avanti Polar Lipids, Alabaster (AL, USA).

2.2. Fluorescence Study of Membrane Fluidity

1. Small Unilamellar Vesicles in 50 mM phosphate buffer, pH 7.
2. The membrane-binding fluorescence probe 1,6-diphenyl-1,3,5-hexatriene, DPH (Sigma).
3. A fluorescence spectrometer, equipped with a polarization attachment.

2.3. NMR Study of Membrane Order and Dynamics

1. Chain-deuterated phospholipids, typically 1,2-dimyristoyl-sn-glycero-3-phosphocholine (DMPC- d_{54}) and 1,2-dihexanoyl-sn-glycero-3-phosphocholine (DHPC- d_{22}); Avanti Polar Lipids, Alabaster (AL, USA).
2. Phosphate buffer, pH 5.5. Usually a 0.2 M stock solution is prepared from which enough is taken for preparing the desired concentration (50 mM).
3. Deuterium-depleted H₂O.
4. Vortex.
5. Oven or water bath.

2.4. Membrane Leakage by Calcein Fluorescence

1. Large Unilamellar Vesicles in 50 mM phosphate buffer, pH 7.
2. Calcein, a fluorescein derivative (Molecular Probes, the Netherlands).
3. The detergent Triton-X (Sigma).

3. Methods

3.1. Preparation of Small Unilamellar Vesicles

The SUVs are sometimes more suitable than LUVs for optical studies since they cause less light scattering than LUVs.

1. Prepare a lipid suspension. The choice of lipids depends on their head-group charges: only zwitterionic, or a mixture of

zwitterionic and negative head-groups, e.g., 80/20 or 70/30 mixtures. Total lipid concentration is typically 1 mM. Mix the lipids in an aqueous solution, such as 50 mM phosphate buffer, pH7. Vortex the mixture. The result is a dispersion of multilamellar vesicles (LMVs), which can be considered as onion-like bilayer structures with water between the bilayers.

2. Sonication: The ice-cooled dispersion is sonicated under nitrogen gas, until the solution is transparent (typically 30 min). The resulting SUVs should have sizes less than 100 nm in diameter (see Note 1).
3. Remove sonifier tip metal particles and lipid debris by centrifugation ($25,000 \times g$). Ultracentrifugation may also be used.
4. The vesicle size and distribution of vesicle sizes may be checked by Dynamic Laser Light scattering (DLS).

3.2. Preparation of Large Unilamellar Vesicles

1. Prepare a lipid suspension. Choice of lipids as described for SUVs. Dissolve the lipids in an organic solvent such as chloroform and vortex.
2. Lyophilize carefully to produce a dry film (see Note 2).
3. Dissolve the dry lipids in buffer, such as 50 mM phosphate buffer, pH 7. Vortexing results in a dispersion of LMVs.
4. Reduce vesicle lamellarity by repeated (typically 4) freeze-thaw cycles.
5. To obtain a well-defined vesicle size, extrude the solution many times (typically 20) through a polycarbonate filter with a pore diameter of 100 nm. This will give LUVs with a diameter of 100 nm and a rather narrow size distribution (see Note 3).
6. The vesicle size and distribution of vesicle sizes may be checked by Dynamic Laser Light scattering (DLS).

3.3. Fluorescence Study of Membrane Fluidity

The fluorescence probe DPH is dissolved in the bilayer of SUVs, and its polarization is used as a measure of membrane fluidity (17).

1. Prepare SUVs according to the above protocol, with a total lipid concentration of about 1 mM.
2. Add DPH from a 1 mM ethanol stock solution to a concentration of 2 μ M. DPH dissolves completely in the bilayer core (18).
3. Measure steady-state fluorescence polarization of DPH (6, 19, 20).

3.4. NMR Study of Membrane Order and Dynamics

1. Preparation of high q -ratio bicelle solution. Mix DMPC- d_{54} in deuterium-depleted water or buffer solution (prepared from deuterium-depleted water). Add an appropriate amount of a 1 M stock solution of DHPC to yield

- [DMPC]/[DHPC]=3.5 (the q -ratio). The total lipid concentration should be around 50–150 mM.
- Heat the mixture to 45°C and cool to below the transition temperature (around 15°C).
 - Vortex and repeat the temperature cycling procedure until a clear solution is obtained.
 - Add the CPP to the ready-made lipid mixture (see note 4).
 - Insert into the NMR magnet and repeat the temperature cycling procedure.
 - NMR experiments should be performed at a temperature between 37 and 45°C.
 - Acquire ^2H spectra with the standard quadrupolar echo sequence $\pi/2-\tau_1-\pi/2-\tau_2$ -acq (21). The recycle delay between scans is typically set to 2 s and the spectral width to 100 kHz. Typically, several thousands of transients are recorded.
 - Measurements of quadrupolar splittings with and without the added CPP can give information about the effect that the peptide has on lipid order (and dynamics) (22).

3.5. Membrane Leakage by Calcein Fluorescence

The fluorescent dye calcein is entrapped in the LUVs, and its fluorescence is self-quenched due to its high concentration. Leakage is detected by observing an increased fluorescence from the calcein (5, 19, 20). The total 100% leakage is defined after adding Triton-X.

- Prepare LUVs according to steps 1 and 2 above. As an alternative to lyophilization in step 2, evaporate the chloroform under argon gas and then place the film under vacuum for at least 1 h to ensure complete removal of the chloroform solvent.
- Prepare a 55 mM solution of calcein in 50 mM potassium phosphate buffer, pH 7.4. Pass through 100-nm polycarbonate filter.
- Use the calcein solution to disperse the dried film from step 1, to a lipid concentration of 10 mM. Vortexing will give LMVs.
- Reduce vesicle lamellarity by repeated (typically 4) freeze-thaw cycles.
- To obtain a well-defined vesicle size, extrude the solution many times (typically 20) through a polycarbonate filter with a pore diameter of 100 nm.
- Pass through three sequential Sephadex-G25 columns to remove nonentrapped calcein. The dilution factor will be about 1.5 for the lipids.
- A sample with total lipid concentration of typically 0.4 mM is placed in a fluorimeter. The background calcein fluorescence

is measured and then CPP is added in aliquots. If leakage of vesicle entrapped calcein occurs, its fluorescence will increase. The fluorescence is measured either as a function of time after each addition or after a fixed time of incubation.

8. At the end of the measurement, the vesicles are lysed by addition of 10% Triton-X, to give the endpoint of 100% leakage.

4. Notes

1. The SUVs are metastable structures and should be used within a few days.
2. It is essential that all of the organic solvent is removed before hydration of the dried lipid film. Remaining solvent will cause problems and errors.
3. LUVs may be stored for weeks, particularly in an inert atmosphere.
4. For preparing magnetically aligned bicelle mixtures with CPPs, it may be useful to add the peptide already with the DMPC lipid. In this way, both the DMPC and the CPP are solubilized by addition of the DHPC solution.

Acknowledgments

The work presented in this article was supported by grants from the Swedish Research Council, the Center for Biomembrane Research, and from the Knut and Alice Wallenberg Foundation. We thank Dr. Jesper Lind for assistance in producing the figure.

References

1. Patel, L.N., Zaro, J.I., and Shen, W.-C. (2007) Cell penetrating peptides: Intracellular pathways and pharmaceutical perspectives *Pharm Res* **24**, 1977–1992.
2. Jones, A.T. (2007) Macropinocytosis: searching for an endocytic identity and a role in the uptake of cell penetrating peptides *J Cell Mol Med* **11**, 670–684.
3. Kerr, M.C., and Teasdale, R.D. (2009) Defining macropinocytosis *Traffic* **10**, 364–371.
4. Wadia, J.S., Stan, R.V., and Dowdy, S.F. (2004) Transducible TAT-HA fusogenic peptide enhances escape of TAT-fusion proteins after lipid raft macropinocytosis *Nat Med* **10**, 310–315.
5. Andersson, A., Danielsson, J., Gräslund, A., and Måler, L. (2007) Kinetic models for peptide-induced leakage from vesicles and cells *Eur Biophys J* **36**, 621–635.
6. Lakowicz, J.R. (1999) Principles of Fluorescence Spectroscopy, 2nd ed., Kluwer Academic/Plenum, New York, Ch. 10.
7. Seelig, J. (1977) Deuterium magnetic resonance: theory and application to lipid membranes *Q Rev Biophys* **10**, 353–418.
8. Schwarz, G. and Arbuzova, A. (1995) Pore kinetics reflected in the dequenching of a lipid vesicle entrapped fluorescent dye *Biochim Biophys Acta* **1239**, 51–57.
9. Bárány-Wallje, E., Gaur, J., Lundberg, P., Langel, Ü., and Gräslund, A. (2007) Differential

- membrane perturbation caused by the cell penetrating peptide Tp10 depending on attached cargo *FEBS Lett* **581**, 2389–2393.
10. Magzoub, M., Pramanik, A., and Gräslund, A. (2005) Modeling the endosomal escape of cell-penetrating peptides: Transmembrane pH gradient driven translocation across phospholipid bilayers *Biochemistry* **44**, 14890–14897.
 11. Björklund, J., Biverstahl, H., Gräslund, A., Mäler, L., and Brzezinski, P. (2006) Real-time transmembrane translocation of penetratin driven by light-generated proton pumping *Biophys J* **91**, L29–L31.
 12. Gräslund, A. and Eriksson, L.E.G. (2002) Biophysical studies of cell-penetrating peptides. In *Cell-Penetrating Peptides: Processes and Applications* (ed. Ü. Langel), pp 223–244, CRC, New York.
 13. Ram, P. and Prestegard, J.H. (1988) Magnetic field induced ordering of bile salt/phospholipid micelles: new media for NMR structural investigations *Biochim Biophys Acta* **940**, 289–294.
 14. Sanders, C.R., Hare, B.J., Howard, K.P., and Prestegard, J.H. (1994) Magnetically-oriented phospholipid micelles as a tool for the study of membrane-associated molecules *Prog NMR Spectrosc* **26**, 421–444.
 15. Sanders, C.R. and Prosser, R.S. (1998) Bicelles: a model membrane system for all seasons? *Structure* **6**, 1227–1234.
 16. Gaemers, S. and Bax, A. (2001) Morphology of three lyotropic liquid crystalline biological NMR media studied by translational diffusion anisotropy *J Am Chem Soc* **123**, 12343–12352.
 17. Magzoub, M., Eriksson, L.E.G., and Gräslund, A. (2003) Comparison of the interaction, positioning, structure induction and membrane perturbation of cell-penetrating peptides and non-translocating variants with phospholipid vesicles *Biophys Chem* **103**, 271–288.
 18. Lakowicz, J.R. (1999) *Principles of Fluorescence Spectroscopy*, 2nd ed., Kluwer Academic/Plenum, New York, p. 72.
 19. Magzoub, M., Oglecka, K., Pramanik, A., Eriksson, L.E.G. and Gräslund, A. (2005) Membrane perturbation effects of peptides derived from the N-termini of unprocessed prion proteins. *Biochim Biophys Acta* **1716**, 126–136.
 20. Oglecka, K., Lundberg, P., Magzoub, M., Langel, Ü., and Gräslund, A. (2008) Relevance of the N-terminal NLS-like sequence of the prion protein for membrane perturbation effects. *Biochim Biophys Acta* **1778**, 206–213.
 21. Davis, J.H., Jeffrey, K.R., Bloom, M., and Valic, M.I. (1976) Quadrupolar echo deuterium magnetic resonance spectroscopy in ordered hydrocarbon chains *Chem Phys Lett* **42**, 390–394.
 22. Biverstahl, H., Andersson, A., Gräslund, A., and Mäler L. (2004) NMR solution structure and membrane interaction of the N-terminal sequence (1-30) of the bovine prion protein *Biochemistry* **43**, 14940–14947.

Chapter 4

Interactions of Amphipathic CPPs with Model Membranes

Sébastien Deshayes, Karidia Konate, Gudrun Aldrian, Frédéric Heitz, and Gilles Divita

Abstract

Due to the poor permeability of the plasma membrane, several strategies are designed to enhance the transfer of therapeutics into cells. Over the last 20 years, small peptides called Cell-Penetrating Peptides (CPPs) have been widely developed to improve the cellular delivery of biomolecules. These small peptides derive from protein transduction domains, chimerical constructs, or model sequences. Several CPPs are primary or secondary amphipathic peptides, depending on whether the distribution of their hydrophobic and hydrophilic domains occurs from their amino-acid sequence or through α -helical folding. Most of the CPPs are able to deliver different therapeutics such as nucleic acids or proteins in vitro and in vivo. Although their mechanisms of internalization are varied and controversial, the understanding of the intrinsic features of CPPs is essential for future developments. This chapter describes several protocols for the investigation of biophysical properties of amphipathic CPPs. Surface physics approaches are specifically applied to characterize the interactions of amphipathic peptides with model membranes. Circular dichroism and infra-red spectroscopy allow the identification of their structural state. These methods are exemplified by the analyses of the main biophysical features of the cell-penetrating peptides MPG, Pep-1, and CADY.

Key words: Cell-penetrating peptides, Interactions, Phospholipids, Membrane, Adsorption, Insertion, Conformation, Versatility

1. Introduction

Since the deciphering of the human genome and analysis of its associated proteome, the development of new potential therapeutics has largely increased. The identification of specific cellular targets and mechanisms allows the conception of novel bioactive agents. However, although most of these compounds display great therapeutic potential, their clinical development is often limited by biological parameters. Indeed, from stability in serum to cellular targeting, most therapeutics are generally restricted by

the same limitations. In this respect, the low permeability of the cell membrane is a clear limiting factor for the delivery of bioactive drugs. To overcome this trouble, several delivery strategies are routinely devised and optimized. From viral to nonviral methods, the existing systems involve chemical, biological, or physical approaches.

Over the last 20 years, carrier peptides called Cell-Penetrating Peptides (CPPs) are designed to enhance the delivery of various kinds of cargoes, including small peptides, proteins, and nucleic acids into a wide variety of cell types from different tissues and organisms (1–3). Although their definition is still evolving, CPPs are generally defined as short peptidic sequences of less than 30 residues. They are usually amphipathic and possess a sufficient number of positively charged amino acids for a final positive net charge. More specifically, their main feature consists in their ability to penetrate biological membranes thereby transferring cargoes into cells (4). CPPs are divided into two groups depending on their mode of transfer of cargoes: some carrier peptides are covalently linked to the cargo, whereas other peptides form stable nanocomplexes with their cargo without any chemical cross-linking or genetic fusion (5, 6). The noncovalent approach allows for better release of the cargo since it does not imply any chemical cleavage inside the targeted cells and offers greater possibilities of development since different formulations can be prepared depending on cell lines or the nature of cargoes. Based on extensive use and studies of their internalization, several mechanisms of CPP cellular uptake have been proposed: from direct translocation models to endocytotic routes or combination of several pathways (7). Several biological and biophysical methods have been applied to elucidate the translocation properties of CPPs. Despite common features, there is no general rule, and the cellular uptake abilities of CPPs, therefore, have to be investigated individually. However, analyses of CPPs tend to show that the intrinsic biophysical properties of CPPs play a crucial role in the internalization process and the mechanism by which they enhance the delivery of biomolecules (2, 8).

Our group has developed three amphipathic CPPs designed for noncovalent use. MPG, Pep-1, and CADY peptides efficiently transfer nucleic acids, proteins, and siRNA, respectively, into cells through the formation of nanocomplexes (9). MPG and Pep-1 are primary amphipathic peptides. Their primary sequence is composed of a hydrophilic domain with positively charged residues associated to another motif mainly constituted of hydrophobic amino acids (10). The hydrophobic domain of MPG derives from the fusion sequence of the HIV-1 protein gp41 (GALFLGFLGAAGSTMGA), while the hydrophilic motif derives from the Nuclear Localization Sequence (NLS) of simian virus 40 (SV40) large T antigen (PKKKRKV). The former is required in

the main interactions with nucleic acids and is required to improve intracellular trafficking of the cargo, while the latter is required for efficient targeting of the cell membrane and internalization (11–14). The integrity of both hydrophilic and hydrophobic segments is preserved, thanks to a three amino-acid spacer (WSQ). The hydrophobic domain of Pep-1 differs from that of MPG and corresponds to a W-rich segment (KETWWETWWTE) derived from HIV-1 reverse transcriptase (15, 16). Finally, CADY is a secondary amphipathic peptide based on the sequences of the chimerical peptide PPTG1, a variant of the fusion peptide JTS1 carrier (17). CADY adopts a helical conformation in solution, and molecular modeling reveals that the lowest energy structural model corresponds to an amphipathic helical conformation stabilized by the stacking and exposure of Trp-residues on one side, of Arg and Lys-charged residues on the other, and of hydrophobic residues on yet another (18, 19).

The present chapter describes several protocols for the investigation of intrinsic biophysical properties of amphipathic CPPs. The interactions of amphipathic peptides with model membranes are studied by using specific surface physics approaches, and peptides structural characteristics are analyzed by circular dichroism and infra-red spectroscopy. In this review, we focus on the main biophysical features of MPG, Pep-1, and CADY.

2. Materials

2.1. Chemicals

1. Chloroform (CHCl_3) and methanol (Merck, cat. no. 1.02447.0500 and 1.06002.0500).
2. Sodium Chloride, suprapur 99.99% (Merck, cat. no. 1.06406.0500) and Sodium Dodecyl Sulfate (SDS), 10% solution in water (w/v) (Merck, cat. no. 1.06022.1000).
3. Pure water is provided by a Milli-Q Gradient A10 from Millipore (Wartford, Royaume-Uni.).

2.2. Phospholipids

1,2-dioleoyl-sn-glycero-3-phosphocholine (DOPC), 1,2-dioleoyl-sn-glycero-3-(1'-rac-glycerol) (DOPG), 1,2-dipalmitoyl-sn-glycero-3-phosphocholine (DPPC), and 1,2-dipalmitoyl-sn-glycero-3-phospho-(1'-rac-glycerol) (DPPG) (Avanti Polar Lipids, Alabaster, USA, cat. no. 850375, 840475, 850355, and 840455, respectively).

2.3. Peptide-Carriers MPG, Pep-1, and CADY

1. MPG is a peptide of 27 residues: GALFLGFLGAAG STMGAWSQPKKRKV (molecular weight: 2,908 Da), where the N-terminus is acetylated and the C-terminus bears a cysteamide group ($\text{NH-CH}_2\text{-CH}_2\text{-SH}$). MPG can be

synthesized in-house or obtained from commercial sources (DeliverX[®], Panomics Inc., Affymetrix). Protocols for the synthesis and purification of MPG are described in references 20, 21. The cysteamide group was shown to be essential for the transfection mechanism and stabilization of the MPG/DNA particle (11, 12). MPG is stable for at least 1 year when stored at -20°C in a lyophilized form.

2. Pep-1 is a peptide of 21 residues: KETWWETWWTEW SQPKKKRKV (molecular weight: 2,907 Da), where the N-terminus is acetylated and the C-terminus bears a cysteamide group ($\text{NH-CH}_2\text{-CH}_2\text{-SH}$). Pep-1 can be synthesized in-house or obtained from commercial sources (Chariot[®], Active Motif). Protocols for the synthesis and purification of Pep-1 are described in reference 15. The cysteamide group was shown to be essential for the transfection mechanism and stabilization of the Pep-1/peptide particle (15). Pep-1 is stable for at least 1 year when stored at -20°C in a lyophilized form.
3. CADY is a peptide of 20 residues: GLWRALWRLRLSL WRLWKA (molecular weight: 2,653 Da), where the N-terminus is acetylated and the C-terminus bears a cysteamide group ($\text{NH-CH}_2\text{-CH}_2\text{-SH}$). CADY can be synthesized in-house or obtained from commercial sources (N-ter[®], Sigma). Protocols for the synthesis and purification of CADY are described in reference 18. The cysteamide group was shown to be essential for the transfection mechanism and stabilization of the CADY/siRNA particle (18, 19). CADY is stable for at least 1 year when stored at -20°C in a lyophilized form.

3. Methods

The methods described below outline (1) preparation of solutions of peptides, phospholipids, and small unilamellar vesicles (SUVs), (2) investigation of membrane interactions at the air–water interface, and (3) analyses of the structural state of peptides in the presence of model membranes.

3.1. Solutions of Carriers, Phospholipids, and Small Unilamellar Vesicles

3.1.1. Preparation of Carrier Solutions

1. Take the vial containing the peptide powder out of the freezer and equilibrate for 30 min at room temperature without opening the vial. This step is required to limit hydration of the peptide powder. Resuspend the peptide at a concentration no greater than 1 mg/ml (concentration around 350 μM , depending on the carrier) in water.
2. Mix gently by tapping the tube and then by vortexing at low speed for 20 s.

3. Measure the ultraviolet (UV) spectrum and calculate the extinction coefficient (ϵ) of the peptide sequence based on UV amino-acid properties. The ϵ value is determined at $\lambda = 280$ nm on the basis of $5,500 \text{ M}^{-1} \text{ cm}^{-1}$ for a Trp residue and $1,490 \text{ M}^{-1} \text{ cm}^{-1}$ for a Tyr residue. Then, Beers law ($A = \epsilon l C$) is used to determine the real concentration of the peptide stock solution. A is the measured absorbance at a given wavelength, l is the path length, and C is the peptide concentration.
4. Repeated freeze/thaw cycles can induce peptide aggregation; therefore, it is recommended that one aliquot the peptide stock solution into tubes containing the amount one expects to use in a typical experiment prior to freezing. The peptide stock solution is stable for about 2 months when stored at 4°C .

3.1.2. Preparation of Phospholipid Solutions

1. Take the vial containing the lipid powder out of the freezer and equilibrate for 30 min at room temperature without opening the vial. As for peptides, this step is essential to limit hydration of the powder. Resuspend the phospholipids powder at a concentration no greater than 100 mg/ml (125 mM) in a chloroform/methanol (3/1, v/v) mixture.
2. Transfer the lipid solution into a glass vial and then mix by vortexing at low speed for 20 s.
3. The lipid stock solution is stable for about 12 months when stored at -20°C .

3.1.3. Preparation of Solutions of Small Unilamellar Vesicles

Small Unilamellar Vesicles (SUV) are prepared from DOPC, DOPG, or a mixture of DOPC and DOPG (80/20, m/m) according to the following protocol.

1. Transfer 5 mg of the phospholipids stock solution (100 mg/ml) into a glass balloon of 10 ml.
2. Evaporate the chloroform/methanol mixture (3/1, v/v) under high vacuum for at least 3 h by using a VV-micro Rotavapor from Heidolph (Schwabach, Germany).
3. Lipids are resuspended in water by vortex mixing with a volume of solution (3 ml) corresponding to a phospholipid concentration of 2 mM.
4. The resulting lipid dispersion is sonicated in one cycle of 20 min at 70% pulse cycle in an ice/water bath, using a 450D Digital Sonicator from Branson (Dietzenbach, Germany).
5. A last centrifugation of the resulting vesicles allows us to remove the remaining titanium particles from the sonication probe.
6. All SUVs preparations are equilibrated overnight at 4°C and used the next day.
7. The SUVs stock solution is stable for about 1 week at 4°C .

3.2. Membrane Interactions at the Air–Water Interface

The cell-penetrating peptides MPG, Pep-1, and CADY are designed on the basis of a primary or secondary amphipathicity. Primary amphipathic peptides, as MPG and Pep-1, are composed of a hydrophobic domain linked to a hydrophilic moiety, whereas the secondary amphipathic peptide CADY presents an amphipathic feature through a helical secondary structure that induces segregation between hydrophobic and hydrophilic domains (8, 9). The amphipathic character of these CPPs makes them surface-active products. In addition, as their biological activity involves lipid membrane interfaces, surface physics are entirely suitable to study their physicochemical and biological properties. Thus, the following methods are based on surface physics that allow the determination of several physicochemical properties of a molecule such as the affinity for interfaces (and especially hydrophobic/hydrophilic ones), the amphipathic character, the insertion into phospholipid monolayers, and the nature of interactions with lipids. These methods, more commonly known as “monolayer techniques,” are potent tools for studying the interfacial features of molecules such as antimicrobial or membrane lytic peptides and are thus entirely adapted for the study of amphipathic CPPs (22–24).

3.2.1. Adsorption at the Air–Water Interface

Amphiphilic molecules are compounds that are able to adsorb at interfaces. They are generally asymmetrical molecules that have a great ability to be oriented at the interface. By definition: a molecule will be adsorbed from solution at an interface if the energy exchange with the surface overcomes the increase in free energy which accompanies the removal of the molecule from the solution (22). In this respect, lipids and detergents are good models of amphipathic molecule. They display a good affinity and hence pronounced adsorption at the air/water interface. Once adsorbed at the air/water interface, these amphiphilic molecules are generally able to organize in a monomolecular film that induces a decrease of the surface tension of pure water. This variation of surface tension corresponds to the surface pressure Π , defined by the relation: $\Pi = \gamma_{\text{water}} - \gamma_{\text{solution}}$, where γ_{water} is the surface tension of pure water and γ_{solution} the surface tension of the solution with the adsorbed monomolecular film. The surface pressure, as the surface tension, is a force per length unit, expressed in mN/m and is generally measured with a tensiometer. For the pure air/water interface, the surface tension is $\gamma_{\text{water}} = 72.8$ mN/m at 20°C. The following protocol is described for standard adsorption measurements (Fig. 1a) that allow the identification of air/water interface affinity as well as amphipathic features of peptides (22). By plotting surface pressure (Π), a function of the concentration of peptide in the subphase (adsorption curve), two crucial values can be determined. The saturating surface pressure (Π_{sat}) indicates

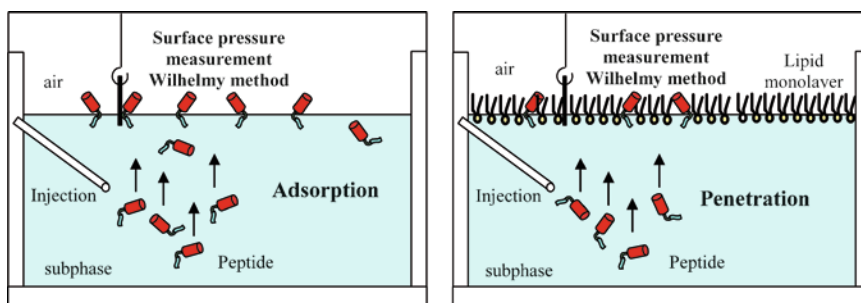


Fig. 1. Schematic representation of surface physics device for air/water interface experiments. *Left panel:* Adsorption principle. Peptides are injected into the subphase at a given concentration, and the subphase is gently stirred with a magnetic stirrer. The monomolecular film formed by peptides at the free lipid air/water interface decreases the surface tension and induces an increase in surface pressure (Π). Adsorption curves consist in plotting Π values as a function of peptide concentration. *Right panel:* Penetrations principle. Insertion measurements display the same principle as adsorption with however an initial monolayer spread at the interface leading to an initial surface pressure (Π_0). The insertion of peptide induces a variation of the surface pressure $\Delta\Pi$. Penetrations curves are obtained by plotting $\Delta\Pi$ values as a function of Π_0 . Surface pressures are expressed in mN/m.

whether the peptide has strong affinity for the air/water interface, i.e., strong amphipathicity. The Critical Micellar Concentration (CMC) corresponds to the maximal concentration for which no further increase in surface pressure is detected.

1. Fill a 71-ml Teflon Langmuir trough with a subphase solution constituted of a NaCl buffer at a concentration of 0.154 M, without any overflowing from the trough (see Note 1).
2. Insert the Langmuir–Blodgett probe, a Wilhelmy platinum plate (22), at the air–solution interface and calibrate the Langmuir–Blodgett film Prolabo (Paris, France) tensiometer on the basis of the surface tension of water ($\gamma_{\text{water}} = 72.8 \text{ mN/m}$ at 20°C) (see Note 2).
3. Inject a small amount of a highly concentrated solution of peptide into the subphase and gently stir with a magnetic stirrer. The effective concentration of peptide in the subphase is calculated on the basis of the dilution in the 71-ml trough. The surface pressure (Π) corresponding to this peptide concentration is measured at equilibrium, after 30 min.
4. Repeat step 3 until no further increase in surface pressure is detected. Surface pressure increase is then plotted as a function of the effective concentration of peptide in the subphase. The final adsorption curve, $\Pi = f(\text{concentration})$, allows us to determine the saturating surface pressure (Π_{sat}) as well as the CMC (Fig. 2) (see Note 3).

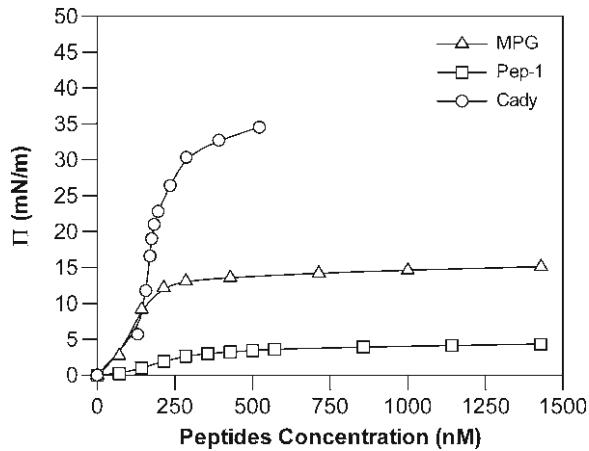


Fig. 2. Adsorption measurements of amphipathic peptides. Pep-1 (*open square*), MPG (*open triangle*), and CADY (*open circle*) are tested with a subphase solution constituted of a 0.154 M NaCl buffer. Adsorption curves allow the identification of Π_{sat} of Pep-1 (5 mN/m), MPG (13 mN/m), and CADY (30 mN/m). These values indicate that CADY is the most amphipathic peptide and that Pep-1 displays the lowest affinity for the free lipid air/water interface. CMC values, 500, 250, and 230 nM for Pep-1, MPG, and CADY, respectively, are close together. However, CMC values are in agreement with the differences observed in the affinity for the air/water interface since CADY displays the lowest CMC whereas Pep-1 the highest one. The more amphipathic peptide, i.e., CADY, has the lowest CMC value.

3.2.2. Insertion in Phospholipid Monolayers

The amphiphilic nature of phospholipids allows us to organize them in a monolayer at the air/water interface. By spreading phospholipids at the interface and by measuring the surface tension, it is possible to form a lipid monolayer at a given surface pressure (Π_i). This approach is very useful when analyzing model membrane insertion of a peptide. Indeed, any peptide that can insert into a phospholipid monolayer will induce a change in the initial surface pressure (Π_i). Then, the variation of surface pressure ($\Delta\Pi$) is indicative of the affinity of the peptide for the monolayer, its insertion in this monolayer, and thus of the peptide/lipid interactions. The following procedure is described for penetration/insertion experiments (Fig. 1b) that allow us to evaluate the affinity of peptides for phospholipid monolayers as well as the determination of the nature of peptide/lipid interactions (22, 24). The variation of surface pressure ($\Delta\Pi$) as a function of different initial surface pressures (Π_i) (penetration curve) allows us to extrapolate the Critical Pressure of Insertion (CPI), which is indicative of the insertion of peptides into phospholipid monolayers.

1. Fill a 71-ml Teflon Langmuir trough with a subphase solution constituted of a sodium chloride NaCl buffer at a concentration of 0.154 M, without any overflowing from the trough (see also Notes 1 and 2).
2. Insert the Langmuir–Blodgett probe, a Wilhelmy platinum plate, at the air–solution interface and calibrate the Langmuir–Blodgett film Prolabo (Paris, France) tensiometer.

3. Gently spread a small amount of highly concentrated solution of lipids in a chloroform/methanol mixture until a significant surface pressure is detected. The initial surface pressure (Π_i) of the phospholipid monolayer is measured at equilibrium after 30 min (see Note 4).
4. Inject a small amount of a highly concentrated solution of peptide into the subphase and gently stir with a magnetic stirrer. The final concentration of peptide in the subphase has to be close to the CMC value determined during adsorption experiments. The variation of surface pressure ($\Delta\Pi$) corresponding to the initial surface pressure (Π_i) of phospholipids is measured at equilibrium, after 30 min.
5. Repeat steps 3 and 4 until a sufficient number of points are achieved (see Note 4). Then, the variation of surface pressure ($\Delta\Pi$) is reported as a function of the initial surface pressure (Π_i) of phospholipids. The final penetration curve, $\Delta\Pi = f(\Pi_i)$, allows us to determine the CPI as well as the evaluation of strength of peptides/lipids interactions (Fig. 3) (see Note 5).

3.3. Membrane Interactions: Structural Investigations

The following protocols are described for the investigation of structural intrinsic properties of peptides using spectroscopic methods. These methods involve both circular dichroism (CD) and Fourier transform-infrared (FT-IR) spectroscopy and allow us to evaluate the conformational state of peptides in several different environments such as water, buffer, lipids vesicles, or other membrane-mimicking solvents (SDS, TFE). In addition, the structural analyses provide information on interactions of peptides with other molecular partners such as lipid/peptide interactions. The following procedures are standard approaches used to investigate structural intrinsic properties of MPG, Pep-1, and CADY.

3.3.1. Structural Analysis by Circular Dichroism Spectroscopy

The measurement of the difference between extinction coefficient of both left-handed and right-handed circularly polarized light is called circular dichroism (CD). All optically active molecules display circular dichroism. A molecule is considered optically active if it does not possess any plan, centre, or axis of symmetry. Every natural amino acid, except Gly, displays an asymmetric carbon, carbon α , which defines the optical activity and contributes to the CD signal of a peptide or protein sequence. Irrespective of their structure, all peptides and proteins exhibit a characteristic CD spectrum. However, the different torsion angles depending on the secondary structure have an impact on the position and intensity of the extrema of the CD spectrum. Thus, CD spectra are specific of the secondary structure of peptides and proteins (25–27). In this regard, an α -helix is characterized by three bands at 193, 207, and 222 nm. For a right-helix, both bands at 207 and 222 nm are minima and the band at 193 nm is a maximum,

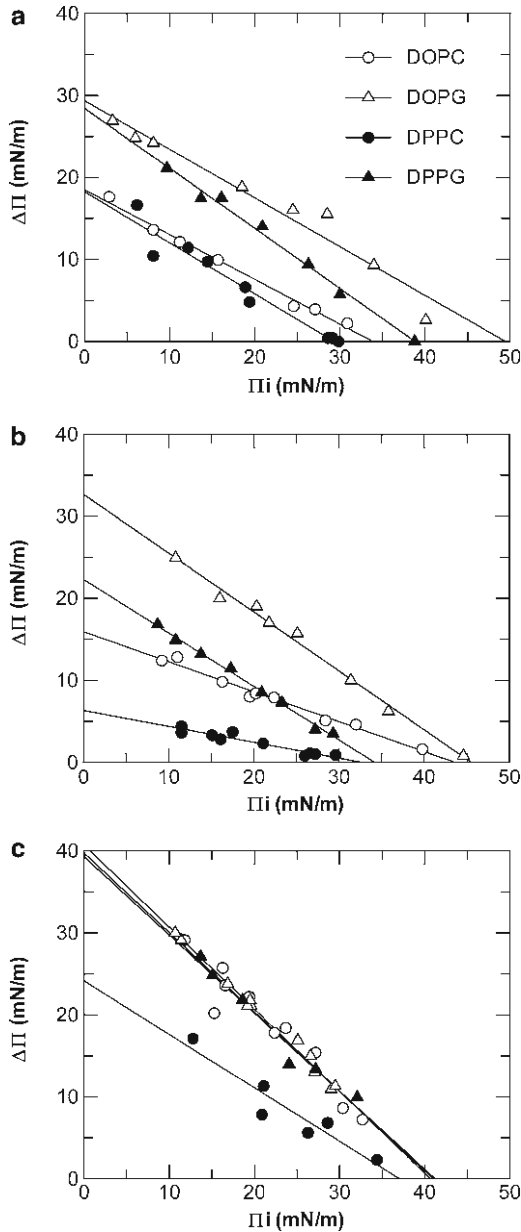


Fig. 3. Insertion of amphipathic peptides into phospholipid monolayers. Penetration curves are reported for MPG (a), Pep-1 (b), and CADY (c) into DOPC (*open circle*), DOPG (*open triangle*), DPPC (*filled circle*), and DPPG (*filled triangle*) phospholipid monolayers. The identification of high CPI values indicates that MPG, Pep-1, and CADY are able to get inserted into the phospholipid monolayers. However, their affinity differs slightly and depends on the polar heads, on the acyl chains, or on both polar heads and acyl chains of lipids.

whereas the spectrum is reversed for a left-helix. CD spectra of β -sheets are composed of two bands centered at 195 and 217 nm, corresponding to a maximum and a minimum, respectively. β turns induce a large variety of CD spectra, leading to problems in their interpretation. Nevertheless, they are generally characterized

by two bands, one negative around 205 nm and the other positive around 222 nm. CD spectra of random coils are composed of a strong minimum at 198 nm and a small positive or negative band around 220 nm.

Finally, the nature of peptide and protein environments (pH, ionic force, solvents, lipids, temperature, pressure, etc.) can influence their secondary structure and therefore the corresponding CD spectrum.

1. Peptide samples are prepared by diluting a stock solution of peptides to a concentration of 75 μM in water (see Note 6).
2. For measurement in solution, samples are prepared by filling in a Hellma Quartz Suprasil cell with an optical path of 1 mm with 200 μl of the 75 μM peptide solution.
3. For measurement in SDS, samples are prepared by filling a Hellma Quartz Suprasil cell with an optical path of 1 mm with 200 μl of the 75 μM peptide solution and increments of stock solution of SDS at 10 mM are added, and peptide concentration is corrected for the dilution.
4. For measurement in SUVs, samples are prepared by filling a Hellma Quartz Suprasil cell with an optical path of 1 mm with 200 μl of the 75 μM peptide solution, and increments of a stock solution of SUVs at 2 mM are added to obtain specific lipid/peptide ratios. Peptide concentration is corrected for the dilution.
5. All the CD spectra are recorded on a Jasco 810 dichrograph from Jasco (Tokyo, Japan) and are obtained from the average of three scans between 190 and 260 nm at an interval of 0.5 nm, a bandwidth of 1 nm, and a standard sensitivity. Blanks are collected on all solvent media and subtracted from the spectra containing peptides.
6. CD spectra are expressed as mean molecular ellipticity per residue ($\text{deg cm}^2/\text{dmol}$).
7. Typical spectra of MPG, Pep-1, and CADY in water, SDS, or SUVs of DOPG are reported in Fig. 4 (see Note 7).

3.3.2. Fourier Transform- Infra Red Spectroscopy

The FT-IR spectroscopy is based on the observation that an infrared beam turned on a molecule can induce vibrations of its molecular bonds (28). The bonding energies are modified and lead to a change in their vibration frequencies that can be detected by an infrared spectrometer. The infrared absorption spectra obtained for peptides and proteins are composed of absorptions bands corresponding to the mode of vibration of amino acids and bands characteristics of the peptidic bond, namely, amide bands (29, 30). There are seven amide bands, but the most frequently used for protein secondary structure investigations is amide I. Two main modes of vibration exist: those resulting from a stretching and

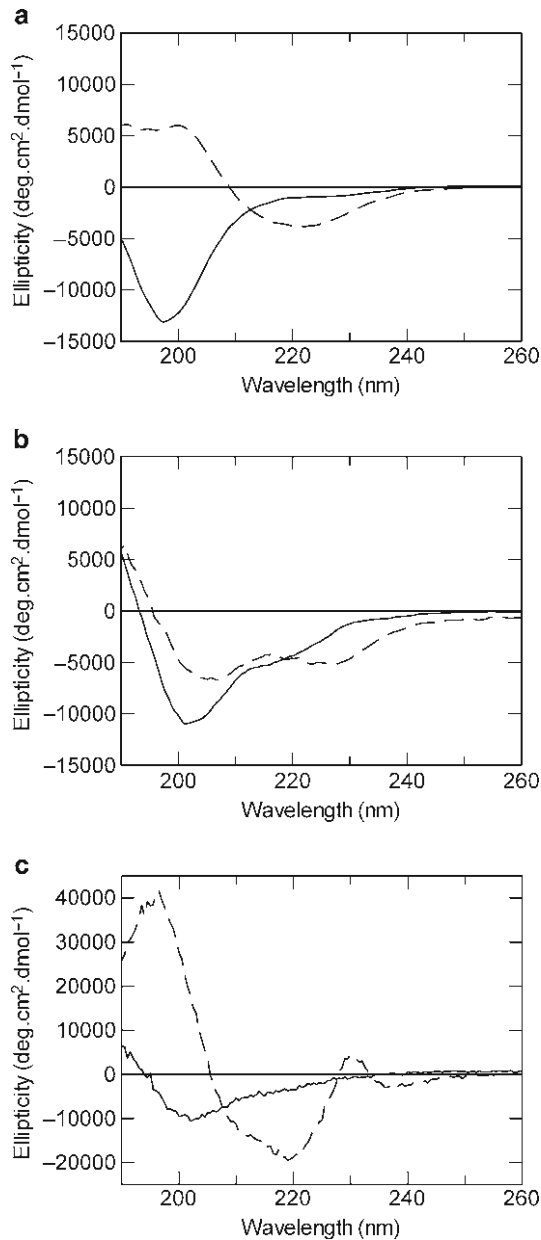


Fig. 4. Conformational analysis of amphipathic CPPs by Circular Dichroism spectroscopy. **(a)** MPG in its free form (*solid line*) and in the presence of 2.20 mM SDS (*dashed line*); **(b)** Pep-1 in its free form (*solid line*) and in the presence of DOPC/DOPG (80/20, m/m) vesicles at 7/1 lipid/peptide ratio (*dashed line*); **(c)** CADY in its free form (*solid line*) and in the presence of DOPG vesicles at 5/1 lipid/peptide ratio. Mean molar ellipticity per residues is expressed in $\text{deg cm}^2/\text{dmol}$. The peptides are mainly random coil in solution and adopt a specific secondary structure in different environments, i.e., partially β -sheet (MPG), partially α -helical (Pep-1), or mainly α -helical (CADY) in the presence of SDS, DOPC/DOPG, and DOPG vesicles, respectively.

those resulting from an angular deformation of the C=O of the peptidic bond. The exact frequency of these vibrations depends on the hydrogen bond between C=O and NH that also depends

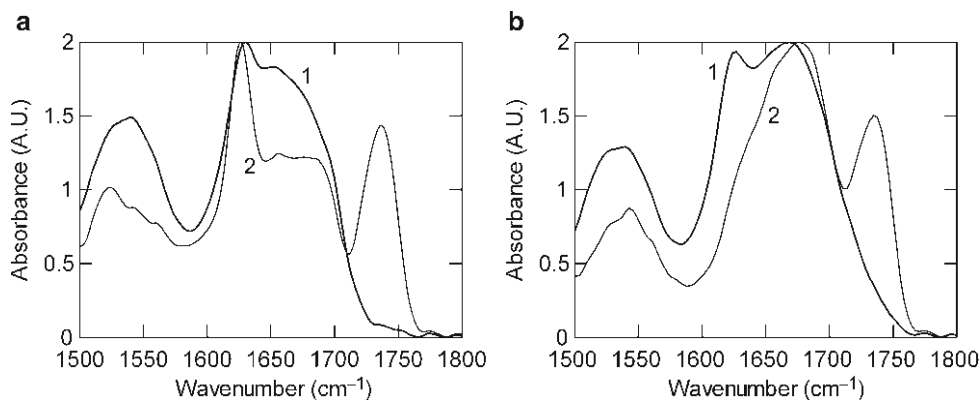


Fig. 5. Conformational analysis of amphipathic CPPs by Fourier Transformed Infra Red spectroscopy. MPG (a) and Pep-1 (b) in their free form (1) and in the presence of DOPC at a 9/1 (mol/mol) lipid/peptide ratio (2). After normalization of spectra, absorbance is expressed in arbitrary units (A.U.). MPG and Pep-1 are able to undergo a conformational transition from a random coil to β -sheet and α -helix conformation in the presence of phospholipids, respectively.

on the secondary structure of peptides and proteins. This structure/frequency relationship allows the attribution of specific bands to each conformation. Thus, the FT-IR spectra of α -helices and β -sheets are characterized by an amide I band centered at $1,655\text{ cm}^{-1}$ and between $1,625$ and $1,640\text{ cm}^{-1}$, respectively. An additional band around $1,680\text{ cm}^{-1}$ is identified for antiparallel sheets. With regard to random coils, a band at $1,650\text{ cm}^{-1}$ is generally observed in the infrared absorption spectrum.

1. Peptide samples are prepared by diluting stock solutions of peptides to a concentration of $75\text{ }\mu\text{M}$ in water.
2. Samples are prepared by depositing solutions of pure peptide and lipid/peptide mixtures at a 9/1 (mol/mol) lipid/peptide ratio onto a fluorine plate where the solvents are allowed to evaporate under a nitrogen flux.
3. FT-IR spectra are recorded on a IFS-28 spectrometer from Bruker (Ettlingen, Germany) equipped with a liquid-nitrogen-cooled MCT detector. Spectra (1,000–2,000 scans) are recorded at a spectral resolution of 4 cm^{-1} and are analyzed using the OPUS/IR2 program.
4. Typical FT-IR spectra of MPG and Pep-1 in their free form and in the presence of DOPC phospholipids are reported in Fig. 5 (see Note 8).

4. Notes

1. Several different Langmuir troughs can be used depending on the amounts and concentrations of the sample studied. For small amounts of peptides or proteins, a 10-ml Teflon

Langmuir trough is generally used and allows the injection of small amounts in the subphase solution. The subphase can be constituted of different solutions such as pure water, NaCl or phosphate buffers at different pH values, ionic force, or concentrations.

2. For small Teflon Langmuir trough, a du Nouy needle probe from Kibron (Espoo, Finland) must be used instead of the Wilhelmy platinum plate to minimize the error induced by the area of the Wilhelmy plate on the final surface area of the trough.
3. Π_{sat} values are determined for peptides, proteins, or other biomolecules with minimal but significant interfacial properties. Indeed, the less a molecule is amphipathic, the less it has affinity for air/water interface and thus lower are the surface pressure increase and Π_{sat} values. For biomolecules without any affinity for air/water interface, there is no increase in surface pressure and thus no Π_{sat} values or CMC. Then, it is strongly advised to check the quality of the experiment by adding a small amount of a specific molecule with high affinity for the air/water interface (lipid, peptide, surfactant, etc.) to induce a given increase in surface pressure.
4. Several different initial surface pressures (Π_i) of phospholipid monolayers are obtained for different spreading of phospholipids. In this regard, it is relatively difficult to obtain exactly the same initial surface pressure from one point to another. Therefore, statistically convincing reproducibility is achieved by increasing the number of measurements until a net tendency in the $\Delta\Pi=f(\Pi_i)$ curves is observed.
5. Critical Pressures of Insertion (CPI) are determined by extrapolation of the Π_i value for $\Delta\Pi=0$. The strength of peptide/lipid interactions is evaluated by extrapolation of the $\Delta\Pi$ value for $\Pi_i=0$ and comparison with the Π_{sat} value. In general, high CPI reveals that the peptides are able to get inserted spontaneously into the phospholipid monolayer. In addition, values >35 mN/m point out a spontaneous insertion into biological membranes. Strong differences between $\Delta\Pi$ for $\Pi_i=0$ and Π_{sat} indicate strong peptide/lipid interactions, while similar values suggest no or weak peptides/lipids interactions.
6. Preliminary studies have shown that for peptides of 20–30 residues, 200 μl of sample at 75 μM in a cell with an optical path of 1 mm allows recording of CD spectra with good signal/noise ratio. Although higher and lower concentrations can be used, several parameters, such as the optical path of the cell and acquisition time, must be adjusted to preserve a good signal/noise ratio.

7. Although several methods allow analysis of CD spectra and determination of percentages of secondary structure, they are often based on protein sets that are not really suitable for small peptides.
8. It is important to remember that in contrast to CD investigations, FT-IR spectroscopy involves dried lipid/peptide samples. This approach may, therefore, sometime favor peptide aggregation and then intermolecular (peptide/peptide) interactions, thus leading to an overestimation of β -sheet structure. Thus, FT-IR studies have to be correlated with other structural analyses.

Acknowledgments

This work was supported in part by the Centre National de la Recherche Scientifique (CNRS) and by grants from the ANR (Agence Nationale de la Recherche, ANR-06-BLAN-0071), and the European Community (QLK2-CT-2001-01451). We thank May C. Morris (CRBM-UMR5237-CNRS) for critical reading of the manuscript and all members of the laboratory and our collaborators for fruitful discussions.

References

1. Dietz, G.P. and Bahr, M. (2004) Delivery of bioactive molecules into the cell: the Trojan horse approach. *Mol. Cell. Neurosci.* **27**, 85–131.
2. Fischer, R., Fotin-Mleczek, M., Hufnagel, H. and Brock, R. (2005) Break on through to the other side—biophysics and cell biology shed light on cell-penetrating peptides. *Chem. Biochem.* **6**, 2126–2142.
3. Heitz, F., Morris, M.C. and Divita, G. (2009) Twenty years of cell-penetrating peptides: from molecular mechanisms to therapeutics. *Br. J. Pharmacol.* **157**, 195–206.
4. Langel, Ü. (2006) Preface, Cell-Penetrating Peptides, 2nd edition. (Ed.: Ü. Langel), CRC Press, Boca Raton.
5. Morris, M.C., Deshayes, S., Heitz, F. and Divita, G. (2008) Cell-penetrating peptides: from molecular mechanisms to therapeutics. *Biol. Cell.* **100**, 201–217.
6. Mano, M., Teodósio, C., Paiva, A., Simões, S. and Pedroso de Lima, M.C. (2005) On the mechanisms of the internalization of S4(13)-PV cell-penetrating peptide. *Biochem. J.* **390**, 603–612.
7. Duchardt, F., Fotin-Mleczek, M., Schwarz, H., Fischer, R. and Brock, R. (2007) A comprehensive model for the cellular uptake of cationic cell-penetrating peptides. *Traffic* **8**, 848–866.
8. Deshayes, S., Morris, M.C., Divita, G. and Heitz, F. (2005) Cell-penetrating peptides: tools for intracellular delivery of therapeutics. *Cell. Mol. Life Sci.* **62**, 1839–1849.
9. Crombez, L., Morris, M.C., Deshayes, S., Heitz, F. and Divita, G. (2008) Peptide-based nanoparticle for ex vivo and in vivo drug delivery. *Curr. Pharm. Des.* **14**, 3656–3665.
10. Deshayes, S., Morris, M.C., Heitz, F. and Divita, G. (2008) Delivery of proteins and nucleic acids using a non-covalent peptide-based strategy. *Adv. Drug Deliv. Rev.* **60**, 537–547.
11. Morris, M.C., Vidal, P., Chaloin, L., Heitz, F. and Divita, G. (1997) A new peptide vector for efficient delivery of oligonucleotides into mammalian cells. *Nucleic Acids Res.* **25**, 2730–2736.

12. Morris, M.C., Chaloin, L., Méry, J., Heitz, F. and Divita, G. (1999) A novel potent strategy for gene delivery using a single peptide vector as a carrier. *Nucleic Acids Res.* **27**, 3510–3517.
13. Simeoni, F., Morris, M.C., Heitz, F. and Divita, G. (2003) Insight into the mechanism of the peptide-based gene delivery system MPG: implications for delivery of siRNA into mammalian cells. *Nucleic Acids Res.* **31**, 2717–2724.
14. Deshayes, S., Gerbal-Chaloin, S., Morris, M.C., Aldrian-Herrada, G., Charnet, P., Divita, G. and Heitz, F. (2004) On the mechanism of non-endosomal peptide-mediated cellular delivery of nucleic acids. *Biochim. Biophys. Acta* **1667**, 141–147.
15. Morris, M.C., Depollier, J., Méry, J., Heitz, F. and Divita, G. (2001) A peptide carrier for the delivery of biologically active proteins into mammalian cells. *Nat. Biotechnol.* **19**, 1173–1176.
16. Deshayes, S., Heitz, A., Morris, M.C., Charnet, P., Divita, G. and Heitz, F. (2004) Insight into the mechanism of internalization of the cell-penetrating carrier peptide Pep-1 through conformational analysis. *Biochemistry* **43**, 1449–1457.
17. Rittner, K., Benavente, A., Bompard-Sorlet, A., Heitz, F., Divita, G., Brasseur, R. and Jacobs, E. (2002) New basic membrane-stabilizing peptides for plasmid-based gene delivery in vitro and in vivo. *Mol. Ther.* **5**, 104–114.
18. Crombez, L., Aldrian-Herrada, G., Konate, K., Nguyen, Q.N., McMaster, G.K., Brasseur, R., Heitz, F. and Divita, G. (2009) A new potent secondary amphipathic cell-penetrating peptide for siRNA delivery into mammalian cells. *Mol. Ther.* **17**, 95–103.
19. Konate, K., Crombez, L., Deshayes, S., Decaffiney, M., Thomas, A., Brasseur, R., Aldrian, G., Heitz, F. and Divita, G. (2010) Insight into the cellular uptake mechanism of a secondary amphipathic cell penetrating peptide for siRNA delivery. *Biochemistry* **49**, 3393–3402.
20. Méry, J., Granier, C., Juin, M. and Brugidou, J. (1993) Disulfide linkage to polyacrylic resin for automated Fmoc peptide synthesis. Immunochemical applications of peptide resins and mercaptoamide peptides. *Int. J. Pept. Protein Res.* **42**, 44–52.
21. Vidal, P., Chaloin, L., Méry, J., Lamb, N., Lautredou, N., Bennes, R. and Heitz, F. (1996) Solid-phase synthesis and cellular localization of a C- and/or N-terminal labelled peptide. *J. Pept. Sci.* **2**, 125–133.
22. Maget-Dana, R. (1999) The monolayer technique: a potent tool for studying the interfacial properties of antimicrobial and membrane-lytic peptides and their interactions with lipid membranes. *Biochim. Biophys. Acta* **1462**, 109–140.
23. Brockman, H. (1999) Lipid monolayers: why use half a membrane to characterize protein-membrane interactions? *Curr. Opin. Struct. Biol.* **9**, 438–443.
24. Calvez, P., Bussi eres, S., Demers, E. and Salesse, C. (2009) Parameters modulating the maximum insertion pressure of proteins and peptides in lipid monolayers. *Biochimie* **91**, 718–733.
25. Greenfield, N. and Fasman, G.D. (1969) Computed circular dichroism spectra for the evaluation of protein conformation. *Biochemistry* **8**, 4108–4116.
26. Chen, Y.H., Yang, J.T. and Chau, K.H. (1974) Determination of the helix and beta form of proteins in aqueous solution by circular dichroism. *Biochemistry* **13**, 3350–3359.
27. Yang, J.T., Wu, C.S. and Martinez, H.M. (1986) Calculation of protein conformation from circular dichroism. *Methods Enzymol.* **130**, 208–269.
28. Griffiths, P.R. and De Haseth, J.A. (1986) Fourier transform infrared spectrometry in Chemical Analysis. John Wiley and Sons Inc., New York.
29. Surewicz, W.K. and Mantsch, H.H. (1988) New insight into protein secondary structure from resolution-enhanced infrared spectra. *Biochim. Biophys. Acta.* **952**, 115–130.
30. Jackson, M. and Mantsch, H.H. (1995) The use and misuse of FTIR spectroscopy in the determination of protein structure. *Crit. Rev. Biochem. Mol. Biol.* **30**, 95–120.

Chapter 5

NMR Studies of Three-Dimensional Structure and Positioning of CPPs in Membrane Model Systems

Lena Mäler and Astrid Gräslund

Abstract

CPPs are generally short cationic peptides that have the capability to interact directly with membranes. Most CPPs attain a three-dimensional structure when interacting with bilayers, while they are more or less unstructured in aqueous solution. To understand the relationship between structure and the effect that CPPs have on membranes, it is of great importance to investigate CPPs with atomic resolution in a suitable membrane model. Nuclear magnetic resonance (NMR) is an excellent technique both for studying solution structures of peptides as well as for investigating their location within a model bilayer. This chapter outlines protocols for producing model membrane systems for NMR investigations as well as the basic NMR tools for determining the three-dimensional structure of CPPs and for investigating the details in lipid–peptide interactions, i.e., the localization of the CPP in the bilayer.

Key words: CPP, Micelle, Bicelle, Membrane, Bilayer, Phospholipid, Nuclear magnetic resonance, Structure

1. Introduction

Cell-penetrating peptides are, from a structural perspective, a class of short, often cationic peptides that have the ability to form various secondary structures under different conditions. In general, these peptides are unstructured in water or buffer solution, but attain secondary structure in the presence of a membrane or a membrane mimetic. Most CPPs have the possibility to adopt amphiphilic α -helical structure under certain membrane conditions (often including somewhat negatively charged bilayer surfaces and not too high peptide/lipid ratio) (1). Some CPPs adopt this structure as a consequence of electrostatic interactions between the positively charged amino-acid residues and a negatively charged bilayer surface, while for others it is found that

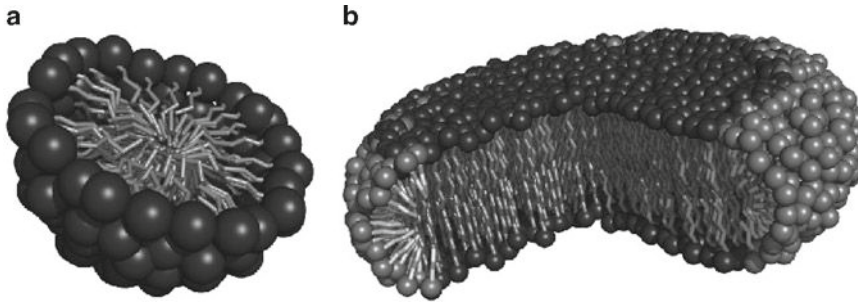


Fig. 1. Schematic picture illustrating the structure of a detergent micelle (a) and a phospholipid bicelle (b), commonly used for studies of CPP-membrane interactions. In (b), the cut-through illustrates the bilayer property of a bicelle.

hydrophobic interactions dominate. The relationship between secondary structure of CPPs and the mechanism by which they act is not entirely understood, and hence, it is important to elucidate this relationship. Some CPPs are toxic and induce membrane leakage, while others do not appear to perturb the membrane, although they interact with the bilayer (2, 3).

The typical biological membrane is a complex structure composed primarily of lipids and proteins. To investigate the molecular details in CPP structure, motion, and location in a bilayer, a model for the lipid bilayer needs to be used (4). Typical membrane models include vesicles (or liposomes), bicelles (5–11) or mixed micelles, and detergent micelles (12) (Fig. 1). The major structural part of a real bilayer is a mixture of various lipids, and one example of a typical eukaryotic neutral (zwitterionic) phospholipid is POPC. This lipid is commonly used to produce vesicles. A large variety of lipids can, however, be used to produce suitable model membranes, for instance, lipids with somewhat shorter acyl chains and lipids with different head-group charge. The simplest membrane mimetic is a suitable detergent, such as sodium dodecyl sulfate (SDS), dodecyl phosphocholine, or dihexanoyl phosphocholine (DHPC) (12). The latter two have been used successfully to determine NMR solution structures of integral membrane proteins as well as that of protein domains. Bicelles are mixtures of phospholipids and a suitable detergent (5–11). These bicelle mixtures have been found to resemble disk-like aggregates, composed of a bilayered phospholipid surface surrounded by detergent molecules (8, 9). The molecular structures of the phospholipids dimyristoylphosphocholine (DMPC), and the negatively charged dimyristoylphosphoglycerol (DMPG), commonly used in bicelles, are shown in Fig. 2.

There are many different methods by which it is possible to study CPP structure, including the relationship between peptide structure and membrane interactions. For all types of structural studies, a suitable membrane model has to be used (4). The choice

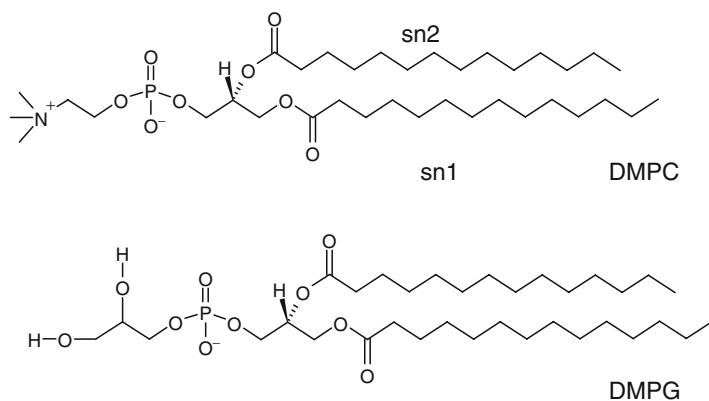


Fig. 2. The molecular structures of two commonly used components in bicelles: 1,2-dimyristoyl-*sn*-glycero-3-phosphocholine (DMPC) and the negatively charged 1,2-dimyristoyl-*sn*-glycero-3-(phospho-(1-glycerol)) (DMPG). The nomenclature for the positioning of the two fatty acyl chains is indicated for DMPC.

of model membrane depends on the technique by which the structure is studied. One of the simplest and fastest spectroscopic methods to investigate secondary structure of peptides and proteins is circular dichroism (CD) spectroscopy, which provides estimates of the content of various secondary structures. Similarly, Fourier transform infrared spectroscopy (FtIR) also provides an overview of the secondary structure content in peptides and proteins

Although these methods give a rapid estimate of the structure, a serious drawback is that they do not, in general, provide information on an atomic level. Solution-state nuclear magnetic resonance (NMR) spectroscopy, on the other hand, does provide atomic level structural information and has been used successfully for the past 30 years to investigate structure as well as motional properties of peptides and proteins (13, 14). The main drawback with NMR is related to the fact that only proteins or peptide-lipid complexes of limited size can be studied. The size limitation is related to molecular mobility, and larger molecules or complexes have slower motions giving rise to severe line broadening in the NMR spectra. Recent advances, including the TROSY experiment (15), have pushed this limit upward, and for example, several solution structures of integral membrane proteins have been reported (16). The size limitations, however, dictate the choice of membrane mimetic, and typically detergent micelles and bicelles have been used to investigate the structure of membrane-bound peptides and proteins. Phospholipid vesicles are generally too large to allow for resolved NMR spectra of incorporated peptides. In favorable situations, small unilamellar vesicles (SUVs) may be used to investigate certain aspects of bound peptides.

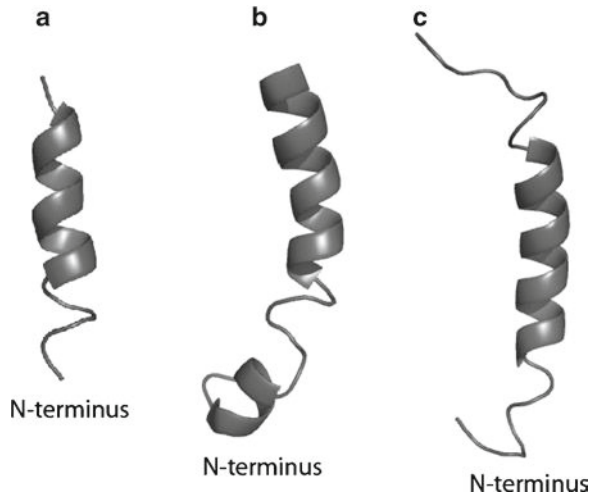


Fig. 3. NMR-derived solution structures of a few CPPs in membrane mimetic media. Structure of penetratin in $q=0.5$ DMPC/DMPG/DHPC phospholipid bilicles (30% PG) (a), of transportan in $q=0.33$ DMPC/DHPC (b), and of the N-terminal fragment (1–30) of the bovine Prion protein in DHPC (c). The figures were generated with PyMol (W.L. DeLano, The PyMol Molecular graphics system (2002) <http://www.pymol.org>). The coordinates were taken from the PDB (<http://www.rcsb.org>) (penetratin: 1OMQ, transportan: 1SMZ and bovine Prion protein-derived peptide: 1SKH).

NMR has been successfully used to elucidate the detailed structure of several CPPs in their membrane-bound form, using a variety of membrane models such as detergents, bilicles, and simple organic solvents (17–23). A wide range of CPPs have been investigated, including penetratin and transportan, as well as peptides derived from the N-terminal fragments of the prion and doppel proteins (Fig. 3). These studies are often based on homonuclear 2D ^1H methods, some of which provide resonance assignments, e.g., correlation experiments such as COSY (24) and TOCSY (25). The important distance constraints, used in the structure calculations, are obtained from nuclear Overhauser enhancements in the NOESY spectrum (26).

Perhaps even more important for understanding the effect that CPPs have on membranes is knowledge about their location within a membrane. Also, for these investigations, there are several methods available. Fluorescence spectroscopy can be used to investigate the location of specific fluorophores (such as intrinsic Trp or Tyr residues within the peptide sequence, or a chemically attached fluorophore) with respect to the bilayer (27–29). Fluorescence quenching by various fluorescence quenchers and fluorescence resonance energy transfer (FRET) between a donor and acceptor fluorophore are particularly useful methods to elucidate the bilayer location of a peptide.

Solution NMR can be used to also give details about the localization of a CPP in a bilayer at atomic resolution. There are several NMR techniques that are useful for this task. ^1H – ^2H

exchange rates for backbone amide hydrogen atoms in the peptide carry information about the bilayer insertion depth of a particular residue within a bilayer. Paramagnetic probes, attached to different parts of a lipid molecule, can be used to monitor the relaxation rate enhancement for resonances close to the probe. These experiments can give a detailed picture of how the various segments of a peptide are located with respect to the lipid molecule. Finally, direct observations of close distances between different parts of a lipid molecule and specific amino-acid residues in a peptide can be obtained through measurements of cross-relaxation. This is conveniently achieved for small peptides in e.g., bicelles by the saturation transfer difference experiment (30), or from selective 1D NOESY experiments (31).

In summary, NMR methods can be used in combination with other spectroscopic techniques to provide models for how CPPs interact with model membranes, revealing not only the three-dimensional structure of a CPP but also the localization of the peptide in a model bilayer. In this chapter, we describe the preparation and use of membrane models that are suitable for NMR investigations of short peptides, such as CPPs. We also outline the basic NMR procedures that are employed in such studies, and we focus on homonuclear two-dimensional ^1H methods for determining structure and localization of CPPs in model membranes. A detailed theoretical and practical description of these experiments is beyond the scope of this review, and we refer the reader to excellent textbooks on modern NMR techniques, such as the one by Cavanagh et al. (14).

2. Materials

Suitable membrane mimetic systems for conducting high-resolution NMR studies include different micelle solutions or bicelle solutions. Depending on the application, different choices can be made: solution structures of CPPs are readily studied in micelle solvents, while for studies of the location of a CPP in a bilayer, a true bilayer, such as that provided by small fast-tumbling bicelles, may be preferred.

2.1. Micelle Preparation

1. Detergents, typically one of the following: sodium dodecyl sulfate (SDS); Sigma (St. Louis, USA), dodecyl phosphocholine (DPC), 1,2-dihexanoyl-sn-glycero-3-phosphocholine (DHPC); Avanti Polar Lipids, Alabaster (AL, USA). For high-resolution NMR studies, deuterated versions of the detergents are often used.
2. Phosphate buffer, pH 5.5–7 (typically 50 mM).

2.2. Preparation of Fast-Tumbling Bicelles (Mixed Bilayered Micelles)

1. Deuterated phospholipids 1,2-dimyristoyl-sn-glycero-3-phosphocholine (DMPC- d_{54}), 1,2-dimyristoyl-sn-glycero-3-(phospho-rac-(1-glycerol)) (DMPG- d_{54}) and 1,2-dihexanoyl-sn-glycero-3-phosphocholine (DHPC- d_{22}), as well as the undeuterated DMPC, DMPG, and DHPC; Avanti Polar Lipids, Alabaster (AL, USA).
2. Phosphate buffer, pH 5.5. Usually a 0.2 M stock solution is prepared from which enough is taken for preparing the desired concentration (50 mM).
3. Lyophilizer.
4. Vortexer.
5. Oven.

2.3. Determining the Location of CPPs in a Bilayer

1. Deuterated water, $^2\text{H}_2\text{O}$.
2. Spin-labeled lipids, 1-palmityl-2-steroyl-(5-DOXYL)-sn-glycero-3-phosphocholine, and/or 1-palmityl-2-steroyl-(12-DOXYL)-sn-glycero-3-phosphocholine and/or 1-palmityl-2-steroyl-(16-DOXYL)-sn-glycero-3-phosphocholine, Avanti Polar Lipids, Alabaster (AL, USA).

3. Methods

Since CPPs are generally short peptides, these are most often obtained by solid-phase synthesis, which for most applications does not allow for cost-effective incorporation of isotopes such as ^{15}N or ^{13}C . Hence, the high-resolution NMR methods used for determining the three-dimensional structure as well as NMR studies of the location of CPPs in bilayers are generally standard homonuclear two-dimensional methods commonly used for investigating small peptides (14).

For structure determination, as well as for investigations on the positioning of CPPs, an almost complete resonance assignment is required. This is generally obtained from a combination of 2D TOCSY and NOESY experiments. In favorable cases, when the overlap between the signals originating from the lipids or detergent and the peptide is minimal, it is also feasible to perform 2D COSY experiments.

For investigations concerning the location of CPPs in model bilayers (bicelles), a combination of $^1\text{H} - ^2\text{H}$ backbone amide exchange experiments, paramagnetically labeled lipids, and determination of peptide-lipid NOEs are useful. The latter can conveniently be determined with the saturation transfer difference experiment.

The samples used for these NMR experiments usually contain a detergent solvent or a mixture of detergents and phospholipids (bicelles) and around 100 μM –1 mM peptide.

3.1. Preparation of CPPs in Micelle Solution

1. Dissolve the desired detergent (typically DPC, DHPC, or SDS) in an aqueous medium (water or phosphate buffer) at a concentration around 50–150 mM.
2. Add the CPP (powder). Typical concentrations range between 0.5 and 1 mM (see Note 1).

3.2. Preparation of CPPs in Fast-Tumbling Bicelles (Mixed Bilayered Micelles)

For high-resolution solution NMR work on peptides or protein fragments in bicelle solution, chain-deuterated lipids (DMPC, DMPG, and DHPC) are frequently used. The final concentration of lipids and detergents should be between 150 and 300 mM. The morphology of mixtures with a total concentration of 300 mM has been carefully investigated. The ratio of lipid/detergent (the q -value) suitable for high-resolution NMR studies is within the range of 0.15–0.5. For a sample of $q=0.5$ DMPC/DHPC bicelles, this implies a final DMPC concentration of 100 mM and a DHPC concentration of 200 mM. Surface-active peptides or protein fragments may be added to ready-made bicelle solution.

1. Mix the desired lipids in an aqueous medium (usually phosphate buffer) and vortex the mixture until a homogeneous slurry is obtained (see Note 2). Typically, chain-deuterated lipids (and detergents) are used for NMR purposes.
2. Prepare a stock solution of the detergent in water (or D₂O if desired for NMR purposes). A 1 M solution of DHPC is convenient for preparing bicelles with a total lipid (phospholipid + detergent) concentration of 300 mM (see Note 3).
3. Add an appropriate amount of the detergent solution to the lipid slurry, to produce the desired q -value (see Notes 4 and 5).
4. The sample is vortexed and heated to well above the melting temperature of the lipid (typically heated to 45°C for DMPC/DHPC mixtures) in several cycles until a transparent low-viscous solution is obtained (see Notes 6 and 7).
5. Add the desired amount of CPP to the ready-made bicelle solution. Typically, for 2D ¹H NMR measurements, a sample volume of 0.5 ml containing around 0.5–1 mM peptide is required (see Note 8).
6. If spin-labeled lipids are used, add a small amount (2.5 μl) of a fairly concentrated solution of labeled lipid in methanol (0.1 M) to the sample.

3.3. Sample Preparation for ¹H – ²H Exchange Experiments

1. Lyophilize the ready-made NMR sample (see Subheading 3.2).
2. Rapidly dissolve the sample in ²H₂O.
3. Transfer to a 5-mm NMR tube and quickly start the NMR experiments.

3.4. NMR Spectroscopy for Three-Dimensional Structure Studies

1. Two-dimensional homonuclear NOESY spectra and TOCSY spectra are recorded as datasets with around $2,048 \times 512$ complex data points using 16–64 scans (see Note 9).
2. The NOESY mixing time is usually set to 100–300 ms (see Note 10).
3. Suitable mixing times for the TOCSY experiment are 30–80 ms.
4. For samples containing deuterated detergent (SDS or DPC), a standard COSY or double-quantum filtered COSY, DQF-COSY (32) may also be recorded, using around 512 increments.
5. Water suppression in the homonuclear experiments is essential and can be achieved either by the excitation sculpting sequence (33) or by Watergate (34) (see Note 11).

3.5. NMR Spectroscopy for Determining the Location of CPPs in Bilayers

1. $^1\text{H} - ^2\text{H}$ exchange experiments are conducted by recording e.g., TOCSY datasets as a function of time (typically one TOCSY experiment takes 1–2 h). By monitoring the reduction of peak intensities, the ability of individual amide hydrogen atoms to exchange with solvent can be determined and hence the location of individual residues in the membrane mimetic.
2. The effect of different paramagnetic probes can be studied by monitoring the effect of a spin-labeled lipid (by paramagnetic relaxation enhancement, PRE) on the signal intensity of individual amino-acid residues in e.g., a TOCSY spectrum. Alternatively, T_1 or T_2 can be measured to enable a more quantitative estimation of the distance between the spin label and individual amino-acid residues.
3. Saturation transfer difference (STD) experiments (30, 35) are performed with a sample containing peptide in undeuterated bicelles. Various DMPC ^1H resonances are saturated with a selective pulse, leading to a series of saturation times. The irradiation can be performed at frequencies corresponding to different parts of the DMPC acyl chain, e.g., methyl protons, the acyl chain methylene protons, or the glycerol-3 methylene protons. A reference spectrum is recorded by moving the carrier 30 ppm from the center of the spectrum (35) and is subtracted from the spectrum recorded with selective acyl chain saturation.

4. Notes

1. A CPP-detergent complex in which the peptide is fully bound to the micelle typically has a molecular size corresponding to 10–30 kDa.

2. For preparation of bicelles, it is essential that the lipids are properly suspended in buffer solution prior to the addition of the DHPC solution. If this is the case, a clear low-viscous solution is formed.
3. It is convenient to use a DHPC stock solution for bicelle preparation. Since DHPC is extremely hygroscopic, it is otherwise difficult to estimate the true amount of DHPC that is actually added to the lipid suspension. Furthermore, unless a stock solution is prepared, DHPC should be handled in a dry atmosphere. It is important for the estimation of bicelle size (related to the q -value) that the relative concentrations of lipids and DHPC can be controlled.
4. It has been shown that some of the DHPC exist as free monomers in solution, which leads to overestimate the DHPC content in the bicelles, and hence underestimate the true bicelle size (related to the q -value).
5. Bicelles with different q -values can be produced using the outlined methodology. It has, however, been reported that a minimum of total lipid concentration (lipid + detergent) of around 100 mM is required to maintain the bicelles' disk shape (36).
6. Bicelle solutions can be stored in the freezer (-20°C) for months. Bicelles made with negatively charged lipids (DMPG) are, however, more sensitive to degradation.
7. Bicelles can be prepared with lipids with varying acyl chain lengths, such as 1,2-dilauroyl-sn-glycero-3-phosphocholine (DLPC, 12 C) and dipalmitoyl-sn-glycero-3-phosphocholine (DPPC, 16 C). It should, however, be noted that the morphology of such mixtures has not yet been fully characterized.
8. A CPP-bicelle complex in which the peptide is fully bound to the bicelle is, for NMR purposes, a large object of more than 50 kDa (37).
9. The NMR experiments used for characterizing CPP structure and membrane location are nicely described in detail in (14).
10. Do not use too long mixing times when recording the NOESY experiment. The peptide-detergent or peptide-bicelle complex can be quite large, and rapid spin diffusion may interfere with the interpretation of NOESY-derived distance constraints.
11. To increase the sensitivity of the homonuclear experiments, it is essential to achieve good water-suppression and to minimize lipid or detergent signals by using deuterated lipids and detergents.

Acknowledgments

The work presented in this chapter was supported by grants from the Swedish Research Council, the Center for Biomembrane Research, and the Carl Trygger Foundation. We thank Dr. Jesper Lind for assistance in producing the figures.

References

1. Gräslund, A. and Eriksson, L.E.G. (2002) Biophysical studies of cell-penetrating peptides. In *Cell penetrating peptides: processes and applications*. Ed. Langel, Ü. CRC, Boca Raton, 223–244.
2. Magzoub, M., Oglecka, K., Pramanik, A., Eriksson, L.E.G., and Gräslund, A. (2005) Membrane perturbation effects of peptides derived from the N-termini of unprocessed prion proteins *Biochim. Biophys. Acta* **15** 126–136.
3. Saar, K., Lindgren, M., Hansen, M., Eiriksdottir, E., Jiang, Y., Rosenthal-Aizman, K., Sassian, M., and Langel, Ü. (2005) Cell-penetrating peptides: a comparative membrane toxicity study *Anal. Biochem.* **345** 55–65.
4. Mäler, L. and Gräslund, A. (2009) Artificial membrane models for the study of macromolecular delivery *Methods Mol. Biol.* **480** 129–139.
5. Sanders, C.R. and Prestegard, J.H. (1990) Magnetically orientable phospholipid bilayers containing small amounts of a bile salt analogue, CHAPSO *Biophys. J.* **58** 447–460.
6. Vold, R.R., Prosser, S.R., and Deese, A.J. (1997) Isotropic solutions of phospholipid bicelles: a new membrane mimetic for high-resolution NMR studies of polypeptides *J. Biomol. NMR* **9** 329–335.
7. Sanders, C.R. and Prosser, R.S. (1998) Bicelles: a model membrane system for all seasons? *Structure* **6** 1227–1234.
8. Chou, J.J., Baber, J.L., and Bax, A. (2004) Characterization of phospholipid mixed micelles by translational diffusion *J. Biomol. NMR* **29** 299–308.
9. Andersson, A. and Mäler, L. (2005) Magnetic resonance investigations of lipid motion in isotropic bicelles *Langmuir* **21** 7702–7709.
10. Marcotte, I. and Auger, M. (2005) Bicelles as model membranes for solid- and solution-state NMR studies of membrane peptides and proteins, *Concepts Magn. Reson.* **24A** 17–37.
11. Prosser, R.S., Evanics, F., Kitevski, J.L., and Al-Abdul-Wahid, M.S. (2006) Current applications of bicelles in NMR studies of membrane-associated amphiphiles and proteins *Biochemistry* **45** 8453–8465.
12. Damberg, P., Jarvet J., and Gräslund, A. (2001) Micellar systems as solvents in peptide and protein structure determination *Methods Enzymol.* **339** 271–285.
13. Wüthrich, K. (1986) *NMR of Proteins and Nucleic Acids*. Wiley-Interscience, New York.
14. Cavanagh, J., Fairbrother, W.J., Palmer, A.G., Rance, M., and Skelton, N.J. (2007) *Protein NMR Spectroscopy. Principles and Practice*. Academic, San Diego.
15. Pervushin, K., Riek, R., Wider, G., and Wüthrich, K. (1997) Attenuated T_2 relaxation by mutual cancellation of dipole-dipole couplings and chemical shift anisotropy indicates an avenue to NMR structures of very large biological macromolecules in solution *Proc. Natl. Acad. Sci. USA* **94** 12366–12371.
16. Tamm, L.K. and Liang, B. (2006) NMR of membrane proteins in solution *Prog. Nucl. Magn. Reson. Spectrosc.* **48** 201–210.
17. Lindberg, M. and Gräslund, A. (2001) The position of the cell penetrating peptide penetratin in SDS micelles determined by NMR *FEBS Lett.* **497** 39–44.
18. Lindberg, M., Jarvet, J., Langel, Ü., and Gräslund, A. (2001) Secondary structure and position of the cell-penetrating peptide transportan in SDS micelles as determined by NMR *Biochemistry* **40** 3141–3149.
19. Lindberg, M., Biverstahl, H., Gräslund, A., and Mäler, L. (2003) Structure and positioning comparison of two variants of penetratin in two different membrane mimicking systems by NMR *Eur. J. Biochem.* **270** 3055–3063.
20. Andersson, A., Almqvist, J., Hagn F., and Mäler, L. (2004) Diffusion and dynamics of penetratin in different membrane mimicking media *Biochim. Biophys. Acta* **1661** 18–26.

21. Bárány-Wallje, E., Andersson, A., Gräslund, A., and Mäler, L. (2004) NMR solution structure and position of transportan in neutral phospholipid bicelles *FEBS Lett.* **567** 265–269.
22. Biverstahl, H., Andersson, A., Gräslund, A., and Mäler, L. (2004) NMR solution structure and membrane interaction studies of the N-terminal sequence (1-30) of the bovine prion protein *Biochemistry* **43** 14940–14947.
23. Bárány-Wallje, E., Andersson, A., Gräslund, A., and Mäler, L. (2006) Dynamics of transportan in bicelles is surface charge dependent *J. Biomol. NMR* **35** 137–147.
24. Aue, W.P., Bartholdi, E., and Ernst, R.R. (1976) Two-dimensional spectroscopy. Applications to nuclear magnetic resonance *J. Chem. Phys.* **64** 2229–2246.
25. Braunschweiler, L. and Ernst, R.R., (1983) Coherence transfer by isotropic mixing: application to proton correlation spectroscopy. *J. Magn. Reson.* **53** 521–528.
26. Jeener, J., Meier, B.H., Bachmann, P., and Ernst, R.R. (1979) Investigation of exchange processes by two-dimensional NMR spectroscopy *J. Chem. Phys.* **71** 4546–4553
27. Lakowicz, J.R. (1999) Principles of Fluorescence Spectroscopy. Kluwer Academic, New York.
28. Chattopadhyay A. and London, E. (1987) Parallax method for direct measurement of membrane penetration depth utilizing fluorescence quenching by spin-labeled phospholipids *Biochemistry* **26** 39–45.
29. Abrams, F.S. and London, E. (1993) Extension of the parallax analysis of membrane penetration depth to the polar region of model membranes: use of fluorescence quenching by a spin-label attached to the phospholipid polar headgroup *Biochemistry* **32** 10826–10831.
30. Mayer, M. and Meyer, B. (2001) Group epitope mapping by saturation transfer difference NMR to identify segments of a ligand in direct contact with a protein receptor *J. Am. Chem. Soc.* **123** 6108–6117.
31. Kessler, H., Mronza, S., and Gemmecker, G. (1991) Multi-dimensional NMR experiments using selective pulses *Magn. Reson. Chem.* **29** 527–557.
32. Piantini, U., Sorensen, O.W., and Ernst, R.R. (1982) Multiple quantum filters for elucidating NMR coupling networks *J. Am. Chem. Soc.* **104** 6800–6801.
33. Hwang, T.-L. and Shaka, A. J. (1995) Water suppression that works. Excitation sculpting using arbitrary waveforms and pulsed field gradients *J. Magn. Reson.* **112** 275–279.
34. Piotto, M., Saudek, V., and Sklená, V. (1992) Gradient-tailored excitation for single-quantum NMR spectroscopy of aqueous solutions *J. Biomol. NMR* **2** 661–665.
35. Wang, J., Schnell, J. R., and Chou, J. J. (2004) Amantadine partition and localization in phospholipid membrane: a solution NMR study *Biochem. Biophys. Res. Commun.* **324** 212–217.
36. Glover, K.J., Whiles, J.A., Wu, G., Yu, N.-J., Deems, R., Struppe, J.O., Stark, R.E., Komives, E.A., and Vold. R.R. (2001) Structural evaluation of phospholipid bicelles for solution-state studies of membrane-associated biomolecules *Biophys. J.* **81** 2163–2171.
37. Lind, J., Nordin, J., and Mäler, L. (2008) Lipid dynamics in fast-tumbling bicelles with varying bilayer thickness: effect of model transmembrane peptides *Biochim. Biophys. Acta* **1778** 256–2534.

Chapter 6

Measurements of the Intracellular Stability of CPPs

Ivo R. Ruttekolk*, Wouter P.R. Verdurmen*, Yi-Da Chung,
and Roland Brock

Abstract

Nowadays, the analysis of the uptake and intracellular distribution of cell-penetrating peptides mostly relies on fluorescence microscopy, using fluorescently labeled CPP analogs. However, fluorescence microscopy does not reveal to which degree fluorescence reflects the intact peptide or only breakdown products. Here, we introduce fluorescence correlation spectroscopy (FCS) as a powerful method to address peptide stability in cells and cell lysates. Measurements in lysates of cells incubated with peptide yield information on degradation of the total cellular peptide content. In combination with protease inhibitors, such measurements enable conclusions on trafficking pathways. Intracellular FCS measurements provide direct information on peptide degradation and association with cellular structures in intact cells.

Key words: Cell-penetrating peptide, Fluorescence correlation spectroscopy, Proteolytic stability, Fluorescence, Microscopy, Peptide degradation

1. Introduction

Conjugation to fluorophores has become the method of choice for analyzing the uptake of cell-penetrating peptides. Using confocal microscopy, the uptake and subcellular distribution can be followed in real time (1–5). Moreover, fluorescence enables a straightforward quantitative comparison of uptake efficiencies using flow cytometry. Nevertheless, most techniques that rely on fluorescence are not able to distinguish between intact, fluorescently labeled molecules and their degradation products which can complicate the interpretation of results obtained with these techniques. In particular, with respect to the subcellular localization,

* Ruttekolk and Verdurmen contributed equally to this work.

it is not clear to which degree the distribution of fluorescence reflects the characteristics of the intact peptide. Moreover, given that proteolytic stability, both extracellular and intracellular, is of major importance for determining the uptake efficiency of a CPP, it is evident that there is an unmet need to follow the stability of CPPs during the course of experiments (6–9). This requirement is furthermore illustrated by the fact that different CPPs and cargo constructs use distinct intracellular endocytotic pathways that differ strongly in proteolytic activity (1, 10–12).

One technique that enables a direct detection of intact CPPs and CPP–cargo constructs and their digestion products without fluorescent labels is mass spectrometry (6, 13, 14). Using stable isotopes as an internal standard, this method can moreover provide information on absolute quantities. However, fully degraded peptides will not be amenable to detection by MS-based techniques. Another way of assessing delivery of intact molecules is through biological assays. The luciferase-based splice correction assay that detects the delivery of CPP-coupled oligonucleotides (15, 16) is a prominent example for these techniques. Nevertheless, in spite of the advancements that both types of techniques have brought to the detection of intact peptide reaching the cytosol, both types of methods fail to provide quantitative information on the sequestration and degradation of peptides in the endolysosomal compartment.

Fluorescence correlation spectroscopy (FCS) is a technique that has the potential to complement these other techniques for providing information on peptide degradation in cell lysates and intact cells. FCS extracts information on the concentration and mobility of fluorescently labeled molecules from temporal fluctuations of the fluorescence intensity in a confocal detection volume the size of an *Escherichia coli* (17). In biological samples, mobility is a function of the size and molecular interactions of a molecule. When combined with imaging, such information can also be obtained for molecules in intact cells (18, 19). This chapter provides protocols for FCS measurements of CPP integrity in cell lysates and intact cells. For obtaining overall information on intracellular peptide breakdown, a protocol for performing FCS experiments in lysates of human cervical carcinoma (HeLa) cells that were incubated with a CPP before lysis is included (see also Fig. 1a–e). Lysosomal protease inhibitors are employed to assess the influence of various classes of lysosomal proteases in the intracellular breakdown of CPPs in endolysosomal compartments. The second protocol describes the measurement of the stability of CPPs composed of D- and L-amino acids in single living Jurkat E1 T cell leukemia cells.

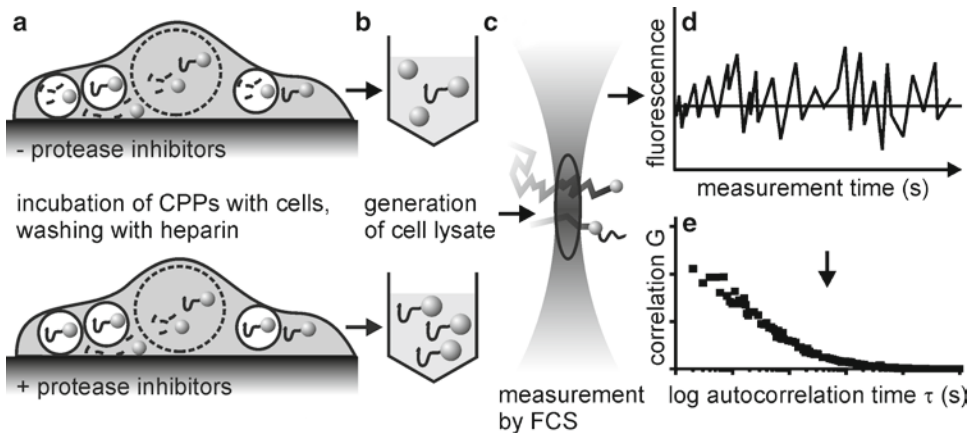


Fig. 1. Schematic overview illustrating sequential steps for the execution of an FCS experiment using cell lysates.

2. Materials

All cell lines are, in principle, amenable to analysis by FCS. For measurements in cell lysates, interactions of peptides with cellular components such as DNA and cellular membranes can complicate especially the quantification of the fraction of intact peptides. Our own experience shows that these molecules are more prone to such interactions than proteolytic fragments. For intracellular FCS measurements, the feasibility and quality of the measurements is influenced to a significant degree by cellular characteristics such as size, morphology, and mobility of cells.

2.1. Preparation of Lysates of HeLa Cells Treated with Lysosomal Protease Inhibitors

1. HeLa cells from the American-Type Culture Collection (ATCC, Manassas, USA); maintained in RPMI 1640 (Pan Biotech, Aidenbach, Germany) supplemented with 10% fetal calf serum (Pan Biotech).
2. 24-well culture plates (Sarstedt, Nümbrecht, Germany).
3. Lysosomal protease inhibitors: Pepstatin A (Sigma–Aldrich, Steinheim, Germany), which can be dissolved at 3 mM in DMSO, and E-64d (Bachem, Heidelberg, Germany), which can be dissolved in DMSO in concentrations up to 50 mM. Inhibitors can be stored at -20°C for months.
4. Lysis buffer: PBS containing 1% (v/v) Triton-X-100 (Sigma–Aldrich). This solution is stable at room temperature (RT) for months. Before each experiment, add a fresh protease inhibitor cocktail from a frozen or dry stock (Roche Diagnostics, Mannheim, Germany).
5. Fluorescein-labeled nona-arginine (R9) (EMC microcollection, Tübingen, Germany). All peptides are dissolved in a minimal

amount of DMSO (peptide concentration ~ 10 mM). Concentration is determined by measuring A_{492} in Tris-HCl buffer (pH 8.8), assuming a molar extinction coefficient of $75,000 \text{ M}^{-1} \text{ cm}^{-1}$. Peptides dissolved in DMSO can be stored for extended periods at 4°C .

6. Heparin (Sigma-Aldrich): Dissolve at 2 mg/ml in H_2O and freeze aliquots at -20°C . Aliquots are stable for months. Do not reuse thawed aliquots.

2.2. FCS

Measurements in HeLa Cell Lysates

1. Trypsin/EDTA solution: PBS containing $400 \text{ }\mu\text{g/ml}$ trypsin and $40 \text{ }\mu\text{g/ml}$ EDTA. Trypsin/EDTA mix was purchased from PAN Biotech.
2. 384-well plate ($175 \text{ }\mu\text{m}$, low-base design, MMI, Eching, Germany).
3. Tris HCl buffer: 100 mM Tris-HCl, pH 8.8.
4. Bovine serum albumin (BSA; Sigma-Aldrich): 5% (w/v) BSA stocks can be prepared by adding BSA to water which will dissolve by itself without mixing. When dissolved, aliquot and freeze at -20°C , where it will be stable for months. Aliquots can be thawed and refrozen several times.
5. TCS SP5 confocal microscope (Leica Microsystems, Mannheim, Germany) equipped with an HCX PL APO $63\times$ N.A. 1.2 water immersion lens and an FCS detection unit fitted with a $500\text{--}550 \text{ nm}$ filter cube (Leica Microsystems, Mannheim, Germany). The carboxyfluorescein moieties were excited by the 488 nm line of an argon-ion laser.
6. ISS VISTA software (ISS inc., Illinois, USA).

2.3. Preparation of Live Cells Treated with Nona-Arginine Composed of D- and L-Amino Acids

1. Jurkat E6.1 T cell leukemia cells (ATCC) maintained in RPMI 1640 supplemented with 10% fetal calf serum (both Pan Biotech).
2. Fluorescein-labeled nona-arginine composed of L- (R9) or D- (r9) amino acids (EMC microcollections).

2.4. Intracellular FCS Measurements in Living Jurkat Cells

1. Items 1–6 as in Subheading 2.2.
2. The microscope was fully encapsulated in an air-heated incubator with humidity control to maintain cell viability during the measurement procedure.
3. Globals for Spectroscopy software (Laboratory for Fluorescence Dynamics Irvine, CA, USA).

3. Methods

3.1. Preparation of Lysates of HeLa Cells Treated with Lysosomal Protease Inhibitors

1. Seed HeLa cells at a density of 80,000 cells/well in a 24-well plate in 800 μ l RPMI + 10% fetal calf serum.
2. Twenty-four hours later, wash cells and preincubate for 30 min with 10 μ M pepstatin A to inhibit aspartic proteases (20) or with 40 μ M E-64d to inhibit cysteine proteases (21). Include two untreated controls (see Note 1) and a control for the vehicle of pepstatin A (0.33% DMSO).
3. Remove medium containing lysosomal protease inhibitors or control vehicle. Incubate for 60 min at 37°C with 5 μ M R9 in RPMI + 10% fetal calf serum in the presence of the inhibitors or control vehicle at the same concentration as during the preincubation.
4. Wash cells twice with RPMI supplemented with 10% fetal calf serum and incubate them twice for 5 min at 37°C with 100 μ g/ml heparin in RPMI containing 10% fetal calf serum, to remove surface-bound peptides (see Note 2).
5. Add 500 μ l of freshly prepared lysis buffer (see Note 3) to the cells and incubate samples for 60 min on ice, for complete lysis.
6. Agitate the lysate by pipetting and centrifuge the lysate for 20 min at 20,000 $\times g$ at 4°C, to remove any remaining membrane debris (see Note 4). Freeze lysates at -20°C until further use (see Note 5).

3.2. FCS Measurements in HeLa Cell Lysates

1. For obtaining a reference of digested peptide, digest R9 with PBS containing trypsin (400 μ g/ml) and EDTA (40 μ g/ml) for 16 h at 37°C.
2. Coat the wells of a 384-well plate with a 0.1% BSA solution in PBS for 30 min at RT, to reduce adsorption of peptides to the walls of the wells. Afterwards, wash twice with PBS.
3. Dilute cell lysates 5 \times in Tris buffer (pH 8.8) (see Note 6) and keep lysates on ice until the measurement.
4. Include a well containing 10 nM fluorescein in PBS as a standard and a well containing pure PBS (see Note 7). Also, include wells for trypsin-degraded R9 and intact R9 in a similar cell lysate/buffer composition as the samples treated with lysosomal protease inhibitors.
5. Determine the laser power that maximizes the signal-to-noise ratio of the signal (see Note 8). Use the FCS wizard of the Leica SP5 software to control the laser power and the

ISS vista software package for the acquisition of the FCS data.

6. Determine the structure parameter and the triplet time using fluorescein (see Note 9).
7. Perform autocorrelation measurements of intact and trypsin-degraded R9 added to 20% cell lysate/80% TRIS-buffer (see Note 10).
8. Add the cell lysates to BSA-coated wells of the 384-well plate and perform autocorrelation measurements of 5×10 s per sample.

3.3. Analysis of Lysate FCS Measurements Using the ISS Software Package

1. Choose a 3D Gaussian model assuming a triplet term and one diffusive component and fix the structure parameter and the triplet term to the values determined for the fluorescein standard.
2. Determine the diffusion autocorrelation time of trypsin-degraded R9, using a 3D Gaussian model assuming one diffusing species. For samples containing different fractions of degraded peptide, which will be fitted with a two-component model, the diffusion autocorrelation time of the fast component will be fixed to this value (representing fully degraded R9). Remaining variables are allowed to vary.
3. Fit the intact R9 using a two-species model. Fix the fast component at the diffusion time of the fully degraded R9. Intact R9, in the presence of lysate, bears two components: (a) a slow component, reflecting peptide interacting with high-molecular-weight molecules from the lysate and (b) a fast component, reflecting peptide molecules that do not interact with molecules from the lysate. Therefore, fitting intact R9 with a two-component fit where the fast component is fixed at the diffusion time of the degraded peptide will also result in a small percentage of fast component (13% in the present experiment). The fraction intact R9 in the lysates from HeLa cells treated with lysosomal protease inhibitors can be calculated by a normalization of the fraction slow component, taking into account the fraction of fast component that is observed for the completely intact R9, according to the following formula:

$$\text{Fraction intact R9}_{\text{sample in lysate}} = \frac{\text{fraction slow component}_{\text{sample in lysate}}}{\left(1 - \text{fraction fast component}_{\text{intact R9 in lysate}}\right)} \quad (\text{Eq. 1})$$

4. Proceed with the fitting procedure for all other measurements, using a 3D Gaussian model assuming two diffusing species

and a fixed fast component, representing degraded R9 as well as intact R9 not interacting with lysate components. Calculate relative quantities of intact R9 according to (Eq. 1).

3.4. Interpretation of Result

Examples of raw autocorrelation curves from an experiment using lysosomal protease inhibitors can be found in Fig. 2a, b. An overlay of representative curves from different treatments illustrates that the autocorrelation curves are unaffected by a treatment with DMSO or pepstatin A, but a clear shift to the right, representing a slower diffusion, is observed for the lysate obtained from HeLa cells treated with E-64d (Fig. 2c). The shift to the right indicates the presence of more intact R9. The slower diffusion time is not just a reflection of the higher molecular weight, but indicates the association with other cellular components present in the lysate, which is not observed for degraded R9. This is illustrated by the differences in diffusion time between degraded and intact R9 in

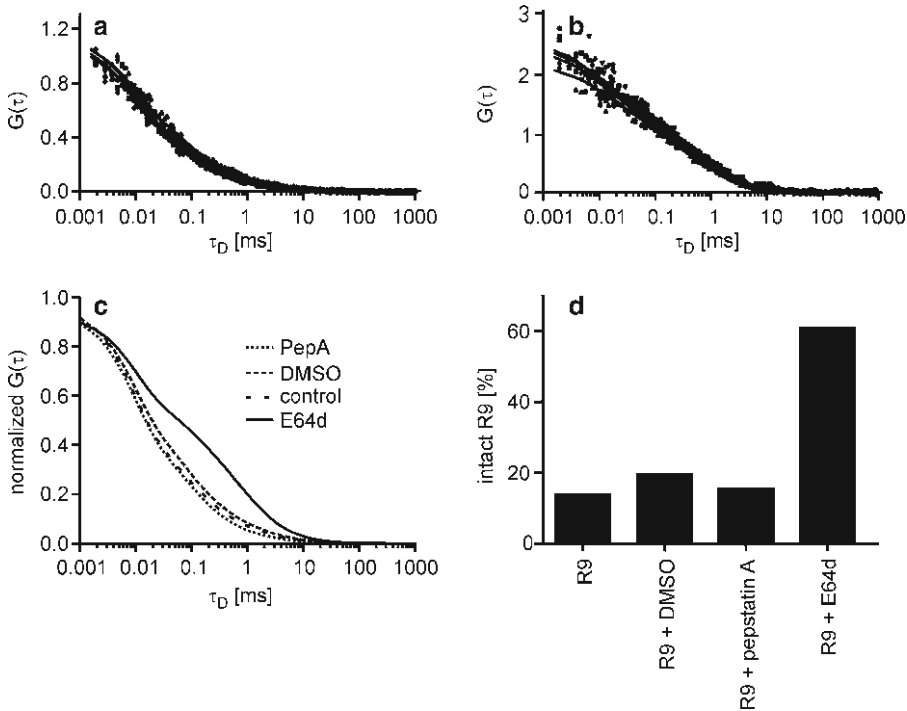


Fig. 2. Fluorescence correlation spectroscopy for the analysis of the stability of R9 in HeLa cells treated with lysosomal protease inhibitors. (a, b) Autocorrelation functions of lysates from HeLa cells incubated with 5 μM R9 for 1 h at 37°C without inhibitor (a) or with 40 μM E-64d (b). Lysates were prepared after the incubation in the presence of protease inhibitors. (c) Comparison of representative fits for autocorrelation curves obtained from HeLa cell lysates obtained as described above. Included are the control treated with peptide only, cells treated with DMSO as a vehicle control, 10 μM pepstatin A, and 40 μM E64d. All lines indicate fits that were obtained using a 3D Gaussian model assuming a triplet state and the presence of a slow-diffusing and a fast-diffusing molecular species. (d) Quantification of intact R9 in HeLa cells treated with lysosomal protease inhibitors. Relative quantities of intact R9 were determined using a two-species 3D Gaussian triplet model with intact and degraded R9 as references.

lysate and in the buffer–lysate mixture. In buffer, degraded R9 shows a diffusion time of about 30 μs , compared to about 47 μs for intact R9 (the actual values will differ between days and between setups). The differences are much larger in the lysate–buffer mix, where degraded R9 has an average diffusion time of 74 μs compared to 900 μs for intact R9. Relative quantities of intact R9 after the incubation in the presence or absence of lysosomal protease inhibitors were calculated. In cells incubated with E-64d, 60% of R9 had remained intact, whereas all other conditions had led to a percentage of intact R9 lower than 20% (Fig. 2d). This result, therefore, demonstrates that in HeLa cells, R9 is mainly degraded by cysteine proteases and that this degradation can be inhibited by the cysteine protease inhibitor E-64d. Besides information on the average diffusion time through the confocal volume, FCS measurements also provide information on the concentration, represented as the average background-corrected fluorescent molecule number in the confocal volume at any given time, which can be calculated as follows:

$$G_{\text{tot}}(0) = 1 + 1/N_{\text{app}} = 1 + \left(1 - \text{CPS}_b / \text{CPS}_t\right)^2 / N_{\text{corr}} \quad (\text{Eq. 2})$$

A comparison of the lysate peptide concentrations from the samples above showed that in the samples treated with E-64d, the concentration, as reflected by the average molecule number N , was substantially lower ($N=0.29$ vs. 1.17–1.38) than for the other three samples. Since we have previously established that E-64d does not affect uptake as witnessed by confocal microscopy in live cells (data not shown), we assume that this observation reflects an increased removal of debris-bound peptide during the centrifugation step included to obtain a homogeneous solution. This furthermore underscores the differences in intracellular association of R9 in cells treated with E-64d compared to other treatments or no treatment (see Note 11).

3.5. Preparation of Live Cells Treated with Nona-Arginine Composed of D- and L-Amino Acids

1. Spin down 300,000 Jurkat E 1 leukemia cells and resuspend in 200 μl RPMI + 10% fetal calf serum containing 500 nM R9 or r9.
2. Incubate for 30 min at 37°C. Wash with RPMI supplemented with 10% fetal calf serum, spin down for 5 min, and resuspend in fresh medium. Seed cells in eight-well microscopy chamber (Nunc, Wiesbaden, Germany) and allow them to settle.

3.6. Intracellular FCS Measurements in Living Jurkat Cells

1. Determine and fix the structure parameter and the triplet time using fluorescein as described above.
2. 1 h after the wash step, single cells are identified by confocal microscopy (see Note 12), and the confocal detection volume is positioned in the nucleus.

- Autocorrelation measurements are acquired in each cell for 5×10 s, using the ISS vista software. Repeat the procedure in at least three or four cells and in the background of the same incubation chamber.

3.7. Analysis of Intracellular FCS Measurements Using Globals for Spectroscopy Software

- Define a 3D Gaussian diffusion model assuming a triplet term and two diffusive components with offset.
- Determine the triplet time (τ_T), the lateral radius of the detection volume (ω_{xy}), and the structure parameter (ratio of ω_z/ω_{xy}), by fitting the autocorrelation function acquired for the fluorescein standard. Fix these values in the fit for the peptide samples. Allow other variables to vary.
- Perform global curve fitting; results for living Jurkat cells are shown in Fig. 3.

3.8. Interpretation of Result

Unlike measurements in cell lysates, intracellular FCS measurements do not give consecutive measurements (10 s each) that can be easily combined, since the calculated autocorrelation functions can differ quite substantially (Fig. 3). In contrast, curves should be inspected individually. Cells were incubated with 500 nM peptide only. This concentration is considerably lower than concentrations

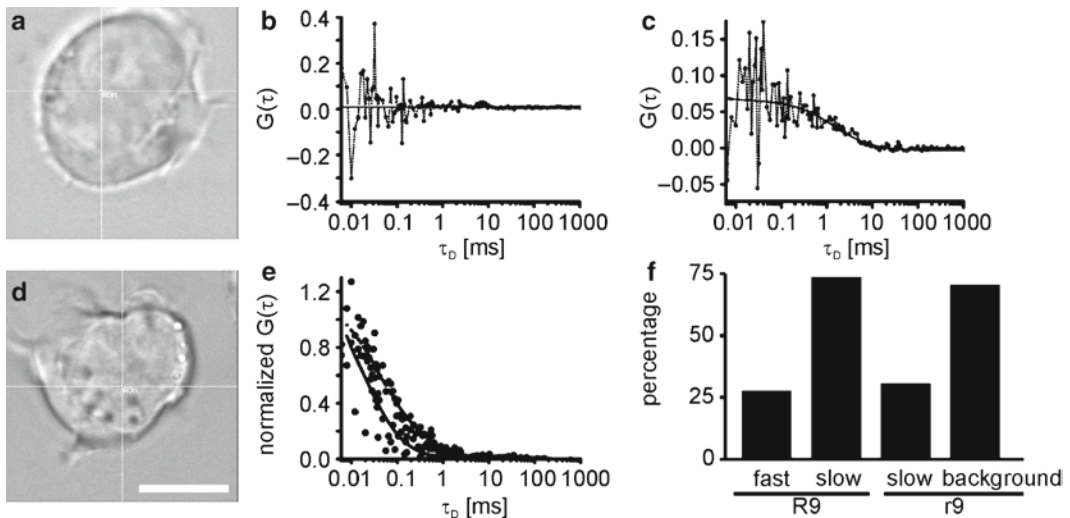


Fig. 3. Intracellular FCS of R9 and r9 in Jurkat cells. Jurkat cells were treated with 500 nM R9 or r9 for 30 min, spun down and washed, and seeded in eight-well microscopy chambers. After 1 h, the detection volume for FCS measurements was placed into the nuclei of living cells identified by transmission microscopy, as indicated in panel (a) (for r9) and (d) (for R9). The cross-hair cursor indicates the position of the detection volume in the optical plane. The scale bar indicates 5 μ m. Representative measurements for r9 (b, c) and R9 (E) are indicated. In panel (f), the relative frequencies of autocorrelation functions with a dominating fast or slow component (R9) or slow component and background signal (r9) are indicated. The result in (f) reflects the average ratio of measurements from 3 (R9) and 4 (r9) different cells. The left autocorrelation function in (e) shows an example in which the fast component was dominant, whereas the dominance of the slow component can be seen in (c) and the *right* curve in (e). (b) shows an uncorrelated background signal from the nucleus of r9-treated cells.

typically used for following the uptake of peptides by confocal imaging. As a consequence, no fluorescence could be seen inside the cells. The positioning of the confocal detection volume was, therefore, based on transmission images (Fig. 3a, d).

In all cases, measurements showed a rapid bleaching at the beginning of the acquisition of autocorrelation functions, indicating the presence of a substantial amount of immobile peptides in the cell. Because no diffusion occurs for this population of peptides, no reliable estimates of the quantity can be made. In addition, we observed that during some 10-s measurement intervals of Jurkat cells treated with R9, species with a high mobility were dominant (Fig. 3e, left curve), reminiscent of free fluorescein. The average molecule number N corresponded to a concentration of free fluorophores of less than 50 nM. During other measurement intervals, a slower diffusive component was more dominant, reflecting intact R9 interacting with cellular components (Fig. 3e, right curve). The slower diffusing component was also observed for r9 (Fig. 3C), in addition to measurement intervals where no signal above the background was present (Fig. 3b). In contrast, no rapidly diffusing molecular species was observed in cells treated with r9, confirming the assumption that the rapidly diffusing species indicates the presence of breakdown products of R9. Moreover, bleaching was more dominant for r9, furthermore indicating a larger immobile fraction of r9.

4. Notes

1. To lysates of untreated controls, intact and degraded R9 will be added. These measurements will serve as references for the analysis of the degree of degradation. The background signal of untreated controls will be applied for correcting particle numbers estimated by the analysis software.
2. In our hands, a heparin treatment at the indicated concentration performs as well as a trypsin treatment to remove surface-bound nona-arginine but is a milder treatment for the cells.
3. The application of a minimal amount of lysis buffer reduces the likelihood of any interferences of the lysis buffer in the FCS measurements due to changes in refractive index.
4. It is expected that some remaining debris-bound peptides will be removed by centrifugation. The amount will depend on the interactions of the peptide with lysate components. Free fluorophores that result from the degradation of labeled peptides are less prone to removal by centrifugation due to less association with lysate components.

5. Of course, FCS experiments can also be conducted without the freezing step. However, for practical reasons, it is often desirable to freeze the lysates on the day that the cellular experiment is conducted. We recommend storing lysates no longer than a few days at -20°C to avoid unwanted storage effects.
6. A buffer with a pH of 8.8 is used because in this pH range, the brightness of the fluorescein moiety attached to the peptides is optimal, which yields a better signal-to-noise ratio in the FCS measurements. In a similar manner, buffering conditions for other fluorophores should be optimized for obtaining optimum fluorescence brightness as well.
7. As FCS measurements provide optimum signal-to-noise ratios for concentrations of fluorophores between 1 and 100 nM, samples should be diluted accordingly. The inclusion of a PBS control for background fluorescence enables the adjustment of the laser intensity to the optimal signal-to-noise ratio (22).
8. Above a certain laser power, the specific fluorescence signal will not increase anymore because of saturation of the fluorophores. Instead, only the background signal will further increase. The optimum laser power yields an optimum ratio of specific signal over background. Especially for more photosensitive dyes such as fluorescein, bleaching of fluorophores at higher laser powers may impose a further constraint.
9. A too large structure parameter is either an indication of a misaligned pinhole or incorrect adjustment of the correction ring for the thickness of the coverslip, or of the presence of several molecular species with similar diffusion autocorrelation times. A structure parameter between four and eight should be obtained.
10. In 384-well plates, a volume 50 μl is standard in our laboratory, although volumes as low as 20 μl are also sufficient.
11. This interpretation assumes equal initial cell numbers and an equal lysis efficiency. An additional control where absolute protein concentrations are determined could be included as further proof.
12. Make sure to identify the cells with a low laser power to minimize photobleaching.

Acknowledgments

The authors acknowledge financial support from the Volkswagen-Foundation (Nachwuchsgruppen an Universitäten, I/77 472) and from the Radboud University Nijmegen Medical Centre to WPRV.

References

1. Duchardt, F., Fotin-Mleczek, M., Schwarz, H., Fischer, R., and Brock, R. (2007) A comprehensive model for the cellular uptake of cationic cell-penetrating peptides, *Traffic*. 8, 848–866.
2. Fotin-Mleczek, M., Welte, S., Mader, O., Duchardt, F., Fischer, R., Hufnagel, H., Scheurich, P., and Brock, R. (2005) Cationic cell-penetrating peptides interfere with TNF signalling by induction of TNF receptor internalization, *J. Cell Sci.* 118, 3339–3351.
3. Herbig, M. E., Weller, K. M., and Merkle, H. P. (2007) Reviewing biophysical and cell biological methodologies in cell-penetrating peptide (CPP) research, *Crit. Rev. Ther. Drug Carrier Syst.* 24, 203–255.
4. Henriques, S. T., Melo, M. N., and Castanho, M. A. (2007) How to address CPP and AMP translocation? Methods to detect and quantify peptide internalization in vitro and in vivo (Review), *Mol. Membr. Biol.* 24, 173–184.
5. Vives, E., Richard, J. P., Rispal, C., and Lebleu, B. (2003) TAT peptide internalization: seeking the mechanism of entry, *Curr. Protein Pept. Sci.* 4, 125–132.
6. Elmquist, A. and Langel, Ü. (2003) In vitro uptake and stability study of pVEC and its all-D analog, *Biol. Chem.* 384, 387–393.
7. Palm, C., Jayamanne, M., Kjellander, M., and Hällbrink, M. (2007) Peptide degradation is a critical determinant for cell-penetrating peptide uptake, *Biochim. Biophys. Acta* 1768, 1769–1776.
8. Trehin, R., Nielsen, H. M., Jahnke, H. G., Krauss, U., Beck-Sickingler, A. G., and Merkle, H. P. (2004) Metabolic cleavage of cell-penetrating peptides in contact with epithelial models: human calcitonin (hCT)-derived peptides, Tat(47–57) and penetratin(43–58), *Biochem. J.* 382, 945–956.
9. Fischer, R., Bachle, D., Fotin-Mleczek, M., Jung, G., Kalbacher, H., and Brock, R. (2006) A targeted protease substrate for a quantitative determination of protease activities in the endolysosomal pathway, *ChemBioChem*. 7, 1428–1434.
10. Pillay, C. S., Elliott, E., and Dennison, C. (2002) Endolysosomal proteolysis and its regulation, *Biochem. J.* 363, 417–429.
11. Räägel, H., Säälük, P., Hansen, M., Langel, U., and Pooga, M. (2009) CPP-protein constructs induce a population of non-acidic vesicles during trafficking through endo-lysosomal pathway, *J. Control Release* 139, 108–117.
12. Tunnemann, G., Martin, R. M., Haupt, S., Patsch, C., Edenhofer, F., and Cardoso, M. C. (2006) Cargo-dependent mode of uptake and bioavailability of TAT-containing proteins and peptides in living cells, *FASEB J.* 20, 1775–1784.
13. Burlina, F., Sagan, S., Bolbach, G., and Chassaing, G. (2005) Quantification of the cellular uptake of cell-penetrating peptides by MALDI-TOF mass spectrometry, *Angew. Chem. Int. Ed. Engl.* 44, 4244–4247.
14. Burlina, F., Sagan, S., Bolbach, G., and Chassaing, G. (2006) A direct approach to quantification of the cellular uptake of cell-penetrating peptides using MALDI-TOF mass spectrometry, *Nat. Protoc.* 1, 200–205.
15. Kang, S. H., Cho, M. J., and Kole, R. (1998) Up-regulation of luciferase gene expression with antisense oligonucleotides: implications and applications in functional assay development, *Biochemistry* 37, 6235–6239.
16. EL Andaloussi, S., Guterstam, P., and Langel, Ü. (2007) Assessing the delivery efficacy and internalization route of cell-penetrating peptides, *Nat. Protoc.* 2, 2043–2047.
17. Rigler, R., Mets, U., Widengren, J., and Kask, P. (1993) Fluorescence correlation spectroscopy with high count rate and low-background – analysis of translational diffusion, *Eur. Biophys. J. Biophys. Lett.* 22, 169–175.
18. Bacia, K. and Schwille, P. (2007) Fluorescence correlation spectroscopy, *Methods Mol. Biol.* 398, 73–84.
19. Waizenegger, T., Fischer, R., and Brock, R. (2002) Intracellular concentration measurements in adherent cells: a comparison of import efficiencies of cell-permeable peptides, *Biol. Chem.* 383, 291–299.
20. Rich, D. H., Bernatowicz, M. S., Agarwal, N. S., Kawai, M., Salituro, F. G., and Schmidt, P. G. (1985) Inhibition of aspartic proteases by pepstatin and 3-methylstatine derivatives of pepstatin. Evidence for collected-substrate enzyme inhibition, *Biochemistry* 24, 3165–3173.
21. Tamai, M., Matsumoto, K., Omura, S., Koyama, I., Ozawa, Y., and Hanada, K. (1986) In vitro and in vivo inhibition of cysteine proteinases by EST, a new analog of E-64, *J. Pharmacobiodyn.* 9, 672–677.
22. Koppel, D. E. (1974) Statistical accuracy in fluorescence correlation spectroscopy, *Phys. Rev. A* 10, 1938–1945.

Chapter 7

Tools for Predicting Binding and Insertion of CPPs into Lipid Bilayers

Paulo F. Almeida

Abstract

The ability to predict properties such as peptide binding and insertion into membranes is an important and time-saving asset in the design of new cell-penetrating peptides (CPPs). Methods to predict those properties are described here, which make use of calculations performed with the Wimley–White hydrophobicity scales. In addition, electrostatic effects can be estimated in a way that provides acceptably close approximations in many cases. Finally, an estimate of the probability of insertion is also discussed. These procedures are illustrated by comparing the calculations with experiments on a few CPPs.

Key words: Binding thermodynamics, Membrane insertion, Interfacial hydrophobicity scale, Octanol hydrophobicity scale, Protein transduction domains, Amphipathic peptides

1. Introduction

The design of new cell-penetrating peptides (CPPs) is essential for the development of this field. The ability to predict the peptide properties can result in significant time savings. Among those properties, the interactions of CPPs with membranes, such as peptide binding and insertion into lipid bilayers, are the most important. Binding of peptides to membranes can be measured experimentally by various methods, including isothermal titration calorimetry, fluorescence spectroscopy, and circular dichroism (CD). While not a replacement for experimental measurements, methods to predict those properties based on simple calculations exist and can be quite useful during the design phase. These tools are freely available to researchers but are not always well-known to new practitioners. The goal of this article is to bring those tools to the attention of researchers in the CPP field, and to show how they can be used by means of a few examples. One of those

examples comes from our own work, but we have also included calculations for the more traditional CPPs, penetratin and the TAT peptide.

The methods described here make use of simple calculations performed with the Wimley–White hydrophobicity scales (1). These scales have been developed over the past decade in Stephen White’s laboratory at the University of California at Irvine. Their description is available on the Internet at <http://www.blanco.biomol.uci.edu>. The calculations involving these scales have been implemented in the software Membrane Protein Explorer (MPEx) (2), which is also freely available through the Internet. All the credit for the development of these scales and tools goes to S.H. White and his collaborators, especially, W. Wimley, K. Hristova, S. Jaysinghe, A. Ladokhin, and C. Snider. However, we have used these resources with much profit in our research and feel they should be brought to the attention of the CPP research community in an easily accessible way.

Two different hydrophobicity scales were developed by White and Wimley, the octanol hydrophobicity scale (1, 3) and the interfacial hydrophobicity scale (1, 4). Four points are worth noting about these scales. First, both scales are derived from experiment, using small peptides where a certain amino acid residue was varied as a means to evaluate its specific contribution to the thermodynamics of transfer from water to *n*-octanol or to the water/membrane interface of a bilayer composed of the zwitterionic lipid 1-palmitoyl-2-oleoylphosphatidylcholine (POPC). Second, these are whole-residue scales; that is, they include the contributions not only of the amino acid side chains, but also of the peptide group (CONH). Third, these scales were derived from partition coefficients determined using mole fraction units for the concentrations in solution. This means that if comparisons are made with experimental values of peptide dissociation (or binding) constants expressed in (reciprocal) molar concentration units, the values of the Gibbs free energies of binding obtained experimentally need to be modified by adding the “cratic correction”, $\Delta G = -RT \ln 55.5 = -2.4$ kcal/mol at room temperature (1), where $R = 1.987$ cal/mol/K is the gas constant, T is the temperature, about 298 K, and 55.5 is the molar concentration of water. Fourth, these scales can be used for an arbitrary peptide, which is especially important in de novo design.

The hydrophobicity scales include three components: (1) the free energy of transfer for each residue, which is composed of the side chain and the peptide group; (2) the free energy of transfer of the end groups, at the N- and C-termini of the peptide; and (3) the free energy of intramolecular hydrogen bonding within the peptide, which arises from the formation of secondary structure (α -helix or β -sheet). A polypeptide is usually represented as shown in Fig. 1a. For the purpose of this discussion, it is useful to

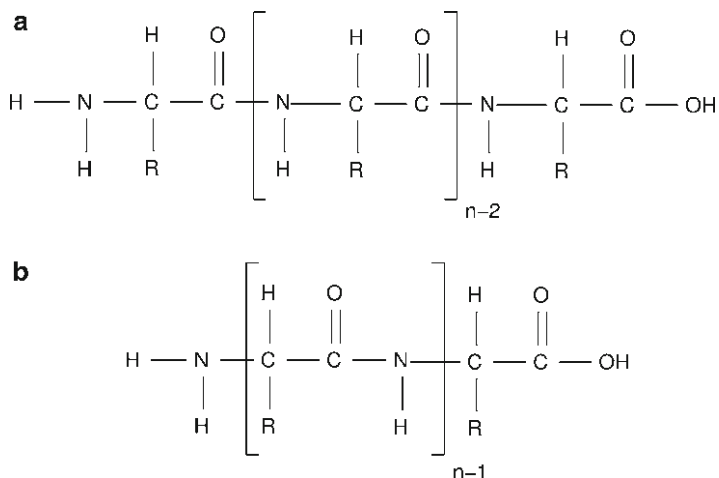


Fig. 1. Polypeptide chain, two representations (a and b).

use the slightly different, but equivalent, subdivision of the chain shown in Fig. 1b, which emphasizes the peptide group as a unit, and is convenient in the calculation of the end-group contributions as well.

An amino acid residue can be considered as composed of three different parts (Fig. 2): the peptide group (CONH), the methylene group (CH_2), and the side chain (R, minus one extra H). The whole-residue hydrophobicity scales for transfer from water to either octanol or the POPC bilayer interface can be constructed by adding the Gibbs free energy contributions of each part. That is, the Gibbs free energy of transfer of a whole residue (ΔG^X) is obtained by adding the contributions of the glycyl group, CH_2CONH (ΔG^{glycyl}), and the side chain (ΔG^{sc}), which is obtained experimentally from differences relative to the glycine residue. The whole-residue scales are then tabulated (Table 1).

The Gibbs free energy of transfer of a polypeptide from water to octanol or to the POPC membrane interface is then computed by simply adding the contributions of each residue (ΔG^X). This does not yet include the effect of N- and C-terminal groups (end groups) or the effect of peptide (intramolecular) hydrogen bonds, which are formed when a regular secondary structure is adopted.

Now the effect of the end groups can be added. The procedure was worked out by Hristova and White (5) for the interfacial scale and is entirely analogous for the octanol scale. To obtain the free energy of transfer of a peptide ending in COOH from water to the bilayer interface, one adds (to the sum of the ΔG_{if}^X for all residues in the sequence) the difference in free energy of transfer of a group ending in COOH relative to the peptide group, CONH (Fig. 3). For polypeptides with different C-terminal end

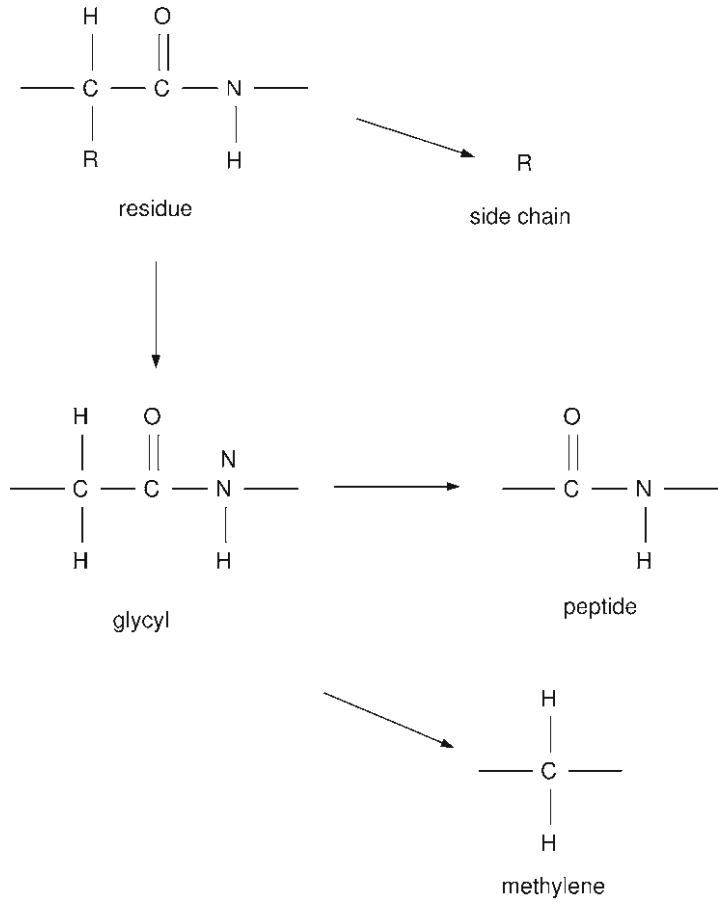


Fig. 2. Decomposition of a residue into side chain, peptide group, and methylene group.

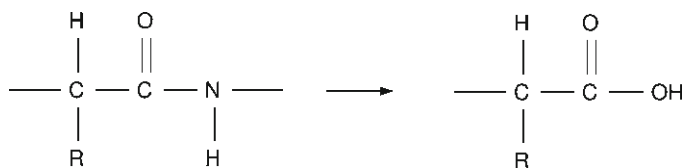


Fig. 3. Thought process to obtain the free energy for a terminal COOH from a peptide group.

groups, the free energies of transfer are calculated by adding the differences relative to the COOH group.

For the N-terminus, the values can be derived from the transfer of an acetylated N-terminus, which comprises the free energies of transfer of the methyl and the peptide groups (Fig. 4). The values to be added to the transfer free energies from water to the interface for other N-terminal versions can be computed from the difference values given by Hristova and White (5). The relations between the various Gibbs free energies are shown schematically in Fig. 5.

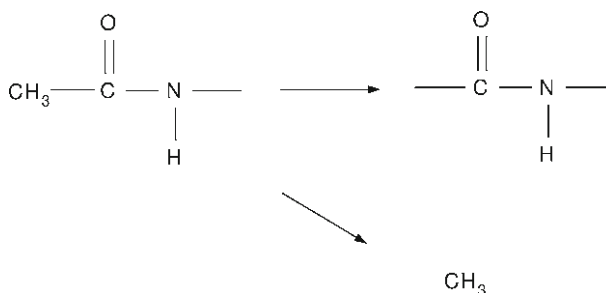


Fig. 4. Decomposition of the acetylamino terminal group into the peptide and methyl groups.

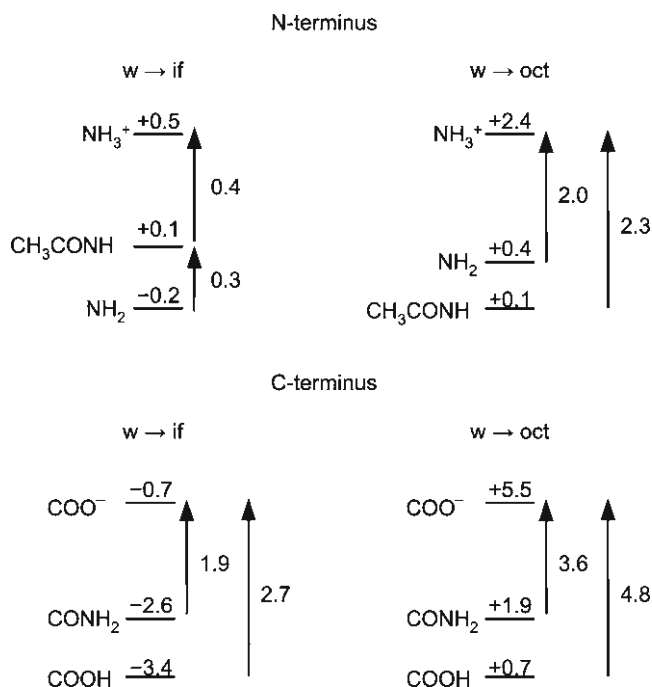


Fig. 5. Gibbs free energies of transfer from water (w) to the interface (if) or to octanol (oct) for the various end groups and their differences (in kcal/mol).

In summary, to calculate the Gibbs free energy of transfer of a peptide with a particular end group, one must add, to the sum of the ΔG_{oct}^X or ΔG_{if}^X for all residues in the sequence, the value listed in Table 3 for the appropriate end group.

To complete the description of the Wimley–White method, we need to address the effect of intramolecular hydrogen bond formation, which occurs when the peptide acquires a regular secondary structure. For the interfacial hydrophobicity scale, based on the folding of melittin to an α -helix at the POPC water/bilayer interface, Ladokhin and White (6) estimated that the Gibbs free energy of the peptide decreases by about 0.4 kcal/mol per residue when it becomes hydrogen-bonded in an α -helix. Wimley et al.

(7) arrived at a similar value, 0.5 kcal/mol, in a β -sheet. Estimates about a factor of 2 smaller for α -helices have been obtained by Seelig's group (8–10). Possible reasons for this discrepancy have been discussed (11). Without making a case for either value, as long as the entire Wimley–White procedure is applied, it is recommendable to use the value of -0.4 kcal/mol per residue to ensure self-consistency of the calculations. Furthermore, a remarkably good agreement is obtained between calculated and experimental binding free energies for a set of six representative amphipathic α -helical peptides if the value of -0.4 kcal/mol is used (12).

For the octanol hydrophobicity scale, although the values obtained for the whole-residue transfer from water to octanol were initially derived for unstructured peptides, they actually represent a good approximation for the transfer of hydrogen-bonded residues (α -helical peptides) from water to the hydrophobic bilayer interior (13).

All the calculations outlined so far refer to the association of a polypeptide with a membrane formed by the zwitterionic lipid POPC at room temperature, which was used in all experiments from which the interfacial hydrophobicity scale was constructed (4–6). These estimates should also apply to other phosphatidylcholines in the fluid state. However, most cationic CPPs bind poorly to zwitterionic lipid membranes and the experiments are usually performed in the presence of an anionic lipid, typically phosphatidylglycerol (PG) or phosphatidylserine (PS). In some cases, the association of particular cationic peptides with anionic membranes was specifically investigated and is well characterized thermodynamically (8–10). But, in general, the estimation of the effect of negatively charged lipids on peptide binding and insertion into membranes rests on much weaker grounds. At this point, only some crude rules of thumb can be offered, based on the results for polycationic peptides (14–17) and also on determinations for amphipathic peptides (18–21), which are useful in obtaining initial estimates of peptide binding to anionic membranes. An estimate that has proved remarkably useful for small polycationic peptides is that the interaction of a positive charge on a peptide with a negatively charged lipid on a membrane contributes about -1 kcal/mol to the Gibbs free energy of binding (14–16). If a PC-based membrane contains about 50 mol% of anionic lipid (PG or PS), or at least more than 30 mol%, a reasonable starting point is to multiply the number of basic residues in the peptide by -1 kcal/mol and add that to the value of the Gibbs energy of binding calculated for a PC membrane; this estimate of the electrostatic free energy is often correct to about 1 kcal/mol. If the membrane only contains 20 mol% anionic lipid, using about half that electrostatic free energy seems to provide a reasonable first estimate.

For cationic amphipathic polypeptides, however, a cautionary statement is required. The above rule of thumb assumes that the

contributions of hydrophobicity and electrostatics to the Gibbs free energy of binding are additive. But, in general, they are not. This nonadditivity of hydrophobic and electrostatic contributions has been clearly demonstrated for the tryptophan-rich peptide indolicidin (21). It also provides a very poor approximation to describe the binding of cecropin A (18). The larger the hydrophobic contribution, the smaller the effect of electrostatics on binding. For indolicidin variants, the effective peptide charge decreases by about 20% for each -3 kcal/mol of hydrophobic binding free energy (21). Furthermore, the effect of peptide charges depends on their position and spacing (17).

Finally, how can these calculations be used to assess the likelihood of CPP insertion? We have proposed the hypothesis that the probability of insertion of amphipathic α -helical peptides is related to the difference between the free energies of transfer to the POPC membrane interface and the bilayer hydrophobic interior (12). These free energies can be estimated using the Wimley–White interfacial and octanol hydrophobicity scales, $\Delta G_{\text{if}}^{\circ}$ and $\Delta G_{\text{oct}}^{\circ}$. Tentatively, we have proposed a value of $\Delta G_{\text{oct-if}}^{\circ} = \Delta G_{\text{oct}}^{\circ} - \Delta G_{\text{if}}^{\circ} \leq 20$ kcal/mol as the threshold for insertion. Below this value, amphipathic peptides would be able to insert transiently into the bilayer, normally accompanied by some membrane reorganization, which could even constitute a small, transient pore. If $\Delta G_{\text{oct-if}}^{\circ}$ is much above that value, peptides will probably not be able to translocate across the membrane without a significant membrane perturbation (12). The value of this hypothesis for cationic CPPs is unclear at this point. If valid, it would suggest that peptides with $\Delta G_{\text{oct-if}}^{\circ} < 20$ kcal/mol would be good candidates as CPPs. However, the presence of negatively charged lipids in the membrane will certainly change the magnitudes of the Gibbs energies of binding and insertion. Yet, based on the data we currently have, it seems that the changes in free energy occur in parallel in both the bound and the inserted state, in such a way that the difference may not vary much (12). If this is so, the presence of negative charge on the membrane becomes important only to determine whether the peptides bind or not. But the insertion would be much less dependent on charge, and the predictions obtained from $\Delta G_{\text{oct-if}}^{\circ}$ calculated for POPC still hold promise. In any case, at this point, the value $\Delta G_{\text{oct-if}}^{\circ}$ should only be used as a measure to compare CPPs, but not as an absolute indicator.

The calculations outlined are illustrated in Subheading 3 with five examples of CPPs: Penetratin (Acetyl-RQIKIWFQNRRMK WKK-amide) (22, 23), HIV-1 TAT 47–57 (YGRKKRRQRRR) (24), Tp10W (AGWLLGKINLKALAALAKKIL-amide) (12, 20), which is variant Y3W of Transportan 10 (25), and, in some aspects, also nonaarginine (Acetyl-R₉-amide) and nonalysine (Acetyl-K₉-amide). All peptides are mainly unstructured in water. When

bound to membranes, Tp10W forms an amphipathic helix (12), penetratin also forms a helix, which is not amphipathic in the traditional sense (22, 23, 26), and TAT appears to be mainly unstructured (23). Heptaarginine-tryptophan (Acetyl-R₇W-amide) also appears unstructured on anionic membranes (23), suggesting that the same is true for nonaarginine and nonalysine.

2. Materials

The “materials” for the calculations are the tables of data on Gibbs energy of transfer from water to octanol or to the bilayer interface.

2.1. Whole-Residue Hydrophobicity Scales (Table 1)

Table 1
Interfacial and octanol hydrophobicity scales: Gibbs free energy of transfer of whole residues (ΔG^X) from water to the bilayer interface or to octanol (1–4)

Amino acid	Interface ΔG_{if}^0 (kcal/mol)	Octanol ΔG_{oct}^0 (kcal/mol)
Ala	0.17 ± 0.06	0.50 ± 0.12
Arg+	0.81 ± 0.11	1.81 ± 0.13
Asn	0.42 ± 0.06	0.85 ± 0.12
Asp−	1.23 ± 0.07	3.64 ± 0.17
Asp0	−0.07 ± 0.11	0.43 ± 0.13
Cys	−0.24 ± 0.06	−0.02 ± 0.13
Gln	0.58 ± 0.08	0.77 ± 0.12
Glu−	2.02 ± 0.11	3.63 ± 0.18
Glu0	−0.01 ± 0.15	0.11 ± 0.12
Gly	0.01 ± 0.05	1.15 ± 0.11
His+	0.96 ± 0.12	2.33 ± 0.11
His0	0.17 ± 0.06	0.11 ± 0.11
Ile	−0.31 ± 0.06	−1.12 ± 0.11
Leu	−0.56 ± 0.04	−1.25 ± 0.11
Lys+	0.99 ± 0.11	2.80 ± 0.11
Met	−0.23 ± 0.06	−0.67 ± 0.11
Phe	−1.13 ± 0.05	−1.71 ± 0.11

(continued)

Table 1
(continued)

Amino acid	Interface ΔG_{if}^0 (kcal/mol)	Octanol ΔG_{oct}^0 (kcal/mol)
Pro	0.45 ± 0.12	0.14 ± 0.11
Ser	0.13 ± 0.08	0.46 ± 0.11
Thr	0.14 ± 0.06	0.25 ± 0.11
Trp	-1.85 ± 0.06	-2.09 ± 0.11
Tyr	-0.94 ± 0.06	-0.71 ± 0.11
Val	0.07 ± 0.05	-0.46 ± 0.11

2.2. Gibbs Energy of Transfer of Some Groups from Water to the Interface or to Octanol (Table 2)

Table 2
Gibbs free energy of transfer of various groups from water to the bilayer interface or to *n*-octanol

	Water → interface (kcal/mol)	Water → octanol (kcal/mol)
ΔG^{glycyl}	0 (4)	+1.15 (3)
ΔG^{CONH}	+1.2 (4)	+2.0 (3)
ΔG^{COOH}	-2.2 (4, 5)	+2.7 (3)
ΔG^{CH_3}	-1.1 (5)	-1.9 (3, 28)

2.3. Gibbs Energy of Transfer of End Groups from Water to the Interface or to Octanol (Table 3)

Table 3
Gibbs free energy of transfer of various N- and C-terminal groups

End group	Water → interface ΔG (kcal/mol)	Water → octanol ΔG (kcal/mol)
N-terminus		
NH ₃ ⁺	+0.5	+2.4
NH ₂	-0.2	+0.4
CH ₃ CONH	+0.1	+0.1
C-terminus		
COOH	-3.4	+0.7
COO ⁻	-0.7	+5.5
CONH ₂	-2.6	+1.9

These values are added to the sum of the free energies of transfer of all the residues to obtain the free energy of transfer for a polypeptide with different end groups. Values are from Hristova and White (5) and calculated in the text, rounded off to one decimal place

3. Methods

3.1. Calculation of the Gibbs Free Energy of Transfer of a Polypeptide from Water to the POPC Membrane Interface or to Octanol

3.1.1. Add the Contributions of All Residues in the Peptide Sequence

The calculations outlined are illustrated with five worked-out examples: penetratin, HIV TAT, Tp10W, nonaarginine (Ac-R₉-amide), and nonalysine (Ac-K₉-amide). These same examples are used to continue the calculations in the following Subheading 3. All the steps in this Subheading 3 can be conveniently performed using the *Totalizer* feature of the program MPEX (2).

The whole-residue hydrophobicity scales are shown in Table 1 (see Note 1). Adding the contributions of all residues in the sequence, one can obtain for transfer from water to octanol and the membrane interface:

Penetratin: $\Delta G_{\text{oct}}^{\circ} = +10.2$ kcal/mol, $\Delta G_{\text{if}}^{\circ} = +2.3$ kcal/mol
(unstructured)

TAT: $\Delta G_{\text{oct}}^{\circ} = +17.7$ kcal/mol, $\Delta G_{\text{if}}^{\circ} = +6.5$ kcal/mol
(unstructured)

Tp10W: $\Delta G_{\text{oct}}^{\circ} = +5.6$ kcal/mol, $\Delta G_{\text{if}}^{\circ} = -0.6$ kcal/mol
(unstructured)

Nonalysine: $\Delta G_{\text{oct}}^{\circ} = +25.2$ kcal/mol, $\Delta G_{\text{if}}^{\circ} = +8.9$ kcal/mol
(unstructured)

Nonaarginine: $\Delta G_{\text{oct}}^{\circ} = +16.3$ kcal/mol, $\Delta G_{\text{if}}^{\circ} = +7.3$ kcal/mol
(unstructured)

3.1.2. Include the Contributions of End Groups

The procedure to obtain the end-group contributions, which are compiled in Table 3, was developed by Hristova and White (5) (see Note 2). In practice, once those values were obtained, the procedure is very simple. To obtain the contribution of a certain type of N- or C-terminus, add the value listed in Table 3 for the appropriate end groups present on the peptide to the sum of the Gibbs energies of transfer of all residues in the sequence. For example, for transfer to the interface, if the peptide has a free, protonated N-terminus (NH_3^+), add 0.5 kcal/mol; if the C-terminus is amidated, add -2.6 kcal/mol.

Thus, for penetratin, nonalysine, and nonaarginine, to account for the acetylated N-terminus add +0.1 kcal/mol (octanol or interface), and for the amidated C-terminus add +1.9 kcal/mol (oct) or -2.6 kcal/mol (if). For TAT, to account for the free (NH_3^+) terminus add +2.4 (oct) or +0.5 (if), and for the free COO^- terminus add +5.5 kcal/mol (oct) or -0.7 kcal/mol (if). For Tp10W, to account for the free (NH_3^+) terminus add +2.4 (oct) or +0.5 (if), and for the amidated

C-terminus add +1.9 kcal/mol (oct) or -2.6 kcal/mol (if). The results become:

Penetratin:	$\Delta G_{\text{oct}}^{\circ} = +12.2$ kcal/mol, $\Delta G_{\text{if}}^{\circ} = -0.3$ kcal/mol (unstructured)
TAT:	$\Delta G_{\text{oct}}^{\circ} = +25.6$ kcal/mol, $\Delta G_{\text{if}}^{\circ} = +6.2$ kcal/mol (unstructured)
Tp10W:	$\Delta G_{\text{oct}}^{\circ} = +9.3$ kcal/mol, $\Delta G_{\text{if}}^{\circ} = -2.8$ kcal/mol (unstructured)
Nonalysine:	$\Delta G_{\text{oct}}^{\circ} = +27.2$ kcal/mol, $\Delta G_{\text{if}}^{\circ} = +6.4$ kcal/mol (unstructured)
Nonaarginine:	$\Delta G_{\text{oct}}^{\circ} = +18.3$ kcal/mol, $\Delta G_{\text{if}}^{\circ} = +4.7$ kcal/mol (unstructured)

3.1.3. Include the Effect of Secondary Structure

To account for α -helix formation, for transfer to the interface, add the product (number of helical residues) \times (-0.4 kcal/mol) to the results above. For transfer to octanol, those results already reflect a hydrogen-bonded, α -helical peptide (see Note 3).

Penetratin is about 60% α -helical when bound to the membrane surface (22, 23, 26), TAT is essentially unstructured (23), and Tp10W is about 60% α -helical (12). This information is necessary to incorporate the effect of peptide hydrogen bonding in the calculation. Taking into account the percent helicity of the peptides, the results become:

Penetratin:	$\Delta G_{\text{oct}}^{\circ} = +12.2$ kcal/mol, $\Delta G_{\text{if}}^{\circ} = -4.1$ kcal/mol (60% helix)
TAT:	$\Delta G_{\text{oct}}^{\circ} = +25.6$ kcal/mol, $\Delta G_{\text{if}}^{\circ} = +6.2$ kcal/mol (unstructured)
Tp10W:	$\Delta G_{\text{oct}}^{\circ} = +9.3$ kcal/mol, $\Delta G_{\text{if}}^{\circ} = -7.8$ kcal/mol (60% helix)

3.2. Calculation of the Gibbs Free Energy of Transfer to the Interface of a Membrane Containing Negatively Charged Lipids (PC/PG or PC/PS Mixtures)

In the absence of any other information, the simplest way to estimate the electrostatic free energy of binding to an anionic lipid membrane is to multiply the net charge on the peptide by -1 kcal/mol. However, this assumes additivity of electrostatic and hydrophobic contributions to binding, which is not valid in general (see Note 4). If the vesicles contain more than 30% negatively charged lipid, use this result directly. Use half that number if the vesicles contain only about 20% negatively charged lipid. With the next section in mind, we will use 25 and 40% PG for penetratin, 25% PG for TAT, and both 20% PS and 50% PS for Tp10W. Penetratin has +7 net charge, add -7 kcal/mol for 40% PG or -3.5 kcal/mol for 25% PG. TAT has +8 net charge, add -4 kcal/mol. Tp10W has +5 net charge, add -2.5 kcal/mol for 20% PG or -5 kcal/mol for 50% PG vesicles. The results are:

Penetratin:	$\Delta G_{\text{if}}^{\circ} = -11.1$ kcal/mol (40%PG), $\Delta G_{\text{if}}^{\circ} = -7.6$ kcal/mol (25%PG)
-------------	--------------------------------------------------------------------------------------------------------------------

TAT:	$\Delta G_{\text{if}}^{\circ} = +2.2$ kcal/mol (unstructured)
Tp10W:	$\Delta G_{\text{if}}^{\circ} = -10.3$ kcal/mol (20%PS), $\Delta G_{\text{if}}^{\circ} = -12.8$ kcal/mol (50%PS)

3.3. Comparison Between Calculated Transfer to the Interface and Experimental Binding to the Membrane

If the experimental dissociation constants (K_{D}) are determined in molar units (binding constants in reciprocal molar units), the Gibbs free energy values derived from those constants, $\Delta G^{\circ} = RT \ln K_{\text{D}}$, must be modified by adding the cratic correction, -2.4 kcal/mol, if the results are to be compared with the calculations performed using the Wimley–White interfacial scale (1).

For penetratin, the experimentally determined dissociation constant from PC/PG 60:40, excluding electrostatics and the cratic correction, is 12 mM (22), which corresponds to $\Delta G^{\circ} = -2.6$ kcal/mol, and the experimental electrostatic contribution is -6.9 kcal/mol (22). Therefore, the complete Gibbs energy of binding becomes $\Delta G_{\text{bind}}^{\circ} = -2.6 - 6.9 - 2.4 = -11.9$ kcal/mol, which compares well to the calculated estimate of $\Delta G_{\text{if}}^{\circ} = -11.1$ kcal/mol. Another experimental estimate for 25% PG, already including the electrostatic free energy, is $K_{\text{D}} = 100 \mu\text{M}$ (27); this corresponds to $\Delta G_{\text{bind}}^{\circ} = RT \ln K_{\text{D}} - 2.4$ kcal/mol $= -7.8$ kcal/mol, which also compares well to the calculated value of $\Delta G_{\text{if}}^{\circ} = -7.6$ kcal/mol.

For the TAT peptide, the experimentally determined dissociation constant from PC/PG 75:25, excluding electrostatics and the cratic correction, is about 0.2 M (24), which corresponds to a $\Delta G^{\circ} = -1$ kcal/mol, and the experimental electrostatic contribution is -4 kcal/mol (24). The complete Gibbs energy of binding becomes $\Delta G_{\text{bind}}^{\circ} = -7.4$ kcal/mol, which is >9 kcal/mol more negative than the estimate (see Note 5).

For Tp10W, the experimentally determined dissociation constant from POPC is $K_{\text{D}} = 140 \mu\text{M}$. Adding the cratic correction, this yields $\Delta G_{\text{bind}}^{\circ} = -7.6$ kcal/mol, which is in very good agreement with the calculation for POPC ($\Delta G_{\text{if}}^{\circ} = -7.8$ kcal/mol). In POPC/POPS 80:20 and 50:50, the experimental dissociation constants are 3 and 0.5 μM , respectively, already including electrostatic components (20). Adding the cratic correction, these K_{D} correspond to $\Delta G_{\text{bind}}^{\circ} = -9.9$ kcal/mol (20%PS) and -11 kcal/mol (50%PS). The corresponding calculated values, $\Delta G_{\text{if}}^{\circ} = -10.3$ kcal/mol (20%PS) and -12.8 kcal/mol (50%PS), are fairly similar, but somewhat overestimated, as expected for amphipathic peptides (21).

3.4. Calculations of Peptide Insertion into the Bilayer

To estimate the likelihood of insertion, the difference between the free energies of the state bound to the interface and the state inserted in the membrane is calculated, as estimated by the free energies of partitioning to the interface and to octanol. This calculation must also take into account the secondary structure of the peptide (hydrogen bonding), and is only valid for zwitterionic

lipid membranes (strictly, POPC). Under the assumption that the membrane lipid charge stabilizes, by similar amounts, the surface-bound and the inserted state, one can apply it tentatively, in a qualitative way, to charged membranes. The absolute values are most certainly not valid, but the relative differences between peptides may be helpful in design (see Note 6).

Penetratin:	$\Delta G_{\text{oct-if}} = +16.9$ kcal/mol (60% helix)
TAT:	$\Delta G_{\text{oct-if}} = +19.4$ kcal/mol (unstructured)
Tp10W:	$\Delta G_{\text{oct-if}} = +17.1$ kcal/mol (60% helix)
Nonalysine:	$\Delta G_{\text{oct-if}} = +20.8$ kcal/mol (unstructured)
Nonaarginine:	$\Delta G_{\text{oct-if}} = +13.6$ kcal/mol (unstructured)

4. Notes

1. The hydrophobicity scales for transfer of a whole residue from water to octanol or to the POPC bilayer interface are built by adding the contributions of the side chain (ΔG^{sc}) and the glycylyl group (ΔG^{glycyl}). Transfer of a nonhydrogen-bonded peptide group (CONH) from water to *n*-octanol has a free energy change $\Delta G_{\text{oct}}^{\text{CONH}} = +2.0$ kcal/mol (1, 3); transfer to the interface corresponds to $\Delta G_{\text{if}}^{\text{CONH}} = +1.2$ kcal/mol (1, 4). Transfer of the glycylyl group (CH₂CONH) from water to octanol is calculated by adding the contributions of the peptide bond and the methylene group (Table 2): $\Delta G_{\text{oct}}^{\text{glycyl}} = \Delta G_{\text{oct}}^{\text{CONH}} + \Delta G_{\text{oct}}^{\text{CH}_2} = +2.0 - 0.85 = +1.15$ kcal/mol (1, 3). Similarly, transfer to the bilayer interface yields $\Delta G_{\text{if}}^{\text{glycyl}} = 0$ (1, 4). The whole-residue scales are then obtained by adding the contributions of the glycylyl group and the side chain. For example, for Ala $\Delta G_{\text{oct}}^{\text{sc}} = -0.65$ (1, 3), so the whole-residue value is $\Delta G_{\text{oct}}^{\text{Ala}} = -0.65 + 1.15 = 0.50$ (1, 3). The side-chain contributions to the Gibbs energies of transfer from water to octanol are given by Wimley et al. (3) and to the bilayer interface by Wimley and White (4). The computed values for the whole residues (1, 2) are listed in Table 1.
2. This note describes how to obtain the values of the end-group contributions to the Gibbs energy of transfer, which are given in Table 3. The procedure to obtain the end-group contributions was developed by Hristova and White (5). For easy reference, ΔG values used in these calculations are listed in Table 2. Let us begin with the interfacial scale. Transfer of the COOH group from water to the interface has a $\Delta G_{\text{if}}^{\text{COOH}} = -2.2$ kcal/mol (5). Hence, the difference of a group ending in COOH relative to the peptide group (Fig. 3)

is $\Delta G_{\text{if}}^{\text{COOH}} - \Delta G_{\text{if}}^{\text{CONH}} = -2.2 - 1.2 = -3.4$ kcal/mol, which is the value given by Hristova and White (5). For polypeptides with different C-terminal end groups, the free energies of transfer are calculated by adding the differences relative to the COOH group (Fig. 5). For example, transfer of the ionized C-terminus (COO^-) to the interface is less favorable by 2.7 kcal/mol (4, 5); thus, we must add $-3.4 + 2.7 = -0.7$ kcal/mol to the sum of the residue contributions. And transfer of an amidated C-terminus (CONH_2) is more favorable than the transfer of an ionized COO^- by 1.9 kcal/mol (5), so we must add $-0.7 - 1.9 = -2.6$ kcal/mol instead. For the N-terminus, the values can be derived from the transfer of an acetylated amino group, which comprises the free energies of transfer of the methyl and the peptide group (Fig. 4). The free energy of transfer of a methyl group to the interface is about -1.1 kcal/mol (5). Thus, $\Delta G_{\text{if}}^{\text{CH}_3\text{CONH}} = \Delta G_{\text{if}}^{\text{CH}_3} + \Delta G_{\text{if}}^{\text{CONH}} = -1.1 + 1.2 = +0.1$ kcal/mol. The values to be added to the free energies of transfer from water to the interface for other N-terminal versions can be computed from the difference values given by Hristova and White (5) and shown in Fig. 5. For example, the free energy of NH_3^+ at the interface is higher than that of CH_3CONH by 0.4 kcal/mol; and ΔG_{if} of NH_2 is lower than that of NH_3^+ by 0.7 kcal/mol, and is lower than that of CH_3CONH by 0.3 kcal/mol. This gives $0.1 - 0.3 = -0.2$ kcal/mol to be added if the N-terminus is the deprotonated NH_2 . The procedure for the octanol scale is entirely analogous. Transfer of the COOH group from water to octanol has a free energy of $\Delta G_{\text{oct}}^{\text{COOH}} = +2.7$ kcal/mol and transfer of the ionized COO^- group is higher by +4.8 kcal/mol (3), yielding $\Delta G_{\text{oct}}^{\text{COO}^-} = +7.5$ kcal/mol. The difference for a group ending in COOH relative to the peptide group (Fig. 3) is $\Delta G_{\text{oct}}^{\text{COOH}} - \Delta G_{\text{oct}}^{\text{CONH}} = +2.7 - 2.0 = +0.7$ kcal/mol. The differences between the free energies of transfer of other C-terminal groups to octanol are $\Delta G_{\text{oct}}^{\text{COO}^-} - \Delta G_{\text{oct}}^{\text{COOH}} = +4.8$ kcal/mol (3) and $\Delta G_{\text{oct}}^{\text{COO}^-} - \Delta G_{\text{oct}}^{\text{CONH}} = +3.6$ kcal/mol (5). Using those differences (Fig. 5) and the value to be added for a COOH end group derived above (+0.7 kcal/mol), we can compute the free energy values to be added to the peptides with various C-terminal groups, which are listed in Table 3. For the N-terminus, as for the interfacial scale, the values can be derived from the transfer of an acetylated amino group. The free energy of transfer of a methyl group to a nonpolar medium is about -2.0 kcal/mol (25). The value derived from the solvation parameter is about -1.9 kcal/mol (3). For the peptide group, the value is +2 kcal/mol (3). Thus, $\Delta G_{\text{oct}}^{\text{CH}_3\text{CONH}} = \Delta G_{\text{oct}}^{\text{CH}_3} + \Delta G_{\text{oct}}^{\text{CONH}} = -1.9 + 2.0 = +0.1$ kcal/mol. The differences between the free energies of transfer of other N-terminal groups to octanol are $\Delta G_{\text{oct}}^{\text{NH}_3^+} - \Delta G_{\text{oct}}^{\text{NH}_2} = +2.0$ kcal/mol

and $\Delta G_{\text{oct}}^{\text{NH}_3^+} - \Delta G_{\text{oct}}^{\text{CH}_3\text{CONH}} = +2.3 \text{ kcal/mol}$ (5). Again, using those differences and the value calculated for the CH_3CONH group, we can compute the free energy values to be added to the peptides with various N-terminal end groups (Table 3 and Fig. 5).

3. The Gibbs energy of transfer of a peptide group (CONH) from water to *n*-octanol ($\Delta G_{\text{oct}}^{\text{CONH}} = +2.0 \text{ kcal/mol}$), although initially derived for small (unstructured) peptides (3), actually provides a reasonable approximation for the transfer of hydrogen-bonded residues (α -helical peptides in the examples discussed here) from water to the hydrophobic bilayer interior (13). For transfer to the interface, Ladokhin and White estimate that the Gibbs energy is reduced by about 0.4 kcal/mol per hydrogen-bonded, helical residue (6).
4. The contribution of about -1 kcal/mol per interaction between a positive charge on the peptide and an anionic lipid, or a lipid membrane with more than 30 mol% anionic lipids, is suggested by a number of results (14–16). It works particularly well for simple polycationic peptides, such as oligolysine (Lys $_n$, $n=3-7$), where a linear correlation is observed between the electrostatic binding free energy and the number of residues in oligolysine (15). A more exact dependence of the electrostatic binding free energy of oligolysine as a function of anionic lipid content of the membrane was provided by Ben-Tal et al. (15). For the strongly cationic CPPs examined here, this simple rule of thumb is in remarkably good agreement with the electrostatic free energy derived from experiment. For penetratin (+7 formal charge) binding to vesicles with a high PG content (>35%), experimental estimates of the electrostatic free energy components are -6.9 kcal/mol (22) and -8.1 kcal/mol (23), while the rule of thumb predicts -7 kcal/mol . For the TAT variant discussed here (+8 formal charge), the electrostatic contribution for binding to vesicles with low PG content (25 mol%) derived from experiment is -4 kcal/mol (24), consistent with the rule's estimate of $-8/2 \text{ kcal/mol}$. For two other TAT variants (also +8 formal charges) binding to vesicles with high PG content (35 mol%), the electrostatic components derived from experiment are -6.4 and -7.1 kcal/mol (23), while the rule predicts -8 kcal/mol . And for an oligoarginine-based peptide (Acetyl-R $_7$ W-amide, +7 formal charge), the value derived from experiment is -7.2 kcal/mol , for 35 mol% PG (23), remarkably close to the -7 kcal/mol suggested by this rule of thumb. However, for amphipathic peptides, the electrostatic and hydrophobic contributions to the binding free energy are not additive in general (21), and deviations from experimental determinations of $\Delta G_{\text{bind}}^{\circ}$ can be quite large.

5. The discrepancy between the calculated and experimental values for TAT is too large to be explained by inaccuracies. Rather, it appears to stem from the value for binding to a neutral (zwitterionic lipid) membrane. The electrostatic contribution suggested by the rule of thumb, to use half of -1 kcal/mol per cationic residue for lipid mixtures containing about 20 mol% PG, amounts to -4 kcal/mol, which is exactly the same value obtained from Seelig's analysis (24). For α -helical peptides, of which Tp10W and penetratin are examples, the Wimley-White estimates are always remarkably close to the experimental determinations of the Gibbs energies of transfer (12). This suggests that the large discrepancy in the TAT case must reveal a real discrepancy between the actual and assumed conformation of the peptide on the membrane. While the CD spectrum of TAT on the membrane is that of a random coil, this information can be misleading. All it says is that TAT does not adopt a regular secondary structure. But if it adopts a well-defined but irregular, hydrogen-bonded structure, the CD spectrum may be identical to that of a truly disordered peptide. If a significant number of intramolecular hydrogen bonds were established by the peptide groups, this would significantly lower the binding free energy. Using -0.4 kcal/mol-residue (6), the maximum contribution from peptide groups alone would be -4.4 kcal/mol. If, in addition, the terminal, free COO^- group establishes a salt bridge with one of the Arg or Lys residues, this could further contribute about -2 kcal/mol to the binding Gibbs energy (12). Altogether, those hydrogen bonds would bring the value of $\Delta G_{\text{if}}^{\circ}$ to -4.2 kcal/mol, which is closer, but still not consistent with the -7.4 kcal/mol derived from experiment. Probably, additional hydrogen bonding within the peptide involving the Arg side chains further lowers the free energy upon binding.
6. We have proposed the hypothesis that, for helical amphipathic peptides such as Tp10W, if $\Delta G_{\text{oct-if}} < 20$ kcal/mol, then these peptides follow a graded mechanism of release of vesicle contents and are likely to be able to translocate across a POPC membrane (12). For highly cationic CPPs, there is no data to support this conjecture, except that, interestingly, $\Delta G_{\text{oct-if}}$ is much smaller for oligoarginine than for oligolysine, and it is well known that CPPs based on Arg are much more efficient than those based on Lys (29–32). Also, penetratin should be a less efficient CPP than nonaarginine. With regard to TAT, the large discrepancy between the binding Gibbs energies calculated using the Wimley-White formalism and derived from experiment recommend caution in the use of the value of $\Delta G_{\text{oct-if}}$ obtained. It probably makes more sense to use the binding free energy derived from experiment $\Delta G_{\text{bind}}^{\circ} = -7.4$ kcal/mol

in place of ΔG_{if}° . Using that value one obtains $\Delta G_{oct-if} = 33$ kcal/mol, suggesting that TAT should not translocate across the bilayer and is a much poorer CPP than nonaarginine, for example, which is consistent with experiment (29–32).

Acknowledgments

This work was supported by National Institutes of Health grant No. GM072507. I thank Steve White and Bill Wimley for their comments on the manuscript.

References

1. White, S. H., and Wimley, W. C. (1999). Membrane protein folding and stability: physical principles. *Annu. Rev. Biophys. Biomol. Struct.* **28**, 319–365.
2. Jaysinghe, S., Hristova, K., Wimley, W., Snider, C., and White, S. H. (2009) Membrane Protein Explorer (MPEx). <http://www.blanco.biomol.uci.edu/mpex>.
3. Wimley, W. C., Creamer, T. P., and White, S. H. (1996) Solvation energies of amino acid side chains and backbone in a family of host–guest pentapeptides. *Biochemistry* **35**, 5109–5124.
4. Wimley, W. C., and White, S. H. (1996) Experimentally determined hydrophobicity scale for proteins at membrane interfaces. *Nat. Struct. Biol.* **3**, 842–848.
5. Hristova, K., and White, S. H. (2005) An experiment-based algorithm for predicting the partitioning of unfolded peptides into phosphatidylcholine bilayer interfaces. *Biochemistry* **44**, 12614–12619.
6. Ladokhin, A. S., and White, S. H. (1999) Folding of amphipathic α -helices on membranes: energetics of helix formation by melittin. *J. Mol. Biol.* **285**, 1363–1369.
7. Wimley, W. C., Hristova, K., Ladokhin, A. S., Silvestro, L., Axelsen, P. H., and White, S. H. (1998) Folding of β -sheet membrane proteins: A hydrophobic hexapeptide model. *J. Mol. Biol.* **277**, 1091–1110.
8. Wieprecht, T., Apostolov, O., Beyermann, M., and Seelig, J. (1999) Thermodynamics of the R-helix-coil transition of amphipathic peptides in a membrane environment: Implications for the peptide-membrane binding equilibrium. *J. Mol. Biol.* **294**, 785–794.
9. Wieprecht, T., Apostolov, O., Beyermann, M., and Seelig, J. (2000) Interaction of a mitochondrial presequence with lipid membranes: Role of helix formation for membrane binding and perturbation. *Biochemistry* **39**, 15297–15305.
10. Klocek, G., Schulthess, T., Shai, Y., and Seelig, J. (2009) Thermodynamics of melittin binding to lipid bilayers. Aggregation and pore formation. *Biochemistry* **48**, 2586–2596.
11. Fernandez-Vidal, M., Jaysinghe, S., Ladokhin, A. S., and White, S. H. (2007) Folding amphipathic helices into membranes: Amphiphilicity trumps hydrophobicity. *J. Mol. Biol.* **370**, 459–470.
12. Almeida, P. F., and Pokorny, A. (2009) Mechanisms of antimicrobial, cytolytic, and cell-penetrating peptides: From kinetics to thermodynamics. *Biochemistry* **48**, 8083–8093.
13. Jaysinghe, S., Hristova, K., and White, S. H. (2001) Energetics, stability, and prediction of transmembrane helices. *J. Mol. Biol.* **312**, 927–934.
14. Kim, J., Mosior, M., Chung, L., Wu, H., and McLaughlin, S. (1991) Binding of peptides with basic residues to membranes containing acidic phospholipids. *Biophys. J.* **60**, 135–148.
15. Ben-Tal, N., Honig, B., Peitzsch, R. M., Denisov, G., and McLaughlin, S. (1996) Binding of small basic peptides to membranes containing acidic lipids: theoretical models and experimental results. *Biophys. J.* **71**, 561–575.
16. Murray, D., Arbuzova, A., Hangyás-Mihályiné, G., Gambhir, A., Ben-Tal, N., Honig, B., and McLaughlin, S. (1999) Electrostatic properties of membranes containing acidic lipids and adsorbed basic peptides: theory and experiment. *Biophys. J.* **77**, 3176–3188.
17. Mosior, M., and McLaughlin, S. (1992) Binding of basic peptides to acidic lipids in membranes: effects of inserting alanine(s)

- between the basic residues. *Biochemistry* **31**, 1767–1773.
18. Gregory, S. M., Cavanaugh, A., Journigan, V., Pokorny, A., and Almeida, P. F. F. (2008) A quantitative model for the all-or-none permeabilization of phospholipid vesicles by the antimicrobial peptide cecropin A. *Biophys. J.* **94**, 1667–1680.
 19. Gregory, S. M., Pokorny, A., and Almeida, P. F. F. (2009) Magainin 2 revisited: a test of the quantitative model for the all-or-none permeabilization of phospholipid vesicles. *Biophys. J.* **96**, 116–131.
 20. Yandek, L. E., Pokorny, A., and Almeida, P. F. F. (2008) Small changes in the primary structure of transportan 10 alter the thermodynamics and kinetics of its interaction with phospholipid vesicles. *Biochemistry* **47**, 3051–3060.
 21. Ladokhin, A. S., and White, S. H. (2001). Protein chemistry at membrane interfaces: non-additivity of electrostatic and hydrophobic interactions. *J. Mol. Biol.* **309**, 543–552.
 22. Persson, D., Thorén, P. E., Herner, M., Lincoln, P., Nordén, B. (2003) Application of a novel analysis to measure the binding of the membrane-translocating peptide penetratin to negatively charged liposomes. *Biochemistry* **42**, 421–429.
 23. Thorén, P. E. G., Persson, D., Esbjorner, E. K., Goksor, M., Lincoln, P., and Nordén, B. (2004) Membrane binding and translocation of cell-penetrating peptides. *Biochemistry* **43**, 3471–3489.
 24. Ziegler, A., Blatter, X. L., Seelig, A., and Seelig, J. (2003) Protein transduction domains of HIV-1 and SIV TAT interact with charged lipid vesicles. Binding mechanism and thermodynamic analysis. *Biochemistry* **42**, 9185–9194.
 25. Yandek, L. E., Pokorny, A., Florén, A., Knoelke, K., Langel, U., and Almeida, P. F. F. (2007) Mechanism of the cell-penetrating peptide transportan 10 permeation of lipid bilayers. *Biophys. J.* **92**, 2434–2444.
 26. Magzoub, M., Eriksson, L. E. G., and Gräslund, A. (2002) Conformational states of the cell-penetrating peptide penetratin when interacting with phospholipid vesicles: effects of surface charge and peptide concentration. *Biochim. Biophys. Acta* **1563**, 53–63.
 27. Binder, H., and Lindblom, G. (2003) Charge-dependent translocation of the trojan peptide penetratin across lipid membranes. *Biophys. J.* **85**, 982–995.
 28. Tanford, C. (1991). The hydrophobic effect: formation of micelles and biological membranes. 2nd Ed., Krieger, Malabar, FL.
 29. Mitchell, D. J., Kim, D. T., Steinman, L., Fathman, C. G., and Rothbard, J. B. (2000) Polyarginine enters cell more efficiently than other polycationic homopolymers. *J. Pept. Res.* **56**, 318–325.
 30. Sakai, N., and Matile, S. (2003) Anion-mediated transfer of polyarginine across liquid and bilayer membranes. *J. Am. Chem. Soc.* **125**, 14348–14356.
 31. Sakai, N., Takeuchi, T., Futaki, S., and Matile, S. (2005) Direct observation of anion mediated translocation of fluorescent oligoarginine carriers into and across bulk liquid and anionic bilayer membranes. *ChemBioChem* **6**, 114–122.
 32. Rothbard, J. B., Jessop, T. C., Lewis, R. S., Murray, B. A., and Wender, P. A. (2004) Role of membrane potential and hydrogen bonding in the mechanism of translocation of guanidinium-rich peptides into cells. *J. Am. Chem. Soc.* **126**, 9506–9507.

Studies of Proteoglycan Involvement in CPP-Mediated Delivery

Anders Wittrup, Si-He Zhang, and Mattias Belting

Abstract

Cell-penetrating peptides (CPPs) are widely used to deliver macromolecular cargoes to intracellular sites of action. Many CPPs have been demonstrated to rely on cell surface heparan sulfate proteoglycans (HSPGs) for efficient cellular entry and delivery. In this chapter, we describe methods for the study of PG involvement in CPP uptake. We provide descriptions of how to determine whether uptake of a CPP of interest is dependent on PGs. We also provide detailed protocols for the purification of PGs by anion-exchange chromatography as well as the characterization of the HSPG core protein composition of a cell line of interest. Finally, we present methods for modulating the expression level of specific HSPG core proteins as a means to determine the core protein specificity in the uptake of a particular CPP.

Key words: Cell-penetrating peptides, CHO cell mutants, Heparan sulfate, Glypican, Proteoglycan, siRNA, Syndecan

1. Introduction

Most gene and protein delivery vehicles [including cell-penetrating peptides (CPPs)] are cationic, and have shown dependence on negatively charged cell surface heparan sulfate proteoglycans (HSPGs) for efficient cell-surface binding and intracellular delivery (1). In an early study, Mislick and Baldeschwieler demonstrated that the uptake of poly-L-lysine/DNA complexes was dependent on HSPG (2). Digestion of cell surface HSPG decreased complex uptake by approximately 80% and the DNA reporter gene expression level was 53-fold lower in PG-deficient cells compared with wild-type CHO cells. The involvement of cell surface PGs, especially HSPGs for the entry of numerous CPPs, has since been demonstrated (3–6).

The PGs are a family of proteins with the common characteristic of one or several glycosaminoglycans (GAGs) attached through a hydroxyl bond to serine residues of the protein. The GAG substituents are heterogeneous disaccharide (hexosamine and glucuronic acid) polymers consisting of 20–150 disaccharide units. GAGs are synthesized by (a) the formation of a tetrasaccharide structure linking the GAG chain to the protein, (b) the polymerization of the polysaccharide chain, and (c) enzymatic modification (mainly by sulfation at various positions) of the chain. Proteins and peptides interact with PGs through interaction with both the core protein and the GAG chains. Usually, highly polybasic domains, containing several clustered basic amino acids (as is typical for CPPs), are the binding motifs for the negatively charged GAGs. Specific saccharide sequences and the spatial organization of such sequences determine the interaction with protein ligands.

Cell surface PGs are mainly HS substituted and belong to two families of proteins: membrane intercalated type I transmembrane syndecans (1–4) and glycosyl–phosphatidyl–inositol anchored glypicans (1–6). Both syndecans and glypicans are endocytosed, either constitutively or upon ligand-induced clustering (7, 8). The role and involvement of individual core proteins in the uptake of CPPs and other HS-binding ligands have, so far, not been studied in great detail. Syndecan-2 has been shown to promote octa-arginine uptake and perlecan, an extracellular matrix PG, has been suggested to mediate the uptake of HIV-Tat in the absence of cell surface HSPGs (9, 10). Recently, our group demonstrated that HSPGs of both the syndecan and glypican type can mediate the uptake of macromolecular cargoes (11).

The main techniques employed to study HSPGs are summarized in Table 1. Below we describe methods to determine whether the uptake of a specific CPP is dependent on PGs. We also present methods for the purification and characterization of the specific HSPGs expressed in a cell line of interest. Finally, we present methods for elucidating the involvement of specific HSPG core proteins in the uptake of, e.g., a certain CPP.

2. Materials

2.1. Interference with HS Synthesis

1. F12K cell growth medium with and without 10% fetal bovine serum (FBS).
2. CHO-K1 and pgsA, B, D, E, F, G, or H cells (ATCC) grown in F12K with 10% FBS supplemented with glutamine and penicillin/streptomycin.

Table 1
Methods used to study HSPGs

Method	Aspect studied	Reference
Radiolabeling and purification		(20)
[³⁵ S]-Sulfate	Sulfation-specific GAG-labeling and detection	Subheading 3.3
[³ H]-Glucosamine	General GAG-labeling	
Anion-exchange chromatography	PG/GAG-purification and structure analysis (charge)	Subheading 3.3
Size-exclusion chromatography	PG/GAG-purification and structure analysis (size)	
Gel electrophoresis	Primarily size separation	Subheading 3.3
Interference with HS synthesis		
Chlorate	General sulfation inhibition	(21)
CHO cell mutants	pgsA; pan-GAG def. (XT-1: xylosyltransferase) pgsB; pan-GAG def. (GalT-I: galactosyltransferase I) pgsG; pan-GAG def. (GlcAT-I: glucuronyltransferase I) pgsD; HS def. (EXT-1: GlcA and GlcNAc transferase) pgsE; undersulf. HS (NDST1: GlcNAc <i>N</i> -deacetylase/ <i>N</i> -sulfotransferase) pgsF; 2-OS def. (HS2ST: HS 2- <i>O</i> -sulfotransferase) pgsH; 6-OS def. (6OST-1: HS 6- <i>O</i> -sulfotransferase)	Subheading 3.1
Conditional knockouts	EXT-1, sulfotransferases	(22, 23)
Interference with HSPG function		
Degradative lyases	Hep lyase I–III	Subheading 3.2
Competition/blocking	Dependent on selectivity of competitor, e.g., heparin	(24)
HSPG antibodies for, e.g., immunoblot analysis		
Core protein-specific antibodies	Specific HSPG core proteins	Subheading 3.4
ΔHS (“anti-stub”) antibody (3G10)	All HSPG core proteins (recognizes a neoepitope generated by Hep lyase III digestion)	Subheading 3.4
Epitope-specific scFv anti-HS antibodies	HS epitopes	(15)

(continued)

Table 1
(continued)

Method	Aspect studied	Reference
Other anti-HS antibodies	10E4 (GlcNAc/GlcNS mixed seq.), JM13 (2-OS, GlcNS, or GlcN), HepSS1 (GlcNS), JM403 (GlcN)	(25)
Modulation of HSPG expression		
siRNA core protein knock-down	Specific HSPG core proteins	Subheading 3.5
Core protein overexpression	Specific HSPG core proteins	Subheading 3.6

-OS O-sulfation

2.2. Interference with HSPG Function

1. Dulbecco's Modified Eagle Medium (DMEM) with and without 10% FBS.
2. HeLa cells (ATCC) grown in DMEM with 10% FBS supplemented with glutamine and penicillin/streptomycin.
3. Forty-eight-Well cell culture plates (Nunc).
4. Eight-well chambered coverglass microscopy slides (Nunc).
5. Phosphate-buffered saline (PBS): 137 mM NaCl, 2.7 mM KCl, 10 mM Na₂HPO₄, 1.8 mM KH₂PO₄, pH 7.4.
6. Heparinase III (E.C. 4.2.2.8, Sigma).
7. Chondroitinase ABC (E.C. 4.2.2.4, Sigma).
8. Digestion buffer: DMEM, supplemented with 20 mM HEPES-HCl, pH 7.4, 0.5% bovine serum albumin (BSA).

2.3. [³⁵S]-Sulfate PG-Labeling and DEAE-Purification

1. DMEM (Invitrogen) with and without 10% FBS.
2. HeLa cells (ATCC) grown in DMEM with 10% FBS supplemented with glutamine and penicillin/streptomycin.
3. Forty-eight-Well cell culture plates (Nunc).
4. PBS: 137 mM NaCl, 2.7 mM KCl, 10 mM Na₂HPO₄, 1.8 mM KH₂PO₄, pH 7.4.
5. Modified Eagle Medium (MEM) w/o MgSO₄ (Invitrogen).
6. [³⁵S]-SO₄ (PerkinElmer).
7. Two % Tx-buffer: 0.15 M NaCl, 10 mM KH₂PO₄, 10 mM EDTA, 5 μg/ml ovalbumin (OVA), pH 7.5, 2% Triton X-100, 1× Complete Protease Inhibitor (Roche).
8. DE52 pre-swollen DEAE-cellulose matrix (Whatman). Reconstitute the dry DEAE-cellulose in water to approximately 50% matrix suspension or slurry (v/v).
9. Poly-Prep chromatography columns (Bio-Rad).

10. PD-10 desalting column (GE Healthcare).
11. Eq.-buffer: 7 M urea, 10 mM Tris-HCl, pH 8.0, 0.1% Triton X-100 (see Note 1).
12. Urea-B: 6 M urea, 0.5 M HAc, 5 µg/ml OVA, pH 5.8, 0.1% Triton X-100.
13. Urea-C: 6 M urea, 10 mM Tris-HCl, 5 µg/ml OVA, pH 8.0, 0.1% Triton X-100.
14. Tris-buffer: 0.05 M Tris-HCl, pH 7.5.
15. Four M Gu-buffer: 4 M Gu-HCl, 50 mM HAc, 5 µg/ml OVA, pH 5.8, 0.2% Triton X-100 (see Note 2).
16. Dextran (Sigma).
17. Dextran-sulfate (Sigma).
18. Resuspension buffer: 1 M NaCl, 10 mM Tris-HCl, pH 7.5, 0.05% Triton X-100.
19. HS'ase buffer: 50 mM NaOAc, 150 mM NaCl, 5 mM CaCl₂, 50 mM HEPES-HCl, pH 6.5, 0.5× complete protease inhibitor w/o EDTA.
20. ABC'ase buffer: 40 mM NaAc, 40 mM Tris-HCl, pH 7.8, 0.5× complete protease inhibitor w/o EDTA.
21. Heparinase III (E.C. 4.2.2.8, Sigma).
22. Chondroitinase ABC (E.C. 4.2.2.4, Sigma).
23. Four×LDS NuPAGE sample buffer (Invitrogen).
24. Four to twelve % NuPAGE Bis-Tris gel (Invitrogen).
25. Glycerol solution: 30% ethanol, 5% acetic acid, and 2.5% glycerol.

2.4. Immunoblot Analysis of HSPGs

1. DMEM with and without 10% FBS.
2. HeLa cells (ATCC) grown in DMEM with 10% FBS supplemented with glutamine and penicillin/streptomycin.
3. DMEM (10% FBS) without antibiotics.
4. Tris-buffered saline (TBS): 25 mM Tris-HCl, 150 mM NaCl, 2 mM KCl, pH 7.4.
5. TTBS, TBS supplemented with 0.5% Tween-20.
6. Dry milk powder.
7. BSA.
8. Mouse monoclonal 3G10 anti-ΔHS antibody (Seikagaku).
9. Mouse monoclonal B-B4 anti-syndecan-1 antibody (Serotec).
10. Goat polyclonal L-18 anti-syndecan-2 antibody (Santa Cruz Biotech).
11. HRP-conjugated sheep anti-mouse (GE Healthcare).
12. HRP-conjugated sheep anti-goat (GE Healthcare).

13. Four×LDS NuPAGE Sample buffer (Invitrogen).
14. Four to twelve % NuPAGE Bis–Tris gel (Invitrogen).

2.5. HSPG Core Protein Knock-Down

1. DMEM with and without 10% FBS.
2. HeLa cells (ATCC) grown in DMEM with 10% FBS supplemented with glutamine and penicillin/streptomycin.
3. DMEM (10% FBS) without antibiotics.
4. Opti-MEM (Invitrogen).
5. Lipofectamine 2000 (Invitrogen).
6. Confirmed functional siRNA sequences (prepare 10 μM stock solutions) (Ambion):
 Silencer® Negative Control siRNA.
 Glypican-1 (Prod. no. s5973).
 Syndecan-1 (Prod. no. 12432).
 Syndecan-2 (Prod. no. s12637).
 Syndecan-4 (Prod. no. 142565).

2.6. HSPG Core Protein Overexpression

1. DMEM with and without 10% FBS.
2. HeLa cells (ATCC) grown in DMEM with 10% FBS supplemented with glutamine and penicillin/streptomycin.
3. DMEM (10% FBS) without antibiotics.
4. Opti-MEM (Invitrogen).
5. Lipofectamine 2000 (Invitrogen).
6. GFP-tagged core protein constructs, e.g., the N-terminal GFP-tagged syndecan-2 and syndecan-3 constructs described by Landgraf et al.: pEGFP-N3/SDC2-MYC and pEGFP-N3/SDC3-MYC (12).

3. Methods

The large number of enzymes involved in PG synthesis and modification (>40) provide numerous possible targets for the interference with PG synthesis. PGs also have several unique physicochemical properties, enabling the isolation and analysis of PGs with a wide variety of techniques.

The extensive sulfation of the GAG chains of PGs enables relatively selective radiolabeling through incubation of cells with [³⁵S]-sulfate in sulfate-depleted medium. In addition, the negative charge of GAGs renders the entire PG highly anionic, making purification by anion-exchange chromatography possible. Often, including in the protocols below, PGs are purified using DEAE-cellulose. The purification results in partially purified PGs with the [³⁵S]-sulfate almost exclusively incorporated into PGs. [³⁵S]-radioactivity can thus

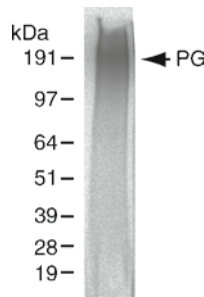


Fig. 1. PG smear. DEAE-purified [^{35}S]-radiolabeled PGs from HeLa cells were separated on a 4–12% polyacrylamide gel. The gel was dried and PGs were visualized by autoradiography. Arrow indicates the center of the PG distribution.

be used as a very sensitive tool to quantify relative amounts of PG in different samples. The [^{35}S]-radioactivity can also be used for PG analysis by autoradiography following, e.g., size separation by electrophoresis (SDS-PAGE).

Most intact PGs are relatively large proteins owing to their GAG substituents. Intact PGs, however, do not have a well-defined molecular weight but rather migrate as a broad smear when separated by electrophoresis (Fig. 1) or size-exclusion chromatography. In order to detect a specific protein “band” on an immunoblot, GAGs attached to the core protein must be digested, usually by enzymatic methods. GAG lyases can either be HS-specific heparinases or CS/DS-specific chondroitinases. Below, heparinase and chondroitinase digestions are performed prior to immunoblot analysis (Subheading 3.4). Similar digestions are also used to determine the presence of HS and CS/DS PG after purification of total cell PG (Subheading 3.3). Furthermore, GAG lyases are used to digest cell surface GAGs, in order to determine the influence of HS and CS/DS on CPP uptake (Subheading 3.2).

3.1. Interference with HS Synthesis

Numerous mutant CHO cell lines, defective in specific enzymes involved in GAG biosynthesis, have been isolated and characterized (13). Clones deficient for enzymes involved in the synthesis of the tetrasaccharide linkage region are deficient in both HS and CS/DS synthesis (pan-GAG deficient, pgsA, pgsB, and pgsG). Clones deficient in the enzyme EXT1 or GlcA/GlcNAc transferase (pgsD) have no HS but express approximately threefold levels of CS/DS when compared with wild-type cells. Finally, clones that are deficient in specific HS-modifying enzymes express HS chains that are deficient in *N*-sulfation, 2-*O*-sulfation, or 6-*O*-sulfation (pgsE, pgsF, and pgsH, respectively). These mutant CHO cell lines are straightforward to apply in the study of a particular CPP. The use of the cell lines can provide answers to whether intact GAG or HS synthesis is required for CPP uptake, as well as elucidate the requirement for certain HS-modifying enzymes in this process.

3.2. Interference with HSPG Function

Below is a protocol for the digestion of cell surface HS and CS/DS. This relatively simple assay can be adapted to most cell types and CPPs, and constitutes an appropriate initial experiment (together with studies in CHO cell mutants) to determine the influence of cell surface GAG on the uptake of a particular CPP in virtually any cell type of choice.

To, in more detail, determine the GAG-structure specificity of a given CPP, it is possible to compete for GAG/CPP binding with an excess of unlabeled GAG-binding compounds with varying specificities potentially allowing the identification of the most important GAG structures involved in CPP binding. The well-characterized epitope-specific single chain anti-HS and anti-CS antibodies developed by the van Kuppevelt laboratory are ideal for this purpose (14, 15):

1. Seed cell type of choice, e.g., HeLa cells, in 48-well plate or 8-well microscopy slide (see Note 3).
2. Allow to grow overnight to reach 50–80% confluency.
3. Wash twice with digestion buffer.
4. Add 0.25 mL/well digestion buffer.
5. Add 2.5 mIU (International Units) heparanase III or 125 mU chondroitinase ABC for each well. Incubate 3 h at 37°C.
6. Wash cells twice with PBS.
7. Perform CPP uptake assay (see Note 4).

3.3. [³⁵S]-Sulfate PG-Labeling and DEAE-Purification

In order to perform several of the PG analyses described in this chapter, purified PGs are required. Below is a protocol for anion-exchange purification of [³⁵S]-labeled membrane PG. The purified PG can be separated by SDS-PAGE and visualized using autoradiography as described below (Fig. 1) or used for immunoblot procedures as described under Subheading 3.3:

1. Seed 3×10^6 HeLa cells in a 75-cm² flask (seed correspondingly fewer cells if a smaller cell culture container is used).
2. Allow the cells to grow for 24 h (to approximately 80% confluency).
3. Rinse the cell layer with 15 mL PBS.
4. Starve cells for 1 h at 37°C in sulfate-free medium (MEM).
5. Aspirate medium, add 10 mL sulfate-free medium supplemented with 100 μ Ci/ml [³⁵S]-sulfate and incubate overnight.
6. Wash cells twice with PBS.
7. Aspirate the PBS and lyse cells in 1.5 mL 2% Tx-buffer for 20–30 min on shaker at RT (use less lysis buffer if fewer cells are processed, e.g., 300 μ L/well in a six-well plate).
8. Scrape the cell culture container and collect the lysate and cell debris.

9. Spin the lysate at $4,500 \times g$ for 10 min, keep the supernatant.
10. Add one volume Eq.-buffer to the supernatant.
11. Purify PGs on an equilibrated DEAE-cellulose column as follows:
 - (a) Load 0.5 mL of DE-52-matrix (see Note 5).
 - (b) Equilibrate column with 5 mL Eq.-buffer.
 - (c) Add 50 μg dextran and 50 μg dextran-sulfate to the sample as carrier.
 - (d) Add the sample to the column. Discard the flow-through.
 - (e) When the sample has passed through the column, wash the column with 5 mL Urea-B.
 - (f) Wash column with 5 mL Urea-C.
 - (g) Wash with 5 mL Tris-buffer.
 - (h) Put a collection tube under the column. Elute the PG by sequential addition 5×0.5 mL Gu-buffer. Allow all liquid from each buffer addition to flow-through, before adding the next volume.
12. Add 50 μg dextran to the sample, take off 1/50 volume (50 μL , for DPM measurement).
13. Precipitate the sample with 4.5 volumes of -20°C pre-cooled 95% ethanol. Make sure the solution is well mixed and keep overnight at -20°C .
14. Spin sample at $4,500 \times g$, 10 min, discard supernatant.
15. Wash once with ice-cold 95% ethanol, air-dry completely.
16. Suspend pellet in 2.5 mL resuspension buffer. Make sure the pellet is dissolved completely (see Note 6).
17. Desalt sample with PD-10 at 4°C . Equilibrate the column in water and elute with 3.5 mL water. Take off 1/50 volume of the eluate (for DPM measurement).
18. Divide sample into three fractions (see Note 7).
19. Put samples in -80°C freezer.
20. Freeze-dry samples to dryness.
21. Dissolve two fractions in 100 μL HS'ase buffer (one sample as nondigested control) and one fraction in 100 μL ABC'ase buffer.
22. Add 0.6 mIU heparinase III to the HS'ase sample and 40 mU chondroitinase ABC to the ABC'ase sample. Add no enzyme to the nondigested control sample in HS'ase buffer.
23. Incubate for 3 h at 37°C .
24. Repeat enzyme additions and incubate at 37°C , overnight. Also keep the nondigested sample in HS'ase buffer at 37°C .

25. Add one-third volume of 4× LDS to all samples (see Note 8).
26. Load at least 5,000–10,000 DPM (as determined at step 17) of each sample on a 4–12% NuPAGE Bis–Tris gel and separate proteins for approximately 1 h at 200 V.
27. Fix and equilibrate gel in glycerol solution for 30 min.
28. Dry gel to a pre-wetted filter paper on a gel-dryer, for 2 h at 80°C or until completely dry.
29. Visualize intact and digested PGs using autoradiographic film or [³⁵S]-sensitive autoradiographic plate after overnight exposure.

3.4. Immunoblot Analysis of HSPG

In order to characterize which HSPG core proteins that are capable of internalizing a specific CPP in a cell line of interest, an appropriate first step is to characterize the HSPG composition of the studied cell line. This can be done using the anti-ΔHS antibody 3G10 (16). This antibody recognizes a neoepitope produced by heparinase III digestion (“HS-stub”). The antibody can thus be used to detect all HSPG core proteins on an immunoblot. Ideally, the identities of the detected bands are confirmed by either core protein-specific antibodies or by siRNA-mediated core protein knock-down (Subheading 3.4). However, certain conclusions can be drawn directly from the molecular weight of the detected bands as the different syndecans have relatively different masses. In contrast, all glypicans are approximately 60 kDa making it difficult to discriminate between these on a ΔHS-blot. Fig. 2 shows a typical anti-ΔHS staining pattern of PGs isolated from HeLa cells:

1. Isolate PGs from at least one well of a six-well plate, according to the method described under Subheading 3.3, steps 1–17 (steps 3–5 can be omitted in order to purify nonradioactive PGs).

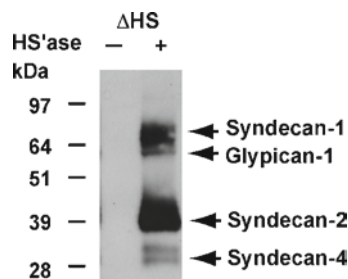


Fig. 2. Identification of HSPG core proteins. DEAE-purified PGs from HeLa cells were either digested with both heparinase III and chondroitinase ABC (+) or left nondigested (-). Proteins were then separated on a 4–12% polyacrylamide gel, electroblotted, and visualized using anti-ΔHS antibody.

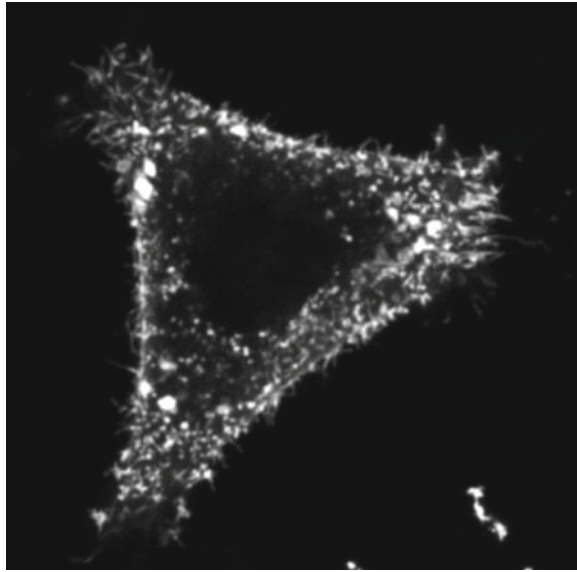


Fig. 3. Typical localization of a GFP-tagged syndecan. Overexpressed GFP-syndecan-2 was visualized using confocal microscopy. Note that the protein localizes to both the cell surface and intracellular vesicles.

2. Divide the desalted purified PG into two fractions.
3. Put samples in -80°C freezer.
4. Freeze-dry samples to dryness.
5. Dissolve the two fractions in 50 μL HS'ase buffer (one digested sample and one nondigested control).
6. Add both 0.6 mIU heparinase III and 40 mU chondroitinase ABC to the sample to be digested (see Note 9).
7. Incubate for 3 h at 37°C .
8. Repeat enzyme additions and incubate at 37°C , overnight. Also keep the nondigested sample in HS'ase buffer at 37°C .
9. Add one-third volume of $4\times$ LDS to all samples.
10. Load, at least, a sample amount corresponding to the material from 2 cm^2 of cells (or 5,000–10,000 DPM, if PGs were labeled with [^{35}S]-sulfate) per lane on a 4–12% NuPAGE Bis-Tris gel and separate proteins for approximately 1 h at 200 V.
11. Transfer proteins to a PVDF membrane for 2 h at 30 V.
12. Block the PVDF membrane for 30 min with 3% BSA in TTBS in case of core protein-specific immunoblot or with 5% dry milk in TTBS if the membrane is to be probed with anti- ΔHIS (3G10) antibody.
13. Probe the membrane with core protein-specific antibodies (e.g., anti-syndecan-1 1:150, anti-syndecan-2 1:200, both in

- 3% BSA in TTBS) or anti- Δ HS (3G10) antibody (1:1,000 in 5% dry milk in TTBS) overnight at 4°C.
14. Wash membrane 3 × 5 min in TTBS.
 15. Probe membrane with appropriate HRP-conjugated secondary antibody.
 16. Visualize protein bands using standard ECL substrate and chemiluminescence detection system (see Note 10).

3.5. HSPG Core Protein Knock-Down

Below is a protocol for siRNA-mediated knock-down of HSPG core proteins in HeLa cells. The protocol is specifically adjusted to allow for studies of the uptake of CPPs and other PG-binding ligands. Standard lipofection reagents, e.g., Lipofectamine, bind cell surface PGs (17, 18) and can potentially interfere with the uptake of other PG-binding ligands. Hence, a washing step to remove remaining cell surface-associated lipofection reagent has been incorporated in the protocol below:

1. Seed 250,000 HeLa cells/well in a six-well plate in DMEM with 10% FCS 24 h prior to transfection (see Note 11).
2. At the day of transfection, dilute siRNAs and Lipofectamine 2000 in Opti-MEM as described below. For each well to be transfected:
 - (a) Dilute 5 μ L of siRNA-stock in 250 μ L Opti-MEM.
 - (b) Dilute 12.5 μ L Lipofectamine 2000 in 250 μ L Opti-MEM, incubate for 10 min at room temperature.
 - (c) Mix 250 μ L of plasmid solution with 250 μ L of lipofectamin solution, incubate for 20 min at room temperature.
3. Wash cells once with DMEM w/o serum and antibiotics.
4. Add 2,000 μ L/well Opti-MEM w/o serum and antibiotics.
5. Add 500 μ L/well of siRNA/Lipofectamine 2000 solutions.
6. Incubate cells at 37°C for 5 h.
7. Wash cells twice with 1 M NaCl in PBS. Do not allow the cells to remain in the hyper osmotic buffer for more than 30 s (see Note 12).
8. Quickly remove the 1 M NaCl buffer and gently wash once with PBS.
9. Add 2,500 μ L/well DMEM with 10% FCS.
10. Incubate cells for 24 h.
11. Purify PGs according to Subheading 3.3, steps 7–17.
12. Validate core protein knock-down in selected wells using Δ HS or core protein-specific antibodies according to the method described under Subheading 3.4.
13. Perform CPP uptake assays in separate wells.

3.6. HSPG Core Protein Overexpression

Overexpression of fluorescently tagged (e.g., GFP-tagged) PG core proteins enables colocalization analysis of internalized CPPs and CPP-delivered cargoes with specific PG core proteins. Detection and localization of endogenous and overexpressed native (i.e., nontagged) core proteins is also possible through the use of core protein-specific antibodies. However, with the exception of antibodies toward syndecan-1, most commercially available core protein antibodies lack specificity for immunofluorescence experiments. Below is a protocol for the overexpression of GFP-tagged HSPG core proteins in HeLa cells:

1. Seed 30,000 HeLa cells/well in eight-well microscopy slide in DMEM with 10% FCS 24 h prior to transfection.
2. At the day of transfection, dilute plasmids (e.g., syndecan-2-GFP and syndecan-3-GFP) and Lipofectamine 2000 in Opti-MEM as described below. For each well to be transfected:
 - (a) Dilute 0.5 μg plasmid in 25 μL Opti-MEM.
 - (b) Dilute 0.75 μL Lipofectamine 2000 in 25 μL Opti-MEM, incubate for 10 min at RT.
 - (c) Mix 25 μL of plasmid solution with 25 μL of lipofectamin solution, incubate for 20 min at RT.
3. Wash the cells once with DMEM w/o serum and antibiotics.
4. Add 200 μL DMEM w/o serum and antibiotics per well.
5. Add 50 μL /well of plasmid/Lipofectamine 2000 solutions.
6. Incubate the cells at 37°C overnight.
7. Wash twice with 250 μL /well of 1 M NaCl in PBS. Do not allow the cells to remain in the hyper osmotic buffer for more than 30 s (see Note 12).
8. Quickly remove the 1 M NaCl buffer and gently wash once with PBS.
9. Remove the PBS and add DMEM w/o serum.
10. Incubate the cells at 37°C for 4–6 h.
11. Incubate cells with fluorescently labeled CPPs or CPP-delivered cargoes (see Note 13).
12. Prepare cells for live-cell fluorescence microscopy.

4. Notes

1. Urea in solution is in equilibrium with ammonium cyanate that can react covalently with proteins. Therefore, dissolve urea in water and prepare buffer immediately after complete dissolution. Do not heat the solution. Alternatively, a dissolved

- urea stock solution can be stored at 4°C and purified by anion-exchange chromatography prior to preparation of buffers.
2. The use of practical grade Gu-HCl requires removal of impurities by activated charcoal. Dissolve practical grade of Gu-HCl in water. Purify the solution by the addition of approximately 10 g/L of activated charcoal. Stir overnight at 4°C and clear solution by filtration two times over two layers of filter paper. Add remaining buffer constituents and adjust pH.
 3. In this chapter, HeLa cells are used throughout. The protocols are, however, intended to serve as prototypical protocols for the study of PG involvement in CPP uptake, in general. Consequently, we encourage the exchange of the specified HeLa cells for other cell lines of interest, if desired.
 4. Several methods for studying CPP uptake and CPP-mediated cargo delivery have been described (19), of which many employ fluorescent compounds; either fluorescently labeled CPPs or labeled cargoes. The uptake of these fluorescent compounds can be studied by fluorescence microscopy or by flow cytometry. Other methods study the intracellular delivery of functional cargo molecules by CPPs. In these methods, the activity of the delivered macromolecule is the final read-out, e.g., reporter-gene activity. The methods described herein are applicable to both types of assays.
 5. Keep pre-swollen 50% (v/v) DE-52 matrix slurry at 4°C. De-gas the slurry for several minutes before packing the columns. Resuspend the slurry with an automatic pipette and be careful not to introduce air-bubbles in the slurry. Pack columns by the addition of approximately two times the intended column matrix volume.
 6. In order to obtain complete enzymatic digestion in subsequent steps, it is, in our experience, very important to remove as much guanidine as possible. Resuspension of the precipitated pellet in a buffer containing 1 M NaCl competes off most guanidine counter-ions bound to PGs. Also make sure the pellet is completely dissolved in this step, as there otherwise will be substantial sample loss.
 7. As the cell-associated PG of most cell types are either HS or CS/DS substituted, the intact PG after heparinase and chondroitinase digestion is primarily CS/DS and HSPG, respectively. If the enzyme digestions are complete, the reduction in [³⁵S]-sulfate radioactivity in the high-molecular weight region after, e.g., heparinase digestion should correspond roughly to the remaining signal intensity after chondroitinase digestion. This signal represents the HSPG pool of the total cell-associated PG and vice versa for the CS/DS PG pool.

8. If additional analyses are to be performed on the purified PG, the sample can be frozen at -80°C before the addition of $4\times$ LDS-buffer which may interfere and make subsequent assays impossible.
9. Certain syndecans can, in addition to being HS substituted, also bear CS chains. In order to obtain well-defined bands at positions reflecting the size of the core protein, it is imperative that all GAG chains are degraded. Samples must, therefore, be both heparinase and chondroitinase treated.
10. HSPG core protein bands appear specifically in GAG-lyase-treated samples and are significantly fainter in nondigested lanes both when detected with core protein-specific antibodies and with anti- ΔHS antibody. In initial experiments, it is prudent to include a lane with no PG, containing only GAG lyases. This is in order to exclude the risk that bands appearing in digested lanes are the result of unspecific detection of constituents of the enzyme preparations.
11. For knock-down experiments, one sample per siRNA sequence is preferably used for the control of knock-down efficiency on the protein level, by either anti- ΔHS or core protein-specific immunoblot, as described. In addition, identically treated samples for CPP uptake assays should be prepared in a format of choice, e.g., 48-well plate or 8-well microscopy slide.
12. The 1 M NaCl wash is incorporated into the lipofection protocol to remove surface-associated lipofection reagent. The cells should be washed gently but relatively quickly to minimize cell lysis and detachment.
13. Note that CPP uptake analysis after overexpression of fluorescently tagged proteins requires the use of CPPs or cargoes labeled with fluorophores spectrally distinct from the fluorescent protein, e.g., GFP combined with Alexa Fluor 546 or similar fluorophores (19).

Acknowledgments

This book chapter is based on work supported by grants from the Swedish Cancer Fund; the Swedish Research Council; the Swedish Foundation for Strategic Research; the Swedish Society of Medicine; the Physiographic Society, Lund; the Crafoordska, Gunnar Nilsson, Lundbergs, and Kamprad Foundations; the Lund University Hospital donation funds; and the governmental funding of clinical research within the National Health Services.

References

- Poon, G. M., and Garipey, J. (2007) Cell-surface proteoglycans as molecular portals for cationic peptide and polymer entry into cells, *Biochem Soc Trans* **35**, 788–793.
- Mislick, K. A., and Baldeschwieler, J. D. (1996) Evidence for the role of proteoglycans in cation-mediated gene transfer, *Proc Natl Acad Sci U S A* **93**, 12349–12354.
- Console, S., Marty, C., Garcia-Echeverria, C., Schwendener, R., and Ballmer-Hofer, K. (2003) Antennapedia and HIV transactivator of transcription (TAT) “protein transduction domains” promote endocytosis of high molecular weight cargo upon binding to cell surface glycosaminoglycans, *J Biol Chem* **278**, 35109–35114.
- Tyagi, M., Rusnati, M., Presta, M., and Giacca, M. (2001) Internalization of HIV-1 tat requires cell surface heparan sulfate proteoglycans, *J Biol Chem* **276**, 3254–3261.
- Sandgren, S., Cheng, F., and Belting, M. (2002) Nuclear targeting of macromolecular polyanions by an HIV-Tat derived peptide. Role for cell-surface proteoglycans, *J Biol Chem* **277**, 38877–38883.
- Sandgren, S., Wittrup, A., Cheng, F., Jonsson, M., Eklund, E., Busch, S., and Belting, M. (2004) The human antimicrobial peptide LL-37 transfers extracellular DNA plasmid to the nuclear compartment of mammalian cells via lipid rafts and proteoglycan-dependent endocytosis, *J Biol Chem* **279**, 17951–17956.
- Tkachenko, E., Lutgens, E., Stan, R. V., and Simons, M. (2004) Fibroblast growth factor 2 endocytosis in endothelial cells proceed via syndecan-4-dependent activation of Rac1 and a Cdc42-dependent macropinocytic pathway, *J Cell Sci* **117**, 3189–3199.
- Yanagishita, M., and Hascall, V. C. (1984) Metabolism of proteoglycans in rat ovarian granulosa cell culture. Multiple intracellular degradative pathways and the effect of chloroquine, *J Biol Chem* **259**, 10270–10283.
- Argyris, E. G., Kulkosky, J., Meyer, M. E., Xu, Y., Mukhtar, M., Pomerantz, R. J., and Williams, K. J. (2004) The perlecan heparan sulfate proteoglycan mediates cellular uptake of HIV-1 Tat through a pathway responsible for biological activity, *Virology* **330**, 481–486.
- Nakase, I., Tadokoro, A., Kawabata, N., Takeuchi, T., Katoh, H., Hiramoto, K., Negishi, M., Nomizu, M., Sugiura, Y., and Futaki, S. (2007) Interaction of arginine-rich peptides with membrane-associated proteoglycans is crucial for induction of actin organization and macropinocytosis, *Biochemistry* **46**, 492–501.
- Wittrup, A., Zhang, S. H., Ten Dam, G. B., van Kuppevelt, T. H., Bengtson, P., Johansson, M., Welch, J., Morgelin, M., and Belting, M. (2009) ScFv antibody-induced translocation of cell-surface heparan sulfate proteoglycan to endocytic vesicles: Evidence for heparan sulfate epitope specificity and role of both syndecan and glypican, *J Biol Chem* **284**, 32959–32967.
- Landgraf, P., Wahle, P., Pape, H. C., Gundelfinger, E. D., and Kreutz, M. R. (2008) The survival-promoting peptide Y-P30 enhances binding of pleiotrophin to syndecan-2 and -3 and supports its neuritogenic activity, *J Biol Chem* **283**, 25036–25045.
- Zhang, L., Lawrence, R., Frazier, B. A., and Esko, J. D. (2006) CHO glycosylation mutants: proteoglycans, *Methods Enzymol* **416**, 205–221.
- Welch, J. E., Bengtson, P., Svensson, K., Wittrup, A., Jenniskens, G. J., Ten Dam, G. B., Van Kuppevelt, T. H., and Belting, M. (2008) Single chain fragment anti-heparan sulfate antibody targets the polyamine transport system and attenuates polyamine-dependent cell proliferation, *Int J Oncol* **32**, 749–756.
- Dennissen, M. A., Jenniskens, G. J., Pieffers, M., Versteeg, E. M., Petitou, M., Veerkamp, J. H., and van Kuppevelt, T. H. (2002) Large, tissue-regulated domain diversity of heparan sulfates demonstrated by phage display antibodies, *J Biol Chem* **277**, 10982–10986.
- David, G., Bai, X. M., Van der Schueren, B., Cassiman, J. J., and Van den Berghe, H. (1992) Developmental changes in heparan sulfate expression: in situ detection with mAbs, *J Cell Biol* **119**, 961–975.
- Belting, M., and Petersson, P. (1999) Intracellular accumulation of secreted proteoglycans inhibits cationic lipid-mediated gene transfer. Co-transfer of glycosaminoglycans to the nucleus, *J Biol Chem* **274**, 19375–19382.
- Belting, M., and Petersson, P. (1999) Protective role for proteoglycans against cationic lipid cytotoxicity allowing optimal transfection efficiency in vitro, *Biochem J* **342**(Pt 2), 281–286.
- Wittrup, A., and Belting, M. (2009) Characterizing peptide-mediated DNA internalization in human cancer cells, *Methods Mol Biol* **480**, 101–112.

20. Iozzo, R. V. (2001) *Proteoglycan Protocols*, Humana Press, Totowa, New Jersey.
21. Humphries, D. E., and Silbert, J. E. (1988) Chlorate: a reversible inhibitor of proteoglycan sulfation, *Biochem Biophys Res Commun* **154**, 365–371.
22. Inatani, M., Irie, F., Plump, A. S., Tessier-Lavigne, M., and Yamaguchi, Y. (2003) Mammalian brain morphogenesis and midline axon guidance require heparan sulfate, *Science* **302**, 1044–1046.
23. Bullock, S. L., Fletcher, J. M., Beddington, R. S., and Wilson, V. A. (1998) Renal agenesis in mice homozygous for a gene trap mutation in the gene encoding heparan sulfate 2-sulfotransferase, *Genes Dev* **12**, 1894–1906.
24. Wittrup, A., Sandgren, S., Lilja, J., Bratt, C., Gustavsson, N., Morgelin, M., and Belting, M. (2007) Identification of proteins released by mammalian cells that mediate DNA internalization through proteoglycan-dependent macropinocytosis, *J Biol Chem* **282**, 27897–27904.
25. van den Born, J., Salmivirta, K., Henttinen, T., Ostman, N., Ishimaru, T., Miyaura, S., Yoshida, K., and Salmivirta, M. (2005) Novel heparan sulfate structures revealed by monoclonal antibodies, *J Biol Chem* **280**, 20516–20523.

Uptake Kinetics of Cell-Penetrating Peptides

Anders Florén, Imre Mäger, and Ülo Langel

Abstract

As our knowledge increases about the diversity in uptake mechanisms displayed by cell-penetrating peptides (CPP), the concept of CPP uptake kinetics becomes increasingly complex. Here, we present three different assays that can be used for studying different kinetic aspects of CPP-mediated delivery: intracellular accumulation and membranolytical effects, intracellular CPP-cargo detachment, and finally a functional readout of a biological action from the delivered cargo. Unlike the traditional end-point measurements that give a static postincubation readout, these assays are all dynamic, real-time, in situ measurements obtained during incubation. A combination of some (or all) of these different assays gives us not only interesting kinetic information about the uptake routes but also provides a simple and valuable methodology for the evaluation of potential drug candidates based on the chemical modification of CPPs by cargo attachment.

Key words: CPP uptake, Kinetics, Flow cytometry, Fluorescence, Bioluminescence, Fluorescence quenching

1. Introduction

The rate of CPP uptake is an important but frequently overlooked parameter when evaluating CPP as drug vectors. The number of studies concentrating on CPP uptake kinetics has remained surprisingly low. Most of the kinetic studies have been performed with fluorescently labeled peptides (1–10), but other methods involving radioactive tagging (11) or biomarkers (12, 13) have been used, as well.

There are a plethora of various other processes competing with intracellular uptake, such as intracellular sequestering, degradation of delivered material, and exocytosis, and in static end-point measurements, these parameters are usually not addressed. For example, in an end-point assay, measuring only a fluorescent signal of a labeled CPP, a poor vector candidate that is retained in the cell

might have the same fluorescence as a very efficient delivery vector that is exocytosed with a high metabolic turnover. Hence, estimating the order of the uptake process, half-life, rate constants, and plateau values might not only prove to be a fruitful approach in shedding some additional light on CPP uptake mechanisms, but it can also give valuable comparative information on the effect of cargo attachments and chemical modifications of CPP-drug candidates.

Our current understanding of CPP uptake relies heavily upon assays utilizing fluorescent labeling, particularly on confocal laser scanning microscopy (CLSM). CLSM is a versatile tool for visualization and identification of different CPP internalization routes and is a dynamic approach as it can monitor uptake in real time on living cells (14–16). Although CLSM on live cells provides us with essential data about internalization mechanisms, the method has several limitations, such as quantification difficulties, problems with controlling the temperature, etc. A more serious matter is that CLSM usually captures only a handful of cells per image, and even a nonbias selection of cells might not give a statistically significant readout.

The lack of kinetic studies (besides CLSM) can only partly be explained by the technical limitations of the measurement equipment. Scaling up a simple end-point assay to a more complicated experimental setup with several parallel experiments and different incubation times is deterring. Here, we present three examples of simple in situ assays that give multiple readouts from the same incubation at different time points. The assays are simple and very flexible and can be modified extensively by the choice of fluorescent label, quencher, temperature, incubation media, chemical modifications, etc. They address different aspects of uptake in terms of intracellular accumulation, intracellular bioavailability, and biological action, using proximity quenched fluorescence, concentration quenched fluorescence, and luminescence. All these assays are conducted in situ during treatment and do not rely on compiling data from several incubations. Not only does this minimize sources of error, but in situ measurements also reduce the consumption of material as each sample can be used for continuous readout throughout the experiment.

1.1. Proximity Quenched Fluorescence Assay

The proximity quenched fluorescence assay is conducted in a fluorescence plate reader for measurements on cells in suspension. We have previously used a version of this assay (9), but it is suitable for a wide range of fluorophores, including UV-fluorophores that are favorable for economical and synthesis reasons. For example, we are using aminobenzoic acid (Abz) attached to a chosen cargo peptide as a fluorophore and nitrotyrosine (NO₂-Tyr) or histidine(dinitrophenyl) (His(DNP)) conjugated to a CPP as a fluorescence quencher (see Fig. 1). The assay is not hampered by background autofluorescence, as long as it is constant. A great advantage of this assay is its capacity to allow quantitative

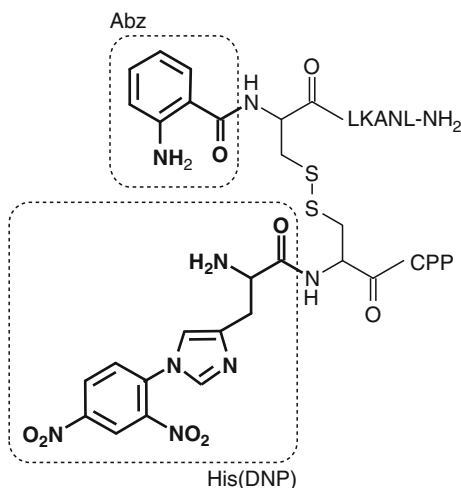


Fig. 1. The structure of cargo-SS-CPP construct used in the quenched fluorescence assay. Aminobenzoic acid (Abz) and histidine(dinitrophenyl) (His(DNP)) moieties are marked in *bold*.

measurements of the total uptake directly in the cell suspension, and since none of the material is wasted during measurement, it is possible to collect the suspension after the incubation for further use.

1.2. Quenched Time-Lapse Uptake and CPP-Induced Membranolysis Assay

This flow cytometry-based assay is suitable for measuring the uptake of carboxyfluorescein (FAM)-labeled peptides into cells in suspension, with a resolution of one sample per minute. The experiment is outlined in Fig. 2. It consists of an ongoing incubation where small samples are taken from the incubation each minute. The incubation is conducted at a controlled temperature (not necessarily 37°C), and the samples are analyzed during incubation. Before analysis, the samples are transferred to FACS tubes containing trypan blue (TB) for analyzing intracellular accumulation, and/or propidium iodide (PI) for analysis of membrane integrity (optionally). TB is a quencher that is confined to the outside of living cells and effectively eliminates FAM-fluorescence by concentration quenching (17, 18). The remaining fluorescence arises from the intracellular-located FAM-CPP that is inaccessible to TB. The secondary (optional) readout is CPP-induced membranolysis, monitored as propidium iodide (PI) accumulation into dead cells. An interesting feature of the secondary assay is that the membranolytic effects can be studied for any molecule; it does not have to be a fluorescently labeled peptide. As compared to CLSM, the quenched readout is based on thousands of cells instead of a handful, and with proper statistical analysis, even minute increases in fluorescence can be detected. Also, flow cytometry gives information as to whether the uptake is uniformly distributed or if some subpopulations are more or less prone to internalize CPP. The drawback of this assay is

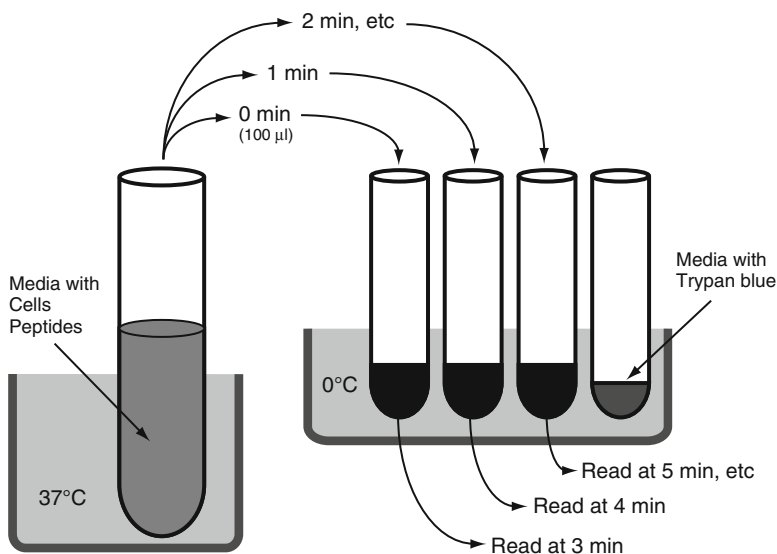


Fig. 2. Time-lapse measurement of CPP uptake using trypan blue to quench the extracellular fluorescence. Optionally, the sample tubes can be supplemented with propidium iodide for monitoring membrane integrity. More detailed explanation is given in the text.

the inability to quantitatively measure the amount of the accumulated material.

1.3. Bioluminescence Assay

In this assay, luciferin is coupled via a cleavable linker to CPPs (12), and the conjugate is delivered into cells which overexpress luciferase enzyme. When reaching the cytoplasm, the linker is cleaved by glutathione, and the released luciferin is converted into its oxidized form by the luciferase enzyme, emitting a photon of light. The luminescence can be read by a luminometer in real time, and the accumulated total uptake at each different time point can be calculated by integrating the acquired luminescence data. An advantage of this assay is that the experiment can be carried out on adherent cells without the need for having the cells in suspension. Also, in this system, the readout monitors a produced biological effect rather than relying on a marker molecule that can detach or be degraded. Any cell line that is stably expressing luciferase, or transiently transfected with a luciferase gene, can be used to characterize the delivery.

2. Materials

General materials:

1. Cell lines and cell culture media required for the corresponding cell line.
2. 10-cm cell culturing plates.

3. Buffers: HEPES-buffered Krebs–Ringer solution (HKR) supplemented with glucose (1 mg/ml), phosphate-buffered saline (PBS).
4. 3 mM ethylenediaminetetraacetic acid (EDTA) dissolved in PBS.

2.1. Quenched Fluorescence Assay

1. Abz-Cys-cargo and His(DNP)-Cys-CPP or Cys-NO₂-Tyr-CPP, conjugated via a disulfide bond (see Fig. 1).
2. Fluorescence plate reader with 320 nm excitation filter and 420 nm emission filter.
3. 0.5 M Tris(2-carboxyethyl)phosphine (TCEP) or dinitrophenol (DTT).

2.2. Quenched Time-Lapse Uptake and CPP-Induced Membranolysis Assay

1. CPP labeled with FAM, diluted in 100 μM stock solutions.
2. Propidium iodide (PI), final concentration 10 μg/ml (15 nM) dissolved in PBS (see Note 1).
3. Trypan blue (TB), 10 mg/ml, dissolved in H₂O (see Note 1).
4. A thermoblock or water bath fixed at 37°C, and a container with ice.
5. Standard 5-ml flow-cytometry tubes and tube racks.
6. A timer.

2.3. Bioluminescence Assay

1. Luciferin-linker-CPP in 100 μM stock solution and free luciferin for control experiments.
2. Cells transfected with luciferase-encoding plasmid, or cells that are stably expressing luciferase.
3. White 96-well plates with transparent bottom and a white base-plate for the 96-well plate to increase signal-to-noise ratio (see Fig. 3).

3. Methods

General methods:

1. Propagate the cells (e.g., HeLa cells, see Note 2) in standard conditions at 37°C and 5% CO₂ concentration in standard cell culture dishes.
2. To render the extracellular matrix intact, instead of trypsinizing the cells, we chose to harvest the cells with 3 mM EDTA (see Note 3).
3. All three assays can be conducted in any desired reaction media (media with or without serum, PBS, HKRg, etc.).

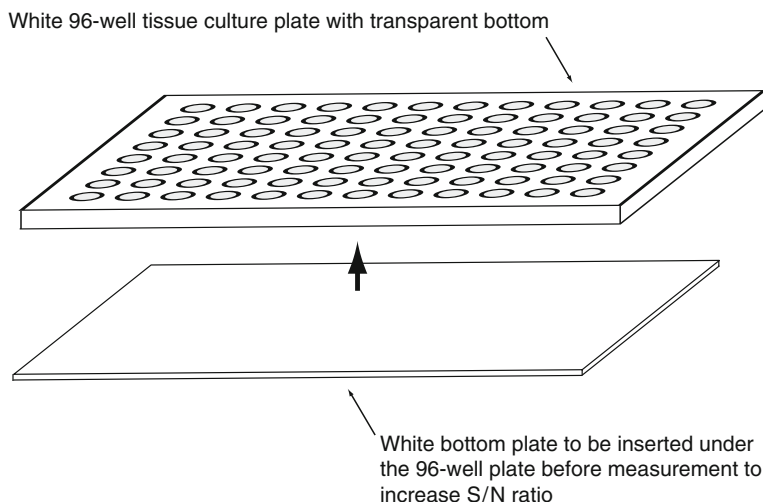


Fig. 3. A white 96-well tissue culture plate with transparent bottom allows verification of the cell culture confluence. Before reading the luminescence, insert a white bottom plate under the 96-well plate to increase the signal-to-noise ratio. The white bottom plate can be custom-made out of white plastic or cardboard.

3.1. Quenched Fluorescence Assay

1. For HeLa cells, seed the cells 2 days prior to the experiment into a 10-cm cell culture dish to reach 90% confluency on the day of the experiment.
2. On the day of the experiment, wash cells with 5 ml PBS and detach the cells by incubating the dish with 1 ml of 3 mM EDTA at 37°C. Add 4 ml of full cell culture media and centrifuge the cells at $500 \times g$ for 10 min; remove the supernatant and resuspend the cells in 1 ml HKRg. Count the cells and dilute them with HKRg to obtain 2.5×10^6 cells/ml (1.25×10^5 cells in 50 μ l buffer/well) (see Note 4).
3. If endocytosis inhibitors are to be used in the experiment, pretreat the cells for 30 min in presence of an inhibitor before adding the cells to the peptide solution (see Note 5).
4. Prepare a white 96-well plate for the experiment. While keeping the plate on ice, add 150 μ l of the cargo-SS-CPP conjugates diluted in HKRg to each well. Remember to include blank samples and positive controls (i.e., unquenched peptide).
5. Set the fluorescence plate reader at 37°C while keeping the plate on ice.
6. After 30 min, add 1.25×10^5 cells in 50 μ l to each well, to reach the final incubation volume of 200 μ l (see Note 6).
7. Immediately, insert the plate into the preheated fluorescence reader and measure the fluorescence (320 nm/420 nm). Make sure to include the blank samples in the recording, to verify that the background autofluorescence is stable. Take readouts at regular intervals (e.g., every 30 s) and be sure to shake the 96-well plate between measurements to keep the cells in suspension.

8. At the end point (e.g., after 60 min), add TCEP or DTT to each well. Be sure to reach a sufficiently high final concentration, e.g., 100 μM , to reduce all remaining disulfide bonds. Use the resulting signal to determine the 100% signal level and normalize the data to this value after subtracting the background from the initial signal. Alternatively, it is also possible to present the data by a simple calculation as picomoles of internalized peptide in the whole cell population.

3.2. Quenched Time-Lapse Uptake and CPP-Induced Membranolysis Assay

The experiment is outlined in Fig. 2. It consists of an ongoing incubation in any desired reaction media (media with or without serum, PBS, etc.), where samples are taken out at fixed time points. Plan your experiment carefully; new samples have to be taken out while simultaneously analyzing the previous samples, and ensure that there is no room for errors when the incubation commences. We suggest you make a practice run with longer time intervals. Samples for both uptake and membranolysis can be taken from the same incubation, but both sets of data cannot be acquired at the same time (see Note 7). The samples are quenched with TB on ice for exactly 3 min followed by immediate data acquisition. Before running the assay, the quenching procedure has to be validated (see Note 8). For each new set of experiments, use control samples (blank FAM positive and PI positive) to determine compensation parameters necessary to eliminate the spectral overlap of the used fluorophores (i.e., FAM and PI).

1. Seed the cells 2 days before the experiment as described above (Subheading 3.1, step 1).
2. Detach the cells using 3 mM EDTA and centrifuge as described above (Subheading 3.1, step 2). Resuspend the cells in 1 ml of the desired reaction media (media with or without serum, PBS, HKRg, etc.) and keep the cells on ice.
3. Take 50 μl of the cell suspension and dilute it into 950 μl of PBS in a sample tube (this will be your blank sample). Run it in the flow cytometer, with the laser set at 488 nm. Record the fluorescence in appropriate channels (for example, FAM at 519/20, PI at 650/LP) and compensate for spectral overlaps. Gate the living population based on the forward/side scattering properties.
4. Use the flow cytometer to calculate the amount of cells in the suspension (see Note 9). Dilute the original cell suspension such that 50 μl yields 200 cells/s when running the blank sample (see Note 10). Remove the tube, add 10 μl of 0.1 mM FAM-labeled peptide, and run the tube again as a FAM-positive control.
5. At each time point, a 100- μl sample will be removed from the incubation. For example, for a 0–9 min monitoring of a 1 μM

CPP incubation on suspended HeLa cells, prepare a 1 ml incubation of 100 μ l from the cell suspension and 890 μ l of reaction media (double these amounts if you want the optional PI samples). Do *NOT* add the FAM-labeled CPP at this stage! Transfer the incubation tube to 37°C and allow it to acclimatize for 1 min.

6. Prepare an array of sample tubes (i.e., one for each time point) and label them (0 min, 1 min, etc.). Pipette 40 μ l of 10 μ g/ml TB and add 260 μ l of reaction media into each tube, and keep the tubes on ice. (Optionally, prepare another array of sample tubes containing 300 μ l reaction media supplemented with 1 μ g/ml (1.5 nM) PI. These samples will be analyzed after the TB-assay.)
7. Start the incubation by adding 10 μ l of 100 μ M CPP solution (20 μ l if PI samples are included) and start the timer. Immediately, remove the first 100 μ l sample from the incubation and put it into the first sample tube (0 min) on ice (optionally also the first sample in the PI array).
8. At 1 min, remove the second 100- μ l sample and transfer it to the second sample tube (labeled 1 min) and leave it on ice. This 100 μ l removal step will be repeated every minute.
9. After 3 min, it is time to start acquiring data from the first ice-incubated TB sample (0 min). Directly after pipetting the 3 min sample, remove the 0 min tube from the ice, load it to into the flow cytometer, and acquire your data. Allow the acquisition to continue until you change tube in the next cycle. Meanwhile, prepare to take out the next sample (4 min).
10. At 4 min, repeat as above and transfer a 100 μ l to the 4 min sample tube. After that, stop the acquisition and change to the next ice-incubated sample tube (1 min) and start to acquire the next file (see Note 11).
11. At 5 min, transfer a 100 μ l to the 5 min sample tube. After that, stop the acquisition and change to the next ice-incubated sample tube (2 min) and start to acquire the next file etc.
12. The experiment will continue like this in 1 min cycles. Work methodically and do not rush; try to complete each step in the same pace. After the last sample is analyzed, rinse the flow cytometer with PBS and analyze the optional PI samples for membrane integrity (see Note 12). Apply extended washing procedures recommended by your supplier.

3.3. Bioluminescence Assay

1. Transfect cells with a luciferase-encoding plasmid (see Note 13) or use a cell line stably expressing luciferase.

- 24 h posttransfection, seed the required number of cells (for HeLa cells, 9,000 cells/well in 100 μ l) onto a white clear bottom 96-well tissue culture plate (see Note 14).
- After another 24 h, prepare the luciferin-linker-CPP solutions in full cell culture media at the desired concentrations. Remove the old growth media from the plate and pipette 150 μ l of the peptide solution into each well. For control experiments, use free luciferin at the same concentration as the luciferin-linker-CPP constructs (see Note 15).
- Measure the luminescence at regular time intervals for at least 1.5 h. As an example, HeLa cells were incubated with 2.5 μ M luciferin-linker-M918 conjugate (see Fig. 4a) for 2 h. The readout was registered in 2 min intervals, and the results are presented as fold increase in luminescence (RLU) compared to untreated cells (see Fig. 4b and Note 16).
- The total uptake at any selected time point can be obtained by integrating the uptake curve presented in Fig. 4b (i.e., by calculating area under curve (AUC) at the selected time point).

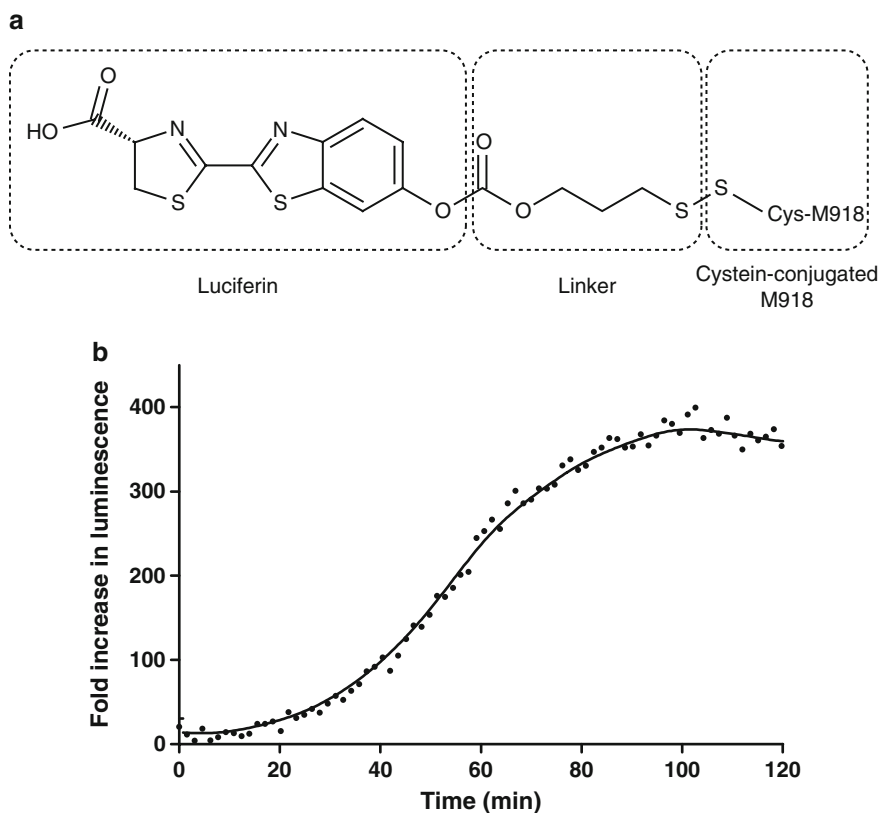


Fig. 4. Example of results from the bioluminescence assay. HeLa cells were incubated with 2.5 μ M Luciferin-linker-M918 conjugate (a). The luminescence was recorded over a period of 2 h; the data is presented as fold increase of luminescence (RLU) compared to the luminescence from untreated cells (b).

4. Notes

1. TB and PI are carcinogenic agents. Check the material safety data sheet and wear proper protective equipment. Dissolve TB in a minimal amount of DMSO (3 $\mu\text{l}/\text{mg}$) and add H_2O to obtain a 10 mg/ml stock solution. Do not store the TB solution in the fridge, as it is prone to precipitate.
2. Any cell line can be used in these assays, including cells growing in suspension. In the examples given in the text regarding seeding and cell counts, all figures refer to standard HeLa cells.
3. In a previous study (9), Bowes human melanoma cells were harvested by scraping. This should be avoided for HeLa and CHO cells, as a large fraction does not survive this treatment. However, it can be used to obtain a PI-positive control, as the harvested cells lose their membrane integrity.
4. When resuspending the cells, take care to obtain the same number of cells per ml in each experiment, as this might affect the measurement results. Count the cells after resuspension.
5. There is a plethora of endocytosis inhibitors that cannot be covered extensively in this chapter; the 30 min incubation might not apply to all inhibitors. Note that chloroquine cannot be used due to its fluorescence in this wavelength range.
6. The pipetting should be done on ice and quickly, preferably with 8-channel pipette since the uptake may be fast even during the first seconds.
7. TB is weakly fluorescent in the PI spectra, and traces of TB will interfere with the PI fluorescence unless it is thoroughly washed away. Use extended washing procedures recommended by your supplier. This is especially important if your cytometer is equipped with a UV-laser, as TB is fluorescent at lower wavelengths.
8. For validation of quenching: Perform a standard uptake on adherent cells using your FAM-labeled CPP on the cell line you will use in your experiment; include a blank sample as a negative control. Wash thoroughly with PBS and harvest the cells with EDTA (see Subheading 3.1, step 2). Prepare three tubes each with positive and negative controls with the same amount of cells as described in Subheading 3.2, step 3. First, run a negative and a positive control to establish a baseline and a positive signal. Then, add the same concentration as used above for your FAM-labeled peptide to the four remaining control tubes and incubate them at room temperature for 30 s. Add the quencher to one positive and one negative sample and incubate all four on ice for 3 min. Now, run the

- unquenched positive and negative controls, both samples should be substantially higher than the previous controls as the CPP associates with the outer cell membrane. Finally, run the quenched positive and negative controls. The quenched positive control should be similar or only slightly higher than the original positive control; the quenched negative should correspondingly be the same or very close to the original negative control.
9. Total number of cells = $20 \times \text{cells per second} \times \text{acquisition time} / \text{flow}$.
 10. This amount depends on the sheath flow and varies between different instruments. The amount of cells should be adjusted so that you are able to record data from at least 2,000 cells during 20 s from the sample tubes, and this should be a fixed amount if you want to compare runs from several experiments.
 11. Most software for flow cytometers has an autosequencing function for run files. We suggest you use it, as there will be no time for typing the file names.
 12. The membranolytic effect should be calculated as the percentage of *all the cells* that are PI positive, not just the gated living population.
 13. The transfection protocol is too lengthy to be included and is beyond the scope of this paper. There are several methods of transfection; we have used Lipofectamine 2000 (Invitrogen) as a transfection agent according to the manufacturer's instructions with successful results.
 14. Use a white plate under the clear-bottomed 96-well plate during the measurement to increase signal-to-noise ratio and sensitivity (see Fig. 3). This bottom plate can be custom-made out of white plastic or cardboard.
 15. For pipetting, use an 8-channel pipette to save time. The uptake is remarkably fast even during the first minutes of the incubation, especially for free luciferin since it is membrane-permeable.
 16. Data normalization may be required as the number of cells and transfection efficacy sometimes fluctuate on a day-to-day basis. Uptake data of free luciferin or untreated cells should always be included for normalization at every experiment.

Acknowledgments

The work presented in this article was supported by: the Swedish Research Council (VR-NT); the Center for Biomembrane Research, Stockholm; the Knut and Alice Wallenberg's

Foundation; the EU through the European Regional Development Fund through the Center of Excellence in Chemical Biology, Estonia; the targeted financing SF0180027s08 from the Estonian Government; the DoRa Program of The European Social Fund; and the Archimedes Foundation.

References

- Polyakov V., Sharma V., Dahlheimer J. L., Pica C. M., Luker G. D., Piwnica-Worms D. (2000) Novel Tat-peptide chelates for direct transduction of technetium-99m and rhenium into human cells for imaging and radiotherapy. *Bioconjug Chem* **11**, 762–71.
- Drin G., Mazel M., Clair P., Mathieu D., Kaczorek M., Tamsamani J. (2001) Physicochemical requirements for cellular uptake of pAntp peptide. Role of lipid-binding affinity. *Eur J Biochem* **268**, 1304–14.
- Drin G., Cottin S., Blanc E., Rees A., Tamsamani J. (2003) Studies on the internalization mechanism of cationic cell-penetrating peptides. *J Biol Chem* **278**, 31192–201.
- Suzuki T., Futaki S., Niwa M., Tanaka S., Ueda K., Sugiura Y. (2002) Possible existence of common internalization mechanisms among arginine-rich peptides. *J Biol Chem* **277**, 2437–43.
- Richard J., Melikov K., Vives E., et al. (2003) Cell-penetrating peptides. A reevaluation of the mechanism of cellular uptake. *J Biol Chem* **278**, 585–90.
- Jones S., Christison R., Bundell K., et al. (2005) Characterisation of cell-penetrating peptide-mediated peptide delivery. *Br J Pharmacol* **145**, 1093–102.
- Li X., Higashikubo R., Taylor J. (2008) Use of multiple carboxylates to increase intracellular retention of fluorescent probes following release from cell penetrating fluorogenic conjugates. *Bioconjug Chem* **19**, 50–6.
- Tünnemann G., Ter-Avetisyan G., Martin R., Stöckl M., Herrmann A., Cardoso M. (2008) Live-cell analysis of cell penetration ability and toxicity of oligo-arginines. *J Pept Sci* **14**, 469–76.
- Hällbrink M., Florén A., Elmquist A., Pooga M., Bartfai T., Langel Ü. (2001) Cargo delivery kinetics of cell-penetrating peptides. *Biochim Biophys Acta* **1515**, 101–9.
- Cheung J. C., Kim Chiaw P., Deber C. M., Bear C. E. (2009) A novel method for monitoring the cytosolic delivery of peptide cargo. *J Control Release* **137**, 2–7.
- Pooga M., Hällbrink M., Zorko M., Langel Ü. (1998) Cell penetration by transportan. *FASEB J* **12**, 67–77.
- Jones L. R., Goun E. A., Shinde R., Rothbard J. B., Contag C. H., Wender P. A. (2006) Releasable luciferin-transporter conjugates: tools for the real-time analysis of cellular uptake and release. *J Am Chem Soc* **128**, 6526–7.
- Wender P. A., Goun E. A., Jones L. R., et al. (2007) Real-time analysis of uptake and bioactivatable cleavage of luciferin-transporter conjugates in transgenic reporter mice. *Proc Natl Acad Sci U S A* **104**, 10340–5.
- Watkins C. L., Schmaljohann D., Futaki S., Jones A. T. (2009) Low concentration thresholds of plasma membranes for rapid energy-independent translocation of a cell penetrating peptide. *Biochem J* **420**, 179–89.
- Duchardt F., Fotin-Mleczek M., Schwarz H., Fischer R., Brock R. (2007) A comprehensive model for the cellular uptake of cationic cell-penetrating peptides. *Traffic* **8**, 848–66.
- Kosuge M., Takeuchi T., Nakase I., Jones A. T., Futaki S. (2008) Cellular internalization and distribution of arginine-rich peptides as a function of extracellular peptide concentration, serum, and plasma membrane associated proteoglycans. *Bioconjug Chem* **19**, 656–64.
- Manceur A., Wu A., Audet J. (2007) Flow cytometric screening of cell-penetrating peptides for their uptake into embryonic and adult stem cells. *Anal Biochem* **364**, 51–9.
- Busetto S., Trevisan E., Patriarca P., Menegazzi R. (2004) A single-step, sensitive flow cytometric assay for the simultaneous assessment of membrane-bound and ingested *Candida albicans* in phagocytosing neutrophils. *Cytometry A* **58**, 201–6.

Thermodynamics of Lipid Interactions with Cell-Penetrating Peptides

Reto Sauder, Joachim Seelig, and André Ziegler

Abstract

Cationic peptides are efficiently taken up by biological cells through different pathways, which can be exploited for delivery of intracellular drugs. For example, their endocytosis is known since 1967, and this typically produces entrapment of the peptides in endocytotic vesicles. The resulting peptide (and cargo) degradation in lysosomes is of little therapeutic interest. Beside endocytosis (and various subtypes thereof), cationic cell-penetrating peptides (CPPs) may also gain access to cytosol and nucleus of living cells. This process is known since 1988, but it is poorly understood whether the cytosolic CPP appearance requires an active cellular machinery with membrane proteins and signaling molecules, or whether this translocation occurs by passive diffusion and thus can be mimicked with model membranes devoid of proteins or glycans. In the present chapter, protocols are presented that allow for testing the membrane binding and disturbance of CPPs on model membranes with special focus on particular CPP properties. Protocols include vesicle preparation, lipid quantification, and analysis of membrane leakage, lipid polymorphism (^{31}P NMR), and membrane binding (isothermal titration calorimetry). Using these protocols, a major difference among CPPs is observed: At low micromolar concentration, nonamphipathic CPPs, such as nona-arginine (WR_9) and penetratin, have only a poor affinity for model membranes with a lipid composition typical of eukaryotic membranes. No membrane leakage is induced by these compounds at low micromolar concentration. In contrast, their amphipathic derivatives, such as acylated WR_9 (C_{14} , C_{16} , C_{18}) or amphipathic penetratin mutant p2AL (Drin et al., *Biochemistry* 40:1824–1834, 2001), bind and disturb lipid model membranes already at low micromolar peptide concentration. This suggests that the mechanism for cytosolic CPP delivery (and potential toxicity) differs among CPPs despite their common name.

Key words: Cell membrane, Drug delivery, Liposomes, Membrane anchor, Protein transport

1. Introduction

Past (1, 2) and current research studies (3–5) have shown that eukaryotic cells take up polycationic compounds, such as cell-penetrating peptides (CPPs) or other cationic homopolymers (e.g., polyethylenimine (6) or DEAE-dextran (7)), at (sub

micromolar concentration by binding them to anionic cell-surface glycans and subsequent endocytosis. Entrapment of CPPs in endocytotic vesicles is of moderate biomedical interest because a CPP-attached cargo (e.g., plasmid DNA, siRNA) would be rapidly degraded when passing from endocytotic vesicles to late endosomes or lysosomes. This way, no or only few cargo molecules would reach their intracellular target, e.g., the nucleus for gene expression.

In this respect, the work of Frankel (8) and Green (9) on the CPP HIV-1 Tat received much attention because the effect of extracellularly added Tat on cellular gene expression suggested that many more Tat molecules reached the nucleus than could be provided by endocytosis. The delivery of CPPs into cytosol and nucleus thus became a focus of high biomedical interest, and the work of Frankel and Green initiated a revival of research on cationic peptides, 20 years after the first studies on polylysine had been published (2).

Subsequent studies with fluorescently labeled CPPs confirmed that various CPPs could indeed enter the cytosol and reach the nucleus of biological cells (10–21). The translocation of CPPs into the cytosol was also observed in cells that were incompetent for endocytosis (e.g., bacteria) (22–24). Both observations were surprising because this meant that some CPPs may overcome the cytoplasmic and/or endosome membrane in spite of their polycationic character that argues against a rapid passive diffusion across lipid bilayers (25). These experimental observations led to rather controversial views on the apparently “magic” (26) uptake into cytosol and cell nucleus.

Some of the observations could have been biased by experimental artifacts: Surface-bound CPP molecules, for example, may enter cells postmortem because the cell treatment with methanol, ethanol, or paraformaldehyde typically used for cell fixation in microscopy can disrupt the membrane (27). This criticism does not apply to studies on living or unfixated cells (10–21). A detailed comparison of the conditions required for this cytosolic CPP entry suggests, however, that the cytosolic delivery of CPPs likely proceeds by more than one mechanism (28).

Some amphipathic CPPs have detergent-like properties. They have a high affinity for charged and uncharged lipids; they partition into the hydrophobic membrane core and disturb model membranes already at low micromolar concentrations – in analogy to many amphipathic antibiotic peptides (29, 30). These amphipathic CPPs translocate almost equally across pure lipid membranes (devoid of membrane proteins or glycans) or the plasma membrane of living cells (31). Molecular pathways of cell entry include, for example, pore and carpet formation – as can be demonstrated in model membranes (32, 33). In some cases, CPPs may also leak out of endosomes (“endosomolytic” or fusogenic peptides) as a result

of their pH-dependent structural change and lipid interaction (11, 34, 35). As a drawback for their intrinsic membrane disturbing property, amphipathic CPPs typically have a higher cell toxicity than nonamphipathic CPPs (36, 37) which might render biomedical applications problematic which is also known from lipid-based transfection reagents.

In contrast, nonamphipathic CPPs, such as homopolymers of arginine, are less toxic (36), but they bind lipid membranes only with poor affinity, since the fraction of anionic lipids encountered in mammalian cells is usually quite low. Also, partitioning into the hydrophobic bilayer core is lacking (38–40). They do not induce membrane leakage at low micromolar concentrations even though they enter the cytosol of living cells at this concentration. This suggests that not the lipids, but other cellular compounds are required for their translocation into the cytosol (28). Their membrane permeation on *model* membranes (devoid of proteins or glycans) has been observed only for special conditions, e.g., high micromolar concentrations (electroporation-like), unphysiological counterions (41, 42), electrochemical gradients (43), repeated lipid phase-cycling (44), or delicate vesicles (45, 46).

The present chapter describes protocols that allow for quantification and comparison of membrane interactions and perturbations of CPPs. Using selected CPPs, it is shown that amphipathic CPPs destabilize model membranes already at low micromolar CPP concentration – in contrast to nonamphipathic CPPs. The distinction of both CPP classes resides on the strategy of making CPPs more amphipathic either by linking a membrane anchor to them (“acylation”) (47) or by a previous report on an amphipathic penetratin mutant (“p2AL”) designed from helical wheel projections (48). Each protocol consists of an initial descriptive on required parameters and related literature, followed by the protocol itself. Conclusions from example data (see Figs. 1–3) are described in Subheading 4.

2. Materials

2.1. Chemicals

1. Ammonium molybdate, $(\text{NH}_4)_6\text{Mo}_7\text{O}_{24} \cdot 4 \text{H}_2\text{O}$ (Merck).
2. ANTS, 8-aminonaphthalene-1,3,6-trisulfonic acid, disodium salt (Molecular Probes).
3. Buffer for leakage experiments: 20 mM Tris, 134 mM NaCl, pH 8.5.
4. Buffer for ITC experiments: 20 mM Tris, 100 mM NaCl, pH 7.4.
5. Calcein (Sigma-Aldrich).
6. Contrad 90 (Socochim).

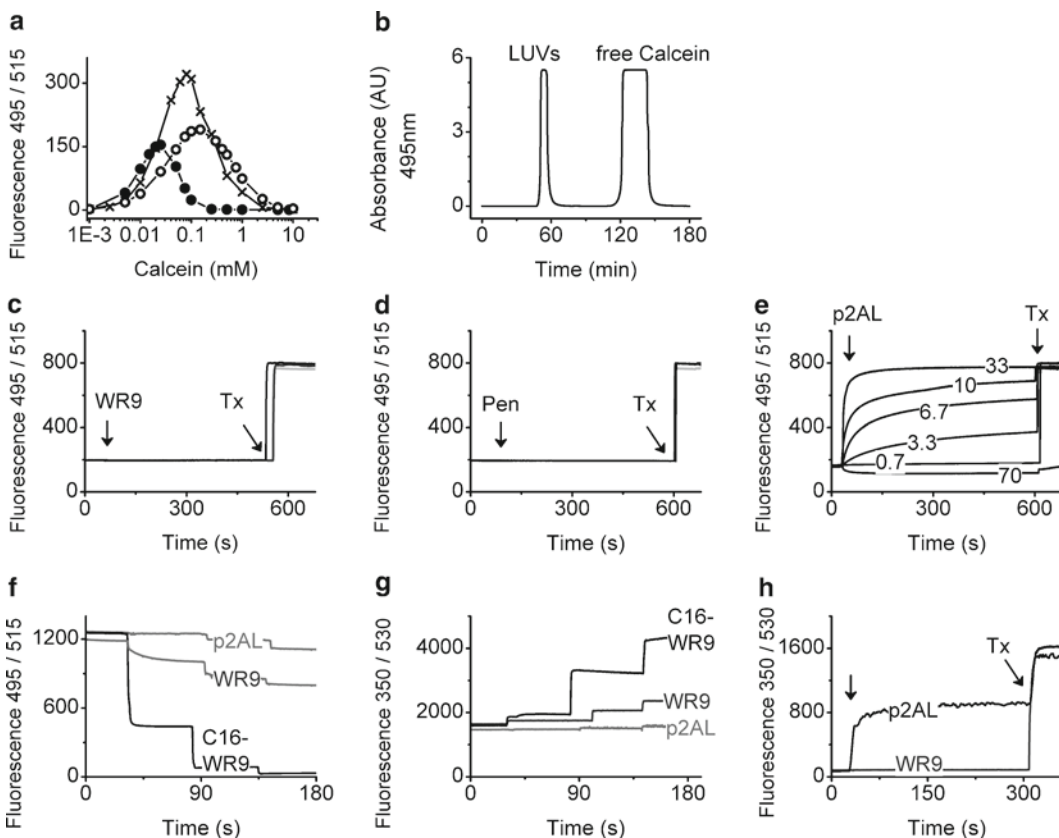


Fig. 1. Membrane leakage assay. **(a)** Because of the high optical absorbance of calcein, the observed maximum fluorescence at given concentration depends not only on quenching but also on cuvette dimensions (i.e., inner-filter effect) as shown for a (filled circle) 10-mm, (times symbol) 5-mm, and (open circle) 2-mm cuvette using same photomultiplier and bandwidth settings for the cuvettes. Small path lengths are thus preferred, especially when working with vesicles that stray light. **(b)** Separation of calcein-loaded LUVs from free calcein on a Sepharose CL-6B column (absorbance detection at 495 nm; 1.6 × 23 cm column, flow rate 0.3 mL/min). **(c)** Leakage assay for nonamphipathic WR₉: under permanent stirring, 100 μ L of 10 μ M (black), 100 μ M (gray) and 1,000 μ M (light gray) WR₉ are added (at 60 s) to 1.4 mL of LUVs (total lipid = 0.45 mM, molar ratio POPC/POPE/POPG/DOPE-PEG = 32/32/31/5; 13 mM calcein). Final peptide concentration is 0.7, 6.7, and 67 μ M, respectively. At 600 s, 100 μ L of 5% Triton X-100 is added to release the entire vesicle content. **(d)** Same leakage assay, but using nonamphipathic penetratin. **(e)** Same leakage assay, but using amphipathic penetratin mutant p2AL. Indicated are final peptide concentrations (μ M). The low fluorescence at highest p2AL concentration (70 μ M) suggests interaction of anionic calcein with cationic CPPs. **(f)** Titration of 1.4 mL of 10 μ M calcein with a 1 mM solution of three different CPPs. 10, 40, and 50 μ L of the CPP are added at 40, 80, and 150 s, respectively, indicating the interaction of anionic dye with cationic CPPs. **(g)** Same titration, but using 100 μ M ANTS. In contrast to **(f)**, the dye-peptide interaction produces a signal *increase*, which is favorable for improved sensitivity of the leakage assay. **(h)** Leakage assay using 12.5 mM of the dye ANTS (and 45 mM of its quencher DPX) inside the vesicles. Despite the improved sensitivity of this assay, no membrane leakage with nonamphipathic WR₉ is observed. Buffer allover: 20 mM Tris, 134 mM NaCl, pH 8.5.

7. DOPE, 1,2-dioleoyl-sn-glycero-3-phosphoethanolamine (Avanti Polar Lipids).

8. DOPE-PEG2000, 1,2-dioleoyl-sn-glycero-3-phosphoethanolamine-*N*-(methoxy(polyethylene glycol)-2000), ammonium salt (Avanti Polar Lipids).

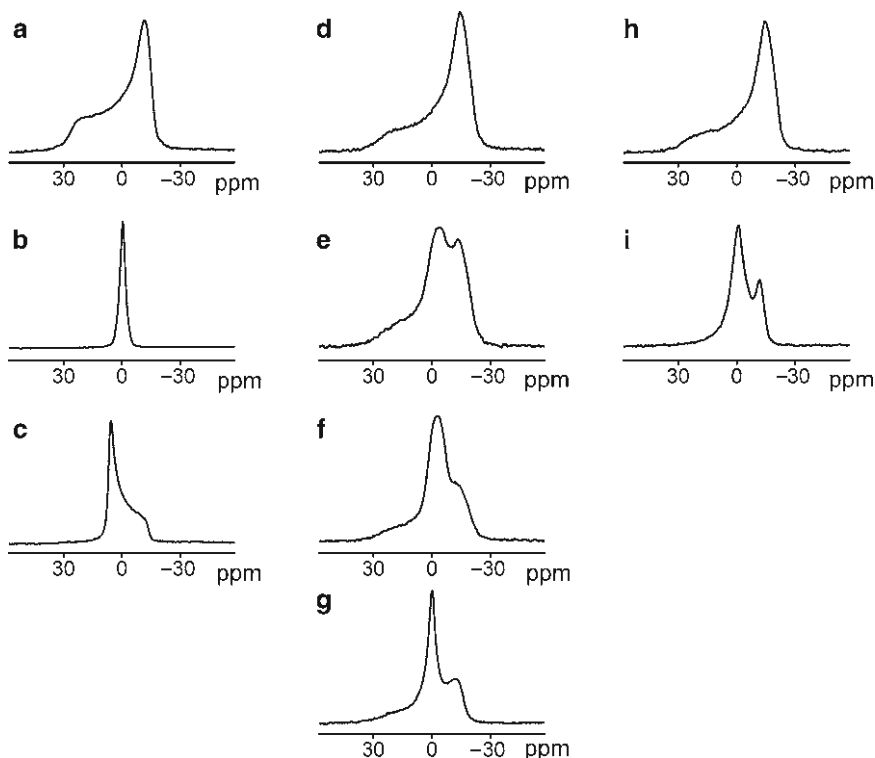


Fig. 2. Polymorphic phase behavior of phospholipids as studied by ^{31}P NMR spectroscopy. *Left column:* (a) intact bilayer of POPC/POPG (=3/1) prepared as MLVs; (b) same bilayer solubilized by Triton; (c) hexagonal phase (DOPE), occasionally termed “inverted micelles” in the CPP field (61). *Middle column:* same bilayer as (a) but prepared in the presence of different CPPs (at 4 mM): (d) nonamphipathic WR_9 , (e) amphiphilic analog $\text{C}_{14}\text{-WR}_9$, (f) $\text{C}_{16}\text{-WR}_9$, and (g) $\text{C}_{18}\text{-WR}_9$. *Right column:* same bilayer as (a), but prepared in the presence of (h) nonamphipathic Antp or its (i) amphiphilic analog p2AL. Spectra were recorded at 25°C and are referenced to external H_3PO_4 85% at 0 ppm. Typically, 5 mg of total lipid, 130 μL of H_2O , and 1.4 mg of peptide were used.

9. Malachite green oxalate (Merck).
10. DPX, *p*-xylene-bis-pyridinium bromide (Molecular Probes).
11. Perchloric acid 70% (Merck).
12. Phosphoric acid 85% (Sigma-Aldrich).
13. POPC, 1-palmitoyl-2-oleoyl-sn-glycero-3-phosphocholine (Avanti Polar Lipids).
14. POPE, 1-palmitoyl-2-oleoyl-sn-glycero-3-phosphoethanolamine (Avanti Polar Lipids).
15. POPG, 1-palmitoyl-2-oleoyl-sn-glycero-3-phospho-(1'-sn-glycerol), sodium salt (Avanti Polar Lipids).
16. Potassium phosphate monobasic, KH_2PO_4 (Sigma-Aldrich).
17. Sepharose CL-6B (Sigma-Aldrich).
18. Tris, Tris(hydroxymethyl)aminomethane (Merck).
19. Triton X-100 (BioChemika).

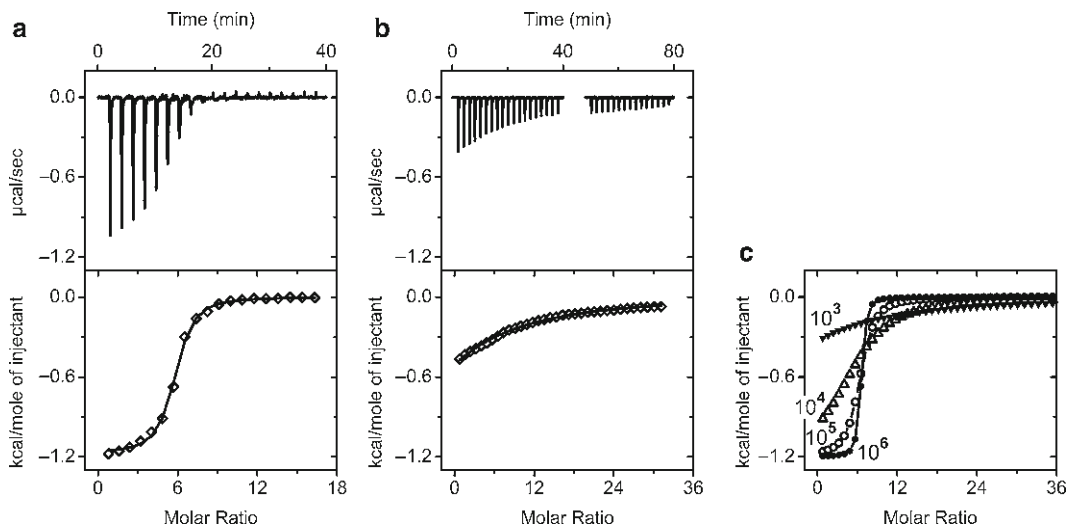


Fig. 3. Isothermal titration calorimetry (ITC). The reaction cell was filled with 204 μL of 60 μM WR_9 . Every 2 min, 2 μL of lipid vesicles (SUVs) composed of neutral POPC and anionic POPG were added (25°C). The concentration of POPG was held constant (8 mM), but POPC was varied in different experiments, so the charge density of the membrane varied as follows: (a) POPG/POPC = 1/1 (typical for bacterial inner membrane), (b) POPG/POPC = 1/9 (typical for eukaryotic cell membrane). The heat release (raw data, *upper panel*) during each injection was integrated to yield the experimental heats of reaction (*diamond*; *lower panel*). The *line* in the *lower panel* represents best fit to the experimental data using a multisite binding model (28), where (a) $K = 1.91 \times 10^5$, $n = 5.51$ POPG/ WR_9 , $\Delta H = -1.18$ kcal/mol POPG_{out}; (b) $K = 1.08 \times 10^3$, $n = 6.12$ POPG/ WR_9 , $\Delta H = -1.69$ kcal/mol POPG_{out}. Because of the low degree of binding in (b), the empty syringe was refilled after the 19th injection (i.e., at 40 min). After refilling, the injection series was continued which is feasible within 10 min using latest ITC technology. Precise determination of even lower binding constants would require much higher peptide and lipid concentrations; however, total lipid concentration is already at a high limit (80 mM in (b)) for obtaining unilamellar vesicles and low polydispersity. (c) Experimental simulations of the binding isotherm according to the multisite binding model using various K (10^6 , 10^5 , 10^4 , and 10^3 , as indicated) and similar conditions as in (a) and (b), i.e., 204 μL of 60 μM WR_9 , 36×2 - μL injections of 8 mM POPG (which is 4.8 mM POPG on outer leaflet of SUVs), fixed $n = 6.0$ POPG_{out}/ WR_9 , and $\Delta H = -1.2$ kcal/mol POPG_{out}.

2.2. Instruments

1. Fluorescence spectrophotometer F-4500 (Hitachi; Tokyo, Japan).
2. Isothermal titration calorimetry (ITC): itc200 (Microcal/GE Healthcare; Northampton, USA) having a reaction cell volume of 203.7 μL and a syringe volume of 38.45 μL .
3. NMR measurements: DRX-400 (Bruker; Karlsruhe, Germany), operating at a resonance frequency of 400 MHz for ^1H and 162 MHz for ^{31}P .
4. UV-visible spectrophotometer 8453 (HP; Waldbronn, Germany).

2.3. Vesicle Preparation (MLVs)

A well-defined physical structure of model membranes facilitates many aspects in the thermodynamic analysis of peptide–lipid interactions, especially when the membrane passage of a peptide (i.e., access to inner leaflets or lamellae) is unknown. We, therefore, start reviewing important steps in the membrane preparation.

When dispersed in water, phospholipids, such as charge-neutral POPC, tend to self-associate: At the air–water interface, they slowly assemble to a monolayer and in the bulk phase rapidly to bilayer forming lipid vesicles (“liposomes”) (49, 50). The dissociation constant of this self-assembly is in the order of 10^{-10} M^{-1} (51); the cross-sectional lipid area of POPC is 68 \AA^2 (52), and the thickness of the hydrophobic core and P-P distance in the fluid state is 27 and 38 \AA , respectively (53). Length, number, and position of double bonds of the acyl chains greatly influence the gel-to-fluid phase transition temperature (T_m), which characterizes the transition from the frozen (L_β ; lamellar gel) to the fluid (L_α ; liquid crystalline) phase. For POPC, this transition temperature is -2°C (54).

Most biological membranes are in the liquid-crystalline phase (55), and cycling across the transition temperature renders bilayers leaky – even to larger compounds (56–58) which is important for observations on CPP leakage across model membranes (44). Lipid polymorphism is regulated, in part, by the ratio between cross-sectional area of lipid head groups compared to the cross-section of the acyl chains. Lipids with a small head group, such as DOPE, do not form contiguous bilayers, but inverted hexagonal (H_{ii}) phases (59). As a result, DOPE is frequently used in transfection reagent mixtures for destabilizing membranes and for improving their membrane translocation (60). In this regard, CPPs have been also proposed to form inverted lipid micellar structures as part of their membrane translocation (61).

Model membranes can be prepared by different methods, such as filter extrusion, sonication, reverse phase evaporation, or detergent dilution (for a review see ref. 62). Resulting vesicles differ not only in size but also in stability, lipid packing density, outer/inner layer lipid stoichiometry, and binding enthalpies. Giant unilamellar vesicles (GUVs), for example, are particularly delicate (63). In contrast, large unilamellar vesicles (LUVs) with a defined diameter of $\sim 100 \text{ nm}$, produced by filter extrusion, have a small polydispersity (64), excellent storage stability, a lateral packing density close to eukaryotes ($28\text{--}35 \text{ mN/m}$) (65, 66), and a balanced inside/outside leaflet lipid stoichiometry. Finally, small unilamellar vesicles (SUVs) with a diameter of $30\text{--}50 \text{ nm}$, produced by sonication, have more lipid molecules on the outside than on the inside leaflet for sterical reasons (67). This is important when considering the lipid binding stoichiometry for peptides that have no access to the inner membrane leaflet. Peptide interactions with SUVs also might have different binding enthalpies in ITC experiments (as compared to LUVs) which can be favorable when working at low concentration (68). The number of water molecules (n_w) required for full hydration of a phospholipid molecule has been estimated to be $17\text{--}38$ (69, 70), so the lipid hydration must exceed $\sim 0.4\text{--}0.9 \text{ g water/g lipid}$, especially

when working with concentrated NMR samples, and additional intravesicular water might be considered (71).

Lipid stock solutions in chloroform (Avanti Polar Lipids, Alabaster, USA) or in dichloromethane are more convenient to aliquot than greasy phospholipid “powders.” On the other hand, the organic solvent requires nonplastic vials/pipettes, pipetting at low room temperatures (the boiling point of dichloromethane and chloroform is 40 and 62°C, respectively, at 760 mmHg), and removal by rotary evaporation.

1. A lipid suspension (16 mM, 2 mL, molar ratio POPG/POPC = 1/1) is prepared as follows.
2. The weight of an empty 5-mL pear-shaped flask is measured. An aliquot of 12.16 mg of POPC (e.g., 0.608 mL of a 20 mg/mL stock) is pipetted into the flask. The solvent is removed by rotary evaporation and subsequent high-vacuum evaporation (0.1 mbar) for >4 h. The weight of the flask is again measured.
3. The second lipid is added, e.g., 12.34 mg POPG (0.617 mL of a 20 mg/mL stock solution), and the solvent is also used to mix the second lipid with the first one. The solvent is removed by rotary evaporation and subsequent high-vacuum evaporation (0.1 mbar) for >4 h. The weight of the flask is measured to determine the lipid weight *ratio*. The total lipid concentration is determined according to Subheading 2.8.
4. Additional lipids, such as pegylated lipids (DOPE-PEG2000), might be added in analogy to item 3 (see also Subheading 2.7), where PEGylated lipids increase the back pressure during filter extrusion.
5. The dry lipid film is hydrated with ~2.0 mL of buffer (the concrete volume is chosen according to measured lipid weight), topped with an Argon layer, vortexed, and hydrated at room temperature during 1 h (72). Thereafter, the flask is again vigorously shaken using a tabletop shaker (“vortex”), resulting in multilamellar vesicles (MLVs) of 16 mM total lipids and a wide size distribution range between 0.5 and 10 μm. Due to the large vesicle size, the light scattering is high, and the appearance is milky. Occasional sediments may exist, originating from slow hydration of inner lamellae, especially if hydration time was too short or if lipid films after solvent evaporation are too thick.
6. LUVs or SUVs are prepared by disrupting the MLVs using sonication (73) or freeze–thaw cycling followed by extrusion through a filter of defined pore size (74), as described under Subheadings 2.5 and 2.4, respectively.

2.4. LUVs

1. The MLV dispersion (prepared under Subheading 2.3) is subjected to five freeze–thaw cycles, which reduces the

- lamellarity (75), vesicle size ($<1\ \mu\text{m}$), and size distribution (76). This is done by placing the flask for 20 min in a -80°C freezer, followed by placing in an ambient-temperature water bath. Typically, no sediments are observed any longer after this step.
2. The suspension is aspirated by a first 2.5-mL Hamilton syringe and extruded into a second Hamilton through a 19-mm syringe filter holder from Avanti Polar Lipids (Alabaster, USA), Avestin (Ottawa, Canada), or Eastern Scientific (Rockville, USA). The filter holder contains a stack of two polyethylene drain disks (art. 230300: Whatman, Maidstone, UK), two polycarbonate nucleopore track-etch membranes with a $0.1\ \mu\text{m}$ pore size (art. 800309: Whatman, Maidstone, UK), and again two drain disks. Importantly, extrusion is performed above the T_m of the lipids, because of the rapid vesicle fusion below T_m (77, 78). Depending on the lipid mixture, a heater block (Avanti Polar Lipids or Eastern Scientific) for the assembly is required. Without disconnecting the assembly, extrusion is repeated between the two syringes for at least 11 cycles (74, 79). The sample is recovered from the second syringe to ensure removal of any larger particles of the original suspension. Pore sizes available are 50, 100, or 200 nm; larger pores no longer produce narrow vesicle size distributions (79). For larger sample volumes, larger Hamilton syringes can be used or barrel extruders (Avestin, Ottawa, Canada or Northern Lipids, Burnaby, Canada).
 3. Because of the vesicle size reduction, the lipid dispersion becomes less opaque. Experimental verification of the vesicle size and distribution is recommended which is performed within a few minutes using dynamic light scattering (DLS).
 4. The prepared vesicles are topped with Argon (to prevent oxidation) and stored at 4°C (to prevent hydrolysis (80)) so that the vesicles can be used during several days before fusion is observed (81). Freezing or cycling across the lipid phase transition temperature should be avoided (82, 83). The vesicle size is checked prior to experiments using DLS. Changes in vesicle size (fusion) and lamellarity occur after days or months, where the kinetics depends on lipid type and cosolutes. Generally, fusion is prevented by higher amounts of charged lipids and promoted by high amounts of divalent ions or PEG. Studies on vesicle stability are summarized elsewhere (81, 83, 84).

2.5. SUVs

1. The MLV dispersion prepared under Subheading 2.3 is sonicated for 40 min with a tip sonicator (e.g., model 250, Branson; Danbury, USA) and 35 W power setting. During sonication, the sample is protected under a nitrogen blanket and cooled with a 20-mL water bath (at a T just higher than T_m of the lipids). Duration, power-to-volume ratio and

ultrasound wavelength are critical to produce SUVs with low polydispersity (85). For instance, a sonication time of >35 min and 50 W is required when using 10 mL volumes (86). Higher power-to-volume ratios might deesterify phospholipids (87). In contrast, bath-type sonicators (e.g., model G112SP1T; Laboratory supplies, Hicksville, USA) are operated at lower relative power settings (80 W/300 mL of water bath) and thus may produce vesicles of higher polydispersity (88) and lamellarity (89); using the latter method, fractions of larger vesicles can be separated by centrifugation or by chromatography with a Sephadex G-50 column (90). Considerations on optimum ultrasound frequency and vesicle formation by acoustic cavitations are published elsewhere (91). Finally, because of higher relative power settings, the tip sonicator can heat the liquid rapidly to temperatures >60°C, which would lead to heat-induced lipid degradation, so cooling is required.

2. After sonication, the SUVs are transferred to two microcentrifugation test tubes (Eppendorf; Hamburg, Germany), and the titanium debris from the sonicator tip (which would disturb optical methods such as DLS) is removed by centrifugation at $16,000\times g$ for 10 min. The prepared vesicles are filled into 4-mL storage vials (art. G075S-14; Infocroma, Zug, Switzerland), topped with Argon, and stored at 4°C. In contrast to LUVs, the outer surface of the vesicle bilayer contains twice as many lipid molecules than the inner leaflet (67), and their high energy curvature causes fusion to larger vesicles already after days (92).

2.6. NMR Samples

MLVs for NMR are prepared in analogy to items 1–5 of Subheading 2.3 with the following exceptions:

1. The membrane passage of CPPs to inner lamella of MLVs cannot be assumed a priori. Therefore, the buffer (see item 5 of Subheading 2.3) contains already the peptide so that the CPP has access to all lamellae.
2. Prior to NMR measurements, the MLVs are subjected to five freeze–thaw cycles to reduce the polydispersity of the vesicles to a diameter of $\sim 1\ \mu\text{m}$ and to accelerate the hydration of inner lamellae and thus to improve spectral quality.
3. In case of rare and expensive lipids, smaller amounts of lipids (typically <5 mg) are dried directly inside the NMR vial (instead of a flask) to prevent losses. The organic solvent is removed by a gentle stream of nitrogen (because of the difficulty to connect it to a Rotavapor). In this respect, chloroform has not been classed as a greenhouse gas (93), but its inhalation might cause liver cancer (94), suggesting to work in a fume hood.

2.7. Lipid Choice

1. A high POPC content is recommended for model membranes because its transition temperature (T_m) is well below ambient temperature and since it is the major lipid in mammalian cell membranes (95). A detailed review on chain length and head-group composition of mammalian cells has been published (96).
2. In view of electrostatic interactions of CPPs, the addition of anionic lipids such as POPG (typical of plants and bacteria) or POPS (typical of eukaryotes) is recommended. The membrane content of anionic lipids can be up to 50–80% in Gram-positive bacteria (97, 98) but is only 2–12% in mammalian cells where they are primarily located in the inner leaflet of the plasma membrane of healthy cells (99). Only after cell death or apoptosis, they appear at the outer membrane leaflet which can be exploited for annexin V binding assays (apoptosis marker) (100). An anionic lipid content of 0–10% is, thus, reasonable for modeling eukaryotic membrane phospholipids.
3. Because of their polycationic character, CPPs may lead to intravesicular aggregation and sedimentation of anionic lipid vesicles (101). This leads to precipitates and light scattering which disturbs optical measurements (e.g., DLS, CD, fluorescence). The vesicle aggregation can be prevented by including 2–4 mol% PEGylated lipids in the lipid mixture (102). At higher ratios (>5–8 mol% depending on PEG chain length), a “mushroom-to-brush” transition of the PEG chains occurs (103–105), which may either increase (106) or diminish peptide binding (107).

2.8. Lipid Quantification

Precise knowledge of the lipid concentration is essential in thermodynamic analysis of peptide–lipid interactions. Especially when preparing SUVs with a tip sonicator, solvent evaporation can occur. Phospholipid content is, thus, measured as phosphate content after oxidation of the phospholipids with perchloric acid. The liberated inorganic phosphate ion reacts with ammonium molybdate to form phosphomolybdic acid, which is measured spectrophotometrically. The sensitivity of the detection is increased in the presence of cationic malachite green (108). Dried KH_2PO_4 at 5–20 nmol is used for calibration. The assay is, thus, incompatible with phosphate-based buffers. When using higher phosphate concentrations and readings later than 20 min after reagent addition, stabilization of the colored complex with surfactants such as Tween 20 is required (109).

1. Wear protection glasses, gloves, and lab coat.
2. Coloring reagent: 1.05 g of ammonium molybdate ($(\text{NH}_4)_6\text{MoO}_{24}\cdot 4\text{H}_2\text{O}$) is dissolved in 15 mL of 6 N HCl; this is added to 0.12 g of Malachite Green previously dissolved in 85 mL of H_2O . After 30 min of stirring, the reagent is filtered

(filter paper #1, Whatman; Maidstone, UK). The reagent is stored at room temperature and is freshly filtered prior to use (0.2- μ m PTFE syringe filter; Whatman, Maidstone, UK). The reagent is stable for 6 weeks. Thereafter, the assay leads to increased OD values and nonlinearity in the standard curve.

3. An aliquot of ~150 nmol of phospholipids (e.g., 30 μ L of a 5 mM POPC suspension) is placed in a 8 \times 60 mm borosilicate glass tube (art. 26.013.201; Glas Keller, Basel, Switzerland)
4. 100 μ L of perchloric acid (70%) is added.
5. Behind a protection shield and in a fume hood, the vial is held with a forceps (tube opening opposed to the body) and is gently boiled with a bunsen burner for approximately 3–4 min so that the solution first turns yellow and, after a short burst of white smoke, gets clear again, leaving ~1/2 of the original volume. After cooling, the solution is made up with water to 1.0 mL.
6. A tenth of it (100 μ L; triplicate) is placed into a disposable plastic cuvette (1 cm path length), and 900 μ L of the freshly filtered coloring reagent is added and immediately mixed.
7. For the blank, 100 μ L of water is placed in a cuvette, and 900 μ L of the coloring reagent is added and mixed.
8. For the standard curve, 5, 10, 15, and 20 μ L of a 1 mM KH_2PO_4 solution are placed in a cuvette, followed by making up with water to 100 μ L and addition of 900 μ L of the coloring reagent.
9. A time scan (light absorbance at 660 nm) of the most concentrated standard is recorded (i.e., 20 nmol of KH_2PO_4), where the OD signal will increase after ~10 min to a Δ OD of ~0.9 (with regard to the blank) and will stay stable for ~30 min.
10. The interval between addition of the coloring reagent and achievement of stable signal (i.e., ~10 min) is kept equal for all samples.

2.9. Peptide Quantification

Precise knowledge of the peptide content is essential – especially for CPPs. Current synthesis and purification procedures typically lead to a peptide purity of >98%, not meaning that the peptide content of the lyophilized powder is >98%: the presence of anionic counterions, such as acetate or trifluoro acetate, is considerably high after purification because of the high content of cationic arginines and lysines in CPPs. The CPP R_n , for example, may contain nine TFA counterions after purification with HPLC using TFA as an ion pairing reagent. As a result, the mass content of TFA in the lyophilized peptide could be 40% or higher. Therefore, elemental analysis (comparing experimental versus theoretical

nitrogen content) or amino-acid analysis (quantifying amino acids with fluorescent tags after acid peptide lysis) (110) are required whenever working with CPPs.

Because spectrophotometers are available in most laboratories, insertion of a light-absorbing amino acid, such as tryptophane, at the N-terminus of the CPP sequence is also a good alternative for peptide quantification (e.g., WR₉). This allows for fast quantification during each peptide handling step using the molar extinction coefficient of 5,500 for tryptophane at 280 nm during denaturation in 6 M guanidine hydrochloride (111).

Peptides used in the present protocols were made by solid-phase peptide synthesis using a Fmoc strategy (112) and a Rink amide resin. The carboxy terminus was amidated and thus uncharged. Acylation at the N-terminus with fatty acids of varying lengths (C₁₄, C₁₆, or C₁₈) was performed on-resin by activation with PyBOP/NMM. The single-letter code for the peptides used are WRRRRRRRRR (WR₉), myristoyl- (C₁₄-WR₉), palmitoyl- (C₁₆-WR₉), and stearoyl-WR₉ (C₁₈-WR₉), RQIKIWFQNRRMKWKK (penetratin; Antp), and RQIKIWFQAARMLWKK (penetratin p2AL, see ref. 48). When observed in a helical wheel projection (113), WR₉ and Antp are considered to be nonamphipathic – in contrast to the acylated WR₉ derivatives (“primary amphipathic” according to refs. 28, 33) and p2AL (“secondary amphipathic” according to refs. 28, 33).

2.10. Fluorescent Membrane Leakage Dyes

Calcein is a zwitterion having a maximum of six negative and two positive charges. Because of the uncertainty about its pK_a (114, 115), the net charge at pH 7 is considered to be -3 (116, 117) or -4 (115). On the basis of published pK_a values, the net charge of further fluorescent leakage dyes, such as ANTS, carboxyfluorescein, and fluorescein, is -3, ~-2.7 (118), and ~-1.6 (114) at pH 7, respectively. Because of its multivalency, the encapsulation of calcein (typically 70 mM) into vesicles produces a high ionic strength. The ionic strength (*I*) of a solution containing *n* ionic species is defined by

$$I = \frac{1}{2} \sum_i^n c_i z_i^2 \quad (1)$$

where *c_i* is the concentration of ion *i*, and *z_i* is its charge number.

Assuming *z* = -3 or -4 for calcein at neutral pH (disodium salt), a 70 mM calcein solution results in an ionic strength of 0.42 or 0.7 M, respectively, which is much higher than that of physiologic saline (0.154 M). This is important when considering ionic gradients as a potential mechanism for CPP membrane disturbance (119).

3. Methods

3.1. Membrane Leakage (Calcein Dequenching)

The fluorescent dyes used in this assay are generally anionic in nature. As a result, they cannot cross the membrane because of the high Born charge energy barrier (25). Spontaneous dye leakage across the membrane proceeds only over days, but dyes of little charge (fluorescein, carboxyfluorescein) leak faster than trivalent dyes (e.g., calcein, ANTS) (116). On the other hand, the multivalency of the latter dyes has the disadvantage of interacting with the cationic peptides (see Fig. 2f and g) and creating a strong ionic gradient across the membrane (see Subheading 2.10).

The membrane leakage assay (116) resides on the principle that the dye is entrapped in vesicles at self-quenching concentrations. Fluorescent dyes such as carboxyfluorescein are self-quenching at concentrations >0.2 M because of nonfluorescent dimer formation and energy transfer to the dimer (120). In addition, the high light absorbance of the dyes causes an inner filter effect so that the concentration for maximum fluorescence is observed already at low micromolar concentration depending on the cuvette dimension (see Fig. 1a). Adding a membrane-perturbing peptide then leads to the release of the dye out of the vesicles. Its dilution into the much larger extravesicular volume results in increased fluorescent signal intensity. In addition to self-quenching, collisional quenchers might be encapsulated (e.g., cationic DPX for anionic dye ANTS) so that their dilution upon membrane leakage causes also an increase of the fluorescence signal.

1. LUVs are prepared as described in Subheading 2.4 (total lipid concentration typically 15 mM) with the exception that the buffer (20 mM Tris) contains calcein (13 mM; ionic strength of 104 mM at pH 8.5), no NaCl, and the pH is 8.5, i.e., 3 pH units higher than pK_{a_3} of calcein. For this purpose, acidic calcein is first dispersed into the buffer, and the pH is adjusted to pH 8.5 using NaOH bringing calcein into solution.
2. Free calcein is removed by SEC using a glass column (i.d. 1.6 cm) filled to a height of 23 cm with Sepharose CL-6B (Sigma-Aldrich; fractionation range of 0.01–4 MDa for globular proteins) as stationary phase and a running buffer of 20 mM Tris, 134 mM NaCl pH 8.5. In order to protect the fluorescent dye against bleaching, the column is wrapped with an aluminum foil. When using carboxyfluorescein as dye, spontaneous dye leakage occurs faster than that for calcein (116), so chromatography at 4°C is recommended.
3. Flow rate of the pump is 0.3 mL/min.
4. Absorbance of calcein is monitored at 495 nm.
5. Fractions of 1 mL are collected into Eppendorf tubes.

6. Fractions between 51 and 57 min (containing calcein-loaded vesicles) are collected (see Fig. 1b)
7. Fractions between 120 and 145 min (containing free calcein) are discarded.
8. The size of the vesicles is checked with DLS.
9. The lipid concentration is measured (see Subheading 2.8). The dilution factor as caused by the present SEC column is typically ~6.
10. Lipids are diluted to a final concentration of 0.1–0.45 mM, i.e., a concentration close to total phospholipid content of cells in culture (e.g., 68 μ M respecting 25 mL culture medium (121)).
11. Using a 1-cm fluorescence cuvette, 1.4 mL of the calcein loaded vesicles are placed in the cuvette containing a magnetic stir bar.
12. Under continuous stirring, a time scan of calcein fluorescence is recorded. After 60 s of baseline recording, a small volume (see Fig. 1e) of the CPP is added to produce a final peptide concentration in the micromolar range.
13. When at equilibrium (e.g., 10 min), 100 μ L of 5% Triton X-100 is added to release the entire vesicle content.
14. The relative membrane leakage (F_{rel}) induced by the CPP can be calculated according to

$$F_{\text{rel}} = \frac{F_{\text{CPP}} - F_0}{F_{\text{triton}} - F_0} \quad (2)$$

where F_0 , F_{CPP} and F_{triton} denote the initial (quenched) fluorescence, increased fluorescence after CPP addition, and maximum fluorescence after triton addition, respectively. Although calcein at self-quenching concentrations in 1-cm cuvettes (>0.2 mM) has almost no fluorescence (see Fig. 1a), F_0 in this assay is typically higher than zero, because of lower inner filter effects when calcein is encapsulated in diluted vesicles.

15. Reporting percentual dye release according to Eq. 2 relies on a linear relation between dye concentration and fluorescence intensity. This is valid only when the fluorescence is not quenched, i.e., at a concentration below the concentration for maximum fluorescence (consider the logarithmic scale in Fig. 1a). The maximum fluorescence for calcein in a 1-cm cuvette, for example, is observed at a concentration of ~20 μ M (see Fig. 1a). Based on a cross-sectional area of 68 \AA^2 per POPC and a sample volume of 1.4 mL, a 0.45 mM POPC LUV preparation (vesicle radius of 50 nm) has a total intravesicular volume of 2.15 μ L. Full membrane leakage, thus, produces a dye dilution factor of 1.4 mL/2.15 μ L = 651.

A linear correlation between fluorescence intensity and concentration is, thus, achieved for a vesicular calcein concentration of $651 \times 20 \mu\text{M} = 13 \text{ mM}$ and lower. When using a higher calcein concentration, the vesicle concentration must be decreased accordingly.

3.2. Membrane Integrity (^{31}P NMR Spectroscopy)

Phosphorous-31 NMR is a simple method to distinguish between lipid bilayers, hexagonal structures, and isotropically moving phospholipids (122). Because of the slow rotation on a NMR time scale, MLVs produce a chemical shift anisotropy (see Fig. 2a). In contrast, rapidly tumbling structures (LUVs, SUVs, detergent-solubilized lipids “mixed micelles”) show an isotropic NMR signal (see Fig. 2b).

The assay, therefore, requires the work with MLVs. Because of potential vesicle aggregation and subsequent precipitation with CPPs (101), a horizontally aligned NMR radiofrequency coil (covering the entire sample tube) is preferred over a standard vertical high-resolution NMR probe head where aggregates sediment out of the sensitive volume of the probe head. Our laboratory typically uses a 4-turn solenoid of $14 \times 8 \text{ mm}$ inner diameter. Sample tubes are borosilicate tubes (Fiolax, Duran; Mainz, Germany) or in-house, custom-made screw vials with internal volumes of 400 and 150 μL , respectively.

1. This assay is incompatible with phosphate-based buffers. MLVs are produced as described under Subheading 2.6. For rare lipids, only 5 mg total lipid and 150 μL of liquid are used, but lipid quantities can be increased up to 100 mg lipid/100 mg of liquid (check hydration number for specific lipid) which leads to more signal and thus to faster experiments.
2. For external calibration, 200 μL of concentrated phosphoric acid (85%) is used (sealed in a borosilicate tube). After magnetic field homogenization with the ^1H frequency (“shimming”) to the vial geometry, the ^{31}P signal of concentrated phosphoric acid is calibrated to 0 ppm (pH dependant). Because of the steady magnetic field drift, this procedure is repeated every day, where one scan typically yields sufficient signal.
3. The lipid samples are subsequently recorded using the same magnetic shim values and chemical shift calibration.
4. Because of the broad chemical shift dispersion, NMR spectra are recorded with a setup for solid-state like compounds, i.e., fast digitizer, high power amplifier, and a probe head that can withstand that power. The inverse relation of excitation bandwidth and pulse length in FT NMR requires 90° pulses in the low μs range (typically 5 μs) for full spectral excitation.

5. ^{31}P NMR spectra are recorded using a Hahn echo sequence ($90^\circ\text{-}\tau\text{-}180^\circ$ with $\tau=40\ \mu\text{s}$), broadband proton decoupling, a recycle delay of 5 s (i.e., ~ 5 times T_1), spectral width of 50 kHz, and 4 K data size. Typically, 8,000 transients are averaged, and the free induction decay is exponentially multiplied prior to Fourier transformation corresponding to a 200 Hz line broadening. Compared to a simple pulse-and-acquire NMR sequence, the delayed acquisition of the Hahn echo sequence reduces contributions of preamplifier and resonance coil ringing after strong radio-frequency pulses (123).

3.3. Membrane Binding (Isothermal Titration Calorimetry)

The membrane binding of peptides can be driven by a variety of forces, such as hydrophobic partitioning, electrostatic attraction to charged lipid head groups, or stabilization through a conformational change (e.g., helix formation). As a consequence, membrane-peptide interactions are characterized by a variety of affinity constants, and these have not only different magnitudes but also different molecular meanings (28, 124): The surface partition constant K_p , as defined here, describes the hydrophobic interaction. The molar amount of peptide bound (n_p) to accessible (i.e., outer leaflet) lipid (n_L), $X_b = n_p/n_L$, is used to calculate

$$K_p = \frac{X_b}{c_m} \quad (3)$$

where c_m is the peptide concentration close to the membrane surface. For uncharged lipids and uncharged peptides, the peptide concentration close to the membrane surface (c_m) equals the free peptide concentration in bulk at equilibrium (c_{eq}), so a plot of c_{eq} versus X_b yields a straight line with the slope K_p (124). However, this correlation is not linear when electrostatic interactions are involved. In this case, the apparent membrane partitioning constant K_{app} is used for both hydrophobic and electrostatic interactions, and we define

$$K_{\text{app}} = \frac{X_b}{c_{\text{eq}}} \quad (4)$$

The electrostatic interactions between cationic peptides and anionic lipids cause the concentration of the peptide near the membrane (c_m) to be higher than in bulk (c_{eq}). Obviously, K_{app} is larger than K_p because of $c_{\text{eq}} \ll c_m$. Characteristically, K_{app} decreases with increasing peptide concentration because of electrostatic screening. Thus, a plot of c_{eq} versus X_b is not linear for charged compounds. Using the Gouy–Chapman theory, c_m and the membrane surface potential (Ψ_0) can be calculated (101, 124–126) which, in turn, allows the calculation of K_p . This way, hydrophobic and electrostatic contributions to the peptide–lipid

interaction can be differentiated, and a plot of c_m versus X_b becomes linear (124).

Several studies agree that nonamphipathic CPPs such as R₉, Tat, and PLL do not partition into the hydrophobic core of model membranes but remain superficially bound (39, 40, 101, 127–129). Their interaction is, thus, best described by a complex (L_nP) formation of n lipids (L) with the peptide (P) according to



This way, peptide binding can be visualized in terms of a multisite binding model. Here, a complex formation constant K of defined stoichiometry is used. In contrast, K_p and K_{app} make no assumptions on the reaction stoichiometry. Assuming n identical binding sites on the multivalent peptide P , the binding of lipid L to individual sites on P can be defined by a single-site (“microscopic”) binding constant

$$K = \frac{[\text{filledsites}]}{[\text{emptysites}][L]} \quad (6)$$

where $[L]$ represents concentration. For statistical reasons (28), the first lipid (i.e., nonsaturating conditions) binds with a higher affinity than the last one (i.e., saturating conditions). Determination of the CPP-lipid affinity by ITC relies on the principle that the peptide in the reaction cell (200 μ L) is progressively saturated by repeated additions ($19 \times 2 \mu$ L) of the lipid while the heat of reaction is recorded during each injection. For a precise fit of experimental data, sufficient data points in the transition region (i.e., 3–10 data points) must be available in the thermogram and, ideally, an initial plateau for the first few titrations (see Fig. 3c). As a rule of thumb, both conditions are met if the starting concentration of the peptide $[P_0]$ in the reaction cell is close to

$$[P_0] = 50K_d / n \quad (7)$$

where K_d is the estimated dissociation constant ($K_d = 1/K$).

Because of the volume ratio of the cell/syringe of ~ 5 and a desired twofold excess of $[L]$ at the end of the titration series, the concentration of the ligand $[L_0]$ is chosen to be $500 K_d$ (which results from $[L_0] = 5 \times 2 n P_0$, where P_0 is equivalent to Eq. 7).

If $[P_0]$ is 2 magnitudes higher than defined in Eq. 7, the transition region of the thermogram is almost rectangular (see Fig. 3c), so the fitted K_d represents only a upper limit of K_d . If P_0 is 2 magnitudes lower than in Eq. 7, the isotherm is very flat and the endpoint is uncertain, so the fit to the data no longer produces clear-cut results (see Fig. 3c). If the concentration cannot be increased in the latter case for experimental reasons (e.g., high polydispersity and lamellarity for lipids >100 mM, or protein self-aggregation at high concentration), the syringe can be

refilled a second time (see Fig. 3b), or the content of syringe and reaction cell can be inverted.

1. Prepare 4 mL of a peptide solution (sufficient for six experiments considering ~ 300 μL per prerun cell rinsing and subsequent titration experiment) and 2 mL of SUVs (sufficient for 30 experiments considering ~ 60 μL per syringe filling) according to Subheading 2.5. The solutions are filled into a 4-mL glass vial and are degassed under stirring (ThermoVac; Microcal, Northampton, USA) at 0.7 atm during 7 min. Degassing is important especially for experiments above room temperature, since air bubbles lead to increased noise and baseline jumps in ITC due to the air compression and friction during stirring at high speeds (typically 1,000 rpm). Prior to filling the instrument, the solutions are kept at experimental temperature to minimize the delay between cell filling and start of the first injection (which is typically 10–20 min for the present instrument).
2. In a first experiment (“blank” experiment), SUVs are titrated into buffer to measure the heat of lipid dilution, which is subtracted in subsequent experiments.
3. After the blank experiment, the reaction cell is cleaned, typically with 2% Contrad 90 (Socochim, Lausanne, Switzerland) for 15 min, followed by ample water rinsing.
4. The cell of the calorimeter, thereafter, contains smaller amounts of water from precedent cleaning procedures which could lead to dilution of the peptide. The cell is, thus, filled once with the peptide, and the content is discarded. Thereafter, the cell is filled again with the peptide for the proper experiment.
5. Selection of the injection volumes is a compromise between sufficient signal/noise per injection and sufficient data points to construct an isotherm: the syringe content (38.5 μL) is typically divided into 19×2 μL aliquots, but the injector could handle smaller volumes with high precision which can be exploited whenever the reaction enthalpy is high. The spacing between the injections depends on the reaction kinetics (and stirrer speed): fast reactions such as ethanol dilutions can be recorded with an interval of 60 s, but the present multisite binding reaction is slower and is best recorded with an interval of 90–120 s (awaiting reaction equilibrium) so that the total experiment time from cell filling to end is typically 1 h.
6. The raw data (see Fig. 3a upper panel) are integrated to yield the heat per injection and thus a binding isotherm when plotting it against the molar ratio of the reactants (see Fig. 3a lower panel). A visual inspection yields a first approximation: in the case of an initial plateau, the ligand is almost completely

bound so that the heat (per mol of ligand) in the plateau region corresponds to the reaction enthalpy. The molar ratio at half of the plateau value allows one to estimate the stoichiometry of the reactants; finally, the slope in the transition region serves as a rough approximation of the binding affinity; in the case of an initial plateau, the dissociation constant k_d is typically $\ll A_0$. Exact values of these parameters are determined by a fit to the data:

7. A fit to the experimental isotherm (see Fig. 3a lower panel) using the multisite binding model (see Eq. 6; for further details see ref. 28) yields K , n , the reaction enthalpy ΔH , and entropy ΔS . Because nonamphipathic CPPs typically do not diffuse across the bilayer (39, 40, 101, 127–129), only the outer leaflet is accessible to the CPP, and this lipid concentration is approximately 60% of the total lipid concentration for SUVs (67).
8. Repeating the experiment at different temperatures is recommended for two reasons: on the one hand, a reaction might be driven entirely by entropy, so the enthalpy would be zero and the calorimeter would not detect any signal (despite the ongoing binding reaction). On the other hand, the slope of ΔH versus T yields the change in molar heat capacity (ΔC_p^0), which gives important information about hydrophobic (typically negative ΔC_p^0) and electrostatic (typically positive ΔC_p^0) contributions to the reaction. Electrostatic contributions to the binding can be also assessed by repeating the experiment at different salt concentrations.
9. Repeating the experiments with different buffers results in valuable information about protonation reactions (e.g., histidine-rich CPPs), which can be detected by ITC because of the different ionization enthalpies of the buffers (130).

4. Notes

1. Membrane leakage (Calcein dequenching). Using this protocol, it is observed that nonamphipathic WR₉ and penetratin do not produce membrane leakage (see Fig. 1c and d). In contrast, the amphipathic penetratin mutant p2AL leads to pronounced membrane leakage already at low micromolar concentrations (see Fig. 1e).

The electrostatic interaction between the anionic dyes and cationic CPPs also affects the result. For example, the interaction of WR₉ with calcein results in a decrease of the fluorescence which could, in principle, mask the membrane leakage (Fig 1f). This effect is even stronger for the acylated WR₉ derivatives (see Fig. 1f) and p2AL at high concentration (see Fig. 1e).

In contrast, the CPP interaction with the dye ANTS leads to an *increase* in fluorescence (see Fig. 1g), so smaller membrane leaks should be detected with improved sensitivity.

Even under these improved conditions using ANTS (see Fig. 1h), no membrane leakage is observed for WR₉. These data agree with previous studies where nonamphipathic CPPs could not produce membrane leakage at physiologically relevant conditions (39, 101, 131–134). However, they have caused membrane leakage under particular conditions such as a higher molar CPP/lipid ratios (>0.2), more permeable dyes (carboxyfluorescein), ionic gradients over the membrane, and pH > 7.5 (135) which is considered to play a limited role in the in vivo CPP transduction (135).

2. Membrane integrity (³¹P NMR spectroscopy). Using this protocol, it is observed (see Fig. 2) that none of the investigated CPPs forms inverted micelles with lipids that are typical for physiological membranes – even at very high peptide concentration (4 mM). However, all amphipathic CPPs damaged the membrane in a detergent-like manner, supporting the membrane leakage data (see Fig. 1). The critical micellar concentration of C₁₈-, C₁₆-, and C₁₄-WR₉ were found to be 26 μM, 49 μM, and ~5 mM, respectively, as determined by surface activity measurements (data not shown).
3. Membrane binding. CPP uptake in biological cells is typically observed at low micromolar concentrations, (=similar concentrations as used in Fig. 3). Using the present ITC protocol, it is observed that the nonamphipathic CPP WR₉ has a poor affinity ($K \sim 10^3$) for model membranes that have an anionic lipid contents typical for mammalian cells (see Fig. 3b). This is in contrast to the high affinity of the CPP for other anionic compounds of the cell membrane such as heparan sulfate ($K \sim 10^5$) (112).

The lipid affinity of nonamphipathic WR₉ becomes, however, important (even at micromolar concentrations) when the membrane has a high anionic lipid content (see Fig. 3a) such as encountered in bacterial membranes. This might be important for species selectivity of transfection reagents.

4. Different types of CPPs. Using a variety of different protocols on model membranes, it is concluded that nonamphipathic CPPs, such as WR₉ and penetratin, likely do not traverse cell membranes by direct interaction with lipids.

This is in stark contrast to amphipathic CPPs such as acylated WR₉ or amphipathic penetratin derivate p2AL both of which considerably disturb the model membrane already at low micromolar concentration.

Acknowledgments

This work was supported by the Swiss National Science Foundation (SNF) Grant # 31.107793.

References

- Morad, N., Ryser, H.J. and Shen, W.C. (1984) Binding sites and endocytosis of heparin and polylysine are changed when the two molecules are given as a complex to Chinese hamster ovary cells. *Biochim. Biophys. Acta.* **801**, 117–126.
- Ryser, H.J. (1967) A membrane effect of basic polymers dependent on molecular size. *Nature* **215**, 934–936.
- Kaplan, I.M., Wadia, J.S. and Dowdy, S.F. (2005) Cationic TAT peptide transduction domain enters cells by macropinocytosis. *J. Control. Release* **102**, 247–253.
- Belting, M., Mani, K., Jonsson, M., Cheng, F., Sandgren, S., Jonsson, S., Ding, K., Delcros, J.G. and Fransson, L.A. (2003) Glypican-1 is a vehicle for polyamine uptake in mammalian cells: a pivotal role for nitrosothiol-derived nitric oxide. *J. Biol. Chem.* **278**, 47181–47189.
- Lundberg, M., Wikstrom, S. and Johansson, M. (2003) Cell surface adherence and endocytosis of protein transduction domains. *Mol. Ther.* **8**, 143–150.
- Kopatz, I., Remy, J.S. and Behr, J.P. (2004) A model for non-viral gene delivery: through syndecan adhesion molecules and powered by actin. *J Gene Med* **6**, 769–776.
- Zenke, M., Steinlein, P., Wagner, E., Cotten, M., Beug, H. and Birnstiel, M.L. (1990) Receptor-mediated endocytosis of transferrin-polycation conjugates: an efficient way to introduce DNA into hematopoietic cells. *Proc. Natl. Acad. Sci. USA* **87**, 3655–3659.
- Frankel, A.D. and Pabo, C.O. (1988) Cellular uptake of the tat protein from human immunodeficiency virus. *Cell* **55**, 1189–1193.
- Green, M. and Loewenstein, P.M. (1988) Autonomous functional domains of chemically synthesized human immunodeficiency virus tat trans-activator protein. *Cell* **55**, 1179–1188.
- Marinova, Z., Vukojevic, V., Surcheva, S., Yakovleva, T., Cebers, G., Pasikova, N., Usynin, I., Hugonin, L., Fang, W., Hallberg, M., Hirschberg, D., Bergman, T., Langel, Ü., Häuser, K.F., Pramanik, A., Aldrich, J.V., Gräslund, A., Terenius, L. and Bakalkin, G. (2005) Translocation of dynorphin neuro-peptides across the plasma membrane. A putative mechanism of signal transmission. *J. Biol. Chem.* **280**, 26360–26370.
- Wadia, J.S., Stan, R.V. and Dowdy, S.F. (2004) Transducible TAT-HA fusogenic peptide enhances escape of TAT-fusion proteins after lipid raft macropinocytosis. *Nat. Med.* **10**, 310–315.
- Fretz, M.M., Penning, N.A., Al-Taei, S., Futaki, S., Takeuchi, T., Nakase, I., Storm, G. and Jones, A.T. (2007) Temperature-, concentration- and cholesterol-dependent translocation of L- and D-octa-arginine across the plasma and nuclear membrane of CD34+ leukaemia cells. *Biochem. J.* **403**, 335–342.
- Zaro, J.L., Rajapaksa, T.E., Okamoto, C.T. and Shen, W.C. (2006) Membrane transduction of oligoarginine in HeLa cells is not mediated by macropinocytosis. *Mol. Pharm.* **3**, 181–186.
- Vives, E., Brodin, P. and Lebleu, B. (1997) A truncated HIV-1 Tat protein basic domain rapidly translocates through the plasma membrane and accumulates in the cell nucleus. *J. Biol. Chem.* **272**, 16010–16017.
- Mitchell, D.J., Kim, D.T., Steinman, L., Fathman, C.G. and Rothbard, J.B. (2000) Polyarginine enters cells more efficiently than other polycationic homopolymers. *J. Pept. Res.* **56**, 318–325.
- Thoren, P.E., Persson, D., Isakson, P., Gokso, M., Onfelt, A. and Norden, B. (2003) Uptake of analogs of penetratin, Tat(48–60) and oligoarginine in live cells. *Biochem. Biophys. Res. Commun.* **307**, 100–107.
- Mano, M., Henriques, A., Paiva, A., Prieto, M., Gavilanes, F., Simoes, S. and Pedrosa de Lima, M.C. (2006) Cellular uptake of S413-PV peptide occurs upon conformational changes induced by peptide-membrane interactions. *Biochim. Biophys. Acta* **1758**, 336–346.

18. Tunnemann, G., Ter-Avetisyan, G., Martin, R.M., Stockl, M., Herrmann, A. and Cardoso, M.C. (2008) Live-cell analysis of cell penetration ability and toxicity of oligo-arginines. *J. Pept. Sci.* **14**, 469–476.
19. Ter-Avetisyan, G., Tunnemann, G., Nowak, D., Nitschke, M., Herrmann, A., Drab, M. and Cardoso, M.C. (2009) Cell entry of arginine-rich peptides is independent of endocytosis. *J. Biol. Chem.* **284**, 3370–3378.
20. Fischer, R., Fotin-Mleczek, M., Hufnagel, H. and Brock, R. (2005) Break on through to the other side—biophysics and cell biology shed light on cell-penetrating peptides. *Chembiochem.* **6**, 2126–2142.
21. Ziegler, A., Nervi, P., Durrenberger, M. and Seelig, J. (2005) The cationic cell-penetrating peptide CPP(TAT) derived from the HIV-1 protein TAT is rapidly transported into living fibroblasts: optical, biophysical, and metabolic evidence. *Biochemistry* **44**, 138–148.
22. Geueke, B., Namoto, K., Agarkova, I., Perriard, J.C., Kohler, H.P. and Seebach, D. (2005) Bacterial cell penetration by beta3-oligohomoarginines: indications for passive transfer through the lipid bilayer. *Chembiochem.* **6**, 982–985.
23. Nekhotiaeva, N., Elmquist, A., Rajarao, G.K., Hällbrink, M., Langel, Ü. and Good, L. (2004) Cell entry and antimicrobial properties of eukaryotic cell-penetrating peptides. *FASEB J.* **18**, 394–396.
24. Holm, T., Netzereab, S., Hansen, M., Langel, Ü. and Hällbrink, M. (2005) Uptake of cell-penetrating peptides in yeasts. *FEBS Lett.* **579**, 5217–5222.
25. Glaeser, R.M. and Jap, B.K. (1984) The “Born Energy” Problem in Bacteriorhodopsin. *Biophys. J.* **45**, 95–97.
26. Nishihara, M., Perret, F., Takeuchi, T., Futaki, S., Lazar, A.N., Coleman, A.W., Sakai, N. and Matile, S. (2005) Arginine magic with new counterions up the sleeve. *Org. Biomol. Chem.* **3**, 1659–1669.
27. Richard, J.P., Melikov, K., Vives, E., Ramos, C., Verbeure, B., Gait, M.J., Chernomordik, L.V. and Lebleu, B. (2003) Cell-penetrating peptides. A reevaluation of the mechanism of cellular uptake. *J. Biol. Chem.* **278**, 585–590.
28. Ziegler, A. (2008) Thermodynamic studies and binding mechanisms of cell-penetrating peptides with lipids and glycosaminoglycans. *Adv. Drug Deliv. Rev.* **60**, 580–597.
29. Scheller, A., Oehlke, J., Wiesner, B., Dathe, M., Krause, E., Beyermann, M., Melzig, M. and Bienert, M. (1999) Structural requirements for cellular uptake of alpha-helical amphipathic peptides. *J. Pept. Sci.* **5**, 185–194.
30. Bechinger, B. and Lohner, K. (2006) Detergent-like actions of linear amphipathic cationic antimicrobial peptides. *Biochim. Biophys. Acta* **1758**, 1529–1539.
31. Takeshima, K., Chikushi, A., Lee, K.K., Yonehara, S. and Matsuzaki, K. (2003) Translocation of analogues of the antimicrobial peptides magainin and buforin across human cell membranes. *J. Biol. Chem.* **278**, 1310–1315.
32. Shai, Y. (1999) Mechanism of the binding, insertion and destabilization of phospholipid bilayer membranes by alpha-helical antimicrobial and cell non-selective membrane-lytic peptides. *Biochim. Biophys. Acta* **1462**, 55–70.
33. Deshayes, S., Plenat, T., Aldrian-Herrada, G., Divita, G., Le Grimellec, C. and Heitz, F. (2004) Primary amphipathic cell-penetrating peptides: structural requirements and interactions with model membranes. *Biochemistry* **43**, 7698–7706.
34. Cho, Y.W., Kim, J.D. and Park, K. (2003) Polycation gene delivery systems: escape from endosomes to cytosol. *J. Pharm. Pharmacol.* **55**, 721–734.
35. Subbarao, N.K., Parente, R.A., Szoka, F.C., Jr., Nadasdi, L. and Pongracz, K. (1987) pH-dependent bilayer destabilization by an amphipathic peptide. *Biochemistry* **26**, 2964–2972.
36. Jones, S.W., Christison, R., Bundell, K., Voyce, C.J., Brockbank, S.M., Newham, P. and Lindsay, M.A. (2005) Characterisation of cell-penetrating peptide-mediated peptide delivery. *Br. J. Pharmacol.* **145**, 1093–1102.
37. Saar, K., Lindgren, M., Hansen, M., Eiriksdottir, E., Jiang, Y., Rosenthal-Aizman, K., Sassian, M. and Langel, Ü. (2005) Cell-penetrating peptides: a comparative membrane toxicity study. *Anal. Biochem.* **345**, 55–65.
38. Macdonald, P.M., Crowell, K.J., Franzin, C.M., Mitrakos, P. and Semchyschyn, D.J. (1998) Polyelectrolyte-induced domains in lipid bilayer membranes: the deuterium NMR perspective. *Biochem. Cell. Biol.* **76**, 452–464.
39. Tiriveedhi, V. and Butko, P. (2007) A fluorescence spectroscopy study on the interactions of the TAT-PTD peptide with model lipid membranes. *Biochemistry* **46**, 3888–3895.
40. Roux, M., Neumann, J.M., Bloom, M. and Devaux, P.F. (1988) 2H and 31P NMR

- study of pentyllysine interaction with head-group deuterated phosphatidylcholine and phosphatidylserine. *Eur. Biophys. J.* **16**, 267–273.
41. Esbjorner, E.K., Lincoln, P. and Norden, B. (2007) Counterion-mediated membrane penetration: Cationic cell-penetrating peptides overcome Born energy barrier by ion-pairing with phospholipids. *Biochim. Biophys. Acta* **1768**, 1550–1558.
 42. Sakai, N., Takeuchi, T., Futaki, S. and Matile, S. (2005) Direct observation of anion-mediated translocation of fluorescent oligoarginine carriers into and across bulk liquid and anionic bilayer membranes. *Chembiochem.* **6**, 114–122.
 43. Henriques, S.T., Costa, J. and Castanho, M.A. (2005) Translocation of beta-galactosidase mediated by the cell-penetrating peptide pep-1 into lipid vesicles and human HeLa cells is driven by membrane electrostatic potential. *Biochemistry* **44**, 10189–10198.
 44. Afonin, S., Frey, A., Bayerl, S., Fischer, D., Wadhvani, P., Weinkauf, S. and Ulrich, A.S. (2006) The cell-penetrating peptide TAT (48–60) induces a non-lamellar phase in DMPC membranes. *Chemphyschem.* **7**, 2134–2142.
 45. Thoren, P.E., Persson, D., Karlsson, M. and Norden, B. (2000) The antennapedia peptide penetratin translocates across lipid bilayers – the first direct observation. *FEBS Lett.* **482**, 265–268.
 46. Thoren, P.E., Persson, D., Esbjorner, E.K., Goksor, M., Lincoln, P. and Norden, B. (2004) Membrane binding and translocation of cell-penetrating peptides. *Biochemistry* **43**, 3471–3489.
 47. Futaki, S., Ohashi, W., Suzuki, T., Niwa, M., Tanaka, S., Ueda, K., Harashima, H. and Sugiura, Y. (2001) Stearylated arginine-rich peptides: a new class of transfection systems. *Bioconjug. Chem.* **12**, 1005–1011.
 48. Drin, G., Demene, H., Tamsamani, J. and Brasseur, R. (2001) Translocation of the pAntp peptide and its amphipathic analogue AP-2AL. *Biochemistry* **40**, 1824–1834.
 49. Schindler, H. (1979) Exchange and interactions between lipid layers at the surface of a liposome solution. *Biochim. Biophys. Acta* **555**, 316–336.
 50. Qiu, R. and MacDonald, R.C. (1994) A metastable state of high surface activity produced by sonication of phospholipids. *Biochim. Biophys. Acta.* **1191**, 343–353.
 51. Smith, R. and Tanford, C. (1972) Critical micelle concentration of L-alpha-dipalmitoylphosphatidylcholine in water and water/methanol solutions. *J. Mol. Biol.* **67**, 75–83.
 52. Altenbach, C. and Seelig, J. (1984) Ca-2+ Binding to phosphatidylcholine bilayers as studied by deuterium magnetic-resonance – evidence for the formation of a Ca-2+ complex with 2 phospholipid molecules. *Biochemistry* **23**, 3913–3920.
 53. Lewis, B.A. and Engelman, D.M. (1983) Lipid bilayer thickness varies linearly with acyl chain length in fluid phosphatidylcholine vesicles. *J. Mol. Biol.* **166**, 211–217.
 54. Santaren, J.F., Rico, M., Guilleme, J. and Ribera, A. (1982) Thermal and ¹³C-NMR study of the dynamic structure of 1-palmitoyl-2-oleyl-sn-glycero-3-phosphocholine and 1-oleyl-2-palmitoyl-sn-glycero-3-phosphocholine in aqueous dispersions. *Biochim. Biophys. Acta* **687**, 231–237.
 55. Cullis, P.R., Hope, M.J. and Tilcock, C.P. (1986) Lipid polymorphism and the roles of lipids in membranes. *Chem. Phys. Lipids* **40**, 127–144.
 56. Langner, M. and Hui, S.W. (1993) Dithionite penetration through phospholipid bilayers as a measure of defects in lipid molecular packing. *Chem. Phys. Lipids* **65**, 23–30.
 57. Fabrie, C.H., de Kruijff, B. and de Gier, J. (1990) Protection by sugars against phase transition-induced leak in hydrated dimyristoylphosphatidylcholine liposomes. *Biochim. Biophys. Acta* **1024**, 380–384.
 58. Volodkin, D., Mohwald, H., Voegel, J.C. and Ball, V. (2007) Coating of negatively charged liposomes by polylysine: drug release study. *J. Control. Release* **117**, 111–120.
 59. Marsh, D. (1996) Intrinsic curvature in normal and inverted lipid structures and in membranes. *Biophys. J.* **70**, 2248–2255.
 60. Felgner, J.H., Kumar, R., Sridhar, C.N., Wheeler, C.J., Tsai, Y.J., Border, R., Ramsey, P., Martin, M. and Felgner, P.L. (1994) Enhanced gene delivery and mechanism studies with a novel series of cationic lipid formulations. *J. Biol. Chem.* **269**, 2550–2561.
 61. Prochiantz, A. (1996) Getting hydrophilic compounds into cells: lessons from homeopeptides. *Curr. Opin. Neurobiol.* **6**, 629–634.
 62. Szoka, F. and Papahadjopoulos, D. (1980) Comparative properties and methods of preparation of lipid vesicles (liposomes). *Annu. Rev. Biophys. Biol.* **9**, 467–508.
 63. Fischer, A., Oberholzer, T. and Luisi, P.L. (2000) Giant vesicles as models to study the interactions between membranes and proteins. *Biochim. Biophys. Acta* **1467**, 177–188.

64. Elorza, B., Elorza, M.A., Sainz, M.C. and Chantres, J.R. (1993) Analysis of the particle size distribution and internal volume of liposomal preparations. *J. Pharm. Sci.* **82**, 1160–1163.
65. Seelig, A. (1987) Local anesthetics and pressure: a comparison of dibucaine binding to lipid monolayers and bilayers. *Biochim. Biophys. Acta* **899**, 196–204.
66. Herbig, M.E., Fromm, U., Leuenberger, J., Krauss, U., Beck-Sickinger, A.G. and Merkle, H.P. (2005) Bilayer interaction and localization of cell penetrating peptides with model membranes: a comparative study of a human calcitonin (hCT)-derived peptide with pVEC and pAntp(43–58). *Biochim. Biophys. Acta* **1712**, 197–211.
67. Michaelson, D.M., Horwitz, A.F. and Klein, M.P. (1973) Transbilayer asymmetry and surface homogeneity of mixed phospholipids in cosonicated vesicles. *Biochemistry* **12**, 2637–2645.
68. Wieprecht, T., Apostolov, O., Beyermann, M. and Seelig, J. (2000) Membrane binding and pore formation of the antibacterial peptide PGLa: thermodynamic and mechanistic aspects. *Biochemistry* **39**, 442–452.
69. Ruocco, M.J. and Shipley, G.G. (1982) Characterization of the sub-transition of hydrated dipalmitoylphosphatidylcholine bilayers – kinetic, hydration and structural study. *Biochim. Biophys. Acta* **691**, 309–320.
70. Zhou, Z., Sayer, B.G., Hughes, D.W., Stark, R.E. and Eband, R.M. (1999) Studies of phospholipid hydration by high-resolution magic-angle spinning nuclear magnetic resonance. *Biophys. J.* **76**, 387–399.
71. Newman, G.C. and Huang, C. (1975) Structural studies on phosphatidylcholine-cholesterol mixed vesicles. *Biochemistry* **14**, 3363–3370.
72. Bangham, A.D., Standish, M.M. and Watkins, J.C. (1965) Diffusion of univalent ions across lamellae of swollen phospholipids. *J. Mol. Biol.* **13**, 238–252.
73. Huang, C. (1969) Studies on phosphatidylcholine vesicles. Formation and physical characteristics. *Biochemistry* **8**, 344–352.
74. Hope, M.J., Bally, M.B., Webb, G. and Cullis, P.R. (1985) Production of large unilamellar vesicles by a rapid extrusion procedure – characterization of size distribution, trapped volume and ability to maintain a membrane-potential. *Biochim. Biophys. Acta* **812**, 55–65.
75. Kaasgaard, T., Mouritsen, O.G. and Jorgensen, K. (2003) Freeze/thaw effects on lipid-bilayer vesicles investigated by differential scanning calorimetry. *Biochim. Biophys. Acta* **1615**, 77–83.
76. Traikia, M., Warschawski, D.E., Recouvreur, M., Cartaud, J. and Devaux, P.F. (2000) Formation of unilamellar vesicles by repetitive freeze-thaw cycles: characterization by electron microscopy and ³¹P-nuclear magnetic resonance. *Eur. Biophys. J.* **29**, 184–195.
77. Larrabee, A.L. (1979) Time-dependent changes in the size distribution of distearoyl-phosphatidylcholine vesicles. *Biochemistry* **18**, 3321–3326.
78. Suurkuusk, J., Lentz, B.R., Barenholz, Y., Biltonen, R.L. and Thompson, T.E. (1976) Calorimetric and fluorescent-probe study of gel-liquid crystalline phase-transition in small, single-lamellar dipalmitoylphosphatidylcholine vesicles. *Biochemistry* **15**, 1393–1401.
79. Mayer, L.D., Hope, M.J. and Cullis, P.R. (1986) Vesicles of variable sizes produced by a rapid extrusion procedure. *Biochim. Biophys. Acta* **858**, 161–168.
80. Grit, M. and Crommelin, D.J.A. (1992) The effect of aging on the physical stability of liposome dispersions. *Chem. Phys. Lipids* **62**, 113–122.
81. Lasic, D.D. (1988) The mechanism of vesicle formation. *Biochem. J.* **256**, 1–11.
82. Petersen, N.O. and Chan, S.I. (1978) Effects of thermal prephase transition and salts on coagulation and flocculation of phosphatidylcholine bilayer vesicles. *Biochim. Biophys. Acta* **509**, 111–128.
83. Lichtenberg, D., Freire, E., Schmidt, C.F., Barenholz, Y., Felgner, P.L. and Thompson, T.E. (1981) Effect of surface curvature on stability, thermodynamic behavior, and osmotic activity of dipalmitoylphosphatidylcholine single lamellar vesicles. *Biochemistry* **20**, 3462–3467.
84. Winterhalter, M. and Lasic, D.D. (1993) Liposome stability and formation – experimental parameters and theories on the size distribution. *Chem. Phys. Lipids* **64**, 35–43.
85. Maulucci, G., De Spirito, M., Arcovito, G., Boffi, F., Castellano, A.C. and Briganti, G. (2005) Particle size distribution in DMPC vesicles solutions undergoing different sonication times. *Biophys. J.* **88**, 3545–3550.
86. Pereira-Lachataignerais, J., Pons, R., Panizza, P., Courbin, L., Rouch, J. and Lopez, O. (2006) Study and formation of vesicle systems with low polydispersity index by ultrasound method. *Chem. Phys. Lipids* **140**, 88–97.

87. Hauser, H.O. (1971) Effect of ultrasonic irradiation on chemical structure of egg lecithin. *Biochem. Biophys. Res. Commun.* **45**, 1049–1055.
88. Woodbury, D.J., Richardson, E.S., Grigg, A.W., Welling, R.D. and Knudson, B.H. (2006) Reducing liposome size with ultrasound: bimodal size distributions. *J. Liposome Res.* **16**, 57–80.
89. Frimer, A.A., Strul, G., Buch, J. and Gottlieb, H.E. (1996) Can superoxide organic chemistry be observed within the liposomal bilayer? *Free Radic. Biol. Med.* **20**, 843–852.
90. Andrews, S.B., Hoffman, R.M. and Borison, A. (1975) Variations of size and distribution in suspensions of sonicated phospholipid bilayers. *Biochem. Biophys. Res. Commun.* **65**, 913–920.
91. Yamaguchi, T., Nomura, M., Matsuoka, T. and Koda, S. (2009) Effects of frequency and power of ultrasound on the size reduction of liposome. *Chem. Phys. Lipids* **160**, 58–62.
92. Martin, F.J. and MacDonald, R.C. (1976) Phospholipid exchange between bilayer membrane vesicles. *Biochemistry* **15**, 321–327.
93. McCulloch, A. (2003) Chloroform in the environment: occurrence, sources, sinks and effects. *Chemosphere* **50**, 1291–1308.
94. Constan, A.A., Wong, B.A., Everitt, J.I. and Butterworth, B.E. (2002) Chloroform inhalation exposure conditions necessary to initiate liver toxicity in female B6C3F1 mice. *Toxicol. Sci.* **66**, 201–208.
95. Blixt, Y., Valeur, A. and Everitt, E. (1990) Cultivation of HeLa cells with fetal bovine serum or Ultrosor G: effects on the plasma membrane constitution. *In Vitro Cell Dev. Biol.* **26**, 691–700.
96. White, D.A. (1973) Phospholipid composition of mammalian tissue. In: Ansell, G.B., Hawthorne, J.A., and Dawson, R.M.C. (editors), 2nd ed., *Form and function of phospholipids*, Elsevier, Amsterdam, pp. 441–482.
97. Epand, R.M. and Epand, R.F. (2009) Lipid domains in bacterial membranes and the action of antimicrobial agents. *Biochim. Biophys. Acta* **1788**, 289–294.
98. Beining, P.R., Huff, E., Prescott, B. and Theodore, T.S. (1975) Characterization of the lipids of mesosomal vesicles and plasma membranes from *Staphylococcus aureus*. *J. Bacteriol.* **121**, 137–143.
99. Devaux, P.F. (1991) Static and dynamic lipid asymmetry in cell membranes. *Biochemistry* **30**, 1163–1173.
100. Martin, S.J., Reutelingsperger, C.P., McGahon, A.J., Rader, J.A., van Schie, R.C., LaFace, D.M. and Green, D.R. (1995) Early redistribution of plasma membrane phosphatidylserine is a general feature of apoptosis regardless of the initiating stimulus: inhibition by overexpression of Bcl-2 and Abl. *J. Exp. Med.* **182**, 1545–1556.
101. Ziegler, A., Blatter, X.L., Seelig, A. and Seelig, J. (2003) Protein transduction domains of HIV-1 and SIV TAT interact with charged lipid vesicles. Binding mechanism and thermodynamic analysis. *Biochemistry* **42**, 9185–9194.
102. Persson, D., Thoren, P.E., Lincoln, P. and Norden, B. (2004) Vesicle membrane interactions of penetratin analogues. *Biochemistry* **43**, 11045–11055.
103. Hristova, K. and Needham, D. (1994) The influence of polymer-grafted lipids on the physical-properties of lipid bilayers – a theoretical-study. *J. Colloid Interface Sci.* **168**, 302–314.
104. Tirosh, O., Barenholz, Y., Katzhendler, J. and Prieve, A. (1998) Hydration of polyethylene glycol-grafted liposomes. *Biophys. J.* **74**, 1371–1379.
105. Garbuzenko, O., Barenholz, Y. and Prieve, A. (2005) Effect of grafted PEG on liposome size and on compressibility and packing of lipid bilayer. *Chem. Phys. Lipids* **135**, 117–129.
106. Allende, D., Simon, S.A. and McIntosh, T.J. (2005) Melittin-induced bilayer leakage depends on lipid material properties: evidence for toroidal pores. *Biophys. J.* **88**, 1828–1837.
107. Kaasgaard, T., Mouritsen, O.G. and Jorgensen, K. (2001) Screening effect of PEG on avidin binding to liposome surface receptors. *Int. J. Pharm.* **214**, 63–65.
108. Itaya, K. and Ui, M. (1966) A new micromethod for the colorimetric determination of inorganic phosphate. *Clin. Chim. Acta* **14**, 361–366.
109. Baykov, A.A., Evtushenko, O.A. and Avaeva, S.M. (1988) A malachite green procedure for orthophosphate determination and its use in alkaline phosphatase-based enzyme immunoassay. *Anal. Biochem.* **171**, 266–270.
110. Vemuri, S. (2005) Comparison of assays for determination of peptide content for lyophilized thymalfasin. *J. Pept. Res.* **65**, 433–439.
111. Edelhoch, H. (1967) Spectroscopic determination of tryptophan and tyrosine in proteins. *Biochemistry* **6**, 1948–1954.
112. Ziegler, A. and Seelig, J. (2008) Binding and clustering of glycosaminoglycans: a common property of mono- and multivalent

- cell-penetrating compounds. *Biophys. J.* **94**, 2142–2149.
113. Schiffer, M. and Edmundson, A.B. (1967) Use of helical wheels to represent the structures of proteins and to identify segments with helical potential. *Biophys. J.* **7**, 121–135.
114. Iritani, N. and Miyahara, T. (1973) Determination of dissociation-constants of calcein by potentiometric method. *Jpn. Anal.* **22**, 174–178.
115. Wallach, D.F.H., Surgenor, D.M., Soderberg, J. and Delano, E. (1959) Preparation and properties of 3, 6-dihydroxy-2, 4-bis-(N, N'-di-(carboxymethyl)-aminomethyl) fluoran – utilization for the ultramicrodetermination of calcium. *Anal. Chem.* **31**, 456–460.
116. Niesman, M.R., Khoobehi, B. and Peyman, G.A. (1992) Encapsulation of sodium fluorescein for dye release studies. *Invest. Ophthalmol. Vis. Sci.* **33**, 2113–2119.
117. Garcia, M.A., Paje, S.E., Villegas, M.A. and Llopis, J. (2002) Preparation and characterization of calcein-doped thin coatings. *Appl. Phys. A Mater.* **74**, 83–88.
118. Aschi, M., D'Archivio, A.A., Fontana, A. and Formiglio, A. (2008) Physicochemical properties of fluorescent probes: experimental and computational determination of the overlapping pKa values of carboxyfluorescein. *J. Org. Chem.* **73**, 3411–3417.
119. Rothbard, J.B., Jessop, T.C., Lewis, R.S., Murray, B.A. and Wender, P.A. (2004) Role of membrane potential and hydrogen bonding in the mechanism of translocation of guanidinium-rich peptides into cells. *J. Am. Chem. Soc.* **126**, 9506–9507.
120. Chen, R.F. and Knutson, J.R. (1988) Mechanism of fluorescence concentration quenching of carboxyfluorescein in liposomes: energy transfer to nonfluorescent dimers. *Anal. Biochem.* **172**, 61–77.
121. Gavino, V.C., Miller, J.S., Dillman, J.M., Milo, G.E. and Cornwell, D.G. (1981) Polyunsaturated fatty acid accumulation in the lipids of cultured fibroblasts and smooth muscle cells. *J. Lipid Res.* **22**, 57–62.
122. Seelig, J. (1978) P-31 Nuclear magnetic-resonance and head group structure of phospholipids in membranes. *Biochim. Biophys. Acta* **515**, 105–140.
123. Soubias, O. and Gawrisch, K. (2007) Nuclear magnetic resonance investigation of oriented lipid membranes. *Methods Mol. Biol.* **400**, 77–88.
124. Seelig, J. (2004) Thermodynamics of lipid-peptide interactions. *Biochim. Biophys. Acta.* **1666**, 40–50.
125. Persson, D., Thoren, P.E., Herner, M., Lincoln, P. and Norden, B. (2003) Application of a novel analysis to measure the binding of the membrane-translocating peptide penetratin to negatively charged liposomes. *Biochemistry* **42**, 421–429.
126. Beschiaschvili, G. and Seelig, J. (1990) Peptide binding to lipid bilayers. Binding isotherms and zeta-potential of a cyclic somatostatin analogue. *Biochemistry* **29**, 10995–11000.
127. Franzin, C.M. and Macdonald, P.M. (2001) Polylysine-induced ²H NMR-observable domains in phosphatidylserine/phosphatidylcholine lipid bilayers. *Biophys. J.* **81**, 3346–3362.
128. Macdonald, P.M., Crowell, K.J., Franzin, C.M., Mitrakos, P. and Semchyschyn, D. (2000) ²H NMR and polyelectrolyte-induced domains in lipid bilayers. *Solid State Nucl. Magn. Reson.* **16**, 21–36.
129. Dennison, S.R., Baker, R.D., Nicholl, I.D. and Phoenix, D.A. (2007) Interactions of cell penetrating peptide Tat with model membranes: a biophysical study. *Biochem. Biophys. Res. Commun.* **363**, 178–182.
130. Baker, B.M. and Murphy, K.P. (1996) Evaluation of linked protonation effects in protein binding reactions using isothermal titration calorimetry. *Biophys. J.* **71**, 2049–2055.
131. Yi, D., Guoming, L., Gao, L. and Wei, L. (2007) Interaction of arginine oligomer with model membrane. *Biochem. Biophys. Res. Commun.* **359**, 1024–1029.
132. Kramer, S.D. and Wunderli-Allenspach, H. (2003) No entry for TAT(44–57) into liposomes and intact MDCK cells: novel approach to study membrane permeation of cell-penetrating peptides. *Biochim. Biophys. Acta.* **1609**, 161–169.
133. Thoren, P.E., Persson, D., Lincoln, P. and Norden, B. (2005) Membrane destabilizing properties of cell-penetrating peptides. *Biophys. Chem.* **114**, 169–179.
134. Lamaziere, A., Burlina, F., Wolf, C., Chassaing, G., Trugnan, G. and Ayala-Sanmartin, J. (2007) Non-metabolic membrane tubulation and permeability induced by bioactive peptides. *PLoS One* **2**, e201.
135. Fuchs, S.M. and Raines, R.T. (2004) Pathway for polyarginine entry into mammalian cells. *Biochemistry* **43**, 2438–2444.

Chapter 11

Calcium and Membrane Repair

Caroline Palm-Apergi and Mattias Hällbrink

Abstract

As more and more studies utilize cell-penetrating peptides to deliver pharmacologically interesting substances, there is a growing need to understand their effect on the plasma membrane. If a cell-penetrating peptide together with its cargo is to be used as a drug, it is necessary to understand how the conjugate interacts with the plasma membrane to enter the cell. A key regulator of the transportation network in the cell is calcium. This chapter describes five methods that can be employed for understanding how the plasma membrane reacts to the presence of cell-penetrating peptides and the involvement of calcium.

Key words: CPP, PTD, Membrane repair response, FURA-2, Propidium iodide, LAMP-2

1. Introduction

The mechanism of cell-penetrating peptides (CPPs) or protein transduction domains (PTDs) has been studied intensely. Several studies have suggested macropinocytosis as the possible uptake mechanism (1, 2). However, there is evidence for other uptake pathways, such as clathrin-dependent endocytosis (3), or that different forms of endocytosis function simultaneously (4, 5) and by blocking one pathway other pathways become more active. It has been shown that uptake is concentration dependent and that the peptides may use two pathways: endocytosis at low concentrations and direct penetration at high concentrations (6). Furthermore, the size of the cargo plays a significant role in translocation and uptake can be divided into at least two functionally distinct uptake mechanisms (7). Thus, it is important to understand how the peptide alone interacts with the plasma membrane.

When the plasma membrane of the cell is exposed to mechanical trauma or stress from the surrounding environment, a repair

system called cellular wound-healing or membrane repair response (MRR) is triggered. The MRR is activated by the local influx of calcium at the site of disruption which in turn leads to mobilization of intracellular vesicles such as endosomes and lysosomes to the plasma membrane to donate their membrane in order to repair the damage (8–11). Even liposomes are able to reseal as the unfavorable energetic state, caused by the exposure of hydrophobic backbone to the hydrophilic solute, results in an increase in free energy promoting resealing (10).

When CPPs bind the cell surface, there will most likely be an increased local concentration of peptides at the plasma membrane which could induce endocytosis. Concurrently the local increase in peptide concentration could cause a mass imbalance followed by a direct translocation (12) or by disrupting the plasma membrane locally, thus inducing membrane resealing and activating the MRR. Since the calcium influx triggers the resealing within seconds, this would explain why no leakage of cytoplasmic contents upon CPP uptake is detected, even though there seems to be a membrane disturbance caused by the peptides. Higher disturbances in the plasma membrane caused by accumulation of peptides are masked and resealed, up to a certain limit, by lysosomal patching induced by the calcium influx and MRR mechanism.

In this chapter, five methods are described that can be used to analyze the effects of CPPs on the plasma membrane and the involvement of calcium and the MRR. The lactate dehydrogenase (LDH) leakage assay is suitable for detecting larger holes in the plasma membrane that eventually could lead to necrosis. The intracellular calcium measurement is a more sensitive method, able to detect much smaller plasma membrane disturbances. Another sensitive assay is the quantification of the lysosomal enzyme β -hexosaminidase (13). This enzyme is situated inside lysosomes and after membrane trauma, it is found outside the cellular membrane as a result of lysosomes being exocytosed in order to reseal the membrane. Furthermore, the exocytosis of lysosomes can be visualized by fluorescence microscopy, by employing antibodies against the lysosomal-associated membrane protein CD107b (LAMP-2) that is not present on the plasma membrane normally. Finally, an HPLC-based method is described, which can be used to assess the importance of calcium during translocation.

2. Materials

2.1. LDH Leakage Assay

1. HeLa or CHO-K1 cells cultured in Dulbecco's Modified Eagle's Media (DMEM) or DMEM/F-12 with Glutamax-I supplemented with 10% FBS, 1% nonessential amino acids, 1% sodium pyruvate, 100 μ g/ml streptomycin, 100 U/ml penicillin.

2. 96-Well culture plates.
3. HEPES-Krebs-Ringer (HKR) buffer (125 mM NaCl, 5 mM KCl, 1.2 mM MgSO₄ · 7H₂O, 1 mM CaCl₂ · 2H₂O, 1.2 mM KH₂PO₄, 25 mM HEPES, 6 mM glucose, pH 7.4) supplemented with 1 g/l D-glucose.
4. Triton-X 200 as positive control.
5. Promega CytoTox-ONE™ assay (Promega).
6. FlexStation II fluorometer (Molecular Devices, USA).

2.2. Intracellular Calcium Measurements

1. HeLa cells cultured in DMEM Glutamax-I supplemented with 10% FBS, 1% nonessential amino acids, 1% sodium pyruvate, 100 µg/ml streptomycin, 100 U/ml penicillin.
2. 96-Well culture plates.
3. HKR buffer supplemented with 1 g/l D-glucose.
4. FURA-2 AM.
5. Ionomycin as positive control.
6. FlexStation II fluorometer (Molecular Devices, USA).

2.3. B-Hexosaminidase Efflux Assay

1. HeLa or CHO-K1 cells cultured in DMEM or DMEM/F-12 with Glutamax-I supplemented with 10% FBS, 1% nonessential amino acids, 1% sodium pyruvate, 100 µg/ml streptomycin, 100 U/ml penicillin.
2. 24-Well culture plates.
3. HKR buffer supplemented with 1 g/l D-glucose.
4. 1 mM 4-methylumbelliferyl N-acetyl-β-D-glucosamide in 0.1 M sodium citrate buffer, pH 4.5.
5. K₂CO₃ buffer (pH 10.5).
6. FlexStation II fluorometer (Molecular Devices, USA).

2.4. Immunohistochemistry Analysis of Translocation of LAMP-2 to the Plasma Membrane

1. HeLa or CHO-K1 cells cultured in DMEM or DMEM/F-12 with Glutamax-I supplemented with 10% FBS, 1% nonessential amino acids, 1% sodium pyruvate, 100 µg/ml streptomycin, 100 U/ml penicillin.
2. 24-Well culture plates.
3. PBS buffer supplemented with 1 g/l D-glucose.
4. 3% paraformaldehyde in phosphate buffer (0.1 M, pH 7.4).
5. Methanol.
6. LAMP-2 monoclonal antibody (H4B4, DSHB, 1:100).
7. Alexa Flour 488 (or 555)-conjugated goat anti-mouse antibody (Invitrogen, 1:400).
8. Perforin (0.1–0.8 µg/ml) as positive control.
9. 10% nonfat dry milk in PBS.

10. 1 µg/ml propidium iodide.
11. Olympus BX61 microscope equipped with CCD camera DP70 or Olympus FV1000 confocal microscope.

2.5. HPLC Analysis of CPP Uptake

1. HeLa or CHO-K1 cells cultured in DMEM or DMEM/F-12 with Glutamax-I supplemented with 10% FBS, 1% nonessential amino acids, 1% sodium pyruvate, 100 µg/ml streptomycin, 100 U/ml penicillin.
2. 24-Well culture plates.
3. HKR buffer supplemented with 1 g/l D-glucose.
4. 0.1% Triton X-100 containing 0.1% trifluoroacetic acid.
5. 400 µl ethanol/water 1/1 v/v containing 2-nitroaniline (0.06 M) and HCl (0.125 M).
6. 50 µl 0.6 M NaNO₂.
7. HPLC coupled to a fluorescence detector.

3. Methods

It is crucial to understand how the cell responds to injury or trauma in order to comprehend the effects the CPPs have on the plasma membrane. When the plasma membrane of the cell is injured, extracellular calcium ions leak into the cytoplasm and activate the MRR. The local increase in cytosolic calcium, caused by the disruption, activates a resealing mechanism that induces exocytosis of intracellular vesicles, which fuse with the broken plasma membrane and reseal it within seconds (10). Lysosomes are believed to be the major contributor to plasma membrane resealing (14) and microinjected antibodies against LAMP-1 cytoplasmic domain have been shown to inhibit resealing and exocytosis of lysosomes due to aggregation (15).

The first method describes the measurement of LDH leakage, an indicative that the membrane damage is too severe for the cell to repair. Although the LDH molecule is large, the test correlates with leakage of even smaller molecules such as deoxyglucose (16, 17). In the second method, a fluorescent dye that fluoresces when it is bound to calcium is utilized to measure calcium influx into the cell. The dye, FURA-2, is modified by an acetomethoxy group that enables it to penetrate the cell membrane. However, well inside the cell, the acetomethoxy group is cleaved off. Therefore FURA-2 cannot exit the cell. As the concentration is approximately 10,000-fold higher outside the cell compared with the inside, even a small increase in calcium can be detected. Thus, the method is highly suitable for detecting membrane disturbances.

A sensitive indication of lysosomal exocytosis is the release of β -hexosaminidase. During exocytosis, β -hexosaminidase is released into the extracellular media as the lysosome donates its membrane and subsequently releases its contents to the extracellular surroundings. The third method exploits the β -hexosaminidase activity, which leads to the conversion of 4-methylumbelliferyl 1-2-acetamido-2-deoxy- β -D-glucopyranoside to 4-methylumbelliferone and can be measured colorimetrically. A significant increase of β -hexosaminidase extracellular activity can be measured at peptide concentrations much lower than those needed for LDH detection.

The fourth method can be utilized to investigate if the MRR is activated during CPP translocation. Antibodies against intraluminal lysosomal proteins on the plasma membrane, e.g., LAMP-2 are used to detect the presence of intraluminal proteins on the plasma membrane. If LAMP-2 is found on the extracellular side of the cell, it indicates that exocytosis occurred most probably due to MRR activation.

The final method analyzes the involvement of calcium during translocation. If there is no calcium in the extracellular media, the MRR will not be activated and therefore the amount of translocated peptide will increase. However, if the extracellular calcium concentration increases the MRR will be activated more efficiently, resulting in less translocated peptide. These methods are good indicators of how the CPP affects the plasma membrane and if calcium or the MRR are involved in translocation (18).

3.1. LDH Leakage Assay

1. Seed 20,000 cells/well HeLa or CHO-K1 cells in 96-well plates in 100 μ l medium in triplicates 1 day before analysis.
2. Wash the cells with HKR buffer supplemented with 1 g/l D-glucose two times.
3. Incubate the cells with 100 μ l peptide dissolved in HKR buffer supplemented with 1 g/l D-glucose at 37°C cells for 25 min.
4. Take 80 μ l of incubation media and add to 80 μ l of CytoTox-ONE™ reagent in a black 96-well plate and incubate at 21°C for 10 min.
5. Measure fluorescence at 560/590 nm.
6. Untreated cells are defined as no leakage and total LDH release by lysing cells with 0.1% Triton X-100 is defined as 100% leakage.

3.2. Intracellular Calcium Measurements

1. Seed 20,000 cells/well HeLa cells in 96-well plates in 100 μ l medium in triplicates 1 day before analysis.
2. Add FURA-2 AM to the medium to a final concentration of 2 μ M and incubate for 30 min at 37°C.

3. Replace the medium with HKR buffer and incubate for an additional 15 min.
4. Measure the ratio of $340_{(\text{calcium-bound FURA-2})}/380_{(\text{FURA-2})}$ nm excitatory wavelengths at 510 nm in FlexStation II fluorometer (Molecular Devices, USA) after the peptide is automatically added (see Note 1).
5. Use 4 s interval 17 s before and 5 or 30 min after the addition of peptide.
6. Untreated cells and cells treated with 10 μM ionomycin are used as controls.

3.3. B-Hexosaminidase Efflux Assay

1. Seed cells in 24-well plates 2 days before analysis.
2. Wash cells twice with HKR buffer.
3. Add 200 μl peptide dissolved in HKR buffer supplemented with 1 g/l D-glucose to cells and incubate for 1 h in 37°C.
4. Transfer 10 μl of cell-exposed buffer into 96-well plates.
5. Add 50 μl 1 mM 4-methylumbelliferyl *N*-acetyl- β -D-glucosamide in 0.1 M sodium citrate buffer, pH 4.5 and incubate for 1 h at 37°C.
6. Add 150 μl of K_2CO_3 buffer (pH 10.5) and measure β -hexosaminidase activity at 365/445 nm em/ex in fluorometer.

3.4. Immunohistochemistry Analysis of Translocation of LAMP-2 to the Plasma Membrane

1. Seed 50,000 HeLa cells/well in 24-well plates on glass cover slips 2 days before analysis.
2. Wash the cells twice with serum-free media.
3. Add 400 μl peptide and incubate in serum-free media for 30 min at 37°C.
4. Wash the cells two times with PBS.
5. Fix the cells with 3% paraformaldehyde in phosphate buffer (0.1 M, pH 7.4) for 30 min (see Note 2).
6. Wash the cells two times with PBS.
7. Permeabilize the control cells with methanol at -20°C for 15 min (see Note 3).
8. Block with 10% nonfat dry milk in PBS for 1 h.
9. Add 30 μl LAMP-2 monoclonal antibody (H4B4, DSHB, 1:100) in Milk/PBS 1:2 to parafilm.
10. Add the glass slide and incubate for 1 h.
11. Wash the cells three times with PBS.
12. Add 30 μl Alexa Flour 488 (or 555)-conjugated goat anti-mouse antibody (Invitrogen, 1:400) in Milk/PBS 1:2 to parafilm.
13. Add the glass slide and incubate 30 min at room temperature in dark.

14. Wash the cells three times for 10 min with PBS.
15. Mount the glass slides onto a cover slip with Fluoromount G (Electron Microscopy Sciences, PA, USA).
16. Analyze the LAMP-2 translocation by fluorescence microscopy.

3.5. HPLC Analysis of CPP Uptake

1. Seed 100,000 HeLa or CHO-K1 cells/well in 24-well plates in 500 μ l medium in triplicates 1 day before analysis.
2. Wash the cells two times with HKR buffer containing different calcium concentrations.
3. Incubate the cells with 200 μ l peptide dissolved in HKR buffer supplemented with 1 g/l D-glucose at 37°C for 1 h.
4. Prepare 400 μ l ethanol/water 1/1 v/v containing 2-nitroaniline (0.06 M) and HCl (0.125 M) (see Note 4).
5. Prepare fresh 50 μ l 0.6 M NaNO₂.
6. Put cells on ice and wash the cells two times with ice-cold HKR buffer containing different calcium concentrations (see Note 5).
7. Add 500 μ l ice-cold HKR buffer containing different calcium concentrations to cells.
8. Mix 50 μ l 0.6 M NaNO₂ with 2-nitroaniline solution (step 4) and let stand for 5 min at ambient temperature.
9. Add 10 μ l of this reagent to the cells in ice-cold HKR covering the cell layer and allow to react for 10 min at 0°C.
10. Aspirate the diazo reagent and wash the cells two times with ice-cold HKR.
11. Lyse cells with 200 μ l 0.1% Triton X-100 containing 0.1% trifluoroacetic acid for 2 h at 0°C.
12. Transfer 180 μ l lysate to a HPLC tube and add 180 μ l water containing 0.1% trifluoroacetic acid.
13. Analyze lysate by HPLC coupled to a fluorescence detector.
14. 10 pmol of parent peptide is used for quantification.

4. Notes

1. Peptide solutions should be prepared in HKR buffer supplemented with 1 g/l D-glucose before experiment and placed in spectrophotometer during the 15 min incubation.
2. Supplement the solution of secondary antibody with 1 μ g/ml propidium iodide to assess that the plasma membrane is intact.
3. This is done to expose all intracellular LAMP-2 antigens.

4. Dissolve 2-nitroaniline in ethanol first then add water.
5. From now on it is important to keep everything on ice.

Acknowledgments

This work was supported by the Jeansson foundation.

References

1. Kaplan, I. M., Wadia, J. S., and Dowdy, S. F. (2005) Cationic TAT peptide transduction domain enters cells by macropinocytosis. *J Control Release* **102**, 247–253.
2. Nakase, I., Tadokoro, A., Kawabata, N., Takeuchi, T., Katoh, H., Hiramoto, K., Negishi, M., Nomizu, M., Sugiura, Y., and Futaki, S. (2007) Interaction of arginine-rich peptides with membrane-associated proteoglycans is crucial for induction of actin organization and macropinocytosis. *Biochemistry* **46**, 492–501.
3. Richard, J. P., Melikov, K., Brooks, H., Prevot, P., Lebleu, B., and Chernomordik, L. V. (2005) Cellular uptake of unconjugated TAT peptide involves clathrin-dependent endocytosis and heparan sulfate receptors. *J Biol Chem* **280**, 15300–15306.
4. Duchardt, F., Fotin-Mleczek, M., Schwarz, H., Fischer, R., and Brock, R. (2007) A comprehensive model for the cellular uptake of cationic cell-penetrating peptides. *Traffic* **8**, 848–866.
5. Padari, K., Säälük, P., Hansen, M., Koppel, K., Raid, R., Langel, Ü., and Pooga, M. (2005) Cell transduction pathways of transportans. *Bioconjug Chem* **16**, 1399–1410.
6. Fretz, M. M., Penning, N. A., Al-Taei, S., Futaki, S., Takeuchi, T., Nakase, I., Storm, G., and Jones, A. T. (2007) Temperature-, concentration- and cholesterol-dependent translocation of L- and D-octa-arginine across the plasma and nuclear membrane of CD34+ leukaemia cells. *Biochem J* **403**, 335–342.
7. Tünnemann, G., Martin, R. M., Haupt, S., Patsch, C., Edenhofer, F., and Cardoso, M. C. (2006) Cargo-dependent mode of uptake and bioavailability of TAT-containing proteins and peptides in living cells. *FASEB J* **20**, 1775–1784.
8. Bi, G. Q., Alderton, J. M., and Steinhardt, R. A. (1995) Calcium-regulated exocytosis is required for cell membrane resealing. *J Cell Biol* **131**, 1747–1758.
9. Togo, T., Alderton, J. M., Bi, G. Q., and Steinhardt, R. A. (1999) The mechanism of facilitated cell membrane resealing. *J Cell Sci* **112**, 719–731.
10. McNeil, P. L. and Steinhardt, R. A. (2003) Plasma membrane disruption: repair, prevention, adaptation. *Annu Rev Cell Dev Biol* **19**, 697–731.
11. Miyake, K. and McNeil, P. L. (1995) Vesicle accumulation and exocytosis at sites of plasma membrane disruption. *J Cell Biol* **131**, 1737–1745.
12. Yandek, L. E., Pokorny, A., Floren, A., Knoelke, K., Langel, Ü., and Almeida, P. F. (2007) Mechanism of the cell-penetrating peptide transportan 10 permeation of lipid bilayers. *Biophys J* **92**, 2434–2444.
13. Howl, J., Jones, S., and Farquhar, M. (2003) Intracellular delivery of bioactive peptides to RBL-2H3 cells induces beta-hexosaminidase secretion and phospholipase D activation. *ChemBiochem* **4**, 1312–1316.
14. McNeil, P. L. (2002) Repairing a torn cell surface: make way, lysosomes to the rescue. *J Cell Sci* **115**, 873–879.
15. Reddy, A., Caler, E. V., and Andrews, N. W. (2001) Plasma membrane repair is mediated by Ca(2+)-regulated exocytosis of lysosomes. *Cell* **106**, 157–169.
16. Saar, K., Lindgren, M., Hansen, M., Eiriksdottir, E., Jiang, Y., Rosenthal-Aizman, K., Sassian, M., and Langel, Ü. (2005) Cell-penetrating peptides: a comparative membrane toxicity study. *Anal Biochem* **345**, 55–65.
17. Johansson, H. J., El Andaloussi, S., Holm, T., Mäe, M., Jänes, J., Maimets, T., and Langel, Ü. (2008) Characterization of a novel cytotoxic cell-penetrating peptide derived from p14ARF protein. *Mol Ther* **16**, 115–123.
18. Palm-Apergi, C., Lorents, A., Padari, K., Pooga, M., and Hällbrink, M. (2009) The membrane repair response masks membrane disturbances caused by cell-penetrating peptide uptake. *FASEB J* **23**, 214–223.

Chapter 12

Mapping of Protein Transduction Pathways with Fluorescent Microscopy

Helin Räägel, Pille Säälük, Ülo Langel, and Margus Pooga

Abstract

The number of various cargo delivered into cells by CPPs demonstrates the effective transport abilities of these short-peptidic sequences. Over the years of research, the translocation process of CPP–cargo complexes has been mapped to being of mostly endocytic nature, however, there is still no consensus on which of the endocytic routes is prevalent and to which extent the interplay between different modes of endocytosis is taking place. The intracellular trafficking of CPPs attached to a cargo molecule is even less understood. Therefore, the internalization and the subsequent intracellular targeting of complexes need clarification in order to define cellular destinations and improve the targeting of the cargo molecule to specific cellular compartments depending on the cargo attached to the transporting vector. This chapter focuses on describing the methods for visualizing the CPP–protein complexes in relation to different endocytic markers, for example transferrin (marker for clathrin-mediated endocytosis) and cholera toxin (ambiguous marker for clathrin-, caveolin-, and flotillin-mediated, but also clathrin- and caveolin-independent endocytosis) to determine the role of the respective pathways during entry to cells, and to different intracellular targets, for instance the lysosomal organelles or the Golgi apparatus. Additionally, antibody staining of respective endocytic vesicles following the internalization of CPP–protein complexes will be discussed.

Key words: Cell-penetrating peptide, Fluorescence microscopy, Protein transduction, Endocytosis, Intracellular trafficking

1. Introduction

The vast number of reports on cell-penetrating peptides (CPPs) being capable of mediating the effective delivery of bioactive cargo both in vitro and in vivo (1–3) has proven their potential as efficient drug delivery vehicles. However, before these promising transport vectors can be used in therapeutic biomedicine, their mechanism of entry and especially intracellular targeting need to be elucidated to ensure that the cargo reaches its required target(s) inside necessary cellular compartment(s).

The primary interaction of the CPP–protein complexes with the plasma membrane of cells involves anchoring to the negatively charged components of the extracellular matrix, for instance heparan sulfate proteoglycans (HSPGs), followed by the induction of endocytosis (4). The information about the subsequent endocytic pathways triggered by the CPP–protein complexes is to this day ambivalent and contradictory since different reports argue for different internalization mechanism(s). For example, clathrin-dependent endocytosis (5), caveolin-dependent endocytosis (6), and macropinocytosis (7) have been proposed to participate in the uptake of CPP–protein complexes to a higher extent. However, it is important to keep in mind that the endocytic route preferred by specific CPP–protein complexes depends highly on the CPP, its concentration and even the properties of the cargo molecule may affect the relevance of different internalization modes during uptake (8, 9).

Once inside the cells, the CPP–protein complexes bypass the recycling endosomes and most of the complexes are trafficked through the endo-lysosomal pathway inside vesicles with varying pH (10). During longer incubation periods, it has been demonstrated that CPPs complexed to a protein cargo are targeted to LAMP-2-labeled degradative organelles (10, 11), but in spite of that, a considerable amount of CPP–protein is detected inside nonacidic vesicles even after 12 h incubation (10). The targeting of CPP–protein complexes to a specific cellular compartment, for example the nucleus, has been shown for some complexes (12), however, the release of the complexes from the entrapping endocytic vesicles is today considered to be the limiting step in CPP-mediated delivery of bioactive cargo molecules.

The analysis of the impact of different endocytic pathways on CPP–protein uptake is done using colocalization studies preferably with live-cell imaging to avoid artifacts of fixation and to get a better picture of what is happening to the complexes inside the cells. Transferrin along with CPP–cargo complexes is used to map the involvement of the clathrin-dependent endocytosis, while cholera toxin is a more ambiguous marker and therefore used to follow vesicles of various origins, that is, formed during clathrin-, caveolin-, and flotillin-mediated but also clathrin- and caveolin-independent endocytosis. Also, the use of fluorescent fusion protein (GFP, YFP, RFP, etc.) constructs of molecules under investigation in transfected cells has been very popular in studying the internalization and intracellular trafficking of CPP–protein complexes. However, the outcome of such experiments depends highly on the specificity, expression level, and accurate localization of the specific fusion protein, thus, it will not be discussed here.

In addition to fluorescence microscopy, the roles of different endocytic routes can be explored by siRNA treatment, where cells are transfected with small RNA dimers, which bind to readily synthesized complementary cellular mRNA, mediate the cleavage

of the oligonucleotide and the subsequent downregulation of the protein of interest (13). This technique allows specific inhibition of distinct endocytic pathways by interfering, for example, with the formation of vesicles requiring the activity or the presence of the particular protein, giving therefore adequate and detailed information about the processes involved in CPP–cargo uptake. However, downregulation of one pathway may activate other entry routes, thus creating false results and underestimations of contributions of specific pathways.

Additionally, the intracellular trafficking of the complexes can be studied using live cell fluorescent probes, for instance LysoSensor for detecting pH drops in endocytic vesicles and ceramide for marking the Golgi apparatus. However, many colocalization experiments are performed using specific antibody staining, which requires fixation of cells, but in return provides numerous possibilities for determining the actual content and entity of the complexes-containing vesicles.

Because of the disadvantages of each particular method, it is important to use different approaches in parallel in order to extract adequate experimental data for further analysis.

2. Materials

2.1. Cell Culture

The following methods can be used in a variety of different cell lines, however, some cell lines are preferred for a particular set of experiments. For example, we recommend using Cos cells derived from the African green monkey kidney cells for visualization of the intracellular pathways (i.e., with LysoSensor), since in Cos cells the recycling and the endo-lysosomal pathways are spatially segregated by the Golgi ring (14) and not as intermixed as in the commonly used HeLa cell line derived from the human cervical carcinoma cells. The present chapter will provide protocols for HeLa and Cos cells, nevertheless, these methods can be applied to other cells as well, for example, NIH 3T3 cells originating from Swiss mouse embryonic fibroblasts are often used for studying the actin cytoskeleton (a method also provided in this chapter).

HeLa or Cos cells cultured in Iscove's Modified Dulbecco's Medium (IMDM) supplemented with 10% fetal bovine serum (FBS), 100 IU/ml penicillin, and 100 µg/ml streptomycin were conventionally used if not stated otherwise.

2.2. Peptides and Cargo Proteins

Various strategies have been used to attach the cargo molecules to CPPs, for example via a reducible disulfide bridge, covalent linkage or by adding the CPP motif to the protein sequence and expressing the fusion protein. The easiest method for complex creation is achieved by simple mixing of CPPs with the desirable cargo, however, this approach requires high affinity of the cargo

molecule to the carrier peptide. The CPP–protein complexes used in the following protocols are formed by mixing of biotinylated CPPs (CPPb) with fluorescently labeled avidin protein (in 3:1 ratio) to ensure binding of all the peptide to the cargo without excess free CPPs in the solution (see Note 1).

Tip: To prevent the degradation and aggregation of CPPs in solution, we recommend aliquoting the water-diluted CPPs and storing at -20°C for longer periods. It is important to avoid repeated freeze–thaw cycles.

2.3. Fixation of Cells

For antibody staining of different endocytic vesicles or intracellular organelles, cells need to be fixed in order to generate a free passage of the antibody molecules into the cell interior. Fixation can be performed with paraformaldehyde, PLP-fixative or methanol, while keeping in mind that depending on the antibody and the localization of the original antigen of interest, one method could result in better recognition than the other.

2.3.1. Paraformaldehyde Fixation

1. 4% Paraformaldehyde in PBS.
2. 0.1% Triton X-100 in PBS for permeabilization [i.e., for anti-caveolin antibody (cat no 610059, BD Transduction Laboratories, Belgium)].

2.3.2. PLP Fixation (Milder Fixation, but Fresh Fixative Has to Be Prepared Each Time)

1. 2% Paraformaldehyde, 75 mM lysine-HCl, and 10 mM sodium periodate in 75 mM phosphate buffer, pH 7.4. Note that the solution of 75 mM lysine-HCl (pH 7.4) is stable for a month.

For permeabilization:

2. 0.5% Saponin in PBS [for anti-PI3P antibody (Echelon Biosciences, UT)] or,
3. 0.01% Saponin in 0.1% bovine serum albumin (BSA) containing PBS solution [for anti-flotillin-1 (Santa Cruz Biotechnology, CA), anti- β 1 integrin (anti-CD29, BD Transduction Laboratories), and anti-Rab5 (Abcam, UK)], which concurrently acts also as a blocking solution.

2.3.3. Methanol Fixation

Methanol fixation is performed with 100% methanol at -20°C .

2.4. Fluorescent Markers and Antibodies for Staining Cellular Organelles

2.4.1. Fluorescent Markers for Live-Cell Imaging

Numerous fluorescent probes exist for visualizing different cellular organelles, still, a lot of them have drawbacks in specificity and performance (see Note 2). Some of the successfully used chemicals are described below.

1. Phosphate-buffered saline (PBS: 137 mM NaCl, 10 mM Na_2HPO_4 , 2.7 mM KCl, pH 7.4).
2. Eight-well chambered coverglasses (Lab-Tek, #155411, Nalge Nunc International, NY) (see Note 3).

3. IMDM supplemented with 100 IU/ml penicillin and 100 µg/ml streptomycin without FBS for incubation of cells with CPP-protein constructs and fluorescent probes (see Note 4).
4. LysoSensor DND-189 (2 µM) (Molecular Probes, Invitrogen, UK) for visualizing the endo-lysosomal pathway and estimating the pH of the endocytic vesicles.
5. Bodipy-TR-C₅ ceramide (0.5 µM, prepared according to the manufacturer's instructions) (Molecular Probes, Invitrogen, UK) for labeling of the Golgi complex.
6. Transferrin labeled with Alexa Fluor 594 (25 µg/ml) (Invitrogen, UK) for mapping the clathrin-mediated endocytosis or,
7. Cholera toxin B subunit labeled, that is, with Alexa Fluor 594 (3 µg/ml) (Invitrogen, UK) for following the caveolin- and flotillin-mediated and clathrin- and caveolin-independent pathways.

2.4.2. Antibody Staining on Fixed Cells

1. HeLa or Cos cells grown in IMDM supplemented with 10% FBS, 100 IU/ml penicillin, and 100 µg/ml streptomycin.
2. 24-Well plates (Greiner BioOne, Germany).
3. Round glass coverslips (Ø 12 mm, no. 1, Menzel-Gläzer, Germany).
4. IMDM supplemented with 100 IU/ml penicillin and 100 µg/ml streptomycin without FBS for incubation of cells with CPP-protein constructs (see Note 4).
5. For fixation of cells, choose the fixation method suitable for the used antibody (see [Subheading 2.3](#)).
6. 10% nonfat dry milk (NFDM) in PBS for blocking of the nonspecific binding sites in the cells (this step can be skipped when using PLP fixation and 0.01% saponin in 0.1% BSA containing PBS solution).
7. Primary antibody against the antigens of interest, for instance hybridoma supernatant solution of LAMP-2 (DSHB, University of Iowa, IA) for visualization of lysosomes, anti-TGN46 (Abcam, UK) for marking of the *trans*-Golgi network and anti-Rab5 (Abcam, UK), anti-flotillin (Santa Cruz Biotechnology, CA), anti-caveolin (cat no 610059, BD Transduction Laboratories, Belgium), and anti-PI3P (Echelon Biosciences, UT) for detecting the corresponding endocytic vesicles.
8. Secondary antibody against the primary antibody used, for instance, anti-Rabbit-Alexa Fluor 488 (Molecular Probes, Invitrogen, UK).
9. Phosphate-buffered saline (PBS).
10. Parafilm.

11. Specimen glasses (Menzel-Gläzer, Germany) for mounting of the coverglasses.
12. 30% Glycerol in PBS for mounting.
13. Colorless nail polish for sealing the edges of the coverglasses.

2.4.3. Staining of the Actin Cytoskeleton

1. HeLa or NIH 3T3 cells grown in IMDM supplemented with 10% FBS, 100 IU/ml penicillin, and 100 µg/ml streptomycin.
2. 24-Well plates (Greiner BioOne, Germany).
3. Round glass coverslips (Ø 12 mm, no. 1, Menzel-Gläzer, Germany).
4. IMDM supplemented with 100 IU/ml penicillin and 100 µg/ml streptomycin without FBS for incubation of cells with CPP-protein constructs (see Note 4).
5. 4% Paraformaldehyde in PBS for fixation.
6. 0.1% Triton X-100 in PBS for permeabilization.
7. 10% NFDm in PBS for blocking of nonspecific binding sites in cells.
8. Phalloidin labeled with a fluorescent dye, for example phalloidin-Alexa Fluor 594.
9. Parafilm.
10. PBS.
11. Specimen glasses (Menzel-Gläzer, Germany) for mounting of the coverglasses.
12. 30% Glycerol in PBS for mounting.
13. Colorless nail polish for sealing the edges of the coverglasses.

2.5. Application of siRNA

siRNA treatment allows downregulation of specific proteins and is therefore frequently used in describing the involvement of certain pathways or molecules in the processes under focus. This chapter provides the detailed working protocol for siRNA-treatment against the membrane raft proteins caveolin-1 and flotillin-1.

1. 24-Well plates (Greiner BioOne, Germany) with round glass coverslips (Ø 12 mm, no. 1, Menzel-Gläzer, Germany).
2. Specific siRNA against protein of interest, for example against caveolin-1 (sc-44202) or flotillin-1 (sc-35391) (Santa Cruz Biotechnology, CA) as in following protocols.
3. Antibiotics-free IMDM supplemented with 10% FBS for seeding cells prior to siRNA treatment (see Note 5).
4. Serum-free and 30% FBS-containing Opti-MEM I (Invitrogen, UK) for incubation of cells with siRNA.
5. Oligofectamine (Invitrogen, UK).

6. IMDM supplemented with 100 IU/ml penicillin and 100 µg/ml streptomycin without FBS for incubation of cells with CPP–protein constructs (see Note 4).
7. If fixation of cells is necessary (for instance for additional antibody staining), see [Subheading 2.4.2](#), items 5–13 for further details.

2.6. Confocal Laser Scanning Fluorescence Microscopy

For colocalization studies, confocal laser scanning microscopy (CLSM) should always be preferred over a regular wide-field fluorescence microscopy in order to better distinguish between overlapping and closely located, but not coinciding signals inside the cells. For live-cell imaging, it is advised to use a microscope with a heated stage or platform and a built-in CO₂ chamber. However, since the cells are viable for up to 30–45 min without the optimum temperature and CO₂ levels, short-term experiments and/or fast image acquisition can be done without the extra equipment. It is also recommended to use 60× oil instead of the 100× oil immersion objective if the numerical aperture (NA) values are identical or approximately the same to avoid laser-caused damage to the cells and the fluorescent labels.

3. Methods

3.1. Live-Cell Imaging of CPP–Protein Complexes in Relation to Markers of Endocytosis (Transferrin or Cholera Toxin B subunit) and Fluorescent Probes (LysoSensor or Ceramide)

3.1.1. Live-Cell Imaging of CPP–Protein Complexes in Relation to Markers of Endocytosis (Transferrin or Cholera Toxin B subunit)

As mentioned earlier, every commercially available fluorescent probe or antibody has its advantages and disadvantages. Therefore, it is recommended, whenever designing an experiment, to pay attention to known drawbacks and use several methods in parallel in order to interpret the data correctly and draw accurate conclusions. For example, when using fluorescent probes for live-cell imaging, it is suggested to perform similar experiments using for instance also the antibody staining on fixed cells and vice versa.

1. Seed 8×10^3 HeLa or Cos cells to eight-well chambered coverglasses a day before the experiment.
2. Wash the cells two times with PBS or serum-free medium (see Note 6).
3. Prepare CPP–protein complexes by mixing biotinylated CPP (CPPb) and fluorophore-labeled protein (for example avidin) at 3:1 ratio, i.e., 1 µM CPPb with 0.33 µM avidin-Texas Red, allowing the complexes to form for approximately 5 min at room temperature. Avoid bright light.
4. Incubate the cells with desired concentration of CPP–protein complexes together with 25 µg/ml transferrin-Alexa Fluor 594 or 3 µg/ml cholera toxin B-Alexa Fluor 594 in 250 µl

serum-free medium for necessary period of time, for example 30 min, 1 h, or 2 h.

5. Wash the cells gently with serum-free medium.
6. Observe and record the results immediately by CLSM. During the imaging cells should be kept either in colorless growth medium or in PBS. To avoid the detachment of cells, supplement PBS with 1 mM calcium chloride and 0.5 mM magnesium chloride.

3.1.2. Live-Cell Imaging of CPP-Protein Complexes in Relation to Fluorescent Probes LysoSensor and Ceramide

1. Seed 8×10^3 HeLa or Cos cells to eight-well chambered coverglasses a day before the experiment.
2. Wash the cells two times with PBS or serum-free medium (see Note 6).
3. Prepare CPP-protein complexes by mixing biotinylated CPP and fluorophore-labeled protein (for example avidin) at 3:1 ratio, i.e., 1 μM biotinylated CPP with 0.33 μM avidin-Texas Red, allowing the complexes to form for approximately 5 min at room temperature. Avoid bright light.
4. Incubate the cells with desired concentration of CPP-protein complexes together with 2 μM LysoSensor DND-189 or 0.5 μM Bodipy-TR- C_5 ceramide in 250 μl serum-free medium for necessary period of time, for example 1 h, or use pulse-chase for longer incubation periods, i.e., pulse the cells with complexes for 2 h, wash the cells, and chase in serum-containing medium for the remaining time, for example 2, 10 h, or other.
5. Tip: We recommend always applying LysoSensor to cells 2 h before recording of the images in spite of the actual length of the incubation, to allow the conventional trafficking of the probe through the endo-lysosomal pathway and ensure its arrival to lysosomes.
6. Wash the cells gently with serum-free medium.
7. Observe and record the results immediately by CLSM.

3.2. Imaging of Fixed Cells Treated with CPP-Protein Complexes and Stained with Antibodies Against Marker Proteins of Endocytic Vesicles, Cellular Organelles or the Cytoskeleton

1. Seed 2.5×10^4 HeLa cells onto round glass coverslips in 24-well plates 2 days before the experiment to allow firm attachment to the surface or 5×10^4 cells per coverslip 1 day before.
2. Prepare CPP-protein complexes by mixing biotinylated CPP and fluorophore-labeled protein (for example avidin) at 3:1 ratio, i.e., 1 μM CPPb with 0.33 μM avidin-Texas Red, allowing the complexes to form for approximately 5 min at room temperature. Avoid bright light.
3. Incubate the cells with desired concentration of CPP-protein complexes in serum-free medium (500 μl per well) for required time, for example 30 min, 1 h, or 2 h (shorter incubation time for

3.2.1. Treatment of Cells with CPP-Protein Complexes in Relation to Specific Endocytic Vesicles or the trans-Golgi Ring Visualized by Antibody Staining

- detecting complexes in earlier endocytic organelles and longer for detecting them further down the endocytic pathway).
4. Wash the cells twice with PBS or serum-free medium (see Note 6).
 5. Fix, permeabilize, and block the cells using one of the following schemes depending on the primary antibody used in the experiment.
 - (a) Fix the cells with 4% paraformaldehyde in PBS on ice for 30 min (500 μ l per well), wash with PBS, permeabilize with 0.1% Triton X-100 in PBS on ice for 5 min (500 μ l per well), wash again with PBS, and block nonspecific binding sites with 10% NFDm in PBS for 45 min to 1 h (500 μ l per well) [use, i.e., in case of anti-caveolin and anti-LAMP-2 staining (lysosomal marker)].
 - (b) Fix with cold methanol at -20°C for 3–5 min (500 μ l per well) (no additional permeabilization is necessary), wash the cells with PBS, and block nonspecific binding sites with 10% NFDm in PBS for 45 min to 1 h (500 μ l per well) [use, i.e., in case of TGN 46 staining (*trans*-Golgi marker)].
 - (c) Fix the cells with 4% paraformaldehyde in PBS at room temperature for 20 min (500 μ l per well), wash the cells three times with TBS (Tris-buffered saline), permeabilize with 0.5% saponin in TBS at room temperature for 15 min (500 μ l per well), wash cells again and block nonspecific binding sites with 10% heat-inactivated goat serum in TBS for 45 min to 1 h (500 μ l per well) (use, i.e., in case of anti-PI3P staining).
 - (d) Fix with freshly made PLP fixative containing 2% paraformaldehyde, 75 mM lysine-HCl and 10 mM sodium periodate in 75 mM phosphate buffer, pH 7.4 at room temperature for 2 h (500 μ l per well), wash the cells, and permeabilize and concurrently block the nonspecific binding sites with 0.01% saponin in 0.1% BSA in PBS for 8 min (500 μ l per well) (use, i.e., in case of anti-Rab5 and anti-flotillin-1 staining).
 6. Wash the cells twice with PBS.
 7. Prepare primary antibody solutions (approximately 0.1–10 $\mu\text{g}/\text{ml}$, start optimization from 1 $\mu\text{g}/\text{ml}$) as follows depending on the antibody used. Note that the primary antibody staining is performed in a droplet of antibody solution (approximately 30 μ l per coverslip) on parafilm (see Note 7).
 - (a) Diluted in 1% NFDm in PBS (in case of LAMP-2, TGN 46, and caveolin).
 - (b) Diluted in 1% heat-inactivated goat serum in TBS (in case of PI3P).

- (c) Diluted in 0.01% saponin in 0.1% BSA in PBS (in case of flotillin and Rab5).
8. Incubate the cells in the droplet of the primary antibody solution at room temperature for 1 h (see Note 8). Be sure to place coverslips on the droplet with cells facing the solution (see Note 7).
 9. Put the coverslips with cells back to the 24-well plate with cells facing up and wash 5×5 min with PBS with gentle rocking (see Note 9).
 10. Prepare secondary antibody solutions using approximately 1:400 dilution of fluorophore-labeled appropriate secondary antibodies, i.e., anti-Rabbit-Alexa Fluor 488, in the solutions described above (see [Subheading 3.2.1](#), step 7 for further details) (see Note 10). Keep in mind that the secondary antibody staining is also performed in a droplet of antibody solution (approximately 30 μ l per coverslip) on parafilm.
 11. Incubate the cells with the secondary antibody solution at room temperature for 45 min (see Note 8). Be sure to place coverslips on the droplet with cells facing the solution.
 12. Put the coverslips with cells back to the 24-well plate with cells facing up and wash 5×5 min with PBS with gentle rocking.
 13. Mount the cells to specimen glasses with 30% glycerol in PBS or anti-fade solution and seal the edges of the coverslips with colorless nail polish (see Note 11).
 14. Examine the specimens with CLSM and store the samples at 4°C in the dark (see Note 12).

3.2.2. Visualization of the Actin Cytoskeleton of Cells Treated with CPP-Protein Complexes

1. Seed 2.5×10^4 HeLa or NIH 3T3 cells onto round glass coverslips in 24-well plates 2 days before the experiment to allow firm attachment to the surface or 5×10^4 cells per coverslip 1 day before.
2. Prepare CPP-protein complexes by mixing biotinylated CPP and fluorophore-labeled protein (for example avidin) at 3:1 ratio, i.e., 1 μ M CPPb with 0.33 μ M avidin-FITC, allowing the complexes to form for approximately 5 min at room temperature. Avoid bright light.
3. Incubate the cells with desired concentration of CPP-protein complexes for required time, for example 30 min, 1 h, or 2 h, in serum-free medium (500 μ l per well).
4. Wash the cells twice with PBS or serum-free medium (see Note 6).
5. Fix the cells with 4% paraformaldehyde in PBS on ice for 30 min (500 μ l per well).
6. Wash with PBS.

7. Permeabilize with 0.1% Triton X-100 in PBS on ice for 5 min (500 μ l per well) (see Note 13).
8. Wash again with PBS.
9. Block nonspecific binding sites with 10% NFDM in PBS for 40 min (500 μ l per well).
10. Wash cells twice with PBS.
11. Prepare phalloidin-Alexa Fluor 594 solution (1.33 U/ml) in 1% NFDM in PBS. Note that the actin cytoskeleton staining is performed in a droplet of fluorophore-labeled phalloidin solution (approximately 30 μ l per coverslip) on parafilm.
12. Incubate the cells in the droplet of phalloidin-containing solution at room temperature for 30 min (see Note 8). Be sure to put coverslips on the droplet with cells facing the solution.
13. Put the coverslips with cells back to the 24-well plate with cells facing up and wash 5 \times 5 min with PBS with gentle rocking (see Note 9).
14. Mount the cells to specimen glasses with 30% glycerol in PBS and seal the edges of the coverslips with colorless nail polish (see Note 11).
15. Examine the specimens with CLSM and store the samples at 4°C in the dark (see Note 12).

3.3. Application of siRNA to Downregulate the Endosomal Pathways

1. Seed 3×10^4 HeLa cells onto round glass coverslips in 24-well plates in antibiotics-free serum-supplemented IMDM 1 day before the experiment (see Note 5).
2. 24 h after seeding the cells perform the first siRNA treatment: apply 100 nM siRNA specific to caveolin-1 (sc-44202) or flotillin-1 (sc-35391) (Santa Cruz Biotechnology, CA) with 1.5 μ l oligofectamine (Invitrogen, UK) in 250 μ l serum-free Opti-MEM I per well (Invitrogen, UK).
3. After 4 h, add 125 μ l Opti-MEM with 30% serum in each well reaching 10% serum content. Incubate overnight.
4. 24 h after the first siRNA treatment repeat the steps 2–3, but use 200 nM concentration instead of 100 nM for caveolin-specific siRNA.
5. 24 h after the second siRNA treatment change the Opti-MEM I on transfected cells to complete IMDM supplemented with antibiotics (500 μ l).
6. After 24 h incubation in full media (48 h from the second siRNA treatment) fix and stain the cells as indicated in [Subheading 3.2.1](#), steps 2–14.

3.4. Visualization by CLSM

When visualizing cells by CLSM, make sure to use low laser intensities to preserve fluorescence and also the cells, latter being

important especially for live-cell imaging. Be sure to use the same settings, i.e., laser intensity and acquisition parameters, when capturing images in parallel or during comparative experiments.

Always check for the bleed-through of fluorophores when using more than one fluorescent label in your specimen. When in doubt, images should be captured separately for each channel to avoid misinterpretation of results. For colocalization studies, always perform a z-scan of the whole cell.

3.5. Quantification of Internalized Protein and Statistical Analysis

In addition to recording the images of cells, many confocal microscopes today are equipped with specific software for the quantification of the overlap of the two analyzed signals. In order to analyze the colocalization of two independent signals (i.e., green and red signal), the region(s) of interest (ROI) must first be designated. For example, examination of the signal in certain vesicles requires marking/highlighting of the vesicles of interest before commencing with the analysis. Keep in mind to precisely track the edges of the organelles of interest for marking of the ROIs and use the images of the whole cell for analysis. After circling the ROIs, follow the manual to correctly examine the overlap of signals.

Colocalization analysis yields a dot blot map of the signal intensities of the two channels under investigation in the studied regions (ROIs). It is advised to optimize the threshold values for each channel to cut off the lower signal intensities that may be caused for example by nonspecific background signal. It is also recommended to use the same threshold values for parallel or comparative studies in order to obtain reliable data. The signal intensities above the threshold value and its contribution to the overall signal can be analyzed further with specific statistical analysis programs or MS Excel.

4. Notes

1. Avidin is a tetrameric protein having four binding sites for biotin, however, its labeling with a fluorophore reduces the number of binding sites. Therefore 3:1 ratio of biotinylated CPP to avidin is used in the experiments to make sure that CPP is bound to the protein cargo and no excess of unbound peptide is present in the solution.
2. You should check the earlier studies performed using a particular antibody or probe before ordering to minimize the possibility of receiving the chemical that is not working properly. It is also advised to perform some positive control experiments with cells to determine whether they work in your hands as they are supposed to and to establish the effective concentrations.

3. Eight-welled chambered coverglasses are an excellent choice for live-cell imaging in order to be economical with the reagents. However, out of the eight wells only four in the center are usable due to limitations of the movement of the stage/platform of some microscopes (e.g. Olympus IX81).
4. Serum-free medium is used for incubation of cells with CPPs because the serum ingredients bind the peptides reducing thus the efficiency of the transporters. Additionally, the serum components may cause degradation of the peptide resulting in the decrease of entry and problems with visualization.
5. According to the manufacturer's instructions, the transfection with Oligofectamine should be performed in the antibiotics-free medium since the presence of antibiotics could decrease cell viability.
6. Be careful when removing the solution from the cells to avoid detachment or dehydration of cells. The solution (medium, PBS, etc.) should be aspirated from one corner while not removing all of it to the last droplet. When in doubt whether all the preceding solution was removed during washing, perform an additional wash.
7. Incubations with antibodies are performed in the droplet of antibody solution to keep the volumes of antibody to the minimum because of its cost. To remove the coverglass from the bottom of the 24-welled plate, use a syringe needle with a bended tip to detach the glass from the bottom of the well and tweezers to carefully take out the glass. Remember the side with attached cells! Do not scratch the coverglass surface with the needle and do not use too much force with tweezers otherwise the glass might break. It is also recommended to tip the edge of the glass cautiously against a paper towel to remove excess liquid before placing the glass on the top of the antibody droplet with cells facing the solution.
8. Incubation with antibodies should be done preferably in a humidified environment to prevent drying of the samples.
9. Washes after antibody or phalloidin treatments must be sufficiently long and performed for several times to ensure the wash-off of unbound chemical and a better/cleaner background for imaging.
10. During antibody treatment keep in mind to use a dye with a spectrum that does not overlap with the one used for labeling of the CPP-protein complexes.
11. The coverglasses are sealed to the specimen glasses with nail polish to create a hydrated microenvironment for the cells and to prevent the glasses from moving during imaging. In order to create the microenvironment, coverglasses with cells are mounted to droplets of 30% glycerol in PBS (before the

experiment make sure that the pH of the glycerol buffer is near 7). To remove the excess solution, place a paper towel over the mounted coverglasses and slide your finger over the glasses using slight pressure. Too much pressure might flatten and damage the cells. It is important to keep the surface of the coverglass parallel to the specimen glass in order to obtain better images. Make sure that the glass stays in its initial place during the treatment with nail polish because the sliding of the cover glass on the specimen glass may cause cells to partially detach and/or fold between the glasses.

12. Note that Alexa Fluor labels are bright and stable even after several weeks, although the signal-to-background ratio decreases in time.
13. Cells fixed/permeabilized with methanol do not stain with phalloidin as methanol can disrupt the actin filaments.

Acknowledgments

The work was supported by grants from Estonian Science Foundation (ESF 7058), Estonian Ministry of Education and Research (0182691s05), Swedish Research Council (VR-NT); Center for Biomembrane Research, Stockholm; and Knut and Alice Wallenberg's Foundation.

References

1. Schwarze S. R., Ho A., Vocero-Akbani A., Dowdy S. F. (1999) In vivo protein transduction: delivery of a biologically active protein into the mouse. *Science*. **285**(5433), 1569–1572.
2. El-Andaloussi S., Johansson H. J., Lundberg P., Langel Ü. (2006) Induction of splice correction by cell-penetrating peptide nucleic acids. *J Gene Med*. **8**(10), 1262–1273.
3. Gitton Y., Tibaldi L., Dupont E., Levi G., Joliot A. (2009) Efficient CPP-mediated Cre protein delivery to developing and adult CNS tissues. *BMC Biotechnol*. **9**, 40.
4. Console S., Marty C., Garcia-Echeverria C., Schwendener R., Ballmer-Hofer K. (2003) Antennapedia and HIV transactivator of transcription (TAT) “protein transduction domains” promote endocytosis of high molecular weight cargo upon binding to cell surface glycosaminoglycans. *J Biol Chem*. **278**(37), 35109–35114.
5. Rinne J., Albarran B., Jylhävä J., Ihalainen T. O., Kankaanpää P., Hytönen V. P., Stayton P. S., Kulomaa M. S., Vihinen-Ranta M. (2007) Internalization of novel non-viral vector TAT-streptavidin into human cells. *BMC Biotechnol*. **7**, 1.
6. Säälük P., Padari K., Niinep A., Lorents A., Hansen M., Jokitalo E., Langel Ü., Pooga M. (2009) Protein delivery with transportans is mediated by caveolae rather than flotillin-dependent pathways. *Bioconjug Chem*. **20**(5), 877–887.
7. Wadia J. S., Stan R. V., Dowdy S. F. (2004) Transducible TAT-HA fusogenic peptide enhances escape of TAT-fusion proteins after lipid raft macropinocytosis. *Nat Med*. **10**(3), 310–315.
8. Tünnemann G., Martin R. M., Haupt S., Patsch C., Edenhofer F., Cardoso M. C. (2006) Cargo-dependent mode of uptake and bioavailability of TAT-containing proteins and peptides in living cells. *Faseb J*. **20**(11), 1775–1784.
9. Duchardt F., Fotin-Mleczek M., Schwarz H., Fischer R., Brock R. (2007) A comprehensive model for the cellular uptake of cationic cell-penetrating peptides. *Traffic*. **8**(7), 848–866.

10. Räägel H., Säälük P., Hansen M., Langel Ü., Pooga M. (2009) CPP-protein constructs induce a population of non-acidic vesicles during trafficking through endo-lysosomal pathway. *J Control Release*. **139**(2), 108–117.
11. Padari K., Säälük P., Hansen M., Koppel K., Raid R., Langel Ü., Pooga M. (2005) Cell transduction pathways of transportans. *Bioconjug Chem*. **16**(6), 1399–1410.
12. Bidwell G. L. 3rd, Davis A. N., Raucher D. (2009) Targeting a c-Myc inhibitory polypeptide to specific intracellular compartments using cell penetrating peptides. *J Control Release*. **135**(1), 2–10.
13. Hamilton A. J., Baulcombe D. C. (1999) A species of small antisense RNA in posttranscriptional gene silencing in plants. *Science*. **286**(5441), 950–952.
14. Misaki R., Nakagawa T., Fukuda M., Taniguchi N., Taguchi T. (2007) Spatial segregation of degradation- and recycling-trafficking pathways in COS-1 cells. *Biochem Biophys Res Commun*. **360**(3), 580–585.

Chapter 13

Insight into Cell-Entry Mechanisms of CPPs by Electron Microscopy

Kärt Padari, Annelly Lorents, Eija Jokitalo, and Margus Pooga

Abstract

Despite the quickly widening application of cell-penetrating peptides (CPP) for the cellular delivery of various macromolecules, the cell entry mechanisms of these peptides have remained elusive so far. The basic features of the translocation of CPPs into cells have been mapped by fluorescence microscopy and activity-based assays revealing that endocytotic mechanisms are mainly responsible for the uptake at physiological temperature. However, the high concentration of CPP or the lowering of the incubation temperature below 10°C (re)activates a nonvesicular cell entry mode. The fluorescence microscopy can hardly provide detailed information about the interaction of CPP molecules with the extracellular structures, the induced changes in the morphology of the plasma membrane, etc. Therefore, application of electron microscopy could help to shed light on the nature of nonvesicular uptake mechanism. Transmission electron microscopy (TEM) has been a valuable tool for the morphological characterization of biological material at high resolution. It can provide useful information at the ultrastructural level about the interaction and arrangement of CPPs on the cell surface, the entrapment in cellular organelles and the translocation to the cytoplasm. In this chapter, we present a method for the tagging of CPPs covalently with a 1.4 nm gold cluster and provide a flat-embedding protocol for the mapping of Nanogold™-labeled CPPs in cultured cells by TEM. This method enables to retain the cell monolayers in their *in situ* orientation. The Nanogold™ tag is putatively not interfering with the uptake of CPPs and enables the production of specimens with excellent morphology and good contrast.

Key words: Cell-penetrating peptide, Transmission electron microscopy, Nanogold-labeled CPP

1. Introduction

CPPs have been used as efficient carriers in drug and gene delivery enabling specific targeting and resulting in high biological response (1–3). However, the current knowledge about how CPPs reach their target compartments inside cells is still far from complete. To better understand the uptake mechanism and distribution of CPPs and their cargo molecules, it is essential to apply

different complementary methods in parallel, which would allow adequate interpretation of experimental data (4). Most of the studies examining the uptake and cellular localization of CPPs have used fluorescence microscopy. Even though fluorescence microscopy is an excellent tool for real-time studies in living cells and can be successfully used for quantitative analysis, it has its limitations. First, the fluorescence signal might be quenched in the cellular environment, especially in the vesicles with low pH or when associated with polyanions, as well as upon interaction with cell surface proteoglycans (5), complicating the interpretation of fluorescence microscopy results. Second, due to the limited resolution of light microscope, it cannot provide detailed information about the interaction of CPPs with the plasma membrane and their exact localization in relation to intracellular compartments. However, detailed information can be acquired by transmission electron microscopy (TEM) that allows visualization of subcellular compartments at the ultrastructural level to study the association with the membranes, the uptake, and the intracellular trafficking of CPPs with very high precision. Still, relatively few studies have applied electron microscopy for assessing the uptake mechanisms of CPPs. The main drawback is the need to fix the specimen that can lead to artifactual redistribution of some peptides into, but also inside of cells (6). Still, not all CPPs redistribute in cells upon fixation (7) and the localization of CPP–cargo conjugates is influenced even less by treatment with fixatives (8), making TEM studies in this field feasible and justified.

TEM has mostly been used in studies focused on the CPP-mediated delivery of proteins (9–11) or gold nanoparticles alone (12–14) rather than for the characterization of internalization mechanisms and intracellular fate of CPPs themselves. For example, the translocation of 16 nm gold nanoparticles modified with Tat-peptide and Penetratin into cell interior was characterized recently and the particles were found in endosomes along with a dispersed signal in the cytosol (12). However, considering that the size of the cargo molecule might determine the uptake mechanism of CPPs (15, 16), a small nanogold tag (1.4 nm) rather than colloidal gold particles (14–16 nm) have to be harnessed in the studies of CPP mechanisms. In addition, the Nanogold™ (NG) cluster is coupled to the CPP molecule by a covalent bond, resulting in homogenous well-defined compound on the contrary to colloidal gold, in which neither the composition of label nor the number of peptide molecules per particle can be exactly defined.

A recent study revealed that the novel CPPs derived from perforin and granzyme do not associate with the cell surface randomly but assemble in spherical structures. The clusters of NG-labeled CPP interfered with the regular packing of the lipid bilayer as the plasma membrane became less distinct in TEM. Although the novel CPPs are taken up by cells mostly by endocytotic

mechanisms, the peptide clusters are not dissociated in the hostile milieu of the endosomes during the first hours (17, 18).

In this chapter, we will discuss the method of TEM for mapping the interaction of NG-labeled CPPs with cells and the following uptake. We present the protocols for the labeling of CPPs with preactivated nanogold tag and embedding the cultured cells in a resin by so-called flat-embedding technique, which retains the orientation and morphology of cells.

2. Materials

2.1. Cell Culture

In this chapter, we describe protocols for cultivating HeLa cells for TEM. HeLa cells are derived from the human cervical carcinoma and have been used in a significant number of other CPP studies. Using the same cell line enables one to complement and compare experimental data with other research groups in the field. However, any other cell line or primary cells can also be used in the studies. Still, for the flat-embedding protocol provided here, only adherent cells can be used.

2.2. Labeling of Peptide

2.2.1. Reagents and Solutions

1. CPP with a thiol group (see Note 1).
2. Monomaleimido nanogold (Nanoprobes Inc., Yaphank, NY) or monomaleimido undecagold.
3. Oxygen-free MilliQ water. Remove air dissolved in MilliQ water by vacuum followed by bubbling through argon for at least 15 min.
4. 50% Methanol ($\geq 99.9\%$) in oxygen-free water.
5. Oxygen-free MilliQ water with 0.1% trifluoroacetic acid (TFA $\geq 99.9\%$) (see Note 2).
6. Acetonitrile with 0.1% TFA.

2.2.2. Materials and Equipment

1. Eppendorf tubes filled with argon.
2. Spectrophotometer (e.g., Nanodrop 1000, Thermo Fischer Scientific Inc.).
3. Thermostat mixer (e.g., Thermomixer Comfort, Eppendorf AB, Germany).
4. Rotational vacuum concentrator (e.g., RVC 2-25, Christ GmbH, Germany, or Savant Speed-Vac SC110, Ramsey, MN).
5. Chromatography system equipped with columns for peptide purification and gel filtration by reversed phase chromatography (see Note 3).

2.3. Preparation of a Specimen for TEM

1. Human cervical carcinoma cell line HeLa cultured in Iscove's Modified Dulbecco's Medium (IMDM) supplemented with 10% fetal bovine serum (FBS), 100 IU/mL penicillin, and 100 µg/mL streptomycin.
2. IMDM supplemented with 100 IU/ml penicillin, 100 µg/ml streptomycin, and 10% FBS for the incubation of cells with CPP–nanogold (CPP–NG) conjugates.
3. Sodium cacodylate buffer: prepare 0.4 M stock solution by dissolving 21.4 g of cacodylic acid sodium salt trihydrate [$\text{Na}(\text{CH}_3)_2\text{AsO}_2 \cdot 3\text{H}_2\text{O}$] in 250 ml MilliQ water (see Note 4). Adjust pH to 7.4 by adding 0.2 M HCl (about 8 ml) to 50 ml of stock solution and add MilliQ water to the volume of 200 ml to make a 0.1 M working solution. Alternatively, to make 0.2 M working solution (for preparing osmium tetroxide solution, see step 9 below) dilute to final volume of 100 ml.
4. Fixative: 2.5% glutaraldehyde in 0.1 M cacodylate buffer, pH 7.4. Always use freshly prepared fixative. Store 25% glutaraldehyde stock [Electron Microscopy Sciences (EMS), Hatfield, PA] in aliquots at -20°C and do not use the reagent that has been thawed and frozen again.
5. Silver enhancement reagent: HQ Silver Kit (Nanoprobes Inc., Yaphank, NY). The components of HQ Silver kit can be aliquoted in amber Eppendorf tubes and stored at -20°C . The components of silver enhancement kit are light sensitive, therefore it is necessary to work in dark room under red safe light conditions while aliquoting or staining specimens.
6. Reagents for gold toning:
 - (a) 2% sodium acetate [$\text{CH}_3\text{COONa} \cdot 3\text{H}_2\text{O}$] in MilliQ water (use freshly made solution).
 - (b) 0.05% gold chloride [$\text{HAuCl}_4 \cdot \text{H}_2\text{O}$] in MilliQ water (can be stored at 4°C for several months).
 - (c) 0.3% sodium thiosulfate pentahydrate [$\text{Na}_2\text{S}_2\text{O}_3 \cdot 5\text{H}_2\text{O}$] in MilliQ water (use freshly prepared solution).
7. Reduced, buffered osmium tetroxide solution for the staining and postfixation of the specimens (see Note 5). Mix equal volumes of 2% OsO_4 in MilliQ water and 0.2 M cacodylate buffer to yield a 1% OsO_4 in 0.1 M cacodylate buffer. Add 15 mg potassium ferrocyanide ($\text{K}_4[\text{Fe}(\text{CN})_6]$) per 1 ml of 1% OsO_4 solution (see Note 6).
8. 70% Ethanol in MilliQ water.
9. 96% Ethanol in MilliQ water.
10. Ethanol ($\geq 99.5\%$).
11. Acetone ($\geq 99.5\%$).

12. Embedding resin: TAAB Premix Embedding Kit (medium, TAAB Laboratories Equipment Ltd, UK) (see Note 7).
13. 2% Uranyl acetate (UA) in 50% ethanol (see Note 8).
14. Lead citrate stain: Add 20 mg of lead citrate [$\text{Pb}_3(\text{C}_6\text{H}_5\text{O}_7)_2 \cdot 3\text{H}_2\text{O}$] to 10 ml of CO_2 -free MilliQ water (boil water for 10 min to make it CO_2 free) (see Note 9). Add 0.1 ml of 10 N NaOH (see Note 10), seal the tube air-tightly and shake vigorously until all the lead citrate is dissolved. Filter the solution through a 0.2 μm Millipore filter before use.
15. Liquid nitrogen for removing coverslips from polymerized resin blocks of specimen.
16. Single-use plastic Pasteur pipettes (transfer pipettes) for changing solutions.
17. Parafilm.
18. Embedding capsules and capsule holder: We use BEEM[®] embedding capsules (size 3) and BEEM[®] capsule holder from EMS. However, any other suitable capsules and holders can be used.
19. Aluminum planchettes or dishes.
20. 24-Well culture plates.
21. Round glass coverslips (Ø 12 mm, no. 1).
22. Cell culture dishes (35 \times 10 mm).

3. Methods

3.1. Labeling of Peptides with Nanogold

1. Dissolve the lyophilized peptide in oxygen-free MilliQ water to yield a 0.5 mM peptide solution. Calculate the volume of water for dissolving the peptide batch based on its weight and molecular mass (see Note 11).
2. Check the concentration of peptide by measuring the optical density of the prepared solution using a suitable dilution, at 280 nm if the peptide contains tryptophan or tyrosine (see Note 12) or at 210 nm. If the weight-based concentration differs from absorbance-based concentration by more than 10%, use the latter.
3. Dissolve monomaleimido nanogold in 50% methanol at 30 μM concentration (see Note 13).
4. Couple the label to peptide by adding CPP solution (2.5-fold molar excess) in small aliquots to nanogold solution upon stirring (see Note 14). Incubate the mixture for 60–90 min at 30°C in dark under mild stirring.

5. Remove methanol and concentrate the solution of conjugate by rotational vacuum concentrator at 30°C to reach ~100 μM concentration (see Note 15).
6. Measure the absorbance of the resulting solution at 280 nm using the suitable dilution and calculate the concentration of conjugate considering that 1 A_{280}/cm corresponds to ~2.1 μM nanogold (see Note 16). Aliquot the conjugate and store in freezer. Store the working aliquot in fridge and use it within 1 month (some conjugates can be stored in fridge less than 1 week). Avoid the repeated freeze–thaw cycles.
7. Purify the conjugate by reversed phase chromatography or gel filtration if necessary (see Note 17).
8. Concentrate the fractions of chromatographic purification by rotational vacuum concentrator (see step 5), pool if necessary and measure the concentration of the conjugate (see Note 15).

3.2. Treatment of Cells with CPP–NG Conjugates and Fixation

1. Clean glass coverslips to remove any dust particles by rinsing multiple (3 to 4) times with 70% ethanol in a 100 ml glass flask. Dry and sterilize coverslips one by one in the flame of gas burner using tweezers.
2. Place the sterilized coverslips to the bottom of cell culture dish (35 \times 10 mm). We recommend having at least three coverslips in one culture dish to get three parallels of each set of experiment for different time points of silver-enhancement procedure (see Subheading 3.3 below). You can also use up to four coverslips (i.e., four different time points of silver enhancement) per one set of experiment.
3. Seed HeLa cells onto coverslips in culture dish and grow for 2 days to reach 80–100% of confluence (see Note 18).
4. Remove the culture medium and incubate the cells with CPP–NG conjugates in IMDM (1 ml solution per culture dish with three coverslips) at desired concentration and temperature for required time depending on your experiment (for example 1 μM of CPP–NG at 37°C for 1 h).
5. Take cells out from the incubator just before the fixation and wash twice with prewarmed IMDM.
6. Remove the medium and immediately apply the fixative. Make sure that the cells do not dry at any stage during the procedures. Fix the cells with 2.5% glutaraldehyde in cacodylate buffer for 30–60 min at room temperature (RT).
7. Wash with cacodylate buffer for three times for 10 min (here you can interrupt the procedure and leave samples in buffer for overnight at 4°C). Continue with silver enhancement (see Subheading 3.3).

3.3. Silver Enhancement

For most applications, the detection of nanogold particles in an electron microscope specimen requires the enlargement of particles in order to visualize these with the magnification range routinely used for imaging cellular organelles. Gold particles act as catalysts in the presence of silver ions and a reducing agent and reduce silver ions to metallic silver. The silver is deposited onto the gold enlarging thereby the 1.4 nm gold particles to about 10 nm diameter or more depending on the enhancement time and temperature. Silver enhancement reaction is time dependent: nanogold particles enlarge particularly rapidly within the first minutes, later the growth rate declines since the surface area of particles increases. After the suggested time of the enhancement, silver may precipitate spontaneously by self-nucleation yielding a background signal. Therefore, it is very important to choose the optimal time for enhancement in order to magnify the nanogold particle without increasing the background staining. Additionally, the deposition of silver onto the gold surface is quicker at higher temperatures. Therefore, we usually prepare two to three specimens in parallel using different duration of silver enhancement. It is particularly important for the protocol provided here because the enhancement is carried out before embedding and if the enhancement proves to be too long (resulting in too large particles) it cannot be reversed.

The following steps of the silver enhancement and gold toning procedures should be carried out in a dark room under red light at 20–22°C.

1. Wash the cells three times with MilliQ water for 3 min.
2. Prepare a 24-well plate for stopping enhancement reaction (see step 5) by filling wells with MilliQ water.
3. Mix equal amounts (for example 200 μ l) of the initiator, moderator, and activator just before use (see instructions of HQ SILVER Enhancement Kit).
4. Place three drops (about 50 μ l) of enhancing solution on parafilm and place coverslips upside down onto the drops to enlarge the particles for 1, 3, and 5 min. If you have four parallels, incubate coverslips for 30 s, 1, 2, and 4 min. Be as precise as possible with incubation times (use a timer) (see Note 19).
5. Stop the reaction by transferring coverslips (cells upside) to MilliQ water in wells of culture plate.
6. Wash twice with MilliQ water for 5 min.
7. Stabilize the silver-deposited particles by gold toning (see Note 20):
 - (a) Wash three times with 2% sodium acetate for 5 min at RT.
 - (b) Treat with 0.05% gold chloride for 10 min on ice.
 - (c) Wash twice with 0.3% sodium thiosulfate (freshly made) for 10 min on ice.

8. Wash three times with MilliQ water for 3 min.
9. Continue with osmication (see Subheading 3.4).

3.4. Embedding of Cells (Flat-Embedding)

1. Osmicate with 1% OsO₄ for 1 h at RT. Avoid direct daylight by covering the culture plate with aluminum foil during osmication.
2. Wash three times with 0.1 M cacodylate buffer for 5 min.
3. Dehydrate once with 70%, once with 96% and twice with absolute ethanol for 1 min each step.
4. Remove the caps from the embedding capsules, place the capsules in holder and fill with embedding resin to maximum. Keep in mind to take resin (if stored in syringes at -20°C) out from freezer before the embedding procedure and let them warm up to RT before use.
5. Dip a coverslip into acetone for couple of seconds and place it onto an aluminum planchette (cells upside).
6. Drop immediately some embedding resin to the cells. Do not allow the complete evaporation of acetone.
7. Place the capsules filled with embedding resin upside down on the top of cells.
8. Keep specimens at RT for 2 h to allow the resin to infiltrate into cells.
9. Transfer the cells to 60°C oven and polymerize overnight (for at least 14 h).
10. After the polymerization, remove the coverslips by dropping samples directly from the oven to liquid nitrogen and crack the coverslip from the block. Make sure that no pieces of glass remain on the resin block; otherwise these could damage the cutting edge of your diamond knife during sectioning (see Note 21).
11. Cut cells embedded in resin into ultrathin sections (30–50 nm, i.e., silver gray sections) and collect on the copper grids (EMS).
12. Stain the sections with 2% UA on parafilm for 1 min.
13. Wash twice in 50% ethanol and let the sections dry in air for 15–20 min.
14. Wash the sections with 0.01 N NaOH for 1 min.
15. Stain the sections with solution of lead citrate for 1–3 min depending on the required contrast.
16. Wash with 0.01 N NaOH and rinse thoroughly (at least three times) by transferring grids from one drop of MilliQ water to another.
17. Let the grids dry and examine in transmission electron microscope operated at 80 kV.

4. Notes

1. Peptides could also be tagged with nanogold on the amino group of lysine or N terminus, but such modification decreases the net positive charge and usually reduces the cellular uptake of CPPs. Therefore the cysteine residue is introduced in CPPs.
2. MilliQ water and acetonitrile with TFA are necessary only if the CPP–nanogold conjugate is purified by reversed phase or gel-filtration (size exclusion) chromatography.
3. In this work, an FPLC system (GE Healthcare/Pharmacia) equipped with absorbance detectors at 280 and 210 nm, an automated fraction collector and the columns Superdex-Peptide HR10/30 (for gel filtration chromatography) and Pro RPC HR5/2 (for reversed phase chromatography) were used.
4. Sodium cacodylate contains arsenic, which is a health hazard if inhaled or absorbed through the skin. Use gloves and fume hood for weighing the reagent and preparing the buffer solution. Do not let the reagent come in contact with acids in order to avoid the production of arsenic gas (19).
5. Osmium tetroxide must be handled with the utmost care because of its high toxicity. Exposure to OsO_4 vapor can cause severe eye, skin, and respiratory problems. Prepare the osmium tetroxide solutions always under the vented hood and handle bottles with disposable gloves. To make 2% aqueous solution of OsO_4 , we use the OsO_4 crystals in the glass ampoule (available from EMS). We recommend immersing the ampoule into liquid nitrogen prior the opening in order to crystallize vaporized osmium tetroxide. OsO_4 is also supplied as an aqueous solution in glass ampoules. Store the solution of 2% OsO_4 at 4°C in a clean brown glass bottle to avoid the contamination by organic matter and exposure to light. Since the vapors of osmium tetroxide can readily leak out of many containers, use double glass bottles sealed with parafilm for storing OsO_4 . All used OsO_4 solutions should be collected into a glass bottle containing vegetable oil (corn oil is preferred because of its high percentage of unsaturated bonds) and stored in the fume hood. For full neutralization, two volumes of unsaturated oil per one volume of 2% osmium tetroxide solution are needed. The neutralized osmium solution is then disposed in accordance to each country's regulations. Contact your environmental health and safety office to obtain local regulation.
6. Osmium tetroxide in combination with ferrocyanide is used for enhancing the contrast of many cellular components, including membranes and glycogen.

7. Components of the embedding kit can be stored at 4°C for 12 months. The mixed and ready-to-use embedding resin can be stored, e.g., in plastic syringes without needle (5 or 2.5 ml) at -20°C for later use for 3 months. Caps for syringes are available from EMS. Most embedding resins are carcinogenic! Cover working area with paper before mixing the components and always use disposable gloves during embedding procedures. Seal used tubes, pipettes, dishes, etc. in a plastic bag and polymerize all resin waste before disposal at 60°C for overnight. Never pour any resin containing solutions down the drain, the resin will polymerize and could clog the tubes.
8. Centrifuge UA solution before use. Care should be taken in the handling and disposal of uranium-containing solutions because of their radioactivity and chemical toxicity. Danger of cumulative effects!
9. Use only carbonate-free MilliQ water and freshly made NaOH to prevent the formation of lead carbonate precipitate. To avoid contamination of the staining solution with carbonate ions, keep the tube tightly sealed from atmospheric carbon dioxide. Use the staining solution within the day of preparation.
10. Prepare 10 N sodium hydroxide by dissolving 4 g of NaOH in 10 ml of CO₂-free distilled water. Be aware that dissolution of sodium hydroxide is highly exothermic.
11. The peptides with a thiol group oxidize very easily to form dimers, therefore, for the labeling procedure do not use the stock solution of peptide, which has been stored for a long time, or is prepared in water that contains oxygen. CPPs can be dissolved at any desired concentration. However, at very high concentration more hydrophobic peptides tend to precipitate upon labeling and low peptide concentrations might result in low labeling yield.
12. Calculate the molar extinction coefficient of your peptide as follows: molar extinction coefficient = (number of tryptophan residues × 5,500) + (number of tyrosine residues × 1,490) (<http://www.encorbio.com/protocols/Prot-MW-Abs.htm>).
13. Reconstitution of 30 nmol batch of monomaleimido nanogold with 1 ml deionized water will yield a 20 mM sodium phosphate buffer at pH 6.5 with 150 mM NaCl, i.e., suitable conditions for selective labeling of thiol groups of peptide. Methanol (or acetonitrile) facilitate the dissolving of the label and reduce precipitation of hydrophobic CPPs during labeling. However, monomaleimido nanogold can be reconstituted in a smaller or a larger volume of solvent if necessary.
14. Perform the coupling reaction in a tube filled with argon to maximize the yield of coupling by excluding the oxidation of thiols. Use a two- to fourfold molar excess of CPP over the

monomaleimide nanogold to assure that most of the label reacts with the peptide. Addition of the CPP solution in water to nanogold solution in 50% methanol decreases the possibility of the peptide/conjugate precipitation during labeling.

15. Check the volume of the conjugate solution during the concentration step regularly (every 30–60 min, depending on the initial volume). Some amphipathic/hydrophobic leucine-rich CPPs may precipitate during methanol removal and concentration. This could be decreased or even avoided by adding some concentrated stock solution of leucine to the reaction mixture before concentration step (final concentration 2–5 mg/ml depending on CPP).
16. Tryptophan contributes to the absorption of a conjugate at 280 nm by $\ll 1\%$ and may therefore not be taken into account. Typically $>90\%$ of nanogold is coupled to the peptide under the used reaction conditions, and the concentration of the conjugate can be calculated based on the total absorption of the solution at 280 nm.
17. The purification of the conjugate to homogeneity is often not necessary and the mixture with unlabeled peptide (the concentrated reaction mixture) can be used in the majority of cellular localization studies. The inactive (hydrolyzed) monomaleimide nanogold (in analogy with cationized or neutral NG) neither strongly binds to the extracellular matrix nor is taken up by cells via endocytosis. The unlabeled CPP remains invisible in TEM and does not interfere with the analysis of the subcellular localization of CPP–NG conjugates. Most importantly, due to their highly cationic nature, CPPs adhere strongly to various surfaces, which lead to high losses of peptides and their conjugates with NG in purifications by chromatographic methods. Run the reversed phase chromatography in C4 to C8 column of minimal necessary volume. We used Pro RPC HR5/2 (Pharmacia, Sweden) and run a steep gradient from 10% acetonitrile in water (both with 0.1%, v/v TFA) to 100% acetonitrile. The CPP–NG conjugate elutes in about 10% higher acetonitrile concentrations than the peptide. Different CPPs elute from the column in different conditions, therefore, optimize the shape of the gradient with a minimal amount of the conjugate before the preparative purification. Gel-filtration chromatography is suggested for the purification of nanogold-labeled proteins and peptides by Nanoprobes Inc. However, the gel filtration chromatography does not separate well the hydrolyzed NG label from the conjugate with CPP due to the small difference in size. Moreover, the conjugates of CPP with NG could be recovered in very low yield (for Superdex peptide HR 10/30 $<50\%$). Addition of a volatile solvent (e.g., acetonitrile up to

- 40%) reduces the losses in purification to some extent, but the recovery yield still remains poor.
18. For electron microscopy, the cells have to be grown on glass coverslips for at least 2 days to guarantee stable adhesion and good morphology of cells in specimens.
 19. We have used HQ SILVER™ Enhancement kit (Nanoprobes) in our studies, which enables controlled silver enhancement and yields homogenous particles. However, it should be kept in mind that the adjacent particles might fuse and form irregular shapes upon growth. Therefore very long incubations that result in large particles should be avoided.
 20. Gold toning is the posttreatment of silver enhanced gold particles with gold chloride. This treatment deposits a thin layer of gold onto the surface of the particles and stabilizes the silver deposition, making the resulting particles of Au–Ag–Au more resistant to the following treatments with osmium tetroxide and UA solutions (20).
 21. Allow blocks to settle at RT for couple of hours before trimming a small pyramid suitable for successful ultrathin sectioning. Small block face facilitates the parallel alignment of block face and knife edge that is important as the specimen thickness is only one cell layer thick thus allowing no trimming from the block face.

Acknowledgments

We thank the people of Electron Microscopy Unit at the University of Helsinki for introducing the silver enhancement method and improving the flat-embedding technique; and M. Kure for excellent technical assistance in electron microscopy. The work was supported by grants from Estonian Science Foundation (ESF 7058) and Estonian Ministry of Education and Research (0182691s05).

References

1. El-Andaloussi, S., Johansson, H., Lundberg, P., and Langel, Ü. (2006) Induction of splice correction by cell-penetrating peptide nucleic acids. *J Gene Med* **8**, 1262–73.
2. Wu, B., Moulton, H. M., Iversen, P. L., Jiang, J., Li, J., Spurney, C. F., Sali, A., Guerron, A. D., Nagaraju, K., Doran, T., Lu, P., Xiao, X., and Lu, Q. L. (2008) Effective rescue of dystrophin improves cardiac function in dystrophin-deficient mice by a modified morpholino oligomer. *Proc Natl Acad Sci USA* **105**, 14814–9.
3. Mäe, M., El-Andaloussi, S., Lundin, P., Oskolkov, N., Johansson, H. J., Guterstam, P., and Langel, Ü. (2009) A stearylated CPP for delivery of splice correcting oligonucleotides using a non-covalent co-incubation strategy. *J Control Release* **134**, 221–7.

4. Holm, T., Johansson, H., Lundberg, P., Pooga, M., Lindgren, M., and Langel, Ü. (2006) Studying the uptake of cell-penetrating peptides. *Nat Protoc* **1**, 1001–5.
5. Ziegler, A., and Seelig, J. (2007) High affinity of the cell-penetrating peptide HIV-1 Tat-PTD for DNA. *Biochemistry* **46**, 8138–45.
6. Lundberg, M., and Johansson, M. (2001) Is VP22 nuclear homing an artifact? *Nat Biotechnol* **19**, 713–4.
7. Mano, M., Teodosio, C., Paiva, A., Simoes, S., and Pedroso de Lima, M. C. (2005) On the mechanisms of the internalization of S4(13)-PV cell-penetrating peptide. *Biochem J* **390**, 603–12.
8. Säälük, P., Elmquist, A., Hansen, M., Padari, K., Saar, K., Viht, K., Langel, Ü., and Pooga, M. (2004) Protein cargo delivery properties of cell-penetrating peptides. A comparative study. *Bioconjug Chem* **15**, 1246–53.
9. Padari, K., Säälük, P., Hansen, M., Koppel, K., Raid, R., Langel, Ü., and Pooga, M. (2005) Cell transduction pathways of transportans. *Bioconjug Chem* **16**, 1399–410.
10. Magzoub, M., Sandgren, S., Lundberg, P., Oglecka, K., Lilja, J., Wittrup, A., Goran Eriksson, L. E., Langel, Ü., Belting, M., and Gräslund, A. (2006) N-terminal peptides from unprocessed prion proteins enter cells by macropinocytosis. *Biochem Biophys Res Commun* **348**, 379–85.
11. Säälük, P., Padari, K., Niinep, A., Lorents, A., Hansen, M., Jokitalo, E., Langel, Ü., and Pooga, M. (2009) Protein delivery with transportans is mediated by caveolae rather than flotillin-dependent pathways. *Bioconjug Chem* **20**, 877–87.
12. Nativo, P., Prior, I. A., and Brust, M. (2008) Uptake and intracellular fate of surface-modified gold nanoparticles. *ACS Nano* **2**, 1639–44.
13. Pujals, S., Bastus, N. G., Pereiro, E., Lopez-Iglesias, C., Puentes, V. F., Kogan, M. J., and Giralt, E. (2009) Shuttling gold nanoparticles into tumoral cells with an amphipathic proline-rich peptide. *ChemBiochem* **10**, 1025–31.
14. Mandal, D., Maran, A., Yaszemski, M. J., Bolander, M. E., and Sarkar, G. (2009) Cellular uptake of gold nanoparticles directly cross-linked with carrier peptides by osteosarcoma cells. *J Mater Sci Mater Med* **20**, 347–50.
15. Tünnemann, G., Martin, R. M., Haupt, S., Patsch, C., Edenhofer, F., and Cardoso, M. C. (2006) Cargo-dependent mode of uptake and bioavailability of TAT-containing proteins and peptides in living cells. *FASEB J* **20**, 1775–84.
16. Duchardt, F., Fotin-Mleczek, M., Schwarz, H., Fischer, R., and Brock, R. (2007) A comprehensive model for the cellular uptake of cationic cell-penetrating peptides. *Traffic* **8**, 848–66.
17. Palm-Apergi, C., Lorents, A., Padari, K., Pooga, M., and Hällbrink, M. (2009) The membrane repair response masks membrane disturbances caused by cell-penetrating peptide uptake. *FASEB J* **23**, 214–23.
18. Koppel, K., Padari, K., Lorents, A., Hällbrink, M., Mano, M., Pedroso de Lima, M. C., and Pooga, M. (2010) S4₁₃-PV cell-penetrating peptide forms nanoparticle-like structures to gain entry into cells. *Bioconjug Chem* **21**, 774–83.
19. Hayat, M. A. Principles and techniques of electron microscopy: biological applications. Fourth edition: Cambridge University Press, Cambridge; 2000.
20. Arai, R., Geffard, M., and Calas, A. (1992) Intensification of labelings of the immunogold silver staining method by gold toning. *Brain Res Bull* **28**, 343–5.

Chapter 14

Toxicity Methods for CPPs

Per Lundin, Samir EL Andaloussi, and Ülo Langel

Abstract

CPPs have for numerous years been utilized as delivery vectors of various pharmaceutically interesting cargoes, both in vitro and in vivo. As CPPs are gradually approaching the bedside, investigating toxicity associated with these highly interesting peptides becomes increasingly important and thorough initial assessment of cytotoxicity in vitro is a first step towards advancing these delivery vehicles in to the clinics. The present chapter describes protocols for four cytotoxicity assays in order to provide a toolbox for toxicity assessment of CPPs. The foci lie on membrane integrity (deoxyglucose leakage and propidium iodide assays) and cell viability (the MTT assay), but the chapter also provides a protocol for assessing an important parameter for future clinical applications, namely the hemolytic properties of CPPs.

Key words: CPP, Toxicity, Membrane integrity, Viability, Deoxyglucose leakage, Propidium iodide, MTT, Hemolysis

1. Introduction

The increasing utilization of cell-penetrating peptides (CPPs) both as research tools and in clinical investigations, necessitates comprehensive evaluation of the toxicity profiles of these intriguing delivery vectors. CPPs have for numerous years been utilized for the delivery of various pharmaceutically interesting cargoes, primarily in vitro, but as their in vivo potential is increasingly harvested (see for instance (1, 2), the need for deeper knowledge regarding the potential cytotoxic effects associated with the delivery is essential. Additionally, a serious concern for further in vivo applications of CPPs is the risk of eliciting an immunological response, especially during longer treatment periods (2). However, such aspects, regardless of their importance, are beyond the scope of this chapter.

As a result of the predominantly cationic nature and the inherent vector capabilities of CPPs, these short peptides can be expected to exert numerous effects on the cell membrane as well as on cellular proliferation and viability. Unsurprisingly, CPPs have been shown to, for instance, induce membrane leakage (3), decrease cell viability at higher concentrations (4), and cause hemolysis (3); effects often associated with stipulated pore formation, membrane perturbation, and leakage (5, 6). However, only relatively few comprehensive studies have assessed the toxicity properties of CPPs in a comparative setting. In one study, the toxic effects of human calcitonin-derived peptide (hCT), Tat(47–57), and penetratin(43–58) on MDCK monolayers, assessed using a commonly utilized leakage assay, were found to be negligible (7). Similar results were obtained in a later study, for the CPPs penetratin, Tat, transportan, and polyarginine, this time employing a toxicity assay based on correlating mitochondrial metabolic activity with cell viability (8). The cytotoxicity induced by most CPPs is thus rather modest, at least considering the highly efficient cargo translocation, but toxicity evaluations are nevertheless pivotal in order to obtain adequate results, especially considering the uncertainty introduced upon covalent cargo attachment (5, 8) and the highly variable toxicity profiles of different CPPs. On a more general note, CPPs exhibiting amphipathic character normally display a higher degree of cytotoxicity, partially as a result of the formation of transmembrane pores (9, 10).

Toxicity assays commonly employed within the field generally aim at detecting membrane leakage and evaluating cell viability, whereas for preclinical assessment other physiologically relevant tests, such as hemolysis assays (3, 11), are also relevant to perform. The present chapter will consequently provide protocols for the deoxyglucose membrane leakage assay, the propidium iodide membrane integrity assay, the MTT viability assay (12), and a hemolysis assay for the detection of detrimental CPP impact on erythrocytes, cf. Fig. 1. The deoxyglucose assay provides an indication of plasma membrane integrity and is based on efflux of radiolabeled, intracellularly phosphorylated, deoxyglucose through a compromised plasma membrane (13). The propidium iodide (PI) assay is based on the exclusion of the fluorescent DNA intercalating agent, a property corresponding with healthy, undamaged cells. The MTT assay assesses mitochondrial dehydrogenase activity, through the enzymatic conversion of a tetrazole into formazan, as an indicator of cellular viability, whereas the hemolysis assay quantifies the hemolytic properties of the CPPs.

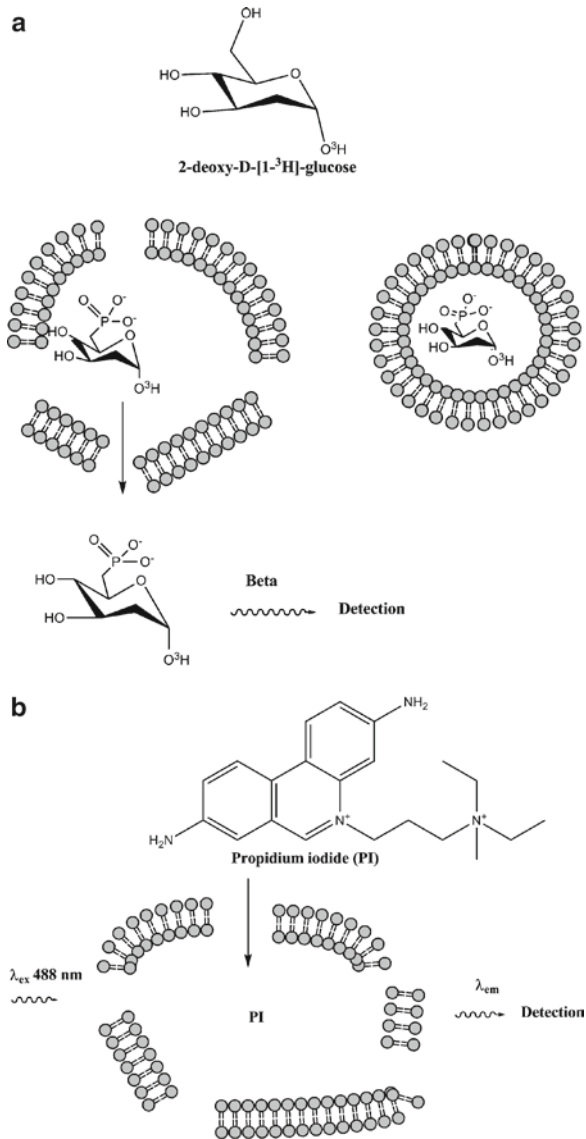


Fig. 1. Schematic overview of utilized methods. **(a)** Deoxyglucose leakage assay, based on the efflux of radiolabeled intracellularly phosphorylated deoxyglucose. **(b)** The propidium iodide (PI) assay relies on healthy cells excluding the fluorescent DNA intercalator. **(c)** Mitochondrial dehydrogenase activity, a property corresponding to healthy cells, is assessed using the MTT assay. **(d)** The hemolysis assay quantifies the hemolytic properties of CPPs.

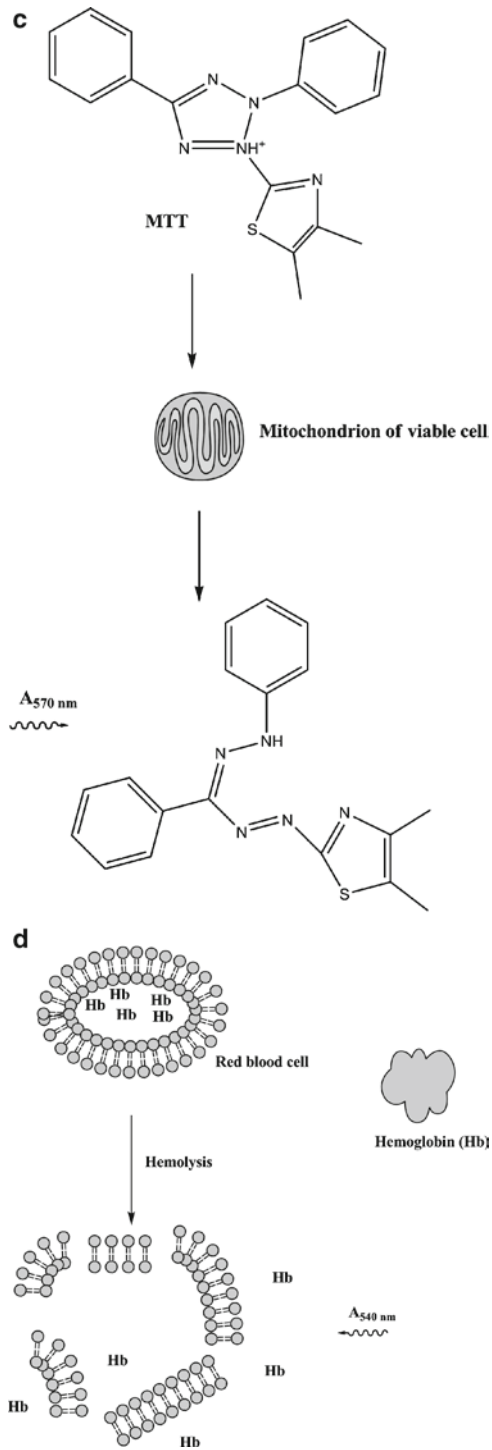


Fig. 1. (continued)

2. Materials

Suitable cell lines and culture media are naturally necessary for carrying out the toxicity assays. A vast number of different cell types, such as HeLa cells, derived from a human cervical carcinoma, Chinese hamster ovary (CHO) cells, and the human breast cancer cell line MDA-MB-231, are commonly utilized within the field. However, in the present chapter, only protocols for HeLa cells will be described, even though it is naturally possible to carry out the experiments using other cell lines as well.

2.1. Deoxyglucose Leakage Assay

1. HeLa cells maintained in Dulbecco's Modified Eagle's Medium (DMEM) with Glutamax, supplemented with 0.1 mM nonessential amino acids, 1.0 mM sodium pyruvate, 10% fetal bovine serum, 100 U/ml penicillin, and 100 mg/ml streptomycin. All reagents purchased from Invitrogen, Sweden.
2. 12-Well culture plates.
3. Aqueous solution of tritiated 2-deoxy-d-glucose (2-deoxy-d-(1-³H)-glucose) (Sigma Aldrich, Sweden). A radioactivity of 0.5 μ Ci (0.185 MBq) is required per well (i.e. per 100,000 cells), plan your experiments accordingly in order to avoid purchasing excessive amounts of radioactive chemicals (see Note 1). Store at or below -20°C .
4. Scintillation fluid, for instance Emulsifier Safe scintillation liquid (Perkin Elmer).
5. HEPES Krebs Ringer (HKR) buffer: 130 mM NaCl, 5 mM KCl, 1.2 mM MgSO_4 , 1.2 mM CaCl_2 , 20 mM HEPES, 1.2 mM Na_2HPO_4 , 10 mM glucose (pH 7.4).
6. 0.2% Triton-X 100 in HKR.

2.2. Propidium Iodide Membrane Integrity Assay

1. HeLa cells maintained in DMEM with Glutamax, supplemented with 0.1 mM nonessential amino acids, 1.0 mM sodium pyruvate, 10% fetal bovine serum, 100 U/ml penicillin, and 100 mg/ml streptomycin. All reagents purchased from Invitrogen, Sweden.
2. 12-Well culture plates.
3. Centrifuge tubes.
4. Phosphate-buffered saline (PBS): 137 mM NaCl, 10 mM Na_2HPO_4 , 2.7 mM KCl, with a pH of 7.4.
5. Trypsin (0.25%) and ethylenediamine tetraacetic acid (EDTA) (1 mM) (Gibco/BRL).
6. PBS containing 0.05 $\mu\text{g}/\text{ml}$ propidium iodide (Sigma Aldrich). Store at or below -20°C .

2.3. MTT Proliferation Assay

1. HeLa cells maintained in DMEM with Glutamax, supplemented with 0.1 mM nonessential amino acids, 1.0 mM sodium pyruvate, 10% fetal bovine serum, 100 U/ml penicillin, and 100 mg/ml streptomycin. All reagents purchased from Invitrogen, Sweden.
2. 96-Well culture plates.
3. MTT (3-(4,5-dimethylthiazol-2-yl)-2,5-diphenyltetrazolium bromide) (5 mg/ml) (Sigma Aldrich) in DMEM. Store at or below -20°C .
4. Absolute isopropanol containing 0.04 M HCl.
5. A highly cytotoxic compound, for instance staurosporine, at an appropriate concentration can with benefit be included as a positive control.

2.4. Hemolysis Assay

1. Bovine blood, supplemented with citrate (see Note 2). Store the blood at or below 4°C and use within the time frame specified by the manufacturer, usually approximately 10 days.
2. PBS and HKR.
3. 0.1% Triton-X 100 in HKR.
4. 1.5 ml Vials and 96-wells culture plates.

3. Methods

The variety of contexts within which CPPs are utilized is steadily increasing. Delivery of proteins, synthetic oligonucleotides and their analogs, plasmids, small-molecule drugs, and even nanoparticles are nowadays mainstream applications of these versatile vectors. Furthermore, the diversity of CPP constructs has also amplified, expanding from the initial covalent conjugates of peptide and cargo into (often relatively ill-defined) complexes and supramolecular structures, such as nanoparticles and aggregates. This spectrum of compounds implies that any arising cytotoxicity might stem from different components in the construct formulation, making it pivotal to determine the exact cause of the toxicity. Including control experiments where both the CPP and its cargo are excluded appears to be a critical determinant behind arriving at accurate conclusions.

The multiple cytotoxic effects potentially exerted by CPP-containing constructs consequently demand a veritable battery of assays evaluating various toxicity aspects. The deoxyglucose leakage assay, as well as the PI assay, is based on the integrity of the plasma membrane, a critical cellular property naturally often affected by CPPs. In spite of their similarities, these two assays evaluate the crossing of the membrane in different directions,

perhaps giving additional clues regarding toxicity mechanisms. The deoxyglucose assay is based on the efflux of the radiolabeled glucose analog, which after cellular uptake is phosphorylated by hexokinases, resulting in a compound unable to penetrate an intact membrane, whereas the PI assay is based on the influx of the DNA intercalator as a measure of membrane integrity.

Assaying for cell viability is naturally absolutely essential for any cytotoxicity assessment and numerous assays are consequently available. The MTT assay (or any one of its many modified variants) offers a fast and relatively simple viability assessment by evaluating mitochondrial dehydrogenase activity, whereas the lysis of erythrocytes gives a hint regarding the behavior in a more clinically relevant setting.

3.1. Deoxyglucose Leakage Assay

1. Determine the radioactivity of the 2-deoxy-d-(1-³H)-glucose solution or, depending on the time of storage, suffice with the manufacturer's information.
2. Harvest the human cervical carcinoma cell line HeLa with trypsin/EDTA when approaching confluence. Subsequently, seed 100,000 cells per well in 12-well culture plates 20 h before treatment.
3. Load the cells with the radiolabeled deoxyglucose for 20 min prior to treatment. A radioactivity of 0.5 μ Ci per well is appropriate but depending on the labeling (specific radioactivity, Ci/mmol) that activity can be modified (see Note 3).
4. Wash the cells three times with HKR to remove all the radiolabeled deoxyglucose present extracellularly.
5. Treat the cells with the desired CPP entities in 500 μ l serum-containing or serum-free DMEM for an appropriate period of time, for instance 1 or 4 h.
6. Remove 100 μ l extracellular aliquots either at a fixed time point after treatment or at several time points during an interval of interest, for instance every 15 min.
7. Lyse the cells with the 0.2% Triton-X 100 in HKR in order to obtain the activity corresponding to total cell lysis.
8. Dilute the obtained samples in 5 ml scintillation fluid, transfer the solution to scintillation vials, and measure the activity on a β -counter.
9. Define the cells treated with 0.2% Triton-X 100 as completely lysed and calculate the cytotoxicity of the respective CPPs. See Fig. 2a, for an example of the results.

3.2. Propidium Iodide Membrane Integrity Assay

1. Harvest the HeLa cells with trypsin/EDTA when approaching confluence. Subsequently, seed 100,000 cells per well in 12-well culture plates 20 h before treatment.

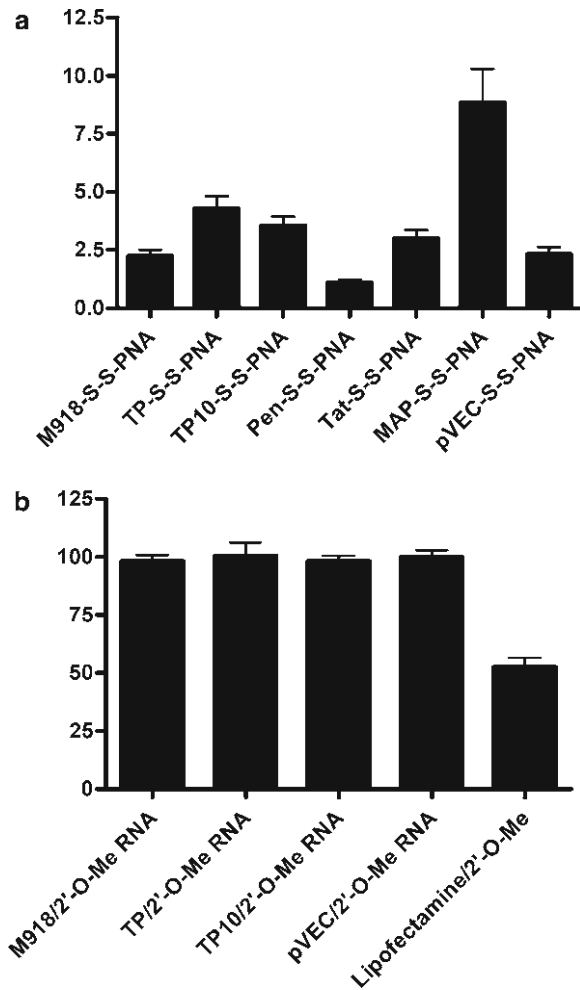


Fig. 2. (a) Deoxyglucose leakage induced in HeLa cells by various CPP-PNA conjugates, at 10 μ M. Total leakage is defined based on cells treated with Triton X-100. Neither conjugate induced a particularly high leakage, except the MAP conjugate, which caused a leakage corresponding to approximately 10% of the effects of the positive control. (b) HeLa cell proliferation assessed using the MTT assay after a 4 h treatment with various noncovalent CPP-oligonucleotide complexes (2 μ M peptide/200 nM 2'-O-Me RNA), with untreated cells defined as 100% viable. Neither CPP-oligonucleotide complex had any significant impact on the cellular proliferation, whereas lipofectamine decreased proliferation by approximately 50%.

2. Prior to the treatment of cells with CPPs, carrying for instance a fluorescently labeled cargo molecule, optionally bioactive, or merely a suitable fluorophore-label on the peptide, a washing step in PBS is applied. Treat the cells with the CPP constructs in 500 μ l serum-containing or serum-free DMEM. After treatment, at least one additional washing step is required in order to detach remaining noninternalized CPPs.

3. The cells are detached with trypsin/EDTA solution for 10 min at 37°C and the reaction is ceased through the addition of 500 µl serum-containing media. The solution containing the detached HeLa cells is transferred to centrifuge tubes and centrifuged at 1,000×*g* for 5 min. After centrifugation, the pellet is washed in PBS and subsequently resuspended in 200 µl PBS containing 0.05 µg/ml PI.
4. Cells are incubated further at 37°C for another 15 min to allow for PI diffusion. Finally, the cell suspension is analyzed using fluorescence-activated cell sorting (FACS) (PI has an excitation wavelength of 488 nm), followed by data processing and analysis in order to assess PI penetration.

3.3. MTT Proliferation Assay

1. HeLa cells are harvested, using trypsin/EDTA, and seeded 20 h before CPP treatment at 10,000 cells per well in 96-well culture plates.
2. Cells are treated with CPPs in 100 µl serum-containing or serum-free DMEM at appropriate concentrations for a predetermined time period, for instance 1, 4, 12, or 24 h.
3. 24 h After treatment, MTT solution is added to the culture medium at a final concentration of 0.5 mg/ml. The cells are exposed to the MTT solution for 4 h at 37°C.
4. The media in each well is replaced with acidic isopropanol containing 0.04 M HCl (see Note 4) in order to solubilize the converted dye.
5. Absorbance is measured in a plate reader at 570 nm, with subtraction of the background absorbance at 670 nm.
6. Cell proliferation can, for instance, be quantified through comparison with untreated cells, where cells in untreated wells are defined as 100% viable. An example of the results is shown in Fig. 2b.

3.4. Hemolysis Assay

1. Bovine blood should generally be used within 10 days of the production date to ensure accurate results. Store blood at 4°C.
2. Centrifuge 10 ml of blood for 10 min at 1,000×*g* (see Note 5).
3. Wash the pellet once with PBS and once with HKR.
4. Resuspend the pellet in HKR to obtain a 4% suspension.
5. Transfer 50 µl to a 1.5 ml vial containing 950 µl CPP solution at an appropriate concentration (see Note 6). Furthermore, create one solution containing the positive control, Triton X-100 in HKR, and one PBS solution constituting the negative control.
6. Incubate for 30 min at 300 rpm and 37°C.

7. Centrifuge the vials at $1,000 \times g$ for 2 min.
8. Transfer 100 μl of supernatant to the 96-wells culture plate and measure absorbance at 540 nm. Define the erythrocytes treated with Triton X-100 as completely lysed and evaluate data accordingly.

4. Notes

1. The half life of ^3H is long (approximately 12 years), thus allowing storage over extended periods of time. ^3H does not pose a significant radiological concern upon external exposure as a result of its weak beta emissions, and it is one of the least radiotoxic radionuclides.
2. Sodium citrate (typically 0.038%) is included as an anticoagulant, as it binds calcium ions required for clotting. Bovine blood can usually be stored for approximately 10 days after the production date, but primarily refer to the manufacturer's instructions.
3. Deoxyglucose is in fact toxic to cells as it interferes with the glucose metabolism. However, the concentrations used in the assay are very low, considering the fact that the specific activity is normally between 5 and 10 Ci/mmol and that the activity per well is approximately 0.5 μCi , and the treatment times are short, wherefore cytotoxicity is not an issue.
4. Complete solubilization of the converted dye is pivotal in order to obtain an accurate assessment of cell proliferation. This can be achieved through careful pipetting up and down several times.
5. Weigh the centrifuge tube prior to centrifugation in order to facilitate calculation of the subsequent suspension.
6. It is worth noting that the concentration intervals likely to arise in an *in vivo* situation do not necessarily correspond to the relevant concentrations for *in vitro* treatments. Consequently, a valid simulation of intravenous injection might require substantial altering of the CPP concentration, depending on the purpose of the potential future application.

Acknowledgments

The work was supported by grants from Swedish Research Council (VR-NT); Center for Biomembrane Research, Stockholm; and Knut and Alice Wallenberg's Foundation.

References

1. Massodi, I., Bidwell, G. L., Davis, A., Tausend, A., Credit, K., Flessner, M., Raucher, D. (2009) Inhibition of ovarian cancer cell metastasis by a fusion polypeptide Tat-ELP. *Clin Exp Metastasis* **26**, 251–260.
2. Wu, B., Moulton, H. M., Iversen, P. L., Jiang, J., Li, J., Li, J., Spurney, C. F., Sali, A., Guerron, A. D., Nagaraju, K., Doran, T., Lu, P., Xiao, X., Lu, Q. L. (2008) Effective rescue of dystrophin improves cardiac function in dystrophin-deficient mice by a modified morpholino oligomer. *Proc Natl Acad Sci U S A* **105**, 14814–14819.
3. Saar, K., Lindgren, M., Hansen, M., Eiriksdottir, E., Jiang, Y., Rosenthal-Aizman, K., Sassian, M., Langel, Ü. (2005) Cell-penetrating peptides: A comparative membrane toxicity study. *Anal Biochem* **345**, 55–65.
4. Mueller, J., Kretzschmar, I., Volkmer, R., Boisguerin, P. (2008) Comparison of cellular uptake using 22 CPPs in 4 different cell lines. *Bioconjug Chem* **19**, 2363–2374.
5. Bárány-Wallje, E., Gaur, J., Lundberg, P., Langel, Ü., Gräslund, A. (2007) Differential membrane perturbation caused by the cell-penetrating peptide Tp10 depending on attached cargo. *FEBS Lett* **581**, 2389–2393.
6. Magzoub, M., Oglecka, K., Pramanik, A., Eriksson, L. E., Gräslund, A. (2005) Membrane perturbation effects of peptides of peptides derived from the N-termini unprocessed prion protein. *Biochim Biophys Acta* **15**, 126–136.
7. Tréhin, R., Krauss, U., Muff, R., Meinecke, M., Beck-Sickingler, A. G., Merkle, H. P. (2004) Cellular internalization of human calcitonin derived peptides in MDCK monolayers: A comparative study with Tat(47-57) and Penetratin(43-58). *Pharm Res* **21**, 33–42.
8. Jones, S. W., Christison, R., Bundell, K., Voyce, C. J., Brockbank, S. M. V., Newham, P., Lindsay, M. A. (2005) Characterisation of cell-penetrating peptide-mediated peptide delivery. *Br J Pharmacol* **145**, 1093–1020.
9. Deshayes, S., Plenat, T., Charnet, P., Divita, G., Molle, F., Heitz, F. (2006) Formation of transmembrane ionic channels of primary amphipathic cell-penetrating peptides. Consequences on the mechanism of cell penetration. *Biochim Biophys Acta* **1758**, 1846–1851.
10. Ziegler, A. (2008) Thermodynamic studies and binding mechanism of cell-penetrating peptides with lipids and glycosaminoglycans. *Adv Drug Deliv Rev* **60**, 580–597.
11. Wu, R. P., Youngblood, D. S., Hassinger, J. N., Lovejoy, C. E., Nelson, M. H., Iversen, P. L., Moulton, H. M. (2007) Cell-penetrating peptides as transporters for morpholino oligomers: effects of amino acid substitution on intracellular delivery and cytotoxicity. *Nucleic Acids Res* **35**, 5182–5191.
12. Mosmann, T. (1983) Rapid colorimetric assay for cellular growth and survival: application to proliferation and cytotoxicity assays. *J Immunol Methods* **65**, 55–63.
13. Walum, E., Peterson, A. (1982) Tritiated 2-deoxy-D-glucose as a probe for cell membrane permeability studies. *Anal Biochem* **120**, 8–11.

Chapter 15

Comparison of CPP Uptake Methods

Tina Holm, Samir EL Andaloussi, and Ülo Langel

Abstract

In the last 15 years, an ever expanding pool of cell-penetrating peptides (CPPs) has been discovered and recently focus has shifted towards improving already existing CPPs by different modifications. Since the number of published peptide sequences with cell-penetrating ability is now reaching several hundreds, the consensus methods to compare the efficacy of these is clearly needed. Many research groups are evaluating the applicability of CPPs as drug delivery vectors, all having their preferred methods of assessing uptake and intracellular distribution. Even when applying the same method, the use of different cell lines, peptide concentrations, exposure conditions, etc. are complicating comparison of data between different groups. This book is a welcome contribution to the CPP research field, hopefully paving the way for standardized protocols to be used in the future. Some of the most common methods used to this date are presented and compared in this chapter.

Key words: CPP, Fluorescence, Microscopy, HPLC, FACS, Spectrofluorometry, Mass spectrometry, Splice correction, Biological response

1. Introduction

Although the first report of a polycationic peptide capable of traversing the cellular plasma membrane was published already in 1965 (1), it was not until 1994 that the potential of this new class of peptides, nowadays called cell-penetrating peptides (CPPs) or protein transduction domains (PTDs), was acknowledged (2). For several years, the general belief was that these peptides entered cells in an energy- and receptor-independent fashion. This hypothesis emanated from studies showing that uptake was not inhibited by lowering the temperature and the fact that peptides of many different origins (β -peptides, peptoids, dendrimers, etc.) were taken up interchangeably. However, in 2001, Lundberg and colleagues reported that nuclear localization of CPPs only

occurred following fixation of the cells, and when using live, unfixed cells, the peptide VP22 only adhered to the plasma membrane (3). In an article published in 2002, the same group also suggested that earlier FACS data could be artifactual, due to extracellularly bound peptides that result in the overestimation of peptide uptake (4). This was later confirmed by Richards et al. (5). Although other groups have demonstrated that fixation has negligible effect on peptide localization (6, 7), working on only live cells is recommended now. Different approaches to discriminate between extracellularly bound and truly internalized peptides have emerged, some of which will be presented later in this chapter, cf. Table 1. The most common strategy is to utilize enzymes in order to degrade peptides bound to the plasma membrane. Unfortunately, peptides buried in the plasma membrane, or bound to the intracellular face of it, are out of range for degradation and will therefore be interpreted as internalized. Furthermore, fluorescence-based assays used for the evaluation of quantitative uptake also suffer from the inability to discriminate truly internalized peptides from those residing in inaccessible vesicular compartments. However, there are methods to address the uptake of CPPs, which discriminates between membrane bound and free bioavailable peptide, such as the splice correcting assay, and these are presented in the end of this chapter. The intracellular fate of peptides following internalization is a question that needs clarification when elucidating new CPPs. Today the general belief is that endocytosis is the major entry route for CPPs, although there are reports that other mechanisms may be involved as well (8–10). The use of different endocytosis inhibitors and markers for specific endocytic pathways has been pivotal to reach that conclusion. Lately, researchers in the field have explored various molecular biology approaches to knockdown or over express essential proteins for the different endocytic pathways (10). Such strategies are more reliable since endocytosis inhibitors are rather toxic and unspecific and tracers are not always internalized exclusively through only one pathway.

Many initial studies, short after the discovery of CPPs, were focusing on the uptake and intracellular distribution of free peptides. However, recent publications suggest that the uptake pattern might differ, when the CPP is coupled to a cargo (11–13). The variation is not only in the level of internalization, but also in the route of uptake (12, 13). Thus, every CPP–cargo complex needs to be investigated individually, and results from free peptides cannot automatically be extrapolated to their cargo-coupled counterpart.

Since there is no single method to unambiguously determine the internalization efficacy of a CPP, a recommendation is to use several in conjunction, thereby circumventing the negative aspects of the different approaches. One combination of methods

Table 1
Overview of the presented methods

Method	End-point	Pros	Cons
Microscopy	Intracellular distribution of fluorophore-labeled peptide	Not biased by membrane bound peptides	Does not discriminate between intact and degraded peptide
HPLC	Peptide degradation and intracellular localization	Possible to determine the amount of internalized and degraded peptide	Restricted to peptides containing primary amines
Fluorescence-activated cell sorting	Cellular uptake of peptide	Possible to assess the percentage of transfected cells and discriminate between live and dead cells	Does not discriminate between internalized and membrane bound peptide or peptides trapped in endosomes
Quantitative uptake by spectrofluorometry	Amount of internalized peptide	Quick, cheap, and easy method for initial screening of new CPPs	Does not discriminate between internalized and membrane bound peptide or peptides trapped in endosomes
Electron microscopy	Intracellular distribution of peptide	High magnification enabling visualization at the organelle level	Laborious sample preparation procedure requiring skilled personnel
Mass spectrometry	Quantitative determination of peptide uptake and degradation	Allows tracking of peptide degradation and identification of the degradation products	Does not discriminate between internalized and membrane bound peptide or peptides trapped in endosomes
Splice correction	Biological activity of CPP-splice correcting oligonucleotide conjugates	Positive readout, thereby avoiding interference from unspecific toxicity. Measures biological activity of the cargo, not only localization	Expensive and requires access to specific cells
Cre-recombinase	Cellular delivery of functional protein	Positive read out, thereby avoiding interference from unspecific toxicity	Requires recombinant expression of CPP-Cre protein
Apoptosis and proliferation	Induction of apoptosis and proliferational arrest	Biological activity of the cargo, not only localization	Might be biased by nonspecific toxicity arising from the peptide per se

providing different pieces to the puzzle could be quantitative uptake by fluorometry and confocal microscopy. However, when push comes to shove, it is a biological effect of the cargo that is the goal of most studies, and this is also the way to demonstrate

the bioavailability of CPP–cargo complexes. Therefore, a complete study of a CPP should ultimately show that it is able to deliver its cargo to the desired intracellular compartment. Some methods based on biological readouts are presented in the end of this chapter.

2. Methods

2.1. Fluorescence-Based Assay

When looking in the rear-view mirror, fluorescence-based techniques are by far the most commonly exploited approaches to assess the uptake of cell-penetrating peptides. Peptides are labeled with a fluorophore, most commonly fluorescein, and the cellular uptake is then measured using different techniques. Although all these techniques provide information regarding peptide uptake, it should be emphasized that uptake of fluorophore-labeled peptides does not necessarily correlate with uptake of free peptides. Furthermore, different fluorophores might affect both uptakes, intracellular distribution, and toxicity of peptides differently (14–16).

2.1.1. Microscopy

As aforementioned, before 2001 most studies on cellular internalization of CPPs were conducted using fluorescence microscopy on fixed cells. However, after the discovery by Lundberg et al. that cell fixation could cause artifactual results, caution is nowadays given to working with fixed cells (3). It is becoming increasingly common to use confocal microscopy, since this technique makes it possible to visualize one focal plane of the cell. As mentioned above, several methods are flawed with poor discrimination between membrane bound and intracellular peptide. These methods are recommended to be used in conjunction with microscopy, which provides further information regarding the exact intracellular localization of peptide.

In mechanistic studies of CPP internalization pathways, fluorescent markers for different endocytic routes enable the determination of the uptake mechanism of CPPs by analyzing the extent of colocalization between CPP and the marker. Another major advantage with microscopy is that viability of cells can be ascertained, both by morphological means by analyzing the cells in bright field and by staining the cells with, e.g., propidium iodide, which only stains cells with impaired cellular membranes. However, microscopy is almost exclusively used as a qualitative measure of peptide uptake. Although possible, the quantitative determination of fluorescent peptide uptake from a cell image is not ideal since it is relatively laborious and not suitable for analysis of multiple samples. Furthermore, the fact that peptides are rather unstable when in contact with cells complicates the picture because

fluorescence inside cells might arise from fluorescent degradation products rather than intact peptides. There are methods to determine peptide degradation with microscopy, e.g., fluorescent resonance energy transfer (FRET), but these are laborious and outside the scope of this chapter. An excellent method based on FRET that enables real-time quantitative measurement of cytosolic uptake in single cells is presented by Adams and Tsien (17, 18). A protocol describing the sample preparation preceding confocal microscopy analysis is presented in Nature Protocols (19).

2.1.2. HPLC

Peptide degradation is an issue that, unfortunately, has not received much attention. Albeit being a well-known problem, only a handful of articles have been published addressing this issue. One excellent method of determining peptide degradation, and simultaneously receiving quantitative information regarding intracellular uptake of CPPs, was developed by Oehlke et al. in 1998 (20). By chemically modifying peptides bound to the extracellular face of the plasma membrane, making them more hydrophobic, it is possible to distinguish these from truly internalized peptides by means of reverse phase HPLC, since modified peptides have a longer retention time. From the chromatograms, it is possible to determine not only the amount of internalized peptide in total, but also the amount of intact and degraded peptides. This assay has been excellently exploited by Palm et al. to determine the extra- and intracellular degradation rates of CPPs (21). Although being an outstanding method for determining peptide uptake and degradation, it is restricted to peptides containing primary amines, i.e., lysine. However, recently Aubry et al. utilized the same method to assess uptake of thiol-containing peptides (22).

2.1.3. Fluorescence-Activated Cell Sorting

Probably the most commonly used method to determine CPP uptake is fluorescence-activated cell sorting (FACS). With this technique, it is possible to discriminate between live and dead cells while quantifying the CPP uptake. As the name implies, it is a fluorescence-based technique that sorts cells at the single cell level. A major advantage with FACS analysis is that it enables measurement of the percentage of cells that have been transfected. After CPP incubation, it is imperative that the cells are subjected to enzymatic treatment, i.e., trypsin or pronase, to remove extracellularly bound peptides (5). However, as with most fluorescence-based techniques, it is not possible to discriminate between truly internalized and membrane bound peptides (peptides that are buried in the membrane or bound to the intracellular face of the membrane) or peptides trapped in endosomes.

2.1.4. Quantitative Uptake by Spectrofluorometry

When having a large number of peptides to be tested for their cell-penetrating ability, a quick and easy screening method to

assess the uptake quantitatively is highly appreciated. Quantitative uptake by spectrofluorometry is a method that makes it possible to determine the amount of internalized, fluorophore-conjugated CPP. In this assay, fluorescently labeled peptides are incubated with cells followed by a mild trypsin treatment to remove peptides bound to the outside of the plasma membrane. By comparing the intracellular fluorescence from cell lysates with fluorescence of exposure solution, it is possible to estimate the number of molecules being internalized. By normalizing against the protein content of the cells, a quantitative value of internalizing capacity is achieved. This method is cheap, only takes a couple of hours and several CPPs can be compared simultaneously. It is very easy to perform and needs no prior experience. When investigating different uptake pathways, different endocytosis inhibitors can be employed to determine the possible uptake mechanisms of CPPs (23). However, a disadvantage is that peptides trapped in endosomes cannot be discriminated from truly internalized peptides. As mentioned earlier, several methods are needed in conjunction to surely determine the cellular uptake. The method presented here is excellent as an initial screening tool; peptides that show no cellular uptake can be excluded from further studies, while the ones generating a positive result are further investigated. A protocol describing this method in more detail is published in *Nature Protocols* (19).

2.2. Electron Microscopy

The important question of where CPPs are localized inside the cell following internalization is probably best answered with the help of electron microscopy. An electron microscope has higher resolving power than an ordinary light microscope, enabling visualization at the organell level. Also, the subcellular localization of peptides does not affect the readout as compared to confocal microscopy, where different fluorophores are quenched differently in different organelles. Although being the method providing the highest magnification, most laboratories are not equipped with electron microscopes and the sample preparation procedure requires an experienced person. For further details regarding the use of electron microscopy for CPP evaluations, consult references from the group of Pooga (24, 25).

2.3. Mass Spectrometry

A major hurdle with the use of peptides as drug delivery tools *in vivo* is their rapid degradation in the presence of serum. The only method that allows simultaneous tracking of peptide degradation and identification of the degradation products is mass spectrometry. However, the presence of serum in the sample to be investigated results in high background and thereby a lower signal-to-noise ratio. The use of ZipTips® (Millipore) is a way to concentrate and purify the peptide from an exposure solution or cell lysate. ZipTips® is a 10- μ l pipette tip with a bed of chromatography media fixed at

its end with no dead volume. Hydrophobic peptides bind to the chromatography media while contaminants are washed away. The concentrated, purified sample is eluted in a small volume of compatible solvent (26). Although being an efficient approach to concentrate peptides, the many washing steps prohibit preparation of many samples at the same time and, more importantly, peptides with low hydrophobicity are lost in the preparation process. Burlina et al. reported a strategy to quantitatively determine uptake and degradation of CPPs (27). Peptide quantification by MALDI-TOF mass spectrometry can only be achieved by using the same peptide labeled with a stable isotope as an internal standard. The CPP and the internal standard are both biotinylated to enable purification from the cell lysate. Following incubation of CPP with cells, a trypsin digestion step is important to remove extracellularly bound peptides. By introducing the internal standard already at the cell lysis step, peptide degradation during sample preparation can be monitored. This method does not only allow a quantitative determination of peptide uptake and degradation, but also the use of mixtures of CPPs, as long as the molecular mass is different. Furthermore, it is possible to accurately discriminate between internalized and membrane bound peptide. A detailed protocol for quantitative uptake determination of CPPs, as well as their cargo, using this approach has been published in Nature Protocols (28).

2.4. Biological Response

Although fluorescence-based assays are very useful for the initial screening of new CPPs, methods based on biological readouts are preferred for more detailed analysis. CPPs are defined as a class of delivery vehicles, meaning that they are exploited for the delivery of different cargos. Therefore, if aiming at for example transfecting oligonucleotides or analogs thereof such as peptide nucleic acids (PNA), it is advised to use assays that measure the activity of the cargo inside cells. Numerous studies have recently emphasized the importance of using functional assays generating biological readouts since uptake of fluorophore-labeled peptides does not inevitably correlate with a biological response. We and others have shown that some fluorophore-labeled CPP-PNA conjugates enter cells efficiently without being able to induce a biological response (23, 29, 30). Also the inverse relation has been reported; low uptake according to fluorescence-based techniques but strong biological response (29, 31, 32). Therefore, some of the assays used to address these issues are further described in this section.

2.4.1. Splice Correction

The use of splice correcting oligonucleotides (SCOs) as a research tool to assess the cargo delivery capacity of CPPs has become common in last years. However, this method and the HeLa pLuc 705 cells upon which the assay is dependent, was developed by Kole and colleagues already in 1998 (33). These cells are stably transfected with a luciferase reporter gene, which is interrupted

by an intron from β -globin pre-mRNA containing an aberrant splice site. The aberrant splice site activates a cryptic splice site and under normal conditions nonfunctional luciferase is produced. Upon introduction of SCOs binding complementary to the aberrant splice site, splicing is redirected and functional luciferase is produced. By coupling different CPPs to SCOs complementary to the cryptic splice site, their capacity as drug delivery vectors can be assessed. Since the splicing event is taking place in the nucleolus, this assay gives information regarding intracellular distribution of the SCO and shows whether fractions of CPP-SCO conjugates have escaped endosomes or not, making this assay superior to many others based on fluorescence techniques. Another major advantage with this method is that it generates a positive biological readout. However, it requires access to the specific cell line, HeLa pLuc 705, upon which the assay is dependent and the luciferase substrate necessary for the detection of luminescence is expensive. A detailed protocol for the splice correcting assay for the assessment of CPP uptake is published in Nature Protocols (34).

2.4.2. Cre-Recombinase

An elegant method to determine protein transduction by CPPs is based on the Cre-*loxP* system. Cre-recombinase is a topoisomerase that catalyzes site-specific recombination of DNA between *loxP* sites. An implementation of this system in the study of cellular protein delivery by CPPs was introduced by Wadia et al. (35). Tat-Cre protein was introduced to mouse reporter T-cells containing a *loxP*-STOP-*loxP* EGFP gene, resulting in the excision of the STOP segment and EGFP expression, which requires nuclear translocation. The positive readout of this method is a clear advantage, since unspecific toxicity is not interfering with the results. Although elegantly designed, this method is not widely used. The main reason for this is that it relies on recombinant expression of CPP-Cre. This is rather laborious and it is difficult to obtain sufficient amounts for multiple experiments. Furthermore, Cre is a rather large cargo that will influence the properties of the CPP.

2.4.3. General: Apoptosis and Proliferation

The vast majority of CPPs are investigated for their potential use as drug delivery vehicles in animals and humans. Cancer research is an area where CPPs have been extensively utilized as transporters of different drugs for chemotherapy; either newly discovered or those currently in use that might need improved cellular delivery. Since the cellular end-points in cancer research is the induction of apoptosis and reduction of proliferation, a plethora of methods has been developed to determine the cellular fate after peptide treatment (36). The main problem with utilizing methods that monitors proliferational arrest is that they might be biased by nonspecific toxicity arising from the peptide per se and not the biological effect of the cargo. Hence, it is extremely important to include all possible controls in order to avoid artifactual results.

3. Conclusions

A plethora of different methods are today used for the assessment of CPP–cargo delivery capacity. Also biophysical approaches, based on the use of small and large unilamellar vesicles, are informative and provide valuable information regarding peptide–membrane interactions without the involvement of other components present in cellular plasma membranes. The simplicity of these systems makes it hard to translate the results to cells but could be used complementary to other cellular-based methods. All methods presented in this chapter have their pros and cons. When evaluating the potency of new potential CPPs, it is recommended to use several methods in conjunction and combining them in such a way that their limitations do not overlap. Although fluorescence-based assays are very useful for initial screening of new CPPs, these should ultimately be combined with methods that address the biological activity of the delivered cargo. In order to obtain a clear and unbiased picture of the characteristics of a new CPP, using a combination of assays is of outermost importance and this chapter provides an overview of some recommended strategies.

Acknowledgments

The work was supported by grants from Swedish Research Council (VR-NT); Center for Biomembrane Research, Stockholm; and Knut and Alice Wallenberg’s Foundation.

References

1. Ryser, H. J. and Hancock, R. (1965) Histones and Basic Polyamino Acids Stimulate the Uptake of Albumin by Tumor Cells in Culture. *Science*. **150**, 501–503.
2. Derossi, D., Joliot, A. H., Chassaing, G., and Prochiantz, A. (1994) The Third Helix of the Antennapedia Homeodomain Translocates through Biological Membranes. *J. Biol. Chem.* **269**, 10444–10450.
3. Lundberg, M. and Johansson, M. (2001) Is VP22 Nuclear Homing an Artifact? *Nat. Biotechnol.* **19**, 713–714.
4. Lundberg, M. and Johansson, M. (2002) Positively Charged DNA-Binding Proteins Cause Apparent Cell Membrane Translocation. *Biochem. Biophys. Res. Commun.* **291**, 367–371.
5. Richard, J. P., Melikov, K., Vives, E., Ramos, C., Verbeure, B., Gait, M. J., Chernomordik, L. V., and Lebleu, B. (2003) Cell-Penetrating Peptides. A Reevaluation of the Mechanism of Cellular Uptake. *J. Biol. Chem.* **278**, 585–590.
6. Säälük, P., Elmquist, A., Hansen, M., Padari, K., Saar, K., Viht, K., Langel, Ü., and Pooga, M. (2004) Protein Cargo Delivery Properties of Cell-Penetrating Peptides. A Comparative Study. *Bioconjug. Chem.* **15**, 1246–1253.
7. Console, S., Marty, C., Garcia-Echeverria, C., Schwendener, R., and Ballmer-Hofer, K. (2003) Antennapedia and HIV Transactivator of Transcription (TAT) “Protein Transduction Domains” Promote Endocytosis of High Molecular Weight Cargo upon Binding to Cell Surface Glycosaminoglycans. *J. Biol. Chem.* **278**, 35109–35114.
8. Duchardt, F., Fotin-Mleczek, M., Schwarz, H., Fischer, R., and Brock, R. (2007) A Comprehensive Model for the Cellular Uptake of Cationic Cell-Penetrating Peptides. *Traffic*. **8**, 848–866.

9. Deshayes, S., Morris, M., Heitz, F., and Divita, G. (2008) Delivery of Proteins and Nucleic Acids using a Non-Covalent Peptide-Based Strategy. *Adv. Drug Deliv. Rev.* **60**, 537–547.
10. Ter-Avetisyan, G., Tünnemann, G., Nowak, D., Nitschke, M., Herrmann, A., Drab, M., and Cardoso, M. C. (2009) Cell Entry of Arginine-Rich Peptides is Independent of Endocytosis. *J. Biol. Chem.* **284**, 3370–3378.
11. El-Andaloussi, S., Järver, P., Johansson, H. J., and Langel, Ü. (2007) Cargo-Dependent Cytotoxicity and Delivery Efficacy of Cell-Penetrating Peptides: A Comparative Study. *Biochem. J.* **407**, 285–292.
12. Tünnemann, G., Martin, R. M., Haupt, S., Patsch, C., Edenhofer, F., and Cardoso, M. C. (2006) Cargo-Dependent Mode of Uptake and Bioavailability of TAT-Containing Proteins and Peptides in Living Cells. *FASEB J.* **20**, 1775–1784.
13. Silhol, M., Tyagi, M., Giacca, M., Lebleu, B., and Vives, E. (2002) Different Mechanisms for Cellular Internalization of the HIV-1 Tat-Derived Cell Penetrating Peptide and Recombinant Proteins Fused to Tat. *Eur. J. Biochem.* **269**, 494–501.
14. Fischer, R., Waizenegger, T., Kohler, K., and Brock, R. (2002) A Quantitative Validation of Fluorophore-Labelled Cell-Permeable Peptide Conjugates: Fluorophore and Cargo Dependence of Import. *Biochim. Biophys. Acta.* **1564**, 365–374.
15. Jones, S. W., Christison, R., Bundell, K., Voyce, C. J., Brockbank, S. M., Newham, P., and Lindsay, M. A. (2005) Characterisation of Cell-Penetrating Peptide-Mediated Peptide Delivery. *Br. J. Pharmacol.* **145**, 1093–1102.
16. Dupont, E., Prochiantz, A., and Joliot, A. (2007) Identification of a Signal Peptide for Unconventional Secretion. *J. Biol. Chem.* **282**, 8994–9000.
17. Adams, S. R. and Tsien, R. Y. (2006) Imaging the Influx of Cell-Penetrating Peptides into the Cytosol of Individual Cells, in *Handbook of Cell-Penetrating Peptides* (Ü. Langel, Ed.) 2nd ed., pp 505–512, CRC, Boca Raton.
18. Adams, S. R. and Tsien, R. Y. (2008) Preparation of the Membrane-Permeant Biarsenicals FIA₅H-EDT2 and ReAs₅H-EDT2 for Fluorescent Labeling of Tetracysteine-Tagged Proteins. *Nat. Protoc.* **3**, 1527–1534.
19. Holm, T., Johansson, H., Lundberg, P., Pooga, M., Lindgren, M., and Langel, Ü. (2006) Studying the Uptake of Cell-Penetrating Peptides. *Nat. Protoc.* **1**, 1001–1005.
20. Oehlke, J., Scheller, A., Wiesner, B., Krause, E., Beyermann, M., Klauschenz, E., Melzig, M., and Bienert, M. (1998) Cellular Uptake of an Alpha-Helical Amphipathic Model Peptide with the Potential to Deliver Polar Compounds into the Cell Interior Non-Endocytically. *Biochim. Biophys. Acta.* **1414**, 127–139.
21. Palm, C., Jayamanne, M., Kjellander, M., and Hällbrink, M. (2007) Peptide Degradation is a Critical Determinant for Cell-Penetrating Peptide Uptake. *Biochim. Biophys. Acta.* **1768**, 1769–1776.
22. Aubry, S., Burlina, F., Dupont, E., Delaroche, D., Joliot, A., Lavielle, S., Chassaing, G., and Sagan, S. (2009) Cell-Surface Thiols Affect Cell Entry of Disulfide-Conjugated Peptides. *FASEB J.* **23**, 2956–2967.
23. Lundin, P., Johansson, H., Guterstam, P., Holm, T., Hansen, M., Langel, Ü., and EL Andaloussi, S. (2008) Distinct Uptake Routes of Cell-Penetrating Peptide Conjugates. *Bioconjug. Chem.* **19**, 2535–2542.
24. Säälilik, P., Padari, K., Niinep, A., Lorents, A., Hansen, M., Jokitalo, E., Langel, Ü., and Pooga, M. (2009) Protein Delivery with Transportans Is Mediated by Caveolae rather than Flotillin-Dependent Pathways. *Bioconjug. Chem.* **20**(5), 877–887.
25. Padari, K., Säälilik, P., Hansen, M., Koppel, K., Raid, R., Langel, Ü., and Pooga, M. (2005) Cell Transduction Pathways of Transportans. *Bioconjug. Chem.* **16**, 1399–1410.
26. Elmquist, A. and Langel, Ü. (2003) In Vitro Uptake and Stability Study of pVEC and its all-D Analog. *Biol. Chem.* **384**, 387–393.
27. Burlina, F., Sagan, S., Bolbach, G., and Chassaing, G. (2005) Quantification of the Cellular Uptake of Cell-Penetrating Peptides by MALDI-TOF Mass Spectrometry. *Angew. Chem. Int. Ed Engl.* **44**, 4244–4247.
28. Burlina, F., Sagan, S., Bolbach, G., and Chassaing, G. (2006) A Direct Approach to Quantification of the Cellular Uptake of Cell-Penetrating Peptides using MALDI-TOF Mass Spectrometry. *Nat. Protoc.* **1**, 200–205.
29. Mäe, M., El Andaloussi, S., Lundin, P., Oskolkov, N., Johansson, H. J., Guterstam, P., and Langel, Ü. (2009) A Stearilated CPP for Delivery of Splice Correcting Oligonucleotides using a Non-Covalent Co-Incubation Strategy. *J. Control. Release.* **134**, 221–227.
30. Abes, S., Moulton, H. M., Clair, P., Prevot, P., Youngblood, D. S., Wu, R. P., Iversen, P. L., and Lebleu, B. (2006) Vectorization of Morpholino Oligomers by the (R-Ahx-R)₄ Peptide Allows Efficient Splicing Correction

- in the Absence of Endosomolytic Agents. *J. Control. Release.* **116**, 304–313.
31. Abes, R., Moulton, H. M., Clair, P., Yang, S. T., Abes, S., Melikov, K., Prevot, P., Youngblood, D. S., Iversen, P. L., Chernomordik, L. V., and Lebleu, B. (2008) Delivery of Steric Block Morpholino Oligomers by (R-X-R)₄ Peptides: Structure-Activity Studies. *Nucleic Acids Res.* **36**, 6343–6354.
 32. Lehto, T., Abes, R., Oskolkov, N., Suhorutsenko, J., Copolovici, D. M., Mäger, I., Viola, J. R., Simonsson, O., Guterstam, P., Eriste, E., Smith, C. I., Lebleu, B., El Andaloussi, S., and Langel, Ü. (2010) Delivery of Nucleic Acids with a Stearylated (RxR)₄ Peptide using a Non-Covalent Co-Incubation Strategy. *J. Control. Release.* **141**(1), 42–51.
 33. Kang, S. H., Cho, M. J., and Kole, R. (1998) Up-Regulation of Luciferase Gene Expression with Antisense Oligonucleotides: Implications and Applications in Functional Assay Development. *Biochemistry.* **37**, 6235–6239.
 34. El Andaloussi, S., Guterstam, P., and Langel, Ü. (2007) Assessing the Delivery Efficacy and Internalization Route of Cell-Penetrating Peptides. *Nat. Protoc.* **2**, 2043–2047.
 35. Wadia, J. S., Stan, R. V., and Dowdy, S. F. (2004) Transducible TAT-HA Fusogenic Peptide Enhances Escape of TAT-Fusion Proteins After Lipid Raft Macropinocytosis. *Nat. Med.* **10**, 310–315.
 36. Aroui, S., Brahim, S., De Waard, M., Breard, J., and Kenani, A. (2009) Efficient Induction of Apoptosis by Doxorubicin Coupled to Cell-Penetrating Peptides Compared to Unconjugated Doxorubicin in the Human Breast Cancer Cell Line MDA-MB 231. *Cancer Lett.* **285**(1), 28–38.

Chapter 16

Characterization of Cellular Internalization Pathways for CPP-Mediated Oligonucleotide Delivery

Peter Guterstam, Samir EL Andaloussi, and Ülo Langel

Abstract

The methods for evaluating internalization pathways of cellular CPP-mediated ON delivery utilizing a pre-mRNA splice correction assay and fluorescence-based quantification are described. Examples for characterization of CPP uptake routes, employing various endocytosis inhibitors, and special treatment conditions are demonstrated. The methods are developed to characterize cellular delivery of pre-mRNA splice switching peptide nucleic acids conjugated to CPPs by disulfide bond.

Key words: Pre-mRNA splicing, Oligonucleotide delivery, Internalization pathways, Endocytosis inhibitors

1. Introduction

Various reporter strategies are used to assess the quantitative and qualitative cellular transduction of CPPs. The most commonly used strategy is the employment of fluorescently labeled CPPs, even though it has been shown that the use of labeled CPPs for the evaluation of delivery efficacy can give artifacts such as false-positive results from CPPs bound to the cellular membrane or entrapment in intracellular vesicles (1). Cellular localization studies using low concentrations of fluorescently labeled CPPs and peptide nucleic acids (PNA) showing no or vague cellular uptake can still give rise to biological effect from the PNA cargo (2). Although fluorescence-based methods offer useful information regarding the localization of peptides and cargo molecules, there are several concerns hampering the utility of fluorescence-based methods. First, different fluorophores can affect the intracellular distribution of peptides differently (3). Second, the fluorophore might affect cellular uptake and cytotoxicity of the peptide (4). Third, and most importantly,

uptake observed with fluorophore-labeled peptides or cargo molecules does not necessarily correlate with bioavailability of the delivered cargo (5). It is therefore appropriate to complement uptake experiments where fluorescently labeled CPPs are utilized with a biological readout strategy where the cargo actually induces conversion of a substrate in living cells. Examples of methods to assess the biologically relevant delivery of proteins and oligonucleotides (ONs) are the cyclization recombination (CRE)-recombinase system (6) and Kole's splice correction assay (7). The first method relies on the use of CRE recombinase–CPP fusion proteins, which requires recombinant expression, making the method less suitable as a first indicator when screening novel CPPs. The latter method is exploited in this protocol and makes use of relatively small (18-mer) neutral antisense PNA ON as cargo. The method described here can also be employed for characterization of CPP-mediated delivery of anionic ONs, such as 2'-*O*-methyl RNA or locked nucleic acids (LNA), complexed to CPPs by noncovalent incubation.

We suggest that a PNA ON is a suitable model cargo for CPPs, as the size of such cargo is in reasonable proportion to the size of CPPs and therefore should not hamper or influence the cell-penetrating function and characteristics of the CPP per se. Additionally, there are several therapeutic applications for ONs, where cellular delivery is a common obstacle, for example, in manipulation of pre-mRNA splicing for the treatment of genetic disorders (8, 9), protein downregulation by mRNA antisense ONs (10) or by siRNA (11). The splice correction assay developed by Kole and coworkers (7) is a cellular assay in which the activity of an antisense ON results in the upregulation of functional, and thereby detectable, luciferase gene expression. Briefly, a plasmid carrying the luciferase coding sequence is interrupted by an insertion of intron 2 from β -globin pre-mRNA carrying an aberrant splice site. Unless this splice site is masked by antisense ONs, the pre-mRNA of luciferase will be improperly processed, resulting in expression of non-functional luciferase proteins. By using HeLa pLuc 705 cells that are stably transfected with this plasmid, various vectors can be evaluated by measuring the luciferase activity in cells. Hence, as this is a positive readout system, it eliminates the flaws associated with functional assays based on protein downregulation.

We describe a protocol, using the above-mentioned splicing correction system, which allows for rapid screening of the delivery efficacy of CPPs. In addition, the very same protocol is utilized to determine the uptake mechanism of CPPs, using various endocytosis inhibitors and treatment at 4°C. The strategy employed to create a transducible entity consists of PNA, targeting the aberrant splice site, covalently conjugated to a CPP by disulfide bridge (12, 13). CPP-mediated delivery of negatively charged ONs, e.g., phosphorothioate 2'-*O*-methyl RNA or LNA, as non-

covalent complexes can also be employed utilizing this method (14–16). The protocol for preparing such noncovalent complexes is described in Chapter 26. By using fluorescently labeled PNA in conjugate with CPP, it is possible to measure not only luciferase activity, i.e., splice correction, but also regular quantitative uptake by fluorometry in the very same cell lysate (17).

Most reports evaluating CPP uptake mechanisms have examined the Tat peptide, either per se or conjugated to various cargo molecules (18, 19). Usually, internalization mechanisms of CPPs are assessed by using different endocytosis inhibitors that act by selectively blocking specific endocytosis pathways. Results are divergent, and depending on study, the uptake has been ascribed to classical clathrin-mediated endocytosis (CME) (18), lipid raft/caveolae-mediated endocytosis (19), macropinocytosis (6), or a combination thereof (20). The differences in results could in part be explained by the fact that different cargo molecules and treatment concentrations have been used. Furthermore, it is probably a reasonable assumption that different CPPs utilize different mechanisms for translocation into cells. In this protocol, we describe the use of three well-known endocytosis inhibitors to distinguish between these pathways. Wortmannin was employed to inhibit both macropinocytosis and clathrin-mediated endocytosis, whereas cytochalasin D and chlorpromazine inhibit macropinocytosis and CME, respectively. To characterize the influence of extracellular structures on CPP-uptake mechanisms, initial cleavage of extracellular proteoglycans by, e.g., heparinase III, cell-incubation in excess of heparin or performing the experiments with heparan sulfate deficient cells is recommended. Chloroquine that buffers intracellular vesicles delaying the lysosomal pathway for endosomes and thereby facilitates potential endosomal release (21) is used to evaluate the contribution of endosomal pathways involved in the cellular uptake of CPP–PNA conjugates. To facilitate the interpretation of experimental results, we have included a table with guidelines for described compounds (Table 1).

The method described here can easily be modified to include alternative strategies for pathway characterization, e.g., by including other available pathway specific inhibitors or tracers provided they are used at effective concentrations without exhibiting cytotoxicity. In Figs. 1 and 2, an example of pathway characterization for the CPP penetratin (22) (RQIKIWFQNRRMKWKK) is shown.

2. Materials

As this protocol for characterizing CPP-uptake pathways is based on delivery of splice-correcting PNA ONs, we have evaluated delivery in the splice correction assay introduced by Kole

Table 1
Guide for characterization CPP-uptake pathways

Cell treatment	Mechanism of action	Suggested pathway if cellular uptake is	
		Increased	Decreased
+4°C	Inhibits endocytosis	Not endocytosis	Endocytosis
Wortmannin	Inhibits macropinocytosis and CME	Clathrin and macropinocytosis independent uptake	Endocytosis or clathrin-mediated uptake
Cytochalasin D	Inhibits macropinocytosis	Not macropinocytosis	Macropinocytosis
Chlorpromazine	Inhibits CME	Clathrin-independent uptake	Clathrin-mediated uptake
Chloroquine	Promotes endosomal release	Endocytosis	Not endocytosis
Heparinase III	Cleaves extracellular heparan sulfates	Uptake independent of heparan sulfates	Heparane sulfate dependent uptake

Expected effect on cellular uptake for various compounds used to characterize translocation pathways for CPP-PNA conjugates

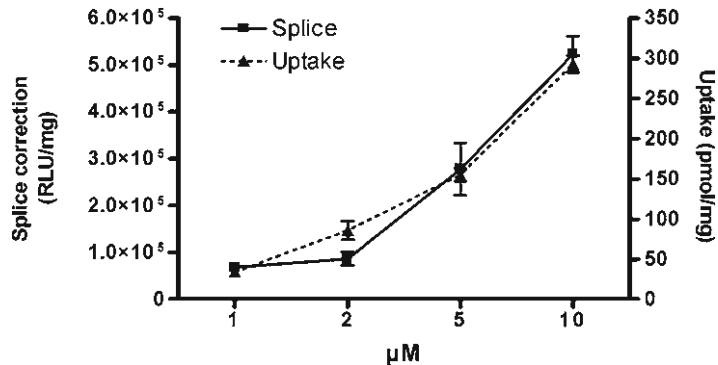


Fig. 1. Bioactivity and quantitative uptake for penetratin. Example of the correlation between splice correction and quantitative uptake of the CPP penetratin conjugated to PNA. Cells were treated at different conjugate concentrations. The qualitative uptake is displayed as RLU per mg cellular protein and quantitative uptake is displayed as pmol conjugate per mg cellular protein. In this case, the quantitative uptake correlates well with observed biological activity. The figure is reprinted from ref. (13) with permission from *Nature protocols*.

and colleagues (7). The assay is based on a human cervical cancer cell line HeLa that has been genetically modified, i.e., HeLa pLuc705 cells. These cells are stably transfected with a plasmid carrying the luciferase coding sequence interrupted by an insertion of intron 2 from β -globin pre-mRNA carrying an aberrant

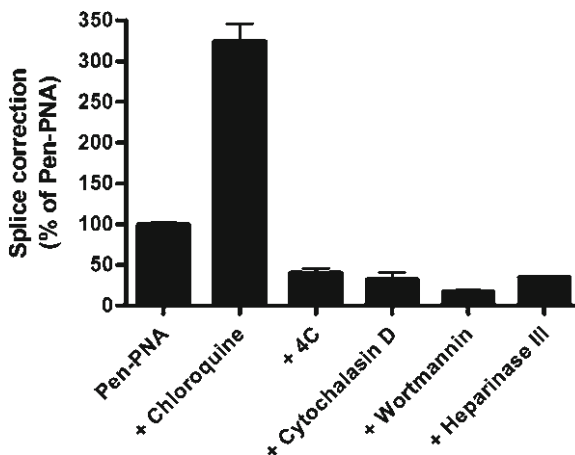


Fig. 2. Characterization of uptake pathway for penetratin. Characterization of the uptake mechanism for penetratin–PNA conjugate. Cells were pretreated with indicated inhibitors or at 4°C according to the protocol, after which 5 μ M of the conjugate was added to the cells. Clearly, the penetratin–PNA conjugate is mainly internalized via macropinocytosis after initial interaction with HS. The figure is reprinted from ref. (13) with permission from *Nature Protocols*.

splice site. Unless the aberrant splice site is masked by an anti-sense ON, the pre-mRNA of luciferase will be improperly processed. Thus, increases in expression of functional luciferase expression reflect successful CPP-mediated delivery of PNA into the nucleus of cells. This protocol can also be employed to characterize pathways for cellular uptake of ONs other than PNA, e.g., anionic ONs. For information regarding preparation of noncovalent complexes of CPP and anionic ONs, see chapter 26.

2.1. Cell-Penetrating Peptides and PNA Conjugates

1. The CPPs have to be synthesized with a 3-nitro-2-pyridinesulfonyl (Npys) modified cysteine in the sequence to enable coupling to PNA. It is crucial, for forming a disulfide bond between CPP and PNA, to also include a terminal cysteine to the PNA splice-correcting sequence (CCTCTTACCTCAGTTACA). It is optional to also include terminal lysine residues in PNA sequence as a mean to enhance solubility. It is beneficial to also include a negative PNA control sequence with four mismatches to target pre-mRNA (CCTCTTACACTCGTTACA) in the experiments. To facilitate solubility of the PNA ONs, we recommended adding two lysine residues in each respective end of the PNA sequences. For quantitative uptake by fluorometry, the PNA sequences have to be labeled with a fluorescent dye, e.g., Cy5 or fluorescein. Modified peptides can be ordered from several suppliers, e.g., Ezbiolab, TAG Copenhagen, or PolyPeptide laboratories, and PNA can be ordered from, e.g., Biosynthesis Inc. or Eurogentec.

2. Conjugation solution for the CPP–PNA conjugation reaction: acetonitrile (20%, v/v) in water.
3. Reversed-phase HPLC system with C-18 column, e.g., Supelco Discovery™ HS C18 (10 μm), for purification CPP–PNA conjugates.
4. Buffers for HPLC purification. Buffer A: 0.1% trifluoroacetic acid (TFA) in distilled water. Buffer B: 0.1% TFA in acetonitrile.
5. MALDI-TOF mass spectrometer, e.g., prO-TOF™ 2000 MALDI O-TOF mass spectrometer (Perkin Elmer) with α-cyano-4-hydroxycinnamic acid (CHCA) matrix, for the analysis of CPP–PNA conjugates (see Note 1).
6. Equipment to dry the purified CPP–PNA conjugates, e.g., freeze-dryer or SpeedVac.
7. Laboratory scale with 0.1 mg accuracy to determine the yield of CPP–PNA conjugation.
8. Distilled water to prepare 100 μM stock solution of CPP–PNA conjugate (see Note 2).

2.2. Cell Culture and CPP–PNA Treatment for Characterization of Uptake Pathways

1. HeLa pLuc 705 cells are maintained in Dulbecco's Modified Eagle's Medium (DMEM) with Glutamax, supplemented with 0.1 mM nonessential amino acids, 1.0 mM sodium pyruvate, 10% fetal bovine serum, 100 U/ml penicillin, and 100 mg/ml streptomycin.
2. Trypsin (0.25%) with 1 mM ethylenediamine tetraacetic acid (EDTA).
3. 24-Well culture plates.
4. Products for the determination of pathway for CPP–PNA uptake. Heparinase III enzyme (e.g., IBEX Technologies, Inc.), chloroquine diphosphate salt (e.g., Sigma-Aldrich), or optional pathway inhibitors, e.g., wortmannin (e.g., Sigma-Aldrich), cytochalasin D (e.g., Sigma-Aldrich), and chlorpromazine hydrochloride (e.g., Sigma-Aldrich).
5. HEPES Krebs Ringer (HKR) buffer: 130 mM NaCl, 5 mM KCl, 1.2 mM MgSO₄, 1.2 mM CaCl₂, 20 mM HEPES, 1.2 mM Na₂HPO₄, 10 mM glucose.

2.3. Luciferase Assay

1. White 96-well plate (e.g., Corning).
2. Cell lysis buffer: 0.1% Triton X-100 in HKR buffer.
3. Luciferase assay substrate mix (Promega).
4. GloMax luminometer (Promega) for the determination of luciferase activity.

2.4. Quantitative Uptake by Fluorometry

1. Black 96-well plate (e.g., Corning).
2. Cell lysis buffer: 0.1 M NaOH in HKR buffer.

3. Fluorescently labeled CPP–PNA conjugate for the establishment of correlation between fluorescence intensity and CPP–PNA concentration.
4. Fluorescence reader, e.g., FlexStation (Molecular Devices).
5. Table-top centrifuge (e.g., Eppendorf) for 1.5 ml Eppendorf tubes.

2.5. Protein Determination

1. Detergent compatible protein determination kit (e.g., Bio-Rad).
2. Transparent 96-well plate (e.g., Corning).
3. Spectrophotometer.

3. Methods

3.1. Cell-Penetrating Peptides and PNA Conjugates

1. Dissolve and mix the PNA and CPP in the conjugation solution. Keep the volumes low so that the respective concentrations do not quote lower than 100 μM .
2. Let the conjugation reaction proceed overnight at 37°C, preferably with agitation.
3. Purify the crude conjugate by HPLC with a gradient from 20% buffer B to 100% buffer B in 80 min.
4. Analyze HPLC fractions by MALDI-TOF (see Note 3).
5. Dry the accurate conjugate fraction, determine the weight by using a laboratory scale with at least 0.1 mg accuracy and prepare 100 μM conjugate stock solutions.

3.2. Endocytosis Inhibitors for Characterization of Internalization Pathway

3.2.1. Preparation of Cells

3.2.2. Preparations for Cellular Transfection

1. Prepare stock solutions of inhibitors and other compound used for pathway characterization in DMEM at 100 \times higher concentration than intended cellular treatment concentration of optional compounds for the characterization of pathways for cellular uptake. Recommended concentrations of the respective stock solutions are 5 μM for wortmannin, 400 μM for cytochalasin D, 1 mM for chlorpromazine, 7.5 mM for chloroquine, and 100 U/ml for heparinase III (see Note 4).
2. The CPP–PNA conjugates are usually effective at cellular treatment concentration ranging from 1 to 10 μM . To prepare CPP–PNA conjugate for 1 μM cellular treatment in one well

of a 24-well plate, take 3 μl from the conjugate stock solution (100 μM) and dilute into 300 μl in DMEM in an 1.5-ml Eppendorf tube.

3. Prepare additional Eppendorf tubes with CPP–PNA conjugates at effective cellular treatment concentrations. Prepare one individual Eppendorf tube for each CPP–PNA concentration and specific compound for pathway characterization.

3.2.3. Transfection of Cells

1. Only for heparinase III pretreatments. If not used, go to step 3. Remove cell medium from the cells, wash once with HKR buffer, and add 297 μl DMEM to each well in the 24-well plate. Add 3 μl of the previously prepared heparinase III stock solution (100 U/ml). Incubate the cells at 37°C for 30 min.
2. Only for treatments at 4°C. If not used, go to step 3. Remove cell medium from the cells, wash once with HKR buffer and add 300 μl DMEM to each well in the 24-well plate. Incubate the cells at 4°C for 30 min.
3. Remove the cell medium, wash once with PBS, and add the previously (Subheading 3.2.2, step 2) prepared CPP–PNA solutions to each well in the 24-well plate.
4. For treatment with inhibitors, add 3 μl of the previously (Subheading 3.2.2, step 1) prepared stock solutions to each well.
5. Incubate the cells for 3 h at 37°C or at 4°C.
6. Remove the cell medium and replace with full growth medium, i.e., including serum, etc.
7. Let cells grow at 37°C for 16 h.

3.2.4. Quantification of Translocation and Uptake

3.2.4.1. Luciferase Activity

1. Remove the cell culture medium.
2. Wash the cells twice with HKR buffer.
3. Add 100 μl of 0.1% Triton X-100 in HKR buffer to each well in the 24-well plate.
4. Let the cells lyse for 15 min at room temperature.
5. Transfer 20 μl of the cell lysate to white 96-well plate.
6. Add 80 μl of luciferase substrate to each well with cell lysate.
7. Read luminescence immediately.

3.2.4.2. Fluorometry

1. Prepare dilution series with fluorophore-labeled CPP–PNA conjugate in 0.1 M NaOH to set up a fluorescence standard curve.
2. Read fluorescence for the dilution series and determine the relationship between fluorescence activity and CPP–PNA concentration.

3. Remove the cell culture medium.
4. Wash the cells twice with HKR buffer.
5. Trypsinize the cells for 10 min at 37°C and transfer the mixture to Eppendorf tubes.
6. Spin down cells at 1,000 × *g* for 5 min at 4°C to collect cells.
7. Remove the supernatant.
8. Add 300 µl of 0.1 M NaOH to each Eppendorf tube and lyse the cells for 60 min at 4°C.
9. Transfer 250 µl of each cell lysate to separate well in a black 96-well plate.
10. Read fluorescence at appropriate ex/em wavelength.
11. Determine the concentration of fluorophore-labeled PNA by referring the measured fluorescence activity to the initially prepared standard curve.

3.2.5. Protein Determination

The protein determination procedure described here is valid for Bio-Rad's detergent protein assay reagent package (see Note 5).

1. Transfer 5 µl of cell lysate from the fluorometry assay or the luciferase assay to a transparent 96-well plate.
2. Add 25 µl of reagent A from the Bio-Rad protein determination kit to each well.
3. Add 200 µl of reagent B from the Bio-Rad protein determination kit to each well.
4. Agitate gently or put the 96-well plate on shake board and let incubate for 15 min at room temperature.
5. Read absorbance at 750 nm and determine the protein content in each sample by using a bovine serum albumin (BSA) standard curve.

3.2.6. Presentation of Data

1. Normalize the luciferase activity to the protein content in the respective cell lysates and present the cellular translocation as relative luminescence units (RLU) per mg of cellular protein. For example with the penetratin CPP, see Fig. 1.
2. Normalize the fluorescence activity to the protein content in the respective cell lysates and present the cellular uptake as pmol PNA per mg of cellular protein. For example with the penetratin CPP, see Fig. 1.
3. Use Table 1 to elucidate cellular uptake pathway for each CPP-PNA conjugate examined (see Note 6). For example with the penetratin CPP, see Fig. 2.

4. Notes

1. We recommend MALDI-TOF for the analysis of the CPP-PNA conjugates but other methods can replace this analysis. For example, it is also possible to use analytical HPLC.
2. Stock solutions of CPP-PNA conjugates and pathway inhibitors can be stored at -20°C for up to 1 year. Avoid repeated freezing and thawing of the stock solutions. Prepare rather several small aliquots.
3. Good crystals for MALDI-TOF analysis are usually made by first adding $1\ \mu\text{l}$ CHCA (saturated solution in acetonitrile) to the analysis plate followed by the addition of $1\ \mu\text{l}$ of the HPLC fraction to be analyzed. Let the matrix and conjugate dry together for about 15 min. If this procedure does not give successful ionization in the MALDI-TOF, try higher proportion of CHCA matrix.
4. Other pathway-specific inhibitors can be used in this assay provided that the used cellular treatment concentration does not induce cytotoxicity. We recommend performing an initial titration to establish a suitable, i.e. active but non-toxic, treatment concentration when using a new inhibitor.
5. The procedure described for protein determination provides the use of the detergent protein assay reagent package (Bio-Rad). Products for protein determination from other suppliers can be used provided that procedure described in Subheading 3.2.5 is modified according to the supplier's recommendations.
6. The compounds presented here for the characterization of cellular CPP-PNA uptake pathways do very seldom generate complete inhibition of a pathway or complete endosomal release. This is normal since none of the compounds is 100% specific. Several compounds and strategies have to be employed to characterize the distinct uptake pathway for a specific CPP-PNA conjugate. For certain CPP-PNA conjugates, the uptake pathway cannot be exactly determined and it is rather a mixture of several uptake routes. The contribution of each uptake route is likely to vary with cellular CPP-PNA treatment concentration in such cases.

Acknowledgments

pLuc705-HeLa cells were kindly provided by R. Kole and B. Lebleu. This work was supported by the Swedish Science

Foundation (VR-NT and VR-MED), the Knut and Alice Wallenberg Foundation, the Swedish Governmental Agency for Innovation Systems (VINNOVA-SAMBIO 2006), and the Swedish Center for Biomembrane Research.

References

- Richard, J. P., Melikov, K., Vivés, E., Ramos, C., Verbeure, B., Gait, M. J., Chernomordik, L. V., and Lebleu, B. (2003) Cell-Penetrating Peptides. A Reevaluation of the Mechanism of Cellular Uptake. *J. Biol. Chem.* **278**, 585–590.
- El-Andaloussi, S., Johansson, H. J., Lundberg, P., and Langel, Ü. (2006) Induction of Splice Correction by Cell-Penetrating Peptide Nucleic Acids. *J. Gene Med.* **8**, 1262–1273.
- Fischer, R., Waizenegger, T., Kohler, K., and Brock, R. (2002) A Quantitative Validation of Fluorophore-Labelled Cell-Permeable Peptide Conjugates: Fluorophore and Cargo Dependence of Import. *Biochim. Biophys. Acta.* **1564**, 365–374.
- El-Andaloussi, S., Järver, P., Johansson, H. J., and Langel, Ü. (2007) Cargo-Dependent Cytotoxicity and Delivery Efficacy of Cell-Penetrating Peptides: A Comparative Study. *Biochem. J.* **407**, 285–292.
- Lundberg, P., El-Andaloussi, S., Sütli, T., Johansson, H., and Langel, Ü. (2007) Delivery of Short Interfering RNA using Endosomolytic Cell-Penetrating Peptides. *FASEB J.* **21**, 2664–2671.
- Wadia, J. S., Stan, R. V., and Dowdy, S. F. (2004) Transducible TAT-HA Fusogenic Peptide Enhances Escape of TAT-Fusion Proteins After Lipid Raft Macropinocytosis. *Nat. Med.* **10**, 310–315.
- Kang, S. H., Cho, M. J., and Kole, R. (1998) Up-Regulation of Luciferase Gene Expression with Antisense ONs: Implications and Applications in Functional Assay Development. *Biochemistry.* **37**, 6235–6239.
- Sazani, P. and Kole, R. (2003) Therapeutic Potential of Antisense ONs as Modulators of Alternative Splicing. *J. Clin. Invest.* **112**, 481–486.
- Faustino, N. A. and Cooper, T. A. (2003) Pre-mRNA Splicing and Human Disease. *Genes Dev.* **17**, 419–437.
- Moreira, J. N., Santos, A., and Simoes, S. (2006) Bcl-2-Targeted Antisense Therapy (Oblimersen Sodium): Towards Clinical Reality. *Rev. Recent. Clin. Trials.* **1**, 217–235.
- Whitehead, K. A., Langer, R., and Anderson, D. G. (2009) Knocking Down Barriers: Advances in siRNA Delivery. *Nat. Rev. Drug Discov.* **8**, 129–138.
- Shiraishi, T. and Nielsen, P. E. (2006) Enhanced Delivery of Cell-Penetrating Peptide-Peptide Nucleic Acid Conjugates by Endosomal Disruption. *Nat. Protoc.* **1**, 633–636.
- El-Andaloussi, S., Guterstam, P., and Langel, Ü. (2007) Assessing the Delivery Efficacy and Internalization Route of Cell-Penetrating Peptides. *Nat. Protoc.* **2**, 2043–2047.
- Kumar, R., Singh, S. K., Koshkin, A. A., Rajwanshi, V. K., Meldgaard, M., and Wengel, J. (1998) The First Analogues of LNA (Locked Nucleic Acids): Phosphorothioate-LNA and 2'-Thio-LNA. *Bioorg. Med. Chem. Lett.* **8**, 2219–2222.
- Wahlestedt, C., Salmi, P., Good, L., Kela, J., Johnsson, T., Hökfelt, T., Broberger, C., Porreca, F., Lai, J., Ren, K., Ossipov, M., Koshkin, A., Jakobsen, N., Skouv, J., Oerum, H., Jacobsen, M. H., and Wengel, J. (2000) Potent and Nontoxic Antisense ONs Containing Locked Nucleic Acids. *Proc. Natl. Acad. Sci. U. S. A.* **97**, 5633–5638.
- Guterstam, P., Lindgren, M., Johansson, H., Tedebark, U., Wengel, J., El Andaloussi, S., and Langel, Ü. (2008) Splice-Switching Efficiency and Specificity for ONs with Locked Nucleic Acid Monomers. *Biochem. J.* **412**, 307–313.
- Holm, T., Johansson, H., Lundberg, P., Pooga, M., Lindgren, M., and Langel, Ü. (2006) Studying the Uptake of Cell-Penetrating Peptides. *Nat. Protoc.* **1**, 1001–1005.
- Richard, J. P., Melikov, K., Brooks, H., Prevot, P., Lebleu, B., and Chernomordik, L. V. (2005) Cellular Uptake of Unconjugated TAT Peptide Involves Clathrin-Dependent Endocytosis and Heparan Sulfate Receptors. *J. Biol. Chem.* **280**, 15300–15306.
- Fittipaldi, A., Ferrari, A., Zoppe, M., Arcangeli, C., Pellegrini, V., Beltram, F., and Giacca, M. (2003) Cell Membrane Lipid Rafts Mediate Caveolar Endocytosis of HIV-1 Tat Fusion Proteins. *J. Biol. Chem.* **278**, 34141–34149.
- Duchardt, F., Fotin-Mleczek, M., Schwarz, H., Fischer, R., and Brock, R. (2007)

- A Comprehensive Model for the Cellular Uptake of Cationic Cell-Penetrating Peptides. *Traffic*. **8**, 848–866.
21. Bevan, A. P., Krook, A., Tikerpaev, J., Seabright, P. J., Siddle, K., and Smith, G. D. (1997) Chloroquine Extends the Lifetime of the Activated Insulin Receptor Complex in Endosomes. *J. Biol. Chem.* **272**, 26833–26840.
22. Derossi, D., Chassaing, G., and Prochiantz, A. (1998) Trojan Peptides: The Penetratin System for Intracellular Delivery. *Trends Cell Biol.* **8**, 84–87.

Part III

Functionality and Cell-Penetrating Peptides

Chapter 17

Mimicry of Protein Function with Cell-Penetrating Peptides

Henrik J. Johansson, Samir EL Andaloussi, and Ülo Langel

Abstract

Proteins are essential components of cellular processes inside cells, and their interactions between each other and with genes are important for the normal physiological functioning of cells as well as for disease states. Modulating protein interactions by different means can potentially control these interactions and restore normal function to diseased cells. The ways to do so are multiple, and such efforts often begin with knowledge of potential target proteins in order to devise mediators that retain the function of the original protein, i.e., mimic the protein functions. An alternative strategy is to utilize protein mimics to inhibit target proteins rather than restoring the activity of a protein. The vast majority of protein mimics exploited to date have been designed to inhibit the activity of oncogenes or activate tumor suppressors for the purpose of tumor therapy. These protein mimics are usually based on small organic compounds or peptides, derived from interaction surfaces of the proteins, and in some cases, full proteins have been exploited. Although peptides and proteins are naturally highly specific and efficient inside cells, they suffer from low bioavailability resulting from their inability to enter cells. One strategy increasingly employed to facilitate the internalization of peptides and proteins has been to chemically conjugate them to cell-penetrating peptides (CPP) or to recombinantly express protein–CPP fusion constructs.

This chapter provides an overview of some of the aspects of perturbing and mimicking protein interactions using peptides and proteins and CPP as transport vectors.

Key words: Cell-penetrating peptide, Protein mimicry, Protein interaction, Linear motif

1. Introduction

The cell controls many of its fundamental processes such as intracellular signaling and gene expression by protein interactions. Thus, modulating protein interactions by different means represents an attractive way to manipulate cellular phenotypes. Agents that modulate protein interactions include small organic molecules, proteins, or peptides derived either from the interacting domains of proteins or discovered by library screens. Since most full-length proteins are essentially cell impermeable and rather

laborious to produce, most attempts to modulate protein interactions involve using parts of proteins or the exploitation of small molecules, thereby simplifying the production of the modulating agent.

2. Protein Interactions as Target

Protein interactions are central to most cellular processes. The best known structures that mediate protein interactions are probably globular domains, which are fairly large and often contain 200–300 amino-acid residues. The number of protein folds has been estimated to be about 1,000 (1, 2). These make up the functional domains of the estimated 4,000–8,000 distinct protein families known to date (2, 3). A difficulty with modulators affecting protein interactions is that many protein interfaces are large and often noncontinuous. This makes it problematic to design small molecules, which otherwise have been successfully exploited for targeting of enzymes where the catalytic site usually is a pocket with rather defined structure and the interacting amino acids are known. However, this traditional view of large interacting surfaces has changed with the finding of peptides capable of interfering with protein interactions. For example, the N-terminal part of the p53 protein forms an α -helix that has three key amino acids that makes up most of the interaction with a hydrophobic groove in MDM2 (4). Using this information, both short peptides and small-molecule inhibitors have been designed (4, 5).

Hence, the typical large interacting surface can be considered to possess “hot spots” highly conserved and crucial for interaction. Another, similar or complementary view is the existence of linear motifs, which are short, functional regions and often correspond to a particular sequence pattern. These motifs are short enough to be synthesized as peptides and sometimes converted into small molecules as mentioned above. Interestingly, the linear motifs seem well represented in the SMAD signaling pathway as reviewed in (6). Another interesting review from Russel and Neduva is recommended for further information regarding linear motifs (7).

Generally, peptides are derived from a single protein by biochemical experiments such as deletion of parts of the protein to elucidate binding and function or screening for peptides in large combinatorial libraries in order to find strong binders. A novel way to discover linear peptide sequences has been recently described by Edwards et al. based on a bioinformatics approach, to identify linear peptides capable of modulating platelet aggregation (8). An *in silico* screen was made for 50 proteins expressed in platelets that were predicted to span the plasma membrane, and within this group, they searched the cytosolic portion of the proteins within 30 amino acids from the membrane. Sequences of ten

amino acids were then searched for within this region that were well conserved among orthologs (corresponding protein in different species) but that differed across paralogs (homologous human proteins). By doing so, they focused the search toward motifs more likely to be specific for a single protein. This gave 52 potential peptides, which were synthesized and palmitylated to allow crossing of the plasma membrane. Interestingly, half of the peptides displayed either agonistic or antagonistic activity in their platelet aggregation assays.

3. Agents to Modulate Protein Interactions

Since proteins are so important for all the activities inside cells, it would be reasonable to exploit them to modulate their own interactions. Unfortunately, proteins are tedious to produce and are, with some exceptions, essentially unable to reach the interior of the cell where most of the protein interactions takes place. They therefore need to be efficiently delivered by some means or expressed from plasmids for example.

Small hydrophobic organic molecules, used to mimic protein function, have the advantage of traversing the lipid membrane; however, they suffer from limited ability to interact with the target in a specific manner due to size constraints. Alternatively, peptides might be more suited as they can be derived from the original protein interaction surface and generate more extensive contacts with proteins. Peptides derived from protein interacting surfaces have been reported to retain functionality after expression from plasmids, either alone or in a construct with a scaffold, e.g., p14ARF peptides (9, 10). Generally, peptides derived from protein interactions sites are used as leads for production of small organic molecules that can traverse the plasma cell membrane to reach their targets (4, 5).

As with proteins, most peptides cannot translocate into cells except for a class of delivery-peptides known as cell-penetrating peptides (CPP). Curiously, the first CPP were derived from proteins, Tat and Antennapedia, suggesting that nature had already foreseen a solution for the transportation of proteins into cells (11–13). However, for the majority of proteins and peptides which cannot enter cells, conjugation to CPP would facilitate their entry.

4. Peptides as Modulators of Protein Interactions

As with all new or modified compounds, the outcome of peptide–protein interactions is not obvious: the peptide may simply bind without affecting the protein, block interactions and activity of its

parent protein, or induce a conformational change either activating or inhibiting the target protein. Additionally, adding to the complexity, a peptide-mediated response may be of a more allosteric nature since only parts of the protein are used, signifying the importance of characterizing new compounds. A peptide that mimics a protein can either function to activate or inhibit, depending on the function of the original parent protein and the region therein from which it was derived. With regard to an activating vs. an inhibiting peptide, mimicking a protein from a pharmacological point of view would favor activating mimics over inhibitors, since lower concentrations can be used. Inhibitory peptides must compete with the native ligands, requiring higher doses, which enhance the risk of nonspecific side effects and immunogenicity. However, screening for potential bioactive peptides mainly identifies inhibitors since it is more straightforward to analyze inhibition rather than function after binding. In addition, since by definition a peptide can only represent a portion of a protein and its potential interacting interfaces and regulatory sites, it is difficult for a peptide mimic to acquire all aspects of the full-length parent protein.

5. Delivery of Full Length Proteins

Since the introduction of functional full-length proteins is desired for modulating cellular function, nature has provided some exceptions from the normal dogma of nontransducible proteins. Accordingly in 1978, autoantibodies to ribonucleoprotein (RNP) from serum could penetrate cells and reach their nuclear target (14). Additional examples of bioactive transducible proteins can be found amongst transcription factors, such as homeoproteins and basic helix-loop-helix (bHLH) proteins, e.g., the Tat transactivator of HIV-1 (12), HoxB4 (15), Engrailed-2 (16), the paired box transcription factor Pax4 involved in vertebrate organogenesis (17), and the bHLH protein NeuroD/BETA2 (18, 19). Such accumulating evidence of transducible proteins and their role in physiological processes together with the observed secretion of Tat (20) and Engrailed (21) raises the question as to whether this mechanism is more widely exploited by nature for communication between cells than was initially believed (see Table 1).

For translocation of nontransducible proteins into cells, effector domains responsible for the natural transduction of full-length proteins have been fused to these proteins. There are numerous reports on protein fusions to CPP, mainly via Tat: for example, fusion of Tat to Bcl-xL for apoptosis protection (22), to E2F1 and p73 to mediate apoptosis in cancer cells (23), and to ubiquitin C-terminal hydroxylase L1 (Uch-1) for neuroprotection

Table 1
A selection of bioactive proteins with translocation ability

Protein	Function	References
IgG	Autoantibody to nuclear RNP	(14)
Tat	Transactivator of HIV-1	(12)
VP22	Herpes simplex virus structural protein	(46)
HoxB4	Homeoprotein, expansion of stem cells	(15)
Engrailed-2	Homeoprotein, retinal axon guiding, rescues dopamine cell loss	(16, 47)
PDX-1	Homeoprotein, transcriptional activation of insulin	(19, 48)
Pax4	Protects against apoptosis	(17)
Pax6	Regulates eye development	(49)
NeuroD/BETA2	Transcriptional activation of insulin	(18, 19)

RNP ribonucleoprotein, PDX-1 pancreatic duodenal homeobox 1, HoxB4 homeobox B4, Pax4 paired box 4

following β -amyloid treatment (24). Additionally, delivery of the proteins GFP and β -galactosidase has been reported by simple coincubation of the proteins with a CPP, Pep-1 (25) (see Table 2). Although an attractive means for conveying proteins into cells, creating protein fusions is still quite a laborious process and coincubation is limited by the properties of the individual protein such as the pI value (26). Since most CPP are cationic in nature, the noncovalent coincubation strategy is limited to the delivery of proteins with a pI below 7. Thus, utilizing smaller peptides derived from full-length proteins, which function either as activating or inhibitory mimics, fused to CPP represents an attractive approach since they can be synthesized on a routine basis.

CPP have been proven capable of conveying a wide range of cargos including peptides and proteins inside cells, which are comprehensively tabularized by Dietz and Bähr until 2004 (27). A selection of proteins and peptides delivered by CPP is presented in Tables 2 and 3.

6. Delivery of Peptides for Protein Mimicry by CPP

As our knowledge of cellular processes and protein interactions accumulates, so too does the number of functional peptides coupled to CPP for shuttling into cells. Examples of peptides reported to inhibit protein–protein interactions include VIVIT, which

Table 2
Selection of proteins delivered by CPPs

CPP	Protein	Biological response	References
Fusion			
Tat	Bcl-xL	Neuroprotection	(22)
Tat	E2F, p73	Induce apoptosis	(23)
Tat	Apoptin	Apoptosis in cancer	(50)
Tat	Uch-1	Neuroprotection	(24)
Tat	Hsp70	Neuroprotection	(51)
Tat	GDNF	Protection against cerebral ischemia	(52)
Tat	PNP	Correction of PNP deficiency in mice	(53)
R ₁₁ , HA2-R ₉	p53	Induce apoptosis and decrease proliferation	(54, 55)
Co-incubation			
Pep-1	GFP, β -gal	Uptake and β -galactosidase activity	(25)
YTA2	β -gal	Uptake and β -galactosidase activity	(56)

Uch-1 ubiquitin C-terminal hydroxylase L1, Hsp70 heat shock protein 70, GDNF glial derived neurotrophic factor, PNP purine nucleoside phosphorylase, HA2 influenza virus hemagglutinin-2 protein, GFP green fluorescent protein, β -gal β -galactosidase

inhibited the calcineurin–NFAT interaction (28, 29), and shepherdin, which blocked the interaction between survivin and Hsp90 (30). The predominant therapeutic target for peptides that inhibit protein interactions has tended to focus on cancer cell progression. However, other pathways are also targeted and examples of which are presented in Table 3.

Peptides that function as activating mimics of the parent protein are rare, and it is sometimes questionable how they should be defined since they preferentially are derived from proteins with an inhibitory/blocking activity. Some examples of peptides, which in this regard mimic the parent proteins, come from the second mitochondria-derived activator of caspases (SMAC) protein. Upon apoptosis induction, SMAC is released into the cytosol where it binds inhibitor of apoptosis proteins (IAPs) and disrupts IAPs sequestering of effector caspases. A SMAC peptide, derived from N-terminal amino acids, position 4–8 conjugated to the CPP, penetratin was reported to bind IAPs and displace caspase-3 to induce apoptosis (31). Using the same system, Fulda et al. used a

Table 3
Selection of peptides as cargos of CPPs

CPP	Peptide	Biological response	References
Inhibitory peptides			
R ₁₁	VIVIT	Inhibited calcineurin–NFAT, immunosuppression	(28, 29)
R ₁₁	CaN AID	Inhibited CaN phosphatase and excitatory cell death	(57)
R ₉	p14ARF derived	Proliferation arrest in tumor cells	(58)
Tat	STAT6-IP	Reduced allergy	(59)
Tat	mGluR1 derived	Neuroprotection against excitotoxicity	(60)
Tat	BPI	Inhibited repressive chromatin induced by BCL6	(61)
Tat	PAK1 derived	Blocked vascular leakage and angiogenesis	(62, 63)
Tat	p15, phage display	Blocked CK2, inhibits tumor growth	(64, 65)
Tat	NR2B9c	Reduced ischemic brain damage	(66)
Pen	Raf-1 derived	Inhibited tumor growth and angiogenesis	(67)
Pen	APP derived	Induced neurite outgrowth	(68)
Pen	Myc derived	Inhibited Myc–Max and proliferation	(69)
Pen	Bak BH3 derived	Antagonized Bcl-xL, induced apoptosis	(70, 71)
Pen	NBD derived	Inhibited NF- κ B, prevented osteoclastogenesis	(72, 73)
Pen	Shepherdin	Inhibited tumor growth	(30)
Potentially inhibitory mimics			
Tat, Pen	Smac peptide	Tumor sensitization and apoptosis	(31, 32)
Tat	JIP-1 derived	Inhibits JNK, prevents cerebral ischemia	(74)
Tat	JIP-1 derived	Inhibited JNK, decreased hyperglycemia	(75, 76)
Tat, Pen	p16 derived	Inhibits Rb phosphorylation and cell cycle	(77, 78)

NFAT nuclear factor of activated T cells, CaN calcium/calmodulin-dependent protein phosphatase, AID autoinhibitory domain, STAT6 signal transducer and activator of transcription 6, mGluR metabotropic glutamate receptor, BPI BCL6 peptide inhibitor, BCL6 B-cell lymphoma-6, PAK1 p21-activated kinase 1, CK2 casein kinase 2, APP amyloid precursor protein, NBD NEMO-binding domain, JIP JNK interacting protein, JNK c-Jun NH₂-terminal kinase, Rb retinoblastoma

SMAC-derived seven-amino-acid-long peptide conjugated to Tat, which conferred antitumor activity in an anticranial xenograft model, sensitizing cells to treatment with cytotoxic drugs (32).

Tat has also been conjugated to a cytotoxic peptide mimic derived from the cyclin-dependent kinase inhibitor p21^{WAF1/CIP1} that displayed translocation to the nucleus in U251 human glioblastoma cells and additionally decreased proliferation in a number

of other cell lines (33). The mimicking peptide contains the PCNA interacting protein (PIP) box, and its construct with Tat colocalized with PCNA.

Despite being highly efficient delivery vectors, one drawback with CPPs is the relative lack of cell-type specificity. One study addressed this matter by incorporating a targeting ligand to a Tat-effector peptide conjugate. By synthesizing an Erb2 peptide ligand in combination with Tat and an effector peptide derived from the transcription factor signal transducer and activator of transcription 3 (STAT3), accumulation in Erb2 overexpressing xenografts was observed with subsequent reduction of tumor proliferation (34). This strategy of incorporation of addressing moieties could prove extremely useful for selective targeting of other tumors.

7. Combining a Peptide Effector Sequence with a CPP

In terms of efficient synthesis of peptides, short is good, since it means less side products and easier purification. In addition, short peptides provide synthesis space for further functional peptides or other moieties. The combination of both an effector and a CPP in the same peptide sequence abolishes the need for an additional CPP, and reports of such constructs can be traced back to 1988. Green and Loewenstein observed that the (polypeptide) Tat-86 peptide/domain from HIV-1 could transverse the cell membrane and stimulate HIV-LTR-driven RNA synthesis (12). Also, Joliot et al. demonstrated in 1991 that a polypeptide of 60 amino acids corresponding to the Antennapedia homeobox enters nerve cells, reaches the nucleus, and modifies the morphology of neurons (13) (see Table 4).

The Ku70 protein is involved in the DNA damage response and mediates its antiapoptotic function by binding Bax in the cytoplasm, thereby preventing Bax translocation to the mitochondria. Recently, Sawada et al. have reported that pentameric peptides derived from the Bax binding domain of Ku70, termed Bax inhibiting peptides, internalized into cells and bound Bax, which prevented translocation of Bax and protected cells against apoptosis (35, 36).

Cytochrome *c* is part of the electron transport chain in mitochondria and is released upon apoptotic stimulus. Howl and Jones found that the Cytochrome *c* sequence harbor sequences with CPP properties (37). Two peptides, denoted Cyt c^{86-101} and Cyt c^{77-101} , derived from Cytochrome *c* were found to decrease cell viability compared to control peptide sequences from Cytochrome *c*. Cyt c^{86-101} and Cyt c^{77-101} also induced DNA fragmentation and caspase-3 activation, which are hallmarks of apoptosis, hence suggesting that the peptides mimic the function of the parent protein.

Table 4
Selection of CPPs as effectors

CPP	Derived from	Biological response	References
Tat-86	Tat	Transactivation of HIV-LTR	(12)
pAntp	Antennapedia	Induced neurite outgrowth in neurons	(13, 79, 80)
Lyp-1	Phage display	Targeted lymphatic tumors and inhibited growth	(81, 82)
M511	AT1AR	Blood vessel contraction	(83)
G53-2	GLP-1R	Induced insulin release	(83)
Cyt c^{86-101}	Cytochrome c	Decreased proliferation and induced apoptosis	(37)
BIPs	Ku70 protein	Cytoprotective	(35, 36)
ARF(1-22)	p14ARF	Decreased proliferation and induced apoptosis	(44)
CDB3	p53-53BP2	Restored p53 function and gene transcription	(84)
MCa	MCa	Scorpion toxin, activated the ryanodine receptor	(85, 86)

HIV-LTR human immunodeficiency virus long terminal repeat, AT1AR angiotensin receptor, GLP-1R glucagon-like peptide receptor, BIPs Bax-inhibiting peptides, ARF alternative reading frame, 53BP2 p53 binding protein 2, MCa maurocalcine

Additionally, the authors suggest the introduction of the term bioportide to denote this class of biologically active proteomimetic CPPs, to distinguish them from the majority of inert CPP sequences.

8. Example of Design of a Combined Effector and CPP for p14ARF

Disruption of cell cycle control mechanisms is a common feature in all types of cancers. The *INK4a/ARF* (or *CDKN2A*) locus encodes two intimately linked but distinct tumor-suppressor proteins, p16INK4a and p14ARF (p19ARF in mouse), in alternative reading frames. The tumor suppressor p14ARF is a small protein of 132 amino acids in length and unusual in the respect that 20% of the amino acids are arginines, which are widely spread throughout the entire protein without any lysines. The human alternative reading frame protein p14ARF and murine double minute (MDM2), denoted HDM2 in humans, and p53 are part of the same regulatory pathway and are modified in virtually all human

cancers. p14ARF is activated by sustained hyperproliferative signals emanating from oncogenes and transcription factors such as Myc (38), Ras (39), AP-1 (40), and E2F1 (41), and the p14ARF activity can be regarded as a surveillance mechanism against excessive oncogene activity. ARF antagonizes the function of HDM2 by preventing its ubiquitin E3 ligase activity and sequesters HDM2 to the nucleolus, leading to the activation of p53 and concomitant cell cycle arrest or apoptosis. Thus, p14ARF prevents tumor transformation mainly by inhibiting the HDM2 protein, though the multiple associations of p14ARF with different signal transduction molecules and transcription factors propounds p14ARF as a central tumor suppressor.

Regarding the design of CPP from the p14ARF protein, regions important for interacting with other proteins were first identified; second, these regions were examined for amino-acid stretches harboring CPP traits. These traits were included of general characteristics of CPP, namely, positively charged side groups, hydrophobic amino acids as well as lack of negative charges. Previously, the N-terminal part of p14ARF had been mapped by deletion mutants and shown to be important for the interaction with HDM2, specifically the 37 first amino acids (42, 43). Peptides from this region expressed in a thioredoxin scaffold or from a plasmid were also found to mimic ARF properties further suggesting that this region could be used to make a protein mimic (9, 10). Based on this information, we designed four different peptides from the N-terminal region ranging from 13 to 37 amino acids in length. Three of the shorter, two 13- and one 22-amino-acid-long peptides proved to be cell-penetrating based on the internalization of their fluoresceinyl-labeled conjugates (44). A peptide corresponding to the 22 N-terminal amino-acids, which were denoted ARF(1-22) decreased proliferation in MCF7 and MDA MB231 cells in a dose-dependent manner. To verify that ARF(1-22) was a CPP with the capability to deliver cargoes into the cell, we conjugated the peptide to a splice-correcting peptide nucleic acid. The ARF(1-22)-PNA conjugate restored aberrant splicing in a splice correction assay in HeLa pLuc 705 cells. Microscopic examination of MCF7 cells revealed nuclear morphology changes associated with apoptosis, and FACS analysis of Annexin V binding suggested that the ARF(1-22) peptide induced apoptosis. Thus, the ARF(1-22)-derived peptide was a CPP, which seemed to mimic the function of the full-length p14ARF protein.

As controls to the ARF peptides, scrambled versions thereof were synthesized. Since a scrambled peptide is distant with regard to amino-acid sequence from its parent peptide, we wanted to introduce a more specific control to the most potent ARF(1-22) peptide. Based on the ARF motif, suggested to be important for interaction (42), amino acids 3–8 were inverted, generating a peptide, which turned out to be an efficient CPP totally inert of

its parent peptides properties. This confirms the specificity of the ARF(1-22) peptide and highlights the importance of short stretches of amino acids for protein interaction. The efficient cell-penetrating properties of the inverted ARF(1-22) peptide were separately explored in another paper where it is denoted M918 (45).

9. Conclusions

As the knowledge about cellular processes increases, so does our ability to pinpoint the key processes mediating different diseases, as for example in cancer. This will open up the possibility to perturb or stimulate key points in regulatory networks to obtain a response that will be beneficial in a disease state. The tools to do so are multiple and use proteins, peptides, or small molecules. However, they all need to reach their target inside the cell, which can be implemented by CPP as exemplified above. Overall, the development of these systems harbors new light to cure multiple diseases.

Acknowledgments

The work was supported by grants from Swedish Research Council (VR-NT), Center for Biomembrane Research, Stockholm, and Knut and Alice Wallenberg's Foundation.

References

- Harrison, A., Pearl, F., Sillitoe, I., Slidel, T., Mott, R., Thornton, J., and Orengo, C. (2003) Recognizing the fold of a protein structure, *Bioinformatics* **19**, 1748–1759.
- Wolf, Y. I., Grishin, N. V., and Koonin, E. V. (2000) Estimating the number of protein folds and families from complete genome data, *J Mol Biol* **299**, 897–905.
- Zhang, C. T. (1997) Relations of the numbers of protein sequences, families and folds, *Protein Eng* **10**, 757–761.
- Chene, P. (2003) Inhibiting the p53-MDM2 interaction: an important target for cancer therapy, *Nat Rev Cancer* **3**, 102–109.
- Vassilev, L. T., Vu, B. T., Graves, B., Carvajal, D., Podlaski, F., Filipovic, Z., Kong, N., Kammlott, U., Lukacs, C., Klein, C., Fotouhi, N., and Liu, E. A. (2004) In vivo activation of the p53 pathway by small-molecule antagonists of MDM2, *Science* **303**, 844–848.
- Neduva, V., and Russell, R. B. (2006) Peptides mediating interaction networks: new leads at last, *Curr Opin Biotechnol* **17**, 465–471.
- Neduva, V., and Russell, R. B. (2005) Linear motifs: evolutionary interaction switches, *FEBS Lett* **579**, 3342–3345.
- Edwards, R. J., Moran, N., Devocelle, M., Kiernan, A., Meade, G., Signac, W., Foy, M., Park, S. D., Dunne, E., Kenny, D., and Shields, D. C. (2007) Bioinformatic discovery of novel bioactive peptides, *Nat Chem Biol* **3**, 108–112.
- Lohrum, M. A., Ashcroft, M., Kubbutat, M. H., and Vousden, K. H. (2000) Contribution of two independent MDM2-binding domains in p14(ARF) to p53 stabilization, *Curr Biol* **10**, 539–542.
- Midgley, C. A., Desterro, J. M., Saville, M. K., Howard, S., Sparks, A., Hay, R. T., and Lane, D. P. (2000) An N-terminal p14ARF

- peptide blocks Mdm2-dependent ubiquitination in vitro and can activate p53 in vivo, *Oncogene* **19**, 2312–2323.
11. Frankel, A. D., and Pabo, C. O. (1988) Cellular uptake of the tat protein from human immunodeficiency virus, *Cell* **55**, 1189–1193.
 12. Green, M., and Loewenstein, P. M. (1988) Autonomous functional domains of chemically synthesized human immunodeficiency virus tat trans-activator protein, *Cell* **55**, 1179–1188.
 13. Joliot, A., Pernelle, C., Deagostini-Bazin, H., and Prochiantz, A. (1991) Antennapedia homeobox peptide regulates neural morphogenesis, *Proc Natl Acad Sci USA* **88**, 1864–1868.
 14. Alarcon-Segovia, D., Ruiz-Arguelles, A., and Fishbein, E. (1978) Antibody to nuclear ribonucleoprotein penetrates live human mononuclear cells through Fc receptors, *Nature* **271**, 67–69.
 15. Amsellem, S., Pflumio, F., Bardin, D., Izac, B., Charneau, P., Romeo, P. H., Dubart-Kupperschmitt, A., and Fichelson, S. (2003) Ex vivo expansion of human hematopoietic stem cells by direct delivery of the HOXB4 homeoprotein, *Nat Med* **9**, 1423–1427.
 16. Brunet, I., Weinl, C., Piper, M., Trembleau, A., Volovitch, M., Harris, W., Prochiantz, A., and Holt, C. (2005) The transcription factor Engrailed-2 guides retinal axons, *Nature* **438**, 94–98.
 17. Lu, J., Li, G., Lan, M. S., Zhang, S., Fan, W., Wang, H., and Lu, D. (2007) Pax4 paired domain mediates direct protein transduction into mammalian cells, *Endocrinology* **148**, 5558–5565.
 18. Chen, J., Li, G., Lu, J., Chen, L., Huang, Y., Wu, H., Zhang, J., and Lu, D. (2006) A novel type of PTD, common helix-loop-helix motif, could efficiently mediate protein transduction into mammalian cells, *Biochem Biophys Res Commun* **347**, 931–940.
 19. Noguchi, H., Matsumoto, S., Okitsu, T., Iwanaga, Y., Yonekawa, Y., Nagata, H., Matsushita, M., Wei, F. Y., Matsui, H., Minami, K., Seino, S., Masui, Y., Futaki, S., and Tanaka, K. (2005) PDX-1 protein is internalized by lipid raft-dependent macropinocytosis, *Cell Transplant* **14**, 637–645.
 20. Helland, D. E., Welles, J. L., Caputo, A., and Haseltine, W. A. (1991) Transcellular transactivation by the human immunodeficiency virus type 1 tat protein, *J Virol* **65**, 4547–4549.
 21. Joliot, A., Maizel, A., Rosenberg, D., Trembleau, A., Dupas, S., Volovitch, M., and Prochiantz, A. (1998) Identification of a signal sequence necessary for the unconventional secretion of Engrailed homeoprotein, *Curr Biol* **8**, 856–863.
 22. Yin, W., Cao, G., Johnnides, M. J., Signore, A. P., Luo, Y., Hickey, R. W., and Chen, J. (2006) TAT-mediated delivery of Bcl-xL protein is neuroprotective against neonatal hypoxic-ischemic brain injury via inhibition of caspases and AIF, *Neurobiol Dis* **21**, 358–371.
 23. Lissy, N. A., Davis, P. K., Irwin, M., Kaelin, W. G., and Dowdy, S. F. (2000) A common E2F-1 and p73 pathway mediates cell death induced by TCR activation, *Nature* **407**, 642–645.
 24. Gong, B., Cao, Z., Zheng, P., Vitolo, O. V., Liu, S., Staniszewski, A., Moolman, D., Zhang, H., Shelanski, M., and Arancio, O. (2006) Ubiquitin hydrolase Uch-L1 rescues beta-amyloid-induced decreases in synaptic function and contextual memory, *Cell* **126**, 775–788.
 25. Morris, M. C., Depollier, J., Mery, J., Heitz, F., and Divita, G. (2001) A peptide carrier for the delivery of biologically active proteins into mammalian cells, *Nat Biotechnol* **19**, 1173–1176.
 26. EL-Andaloussi, S., Järver, P., Johansson, H. J., and Langel, Ü. (2007) Cargo-dependent cytotoxicity and delivery efficacy of cell-penetrating peptides: a comparative study, *Biochem J* **407**, 285–292.
 27. Dietz, G. P., and Bähr, M. (2004) Delivery of bioactive molecules into the cell: the Trojan horse approach, *Mol Cell Neurosci* **27**, 85–131.
 28. Noguchi, H., Matsushita, M., Okitsu, T., Moriwaki, A., Tomizawa, K., Kang, S., Li, S. T., Kobayashi, N., Matsumoto, S., Tanaka, K., Tanaka, N., and Matsui, H. (2004) A new cell-permeable peptide allows successful allogeneic islet transplantation in mice, *Nat Med* **10**, 305–309.
 29. Yu, H., Sliedregt-Bol, K., Overkleeft, H., van der Marel, G. A., van Berkel, T. J., and Biessen, E. A. (2006) Therapeutic potential of a synthetic peptide inhibitor of nuclear factor of activated T cells as antirestenotic agent, *Arterioscler Thromb Vasc Biol* **26**, 1531–1537.
 30. Plescia, J., Salz, W., Xia, F., Pennati, M., Zaffaroni, N., Daidone, M. G., Meli, M., Dohi, T., Fortugno, P., Nefedova, Y., Gabrilovich, D. I., Colombo, G., and Altieri, D. C. (2005) Rational design of shepherdin, a novel anticancer agent, *Cancer Cell* **7**, 457–468.
 31. Arnt, C. R., Chiorean, M. V., Heldebrandt, M. P., Gores, G. J., and Kaufmann, S. H. (2002) Synthetic Smac/DIABLO peptides enhance the effects of chemotherapeutic agents by

- binding XIAP and cIAP1 in situ, *J Biol Chem* **277**, 44236–44243.
32. Fulda, S., Wick, W., Weller, M., and Debatin, K. M. (2002) Smac agonists sensitize for Apo2L/TRAIL- or anticancer drug-induced apoptosis and induce regression of malignant glioma in vivo, *Nat Med* **8**, 808–815.
 33. Baker, R. D., Howl, J., and Nicholl, I. D. (2007) A synchological cell penetrating peptide mimic of p21(WAF1/CIP1) is pro-apoptogenic, *Peptides* **28**, 731–740.
 34. Tan, M., Lan, K. H., Yao, J., Lu, C. H., Sun, M., Neal, C. L., Lu, J., and Yu, D. (2006) Selective inhibition of ErbB2-overexpressing breast cancer in vivo by a novel TAT-based ErbB2-targeting signal transducers and activators of transcription 3-blocking peptide, *Cancer Res* **66**, 3764–3772.
 35. Sawada, M., Hayes, P., and Matsuyama, S. (2003) Cytoprotective membrane-permeable peptides designed from the Bax-binding domain of Ku70, *Nat Cell Biol* **5**, 352–357.
 36. Yoshida, T., Tomioka, I., Nagahara, T., Holyst, T., Sawada, M., Hayes, P., Gama, V., Okuno, M., Chen, Y., Abe, Y., Kanouchi, T., Sasada, H., Wang, D., Yokota, T., Sato, E., and Matsuyama, S. (2004) Bax-inhibiting peptide derived from mouse and rat Ku70, *Biochem Biophys Res Commun* **321**, 961–966.
 37. Howl, J., and Jones, S. (2008) Proteomimetic cell penetrating peptides, *Int J Pept Res Ther* **14**, 359–366.
 38. Zindy, F., Eischen, C. M., Randle, D. H., Kamijo, T., Cleveland, J. L., Sherr, C. J., and Roussel, M. F. (1998) Myc signaling via the ARF tumor suppressor regulates p53-dependent apoptosis and immortalization, *Genes Dev* **12**, 2424–2433.
 39. Palmero, I., Pantoja, C., and Serrano, M. (1998) p19ARF links the tumour suppressor p53 to Ras, *Nature* **395**, 125–126.
 40. Ameyar-Zazoua, M., Wisniewska, M. B., Bakiri, L., Wagner, E. F., Yaniv, M., and Weitzman, J. B. (2005) AP-1 dimers regulate transcription of the p14/p19ARF tumor suppressor gene, *Oncogene* **24**, 2298–2306.
 41. Bates, S., Phillips, A. C., Clark, P. A., Stott, F., Peters, G., Ludwig, R. L., and Vousden, K. H. (1998) p14ARF links the tumour suppressors RB and p53, *Nature* **395**, 124–125.
 42. Bothner, B., Lewis, W. S., DiGiammarino, E. L., Weber, J. D., Bothner, S. J., and Kriwacki, R. W. (2001) Defining the molecular basis of Arf and Hdm2 interactions, *J Mol Biol* **314**, 263–277.
 43. DiGiammarino, E. L., Filippov, I., Weber, J. D., Bothner, B., and Kriwacki, R. W. (2001) Solution structure of the p53 regulatory domain of the p19Arf tumor suppressor protein, *Biochemistry* **40**, 2379–2386.
 44. Johansson, H. J., EL-Andaloussi, S., Holm, T., Mäe, M., Janes, J., Maimets, T., and Langel, Ü. (2008) Characterization of a novel cytotoxic cell-penetrating peptide derived from p14ARF protein, *Mol Ther* **16**, 115–123.
 45. EL-Andaloussi, S., Johansson, H. J., Holm, T., and Langel, Ü. (2007) A novel cell-penetrating peptide, M918, for efficient delivery of proteins and peptide nucleic acids, *Mol Ther* **15**, 1820–1826.
 46. Elliott, G., and O'Hare, P. (1997) Intercellular trafficking and protein delivery by a herpesvirus structural protein, *Cell* **88**, 223–233.
 47. Sonnier, L., Le Pen, G., Hartmann, A., Bizot, J. C., Trovero, F., Krebs, M. O., and Prochiantz, A. (2007) Progressive loss of dopaminergic neurons in the ventral midbrain of adult mice heterozygote for Engrailed1, *J Neurosci* **27**, 1063–1071.
 48. Noguchi, H., Kaneto, H., Weir, G. C., and Bonner-Weir, S. (2003) PDX-1 protein containing its own antennapedia-like protein transduction domain can transduce pancreatic duct and islet cells, *Diabetes* **52**, 1732–1737.
 49. Lesaffre, B., Joliot, A., Prochiantz, A., and Volovitch, M. (2007) Direct non-cell autonomous Pax6 activity regulates eye development in the zebrafish, *Neural Dev* **2**, 2.
 50. Guelen, L., Paterson, H., Gaken, J., Meyers, M., Farzaneh, F., and Tavassoli, M. (2004) TAT-apoptin is efficiently delivered and induces apoptosis in cancer cells, *Oncogene* **23**, 1153–1165.
 51. Lai, Y., Du, L., Dunsmore, K. E., Jenkins, L. W., Wong, H. R., and Clark, R. S. (2005) Selectively increasing inducible heat shock protein 70 via TAT-protein transduction protects neurons from nitrosative stress and excitotoxicity, *J Neurochem* **94**, 360–366.
 52. Kilic, U., Kilic, E., Dietz, G. P., and Bahr, M. (2003) Intravenous TAT-GDNF is protective after focal cerebral ischemia in mice, *Stroke* **34**, 1304–1310.
 53. Toro, A., and Grunebaum, E. (2006) TAT-mediated intracellular delivery of purine nucleoside phosphorylase corrects its deficiency in mice, *J Clin Invest* **116**, 2717–2726.
 54. Michiue, H., Tomizawa, K., Wei, F. Y., Matsushita, M., Lu, Y. F., Ichikawa, T., Tamiya, T., Date, I., and Matsui, H. (2005) The NH2 terminus of influenza virus hemagglutinin-2 subunit peptides enhances the antitumor potency of polyarginine-mediated p53 protein transduction, *J Biol Chem* **280**, 8285–8289.

55. Michiue, H., Tomizawa, K., Matsushita, M., Tamiya, T., Lu, Y. F., Ichikawa, T., Date, I., and Matsui, H. (2005) Ubiquitination-resistant p53 protein transduction therapy facilitates anti-cancer effect on the growth of human malignant glioma cells, *FEBS Lett* **579**, 3965–3969.
56. Myrberg, H., Lindgren, M., and Langel, Ü. (2007) Protein delivery by the cell-penetrating peptide YTA2, *Bioconjug Chem* **18**, 170–174.
57. Terada, H., Matsushita, M., Lu, Y. F., Shirai, T., Li, S. T., Tomizawa, K., Moriwaki, A., Nishio, S., Date, I., Ohmoto, T., and Matsui, H. (2003) Inhibition of excitatory neuronal cell death by cell-permeable calcineurin autoinhibitory peptide, *J Neurochem* **87**, 1145–1151.
58. Gusarova, G. A., Wang, I. C., Major, M. L., Kalinichenko, V. V., Ackerson, T., Petrovic, V., and Costa, R. H. (2007) A cell-penetrating ARF peptide inhibitor of FoxM1 in mouse hepatocellular carcinoma treatment, *J Clin Invest* **117**, 99–111.
59. McCusker, C. T., Wang, Y., Shan, J., Kinyanjui, M. W., Villeneuve, A., Michael, H., and Fixman, E. D. (2007) Inhibition of experimental allergic airways disease by local application of a cell-penetrating dominant-negative STAT-6 peptide, *J Immunol* **179**, 2556–2564.
60. Xu, W., Wong, T. P., Chery, N., Gaertner, T., Wang, Y. T., and Baudry, M. (2007) Calpain-mediated mGluR1alpha truncation: a key step in excitotoxicity, *Neuron* **53**, 399–412.
61. Polo, J. M., Dell'Oso, T., Ranuncolo, S. M., Cerchiatti, L., Beck, D., Da Silva, G. F., Prive, G. G., Licht, J. D., and Melnick, A. (2004) Specific peptide interference reveals BCL6 transcriptional and oncogenic mechanisms in B-cell lymphoma cells, *Nat Med* **10**, 1329–1335.
62. Stockton, R. A., Schaefer, E., and Schwartz, M. A. (2004) p21-activated kinase regulates endothelial permeability through modulation of contractility, *J Biol Chem* **279**, 46621–46630.
63. Kiosses, W. B., Hood, J., Yang, S., Gerritsen, M. E., Chersesh, D. A., Alderson, N., and Schwartz, M. A. (2002) A dominant-negative p65 PAK peptide inhibits angiogenesis, *Circ Res* **90**, 697–702.
64. Perea, S. E., Reyes, O., Puchades, Y., Mendoza, O., Vispo, N. S., Torrens, I., Santos, A., Silva, R., Acevedo, B., Lopez, E., Falcon, V., and Alonso, D. F. (2004) Antitumor effect of a novel proapoptotic peptide that impairs the phosphorylation by the protein kinase 2 (casein kinase 2), *Cancer Res* **64**, 7127–7129.
65. Perera, Y., Farina, H. G., Hernandez, I., Mendoza, O., Serrano, J. M., Reyes, O., Gomez, D. E., Gomez, R. E., Acevedo, B. E., Alonso, D. F., and Perea, S. E. (2008) Systemic administration of a peptide that impairs the protein kinase (CK2) phosphorylation reduces solid tumor growth in mice, *Int J Cancer* **122**, 57–62.
66. Aarts, M., Liu, Y., Liu, L., Besshoh, S., Arundine, M., Gurd, J. W., Wang, Y. T., Salter, M. W., and Tymianski, M. (2002) Treatment of ischemic brain damage by perturbing NMDA receptor-PSD-95 protein interactions, *Science* **298**, 846–850.
67. Dasgupta, P., Sun, J., Wang, S., Fusaro, G., Betts, V., Padmanabhan, J., Sebti, S. M., and Chellappan, S. P. (2004) Disruption of the Rb – Raf-1 interaction inhibits tumor growth and angiogenesis, *Mol Cell Biol* **24**, 9527–9541.
68. Hoareau, C., Borrell, V., Soriano, E., Krebs, M. O., Prochiantz, A., and Allinquant, B. (2008) APP cytoplasmic domain antagonizes reelin neurite outgrowth inhibition of hippocampal neurons, *Neurobiol Aging* **29**(4), 542–553.
69. Giorello, L., Clerico, L., Pescarolo, M. P., Vikhanskaya, F., Salmona, M., Colella, G., Bruno, S., Mancuso, T., Bagnasco, L., Russo, P., and Parodi, S. (1998) Inhibition of cancer cell growth and c-Myc transcriptional activity by a c-Myc helix 1-type peptide fused to an internalization sequence, *Cancer Res* **58**, 3654–3659.
70. Holinger, E. P., Chittenden, T., and Lutz, R. J. (1999) Bak BH3 peptides antagonize Bcl-xL function and induce apoptosis through cytochrome *c*-independent activation of caspases, *J Biol Chem* **274**, 13298–13304.
71. Vieira, H. L., Boya, P., Cohen, I., El Hamel, C., Haouzi, D., Druillenec, S., Belzacq, A. S., Brenner, C., Roques, B., and Kroemer, G. (2002) Cell permeable BH3-peptides overcome the cytoprotective effect of Bcl-2 and Bcl-X(L), *Oncogene* **21**, 1963–1977.
72. Jimi, E., Aoki, K., Saito, H., D'Acquisto, F., May, M. J., Nakamura, I., Sudo, T., Kojima, T., Okamoto, F., Fukushima, H., Okabe, K., Ohya, K., and Ghosh, S. (2004) Selective inhibition of NF-kappa B blocks osteoclastogenesis and prevents inflammatory bone destruction in vivo, *Nat Med* **10**, 617–624.
73. May, M. J., D'Acquisto, F., Madge, L. A., Glockner, J., Poher, J. S., and Ghosh, S. (2000) Selective inhibition of NF-kappaB activation by a peptide that blocks the interaction

- of NEMO with the I κ B kinase complex, *Science* **289**, 1550–1554.
74. Borsello, T., Clarke, P. G., Hirt, L., Vercelli, A., Repici, M., Schorderet, D. F., Bogousslavsky, J., and Bonny, C. (2003) A peptide inhibitor of c-Jun N-terminal kinase protects against excitotoxicity and cerebral ischemia, *Nat Med* **9**, 1180–1186.
 75. Kaneto, H., Nakatani, Y., Miyatsuka, T., Kawamori, D., Matsuoka, T. A., Matsuhisa, M., Kajimoto, Y., Ichijo, H., Yamasaki, Y., and Hori, M. (2004) Possible novel therapy for diabetes with cell-permeable JNK-inhibitory peptide, *Nat Med* **10**, 1128–1132.
 76. Bonny, C., Oberson, A., Negri, S., Sauser, C., and Schorderet, D. F. (2001) Cell-permeable peptide inhibitors of JNK: novel blockers of beta-cell death, *Diabetes* **50**, 77–82.
 77. Fahraeus, R., Paramio, J. M., Ball, K. L., Lain, S., and Lane, D. P. (1996) Inhibition of pRb phosphorylation and cell-cycle progression by a 20-residue peptide derived from p16CDKN2/INK4A, *Curr Biol* **6**, 84–91.
 78. Gius, D. R., Ezhevsky, S. A., Becker-Hapak, M., Nagahara, H., Wei, M. C., and Dowdy, S. F. (1999) Transduced p16INK4a peptides inhibit hypophosphorylation of the retinoblastoma protein and cell cycle progression prior to activation of Cdk2 complexes in late G1, *Cancer Res* **59**, 2577–2580.
 79. Le Roux, I., Joliot, A. H., Bloch-Gallego, E., Prochiantz, A., and Volovitch, M. (1993) Neurotrophic activity of the Antennapedia homeodomain depends on its specific DNA-binding properties, *Proc Natl Acad Sci U S A* **90**, 9120–9124.
 80. Bloch-Gallego, E., Le Roux, I., Joliot, A. H., Volovitch, M., Henderson, C. E., and Prochiantz, A. (1993) Antennapedia homeobox peptide enhances growth and branching of embryonic chicken motoneurons in vitro, *J Cell Biol* **120**, 485–492.
 81. Laakkonen, P., Porkka, K., Hoffman, J. A., and Ruoslahti, E. (2002) A tumor-homing peptide with a targeting specificity related to lymphatic vessels, *Nat Med* **8**, 751–755.
 82. Laakkonen, P., Akerman, M. E., Biliran, H., Yang, M., Ferrer, F., Karpanen, T., Hoffman, R. M., and Ruoslahti, E. (2004) Antitumor activity of a homing peptide that targets tumor lymphatics and tumor cells, *Proc Natl Acad Sci U S A* **101**, 9381–9386.
 83. Östlund, P., Kilk, K., Lindgren, M., Hällbrink, M., Jiang, Y., Budihna, M., Cerne, K., Bavec, A., Östenson, C.-G., Zorko, M., and Langel, Ü. (2005) Cell-penetrating mimics of agonist-activated G-protein coupled receptors, *Int J Pept Res Ther* **11**, 237–247.
 84. Issaeva, N., Friedler, A., Bozko, P., Wiman, K. G., Fersht, A. R., and Selivanova, G. (2003) Rescue of mutants of the tumor suppressor p53 in cancer cells by a designed peptide, *Proc Natl Acad Sci U S A* **100**, 13303–13307.
 85. Esteve, E., Mabrouk, K., Dupuis, A., Smida-Rezgui, S., Altafaj, X., Grunwald, D., Platel, J. C., Andreotti, N., Marty, I., Sabatier, J. M., Ronjat, M., and De Waard, M. (2005) Transduction of the scorpion toxin maurocalcine into cells. Evidence that the toxin crosses the plasma membrane, *J Biol Chem* **280**, 12833–12839.
 86. Boisseau, S., Mabrouk, K., Ram, N., Garmy, N., Collin, V., Tadmouri, A., Mikati, M., Sabatier, J. M., Ronjat, M., Fantini, J., and De Waard, M. (2006) Cell penetration properties of maurocalcine, a natural venom peptide active on the intracellular ryanodine receptor, *Biochim Biophys Acta* **1758**, 308–319.

Chapter 18

Homeoprotein Intercellular Transfer, the Hidden Face of Cell-Penetrating Peptides

Alain Prochiantz

Abstract

Cell-Penetrating Peptides (CPPs) are small peptides internalized by live cells, gaining access to their cytoplasm and intracellular organelles (i.e., mitochondria, nucleus) and are used as pharmacological tools. This is indeed a very important issue, fully justifying the efforts of several groups to better understand the mechanisms of peptide transduction and to verify if and how this strategy can be translated into therapeutic improvements. However, the discovery of peptide transduction is a consequence of that of a novel signaling mechanism based on the intercellular transfer of homeoprotein transcription factors. Indeed, the first and probably most popular CPPs (Tat and Penetratin) correspond to domains that drive TAT (HIV) and homeoprotein transcription factors into the cells. These findings have fostered several studies on transduction and allowed the design of “nonnatural” CPPs. As useful as they are, these lines of research have, in general, neglected the fact that protein transduction is a signaling mechanism, in its own right, with important physiological functions. In this chapter, I describe some of these functions and propose that this class of signaling molecules, in particular homeoproteins, may also be used as therapeutic agents.

Key words: Signaling, Homeoprotein transcription factors, Morphogens, Patterns, Axon guidance, Critical periods, Plasticity, Neurology, Psychiatry

1. Introduction

The first mention that transcription factors could be internalized by live cells can be traced back to the work of Frankel and colleagues and concerned TAT, the Human Immunodeficiency Virus (HIV) transcription factor (1). This observation was never fully developed, in spite of its potential interest for our understanding of HIV infectivity. In fact, since the early 1990s, most of the physiological studies on the intercellular transfer of transcription factors have been centered on homeoprotein transcription factors, in

plants and animals (2). Homeoprotein transfer in plants was easily accepted because of the existence of intercellular bridges or “corridors” called plasmodesmata (3). I will not develop this aspect of homeoprotein transduction, but I recommend the reading of the work done by Joliot and colleagues, demonstrating that Knotted-1, a TALE-class plant homeoprotein, and Engrailed, an animal homeoprotein, share similar transduction properties and mechanisms (4).

I just refer to the plasmodesmata for easy explanation to underscore that one of the main obstacles to the acceptance of this novel signaling mechanism is a conservative conception of what a membrane should be. In contrast with what is commonly believed, biological membranes are not Berlin walls but living structures that can be disturbed and repaired (as most biological structures), and there is no reason to believe that the local and transient perturbation of a membrane is not a physiological way to internalize a macromolecule. This is acceptable on two conditions. The first condition is that the internalized protein has developed specific destabilizing properties and the second one is that repair mechanisms will rapidly seal the membranes. It is beyond doubt that homeoproteins, through the unique structure of their third helix (5), have this “disturbance properties” and that repair mechanisms exist (6). It would be important to verify if they are activated in the course of homeoprotein transduction.

It remains that in the past 20 years, with a recent acceleration, several laboratories have explored homeoprotein transduction at the mechanistic and the physiological levels. I will not further discuss the mechanisms of secretion and internalization which are the object of other chapters and will concentrate the discussion on the recently discovered physiological functions of this unexpected signaling mechanism.

2. Boundaries and Compartments During Development

Fly genetics has popularized the concept of boundaries. GAP genes, homeotic genes and tissue polarity genes, often encoding homeoprotein transcription factors, participate in the definition of territory position, size, identity, and polarity. These developmental genes of the homeoprotein family also exist in vertebrates where they direct, also through a combinatorial code, the development of distinct territories. This process takes place in many organs but has been abundantly documented in the nervous system with the formation of boundaries in the developing neuroepithelium. Good examples are the formation of the isthmus defined by the abutting expression territories of *Otx2* and *Gbx2*, or the dorsal-ventral segmentation of the neural tube where a combinatorial

code of expression of several homeoproteins is at the origin of the differentiation of neural and glial subpopulations (7, 8).

An extreme situation is provided by Pax6, a gene encoding a homeoprotein that has a master function in eye development. Indeed, it was shown that Pax6 invalidation leads to a eyeless or small-eye phenotype in the fly and mouse, respectively (9, 10). Conversely, and more surprisingly, a gain of function of Pax6 induces the formation of eye structures in unexpected territories: the leg or the antenna in the fly, the belly in *Xenopus* (11, 12).

We have proposed (13, 14) that the development of the eye territory starts with the induction, by a growth factor, of Pax6 within a limited domain but that this territory extends through a nonautonomous autoinduction of Pax6 (Fig. 1). In this model, secreted Pax6 gains access to abutting cells where it activates its own transcription. This process is reiterated, allowing a homeogenetic expansion of the Pax6 territory. The process stops when Pax6 is internalized by cells that are not permissive to its autoinduction, for example, Pax2 expressing cells.

As proposed in recent reviews (14), this model would explain why boundaries form where homeoproteins meet as observed in several regions of the developing neuroepithelium. To test this model, we have developed a strategy aimed at blocking Pax6 transfer in the developing zebra-fish embryo and consisting of injecting or expressing anti-Pax6 antibodies in the extracellular space at the blastula stage. As a result, we observed very specific eye phenotypes ranging from no eye to unilateral eyes and small eye (unilateral or bilateral) phenotypes. The phenotypes were extremely specific and antagonized by the extracellular neutralization of the antibody, precluding that the antibody has an intracellular activity (15).

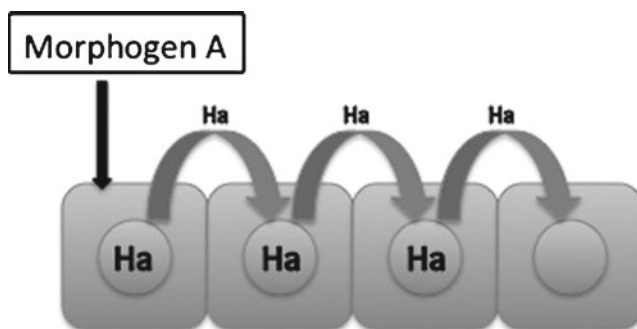


Fig. 1. Homeogenetic induction by homeoprotein transfer. In this model, a primary morphogen A induces the expression of homeoprotein Ha in a small number of cells (one cell in this schematic drawing). The homeoprotein is transported into abutting cells where it induces its own synthesis. This process is reiterated, leading to a homeogenetic expansion of the “marked” territory until Ha reaches a cell nonpermissive for its synthesis. This model was developed by Prochiantz and colleagues (2, 13, 14) and was illustrated for Pax6 in the formation of the zebra-fish eye anlagen (15).

This type of approach demonstrating a noncell autonomous component in Pax6 activity during zebra-fish eye anlagen formation is presently used in the chick where we explore the effect of blocking homeoprotein transfer in the positioning of boundaries along the dorsal–ventral axis of the neural tube.

3. Axon Guidance

Axon guidance is a very important way to ensure the construction of physiological neuronal circuits during development. In fact, some axons have to travel distances several hundred times the diameter of their cell bodies. Navigation is made by growth cones, structures present at the extremities of axons (also of dendrites) capable of reading their position and of responding to this information by an appropriate behavior (stop-go-turn).

Ever since Sperry (16), one of the most popular models for the study of axon guidance is the patterning of the projections of the retina in the tectum (superior colliculus in the mouse), a dorsal mesencephalic structure. Indeed, the two axes of the retina (dorsal–ventral and nasal–temporal) project on two axes of the tectum. In this review, we concentrate on the projection of the temporal–nasal axis of the retina onto the anterior–posterior axis of the tectum. Many guidance cues have been proposed. Among them, the Ephrin/Eph system is particularly elegant. Indeed, Ephrins (EphrinA5) are expressed in a low anterior/high posterior gradient at the surface of the tectum, whereas their Eph receptors (EphA3) are expressed in a low nasal/high temporal gradient in the retinal ganglion cells (RGCs) including at the level of their growth cones. Thus, temporal axons activate the stop signal associated with high Ephrin signaling when they arrive in the posterior regions of the tectum (17, 18).

Engrailed homeoprotein is also expressed in a low anterior/high posterior gradient in the tectum. Gain-of-function experiments demonstrate that it participates in axon guidance along this axis, through the regulation of EphrinA5 expression (19). At least, this was the explanation until a series of recent experiments (20) showed that Engrailed is internalized by growth cones and exerts a contrasted action on nasal and temporal axons, repelling the latter and attracting the former (Fig. 2). Engrailed guidance activity requires its internalization by growth cones and involves the translation of localized mRNAs. This patterning activity of extracellular Engrailed also takes place *in vivo* (21), and the mode of action involves a translation-dependent physiological interaction with EphrinA5. Indeed, low levels of EphrinA5 are incapable of repelling temporal growth cones unless Engrailed is present (21).

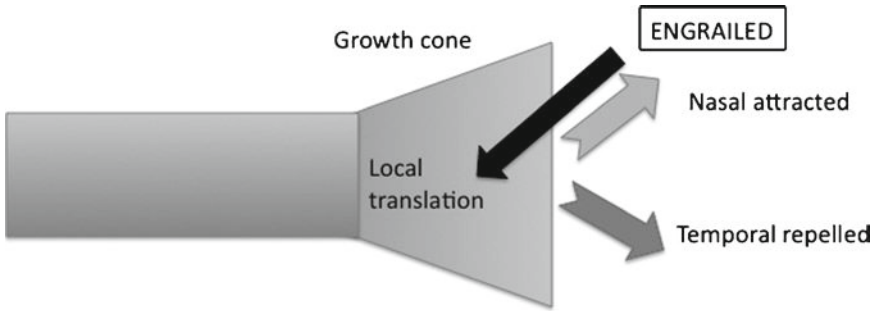


Fig. 2. Engrailed as a guidance molecule for Retinal Ganglion Cells (RGCs). Within an Engrailed gradient, temporal and nasal RGC growth cones are repelled and attracted, respectively (20). These effects require Engrailed internalization and the translation of local mRNAs. In vivo, blocking Engrailed extracellular activity perturbs the navigation of RGC temporal axons, which invade posterior regions of the tectum in spite of their high levels of Engrailed expression (21).

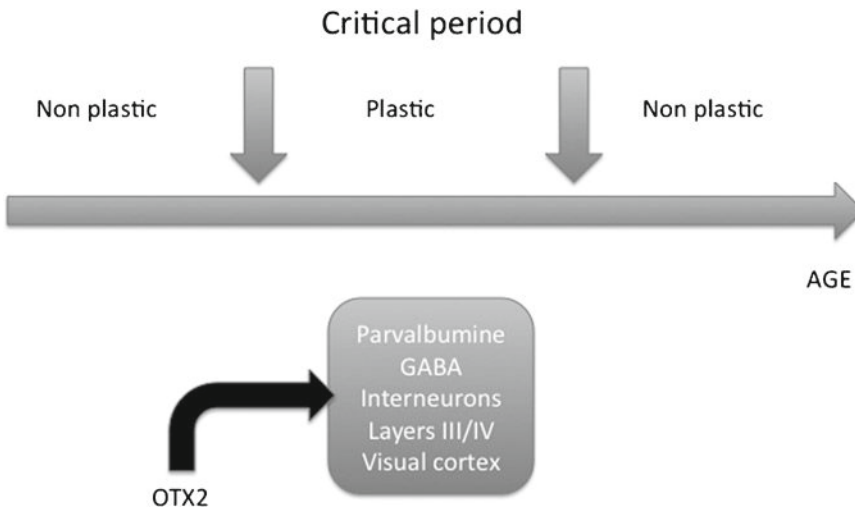


Fig. 3. Otx2 regulates critical period (CP) opening and closure in the binocular visual cortex. During postnatal development, the cortical synaptic architecture is highly sensitive to sensory information. This transitory period of plasticity is called critical period. In the binocular visual cortex, the critical period (when the two eyes can compete for cortical representation) is triggered by the maturation of Parvalbumine GABAergic neurons. Indeed, the maturation of these neurons (that inhibit pyramidal cell activity) opens a plasticity period at postnatal day 20 (P20) in the mouse and closes it at P40. Otx2 internalization by these interneuron is necessary and sufficient for PV maturation and thus regulates CP opening and closure (22).

4. Critical Period for Binocular Vision

The final – not so final – wiring of the thalamocortical projections that transport sensory information into layers III and IV of the cortex takes place rather late in development and is activity-dependent. This period during which the formation of connections is dependent upon sensory information is called the critical period (CP). CP is indeed critical as it is temporary, opening and closing at precise developmental times, and of prime importance for learning (Fig. 3).

A model system that has enabled the acquisition of a huge amount of information on CP regulation is the binocular visual cortex. In animals with binocular vision, projections from the two eyes compete for the innervation of a specific domain in the dorsal thalamus. Neurons from this thalamic relay also compete for space occupancy and synaptic activity in layers III and IV of the binocular visual cortex. Before or after plasticity, a short monocular deprivation has no consequence on ocular dominance, characterized by the respective representation of the two eyes at the cortical level. However, such a deprivation during CP will shift dominance toward the “active” eye. This shift is brought about by a morphological reorganization of the nerve terminals. Interestingly, CP is marked by the maturation of a specific class of GABAergic interneurons, the Parvalbumine (PV) large basket cells. Indeed, CP opening is induced by the maturation of these cells, and CP closure is obtained when the same cells are fully mature and exert their full inhibitory activity on descending pyramidal glutamatergic neurons (Fig. 3).

Many candidate factors have been proposed as being responsible for activity-dependent CP opening. In a recent report, we have brought a series of evidence in favor of a mechanism involving the transfer of Otx2, a homeoprotein transcription factor, into PV cells (22). These experiments establish that Otx2 internalization by PV cells is necessary and sufficient (loss and gain of function) to open CP and close it 20 days later in the mouse. An important observation is that Otx2 directly infused into the brain is specifically captured by PV cells, suggesting the existence of specific binding sites. The nature of these sites and the domain of Otx2 responsible for PV cell recognition is presently under investigation. However, preliminary results strongly suggest that complex sugars degraded by chondroitinase ABC participate in this recognition.

5. Therapeutic Proteins

Homeogene expression is extremely important in the course of development, and, in fact, it has been hypothesized that defects in their expression is at the origin of several pathologies, including psychiatric diseases (23–25). However, these genes are still expressed in the adult where their exact function is by large unknown. A case that has attracted attention is that of Engrailed and of its expression by adult mesencephalic dopaminergic neurons (mDA) in the substantia nigra (SN) and ventral tegmental area (VTA). It was proposed by Simon and colleagues that Engrailed (Engrailed1 and Engrailed2) is a survival factor for mDA neurons (26).

This hypothesis was further studied by Sonnier et al. (27) who followed the death of mDA neurons in adult mice heterozygote for

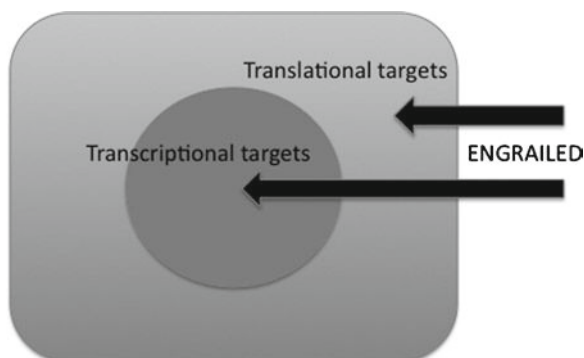


Fig. 4. Homeoproteins as therapeutic proteins and tools to identify therapeutic targets. This figure illustrates the role of Engrailed as a survival factor for mesencephalic dopaminergic neurons (27). It also illustrates that Engrailed transduction may shed light on the pathology and help in the identification of the new therapeutic targets.

Engrailed1 but expressing normal amounts of Engrailed2. In these mice which have lost one Engrailed allele out of four, mDA neurons start to die 6 weeks after birth, and this death is both progressive (40% loss of SN mDA neurons after 1 year) and higher in the SN than in the VTA (20% loss only after 1 year). This progressive loss affecting preferentially the SN (in comparison with the VTA) is very reminiscent of Parkinson disease, a pathology that affects a significant percentage of people beyond the age of 65.

Because Engrailed can be internalized by live cells, Sonnier and colleagues have infused it in the midbrain and shown that the exogenous molecule can save mDA neurons from death (27). This experiment illustrates the fact that homeoproteins, in specific cases, may be used as “therapeutic proteins,” at least in the mouse. Indeed, we are only at the beginning of this type of development, but what is extremely encouraging is the use of these gain-of-function strategies to identify downstream targets, also potential pharmacological targets, at the transcription and translation levels (Fig. 4). We have started to do so, and although, it is too early to draw firm conclusions, it is noteworthy that Engrailed acts as a “therapeutic protein” in animal models of Parkinson disease and that the identity of many of Engrailed targets in the SN is not at odds with the idea that this transcription factor is in the Parkinson pathway.

6. Conclusions

The field of cell penetrating peptides or transduction peptides is now flourishing and has acquired a true status of independence. But, if one wants to see forward, beyond the need to develop new drugs that can gain access to the cell interior, it is clear that one

needs to better understand very basic questions. Although the interest of my laboratory bends toward the physiological meaning of this novel transduction pathway (with the hope to shed light on pathologies of unknown etiology, in particular psychiatric diseases), we still see it as a priority to work on unconventional secretion and internalization, in particular on the endocytosis-independent mechanism of import that goes so much against “established” proof that even prominent researchers in the domain have hesitated to recognize the evidence. Working on unconventional internalization means pursuing the studies on peptide/lipid interactions and on the role of negative charges carried by complex sugars, but above all it means understanding membrane plasticity in terms of continuous disruption and repair. If our community can understand these processes and control them, there is little doubt that this will open new perspectives for the development of a new generation of drugs with intracellular activity.

Acknowledgments

This work was supported by Centre national de la Recherche Scientifique, Ecole normale supérieure and Collège de France. I want to thank Elizabeth Di Lullo for her useful comments and careful rereading of the manuscript.

References

1. Frankel AD, Brecht DS, Pabo CO. Tat protein from human immunodeficiency virus forms a metal-linked dimer. *Science* 1988;240:70–3.
2. Prochiantz A, Joliot A. Can transcription factors function as cell-cell signalling molecules? *Nat Rev Mol Cell Biol* 2003;4:814–9.
3. Lucas WJ, Bouche-Pillon S, Jackson DP, et al. Selective trafficking of KNOTTED1 homeodomain protein and its mRNA through plasmodesmata. *Science* 1995;270:1980–3.
4. Tassetto M, Maizel A, Osorio J, Joliot A. Plant and animal homeodomains use convergent mechanisms for intercellular transfer. *EMBO Rep* 2005;6:885–90.
5. Joliot A, Prochiantz A. Transduction peptides: from technology to physiology. *Nat Cell Biol* 2004;6:189–96.
6. Cai C, Masumiya H, Weisleder N, et al. MG53 nucleates assembly of cell membrane repair machinery. *Nat Cell Biol* 2009;11:56–64.
7. Simeone A. Positioning the isthmic organizer where *Otx2* and *Gbx2* meet. *Trends Genet* 2000;16:237–40.
8. Briscoe J, Pierani A, Jessell TM, Ericson J. A homeodomain protein code specifies progenitor cell identity and neuronal fate in the ventral neural tube. *Cell* 2000;101:435–45.
9. Callaerts P, Halder G, Gehring WJ. PAX-6 in development and evolution. *Annu Rev Neurosci* 1997;20:483–532.
10. Quiring R, Walldorf U, Kloter U, Gehring WJ. Homology of the *eyeless* gene of *Drosophila* to the *Small eye* gene in mice and *Aniridia* in humans. *Science* 1994;265:785–9.
11. Halder G, Callaerts P, Gehring WJ. Induction of ectopic eyes by targeted expression of the *eyeless* gene in *Drosophila*. *Science* 1995;267:1788–92.
12. Chow RL, Altmann CR, Lang RA, Hemmati-Brivanlou A. Pax6 induces ectopic eyes in a vertebrate. *Development* 1999;126:4213–22.
13. Brunet I, Di Nardo AA, Sonnier L, Beurdeley M, Prochiantz A. The topological role of homeoproteins in the developing central nervous system. *Trends Neurosci* 2007;30:260–7.

14. Holcman D, Kasatkin V, Prochiantz A. Modeling homeoprotein intercellular transfer unveils a parsimonious mechanism for gradient and boundary formation in early brain development. *J Theor Biol* 2007;249:503–17.
15. Lesaffre B, Joliot A, Prochiantz A, Volovitch M. Direct non-cell autonomous Pax6 activity regulates eye development in the zebrafish. *Neural Dev* 2007;2:2.
16. Sperry RW. Chemoaffinity in the orderly growth of nerve fiber patterns and connections. *Proc Natl Acad Sci USA* 1963;50:703–10.
17. Flanagan JG, Vanderhaeghen P. The ephrins and Eph receptors in neural development. *Annu Rev Neurosci* 1998;21:309–45.
18. Flanagan JG. Neural map specification by gradients. *Curr Opin Neurobiol* 2006;16:59–66.
19. McLaughlin T, O’Leary DD. Molecular gradients and development of retinotopic maps. *Annu Rev Neurosci* 2005;28:327–55.
20. Brunet I, Weinl C, Piper M, et al. The transcription factor Engrailed-2 guides retinal axons. *Nature* 2005;438:94–8.
21. Wizenmann A, Brunet I, Lam JSY, et al. Extracellular Engrailed participates in the topographic guidance of retinal axons in vivo. *Neuron* 2009;64(3):355–66.
22. Sugiyama S, Di Nardo AA, Aizawa S, et al. Experience-dependent transfer of Otx2 homeoprotein into the visual cortex activates postnatal plasticity. *Cell* 2008;134:508–20.
23. Kennedy DP, Courchesne E. The intrinsic functional organization of the brain is altered in autism. *Neuroimage* 2008;39:1877–85.
24. Harrison PJ. Schizophrenia susceptibility genes and neurodevelopment. *Biol Psychiatry* 2007;61:1119–20.
25. Walsh CA, Morrow EM, Rubenstein JL. Autism and brain development. *Cell* 2008;135:396–400.
26. Simon HH, Thuret S, Alberi L. Midbrain dopaminergic neurons: control of their cell fate by the engrailed transcription factors. *Cell Tissue Res* 2004;318:53–61.
27. Sonnier L, Le Pen G, Hartmann A, et al. Progressive loss of dopaminergic neurons in the ventral midbrain of adult mice heterozygote for Engrailed1. *J Neurosci* 2007;27:1063–71.

Pharmacology, Biodistribution, and Efficacy of GPCR-Based Pepducins in Disease Models

Sarah L. Tressel, Georgios Koukos, Boris Tchernychev, Suzanne L. Jacques, Lidija Covic, and Athan Kuliopulos

Abstract

G protein-coupled receptors (GPCR) are a superfamily of receptors that are vital in a wide array of physiological processes. Modulation of GPCR signaling has been an intensive area of therapeutic study, mainly due to the diverse pathophysiological significance of GPCRs. Pepducins are cell-penetrating lipidated peptides designed to target the intracellular loops of the GPCR of interest. Pepducins can function as agonists or antagonists of their cognate receptor, making them highly useful compounds for the study of GPCR signaling. Pepducins have been used to control platelet-dependent hemostasis and thrombosis, tumor growth, invasion, and angiogenesis, as well as to improve sepsis outcomes in mice. Pepducins have been successfully designed against a wide variety of GPCRs including the protease-activated receptors (PAR1, 2, 4), the chemokine receptors (CXCR1, 2, 4), the sphingosine-1-phosphate receptor (S1P3), the adrenergic receptor (ADRA1B), and have the potential to help reveal the functions of intractable GPCRs. Pharmacokinetic, pharmacodynamic, and biodistribution studies have showed that pepducins are widely distributed throughout the body except the brain and possess appropriate drug-like properties for use in vivo. Here, we discuss the delivery, pharmacology, and biodistribution of pepducins, as well as the effects of pepducins in models of inflammation, cardiovascular disease, cancer, and angiogenesis.

Key words: Pepducin, GPCR, Inflammation, Sepsis, Thrombosis, Cancer, Angiogenesis, PAR1, PAR4, CXCR1, CXCR2, CXCR4

1. Introduction

G protein-coupled receptors (GPCR) are a superfamily of receptors that are vital in a wide array of physiological processes. GPCRs share a unique seven transmembrane structure that transmits extracellular signals across the plasma membrane and activate intracellular signal transduction pathways through G proteins (1). Modulation of GPCR signaling has been an intensive area of therapeutic study,

mainly due to the diverse pathophysiological significance of GPCRs (2, 3). Essentially, all small-molecule drugs directed at GPCRs interact with the ligand binding site on the extracellular surface of the receptor. By comparison, pepducins exploit the importance of the G protein and modulate the interactions of the receptor with the G protein on the intracellular surface (4). Pepducins are cell-penetrating lipidated peptides designed to target the intracellular loops of the GPCR of interest (4). Pepducins can function as agonists or antagonists of their cognate receptor, making them highly useful compounds for the study of GPCR signaling.

Pepducins have been used to target GPCR signaling pathways in many disease models, including inflammation, thrombosis, and cancer. We and others have shown that pepducins can be used to control platelet-dependent hemostasis and thrombosis (5–7), tumor growth, invasion, and angiogenesis (8–10), as well as to improve sepsis outcomes in mice (11, 12). Pepducins have been successfully designed against a wide variety of GPCRs including protease-activated receptors (PAR1, 2, 4), chemokine receptors (CXCR1, 2, 4), the sphingosine-1-phosphate receptor (S1P3) (13), the adrenergic receptor (ADRA1B) (14), and have the potential to help reveal the functions of intractable GPCRs. Here, we discuss the delivery, pharmacology, and biodistribution of pepducins, as well as the effects of pepducins in models of inflammation, cardiovascular disease, cancer, and angiogenesis.

2. Pepducin Delivery, Pharmacology, and Biodistribution

The seven transmembrane domains of GPCRs are joined by intracellular loops (i1–i3) and extracellular loops (e2–e4), and are flanked by an N-terminal e1 extracellular domain and an i4 C-terminal intracellular domain. Pepducins are created by attaching a lipidated group, such as an acyl chain (e.g., C₁₂–C₁₈) or steroid to a peptide corresponding to the i1–i4 loops of the GPCR of interest (2, 4, 11, 13–17). Mechanistic studies suggest that the hydrophobic lipid group partitions into the plasma membrane and “flips” across the bilayer, thus shuttling the attached peptide to the inner leaflet of the plasma membrane in a reversible manner (Fig. 1) (2, 4, 18, 19). Mutagenesis analysis of the receptor and pepducin indicate that the peptide can interact with the intracellular domains of the GPCR of interest (4).

The delivery of PAR1- and PAR4-based pepducins to circulating platelets confirmed that pepducins can partition to the plasma membrane of the target cells of animals (2, 18). Fluorescein-tagged palmitoylated or nonpalmitoylated peptides were injected intravenously in mice (2). Flow cytometry of circulating platelets,

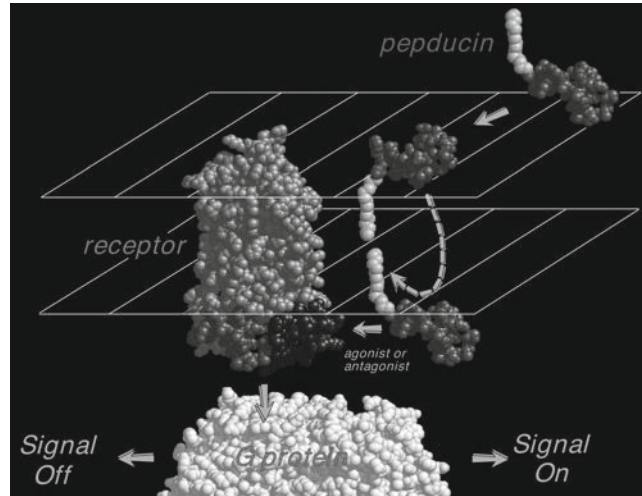


Fig. 1. Proposed mechanism of modulation of GPCR signaling by its cognate pepducin. Cell-penetrating pepducins with a covalently attached palmitate are shown inserting and flipping across to the intracellular surface of the plasma membrane where they interact with the GPCR and G protein to either turn off or turn on signaling.

after using pronase to remove peripherally bound peptides from the platelet surface, revealed significantly higher levels of fluorescence in the mice treated with the palmitoylated peptide as compared to those treated with the nonpalmitoylated peptide. Confirmation that the palmitoylated peptides can flip across the lipid bilayer was provided by Wielders and colleagues, who used a FRET-based assay with differentially labeled phospholipids that were distributed either to the outer leaflet (NBD-phosphocholine as donor) or inner leaflet (NBD-phospho-L-serine as donor) of the plasma membrane (18). They demonstrated that rhodamine-labeled PAR1 pepducins (Rho-P1pal-12 as an acceptor) are present in both inner and outer leaflets of the bilayer. Together, these data support the proposed mechanism in Fig. 1 that palmitoylation is sufficient for delivery of the peptide across the plasma membrane of the cell.

Many studies have been conducted to determine the specificity of various pepducins to their cognate receptors (2, 11–13, 20, 21). Early work with the PAR1 i3 loop antagonist P1pal-12 indicated that the pepducin was highly specific for PAR1. Treatment of human platelets with 5 μ M P1pal-12 for 1 min resulted in a 75–95% decrease in SFLLRN (PAR1 agonist)-induced aggregation and complete blockade of aggregation in response to 3 nM thrombin (2). The specificity of P1pal-12 was demonstrated by the lack of an effect in the aggregation of platelets induced by a series of agonists for the thromboxane, ADP, collagen, or GPIIb/IX/V receptors. Furthermore, P1pal-12 had no effect in endothelial cells on the responses to IL8, SDF-1 α ,

S1P, thromboxane, MCP-1, RANTES, or the migration of recombinantly transfected HEK293 cells to ligands for PAR2, PAR4, CXCR1, CXCR2, S1P1, S1P3, or CCR5 receptors (12). A PAR4 i3 loop-based pepducin, P4pal-10, completely blocked AYPGKF (PAR4 agonist)-induced aggregation and had the ability to partially block PAR1 activation at higher concentrations but did not affect ADP, thromboxane, and GPIb/IX/V receptors (2). Hollenberg and colleagues verified that P4pal-10, but not the reverse-sequence pepducin rev-P4pal-10, inhibited human platelet aggregation to PAR4 agonists (20). Slofstra et al. demonstrated that P4pal-10 had no effect on migration of human neutrophils to IP-10, SDF-1 α , and S1P but completely blocked migration to thrombin (21).

The pharmacokinetics (PK), pharmacodynamics (PD), and bioavailability of pepducins were determined using fluorescent (2) and radioactively labeled pepducins. To perform PK and PD studies, the PAR4 pepducin P4pal-10 was labeled with Alexa Fluor (P4pal-10-Alexafluor) and injected into mice intravenously (19). Bolus intravenous injection of P4pal-10-Alexafluor resulted in high plasma and platelet pepducin levels for 5 h followed by elimination with a half-life of 3.5 h (19). We had previously showed that P4pal-10 inhibits murine platelet function by antagonizing PAR4, a major hemostasis receptor in rodents (2). Therefore, PD studies were carried out by measuring the effect of P4pal-10 on bleeding time in mice (19). Intravenous injection of P4pal-10 increased bleeding time threefold to fivefold after 5 min which was maintained for 1 h after injection. P4pal-10 extended bleeding time approximately twofold at the 4 h point and returned to baseline at the 24 h time point. Subcutaneous injection of 3 mg/kg P4pal-10 resulted in a sixfold prolongation of bleeding time 4 h after injection and gave a more prolonged PD half-life of approximately 14 h.

To begin to study the biodistribution of pepducins, P4pal-10C (pal-CGRRYGHALR) was radioactively labeled with (¹⁴C)-acetamide on a cysteine residue ([¹⁴C]-P4pal-10C) and injected subcutaneously or intravenously into mice at four different doses. After 4 h, the localization of radioactive pepducin was measured in various organs and tissues (Fig. 2). Intravenous injection of [¹⁴C]-P4pal-10C with a therapeutic dose of 1.4 mg/kg P4pal-10 resulted in the appearance of radioactivity in the liver, kidney, lungs, and spleen, and lesser amounts to other tissues (Fig. 2a). Intravenous injection with a high dose of 14 mg/kg P4pal-10 resulted in appearance of radioactivity in highly perfused tissues such as the kidney, lungs, liver, and spleen with lesser radioactivity appearing in the heart, blood, muscle, and fat, but not the brain. Subcutaneous injection of [¹⁴C]-P4pal-10C with a therapeutic dose of 1 mg/kg P4pal-10 resulted in appearance of radioactivity in the liver, kidney, lungs, and blood. Subcutaneous injection at a higher dose of 10 mg/kg gave a fairly even distribution

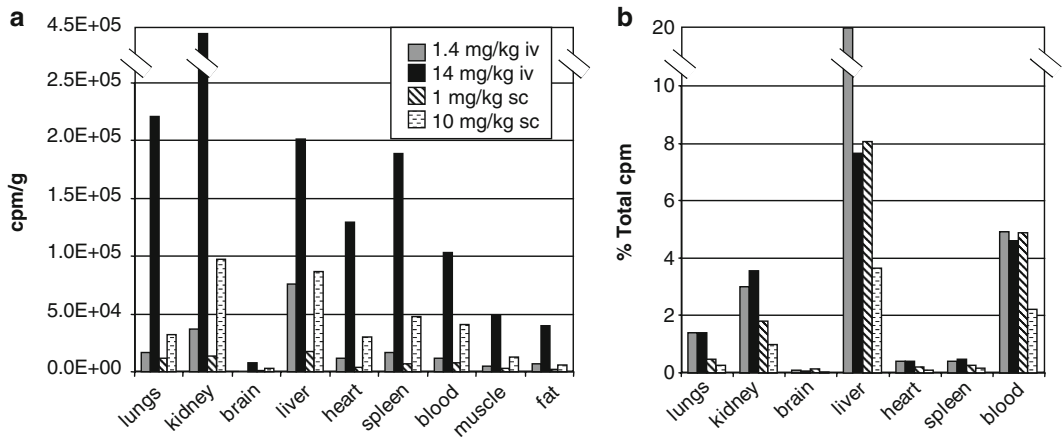


Fig. 2. Pepducin biodistribution. Mice were injected intravenously (1.4 mg/kg or 14 mg/kg) or subcutaneously (1 mg/kg or 10 mg/kg) with P4pal-10 radioactively labeled pepducin, [^{14}C]-P4pal-10C. After 4 h the distribution of [^{14}C]-P4pal-10C was measured in various organs and tissues by radioactive count in counts per million (cpm). Data are represented as (a) cpm/g tissue or (b) as a percent of the total cpm.

of radioactivity to the kidney, liver, spleen, blood, heart, and lungs, with lesser amounts to muscle and fat, but not to brain. This pattern is consistent with a biodistribution of [^{14}C]-P4pal-10C to highly vascularized tissues. More detailed examination of blood components revealed that 50% of the [^{14}C]-P4pal-10C radioactivity partitioned to red blood cells, 40% to plasma, and the remaining 10% was detected in white blood cells and platelets 4 h after intravenous or subcutaneous injection (Fig. 3a). By 1 h, radioactivity was detected in urine, with a fivefold increase in urine at 4 h (Fig. 3b). Radioactivity appeared in mouse blood in a linearly increasing manner following subcutaneous injection (Fig. 3c). Together, these findings suggest that the P4pal-10 pepducin is widely distributed throughout the body and blood components, is biologically active, and is excreted into the urine.

3. Efficacy of Pepducins in Disease Models

3.1. Inflammation

GPCRs have been implicated in many inflammatory diseases, including sepsis and systemic inflammatory response syndrome, rheumatoid arthritis, ulcerative colitis, atherosclerosis, and psoriasis. Leukocytes and other cells, such as endothelial cells, fibroblasts, epithelium, and glial cells, contribute to the inflammatory response by the secretion of proinflammatory mediators. This often results in an overzealous immune response that does more harm than good and is responsible for much of the morbidity and mortality associated with inflammatory conditions. Pepducins

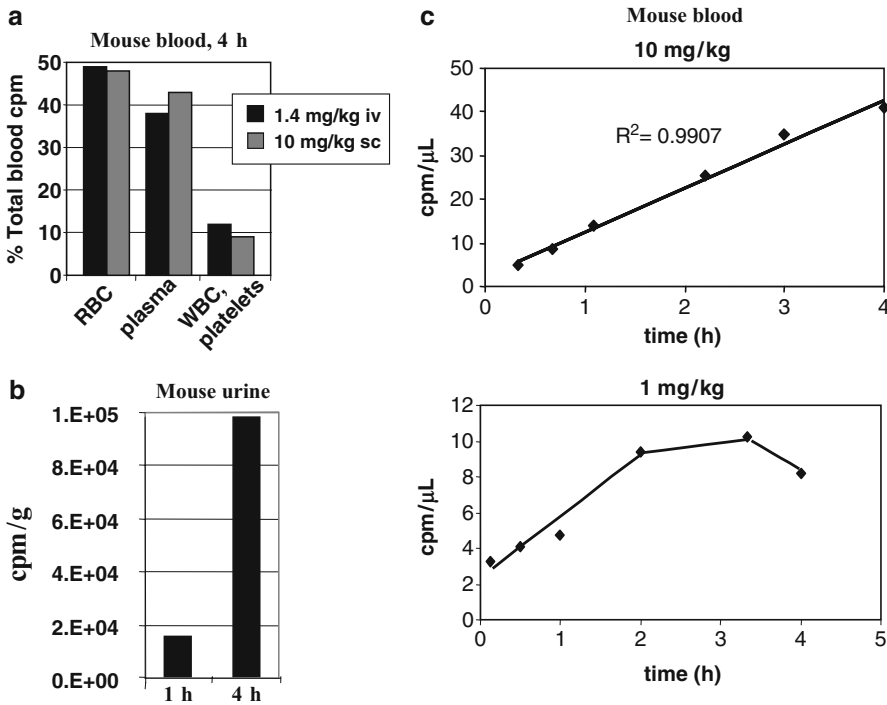


Fig. 3. Pharmacokinetics of pepducins in mouse blood and urine. (a) Mice were injected with 1.4 mg/kg intravenously or 10 mg/kg subcutaneously with [^{14}C]-P4pal-10. After 4 h, radioactivity was measured in red blood cells (RBC), plasma, and white blood cells (WBC)/platelets and represented as a percent of the total counts per million (cpm) in whole blood. (b) Mice were injected with [^{14}C]-P4pal-10C. After 1 and 4 h radioactivity was measured in the urine. (c) Mice were injected subcutaneously with 10 mg/kg or 1 mg/kg ^{14}C -P4pal-10C. Radioactivity was measured in the blood over time.

targeted against PAR1, PAR2, PAR4, CXCR1, CXCR2, and CXCR4 have been used to study the role of these receptors in specific inflammatory diseases (Table 1) and could potentially be used as therapeutics for these conditions (11, 20–26).

Sepsis and systemic inflammatory response syndrome (SIRS) are a leading cause of mortality in intensive care units (27). Sepsis can lead to systemic inflammation and overactivation of the coagulation system – a condition termed disseminated intravascular coagulation (DIC) (28). Pepducins have been used to study the role of neutrophil, platelet, and endothelial cell PAR1, PAR2, PAR4, CXCR1, CXCR2, CXCR4 in sepsis and systemic inflammation (11, 12, 21). Chemokine receptor pepducins for CXCR1 and CXCR2 were found to improve survival and prevent DIC in septic mice (11). Antagonist pepducins were designed against the i1 and i3 loops of CXCR1 and CXCR2 (x1/2pal-i3, x1/2LCA-i1), and CXCR4 (x4pal-i1, x4pal-i2). Treatment with the CXCR1/2 pepducins blocked neutrophil chemotaxis toward IL-8, improved survival, and reversed DIC and liver failure in septic mice. However, treatment with a CXCR4 pepducin had no effect on survival but caused massive leukocytosis consistent with the role of CXCR4 in

Table 1
Pepducin applications and outcomes in inflammatory disease models in mice

Disease model	Pepducin	Sequence	Target	Outcome	References
Inflammation/ paw edema	P4pal-10	<i>N-pal</i> -SGRRYGHALR-NH ₂	PAR4	Reduced edema and granulocyte recruitment induced by carrageenan	(20, 22)
Sepsis, systemic inflammatory response syndrome (SIRS), and disseminated intravascular coagulation (DIC)	P1pal-12	<i>N-pal</i> -RCLSSAVANRS-NH ₂	PAR1	Reduced organ damage and inflammatory mediators, inhibited neutrophil migration	(21)
	P4pal-10	<i>N-pal</i> -SGRRYGHALR-NH ₂	PAR4		
	x1/2pal-i3	<i>N-pal</i> -RTLFLKAHMGQKHRAMR-NH ₂	CXCR1/2	CXCR1/2 pepducins reduced organ damage, inhibited neutrophil migration, improved survival, and inhibited DIC	(11)
	x1/2LCA-i1	<i>N-LCA</i> -YSRVGRSVTD-NH ₂	CXCR1/2		
x4pal-i1	<i>N-pal</i> -MGYQKKLRSMTD-NH ₂	CXCR4			
Ulcerative colitis	P1pal-12S	<i>N-pal</i> -RSLSSAVANRS-NH ₂	PAR1	Temporally modulated survival, vascular leakage, and DIC	(12)
	P1pal-13	<i>N-pal</i> -AVANRSKKSRLF-NH ₂	PAR1 (agonist)		
	P4pal-10	<i>N-pal</i> -SGRRYGHALR-NH ₂	PAR4	Decreased epithelial cell permeability in murine colonic strips	(24, 25)
Rheumatoid arthritis	P4pal-10	<i>N-pal</i> -SGRRYGHALR-NH ₂	PAR4	Reduced agonist induced joint vascular conductance and edema	(26)

pal palmitoyl, *LCA* lithicholic

SDF-1 α neutrophil homeostasis. Slofstra and colleagues used the PAR4 antagonist pepducin, P4pal-10, to study the role of PAR4 in sepsis and discovered that PAR4 inhibition of neutrophils protected against systemic inflammation and DIC (21).

PAR1 i3 loop agonist and i3 loop antagonist pepducins were used to study the role of PAR1 at different stages of sepsis in mice (12). Treatment with the PAR1 antagonist pepducin, P1pal-12S, at early time points but not late time points, improved survival and prevented DIC in septic mice. Interestingly, treatment with the PAR1 agonist pepducin, P1pal-13, at late time points improved survival and prevented DIC in septic mice by inhibiting leakage of endothelial cell tight junctions. These findings suggested that PAR1 switches from being a vascular-disruptive receptor to a vascular-protective receptor during sepsis. Further studies demonstrated that transactivation of PAR2 by PAR1 within a PAR1–PAR2 heterodimer mediated the protective effects of the PAR1 agonist pepducin seen in later stages of sepsis which was lost in either the PAR1^{-/-} or PAR2^{-/-} mice. PAR1 antagonist pepducins did not prevent the transactivation of PAR2 by the PAR1 tethered ligand, suggesting that the pepducins did not cause dissociation of the PAR1–PAR2 heterodimer complex. Thus, pepducins revealed a novel transactivation of PAR2 by the PAR1 tethered ligand, which complemented the genetic approaches (12).

PAR4 pepducins have been used to study ulcerative colitis, irritable bowel syndrome, and rheumatoid arthritis (24–26). Dabek and colleagues (25) used the PAR4 antagonist pepducin, P4pal-10, to study the role of PAR4 and its activator cathepsin G in colonic epithelial barrier function and neutrophil activity in ulcerative colitis. Treatment of mice with fecal supernatants from ulcerative colitis patients increased epithelial cell permeability, which was blocked by P4pal-10. Furthermore, P4pal-10 was used to study joint pain and inflammation in a model of rheumatoid arthritis (26). McDougall et al. (26) treated mice with P4pal-10 and found that the pepducin could block the proinflammatory and pronociceptive effects of a PAR4 agonist in the mouse knee joint and alleviate acute joint inflammation. Together, these animal studies demonstrate that pepducins designed for a specific GPCR target can be successfully used to study a wide variety of inflammatory diseases.

3.2. Cardiovascular Disease

Major cardiovascular diseases include atherosclerosis, coronary artery disease, thrombosis, restenosis, hypertension, and heart failure. Cardiovascular disease is the major cause of death in the developed world, and significant resources have been invested in finding new therapies to treat these diseases. The technology of pepducins has helped elucidate the role of various GPCRs in the pathophysiology of arteriothrombosis, myocardial ischemia, and blood vessel inflammation (Table 2).

Table 2
Peptiducin applications and outcomes in cardiovascular disease in animal models

Peptiducin	Sequence	Target	Outcome	References
P1pal-7	<i>N-pal</i> -KKSRALF- NH_2	PAR1 antagonist	Inhibition of guinea pigs platelet aggregation Prolonged collagen-induced arterial occlusion time in guinea pigs	(7)
P1pal-12	<i>N-pal</i> -RCLSSSAVANRS- NH_2	PAR1 antagonist	Inhibition of collagen-induced platelet aggregation Delayed thrombin generation Decreased collagen-induced calcium signal Decreased thrombin-induced relaxation in rat aortic rings	(7) (18) (5) (33)
P1pal-12S	<i>N-pal</i> -RSLSSSAVANRS- NH_2	PAR1 antagonist	Increased transendothelial migration of murine monocytes	(32)
P1pal-19	<i>N-pal</i> -RCLSSSAVANRSKKSRALF- NH_2	PAR1 agonist	Promotes Ca^{2+} signal, relaxation of rat aortic rings, and prostaglandin E2 release	(33)
P4pal-10	<i>N-pal</i> -SGRRYGHALR- NH_2	PAR4 antagonist and PAR1 partial antagonist	Delayed thrombin generation Delayed platelet accumulation Prolonged tail bleeding time in mice Reduced infarct size in ischemia/reperfusion in rats	(18) (18, 20) (2, 19) (34)
Rev-P4pal-10	<i>N-pal</i> -RLAHGYRRGS- NH_2	Inactive		(20)
P4pal-i1	<i>N-pal</i> -ATGAPRLPST- NH_2	PAR4 antagonist	Inhibition of arterial occlusion in guinea pigs, when combined with bivalirudin or P1pal-7 Inhibition of epinephrine-induced Ca^{2+} flux	(6) (30)

pal-palmitoyl

The first *in vivo* studies using pepducins explored the contribution of thrombin receptor signaling to hemostasis, thrombosis, and systemic platelet activation. In accordance with the tail-bleeding phenotype observed in PAR4 knockout mice (29), mice infused with P4pal-10 exhibited prolonged tail-bleeding times and unstable thrombi formation as compared to P1pal-12 or vehicle-treated mice (2). Infusion of mice with P4pal-10 also protected against systemic thrombus formation induced by the PAR4-agonist peptide AYPGKF plus epinephrine (2). Wienders and colleagues (18) showed that P4pal-10 delayed the generation of thrombin. Fluorescent platelets were monitored by real-time accumulation at the site of wire injury to the carotid artery of mice. P4pal-10-inhibited platelets had a significant delay in accumulation at the site of vascular injury (18).

To study the distinct functions of PAR1 versus PAR4 in human platelets, a PAR4 pepducin based on the i1 loop, P4pal-i1, was developed (6). P4pal-i1 proved to be selective for PAR4 without affecting PAR1-induced platelet aggregation. Using P4pal-i1 in a carotid injury model in guinea pigs, which express PAR1 and PAR4 on their platelets, it was shown that blocking PAR4 decreases arterial occlusion by approximately 50%. Inhibition of PAR1 with P1pal-7 (0.3 mg/kg *i.v.*) in the same injury model (7) also gave approximately 50% prolongation of the occlusion time. When PAR1 and PAR4 inhibitors were combined, it resulted in a great increase in the arterial occlusion time in the guinea pig model (7). Also, when P4pal-i1 was combined with bivalirudin, a direct thrombin inhibitor widely used in patients with acute coronary syndromes, there was a significant inhibition of human platelet aggregation and suppression of arterial thrombosis in guinea pigs to a much higher degree than bivalirudin alone (6). The P4pal-i1 pepducin was also used by Grenegard et al. (30) to study the activation of human platelets. In thrombin-preactivated platelets, P4pal-i1 inhibited the epinephrine-induced increase of calcium concentration $[Ca^{2+}]$ and aggregation. The above observations support the role of both PAR1 and PAR4 in platelet-driven arterial thrombosis (6, 31).

Pepducins have been used to help elucidate the mechanisms of platelet procoagulant activity. Keuren and colleagues used the pepducins P1pal-12 and P4pal-10 to study the synergistic action of thrombin and collagen in generating procoagulant platelet surfaces (5). P1pal-12 significantly decreased the thrombin plus collagen-induced calcium signal and decreased the prothrombinase activity to levels induced by collagen alone. These data suggest that PAR1 activation is a prerequisite for both sustained elevations in $[Ca^{2+}]$ and that procoagulant activity is induced by a combination of collagen and thrombin through PAR1 (5). A slightly modified version of P1pal-12, P1pal-12S (12), has been recently used as a PAR1 antagonist in leukocyte inflammatory

studies in mice (32). Monocytes derived from hypercoagulable mice (TM^{Pro/Pro}) treated with P1pal-12S showed increased transendothelial migration towards human complement factor 5a, suggesting a role of PAR1 in monocyte inflammatory responses.

The pepducins P1pal-12 and P1pal-7 were also used to study collagen-dependent aggregation in human platelets (7). These PAR1 pepducins led to inhibition of collagen-induced platelet aggregation, blocked p38 MAPK activation, and significantly reduced the propagation of platelet–platelet thrombi in human whole blood, under arterial flow conditions. Intravenous administration of P1pal-7 in guinea pigs protected from collagen-induced thrombocytopenia and prolonged the mean occlusion time in a carotid artery FeCl₃ injury model.

PAR1-based pepducins have been valuable in studying other cell types involved in cardiovascular diseases. Kubo et al. (33) investigated the activity of PAR1 pepducins P1pal-19 and P1pal-12 in vascular tissue preparations and compared their activity to that of soluble activating peptides. They found that the P1pal-19 agonist can promote Ca²⁺ signals, prostaglandin E2 release, and persistent relaxation of rat aortic rings in a concentration-dependent manner. When using P1pal-12 in precontracted rat aortic rings, there was decreased relaxation induced by TFLLRN or P1pal-19, in agreement with the contractile role of PAR1 in cells of the blood vessel wall.

The role of PAR4 in ischemic injury of the heart was the focus of Strande and colleagues (34). P4pal-10 was administered as an intravenous bolus of 10 µg/kg to rats, and it significantly reduced the myocardium infarct size by approximately 20% in an ischemia/reperfusion (I/R) injury model. According to this study, by blocking PAR4 with P4pal-10, they further revealed the protective effects of adenosine signaling in the myocardium.

Other GPCRs that play key roles in the cardiovascular system have also been targeted with pepducins. A high-throughput functional assay developed by Edwards et al. (14) identified a number of palmitoylated cell-permeable oligopeptides that acted either as agonists or antagonists of GPCRs involved in platelet function including prostaglandin, LPA, and adrenergic receptors.

3.3. Cancer and Angiogenesis

GPCRs such as PAR1 and PAR2 play critical roles in cancer progression, invasion, and metastasis (35). In this section, we discuss the utility of pepducins targeted against the intracellular loops of PAR1, PAR2, Smoothed (SMO), S1P3, and CXCR4 in cancer and angiogenesis.

In addition to its well-recognized roles in platelet and vascular biology, PAR1 has been proposed to be involved in the invasive and metastatic processes of breast cancer (36, 37), pancreatic cancer (38), and melanoma (39–41) and has been identified as an oncogene in the transformation of NIH3T3 mouse fibroblasts

(42, 43). PAR1 can stimulate $G\alpha_i$, $G\alpha_q$, and $G\alpha_{12/13}$ pathways, which contribute to various processes involved in the regulation of tumor cell biology.

We have extensively tested the efficacy of the i3 loop-derived PAR1 pepducin, P1pal-7, as a monotherapy and in combination with taxotere in breast (9, 44) and ovarian (45) xenograft mouse models (Table 3). The effective pepducin therapeutic dose range in several xenograft cancer efficacy models is 3–10 mg/kg. To examine the *in vivo* efficacy of pepducins in tumor growth, the mammary fat pads of mice were injected with two different PAR1 expressing cell lines: PAR1-MCF7/N55 or MDA-MB-231 cells. Inhibition of PAR1 with P1pal-7 significantly reduced tumor growth of both PAR1-MCF7/N55 and MDA-MB-231 breast tumors by 62% ($p < 0.01$) as monotherapy (9), and 95% ($p < 0.01$) as dual therapy (44), respectively. In another set of studies, P1pal-7 gave a highly significant 88% reduction in metastasis to lung with tail vein injected breast cancer GFP/MDA-MB-231 cells ($p < 0.001$) as monotherapy (44) and significant reduction of ovarian OVCAR4 peritoneal dissemination ($p < 0.005$) as dual therapy with docetaxel (45). There were no obvious toxicities associated with multiday dosing of P1pal-7 up to 70 days in mice. These data provide an *in vivo* validation that targeting PAR1 may be a novel therapeutic approach in the treatment of breast and ovarian carcinomas.

Pepducins have also been successfully used to study angiogenesis and proangiogenic activities in endothelial cell migration and proliferation. P1pal-7 almost completely blocked angiogenesis of peritoneal ovarian (45) and breast cancers (9). Moreover, P1pal-7 significantly inhibited ascites production in peritoneal ovarian cancer (45) due to blockade of PAR1-dependent endothelial barrier function (12). P1pal-7 monotherapy gave complete inhibition of ascites formation with SKOV3 peritoneal carcinomatosis and 60% ($p < 0.005$) reduction with OVCAR4 ovarian cells. Licht et al. developed a pepducin to the i2 loop of S1P3 called KRX-725 (13), using a myristoyl-glycine attached to the N-terminus of the peptide. KRX-725 was found to have agonist activity for S1P3 and mimicked the effects of sphingosine 1-phosphate, the ligand for S1P3, in endothelial cells. KRX-725 induced angiogenesis *in vitro* and *in vivo* in the mouse corneal pocket assay.

In other studies, pepducins were used to delineate the contribution of PAR1 to the Akt survival pathways in breast cancers. P1pal-7 inhibited the viability of PAR1-expressing breast cancer cells through Akt (44). Phosphorylation of Akt was significantly inhibited in established tumors treated with P1pal-7 for 5 days and gave significant attenuation of the survival pathway. The P1pal-7 protective effect was rescued by constitutively active Akt, suggesting that P1pal-7 and PAR1 act upstream of Akt.

Table 3
Pharmacology of P1pal-7 ($C_{15}H_{31}CONH-KKSRLF-NH_2$) in human tumor xenograft models

Tumor type	Cell line	Dosing regimen	Efficacy	References
Breast carcinoma	PARI-MCF7/N55 (s.q.)	10 mg/kg (s.c. q2d), <i>single agent</i>	Tumor burden, significant 62% reduction ($p < 0.01$) in tumor growth	(9)
Breast carcinoma	MDA-MB-231 (s.q.)	10 mg/kg (i.p. q2d) <i>combination with docetaxel</i> (10 mg/kg i.p. once weekly)	Tumor burden, significant 95% reduction ($p < 0.01$) in tumor growth	(44)
Ovarian carcinoma	OVCAR4 (i.p.)	3.6 mg/kg (i.p. q2d) <i>combination with docetaxel</i> (10 mg/kg i.p. once weekly)	Significant reduction in diaphragm metastasis ($p < 0.005$)	(45)
Breast carcinoma	GFP/MDA-MB-231 (i.v.)	10 mg/kg (s.c. 5 days per week), <i>single agent</i>	Metastasis, significant 88% reduction ($p < 0.001$) in metastasis to lung	(44)
Breast carcinoma	PARI-MCF7/N55 (s.q.)	10 mg/kg (s.c. q2d), <i>single agent</i>	Vascularity, significant 75% inhibition ($p < 0.006$) in angiogenesis	(9)
Ovarian carcinoma	OVCAR4 (i.p.)	3.6 mg/kg (i.p. q2d) <i>combination with docetaxel</i> (10 mg/kg i.p. once weekly)	Vascularity, significant 75% inhibition ($p < 0.0001$) in angiogenesis	(45)
Ovarian carcinoma	SKOV3 (i.p.)	10 mg/kg (s.c. 5 days per week), <i>single agent</i>	Ascites formation, complete inhibition of ascites	(45)
Ovarian carcinoma	OVCAR4 (i.p.)	10 mg/kg (i.p. q2d), <i>single agent</i>	Ascites formation, significant 60% inhibition ($p = 0017$) in ascites formation	(45)

s.q. subcutaneous, *i.p.* intraperitoneal, *i.v.* intravenous

Majumdar et al. (8) used the PAR1 pepducin P1pal-12 (4) to demonstrate that plasmin induced migration of α_9 integrin-expressing CHO cells through PAR1. The PAR4 pepducin served as a negative control and had no effect on plasmin-induced migration of α_9 -CHO cells. A recent publication by Kaufmann and colleagues (46) investigated the role of PAR2 in the proliferation, spread, and invasion of hepatocellular carcinoma (HCC). The PAR2 pepducin antagonist P2-pal-21, which has an IC_{50} of 1 μ M for PAR2 (2), completely blocked the PAR2-dependent invasion of HCCs.

Hedgehog signaling is regulated by the seven-transmembrane receptor, Smoothed (SMO). The aberrant regulation of the Hedgehog-SMO pathway has been implicated in tumor progression (47, 48). Remsberg and colleagues (10) synthesized N-palmitoylated peptides spanning the intracellular loops of SMO (i1, i2, and i3). A series of N-terminal and C-terminal truncations of the loops were generated and tested for inhibition of growth of breast MCF-7 cells and melanoma SK-Mel2 cells. The most potent peptide was derived from the i2 loop SMO-i2-12 (Pal-LTYAWHTSFK) with an IC_{50} of 0.06 μ M. Substitution of the palmitoyl lipid with a myristoyl resulted in a loss of potency. Synthesis of metabolically stable retroinverse derivatives using all D-amino acids were found to improve the potency over the parent compound.

4. Conclusion

GPCRs play diverse roles in many physiological processes, yet relatively few have been successfully targeted. Pepducins can function as antagonists or agonists of their cognate receptor and prove to be useful compounds for the study of GPCRs that are difficult to target with small-molecule approaches. Pepducins provide a useful complement to genetic approaches and may help uncover novel functions of GPCRs, such as the transactivation of PAR2 by PAR1 within a PAR1-PAR2 heterodimer. Pepducins have been extensively tested in animal models of systemic inflammation, sepsis, thrombosis, atherosclerosis, cancer, and angiogenesis. Pharmacodynamic, pharmacokinetic, and biodistribution studies in mice have demonstrated that pepducins are widely distributed throughout the body and suggest that pepducins possess appropriate drug-like properties for use in vivo. Toxicity studies have also been performed and have found pepducins to be well tolerated in animals. Together, pepducins are a promising new class of compounds for the study of GPCRs and may ultimately be developed as therapeutics in a variety of diseases.

Acknowledgments

This research was supported by NIH grants CA104406 (L. Covic) and CA122992, HL64701, and HL57905 (A. Kuliopulos).

References

1. Palczewski, K., Kumasaka, T., Hori, T., Behnke, C. A., Motoshima, H., Fox, B. A., Le Trong, I., Teller, D. C., Okada, T., Stenkamp, R. E., Yamamoto, M., and Miyano, M. (2000) Crystal structure of rhodopsin: a G protein-coupled receptor, *Science* **289**, 739–745.
2. Covic, L., Misra, M., Badar, J., Singh, C., and Kuliopulos, A. (2002) Pepducin-based intervention of thrombin-receptor signaling and systemic platelet activation, *Nat Med* **8**, 1161–1165.
3. Kuliopulos, A., and Covic, L. (2003) Blocking receptors on the inside: pepducin-based intervention of PAR signaling and thrombosis, *Life Sci* **74**, 255–262.
4. Covic, L., Gresser, A. L., Talavera, J., Swift, S., and Kuliopulos, A. (2002) Activation and inhibition of G protein-coupled receptors by cell-penetrating membrane-tethered peptides, *Proc Natl Acad Sci USA* **99**, 643–648.
5. Keuren, J. F., Wielders, S. J., Ulrichs, H., Hackeng, T., Heemskerk, J. W., Deckmyn, H., Bevers, E. M., and Lindhout, T. (2005) Synergistic effect of thrombin on collagen-induced platelet procoagulant activity is mediated through protease-activated receptor-1, *Arterioscler Thromb Vasc Biol* **25**, 1499–1505.
6. Leger, A. J., Jacques, S. L., Badar, J., Kaneider, N. C., Derian, C. K., Andrade-Gordon, P., Covic, L., and Kuliopulos, A. (2006) Blocking the protease-activated receptor 1–4 heterodimer in platelet-mediated thrombosis, *Circulation* **113**, 1244–1254.
7. Trivedi, V., Boire, A., Tchernychev, B., Kaneider, N. C., Leger, A. J., O’Callaghan, K., Covic, L., and Kuliopulos, A. (2009) Platelet matrix metalloprotease-1 mediates thrombogenesis by activating PAR1 at a cryptic ligand site, *Cell* **137**, 332–343.
8. Majumdar, M., Tarui, T., Shi, B., Akakura, N., Ruf, W., and Takada, Y. (2004) Plasmin-induced migration requires signaling through protease-activated receptor 1 and integrin alpha(9) beta(1), *J Biol Chem* **279**, 37528–37534.
9. Boire, A., Covic, L., Agarwal, A., Jacques, S., Sherifi, S., and Kuliopulos, A. (2005) PAR1 is a matrix metalloprotease-1 receptor that promotes invasion and tumorigenesis of breast cancer cells, *Cell* **120**, 303–313.
10. Remsberg, J. R., Lou, H., Tarasov, S. G., Dean, M., and Tarasova, N. I. (2007) Structural analogues of smoothened intracellular loops as potent inhibitors of Hedgehog pathway and cancer cell growth, *J Med Chem* **50**, 4534–4538.
11. Kaneider, N. C., Agarwal, A., Leger, A. J., and Kuliopulos, A. (2005) Reversing systemic inflammatory response syndrome with chemokine receptor pepducins, *Nat Med* **11**, 661–665.
12. Kaneider, N. C., Leger, A. J., Agarwal, A., Nguyen, N., Perides, G., Derian, C., Covic, L., and Kuliopulos, A. (2007) ‘Role reversal’ for the receptor PAR1 in sepsis-induced vascular damage, *Nat Immunol* **8**, 1303–1312.
13. Licht, T., Tsurulnikov, L., Reuveni, H., Yarnitzky, T., and Ben-Sasson, S. A. (2003) Induction of pro-angiogenic signaling by a synthetic peptide derived from the second intracellular loop of S1P3 (EDG3), *Blood* **102**, 2099–2107.
14. Edwards, R. J., Moran, N., Devocelle, M., Kiernan, A., Meade, G., Signac, W., Foy, M., Park, S. D., Dunne, E., Kenny, D., and Shields, D. C. (2007) Bioinformatic discovery of novel bioactive peptides, *Nat Chem Biol* **3**, 108–112.
15. Shpakov, A. O., Pertseva, M. N., Guryanov, I. A., and Vlasov, G. P. (2005) Influence of synthetic peptides derived from the third cytoplasmic loop of the type 1 relaxin receptor on the stimulation of G-protein GTP-binding activity by relaxin, *Biol Membrany* **22**, 450–457.
16. Swift, S., Leger, A. J., Talavera, J., Zhang, L., Bohm, A., and Kuliopulos, A. (2006) Role of the PAR1 receptor 8th helix in signaling: the 7-8-1 receptor activation mechanism, *J Biol Chem* **281**, 4109–4116.
17. Shpakov, A. O., Gur’yanov, I. A., Kuznetsova, L. A., Plesneva, S. A., Shpakova, E. A., Vlasov, G. P., and Pertseva, M. N. (2007) Studies of the molecular mechanisms of action of relaxin

- on the adenylyl cyclase signaling system using synthetic peptides derived from the LGR7 relaxin receptor, *Neurosci Behav Physiol* **37**, 705–714.
18. Wielders, S. J., Bennaghmouch, A., Reutelingsperger, C. P., Bevers, E. M., and Lindhout, T. (2007) Anticoagulant and anti-thrombotic properties of intracellular protease-activated receptor antagonists, *J Thromb Haemost* **5**, 571–576.
 19. Covic, L., Tchernychev, B., Jacques, S., and Kuliopulos, A. (2007) Pharmacology and In Vivo Efficacy of Pepducins in Hemostasis and Arterial Thrombosis, in *Handbook of Cell-Penetrating Peptides* (Langel, U., Ed.), pp. 245–257, CRC Press, Boca Raton, FL.
 20. Hollenberg, M. D., Saifeddine, M., Sandhu, S., Houle, S., and Vergnolle, N. (2004) Proteinase-activated receptor-4: evaluation of tethered ligand-derived peptides as probes for receptor function and as inflammatory agonists in vivo, *Br J Pharmacol* **143**, 443–454.
 21. Slofstra, S. H., Bijlsma, M. F., Groot, A. P., Reitsma, P. H., Lindhout, T., ten Cate, H., and Spek, C. A. (2007) Protease-activated receptor-4 inhibition protects from multiorgan failure in a murine model of systemic inflammation, *Blood* **110**, 3176–3182.
 22. Houle, S., Papez, M. D., Ferazzini, M., Hollenberg, M. D., and Vergnolle, N. (2005) Neutrophils and the kallikrein–kinin system in proteinase-activated receptor 4-mediated inflammation in rodents, *Br J Pharmacol* **146**, 670–678.
 23. Zhang, G., Kernan, K. A., Collins, S. J., Cai, X., Lopez-Guisa, J. M., Degen, J. L., Shvil, Y., and Eddy, A. A. (2007) Plasmin(ogen) promotes renal interstitial fibrosis by promoting epithelial-to-mesenchymal transition: role of plasmin-activated signals, *J Am Soc Nephrol* **18**, 846–859.
 24. Annahazi, A., Gecse, K., Dabek, M., Ait-Belgnaoui, A., Rosztoczy, A., Roka, R., Molnar, T., Theodorou, V., Wittmann, T., Bueno, L., and Eutamene, H. (2009) Fecal proteases from diarrheic-IBS and ulcerative colitis patients exert opposite effect on visceral sensitivity in mice, *Pain* **144**, 209–217.
 25. Dabek, M., Ferrier, L., Roka, R., Gecse, K., Annahazi, A., Moreau, J., Escourrou, J., Cartier, C., Chaumaz, G., Leveque, M., Ait-Belgnaoui, A., Wittmann, T., Theodorou, V., and Bueno, L. (2009) Luminal cathepsin g and protease-activated receptor 4: a duet involved in alterations of the colonic epithelial barrier in ulcerative colitis, *Am J Pathol* **175**, 207–214.
 26. McDougall, J. J., Zhang, C., Cellars, L., Joubert, E., Dixon, C. M., and Vergnolle, N. (2009) Triggering of proteinase-activated receptor 4 leads to joint pain and inflammation in mice, *Arthritis Rheum* **60**, 728–737.
 27. Hotchkiss, R. S., and Karl, I. E. (2003) The pathophysiology and treatment of sepsis, *N Engl J Med* **348**, 138–150.
 28. Riedemann, N. C., Guo, R. F., and Ward, P. A. (2003) Novel strategies for the treatment of sepsis, *Nat Med* **9**, 517–524.
 29. Sambrano, G. R., Weiss, E. J., Zheng, Y. W., Huang, W., and Coughlin, S. R. (2001) Role of thrombin signalling in platelets in haemostasis and thrombosis, *Nature* **413**, 74–78.
 30. Grenegard, M., Vretenbrant-Oberg, K., Nylander, M., Desilets, S., Lindstrom, E. G., Larsson, A., Ramstrom, I., Ramstrom, S., and Lindahl, T. L. (2008) The ATP-gated P2X1 receptor plays a pivotal role in activation of aspirin-treated platelets by thrombin and epinephrine, *J Biol Chem* **283**, 18493–18504.
 31. Leger, A. J., Covic, L., and Kuliopulos, A. (2006) Protease-activated receptors in cardiovascular diseases, *Circulation* **114**, 1070–1077.
 32. Seehaus, S., Shahzad, K., Kashif, M., Vinnikov, I. A., Schiller, M., Wang, H., Madhusudhan, T., Eckstein, V., Bierhaus, A., Bea, F., Blessing, E., Weiler, H., Frommhold, D., Nawroth, P. P., and Isermann, B. (2009) Hypercoagulability inhibits monocyte transendothelial migration through protease-activated receptor-1-, phospholipase-Cbeta-, phosphoinositide 3-kinase-, and nitric oxide-dependent signaling in monocytes and promotes plaque stability, *Circulation* **120**, 774–784.
 33. Kubo, S., Ishiki, T., Doe, I., Sekiguchi, F., Nishikawa, H., Kawai, K., Matsui, H., and Kawabata, A. (2006) Distinct activity of peptide mimetic intracellular ligands (pepducins) for proteinase-activated receptor-1 in multiple cells/tissues, *Ann N Y Acad Sci* **1091**, 445–459.
 34. Strande, J. L., Hsu, A., Su, J., Fu, X., Gross, G. J., and Baker, J. E. (2008) Inhibiting protease-activated receptor 4 limits myocardial ischemia/reperfusion injury in rat hearts by unmasking adenosine signaling, *J Pharmacol Exp Ther* **324**, 1045–1054.
 35. Dorsam, R. T., and Gutkind, J. S. (2007) G-protein-coupled receptors and cancer, *Nat Rev Cancer* **7**, 79–94.
 36. Even-Ram, S., Uziely, B., Cohen, P., Grisaru-Granovsky, S., Maoz, M., Ginzburg, Y., Reich, R., Vlodaysky, I., and Bar-Shavit, R. (1998) Thrombin receptor overexpression in malignant

- and physiological invasion processes, *Nat Med* **4**, 909–914.
37. Henrikson, K. P., Jazin, E. E., Greenwood, J. A., and Dickerman, H. W. (1990) Prothrombin levels are increased in the estrogen-treated immature rat uterus, *Endocrinology* **126**, 167–175.
 38. Rudroff, C., Seibold, S., Kaufmann, R., Zetina, C. C., Reise, K., Schafer, U., Schneider, A., Brockmann, M., Scheele, J., and Neugebauer, E. A. (2002) Expression of the thrombin receptor PAR-1 correlates with tumour cell differentiation of pancreatic adenocarcinoma in vitro, *Clin Exp Metastasis* **19**, 181–189.
 39. Nierodzik, M. L., Chen, K., Takeshita, K., Li, J. J., Huang, Y. Q., Feng, X. S., D'Andrea, M. R., Andrade-Gordon, P., and Karparkin, S. (1998) Protease-activated receptor 1 (PAR-1) is required and rate-limiting for thrombin-enhanced experimental pulmonary metastasis, *Blood* **92**, 3694–3700.
 40. Even-Ram, S. C., Maoz, M., Pokroy, E., Reich, R., Katz, B. Z., Gutwein, P., Altevogt, P., and Bar-Shavit, R. (2001) Tumor cell invasion is promoted by activation of protease activated receptor-1 in cooperation with the alpha v beta 5 integrin, *J Biol Chem* **276**, 10952–10962.
 41. Nierodzik, M. L., Kajumo, F., and Karparkin, S. (1992) Effect of thrombin treatment of tumor cells on adhesion of tumor cells to platelets in vitro and tumor metastasis in vivo, *Cancer Res* **52**, 3267–3272.
 42. Whitehead, I., Kirk, H., and Kay, R. (1995) Expression cloning of oncogenes by retroviral transfer of cDNA libraries, *Mol Cell Biol* **15**, 704–710.
 43. Martin, C. B., Mahon, G. M., Klinger, M. B., Kay, R. J., Symons, M., Der, C. J., and Whitehead, I. P. (2001) The thrombin receptor, PAR-1, causes transformation by activation of Rho-mediated signaling pathways, *Oncogene* **20**, 1953–1963.
 44. Yang, E., Boire, A., Agarwal, A., Nguyen, N., O'Callaghan, K., Tu, P., Kuliopulos, A., and Covic, L. (2009) Blockade of PAR1 signaling with cell-penetrating pепducins inhibits Akt survival pathways in breast cancer cells and suppresses tumor survival and metastasis, *Cancer Res* **69**, 6223–6231.
 45. Agarwal, A., Covic, L., Sevigny, L. M., Kaneider, N. C., Lazarides, K., Azabdaftari, G., Sharifi, S., and Kuliopulos, A. (2008) Targeting a metalloprotease-PAR1 signaling system with cell-penetrating pепducins inhibits angiogenesis, ascites, and progression of ovarian cancer, *Mol Cancer Ther* **7**, 2746–2757.
 46. Kaufmann, R., Oettel, C., Horn, A., Halbhuber, K. J., Eitner, A., Krieg, R., Katenkamp, K., Henklein, P., Westermann, M., Bohmer, F. D., Ramachandran, R., Saifeddine, M., Hollenberg, M. D., and Settmacher, U. (2009) Met receptor tyrosine kinase transactivation is involved in protease-activated receptor-2-mediated hepatocellular carcinoma cell invasion, *Carcinogenesis* **30**, 1487–1496.
 47. Bailey, J. M., Mohr, A. M., and Hollingsworth, M. A. (2009) Sonic hedgehog paracrine signaling regulates metastasis and lymphangiogenesis in pancreatic cancer, *Oncogene* **28**, 3513–3525.
 48. Theunissen, J. W., and de Sauvage, F. J. (2009) Paracrine Hedgehog signaling in cancer, *Cancer Res* **69**, 6007–6010.

Identification and Characterization of Tissue-Specific Protein Transduction Domains Using Peptide Phage Display

Maliha Zahid and Paul D. Robbins

Abstract

Protein transduction domains (PTD) or cell-penetrating peptides (CPPs) are small peptides that are able to carry proteins, nucleic acid, and particles across the cellular membranes into cells. PTDs can be classified into three types: (1) positively charged, cationic peptides, comprised of homopolymers of arginine, ornithine, or lysine; (2) hydrophobic peptides, derived from leader sequences of secreted proteins, and cell-type specific peptides; (3) tissue-specific, mainly amphipathic peptides identified by screening of peptide displaying phage libraries. The cationic and hydrophobic PTDs can efficiently transduce a variety of cell types in culture and in vivo, but in a nonspecific manner. In contrast, the tissue-specific transduction domains have more restricted transduction properties and presumably transduce cells through a different mechanism. In this chapter, we described methods for screening peptide phage display libraries for cell and tissue-specific transduction peptides both in cell culture and in vivo and for functional analysis of transduction.

Key words: Phage display, Biopanning, Protein transduction domains, In vivo

1. Introduction

1.1. Protein Transduction Domains

Protein transduction domains (PTD) or cell-penetrating peptides (CPP) are small peptides that are able to carry a variety of cargos including full-length proteins, oligonucleotides, nanoparticles, and nucleic acid across cellular membranes. These transduction peptides are classified under three broad classes: (1) cationic; (2) hydrophobic or protein leader sequence-derived domains; and (3) tissue-specific transduction peptides (1–3). The cationic peptides in particular, have been used extensively in cell culture and in mouse models for delivery of therapeutic cargos. However, tissue-specific transduction peptides, which presumably enter the cell through a different mechanism than cationic peptides, have

advantages in regard to reducing side effects and increasing therapeutic efficacy. Tissue-specific transduction domains can be identified by screening of peptides phage display libraries for peptides that are able to facilitate internalization of intact phage (4).

1.2. Biopanning Using Phage Peptide Display Libraries

Initial studies utilizing phage peptide display libraries were limited to *in vitro* studies, phage display being carried out against immobilized antigen targets or cell-specific ligands (5). Phage display also was used *in vivo* to identify peptides that are able to home to the tumor vasculature for anti-cancer therapy (1). Further *in vivo* work has shown that not only tumor vasculature but also normal organs and cells can be targeted by *in vivo* phage display (6, 7). However, these studies focused on identifying peptides that are able to bind to the surface of the cell, not necessarily for facilitating internalization.

As outlined below, we have developed a biopanning methodology using peptide phage display to identify tissue-specific transduction peptides that are able to facilitate transduction of specific cell and/or tissues types. The approach for biopanning for transduction peptides using phage display involves exposing the cell or tissue type of interest to a large, randomized library of phage, usually M13, expressing a peptide library on a surface coat protein. After binding, the non-relevant phage is washed away, the cell trypsinized to release bound phage, and internalized phage recovered by cell lysis. The released phage is expanded in bacteria and reexposed to the target of interest. Four to six cycles of biopanning lead to adequate enrichment with the relevant clone phage, which can subsequently be sequenced, and the peptide motif carried as a fusion coat protein identified. The biopanning can be performed in cultured cells, *in vivo* or using a combination of cell culture and *in vivo* approaches.

We have used biopanning of a peptide phage display library to identify synovial fibroblast, airway epithelial, and tumor-specific and cardiac-tissue-specific transduction peptides (2, 3). Below is described a protocol for identifying internalizing peptides by screening a peptide phage display library both in cell culture and *in vivo*. The protocol described is for a rat cardiomyoblast cell line, or H9C2 cells, as an example of a cell type targeted, utilizing a commercially available (New England Biolabs, cat. no. E8110S) M13, 12 amino acid peptide phage display library. This protocol can be modified to target specific tissue types/organs *in vivo*. The process is complicated by the heterogeneity and complexity of the tissue being targeted, the sequestration of injected phage by organs of the reticuloendothelial system, largely the liver and spleen, and a large pool of contaminating, nonspecific circulating phage. In addition, the rigorous conditions that the phage displaying peptides are put through leads to loss of infective phage over subsequent cycles. Here we provide a protocol to identify peptides transducing the heart as an example with kidney being

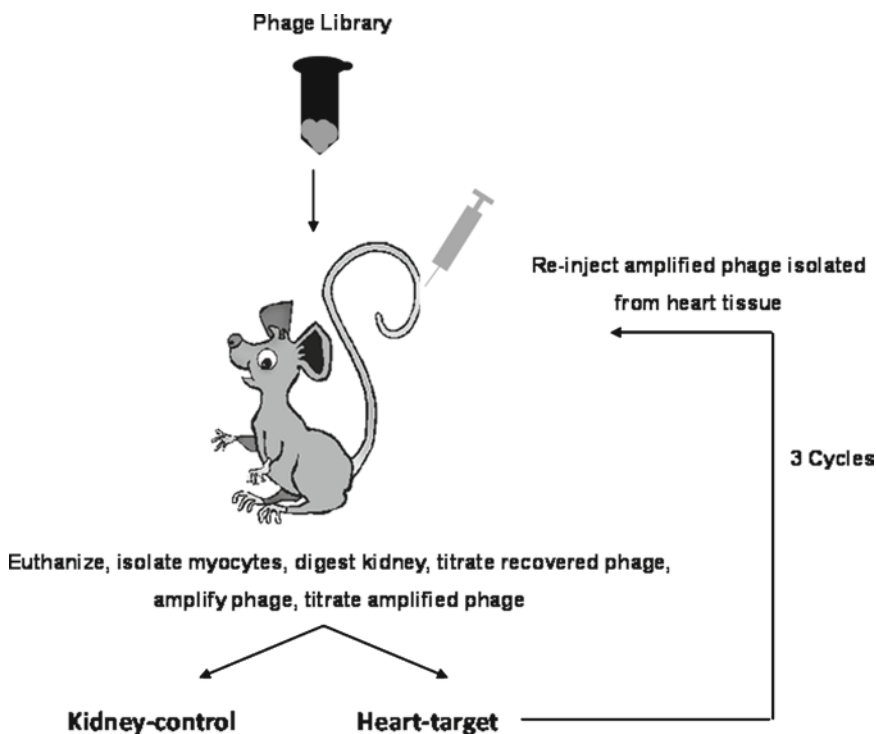


Fig. 1. Schematic representation of in vivo peptide phage display experimental design, using heart as target and kidney as control organs.

used as a control tissue, Fig. 1. However, this protocol can be modified to target various organs with helpful hints provided in Subheading 4 to maximize a researcher's chances of success.

2. Materials

2.1. Cell Culture

1. Dulbecco's modified eagle's medium (DMEM; GIBCO/BRL).
2. Heat-inactivated fetal bovine serum (FBS; GIBCO/BRL).
3. Pen Strep stock solution (GIBCO; 15140).
4. HEPES buffer solution 1 M (GIBCO; 15630).
5. Rat Cardiomyoblast Cell Line (H9C2 Cells) Media. Make the H9C2 cell media by adding 50 ml of heat-inactivated FBS, 5 ml of HEPES, and 5 ml of Pen Strep to 500 ml of DMEM. Filter the mixture and store at 4°C.
6. Solution of trypsin (0.25%) and ethylenediamine tetraacetic acid (EDTA-1 mM; GIBCO).

2.2. Phage Display

1. M13 12-mer peptide phage display library containing:
 - (a) Phage display peptide library, 100 μ l, $\sim 1 \times 10^{13}$ pfu/ml, in TBS with 50% glycerol.
 - (b) -96 gIII sequencing primer 5'- CCC TCA TAG TTA GCG TAA CG -3', 100 pmol, 1 pmol/ μ l.
 - (c) -28 gIII sequencing primer 5'- GTA TGG GAT TTT GCT AAA CAA C -3', 100 pmol, 1 pmol/ μ l.
 - (d) *E. coli* ER2738. Host strain supplied as 50% glycerol culture; not competent. Store at -70°C .
2. LB Medium: 10 g Bacto-Tryptone, 5 g yeast extract, 5 g NaCl in 1 L of H_2O . Autoclave, store at 4°C .
3. IPTG/Xgal Stock Solution: Mix 1.25 g IPTG (isopropyl- β -d-thiogalactoside) and 1 g Xgal (5-Bromo-4-chloro-3-indolyl- β -d-galactoside) in 25 ml DMF (dimethyl formamide). Solution should be stored at -20°C .
4. LB/IPTG/Xgal Plates: 1 LLB medium + 15 g/l agar. Autoclave, cool to $<70^{\circ}\text{C}$, add 1 ml IPTG/Xgal Stock per liter and pour. Store plates at 4°C in the dark.
5. Agar Top: 10 g Bacto-Tryptone, 5 g yeast extract, 5 g NaCl, 7 g Bacto-Agar in 1 L of deionized H_2O . Autoclave, dispense into 50 ml aliquots. Store at room temperature (will be solid).
6. Tetracycline Stock Solution: 20 mg/ml of tetracycline powder in a 1:1 ethanol:water. Store at -20°C , light protected. Vortex before use.
7. LB + Tetracycline Media: To 1 L of H_2O add 10 g Bacto-Tryptone, 5 g yeast extract, and 5 g NaCl. Autoclave, and allow to cool down to $<70^{\circ}\text{C}$ or until lukewarm to touch. Add 1 ml of Tetracycline stock solution, mix and store at 4°C , light-protected, until ready for use. Do not use if color turns from yellow to brown or black.
8. LB/Tetracycline Plates: Add 15 g of Agar to a liter of LB medium. Autoclave and allow to cool to $<70^{\circ}\text{C}$, add 1 ml of tetracycline stock solution, pour into plates and allow to solidify. Store plates at 4°C , light-protected. Do not use plates if they turn brown or black.
9. TBS: 50 mM Tris-HCl (pH 7.5), 150 mM NaCl. Autoclave and store at room temperature.
10. PEG/NaCl: 20% (w/v) polyethylene glycol - 8000, 2.5 M NaCl. Autoclave, mix well to combine separated layers while still warm. Store at room temperature.
11. Iodide Buffer: 10 mM Tris-HCl (pH 8.0), 1 mM EDTA, 4 M sodium iodide (NaI). Store at room temperature in the dark. Discard if color is evident.

2.3. Phage Display in Mice

1. Eight- to twelve-week-old albino, male or female mice (Balb/c or FVB; Jackson Labs).
2. 0.5-ml Insulin syringes.
3. Sterile phosphate-buffered saline (PBS; GIBCO).
4. Avertin stock solution: Avertin (2, 2, 2-Tribromoethanol; Sigma-Aldrich) is mixed with 15. 5 ml *tert*-Amyl Alcohol (2-methyl-2-butanol; Fisher) for ~12 h in a dark bottle at room temperature. Allow the mixture to go completely into solution, sterile filter and store at 4°C, light protected. On the day of use, mix 200 µl of this stock solution with 10 ml of PBS, sterile filter and wrap in foil before use. This will be the 2% Avertin working solution.
5. HBSS (Cellgro).
6. 10% Glucose. Dissolve 10 g of glucose in 100 ml of deionized H₂O, sterile filter in a hood and store for later use.
7. Heparin 1,000 U/ml (Lymphomed).
8. Collagenase II (50 mg/ml; Worthington).
9. DNase I (20 mg/ml; Roche).
10. Dulbecco's Modified Eagle's Medium 50:50/F12 (Cellgro).
11. Heat-inactivated fetal bovine serum (FBS; GIBCO/BRL).
12. Gentamycin 50 mg/ml (1,000×; GIBCO).
13. 75-µM cell filters.
14. Solution of trypsin (0.25%) and ethylenediamine tetraacetic acid (EDTA-1 mM; GIBCO).
15. HBSS-G: To 90 ml of HBSS, add 10 ml of 10% glucose solution.
16. HBSS-G-Heparin: To 50 ml of HBSS-G, add 500 µl of Heparin (1,000 U/ml stock solution). Make fresh on the day of use.
17. Digestion Enzyme: To 39 ml of HBSS-G add 40 µl of DNase I and 1.2 ml of Collagenase II. Make fresh on the day of use.
18. Plating medium: To 90 ml of DMEM 50:50/F12 add 10 ml of the heat-inactivated FBS and 100 µl of Gentamycin stock solution.
19. 0.75% collagenase II: Add 75 mg of collagenase II to 10 ml of PBS. Make fresh on the day of use.
20. DMEM 50:50/F12/25% FBS: add 7.5 ml DMEM/F12 to 2.5 ml FBS. Will need 10 cc for each heart.

3. Methods

3.1. Peptide Phage Display

1. Passage the rat cardiomyoblast cell line, H9C2 cells, for a minimum of three passages (after thawing from -180°C). Cells should be passaged once they are $\sim 70\%$ confluent. Do not allow to grow to complete confluency as they will begin to differentiate.
2. After the third passage, trypsinize cells with Trypsin/EDTA and plate in a six-well plate at a cell density of 2×10^5 cells/well. Twenty-four hours post-plating, aspirate and replace with prewarmed media, and add 10 μl of the M13 peptide phage library ($\sim 10^{11}$ phage) to the media. Return cells to incubator for 6 h. (see Note 1)
3. After the incubation period, wash cell extensively (at least $6\times$) with prewarmed PBS, trypsinized cells, and centrifuge to collect cell pellet. Wash the cell pellet one to two times more with media. Aspirate the supernatant media above the cell pellet but not completely. Cell pellet may be stored at -80°C for later lysis and phage titration.
4. Release internalized phage by subjecting the cell pellet to one freeze-thaw cycle by bringing the cell pellet from -80°C to either room temperature, or by placing in a 37°C water-bath. Pellet out the cell debris and use the supernatant for phage titration as detailed below.

3.2. Phage Titration

1. Inoculate 100 ml LB + tetracycline media in a round-bottomed flask with 10 μl of *E. coli*, provided with the phage display library. Grow overnight at 37°C with gentle shaking (225 rpm). This will be the starter culture.
2. Inoculate another 100 ml of LB + tetracycline media with one to two drops of the starter culture. Incubate at 37°C for 1 h with gentle shaking.
3. Melt agarose top in a microwave until liquid. Vortex to make sure it is homogenous. Dispense 3 ml into six sterile culture tubes. Place the six culture tubes in a water-bath with temperature set to 45°C and maintain at this temperature until ready for use. (see Note 2)
4. To carry out infection, add 20 μl of cell extract (from step 3.1,4) to 200 μl of *E. coli* culture (from step 3.2,2), vortex quickly, and incubate at room temperature for 1–5 min. This will be the 1×10^0 dilution. Take 20 μl of this and add to another 200 μl of the starter culture (1×10^1) and so on until you have 1×10^6 dilutions. Use a new tip for each serial dilution.
5. Transfer 200 μl of each of these to the culture tubes containing 3 ml of the melted agar top at 45°C , one infection at a time

(from Subheading 3.2, item 4), vortex briefly, and immediately pour culture onto a prewarmed LB + Tetracycline plate or IPTG/X-gal plate (labeled 1×10^0 to 1×10^6). Pre-warm, for at least 1 h, one LB/IPTG/Xgal plate per expected dilution at 37°C until ready for use. Gently tilt and rotate plate to spread top agar evenly.

6. Allow the plates to cool for 5 min, invert, and incubate overnight at 37°C. Place in 37°C, light-protected (for either type of plates) for overnight growth.
7. Next day count either the clear plaques in the case of LB + Tetracycline plates or blue plaques in the case of Xgal plates. Some plates will have too numerous to count plaques and some might have too few. Count the ones with 10–200 plaques, multiply by the dilution factor and that will provide the number of phage per 20 μ l of the cell lysate. The total number of phage can be calculated by multiplying this number by the total lysate cell supernatant volume (in μ l) divided by 20.

$$\text{Total No of Phage} = \text{Number of plaques in a plate} \times \text{Dilution factor of the plate} \times \text{total cell lysate volume} / 20$$

3.3. Phage Amplification

1. Inoculate 100 ml LB + tetracycline media in a round-bottomed flask with 10 μ l of *E. coli*, provided with the phage display library. Grow overnight at 37°C with gentle shaking (225 rpm). This will be the starter culture.
2. Inoculate another 100 ml of LB + tetracycline media with one to two drops of the starter culture. Incubate at 37°C for 1 h with gentle shaking.
3. Take 32 ml of this culture and add 1–1.5 ml of the cell lysate (from Subheading 3.1, step 4 above) to it and grow for 4 h at 37°C with gentle shaking (225 rpm).
4. Spin down at 24,000 *g*-force at 4°C for 20 min.
5. Discard the pellet. Take the 30 ml of the supernatant and add 6 ml of PEG/NaCl and keep at 4°C overnight.
6. Next day spin the tube at 30,000 *g*-force for 20 min at 4°C.
7. Discard the supernatant and dissolve the pellet in 1 cc of TBS (in the hood). Transfer to Eppendorf tube and add 200 μ l of PEG/NaCl (all in the hood). Place on ice for 1 h.
8. Spin the tube in cold room at 20,000 *g*-force for 5 min.
9. Discard the supernatant. Resuspend the pellet in 200 μ l of TBS. This is your amplified phage. Titer this amplified phage using the protocol detailed in Subheading 3.2. This will be the amplified and tittered phage used for next cycle of phage display.

3.4. Phage Sequencing

After three to six cycles (generally four are adequate) a cell-specific clone will emerge. From the plate with <100 plaques, pick 10–20 for amplification and subsequent sequencing.

1. Dilute an overnight culture of *E. coli* 1:100 in LB. Dispense 1 ml of diluted culture into culture tubes, one for each clone to be characterized.
2. Use a sterile wooden stick or pipette tip to stab a plaque from a titering plate (important: plates should be <1–3 days old, stored at 4°C and have <100 plaques) and transfer to a tube containing the diluted culture. Pick well-separated plaques. This will ensure that each plaque contains a single DNA sequence.
3. Incubate the tubes at 37°C with shaking for 4.5–5 h (no longer).
4. Transfer the cultures to microcentrifuge tubes, and centrifuge at 20,000 *g*-force for 30 s. Transfer the supernatant to a fresh tube and re-spin. Using a pipette, transfer the upper 80% of the supernatant to a fresh tube. This is the amplified phage stock and can be stored at 4°C for several weeks with little loss of titer. For long-term storage (up to several years), dilute 1:1 with sterile glycerol and store at –20°C.
5. Transfer 500 µl of the amplified phage stock to a fresh microfuge tube. Add 200 µl of 20% PEG/2.5 M NaCl. Invert several times to mix, and let stand for 10–20 min at room temperature.
6. Microfuge at 20,000 *g*-force for 10 min at 4°C and discard the supernatant. Phage pellet may not be visible. Re-spin briefly. Carefully pipet away and discard any remaining supernatant.
7. Suspend the pellet thoroughly in 100 µl of Iodide Buffer by vigorously tapping the tube. Add 250 µl of ethanol and incubate 10–20 min at room temperature. Short incubation at room temperature will preferentially precipitate single-stranded phage DNA, leaving most phage protein in solution.
8. Spin in a microfuge at 20,000 *g*-force for 10 min at 4°C, and discard the supernatant. Wash the pellet with 0.5 ml of 70% ethanol (stored at –20°C), re-spin, discard the supernatant, and briefly dry the pellet under vacuum or at room air.
9. Resuspend the pellet in 30 µl of TE buffer. The template can be suspended in H₂O instead of TE if desired, but this is not recommended for long-term storage. In TE buffer, the phage DNA should be stable indefinitely at –20°C. Sequence this DNA using the sequencing primers provided with the peptide phage display library.

3.5. In Vivo Peptide Phage Display

Weigh the mouse on a small animal scale and anesthetize using 12 µl/gm of tissue weight of 2% Avertin solution administered intraperitoneally. Mouse will be anesthetized in 2–5 min. Inject 10 µl

of the peptide phage display library ($\sim 10^{11}$ pfu) intravenously, either retro-orbitally or through a tail vein injection. The M13 phage, after an intravenous injection, has a half-life of 4.5 h, in the circulation. Allow the mouse to recover and circulate the phage for the desired number of half-lives (~ 3 – 6 half-lives). (see Note 3)

3.6. Isolating Cardiac Myocytes

1. After the desired time of circulation, re-anesthetize the mouse using 2% Avertin, euthanize using either a CO₂ chamber or cervical dislocation, and open the chest cavity. Now place a nick in either the right atrium or right ventricle and using a small bore needle, inject the left ventricle with 3–5 ml of HBSS-G-Heparin, so as to flush out all the red blood cells from the ventricular cavity and the coronary circulation.
2. Dissect out the heart, trim the atria and great vessels, and weigh the resulting trimmed heart.
3. Place a petri dish on ice, add 2–4 ml of HBSS-G-Heparin, place heart pieces in it and chop as finely as possible.
4. Transfer all of this to a round bottom 5 cc tube and discard the supernatant.
5. Add 2 ml of Digestion Enzyme to the pieces, incubate (with rocking) at 37°C for 5 min.
6. Collect the supernatant into DMEM 50:50/F12/25% FBS (10 ml for each heart) media; keep at 37°C.
7. Repeat the steps 5 and 6 above until all the tissue pieces are digested.
8. Now place the accumulated tissue + DMEM + FBS through a 70- μ m filter.
9. Centrifuge the filtered cells for 4 min at 1,000 rpm.
10. Aspirate off the media, keep the pellet and resuspend the cells in 5–6 ml of the plating medium.
11. Now place the cells and media in a 6-in cell culture plate (to plate out the fibroblasts) and place in an incubator at 37°C for 2 h (without disturbing).
12. At the end of 2 h, aspirate the top media, pellet the cells, resuspend in 1 ml of PBS, transfer to an Eppendorf tube and place in -80°C to freeze.
13. Put the cell pellet through one freeze–thaw cycle to lyse the cells and release the internalized phage. Pellet the cell debris by centrifuging at maximum speed for 60 s in a table-top centrifuge. Use 20 μ l of this cell lysate/supernatant to titrate the released phage as detailed in Subheading 3.2. This phage population is the population of interest that will be put through subsequent cycles of phage amplification (as detailed in Subheading 3.3) and reinjected into a mouse for a second cycle of peptide phage display. The number of phage recovered from the heart will be normalized to the weight of the heart (in grams).

3.7. Isolating Kidney Cells

1. Inject phage library intravenously (reto-orbitally or via a tail vein injection) and allow to circulate for the decided number of hours.
2. After the desired time of circulation, re-anesthetize the mouse using 2% Avertin, euthanize using either a CO₂ chamber or cervical dislocation, and open the chest cavity. Now place a nick in either the right atrium or right ventricle and using a small bore needle, inject the left ventricle with 3–5 ml of HBSS-G-Heparin, so as to flush out all the red blood cells from the ventricular cavity and the coronary circulation.
3. Dissect the kidney out and rinse in PBS.
4. In a cell culture hood, cut the kidney into small pieces with autoclaved/sterile razor blade.
5. Digest the minced tissue with 0.75% collagenase II at 37°C for 30–45 min.
6. Pipette the digested tissue up and down.
7. Filter the cells with 75- μ m filter.
8. Trypsinize the cells for 10 min at room temperature.
9. Spin down the cells and wash with PBS twice.
10. Resuspend in 1 ml of PBS.
11. Store in Eppendorf tubes at –80°C.
12. Put the cell pellet through one freeze–thaw cycle to lyse the cells and release the internalized phage. Pellet the cell debris by centrifuging at maximum speed for 60 s in a table-top centrifuge. Use 20 μ l of this cell lysate/supernatant to titrate the released phage as detailed in Subheading 3.2. This phage population is the control phage and the released phage from heart, the target organ of interest, will be expressed as a ratio of the number of phage recovered from kidney. The number of phage recovered from the kidney will be normalized to the weight of the kidney (in grams). The figure below (Fig. 1) details the experimental protocol as a schematic diagram.
13. After three or four cycles of in vivo peptide phage display, 10–20 plaques are picked from phage recovered from the target organ, amplified and sequenced as detailed in Subheading 3.4. A consensus sequence should emerge after 4 cycles of phage display. (To test the transduction ability of the identified peptide, see Note 4)

4. Notes

1. *Phage contamination*: The potential for contamination with environmental bacteriophage can be minimized by using aerosol-resistant pipette tips and wearing gloves for all protocols.

With phage work in the hood as much as possible to avoid contamination and when out of the hood, keep phage on wet ice. Also, to prevent contamination, all solutions should be autoclaved where possible and solutions containing heat-labile components should be made fresh, sterile filtered and stored under appropriate conditions. The M13 peptide phage display library used as an example in this chapter, utilizes the library cloning vector M13KE which is derived from the common cloning vector M13mp19. This vector carries the lacZ α gene, and phage plaques appear blue when plated on culture plates containing IPTG/Xgal. Environmental filamentous phage will typically yield colorless plaques when plated on the same media. These plaques are also larger and “fuzzier” than the library phage plaques. If contaminated, environmental phage appear to be a concern, we recommend plating on LB/IPTG/Xgal plates for all titrating steps and, if white plaques are evident, picking only blue plaques for sequencing.

2. *Phage viability*: Phage are temperature sensitive. After melting the agar top in a microwave and dispensing into culture tubes, place in a water-bath brought to 45°C and maintain at that temperature. Fluctuations, especially increase in temperature, will reduce phage infectivity and subsequent yield. Also culture plates (either LB + Tetracycline or IPTG/Xgal plates) need to be prewarmed before plating culture media containing phage onto them. Pre-warm plates to 37°C for an hour before use. Also once agar top and culture media of *E. coli* incubated with M13 phage are mixed together, *immediately* mix and transfer to plates. Letting the mixture stand for any length of time will reduce phage viability. Also as the phage are put through repeated cycles of display to enrich for the relevant clone, phage viability has a tendency to decrease. Minimize this loss of infectivity by putting cell lines through only one cycle of freeze–thaw to lyse the cells and release internalized phage. In addition minimize time delays and storage of phage in-between cycles. To theoretically increase the chances of recovering infective phage, cell lines may be pretreated with Chloroquine, an agent known to increase intra-lysosomal pH and hence decrease intra-cellular breakdown of internalized phage.

Phage viability is an even bigger concern in the case of *in vivo* phage display compared to phage display in cell culture. Infectivity will decrease over time and subsequent cycles of phage display. To maximize the chances of recovering infective phage, subject lysed/digested tissue to only one cycle of freeze–thaw to release the phage. Amplified phage should be stored in –20°C until ready for injection. Do not repeat freeze–thaw the stored phage. Minimize the time delays between subsequent cycles of phage display. To increase the

chances of recovering internalized phage, breakdown of internalized phage can theoretically be minimized by pre-treating the rodents with Chloroquine (20 mg/kg dose) prior to injecting with the phage. The pretreatment with Chloroquine should precede the phage injection by an adequate interval of time for it to be effective (for example 24 or 48 h before as well as on the day of phage injection).

3. *Target organ*: In vivo phage display is complicated by the nature of the target being more complex and issues of a large pool of contaminating/nonspecific phage in the circulating blood pool (in the case of intravenous injection). This is of greater concern in the case of highly vascular organs, for example heart or kidneys, and less so with less vascular tissue as in the case of brain. The problem of contaminating blood pool can be minimized by allowing for long enough circulation times (three to six half-lives) for the phage to clear the blood stream. Also the first cycle of phage display can be done in vitro in an appropriate cell line in order to enrich for relevant phage, with subsequent cycles being performed in vivo.
4. *Testing activity of the identified peptide*: Once candidate tissue specific transduction peptides are identified, it is then necessary to demonstrate transduction of the appropriate target cells or tissues. Initially, transduction can be analyzed using the peptide coupled or conjugated to a fluorescent marker like 6-carboxyfluorescein, streptavidin-alexa488, eGFP or β -galactosidase. However, this approach only demonstrates that the peptide allows entry of cargos inside the cells. To demonstrate functional delivery of agents into the cell, we have used approaches involving delivery of biologically active peptides into cells. For example, a peptide inhibitor of the transcription factor NF- κ B, a ubiquitously expressed transcription factor that is evolutionarily conserved, can be used. A small, 11 amino acid peptide, termed the NEMO-binding domain (NBD), has been identified as able to block the kinase responsible for activating the kinase, IKK, that activates NF- κ B (8). Delivery of the NBD using a tissue-specific protein transduction domain leads to a dose-dependent inhibition of NF- κ B signaling in tissue culture and in animal models. Thus tissue-specific transduction peptide-mediated delivery of NBD can be used to assess and compare efficacy of functional transduction using a NF- κ B reporter assay (9).

An alternative approach to using the NBD peptide as an assay for functional transduction is the use of an anti-microbial peptide to induce apoptosis (10). Anti-microbial peptides, able to disrupt bacterial membranes, also can disrupt the integrity of mitochondrial membranes, resulting in release of cytochrome C and induction of apoptosis. PTD-mediated

delivery of anti-microbial peptides results in rapid and efficient disruption of the mitochondrial membrane and induction of apoptosis in contrast to the anti-microbial peptide alone. Thus we also have used extent and rate of induction of apoptosis by anti-microbial peptides, such as KLAKLAK, fused to tissue-specific transduction domains, as an indicator of functional transduction of cells.

References

1. Arap, W., R. Pasqualini, and E. Ruoslahti, *Cancer treatment by targeted drug delivery to tumor vasculature in a mouse model*. Science, 1998. **279**(5349): pp. 377–80.
2. Mi, Z., et al., *Identification of a synovial fibroblast-specific protein transduction domain for delivery of apoptotic agents to hyperplastic synovium*. Mol Ther, 2003. **8**(2): pp. 295–305.
3. Rehman, K.K., et al., *Protection of islets by in situ peptide-mediated transduction of the Ikappa B kinase inhibitor Nemo-binding domain peptide*. J Biol Chem, 2003. **278**(11): pp. 9862–8.
4. Ardel, P.U., et al., *Targeting urothelium: ex vivo assay standardization and selection of internalizing ligands*. J Urol, 2003. **169**(4): pp. 1535–40.
5. Scott, J.K. and G.P. Smith, *Searching for peptide ligands with an epitope library*. Science, 1990. **249**(4967): pp. 386–90.
6. Arap, W., et al., *Steps toward mapping the human vasculature by phage display*. Nat Med, 2002. **8**(2): pp. 121–7.
7. Zhang, L., J.A. Hoffman, and E. Ruoslahti, *Molecular profiling of heart endothelial cells*. Circulation, 2005. **112**(11): pp. 1601–11.
8. May, M.J., et al., *Selective inhibition of NF-kappaB activation by a peptide that blocks the interaction of NEMO with the IkappaB kinase complex*. Science, 2000. **289**(5484): pp. 1550–4.
9. Madge, L.A. and M.J. May, *Inhibiting proinflammatory NF-kappaB signaling using cell-penetrating NEMO binding domain peptides*. Methods Mol Biol, 2009. **512**: pp. 209–32.
10. Mai, J.C., et al., *A proapoptotic peptide for the treatment of solid tumors*. Cancer Res, 2001. **61**(21): pp. 7709–12.

Applications of Cell-Penetrating Peptides as Signal Transduction Modulators for the Selective Induction of Apoptosis

Sarah Jones and John Howl

Abstract

The discovery of cell-penetrating peptides (CPP) has provided the scientific community with relatively small and increasingly cost-effective molecular agents that readily cross the normally impermeable cell membrane. Thus, as either inert delivery vectors or biologically active agents, CPP can be used to selectively modulate intracellular signal transduction events. Indeed, the survival of many cancer cells is associated with alterations in the function of key intracellular signalling proteins. Accordingly, CPP constructs have been developed to access intracellular target loci in both normal and transformed cells. Thus, CPP are a novel, generic class of signal transduction modulator which can be utilized to specifically induce apoptosis in tumour cells as a potential therapeutic option. However, and particularly at higher concentrations, CPP can induce non-specific membrane perturbations, thus leading to cell death by necrotic mechanisms. This chapter, therefore, focuses on methodologies for the assessment of apoptotic events, including *in situ* TUNEL analysis, activation of caspase-3, and the MTT assay, whilst also discussing dual Annexin V and propidium iodide staining, an assay used for the quantification of cell populations undergoing apoptosis and/or necrosis.

Key words: CPP, Apoptosis, Signal transduction, Proteomimetic, TUNEL, Annexin V, Propidium iodide, MTT, Caspase-3

1. Introduction

The past decade has witnessed a resurgent interest in the therapeutic applications of peptides. Accordingly, CPP technologies have successfully been employed as intracellular signal transduction modulators for the selective induction of apoptosis in tumour cells. For instance, mitochondria-targeting CPP have been shown to induce apoptosis of tumour cells (1) and the intracellular delivery of a peptide that activates p53 has proven to be an effective

tumour suppressor of malignant cells *in vivo* (2). For reasons of clarification, and based upon a consideration of structural organization, we have chosen to delineate apoptogenic CPP into two separate groups:

1.1. Apoptogenic CPP of Synchronologic Organization

This quantitatively dominant type of construct utilizes a variety of different CPPs as biologically inert vectors. Their synchronologic organization is composed of a bioactive apoptogenic cargo (*message*) chemically conjugated in a tandem fashion to the CPP (*address*). The CPP is designed to act only as an inert delivery vector for the intracellular translocation of apoptogenic moieties, be they peptidyl modulators of signal transduction (3, 4) or pharmacotherapeutics (5, 6).

1.2. Apoptogenic CPP that Are Intrinsically Cell Penetrant

A component of our investigations into the utility of apoptogenic CPP has advanced following the development of a prediction algorithm which identifies cell-penetrant peptide sequences within key intracellular signalling proteins (7). Also termed proteomimetic CPP (8), these novel constructs are of *rhemylogic* organization, with discontinuously arranged pharmacophores within a single peptide chain. These CPP possess the dual function of modulating intracellular events whilst being intrinsically cell penetrant, thus circumventing the need of a sometimes difficult conjugation step between CPP and bioactive cargo. One such peptide is Cyt c^{77-101} (*H-GTKMIFVGIKKKEERADLIAYLKKA-NH₂*), a cryptic sequence identified within the apoptogenic protein cytochrome *c*. Cyt c^{77-101} and its N-terminally extended target-selective analogues display a strong propensity for both cellular penetration and apoptotic induction in U373MG astrocytoma cells (8).

A second component of our studies using apoptogenic CPP, which are intrinsically cell penetrant, has developed from synthetic analogues of the heterotrimeric G protein activating tetradecapeptide mastoparan (MP), isolated from wasp venom. Mitoparan ([Lys^{5,8}Aib¹⁰]MP; (1)), a highly potent MP analogue, specifically promotes apoptosis of human cancer cells as confirmed in our laboratory using common methodologies for the detection of apoptotic events such as, *in situ* TUNEL staining, activation of caspase-3 and translocation of phosphatidylserine to the outer cell membrane. Intriguingly, mitoparan penetrates plasma membranes and redistributes to co-localize with mitochondria. Further investigations demonstrated that through cooperation with a permeability transition pore protein VDAC (voltage-dependent anion channel), mitoparan induces mitochondrial swelling and permeabilization, leading to the subsequent release of cytochrome *c*.

Whilst CPP provide valuable tools for the therapeutic induction of apoptosis, higher concentrations of CPP, perhaps 5 μ M and above for a majority of those CPP studied to date, can induce membrane perturbations and subsequent necrotic events probably

resulting from an uncontrolled influx of Ca^{2+} . Thus, to harness the specific apoptogenic potential of CPP, in the absence of more generalized necrosis, it is essential to precisely determine the mechanisms of cell death induced by peptide exposure. Similar assays are also valuable to select CPP that can be used for other applications in the absence of detrimental changes in cellular viability.

Initial screening of apoptogenic CPP can be carried out by measuring cell viability and 3-(4,5-dimethylthazol-2-yl)-2,5-diphenyl tetrazolium bromide (MTT) assays are routinely used for this purpose (9). However, whilst the MTT assay provides a simple and cost-effective assessment of the ability of apoptogenic CPP to reduce cell viability, firm establishment of apoptosis, through assays such as TUNEL staining are also imperative. For a more rigorous assessment of apoptosis, whilst also discounting necrosis, dual Annexin V and propidium iodide (PI) staining are thoroughly recommended. There are of course numerous other methodologies for the measurement of apoptosis. Assessing the real-time activation of caspase-3, the final executioner in the caspase cascade, is a common methodology routinely used within our laboratory.

Most of the studies reported herein have utilized the U373MG cell line as representative of high grade human glioma, though the methods presented are certainly applicable to the study of other eukaryotic cell types.

2. Materials

2.1. Cell Culture and Peptide Preparation

1. Cell culture medium: Dulbecco's Modified Eagle's Medium with L-glutamine (0.1 mg/ml) (DMEM) (Sigma) supplemented with 10% (w/v) fetal bovine serum (FBS) (Sigma), penicillin (100 U/ml), and streptomycin (100 µg/ml).
2. Trypsin/EDTA: 0.5 g/l porcine trypsin and 0.2 g/l EDTA.4Na in Hanks Balanced Salt Solution (Sigma).
3. Hanks Balanced Salt Solution (HBSS) (Sigma).
4. Sterile T75 cm² vented flasks.
5. Laminar Flow Class II tissue culture fume hood (Clean Air).
6. CO₂ incubator (Jencons, Millennium).
7. Purified and lyophilized peptides.
8. dH₂O.
9. Sterile syringes.
10. Sterile filters.
11. Sterile Eppendorf tubes.

2.2. Measurement of Cell Viability

1. Sterile 96-well plates.
2. Cell culture medium pre-warmed to 37°C.
3. HBSS.
4. 3-(4,5-Dimethylthiazol-2-yl)-2,5-diphenyltetrazolium bromide (MTT) solution (0.5 mg/ml): Prepare a 5 mg/ml stock solution of MTT (Sigma) in pre-warmed DMEM. 0.02 g MTT in 4 ml of medium should be sufficient for two 96-well plates. This preparation may require sonification to fully dissolve the MTT. Dilute the MTT stock solution by 1:10 in DMEM (3 ml of the above stock solution in 30 ml medium is sufficient for two 96-well plates).
5. 96-Well plate reader.

2.3. Measurement of Apoptosis: Detection of DNA Fragmentation In Situ by TUNEL Assay

1. Sterile six-well plates.
2. Glass cover slips (18 × 18 mm).
3. Forceps.
4. Cell culture medium pre-warmed to 37°C.
5. Phosphate-buffered saline (PBS), pH 7.4 (500 ml).
6. Paraformaldehyde: 4% (wt/vol) solution in PBS (see Note 1).
7. Permeabilization solution: 0.1% (vol/vol) Triton X-100 in 0.1% (wt/vol) sodium citrate.
8. Nuclear DNA fragmentation, a feature of apoptosis can be measured by Tdt (terminal deoxynucleotidyl transferase)-mediated dUTP nick end labelling (TUNEL). Many convenient kits are available including the “In Situ Cell Death Detection kit” (TMR red, Roche, UK).
9. DNase 1, grade 1: 3,000 U/ml in 50 mM Tris-HCl, pH 7.5, 1 mg/ml BSA (Roche, UK).
10. Vectashield™ (Vector Laboratories Inc, Peterborough, UK) containing 4',6' Diamidino-8-phenylindole dihydrochloride (DAPI).
11. Glass slides (26 × 76 mm).
12. Clear nail varnish.

2.4. Measurement of Apoptosis and Necrosis: Quantitative Determination of Annexin V and Propidium Iodide Staining Using Flow Cytometry

1. HBSS without phenol red (Sigma).
2. Trypsin/EDTA without phenol red: 0.5 g/l porcine trypsin and 0.2 g/l EDTA.4Na in HBSS (Sigma).
3. 5-ml Polystyrene round bottom tubes, 12 × 75 mm (BD, Falcon).
4. Annexin-V-FLUOS staining kit (Roche, UK).
5. Flow cytometer (BD FACS Calibur).
6. BD Cell Quest Pro software.

2.5. Caspase-3 Activation

1. 35-mm Sterile glass base dishes (IWAKI).
2. DMEM without phenol red.
3. DEVD-NucView™ 488 Caspase-3 Substrate (Biotium Inc, Cambridge Bioscience, Cambridge, UK).
4. Caspase-3 inhibitor Ac-DEVD-CHO (Biotium Inc, Cambridge Bioscience, Cambridge, UK).
5. Confocal microscope with a live cell imaging chamber (Carl Zeiss LSM 510 Meta).

3. Methods

3.1. Cell Culture and Peptide Preparation

1. U373MG human astrocytoma cells (Pontén and Macintyre, 1968) are routinely maintained in cell culture medium, in a humidified atmosphere of 5% CO₂ at 37°C (CO₂ incubator) and routinely passaged when approaching confluence with trypsin/EDTA. To ensure sterility, cell culture should be carried out in a laminar Class II fume hood, whilst wearing gloves throughout.
2. U373MG cells are an adherent cell line thus all of the protocols below are tailored for adherent cultures.
3. Purified peptides are dissolved in dH₂O to a final concentration of 1 mM, filter sterilized and stored in sterile Eppendorfs at -20°C (see Note 2).

3.2. Measurement of Cell Viability

Cell viability can be measured by MTT conversion. MTT is reduced, by metabolically active cells only, to a coloured water-insoluble formazan salt. Following solubilization and colorimetric measurement, only viable cells are therefore detected. Many similar methods using the reduction of tetrazolium salts are also available.

To ensure sterility, the procedure below should be carried out in a Class II laminar flow hood using aseptic tissue culture techniques. From step 6 onwards, however, the procedure can be carried out on an open bench.

1. Cells are passaged as above (see Subheading 3.1) and grown to 75% confluence in 96-well plates (see Note 3) and washed in culture medium (200 µl/well) prior to assay.
2. Treat cells with 200 µl medium/well containing apoptogenic CPP or vehicle (medium alone) for the designated time periods at 37°C.
3. To six empty wells, add 200 µl of stimulation medium alone as to detect any background absorbance readings.
4. To terminate the reaction, aspirate off the stimulation medium.

5. Add the prepared MTT solution (0.5 mg/ml) at 200 μ l/well and incubate for 3 h at 37°C (see Note 4).
6. Aspirate medium taking care not to disturb the cell monolayer and insoluble coloured product.
7. Solubilize in warm DMSO at 200 μ l/well.
8. Incubate for a further 15 min at 37°C.
9. Gently agitate and read absorbance at 540 nm on a 96 well plate reader.
10. Cell viability is expressed as a percentage of cells treated with vehicle (medium) alone. An average value for the background readings is calculated and subtracted from all values prior to the determination of % cell viability. Results are expressed as mean \pm S.E.M.

3.3. Measurement of Apoptosis: Detection of DNA Fragmentation In Situ by TUNEL Assay

As previously mentioned, CPP, particularly at higher concentrations, tend to induce cell death by non-specific membrane perturbations, it is therefore of utmost importance to establish that apoptosis is indeed the mechanism of cell death. Nuclear DNA fragmentation is a well-established characteristic of apoptosis and can be easily detected by TUNEL assay (see Note 5). As in Subheading 3.2, sterility should be maintained whilst plating out cells and throughout the duration of their stimulation with apoptogenic CPP.

1. Cells are passaged as above (see Subheading 3.1) and grown to 75% confluence on cover-slips in six-well plates. When plating out cells onto cover-slips, it is imperative that the cover-slips are first sterilized by holding with forceps and spraying them with 95% ethanol. Allow the cover-slips to dry then gently transfer 1 coverslip/well to the chambers of a six-well plate.
2. Wash once in fresh cell culture medium and treat with peptides or vehicle alone (medium) in medium, for the designated time periods in a humidified atmosphere of 5% CO₂ at 37°C.
3. Wash cells with phosphate-buffered saline (PBS), pH 7.4 and fixed with 4% (wt/vol) paraformaldehyde in PBS 4% (wt/vol) for 1 h at room temperature.
4. Fixed cells are permeabilized with 0.1% (vol/vol) Triton X-100 in 0.1% (wt/vol) sodium citrate at 4°C for 2 min, then incubated for 1 h at 37°C in a humidified atmosphere in the dark with TUNEL reaction mixture containing terminal deoxynucleotidyl transferase (Tdt) and TMR red-dUTP to label free 3'OH ends in the DNA. Positive controls are achieved by incubating fixed and permeabilized cells with DNase 1, grade 1 for 10 min at room temperature to induced DNA strand breaks, prior to the labelling procedure.

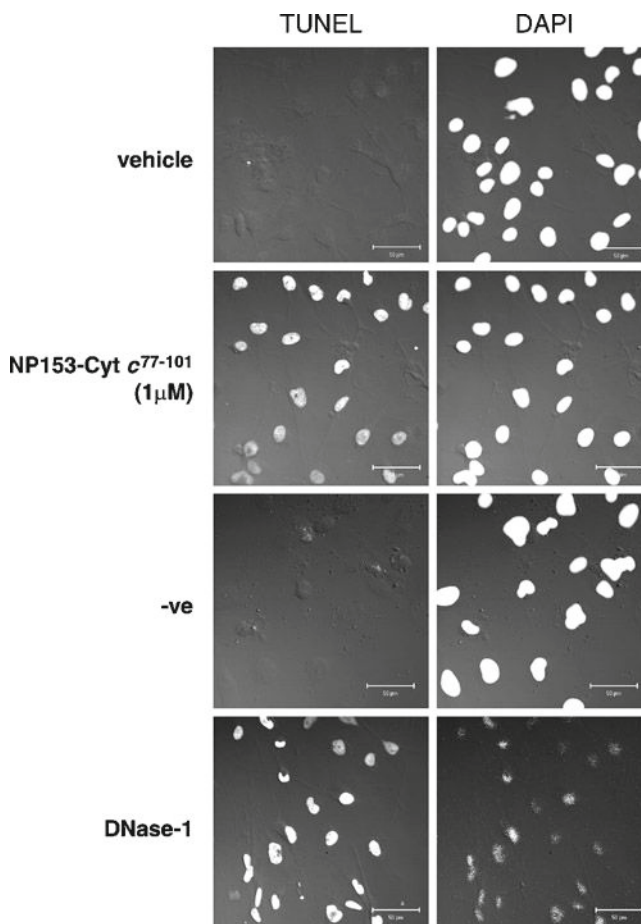


Fig. 1. An N-terminally extended target-selective analogue of the proteomimetic peptide Cyt c^{77-101} (NP153-Cyt c^{77-101}) induces apoptosis of U373MG astrocytoma as confirmed by nuclear DNA fragmentation. U373MG cells were treated with NP153-Cyt c^{77-101} or with vehicle alone for 18 h. Nuclear DNA fragmentation was detected by TUNEL in situ cell detection assay, TMR red (Roche) and cells were counterstained with DAPI to visualize nuclear DNA. The appearance of fluorescence located in the nuclei of NP153-Cyt c^{77-101} -treated cells provides evidence of apoptosis, whereas DNA fragmentation is not evident in cells treated with vehicle alone (medium). Fixed and permeabilized cells were incubated with Dnase-1 (3,000 U/ml) to induce DNA strand breaks, prior to the labelling procedure and therefore acts as a positive control (Dnase-1). DNA fragmentation is comparable to cells treated with NP153-Cyt c^{77-101} . As a negative control, fixed and permeabilized cells were treated with labelling solution without Tdt (-ve).

5. Negative controls are achieved by incubating fixed and permeabilized cells in TUNEL reaction mixture without Tdt.
6. Cover slips are washed in PBS, air-dried and mounted on slides with Vectashield™ containing DAPI to counter stain double-stranded DNA in the nuclei (see Notes 6 and 7).
7. Samples are analyzed using fluorescence or confocal microscopy (see Fig. 1.) or can be kept in the dark at 4°C until viewing.

3.4. Measurement of Apoptosis and Necrosis: Quantitative Determination of Annexin V and Propidium Iodide Staining Using Flow Cytometry

One must be aware of reports that suggest that TUNEL staining may give false positives (10, 11). It is therefore preferable to carry out an additional assay, or assays, for the detection of apoptosis. Dual Annexin V and PI staining not only acts as an additional detector assay for apoptotic events, but also provides a means of measuring the percentage of cells that are undergoing apoptosis and/or necrosis. Phosphatidylserine translocation to the outer plasma membrane is a feature of early apoptosis and can be measured by Annexin-V staining and flow cytometric analysis. Annexin V is a Ca^{2+} -dependent phospholipid-binding protein with high affinity for phosphatidyl serine. Since necrotic cells also expose phosphatidylserine owing to loss of membrane integrity, PI exclusion needs to be carried out to discriminate between apoptosis (Annexin V⁺/PI⁻) and necrosis (Annexin-V⁺/PI⁺). PI is membrane impermeable and is therefore excluded from viable cells with an intact plasma membrane.

1. Treat 10^6 cells with apoptogenic CPP or medium alone (untreated, $\times 2$).
2. Wash cells in HBSS, trypsinize and transfer to a 5-ml polystyrene round bottom tube.
3. Centrifuge samples at $200 \times g$ for 5 min.
4. Resuspend the cell pellet in 100 μl Annexin-V-FLUOS labelling solution containing Annexin-V-fluorescein and PI and incubate for 15 min at 15–25°C. NB. Retain one untreated and unstained sample for establishment of instrument settings on the flow cytometer.
5. Add 0.5 ml HEPES incubation buffer to each sample.
6. Unstained and untreated cells are used to establish instrument settings on the BD FACS Calibar.
7. Fluorescence of Annexin-V-fluorescein and PI is detected in FL-1 and FL-3 channels, respectively.
8. FL-1 and FL-3 cell populations are isolated to the first log decade.
9. Stained and untreated cells are used to establish quadrant settings for dot plot analysis.
10. Statistical analyses are performed using BD Cell Quest Pro software (see Figs. 2 and 3).

3.5. Caspase-3 Activation

Using the DEVD-NucView™ 488 Caspase-3 Substrate allows for the real-time detection of caspase-3 activity in living cells (see Note 8). Though confocal microscopy methods are beyond the scope of this chapter, it is nonetheless useful to the reader to be advised on some common guidelines for live cell imaging analysis. Some of these “tips” can also be applied to viewing the sub-cellular localization of fluorescently labelled CPP.

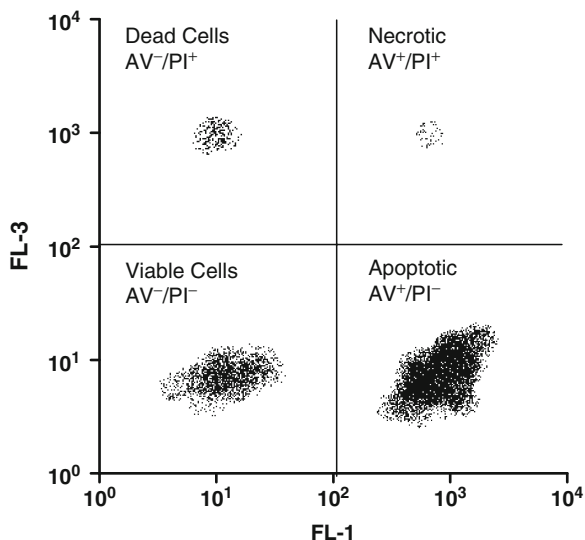


Fig. 2. A schematic representation of expected results for *dot plot* analysis of cells that have undergone dual staining with Annexin V (AV) and PI. *Dot plot* analysis will show cell populations undergoing early apoptotic events (AV⁺/PI⁻), viable cells (AV⁻/PI⁻), cells undergoing necrosis (AV⁺/PI⁺), and dead cells (AV⁻/PI⁺). Quadrant statistics can then be either tabulated or represented graphically.

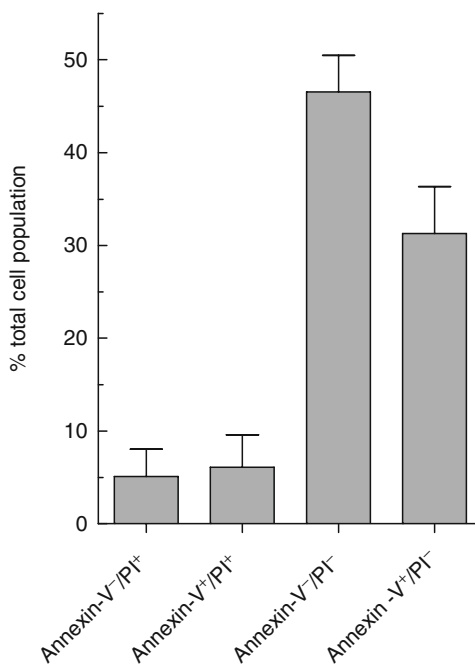


Fig. 3. Flow cytometric analysis of Annexin-V-fluorescein and propidium iodide (PI) staining of U373MG cells treated with the apoptogenic CPP mitP (10 μ M). Quadrant statistics from four separate experiments were combined, represented graphically and show predominant cell populations undergoing early apoptosis and viable cells compared to necrotic and dead cells. Data for this figure were taken from Jones et al. (1).

1. U373MG cells are passaged as above (see Subheading 3.1) and grown to 75% confluence in 35 mm sterile glass base dishes (see Note 9).
2. Treat cells with peptides or vehicle (medium) alone for the designated time periods in a humidified atmosphere of 5% CO₂ at 37°C.
3. Peptides should be dissolved in DMEM without phenol red. Depending on the potency of your apoptogenic CPP, an optimum concentration and duration of treatment must be first established (see Note 10).
4. 1 h, prior to the viewing of cells under the confocal microscope, commence heating of the live cell imaging chamber to 37°C.
5. Add DEVD-NucView™ 488 Caspase-3 substrate at a final concentration of 5 μM for a further 30 min. As an additional control, treated cells can be incubated with the caspase-3 inhibitor Ac-DEVD-CHO (25 μM), 30 min prior to substrate addition.
6. Nuclear staining and fluorescence are observed using a Carl Zeiss LSM 510 Meta confocal microscope equipped with a live cell imaging chamber supplemented with CO₂.
7. When capturing images it is advisable to take both the fluorescent image and a differential interference contrast (DIC) image. Superimposing the former onto the latter will assist in ascertaining the intracellular distribution of the fluorescent moiety (see Fig. 4).

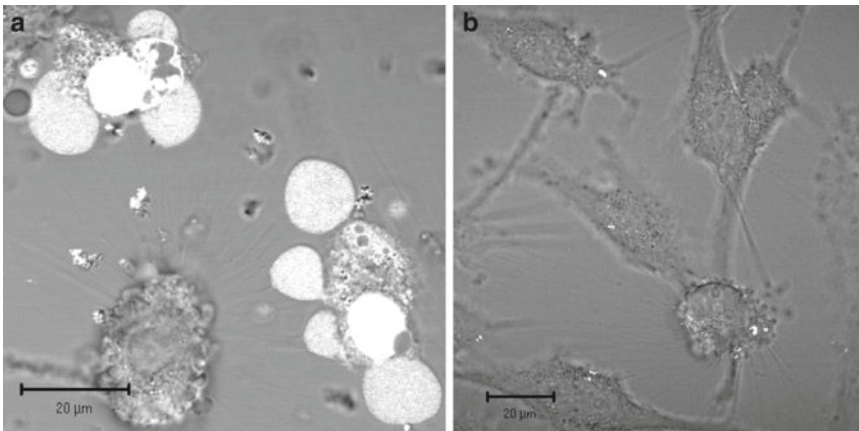


Fig. 4. NP153-Cyt c^{77-101} induces apoptosis of U373MG astrocytoma as confirmed by activation of caspase-3. U373MG cells were treated with NP153-Cyt c^{77-101} (3 μM) for 4 h. The cell-permeable construct DEVD-NucView™ 488 Caspase-3 Substrate consists of a functional high-affinity DNA-binding dye that is rendered inert by the highly negatively charged DEVD peptide substrate. Upon activation of caspase-3, the substrate is cleaved to release a functional DNA dye that subsequently migrates to the nucleus. Fluorescence seen in the nuclei of NP153-Cyt c^{77-101} -treated cells (a) indicates activation of caspase-3, compared to cells treated with vehicle alone (medium) (b). Fluorescent images have been superimposed onto DIC images taken immediately after the acquisition of the fluorescent observations.

4. Notes

1. 4% paraformaldehyde. When making up 4% (wt/v) paraformaldehyde, it is essential to carry out the procedure in a fume cupboard whilst wearing gloves. Inhalation of the dust can cause irritation to the respiratory tract, whilst eye contact can result in corneal damage and blindness. So, in the fume cupboard, weigh out the paraformaldehyde and make up to 4% in PBS. Whilst still in the hood, transfer to a combined stirrer and hotblock. Paraformaldehyde will not go into solution easily, so using a magnetic stirrer and increasing the temperature is advisable. A fail-safe approach, however, is to raise the pH; one sodium hydroxide pellet in approximately 200 ml of solution is sufficient. To air on the side of caution, in our laboratory we carry out the procedure in the fume hood until the coverslips are transferred to the slides and the samples have undergone many washes with PBS.
2. Repeating freeze–thawing of peptides should be avoided at all costs. So, it is essential that following solubilization in dH_2O , peptides are aliquotted into Eppendorfs and stored at -20°C . Filter sterilization of the peptide is also recommended since peptides can be incubated with cell cultures for 18 h or longer. The latter procedure makes for convenient preparation whilst assaying your peptide.
3. It is strongly advised to plate cells out into 96-well plates the day before the assay and not to “grow up” cells in 96-well plates over a period of days. Cell growth rates will depend upon the cell type being used. Culturing U373MG cells, for example, will require one sub-confluent T75 cm^2 flask of cells to be trypsinized and equally dispersed in 45 ml cell culture medium. This should be more than sufficient for plating cells out into two 96-well plates (200 μl /well), so that 75% confluence is achieved the following day. Do not use outer wells of the 96-well plates, but fill them with 200 μl /well sterile HBSS.
4. After 3 h, a purple monolayer should be evident on the bottom of the wells containing viable cells. Incubating the MTT solution for longer than 4 h can lead to “clumping” and “loose” formazan salts, which carry the risk of being removed alongside the removal of the culture medium, thus greatly affecting your results.
5. A typical feature of apoptosis is DNA fragmentation. TUNEL staining allows for the detection of these breaks by using the enzyme Tdt to catalyse the polymerization of fluorescently labelled nucleotides (e.g. TMR red-dUTP) with the exposed 3'OH ends in the DNA. It is noteworthy that random digestion of DNA also occurs during necrosis. Since the Tdt reaction

preferentially labels internucleosomal DNA degradation, characteristic of apoptosis as opposed to random DNA digestion, typical of late necrosis (12), TUNEL staining is used as a more specific indicator of apoptosis.

6. Though this may appear as an apparently simple step, it is very easy at this stage to lose track of which coverslips are which and upon which side of the coverslips the stained cells are. Thus, after washing with PBS it is best to place the tops or bottoms of small petri-dishes (which have been labelled with each treatment condition) onto some paper towelling. With forceps, gently remove each coverslip from each well and with the stained side facing away from the petridish, stand the coverslip up against its respective dish. The paper towelling will help to absorb the excess moisture. Once the coverslips have dried, place a glass microscope slide on the bench and dispense a small droplet of Vectashield™ containing DAPI onto the centre of the slide. Gently place your coverslip (cells and stained side down) onto the Vectashield mounting medium, the mounting medium will disperse and the sides of the coverslips can be sealed with clear nail varnish and allowed to dry in the dark. Carefully placing foil over the slides should suffice.
7. It may be difficult to remove the coverslips from the wells of the six-well plates. It is recommended that, before removing the coverslips with forceps, 2 ml PBS is added to each well to prevent the coverslips adhering to the bottom of the well.
8. Although samples may be fixed using this method, for the aim of long-term storage, data from our laboratory would indicate that non-specific background staining is enhanced following fixation.
9. As in Note 3 it is strongly recommended not to grow up cells over a long period in 35-mm sterile glass-based dishes. Always plate out the day before. Half of a sub-confluent T75 cm² flask of cells should be sufficient for plating cells into four 35-mm glass-based dishes at 4 ml cell suspension per dish.
10. Depending on the potency of your apoptogenic CPP, an optimum concentration and duration of treatment must be first established. Time courses and dose-dependent observations are therefore advisable to establish the concentration needed to assess the biological effect (caspase-3 activation) without severely reducing cell viability.

Acknowledgments

Our studies with brain tumour cells have been supported by the Samantha Dickson Brain Tumour Trust.

References

1. Jones, S., Martel, C., Belzacq-Casagrande, A.S., Brenner, C., and Howl, J. (2008) Mitoparan and target-selective chimeric analogues: membrane translocation and intracellular redistribution induces mitochondrial apoptosis. *Biochim. Biophys. Acta* **1783**, 849–863.
2. Snyder, E.L., Meade, B.R., Saenz, C.C., and Dowdy, S.F. (2004) Treatment of terminal peritoneal carcinomatosis by a transducible p53-activating peptide. *PLoS Biol.* **2**, 186–193.
3. Yang, L., Mashima, T., Sato, S., Mochizuki, M., Yamori, T., Oh-Hara, T., and Tsuruo, T. (2003) Predominant suppression of apoptosis by inhibitor of apoptosis protein in non-small cell lung cancer H460 cells: therapeutic effect of a novel polyarginine-conjugated Smac peptide. *Cancer Res.* **63**, 831–837.
4. Muthumani, K., Lambert, V.M., Shanmugam, M., Thieu, K.P., Choo, A.Y., Chung, J.C., Satishchandran, A., Kim, J.J., Weiner, D.B., and Ugen, K.E. (2009) Anti-tumour activity mediated by protein and peptide transduction of HIV viral protein R (Vpr). *Cancer Biol. Ther.* **8**, 180–187.
5. Lindgren, M., Rosenthal-aizman, K., Saar, K., Eiriksdottir, E., Jiang, Y., Sassian, M., Ostlund, P., Hallbrink, M., and Langel, U. (2006) Overcoming methotrexate resistance in breast cancer tumour cells by the use of a new cell penetrating peptide. *Biochem. Pharmacol.* **71**, 416–425.
6. Myrberg, H., Zhang, L., Mäe, M., and Langel, U. (2008) Design of a tumour-homing cell-penetrating peptide. *Bioconjug. Chem.* **19**, 70–75.
7. Hallbrink, M., Kilk, K., Elmquist, A., Lundberg, P., Lindgren, M., Jiang, Y., Pooga, M., Soomets, U., and Langel, U. (2005) Prediction of cell-penetrating peptides. *Int. J. Pept. Res. Ther.* **11**, 249–259.
8. Howl, J., and Jones, S. (2008) Proteomimetic cell penetrating peptides. *Int. J. Pept. Res. Ther.* **14**, 359–366.
9. Carmichael, J., DeGraff, W.G., Gazdar, A.F., Minna, J.D., and Mitchell, J.B. (1987) Evaluation of a tetrazolium-based semiautomated colorimetric assay: assessment of chemosensitivity testing. *Cancer Res.* **47**, 936–942.
10. Stahelin, B.J., Marti, U., Solioz, M., Zimmerman, H., and Keichen, J. (1998) False-positive staining in the TUNEL assay to detect apoptosis in liver and intestine is caused by endogenous nucleases and inhibited by pyrocarbonate. *Mol. Pathol.* **51**, 204–208.
11. Pulkkanen, K.J., Laukkanen, M.O., Naarala, J., and Yla-Herttuala, S. (2000) False positive apoptosis signal in mouse kidney and liver detected in TUNEL assay. *Apoptosis* **5**, 329–333.
12. Gold, R., Schmied, M., Giegerich, G., Breitschopf, H., Hartung, H.P., Toyka, K.V., and Lassmann, H. (1994) Differentiation between cellular apoptosis and necrosis by the combined use of in situ tailing and nick translation techniques. *Lab. Invest.* **71**, 219–25.

Part IV

Applications of CPPs in Gene Modulation

Splice Redirection as a Convenient Assay to Monitor CPP–ON Efficiency and Mechanism

Rachida Abes, Andrey A. Arzumanov, Amer F. Saleh, Fatouma Said Hassane, Michael J. Gait, and Bernard Lebleu

Abstract

Several strategies based on synthetic oligonucleotides (ON) have been proposed to control gene expression. As for most biomolecules, however, delivery has remained a major roadblock for in vivo applications. Conjugation of steric-block neutral DNA mimics, such as peptide nucleic acids (PNA) or phosphorodiamidate morpholino oligonucleotides (PMO), to cell-penetrating peptides (CPP) has recently been proposed as a new delivery strategy. It is particularly suitable for sequence-specific interference with pre-mRNA splicing, thus offering various applications in fundamental research and in therapeutics. The chemical synthesis of these CPP–ON conjugates will be described as well as easy-to-implement assays to monitor cellular uptake, endosome leakage, and efficiency of splicing redirection.

Key words: Cell-penetrating peptides, Oligonucleotides, Splicing regulation, Delivery, Liposome leakage

1. Introduction

Alternative splicing allows the production of several mRNAs from a single pre-mRNA gene transcript. The majority of genes in higher eukaryotes are alternatively spliced, which contributes largely to transcriptome and proteome complexity. Of importance in medicine, a large proportion of human genetic diseases are caused by mutations affecting splicing. For example, intronic mutations in human β -globin thalassemic genes activate cryptic splice sites and result in the production of truncated non-functional proteins.

This has prompted oligonucleotide (ON)-based strategies aimed at redirecting the splicing machinery towards the correct use of splicing signals. In the case of β -thalassemia, for example,

masking the mutated intronic site by an ON (often named splice-switching ON or SSO) has been proposed by Kole and his colleagues to down-regulate the use of the cryptic splice site and to promote the production of functional β -globin mRNA and protein.

Regulation of alternative splicing by SSOs has many potential applications relating to several human diseases (1). For example, in a potential cancer application, alternative splicing of the Bcl-x pre-mRNA leads to the production of both pro- and anti-apoptotic forms. The latter is over-expressed in cancer cells and contributes to chemotherapy resistance.

ON-induced exon skipping represents a strategy to redirect the splicing machinery with potential clinical benefits. This is best exemplified in the case of Duchenne muscular dystrophy (DMD), which is a high-incidence human genetic disease (1 in 3,500 in young boys) caused by exonic mutations leading to out-of-frame translation of dystrophin mRNA. ON hybridization to acceptor or donor splice sites allows the exclusion of mutated exons (exon skipping) and the production of a shorter but in-frame and importantly functional dystrophin mRNA. Encouraging data obtained by several groups in the murine *mdx* model of DMD have fostered the launch of human clinical trials with SSOs in several countries (2). Redirection of the splicing machinery requires the nuclear delivery of steric-block ON analogues. Peptide nucleic acids (PNA) and phosphorodiamidate morpholino oligomers (PMO) are particularly well suited, since they hybridize to complementary RNA with high affinity, they have an elevated metabolic stability and, importantly for steric-blocking applications, they do not promote the destruction of their RNA target. RNase H-competent ON analogues and siRNAs thus cannot be used in these applications. Unfortunately, neutral ONs cannot be transfected with commonly used delivery vectors (for example, cationic lipids) that rely on electrostatic interactions. However, cell-penetrating peptides (CPP) can be chemically conjugated easily to PNA and PMO (as described in this chapter) and have appeared as a particularly well-adapted delivery strategy for PNA and PMO.

The splicing redirection assay proposed by Kole (3) (Fig. 1) has been adopted by many groups in the field to assay steric-block ONs and their delivery vectors. It is advantageous in being easy to implement, in providing a positive read-out over a low background, and in being sequence-specific. It will be described in detail in this chapter. Nevertheless, CPP delivery of ONs is still limited by escape from endocytotic vesicles. We found that saponin permeabilization of the plasma membrane is a rather convenient assay to assess splicing redirection achieved that overrides endocytosis and its limitations. Finally, we will describe liposome leakage as an assay to evaluate the membrane destabilizing potential of CPP delivery vectors.

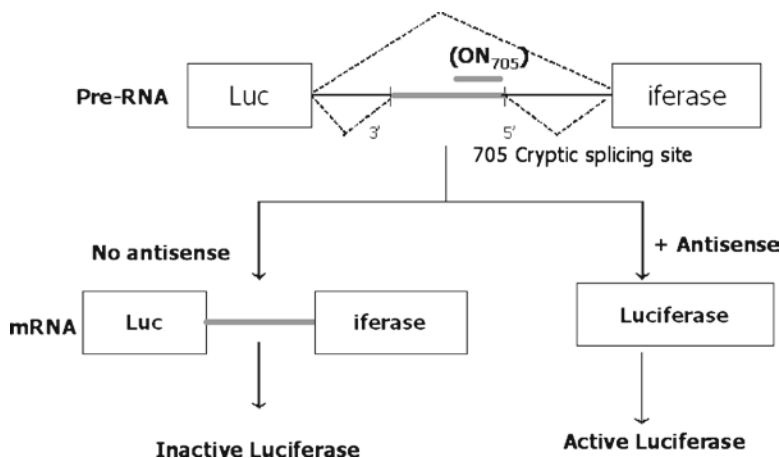


Fig. 1. Splicing redirection assay. HeLa pLuc705 cells contain a stably integrated luciferase reporter gene that is interrupted by the human β -thalassemia intron 2 (IVS2-705) containing a cryptic splice site. Aberrant splicing leads to the production of a non-functional luciferase protein. The hybridization of an oligonucleotide (ON 705) to the cryptic splice site restores luciferase expression, which can be monitored by luminescence and PCR assays.

2. Materials

2.1. Cell Culture

1. DMEM (Gibco) supplemented with 10% foetal bovine serum (BioWest), 5 ml MEM Non-Essential Amino Acids (100 \times) (Gibco), 5 ml sodium pyruvate MEM (100 mM, Gibco) and 5 ml Penicillin–Streptomycin–Neomycin (PSN) antibiotic mixture (Gibco) for HeLa pLuc705 cell culture.
2. MycoAlert[®] mycoplasma Detection Kit (LONZA) for mycoplasma Detection.
3. Opti-MEM[®] I Reduced Serum Medium (1 \times) with l-Glutamine (Gibco) for serum-free experiments.
4. Trypsin–Ethylenediamine-tetraacetic acid 0.05% Trypsin with 0.35 mM EDTA 4Na 1 \times (Gibco) for cell detachment.
5. Dulbecco's phosphate-buffered saline (D-PBS) (1 \times) (Gibco) for cell washing.
6. Forma Direct Heat CO₂ Incubator HEPA Class 100 (Thermo Electron Corporation) for cell cultures.
7. Laboratory laminar airflow cabinet BH-EN 2004-S. Type II, Catégorie 2 (Microbiological Safety Cabinets) for cell manipulations in sterile conditions.
8. Allegra[™] 25R low-speed Beckmann centrifuge or Eppendorf Centrifuge 5417R for cell recovery.
9. Axiovert 40 C (transmitted light) (Carl Zeiss, Oberkochen, Germany) and Thoma cell for cell integrity routine checking and counting.

2.2. Synthesis of PNA–Peptide and PMO–Peptide Conjugates

1. Conjugation reagents for PNA–peptide conjugates: Purchase PNA with either N-terminal (NPys)Cys or N-terminal bromoacetyl (Panagene, Korea) or synthesize PNA as previously described (4). Peptides with C-terminal Cys can be purchased from many suppliers (e.g. ABL Ltd, Oldham, UK) or synthesized as previously described (4). Other reagents are formamide (>99.5%, Fluka), BisTris.HBr buffer (pH 7.5), ammonium acetate (NH₄Ac). For reversed-phase HPLC, use a C-18 Jupiter reversed-phase (250 × 10 mm, 10 μm pore size) column (semi-preparative, Phenomenex). 2.0 M triethylammonium acetate, pH 7 (TEAA, Glen Research), hydrochloric acid solution (HCl, AnalaR-grade, BDH Chemicals), trifluoroacetic acid (TFA, >99.9%, Romil), acetonitrile (Fisher Scientific, HPLC grade) and water (HPLC grade) are used as solvents.
2. Conjugation reagents for PMO–peptide conjugates: Purchase PMO with 5'-amino linker (Gene Tools LLC). Other reagents are *N*-[γ-maleimidobutyryloxy]succinimide ester (GMBS, Thermo Scientific), acetone (>99%, Fisher Scientific, Laboratory reagent grade) and dimethyl sulfoxide (DMSO, >99.9%, Aldrich). For reversed-phase HPLC, use a C-18 Jupiter reversed-phase (250 × 10 mm, 10 μm pore size) column (semi-preparative, Phenomenex). Hydrochloric acid solution (HCl, AnalaR-grade, BHD Chemicals), heptafluorobutyric acid (HFBA, >99.5%, Fluka), acetonitrile (Fisher Scientific, HPLC grade) and water (HPLC grade) are used as solvents.

2.3. FACS Analysis of CPP–ON Cellular Uptake

1. FACSCanto™ flow cytometer (BD Biosciences, San Jose, CA) using Facs Diva® software for PNA and PMO–peptide conjugates uptake.
2. Propidium Iodide (Molecular Probes, Eugene, OR) used at final concentration of 0.05 μg/ml for cell permeability quantification.

2.4. Luciferase Assay of Splicing Redirection

1. BCA™ Protein Assay Kit (Pierce, Rockford, IL) and ELISA plate reader (Dynatech MR 5000, Dynatech Labs, Chantilly, VA) for the quantification of cellular protein concentrations.
2. Berthold Centro LB 960 luminometer (Berthold Technologies, Bad Wildbad, Germany) and Luciferase Assay System with Reporter Lysis Buffer (Promega) for luciferase activity quantification.

2.5. RT-PCR Evaluation of Splicing Redirection

1. Forward 5' TTG ATATGT GGA TTTCGA GTC GTC 3' and reverse 5' TGT CAA TCA GAG TGC TTT TGG CG 3' luciferase primers from Eurogentec, Belgium.
2. TRI REAGENT™ (Sigma Aldrich), chloroform, isopropanol, and ethanol (Carlo Erba reagents) for RNA extraction.
3. Concentrator 5301 from Eppendorf for RNA pellets drying.

4. SuperScript III one-step RT-PCR system with Platinum® Taq polymerase (Invitrogen) and MJ Research PTC200 Peltier Thermal cycler for amplification.
5. Eppendorf BioPhotometer for amplification products quantification.
6. Agarose and ethidium bromide Powder (Sigma Aldrich) for gel electrophoresis using Amilabo electrophoresis Power supply.
7. Lumi imager F1 Roche for image acquisition or a Genius Bio Imaging system (Syngene) with Gene Tools software.
8. *DpnI*, *AvaI*, and *XbaI* restriction enzymes (Promega) for pLuc 705 plasmid DNA digestion.

2.6. Splicing Redirection in Saponin-Permeabilized Cells

1. Saponin (Fluka BioChemika) to permeabilize cells and bypass endocytosis.
2. BCA™ Protein Assay Kit (Pierce, Rockford, IL) and ELISA plate reader (Dynatech MR 5000, Dynatech Labs, Chantilly, VA) for the quantification of cellular protein concentrations.
3. Berthold Centro LB 960 luminometer (Berthold Technologies, Bad Wildbad, Germany) and Luciferase Assay System with Reporter Lysis Buffer (Promega) for Luciferase activity quantification.

2.7. Liposome Leakage Assay

1. Phospholipids DOPC, DOPE, PI, LBPA from Avanti Polar Lipids (USA)
 - DOPC = 1,2-dioleoyl-*sn*-glycerol-3-phosphocholine.
 - DOPE = 1,2-dioleoyl-*sn*-glycero-3-phosphoethanolamine.
 - PI = L- α -phosphatidylinositol sodium salt (from soy).
 - LBPA = BMP (*S,R*) = bis(monooleoylglycero)phosphate (ammonium salt).
2. MES and HEPES buffer (Sigma Aldrich).
3. NaCl (Carlo Erba).
4. ANTS (8-aminonaphthalene-1,3,6-trisulfonic acid, disodium salt) and DPX (p-xylene-bis-pyridinium bromide) as fluorescent dye and quencher (Invitrogen).
5. Mini-extruder for liposome preparation (Avanti Polar Lipids).
6. Chromatography column (1 × 10 cm) (Sigma Aldrich) for liposome purification.
7. Labassay phospholipid kit for DOPC quantification (Wako, GmbH).
8. Microplate plate reader (Dynatech MR 5000).
9. Luminescence Spectrometer LS 35 (Perkin Elmer, USA).

3. Methods

3.1. Cell Culture and Cell Dissociation

1. Culture HeLa pLuc 705 cells as exponentially growing sub-confluent monolayers in DMEM medium supplemented with 10% foetal bovine serum, sodium pyruvate, non-essential amino acids and antibiotics (see Note 1).
2. Wash cells twice with PBS and passage with Trypsin/EDTA every other day on 175 cm² flasks for routine maintenance for a maximum of ten passages. For experiments, plate cells overnight on 24-well plates (1.75×10^5 cells/well).
3. Test cells for the absence of mycoplasma contamination every month as described in the Lonza kit on 100 μ l cell culture supernatant.

3.2. Synthesis of CPP-PNA and CPP-PMO Conjugates

3.2.1. Synthesis of Disulfide-Linked CPP-PNA Conjugates (Fig. 2)

1. Place 250 μ l of formamide in a microfuge tube.
2. Add 10 μ l of a 10 mM aqueous solution of activated oligonucleotide ((NPys)-Cys-PNA) and 25 μ l of a 10 mM aqueous solution of C-terminal Cys-containing peptide.
3. Add 50 μ l of 1cM NH₄Ac solution stir with a Vortex, centrifuge briefly, and allow to stand for 30–60 min at room temperature.
4. Purify the conjugate using C18 reversed-phase HPLC in two injections with the following conditions:
Buffer A: 0.1% TFA
Buffer B: 90% acetonitrile, 10% buffer A
Gradient: 15–35% buffer B in 25 min
Flow rate: 3.5 ml/min
Detection: 260 nm
5. Collect the purified product and lyophilize.
6. Dissolve the conjugate in sterile water, analyse by HPLC and MALDI-TOF-mass spectrometry.
7. Quantify by measuring the UV absorbance at 260 nm in 0.1 M TEAA (pH 7).

3.2.2. Synthesis of Thioether-Linked CPP-PNA Conjugates (Fig. 2)

1. Place 10 μ l of a 10 mM aqueous solution of bromoacetyl PNA in a microfuge tube.
2. Add 100 μ l of formamide and 50 μ l of 1 M BisTris.HBr buffer (pH 7.5).
3. Add 25 μ l of a 10 mM aqueous solution of C-terminal Cys-containing peptide.
4. Heat the solution at 45°C for 2 h.

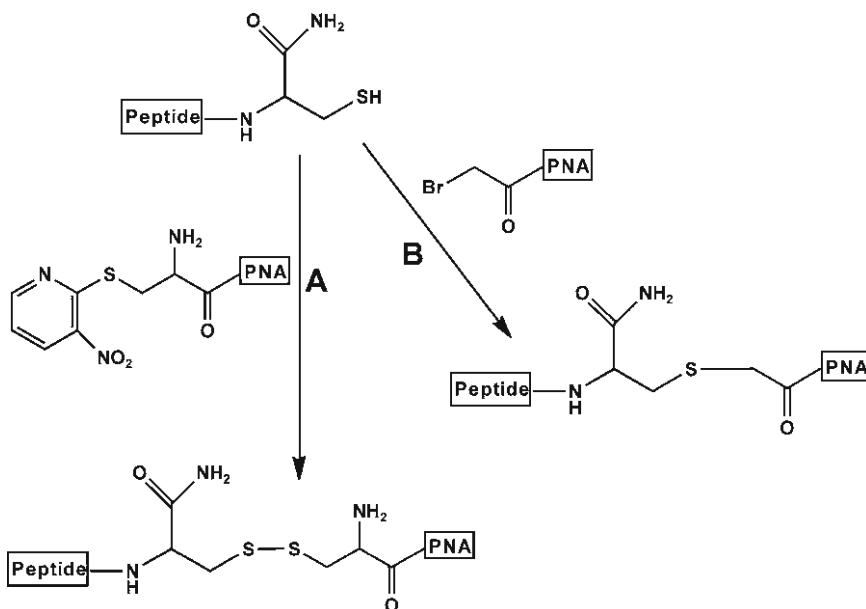


Fig. 2. Peptide conjugation to PNA by (A) disulfide linkage, (B) thioether linkage.

5. Purify the conjugate by reversed-phase HPLC in two injections with the following conditions:
 - Buffer A: 5 mM HCl
 - Buffer B: 90% acetonitrile, 10% water, 5 mM HCl
 - Gradient: 5–20% buffer B in 25 min
 - Flow rate: 3.5 ml/min
 - Detection: 260 nm
6. Collect the purified product and lyophilize.
7. Dissolve the product in sterile water, and use a speed vacuum (at medium drying rate) until 20 μ l solution remains in the tube.
8. Add 600 μ l of sterile water, and evaporate again as in step 7. Repeat this step again but to complete dryness this time.
9. Re-dissolve the conjugate in sterile water.
10. Analyse by HPLC and MALDI-TOF mass spectrometry and quantify by measuring the UV absorbance at 260 nm in 0.1 M TEAA (pH 7) (see Note 2).

3.2.3. Synthesis of Thioether (Maleimide)-Linked PMO–Peptide Conjugates (Fig. 3)

1. Prepare a 10 mM stock solution of PMO by dissolving 1,000 nmol of PMO in a 100 μ l of 50 mM sodium phosphate buffer (pH 7.2) containing 20% acetonitrile.
2. Place 10 μ l of a 10 mM PMO stock solution (see step 1) in a microfuge tube.

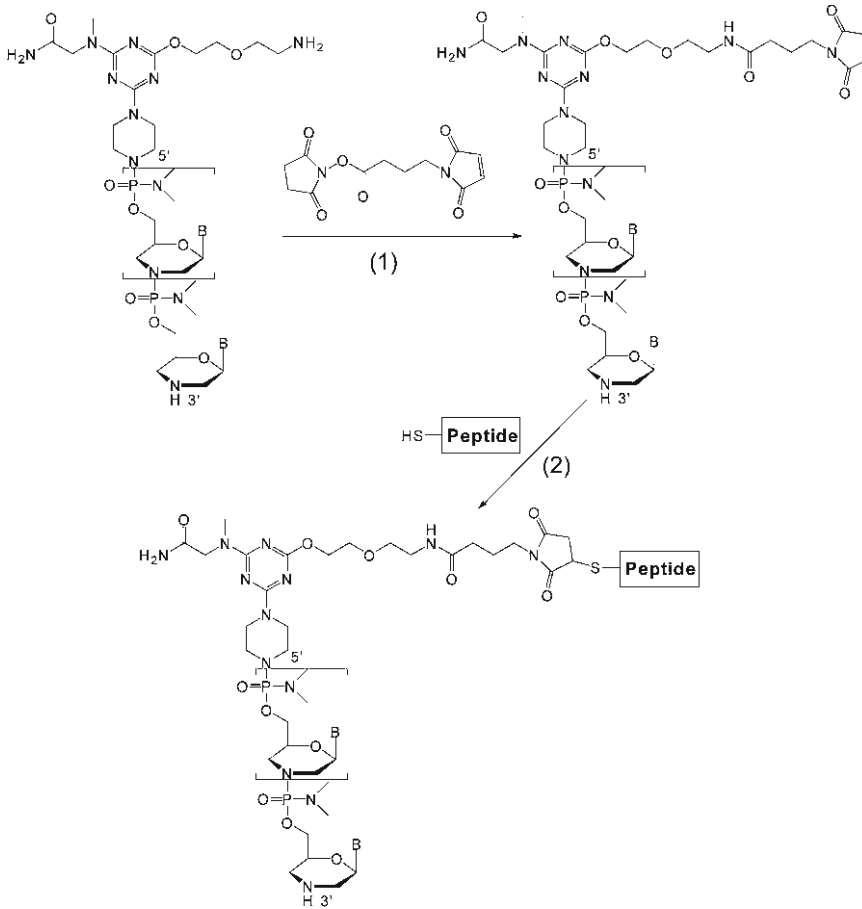


Fig. 3. Peptide conjugation to PMO via GMBS cross-linker.

3. Add 13 μ l of 50 mM sodium phosphate buffer (pH 7.2) containing 20% acetonitrile.
4. Add 2 μ l of a 100 mM GMBS solution in DMSO, vortex, and allow to stand for 1 h at room temperature in the dark.
5. Add 750 μ l of cold acetone, vortex, and centrifuge for 2 min at 15,000*g* at room temperature.
6. Decant off the acetone and allow the precipitate to dry for 30 min.
7. Dissolve the precipitate in 30 μ l of 50 mM sodium phosphate buffer (pH 6.5) containing 20% acetonitrile.
8. Add 20 μ l of a 10 mM aqueous solution of C-terminal Cys-containing peptide, stir with a Vortex and allow to stand at room temperature for 2 h in the dark.

9. Purify the conjugate using C-18 reversed-phase HPLC in one injection with the following conditions:
 Buffer A: 0.1% HFBA
 Buffer B: 90% acetonitrile, 10% buffer A
 Gradient: 38–50% buffer B in 20 min
 Flow rate: 3.5 ml/min
 Detection: 260 nm wavelength
10. Collect the purified product and lyophilize.
11. Analyse by HPLC and MALDI-TOS mass spectrometry and quantify by measuring the UV absorbance at 265 nm in 0.1 M HCl.

3.3. FACS Analysis of ON-Peptide Conjugates Cellular Uptake and Cell Permeability Assay

1. Wash exponentially growing HeLa pLuc705 cells with PBS to remove cell culture medium, treat with trypsin/EDTA for 5 min, centrifuge at $900 \times g$ at 4°C for 5 min, wash twice with PBS, centrifuge again, resuspend in DMEM, plate on 24-well plates (1.75×10^5 cells/well) and culture overnight.
2. Discard the culture medium and wash cells twice with PBS.
3. Discard PBS and incubate cells with fluorescently labelled conjugates diluted in Opti-MEM or DMEM (see Notes 3 and 4).
4. After incubation for the appropriate period, wash the cells twice with PBS and treat with trypsin/EDTA for 5 min at 37°C.
5. Resuspend cells in PBS 5% FCS, centrifuge at $900 \times g$ (5 min, 4°C) and resuspend in PBS 0.5% FCS containing 0.05 µg/ml propidium iodide (PI).
6. Analyse fluorescence with a FACS fluorescence activated sorter for cellular uptake and PI permeabilization using FACS Diva software. Exclude PI-stained cells from further analysis by appropriate gating. Analyse a minimum of 20,000 events per sample.

3.4. Luciferase Assay of Splicing Redirection

1. Detach exponentially growing HeLa pLuc705 cells with trypsin/EDTA, plate on 24-well plates (1.75×10^5 cells/well) and culture overnight.
2. Wash twice with PBS and incubate with the splice correcting conjugates (or its scrambled version) at the appropriate concentrations usually between 0.5 and 4 h in Opti-MEM medium (see Notes 3, 4 and 6).
3. Wash cells and continue incubation for 20 h in complete DMEM medium containing 10% FCS.
4. Wash cells twice with PBS and lyse with Reporter Lysis Buffer.

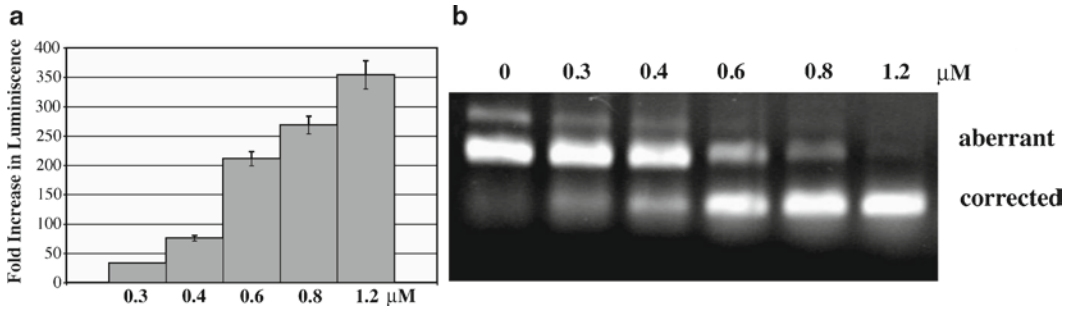


Fig. 4. Assay of splicing redirection. **(a)** Luciferase assay and **(b)** RT-PCR evaluation from which EC_{50} can be determined. Concentrations of conjugates are as shown.

5. Quantify luciferase activity in a luminometer using the Luciferase Assay System substrate. Perform all experiments in triplicate.
6. Measure cellular protein concentrations with the BCA™ Protein Assay Kit and read using an ELISA plate reader at 550 nm. Perform all experiments in triplicate.
7. Express luciferase activities as relative luminescence units (RLU) per μg protein. Average each data point over the three replicates (see Fig. 4, for an assay example).
8. The remainder of the lysate (usually 270 μl) may be used for RT-PCR analysis (Subheading 3.6).

3.5. Luciferase Assay of Splicing Redirection in Saponin-Permeabilized Cells

1. Detach exponentially growing HeLa pLuc705 cells with trypsin/EDTA, plate on 24-well plates (1.75×10^5 cells/well) and culture overnight.
2. Wash twice with PBS and co-incubate the cells with 20 μg/ml saponin and with the splice redirecting conjugates or its scrambled version at the appropriate concentrations for 0.5 h in Opti-MEM medium (see Note 5).
3. Wash cells and continue incubation for 23 h in complete DMEM medium containing 10% FCS.
4. Wash cells twice with PBS and lyse with Reporter Lysis Buffer.
5. Quantify luciferase activity in a luminometer using the Luciferase Assay System substrate. Perform all experiments in triplicate.

3.6. RT-PCR Evaluation of Splicing Redirection

1. Extract total RNA using 1 ml of TRI REAGENT™/well after measurement of luciferase. Add 300 μl of chloroform, mix vigorously and incubate 10 min at room temperature.
2. Centrifuge at $12,000 \times g$ for 15 min at 4°C and add an equal volume of isopropanol to the aqueous phase. Mix well and incubate for 10 min at room temperature.

3. Centrifuge at $12,000 \times g$ for 15 min at 4°C and resuspend the pellet in 1 ml of cold (-20°C) 75% ethanol. Mix and centrifuge at $12,000 \times g$ for 5 min at 4°C . Discard the supernatant. Evaporate off the ethanol using an Eppendorf Concentrator 5301 for 1 min at 60°C .
4. Add 20 μl of Nuclease-Free Water.
5. Quantify total RNA using Eppendorf BioPhotometer and control quality by 1% agarose gel electrophoresis on Amilabo electrophoresis Power supply st 1006T.
6. Amplify 1 μg total RNA using SuperScript III one-step RT-PCR system with Platinum® Taq polymerase in the presence of Luciferase specific primers with MJ Research PTC200 Peltier Thermal cycler.
7. Analyse PCR products by electrophoresis using 2% agarose gel. Use digestion products of the plasmid pLuc705 by *DpnI*, *XbaI*, and *AvaI* restriction enzymes as molecular weight markers (see Fig. 4, for an assay example)
8. For EC_{50} measurement, where experiments are carried out over a range of concentrations, analyse the gel using the imaging software to determine the EC_{50} .

3.7. Liposome Leakage Assay

3.7.1. Liposome Formulation

1. Dissolve phospholipids in chloroform or in chloroform/methanol (9/1).
2. Mix phospholipids DOPC/DOPE/PI/LBPA in molar ratio 5/3/2/1 (10 μmol total lipids) and evaporate lipids solution under high vacuum for 1 h.
3. Hydrate lipidic film with 1 ml of buffer containing quenched dye (20 mM MES, 75 mM NaCl, 12.5 mM ANTS, 45 mM DPX, (pH 5.5) to obtain 10 mM lipids and stir with a Vortex for 5 min.
4. Immerse alternatively suspension solution in liquid nitrogen and water bath at 37°C for five cycles of freezing/thawing.
5. Extrude liposome using a mini-extruder and one polycarbonate filter (100 nm diameter) and four pre-filters. Twenty-one passages through the filter are necessary to obtain a homogeneous population of LUV (Large Unilamellar Vesicle)
6. Purify liposomes by chromatographic exclusion on Sephadex G-50 column (1×10) to remove non-encapsulated dye and quencher. Equilibrate the column first with acidic buffer (20 mM MES, 145 mM NaCl, pH 5.5) and elute liposomes with the same buffer.
7. Quantify DOPC using the phospholipids kit to estimate phospholipid yield after formulation and purification.
8. Measure liposome size on a Coulter N4 Particle Size Analyzer. Mean size should be between 105 and 115 nm.

3.7.2. Liposome Leakage Assay

1. Quantify leakage in acidic (20 mM MES, 145 mM NaCl, pH 5.5) or neutral (20 mM Hepes, 145 mM NaCl, pH 7.4) buffer.
2. Add 100 μ M phospholipids in a final volume of 2 ml of buffer and measure initial fluorescence (F_0) at ex 360 and 530 nm under stirring at room temperature.
3. Add 40 μ l of 10% Triton X100 to obtain maximal fluorescence (F_{\max}).
4. Determine destabilization level for each peptide by measuring F_0 before adding the peptide (lipid/peptide ratio: 5/1).
5. Carry out kinetic studies under stirring at room temperature (see Note 8).
6. Determine leakage percentage by the formula: % leakage = $100 \times (F_t - F_0) / (F_{\max} - F_0)$.

4. Notes

1. HeLa pLuc 705 cells are stably transfected by a luciferase construction (Fig. 1) that allows the quantitative assessment of nuclear delivery and biological activity of CPP-ON conjugates. Cells should not be passaged more than ten times and should be controlled routinely for the absence of mycoplasma contamination.
2. In peptide-PNA conjugation, the synthesis of (NPys)Cys-PNA and synthesis of C-terminal Cys-containing peptides was described in a previous protocols chapter (4). Maintenance of full solubility in the conjugation reaction is essential and it is preferable to add formamide in all conjugation reactions to ensure solubility of peptide, PNA, and conjugate. A mixture of formamide and acetonitrile may be helpful to maintain solubility in the case of hydrophobic peptides (e.g. Transportan). In some cases, adjustment of the acetonitrile gradient conditions is needed. Conjugations yields achieved are typically 40–60%. In PMO-peptide conjugation, it is advisable to have high concentrations of the starting reactants to ensure a rapid conjugation. The thioether (thiomaleimide) linkage formation should be complete within 2 h. There is no harm in leaving the reaction overnight at 4°C. For MALDI-TOF mass spectrometry analysis, it is best to use a matrix of 2, 6-dihydroxyacetophenone (20 mg/ml) in methanol/diammonium hydrogen citrate. Yields vary between 20 and 35% depending on the sequence and the quality of the starting peptide and PMO.
3. For mechanistic studies, different drugs or treatments interfering with endocytosis may be used. In this case, pre-treat the cells

with the inhibitors for the appropriate time and concentration. Inhibitors should also be present during incubation with the CPP-ON conjugates. Most endocytosis inhibitors tend to be cytotoxic and should be used for the shortest possible period of time (5).

Treatment with trypsin before FACS analysis is required to eliminate membrane-bound CPP-ON conjugates (5).

4. CPP-ON conjugates should preferably be used at low concentrations (below 2.5 μM) to avoid cell permeabilization.
5. Saponin treatment should not exceed 0.5 h to permeabilize transiently the cell membrane without cytotoxicity.
6. We have described various cell-penetrating peptides for conjugation to PNA and PMO, including R6Pen (4, 6, 7), Pip (8), and (R-Ahx-R)₄ (9). Such PNA and PMO conjugates allow splicing redirection in this assay with submicromolar EC₅₀ values.
7. Programme used for reverse transcription and amplification:
 - Reverse Transcription: 1 cycle
 - cDNA production: 30 min at 55°C
 - Denaturation: 2 min at 94°C
 - Amplification: 30 cycles
 - Denaturation: 20 s at 94°C
 - Hybridization: 30 s at 60°C
 - Elongation: 30 s at 68°C
 - Elongation: 1 cycle for 5 min at 68°C
 - Store PCR products at -20°C.
8. Some peptides and peptide-ON conjugates unfortunately give rise to liposome precipitation which prevents observation of membrane destabilization.

Acknowledgments

We thank R. Kole (University North Carolina) for providing the HeLa pLuc705 cell line. Amer Saleh was supported by the MRC-Technology Development Gap Fund and also by Action Duchenne. Rachida Abes was supported by Ligue Française contre le Cancer PhD fellowship and Fatouma Said Hassane by Association Française contre les Myopathies.

Studies funded by EC grant QLK3-CT-2002-01989 and CEFIPRA grant 3205.

References

1. Bauman, J., Jearawiriyapaisam N. and Kole, R. (2009) Therapeutic potential of splice-switching oligonucleotides. *Oligonucleotides* **19**, 1–13.
2. Wilton, S.D. and Fletcher, S. (2008) Exon skipping and Duchenne muscular dystrophy: Hope, hype and how feasible. *Neurol. India* **56**, 254–262.
3. Kang, S.H., Cho, M.J. and Kole, R. (1998) Up-regulation of luciferase gene expression with antisense oligonucleotides: implications and applications in functional assay development. *Biochemistry* **37**, 6235–6239.
4. Abes, S., Turner, J.J., Abes, R., Arzumanov, A.A., Williams, D., Owen, D., Lebleu, B. and Gait, M.J. (2009) Peptide-based delivery of steric-block PNA oligonucleotides. *Methods Mol. Biol.* **480**, 85–99.
5. Richard, J.P., Melikov, K., Vives, E., Ramos, C., Verbeure, B., Gait, M.J., Chernomordik, L.V. and Lebleu, B. (2003) Cell-penetrating peptides. A re-evaluation of the mechanism of cellular uptake. *J. Biol. Chem.* **278**, 585–590.
6. Turner, J.J., Ivanova, G.D., Verbeure, B., Williams, D., Arzumanov, A.A., Abes, S., Lebleu, B. and Gait, M.J. (2005) Cell-penetrating peptide conjugates of peptide nucleic acids (PNA) as inhibitors of HIV-1 Tat-dependent trans-activation in cells. *Nucleic Acids Res.* **33**, 6837–6849.
7. Abes, S., Turner, J.J., Owen, D., Ivanova, G.D., Verbeure, B., Williams, D., Arzumanov, A.A., Clair, P., Gait, M.J. and Lebleu, B. (2007) Efficient splicing correction by PNA conjugation to an R6-Penetratin delivery peptide. *Nucleic Acids Res.* **35**, 4495–4502.
8. Ivanova, G.D., et al. (2008) Improved cell-penetrating peptide-PNA conjugates for splicing redirection in HeLa cells and exon skipping in mdx mouse muscle. *Nucleic Acids Res.* **36**, 6418–6428.
9. Abes, S., et al. (2006) Vectorization of morpholino oligomers by the (R-Ahx-R)₄ peptide allows efficient splicing correction in the absence of endosomolytic agents. *J. Control. Release* **116**, 304–313.

CPP-Directed Oligonucleotide Exon Skipping in Animal Models of Duchenne Muscular Dystrophy

HaiFang Yin, Hong Moulton, Corinne Betts, and Matthew Wood

Abstract

Antisense oligonucleotides (AOs) are effective splice switching agents and have potential as therapeutics via the exclusion or inclusion of specific target gene exons to ameliorate and modify disease progression. The leading example is Duchenne muscular dystrophy (DMD), a fatal muscle degenerative disease, where AO-mediated skipping of specific *DMD* gene exons can restore the disrupted *DMD* open reading frame, leading to the production of functional dystrophin protein and ameliorate the DMD phenotype in animal models. Clinical proof-of-concept has recently been shown in two successful, independent Phase I clinical trials. These trials both followed local intramuscular treatments, and the challenge now is to develop and test systemic protocols, which will be required for treatment-aimed disease modification. Recently, a number of groups have demonstrated the promise of AOs directly conjugated to cell-penetrating peptides (CPPs) as having significant potential for systemic delivery and therapeutic correction in DMD animal models. Here, we review the background to this work and describe in detail the experimental protocols used in studies aimed at investigating CPP-conjugated AOs as systemic splice correcting agents in animal models of DMD.

Key words: Antisense oligonucleotide, Morpholino, Cell-penetrating peptide, Splice correction, Exon skipping, Duchenne muscular dystrophy, Dystrophin, Muscle, Heart, Systemic delivery

1. Introduction

Antisense oligonucleotides (AOs) have significant potential as compounds for splice switching and splice correction therapies in a range of human disease states, the leading clinical example being for Duchenne muscular dystrophy (DMD). DMD is an X-linked, monogenic, degenerative muscle disorder affecting approximately 1 in 3,500 newborn boys, as a result of mutations in the *DMD* gene, leading to loss of the essential muscle protein dystrophin. As a result, this causes progressive muscle degeneration and weakness, cardiomyopathy, respiratory failure, and ultimately premature

death, with affected DMD boys typically surviving into their 20s without any treatment. The absence of dystrophin protein arises primarily due to not only deletions but also duplications, point mutations, or other smaller gene rearrangements that interrupt the open reading frame of the *DMD* gene, thus inhibiting effective transcription and translation of functional dystrophin protein (1). This loss of dystrophin protein leads to a series of deleterious pathophysiological changes principally in muscle cells, including reduced muscle membrane stability and increased intracellular calcium influx, ultimately leading to muscle fibre degeneration and disease onset. Interestingly, despite such mutations leading to an absence of dystrophin protein, up to 50% of all DMD patients have occasional dystrophin-positive, so-called revertant, muscle fibres. These are thought to arise due to alternative processing of the *DMD* pre-mRNA, which as a result spontaneously restores the *DMD* open reading frame, leading to effective dystrophin expression in muscle cells. Such revertant dystrophin protein is found to be functional, being correctly localised to the muscle membrane and leading to the normal and essential assembly of a critical network of dystrophin-related proteins (the dystrophin-associated protein complex (DAPC)), which indicates that the restored dystrophin protein has structural integrity comprising the presence of the necessary functional domains for normal biochemical activity. This finding of revertant fibres in many DMD patients together with the existence of mildly affected individuals with a related allelic disorder known as Becker muscular dystrophy (BMD) (2), in which these patients harbour in-frame *DMD* gene deletions, hinted at the possibility that exogenous modification of dystrophin pre-mRNA processing (via the splice modification to exclude or skip specific *DMD* exons) could lead to restoration of the *DMD* gene open reading frame and induce the expression of functional dystrophin protein in DMD patients (3). In recent years, the use of AOs to mediate such splice correction therapy in DMD has been effectively demonstrated in a range of experimental systems, including human DMD muscle cells, via intramuscular and systemic injection in dystrophin-deficient *mdx* mice (4–13), and most importantly in two recent Phase I clinical trials, following direct intramuscular injection in DMD patients (14, 15). AO splice correction therapy, thus, has clear therapeutic potential, and it has been estimated from information on the Leiden muscular dystrophy database that such a treatment could benefit up to 83% of all DMD patients (16).

While very encouraging, the clinical trial data referred to above was obtained following local intramuscular AO administration in single lower limb muscles in DMD patients. Thus, a major challenge for the future application of this AO-mediated exon skipping therapy for DMD will be to establish methods for effective systemic AO delivery to all muscles and other tissues affected

by the DMD disease process. Two early studies in *mdx* mice using 2'OMePS and morpholino phosphorodiamidate oligomer (PMO) AOs both reported low dystrophin splice correction in peripheral muscle groups, following systemic intravenous administration (5, 8). In the latter study, high systemic intravenous doses and a multiple injection regimen (with seven repeat doses at 100 mg/kg) were required, and despite these experimental conditions, splice correction efficiency remained relatively low with inter-muscle variation, and with no observed dystrophin splice correction in heart. Subsequently, a number of groups have explored the potential use of covalently attached arginine-rich cell-penetrating peptide (CPP) sequences to enhance PMO delivery in DMD animal models (17). Such peptide-PMO conjugates, initially based on the well-characterised (RXR)₄ peptide and related CPPs, were shown to dramatically improve the efficiency of systemic splice correction in dystrophin-deficient *mdx* mice, with restoration of dystrophin protein to more than 50% of normal levels in all peripheral muscles and with evidence of restored cardiac dystrophin protein observed for the first time (6, 10, 12, 18, 19). Subsequently, Ivanova and colleagues have reported the discovery and development of novel CPPs, initially based on an R6-Penetratin motif, which have significant potential for enhanced systemic AO uptake and function in DMD models (20, 21). While the application of such CPPs has encouraging potential for enhancing systemic PMO delivery for dystrophin splice correction, such peptides do not typically confer targeted cell specificity. Thus recently, Yin et al. have demonstrated for the first time that a chimeric peptide-PMO conjugate, incorporating muscle-specific heptapeptide and arginine-rich CPP domains, could yield targeted PMO delivery and improved splice correction in *mdx* mice (22). Thus, CPP-directed AO delivery has demonstrated potential for achieving restored dystrophin expression with amelioration of the disease phenotype in DMD animal models. Further developments in CPP and related peptide-AO methods are in progress for DMD, and the first clinical trial to evaluate a peptide-PMO therapeutic agent for DMD is planned in 2010.

2. Materials

Unless stated otherwise, all solutions should be prepared in double distilled water. This standard is referred to as “water” in this text.

2.1. RNA Extraction and RT-PCR

1. Iso-Pentane (VWR BDH Prolabo, Briare, France). This substance is highly flammable; therefore, store in a cool, dry, and well-ventilated area.

2. TRIzol[®] Reagent (Invitrogen, Paisley, UK). This substance is highly toxic and a possible mutagen (see Note 1). Prevent product from entering drains. Store at 2–8°C.
3. Chloroform, analytical reagent grade (Fisher Scientific, Leicestershire, UK). This substance is carcinogenic and a possible teratogen (see Note 1). Prevent product from entering drains. This substance is also light-sensitive and should be stored in a cool, dry area.
4. 2-Propanol (Sigma) for molecular biology, minimum 99%. This substance is highly flammable; therefore, store in a cool, dry, and well-ventilated area.
5. RNA wash: 75% v/v ethanol, absolute, 200 proof, for molecular biology (Sigma); 25% v/v RNA free water. Ethanol is highly flammable; therefore, store in a cool, dry area.
6. RT-PCR: QIAGEN One Step RT-PCR Kit (QIAGEN, Hilden, Germany). Store at –20°C (see Note 2).
7. Nested PCR: Hot Star *Taq* DNA Polymerase kit (QIAGEN). Store at –20°C (see Note 2).
8. TAE Buffer (50×): 2 M Tris-Base; 10% (v/v) 0.5 M EDTA (Sigma), pH 8.0; 5.7% (v/v) glacial acetic acid (VWR) 100%. Combine reagents and make up to 900 ml with water; pH 7.6–7.8. To make 1× TAE buffer, dilute 20 ml in 980 ml of water to make up to 1 l.
9. Agarose Gel: 2% (w/v) Agarose (Bioline, Taunton, MA) in 1× TAE buffer. Add between 2 and 4 µl of ethidium bromide (EB; Sigma) for visualisation of bands. The electrophoresis tank should be filled with TAE buffer. EB is highly toxic, and chronic exposure may be mutagenic. Do not allow to enter drains (see Note 3).

2.2. Preparation of Protein Samples

1. Lysis buffer: 75 mM Tris-HCl (Sigma), pH 6.5; 10% sodium dodecyl sulphate (SDS; Sigma), for electrophoresis, approximately 99% pure. Store at room temperature. Prior to lysing samples, add 5% 2-Mercaptoethanol, 99% extra pure (Acros Organics, New Jersey, USA), and 3% Protease Inhibitor Cocktail (Sigma) to the aliquot. The protease inhibitor needs to be reconstituted prior to use and aliquoted into tubes. Store at –20°C.

2.3. SDS-Polyacrylamide Gel Electrophoresis (SDS-PAGE)

1. Separating buffer (4×): 1.5 M Tris-HCl, pH 8.8. Store at room temperature.
2. Stacking buffer (4×): 0.5 M Tris-HCl, pH 6.8. Store at room temperature.
3. Thirty percent acrylamide/bis-acrylamide solution, Electrophoresis Reagent, 37.5:1 (Sigma). This may cause cancer and heritable genetic damage, so care should be taken not to make contact with the substance. Store at 2–8°C.

4. *N,N,N,N'*-Tetramethyl-ethylenediamine (TEMED; Sigma) for electrophoresis, approximately 99%. This substance is harmful by inhalation or ingestion. It is also highly flammable therefore store in a cool, dry and well ventilated area (see Note 4).
5. Ammonium persulfate (Sigma): Dissolve the powder to make a 10% (w/v) solution in water. Aliquot the solution and freeze at -20°C .
6. SDS: Prepare a 20% (w/v) solution in water and dissolve thoroughly. This substance is highly flammable; therefore, store in a cool, dry, and well-ventilated area. Avoid contact with skin and eyes, and dust formation as this substance may be harmful.
7. Glycerol (Sigma), ReagentPlus[®], $\geq 99.0\%$ (GC). Store at room temperature.
8. Running buffer (10 \times): 247.7 mM Tris, 1.91 M glycine (Sigma), 1% (w/v) SDS. Store at room temperature.
9. Laemmli SDS sample buffer: 0.1 M Tris-HCl, pH 6.6; 2% (w/v) SDS; 2% 2-Mercaptoethanol; 20% (v/v) glycerol; 0.01% (w/v) Bromophenol Blue (Sigma). Store at $2-8^{\circ}\text{C}$.

2.4. Western Blotting for Dystrophin Protein

1. Transfer buffer (10 \times): 247.7 mM Tris, 1.91 M glycine. Store at room temperature.
2. Transfer buffer: 10% (v/v) 10 \times transfer buffer; 10% (v/v) methanol (Fisher Scientific, Leicestershire, UK), analytical reagent grade. Methanol is highly flammable and toxic by inhalation, contact with skin, and if ingested. Keep container tightly closed and store at room temperature in a flammables cupboard, away from sources of ignition. Add 0.01% (w/v) SDS and make up the volume with water (see Note 5).
3. Immobolin-P membrane, PVDF, 0.45 μm (Millipore, Bedford, MA) and 11 μm filter paper (Whatman, Maidstone, UK).
4. Wash solution: Prepare phosphate-buffered saline (PBS; Sigma) with 0.1% (v/v) Tween (Sigma) to make PBST; 5% 5 M NaCl.
5. Blocking buffer: 5% (w/v) Non-fat dry milk in PBST.
6. Primary antibody: NCL DYS-1 (Leica-Novocastra, Newcastle, UK) (see Note 6).
7. Secondary antibody: Anti-mouse IgG whole monoclonal peroxidase, produced in goat (Sigma).
8. Develop using Chemiluminescent HRP substrate, Immobilon Western (Millipore, Bedford, MA); and Kodak Biomax XAR film (Sigma) (see Note 7).

2.5. Immunohistochemistry for Dystrophin

1. Microscope coverslips: Borosilicate glass, 22 mm×40 mm×0.15 mm (VWR, Geldenaaksebaan, Leuven).
2. Microscope slides: Superfrost® Plus (VWR).
3. Blocking solution: 20% (v/v) Normal goat serum (NGS; Sigma), 20% (v/v) foetal calf serum (FCS; Invitrogen) in PBS.
4. PBS is used as a washing solution.
5. Primary diluent solution: 20% (v/v) NGS in PBS.
6. Primary antibody: Rabbit polyclonal antibody targeting at the C-terminal of dystrophin, (Abcam, Cambridge, MA). Store at 2–8°C.
7. Secondary antibody: Alexa Flour® 594, Goat anti-rabbit IgG (Invitrogen, Oregon, USA). Store at 2–8°C.
8. Nuclear stain: 1.34 µg/ml DAPI (4,6-diamidino-2-phenylindole) in DMSO (Sigma) (see Note 8).
9. Mounting medium: Dako fluorescent mounting medium (Dako, Carpinteria, CA). Store at 2–8°C.

2.6. Immunohistochemistry for Dystrophin-Associated Protein Complex

1. Microscope coverslips: Borosilicate glass, 22 mm×40 mm×0.15 mm.
2. Microscope slides: Superfrost® Plus.
3. Blocking solution: Biotin/Avidin Blocking System (Vector, Burlingame, CA). Store at 2–8°C.
4. Washing solution: 0.1% Tween 20 in PBS (PBST).
5. MOM Blocking Solution: Dilute two drops of MOM Blocking Solution in PBS.
6. MOM diluent solution: Dilute MOM Protein Concentrate (Vector) 1:125 in PBS. Store at 2–8°C.
7. Primary Antibody: β-Sarcoglycan: NCL-L-b-SARC, α-Sarcoglycan: NCL-l-a-SARC, and β-Dystroglycan: NCL-b-DG (Leica-Novocastra) are diluted in MOM Diluent Buffer (see Note 6).
8. Secondary antibody: Biotinylated Anti-mouse IgG reagent (Vector) is diluted in MOM Diluent Buffer.
9. Texas Red Streptavidin (Vector) is diluted 1:250 in MOM Diluent Buffer. Store at 2–8°C.

3. Methods

Recent exciting progress in the treatment of DMD, especially the success of two phase I clinical trials with antisense oligonucleotide-mediated exon skipping (14, 15), makes it an ideal model system

for evaluating numerous newly developed antisense oligonucleotides (AOs). In particular, the CPP-conjugated PMOs have been shown to restore high levels of dystrophin expression in multiple muscle groups including heart and have averted the progression of the disease in dystrophin-deficient *mdx* mice (6, 10, 12, 18, 19). Therefore, it is pivotal to determine the level of the exon skipping and functional correction of dystrophin protein induced by the CPP AO conjugates in *mdx* mice.

There are a number of different parameters that may be applied to determine the efficacy of the CPP AO conjugates; among them, the most essential assays are the measurement at the RNA, protein level and phenotypical restoration. RT-PCR is used routinely to test the percent of exon skipping in the dystrophin transcript, which is based on the relative percent of skipped transcript to full-length unskipped dystrophin mRNA. Western blot is most commonly used to quantify the total amount of restored dystrophin protein after the treatment, which is the most critical parameter for the functional correction of dystrophic muscles. Immunohistochemical staining is important to show the correct localization and distribution of the restored dystrophin protein in muscle fibres, which can reflect the efficiency of CPP AO conjugate delivery in terms of the number of dystrophin-positive fibres. The number of dystrophin-positive fibres has a direct correlation with the muscle force recovery.

Dystrophin is a key component of DAPC, which bridges the cytoskeleton and extracellular matrix and stabilises the sarcolemmal membrane (1). In the absence of dystrophin, other DAPC components fail to localise to the sarcolemma and diffuses into the cytoplasm. Therefore, it is an important functional parameter to look at for evaluating the efficacy of CPP AO conjugates. Here, we show the methods for immunostaining of the β -sarcoglycan, α -sarcoglycan, and β -dystroglycan components of the DAPC.

3.1. RNA Extraction and RT-PCR

1. The muscle tissues are harvested and snap-frozen in liquid nitrogen or dry-ice-cold isopentane and stored at -80°C .
2. Collect 20–30 muscle cryosections of 15 μm thickness into sterile 1.5-ml Eppendorf tubes placed on dry ice.
3. Put 1 ml of Trizol into the Eppendorf and carry out the subsequent steps according to the manufacturer's instructions for Trizol. Measure the total RNA concentration by spectrophotometer (Nanodrop).
4. Use 200 ng of RNA template for a 20- μl RT-PCR with the OneStep RT-PCR kit. The primer sequences for the initial RT-PCR are Exon20Fo 5'-CAGAATTCTGCCAATTGCTGAG-3' and Ex26Ro 5'-TTCTTCAGCTTGTGTCATCC-3' which allows amplification of messenger RNA from exons 20 to 26. The cycle conditions are 95°C for 30 s, 55°C for 1 min,

and 72°C for 2 min for 25 cycles. RT-PCR product (1 µl) is then used as the template for secondary PCR performed in 25 µl with 0.5 U Taq DNA polymerase (see Note 9). The primer sequences for the second round are Ex20Fi 5'-CCCAGTCTACCACCCTATCAGAGC-3' and Ex24Ri 5'-CAGCCATCCATTTCTGTAAGG-3'. The cycle conditions are 95°C for 1 min, 57°C for 1 min, and 72°C for 2 min for 25 cycles.

5. The PCR products are examined by electrophoresis on a 2% agarose gel. An example for RT-PCR is shown as Fig. 1a.

3.2. Preparation of Samples for Assay of Dystrophin by Western Blotting

1. Collect 30–40 cryosections of 15-µm thickness in 1.5-ml Eppendorf tubes placed on dry ice (fill up to 0.5 ml mark).
2. Remove samples from the ice, add 150-µl protein lysis buffer (see Note 10), and homogenize by gently pipetting up and down until the sections are dissolved.
3. Boil at 100°C for 3–5 min (punch a hole into the cap with a needle) and centrifuge for 15 min, at 12,000 × *g* or maximum speed.
4. Collect the supernatant and keep the aliquot at –80°C for long storage.
5. Measure protein concentration by Bradford reagent using 1:100 dilution (see Note 11) according to the manufacturer's instruction.
6. Prepare samples in Eppendorf with the required amount of protein and mix the samples with 2× or 5× Laemmli SDS sample loading buffer.
7. Boil the samples for 3–5 min and then spin them down at maximum speed for 5 min; the samples are ready for loading.

3.3. SDS-PAGE

1. These instructions are based on the Bio-Rad mini-gel system with 0.75-mm thick gel plates. They are easily adjusted to other systems. It is important to ensure that all the glass plates are clean.
2. Assemble the gel plates in a green plastic gel holder. Ensure that the glass plates are correctly aligned and level with the bench.
3. Place gel holder and plates into the transparent rack. Press down on the gel holder to ensure that there is a tight seal with the rubber pad underneath so that the gel mixture does not leak out.
4. Prepare 5 ml of 6% resolving gel in a Falcon tube by mixing 1.25 ml of 4× Resolving gel buffer with 1 ml of 30% acryl amide/bis-acrylamide (37.5:1) solution, 2.45 ml of water, 0.25 ml of glycerol, 42.5 µl of 20% SDS, 50 µl of ammonium

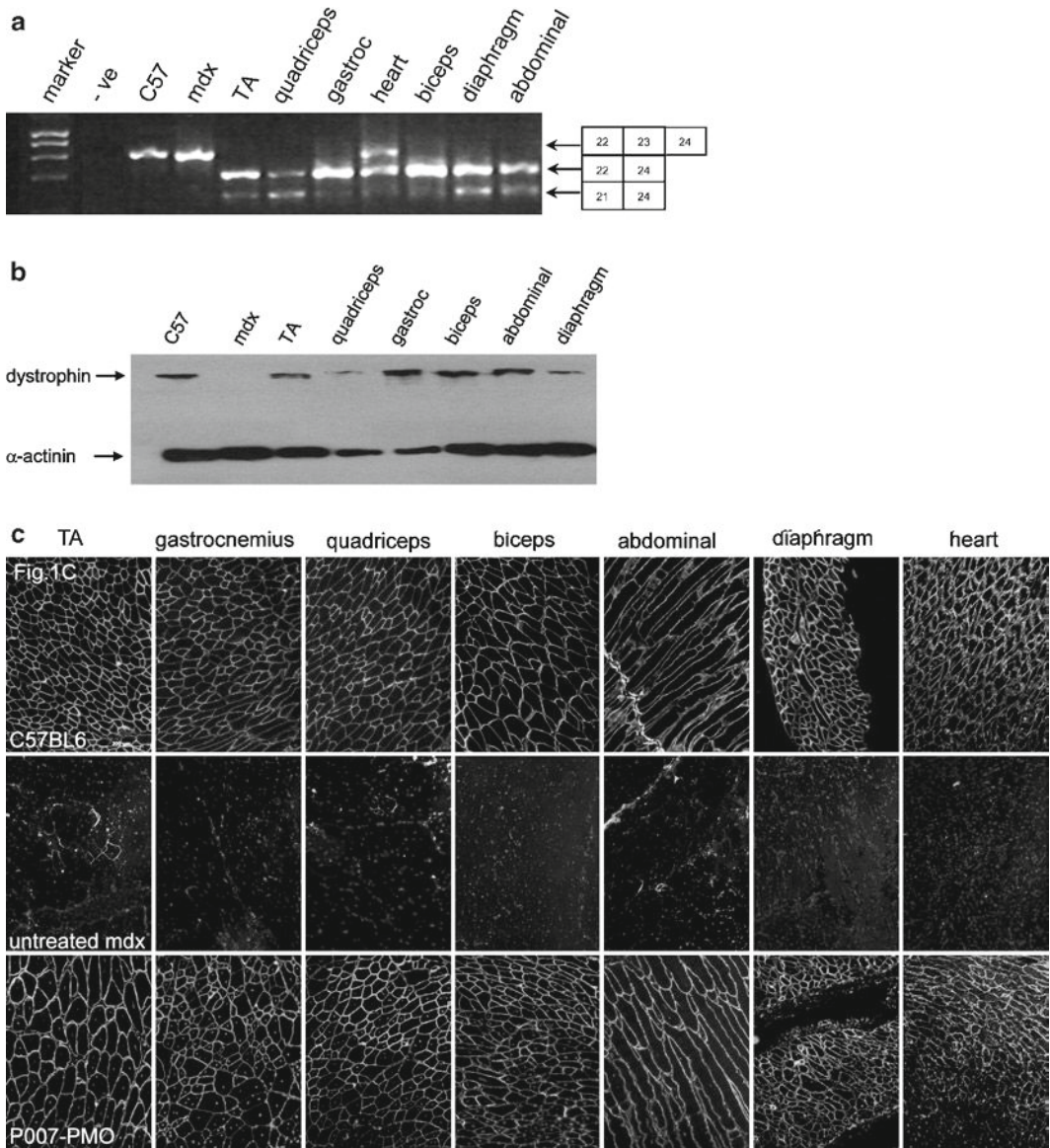


Fig. 1. Restoration of muscle and cardiac dystrophin expression in mdx mice. Restoration of dystrophin expression following single 25 mg/kg intravenous injections of the P007-PMO AO conjugate in adult mdx mice. (a) Immunostaining of muscle tissue cross-sections to detect dystrophin protein expression and localisation in C57BL6 normal control mice (*top panel*), untreated mdx mice (*middle panel*), and P007-PMO treated mdx mice (*lower panel*), showing near normal levels of dystrophin expression in the treated mice. Muscle tissues analysed were from tibialis anterior (TA), gastrocnemius, quadriceps, biceps, abdominal wall, diaphragm, and heart muscles (scale bar = 200 μ m). (b) RT-PCR to detect exon skipping efficiency at the RNA level demonstrated almost complete exon 23 skipping in the peripheral skeletal muscles indicated and about 50% exon skipping in heart in treated mdx mice. This is shown by shorter exon-skipped bands (indicated by the boxed numbered 22–24 – for exon 23 skipping). Truncated transcripts deleted for both exons 22 and 23 were also seen as indicated by the box 21–24. (c) Western blot for dystrophin expression in peripheral skeletal muscles showed about 100% dystrophin restoration in all skeletal muscles except the diaphragm and with P007-PMO conjugate treatment compared with levels found in normal C57BL6 mice. Equal loading of 10 μ g protein is shown for each sample with α -actinin expression as a loading control.

- persulfate solution, and 5 μ l of TEMED. Invert the Falcon tube several times to mix (see Note 12). Pour the gel mixture between the glass plates until it is two thirds full. Leave one third for stacking gel.
5. Pipette water on top of the resolving gel to ensure that the gel does not dry out. The gel may visibly deform under the pressure of the water at this stage. The level of the gel should settle out as the gel sets (unless too much TEMED was used or the gel was poured too late after the TEMED was added).
 6. The gel should take 45–60 min to set. The remaining gel mixture in the Falcon tube can be used as a guide as to when the gel has set.
 7. Remove the gel holder from the transparent rack and pour the water off into the sink.
 8. Prepare 2.5 ml of 4% stacking gel by mixing 625 μ l of 4 \times Stacking gel buffer with 325 μ l of 30% acryl amide/bis-acrylamide (37.5:1) solution, 1.4 ml of water, 25 μ l of 20% SDS, 125 μ l of glycerol, 25 μ l of ammonium persulfate solution, and 2.5 μ l of TEMED in a Falcon tube and mix by inversion. Immediately pipette the stacking gel mixture between the glass plates and on top of the resolving gel.
 9. Fit the comb between the glass plates and clean off displaced stacking gel mixture. Avoid air bubbles between the comb and the gel.
 10. The gel should take 30–45 min to set. The remaining gel mixture in the Falcon tube can be used as a guide as to when the gel has set (see Note 13).
 11. Prepare the 1 \times SDS Running buffer by diluting 100 ml of the 10 \times SDS Running buffer with 900 ml water in a measuring cylinder.
 12. Pour 1 \times SDS Running Buffer into the tank so that the level of buffer is full between the two gels and a third full for the rest of the tank. If there is any leakage into the main tank, more buffer needs to be poured into the tank. Gently remove the comb from the top of the gel by pulling directly upwards. Be careful not to deform the wells. Using a P200 micropipette, clean the wells with SDS Running Buffer. The wells are easily viewed from above and from front. When buffer is pipetted into a well, the bottom of the well should visibly flatten out. This produces even-shaped wells and makes them easier to visualise from the front of the apparatus.
 13. Load the pre-stained protein molecular weight marker in the first lane and the samples in the subsequent lanes.
 14. Set up the gel unit and connect to a power supply. The gel can be run either overnight at 50 V in a cold room or at 150 V for 3 h (see Note 14).

3.4. Western Blotting for Dystrophin

1. Remove the gel plates from the gel tank. The SDS Running Buffer may be discarded or recycled one more time.
2. Separate the glass plates using a plastic wedge. The gel should stick to one of the plates.
3. Cut away the stacking gel and the edges of the gel so as to loosen it from the glass plates.
4. Place the glass plate with the gel attached in a container with 1× transfer buffer.
5. Cut a PVDF membrane to the size of the gel and cut away one corner for identification (see Note 15).
6. Soak the membrane in methanol for approximately 1 min (see Note 16).
7. Cut two pieces of filter paper to the size of the membrane.
8. Soak two sponges and the two pieces of filter paper in transfer buffer.
9. Briefly wash the PVDF membrane in transfer buffer.
10. Assemble the cassette as follows from bottom to top: black side of transfer cassette, one sponge, one filter paper, gel, membrane, one filter paper, one sponge.
11. Then, load the cassette(s) into the rack with the black sides aligned and make sure that the membrane is between the gel and anode. It is vital to ensure this orientation, or the proteins will be lost from the gel into the buffer rather than transferred onto PVDF membrane.
12. Place the rack (and cassette) into the gel tank.
13. Fill the tank with 1× SDS transfer buffer, place the lid on the tank, and start the power supply.
14. Transfer overnight at 50 V at 4°C.
15. Once the transfer is complete, the cassette can be taken out of the tank and carefully disassembled.
16. Take the membrane out and briefly rinse with PBS (see Note 17).
17. Block the membrane with 20-ml blocking solution for 1–2 h (see Note 18).
18. After blocking, incubate the membrane with dystrophin primary antibody (1:200 diluted in blocking solution) overnight on a shaker in the cold room.
19. Wash the membrane four times with blocking solution containing 200 mM NaCl (1 for 10 min, 3 for 5 min) (see Note 19).
20. Incubate the membrane with secondary antibody (1:9,000 diluted in blocking solution) on a shaker for 1 h at room temperature.

21. Wash the membrane three times with PBST containing 200 mM NaCl for 15 min each time.
22. After the final wash, pick up the membrane(s) using tweezers and place on the top of an OHP transparency film/piece of cling wrap.
23. Place 250 μ l of each ECL reagent (1:1 ratio) into a 1.5-ml Eppendorf (roughly 500 μ l of developing reagent is required for one membrane).
24. Pipette 500 μ l of premixed ECL reagent onto each membrane (~4 cm \times 6 cm). Ensure that the entire membrane is covered with reagent.
25. Cover the membrane with a second OHP transparency and fold over the cling wrap. Ensure that there are no bubbles between the plastic and the membrane.
26. Place the covered membrane into the cassette. Position the membrane to allow for easy identification later on (see Note 20).
27. The remaining steps are done in a dark room under safe light conditions.
28. Open the X-ray film and cut a piece to the size of the membrane and fold or cut a corner for identification.
29. Place the film on top of the wrapped membrane in the cassette, immediately close the cassette, and start the timer.
30. Useful exposure times range between 1 and 15 min. A good starting point is 1 min. When the exposure time is up, remove the film from the cassette and place in the X-O-graph for developing (see Note 21).
31. Open the cassette and align the developed film on top of the membrane. Use a fine-liner pen to mark on the position of the protein markers for size determination.
32. Keep the membrane(s) in PBS if they are required for further experimentation (see Note 22). An example of Western blotting is shown as Fig. 1b.

3.5. Immunohistochemistry for Dystrophin

1. Cryosections of 8 μ m are cut from at least two-thirds deep into the muscle at 100 μ m intervals (see Note 23).
2. Air-dry the cryosections on the slide for 10 min.
3. Circle the section with a Blocking Pen (see Note 24).
4. Soak the slides in PBS for 10 min.
5. Block the sections with 20% FCS and 20% NGS in PBS at room temperature for 1 h.
6. Tip the blocking buffer away from the sections and incubate the sections with dystrophin primary antibody at a dilution of

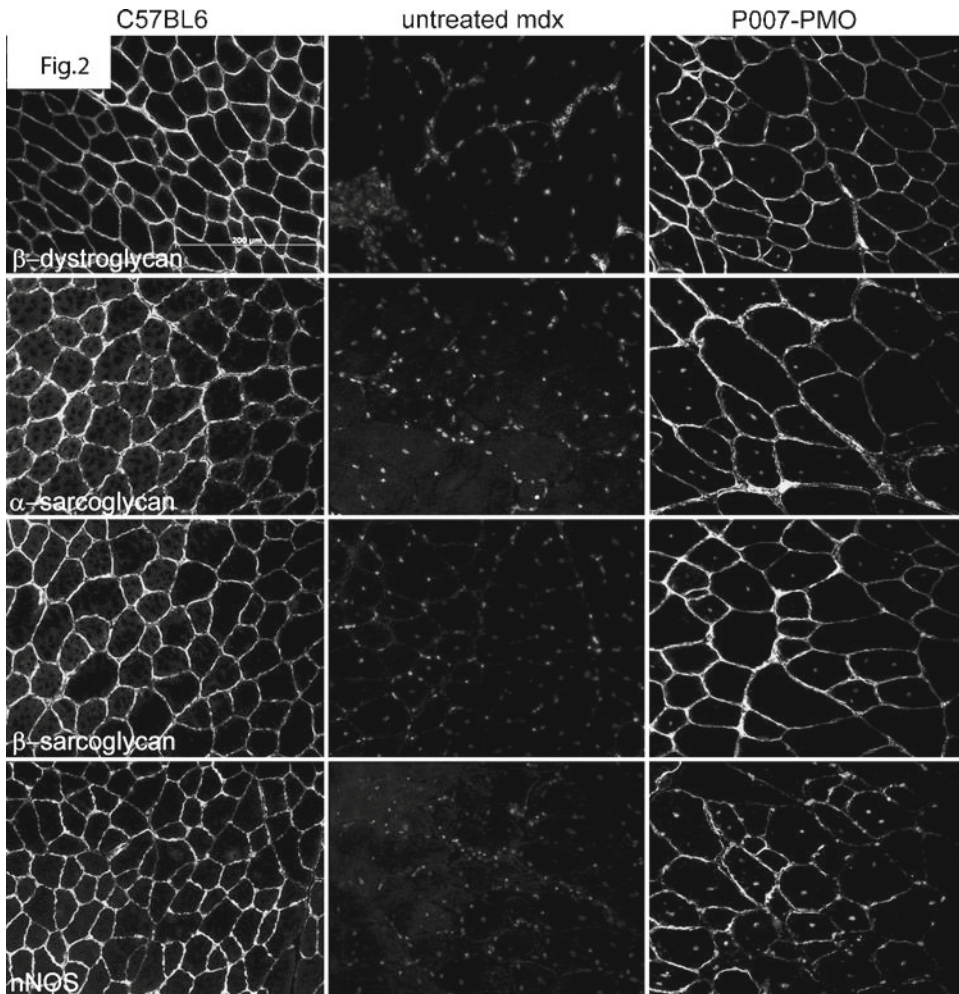


Fig. 2. Functional evaluation of mdx skeletal muscles following treatment with the P007-PMO conjugate. Restoration of the dystrophin-associated protein complex (DAPC) in mdx mice treated with P007-PMO at 25 mg/kg was studied to assess dystrophin function and recovery of normal myoarchitecture. DAPC protein components β -dystroglycan, α and β -sarcoglycan, and nNOS were detected by immunostaining in tissue cross-sections of TA muscles from treated mdx mice compared with C57BL6 normal mice and untreated mdx control mice. All detected DAPC components are found to be successfully relocalised to the mdx muscle sarcolemma after treatment.

- 1:2,500 (see Note 25) with 20% NGS for 1 h at room temperature.
7. Remove the primary antibody and briefly wash the slide three times with PBS.
 8. Incubate the sections with fluorophore-labelled secondary antibody (goat anti-rabbit IgG) at a dilution of 1:200 in PBS for 1 h at room temperature.
 9. Remove the secondary antibody and briefly wash the slides three times with PBS.

10. Tip the PBS away from the slides and mount the slides with DAPI-mounting medium and wrap in foil (see Note 26).
11. The slides are viewed through the fluorescence microscope. Excitation at 543 nm induces the Cy3 fluorescence (red emission) for the dystrophin protein, while excitation at 364 nm induces DAPI fluorescence (blue emission). An example of the result is shown as Fig. 1c.

3.6. Immunohistochemistry for Dystrophin-Associated Protein Complex

1. Cryosections of 8 μm are cut from at least two-thirds deep into the muscle at 100- μm intervals.
2. Air-dry the cryosections for 30 min.
3. Circle the section with a Blocking Pen.
4. Block the endogenous biotin with the Vector biotin blocking system and incubate the sections with avidin solution for 15 min (see Note 27).
5. Remove the avidin buffer and briefly wash the slide with PBST.
6. Incubate the slide with biotin solution for 15 min.
7. Remove the biotin solution and briefly wash with PBST.
8. After washing, add M.O.M blocking solution and incubate at room temperature for 1 h (see Note 28).
9. Wash the slides three times for 3 min with PBST.
10. Add M.O.M diluent solution to the slide and incubate for 5 min.
11. Tip the diluent solution away from the slide and incubate with the primary antibodies (α -sarcoglycan, β -sarcoglycan, and β -dystroglycan monoclonal mouse antibodies) in diluent solution at a 1:100 dilution for 1 h (see Note 29).
12. Tip the primary antibody away from the slides and wash the slides three times with PBST for 3 min each time.
13. Add anti-mouse-IgG from the MOM kit and incubate for 10 min (see Note 30).
14. Remove the solution and briefly wash the slides three times with PBST for 3 min each time.
15. Add avidin-fluorescence and incubate for 5 min (see Note 31).
16. Remove the secondary antibody and wash the slides three times for 3 min.
17. Mount the slides with DAPI-mounting medium and wrap in foil.
18. The slides are viewed through the fluorescence microscope. Excitation at 543 nm induces the Cy3 fluorescence (red emission) for the dystrophin-associated protein complex, while excitation at 364 nm induces DAPI fluorescence (blue emission). An example of the result is shown as Fig. 2.

4. Notes

1. It should only be handled in a fume hood, and safety goggles and impervious gloves should be worn at all times. Contaminated waste should be disposed of in special waste appropriately.
2. Thaw reagents directly before use; however, the enzyme mix or *Taq* should be kept on ice at all times.
3. Keep the container tightly closed and in the designated EB contamination area. Heavily contaminated waste should be disposed of in special waste; however, gels and tips may be discarded in clinical bins.
4. TEMED may decline in quality over time; therefore, it is best to buy small bottles.
5. Transfer buffer can be used for up to two to three transfers before it is discarded. In order to keep the transfer buffer cooler than room temperature whilst running, the experiment and transfer apparatus may be kept on ice or stored in the cold room.
6. The enzyme is stable in a freeze-dried conjugate form. It, therefore, requires reconstitution in 2.5 ml of water prior to use. Aliquot into tubes and store at -20°C . Tubes may be removed from the freezer one at a time and stored at $2-8^{\circ}\text{C}$.
7. If quantification is required, the film may be scanned and programmes such as ImageJ utilised to compare the scanning densitometry. Alternatively, an instrument such as FujiFilm LAS-100 plus may be used.
8. Once the DAPI has been added to the Dako, shake the bottle well and wrap in foil as DAPI is light-sensitive.
9. For RT-PCRs, nested PCR is not necessary for highly efficient exon skipping, and one round of RT-PCR would be sufficient for the detection of exon skipping bands.
10. The volume of protein lysis buffer can be adjusted depending on the amount of tissue sections.
11. Protein concentration measurement may be carried out by BCA or the Bradford assay, but we have found that the Bradford assay is simple, quick, and reliable. Please check carefully for the interference factors for Bradford, especially for the concentration of SDS in the mentioned lysis buffer; we always dilute the protein sample 1:100.
12. TEMED catalyses polymerization of the resolving gel, so the gel mixture must immediately be pipetted between the glass plates to prevent the gel from setting too early. Around 2 ml of gel mixture is required per 75 mm mini-gel.

13. When the stacking gel has set, gels may be removed from the green plastic holders, wrapped in a damp paper towel, and then wrapped in cling film and stored at 4°C.
14. Place the gel tank into an icebox when the gel is running at room temperature for 3 h at 150 V to prevent the running buffer from overheating.
15. If there is more than one membrane, number the corners with a pencil. Do not handle the membrane with bare hands.
16. Soaking the PVDF membrane in methanol prevents proteins from passing straight through the membrane.
17. After the transfer, you can stain the gel with Coomassie blue to check whether the transfer is complete.
18. Non-fat dry milk in PBST is a typical and cheap blocking solution. Alternatively, 2% BSA in PBST also works well.
19. It is very important to use sufficient wash solution. For a typical membrane in a small container (i.e. empty tip-box lid), 15–20 ml is optimal. Insufficient washing will result in high background, and salt helps reduce the background.
20. Always develop in the dark room as this allows the incubation period in ECL reagent to be accurately controlled and prevents problems arising from the dark room availability.
21. Ensure that the film is sealed away before turning on the white light or opening the door as this will expose the film and render it useless.
22. Membranes can be stored in PBS at 4°C indefinitely and also can be stained by Coomassie blue for checking the transfer.
23. Prepare duplicate or triplicate cryosection slides in case you need to repeat immunostaining, and all the cryosections can be kept in the slide box and stored at –80°C.
24. The liquid-repellent slide marker prevents the sections from detaching from the slides.
25. We have tested three different dystrophin primary antibodies, including two in-house rabbit polyclonal antibodies and one commercially available rabbit polyclonal antibody, and found that they all work well although the commercial antibody has slightly high background.
26. DAPI for nuclei counterstaining and the slides can be stored in room temperature up to 3 months.
27. Two drops of avidin/biotin is sufficient to cover the sections on the slide.
28. The blocking time can be adjusted according to the background.

29. For nNOS staining, the whole procedure is the same as for dystrophin except the incubation with primary antibody is overnight at 4°C.
30. The time needs to be accurate at this step.
31. The incubation time can be optimised according to the intensity of the signals, but ensure that you always have a negative control (for secondary antibody only).

Acknowledgments

This work was supported by UK Department of Health and the UK Muscular Dystrophy Campaign. The authors would like to thank the UK MDEX Consortium for helpful discussions and support. They would also like to thank Professor Kay Davies, Department of Physiology, Anatomy and Genetics, University of Oxford for providing access to facilities including the *mdx* mouse colony.

References

1. Davies, K. E. and Nowak, K. J. (2006) Molecular mechanisms of muscular dystrophies: old and new players, *Nat Rev Mol Cell Biol* **7**, 762–773.
2. Muntoni, F., Torelli, S., and Ferlini, A. (2003) Dystrophin and mutations: one gene, several proteins, multiple phenotypes, *Lancet Neurol* **2**, 731–740.
3. van Deutekom, J. C. and van Ommen, G. J. (2003) Advances in Duchenne muscular dystrophy gene therapy, *Nat Rev Genet* **4**, 774–783.
4. Aartsma-Rus, A., Janson, A. A., Kaman, W. E., Bremmer-Bout, M., den Dunnen, J. T., Baas, F., van Ommen, G. J., and van Deutekom, J. C. (2003) Therapeutic antisense-induced exon skipping in cultured muscle cells from six different DMD patients, *Hum Mol Genet* **12**, 907–914.
5. Alter, J., Lou, F., Rabinowitz, A., Yin, H., Rosenfeld, J., Wilton, S. D., Partridge, T. A., and Lu, Q. L. (2006) Systemic delivery of morpholino oligonucleotide restores dystrophin expression bodywide and improves dystrophic pathology, *Nat Med* **12**, 175–177.
6. Jearawiriyapaisarn, N., Moulton, H. M., Buckley, B., Roberts, J., Sazani, P., Fucharoen, S., Iversen, P. L., and Kole, R. (2008) Sustained dystrophin expression induced by peptide-conjugated morpholino oligomers in the muscles of *mdx* mice, *Mol Ther* **16**, 1624–1629.
7. Lu, Q. L., Mann, C. J., Lou, F., Bou-Gharios, G., Morris, G. E., Xue, S. A., Fletcher, S., Partridge, T. A., and Wilton, S. D. (2003) Functional amounts of dystrophin produced by skipping the mutated exon in the *mdx* dystrophic mouse, *Nat Med* **9**, 1009–1014.
8. Lu, Q. L., Rabinowitz, A., Chen, Y. C., Yokota, T., Yin, H., Alter, J., Jadoon, A., Bou-Gharios, G., and Partridge, T. (2005) Systemic delivery of antisense oligoribonucleotide restores dystrophin expression in body-wide skeletal muscles, *Proc Natl Acad Sci U S A* **102**, 198–203.
9. van Deutekom, J. C., Bremmer-Bout, M., Janson, A. A., Ginjaar, I. B., Baas, F., den Dunnen, J. T., and van Ommen, G. J. (2001) Antisense-induced exon skipping restores dystrophin expression in DMD patient derived muscle cells, *Hum Mol Genet* **10**, 1547–1554.
10. Wu, B., Moulton, H. M., Iversen, P. L., Jiang, J., Li, J., Spurney, C. F., Sali, A., Guerron, A. D., Nagaraju, K., Doran, T., Lu, P., Xiao, X., and Lu, Q. L. (2008) Effective rescue of dystrophin improves cardiac function in dystrophin-deficient mice by a modified morpholino oligomer, *Proc Natl Acad Sci U S A* **105**, 14814–14819.

11. Yin, H., Lu, Q., and Wood, M. (2008) Effective exon skipping and restoration of dystrophin expression by peptide nucleic acid antisense oligonucleotides in mdx mice, *Mol Ther* **16**, 38–45.
12. Yin, H., Moulton, H. M., Seow, Y., Boyd, C., Boutilier, J., Iverson, P., and Wood, M. J. (2008) Cell-penetrating peptide-conjugated antisense oligonucleotides restore systemic muscle and cardiac dystrophin expression and function, *Hum Mol Genet* **17**, 3909–3918.
13. Arechavala-Gomez, V., Graham, I. R., Popplewell, L. J., Adams, A. M., Aartsma-Rus, A., Kinali, M., Morgan, J. E., van Deutekom, J. C., Wilton, S. D., Dickson, G., and Muntoni, F. (2007) Comparative analysis of antisense oligonucleotide sequences for targeted skipping of exon 51 during dystrophin pre-mRNA splicing in human muscle, *Hum Gene Ther* **18**, 798–810.
14. Kinali, M., Arechavala-Gomez, V., Feng, L., Cirak, S., Hunt, D., Adkin, C., Guglieri, M., Ashton, E., Abbs, S., Nihoyannopoulos, P., Garralda, M. E., Rutherford, M., McCulley, C., Popplewell, L., Graham, I. R., Dickson, G., Wood, M. J., Wells, D. J., Wilton, S. D., Kole, R., Straub, V., Bushby, K., Sewry, C., Morgan, J. E., and Muntoni, F. (2009) Local restoration of dystrophin expression with the morpholino oligomer AVI-4658 in Duchenne muscular dystrophy: a single-blind, placebo-controlled, dose-escalation, proof-of-concept study, *Lancet Neurol* **8**, 918–928.
15. van Deutekom, J. C., Janson, A. A., Ginjaar, I. B., Frankhuizen, W. S., Aartsma-Rus, A., Bremmer-Bout, M., den Dunnen, J. T., Koop, K., van der Kooi, A. J., Goemans, N. M., de Kimpe, S. J., Ekhardt, P. F., Venneker, E. H., Platenburg, G. J., Verschuuren, J. J., and van Ommen, G. J. (2007) Local dystrophin restoration with antisense oligonucleotide PRO051, *N Engl J Med* **357**, 2677–2686.
16. Aartsma-Rus, A., Fokkema, I., Verschuuren, J., Ginjaar, I., van Deutekom, J., van Ommen, G. J., and den Dunnen, J. T. (2009) Theoretic applicability of antisense-mediated exon skipping for Duchenne muscular dystrophy mutations, *Hum Mutat* **30**, 293–299.
17. Moulton, H. M., Fletcher, S., Neuman, B. W., McClorey, G., Stein, D. A., Abes, S., Wilton, S. D., Buchmeier, M. J., Lebleu, B., and Iverson, P. L. (2007) Cell-penetrating peptide-morpholino conjugates alter pre-mRNA splicing of DMD (Duchenne muscular dystrophy) and inhibit murine coronavirus replication in vivo, *Biochem Soc Trans* **35**, 826–828.
18. Wu, B., Li, Y., Morcos, P. A., Doran, T. J., Lu, P., and Lu, Q. L. (2009) Octa-guanidine morpholino restores dystrophin expression in cardiac and skeletal muscles and ameliorates pathology in dystrophic mdx mice, *Mol Ther* **17**, 864–871.
19. Yokota, T., Lu, Q. L., Partridge, T., Kobayashi, M., Nakamura, A., Takeda, S., and Hoffman, E. (2009) Efficacy of systemic morpholino exon-skipping in duchenne dystrophy dogs, *Ann Neurol* **65**, 667–76.
20. Ivanova, G. D., Arzumanov, A., Abes, R., Yin, H., Wood, M. J., Lebleu, B., and Gait, M. J. (2008) Improved cell-penetrating peptide-PNA conjugates for splicing redirection in HeLa cells and exon skipping in mdx mouse muscle, *Nucleic Acids Res* **36**, 6418–6428.
21. Ivanova, G. D., Fabani, M. M., Arzumanov, A. A., Abes, R., Yin, H., Lebleu, B., Wood, M., and Gait, M. J. (2008) PNA-peptide conjugates as intracellular gene control agents, *Nucleic Acids Symp Ser (Oxf)* **31**–32.
22. Yin, H., Moulton, H. M., Betts, C., Seow, Y., Boutilier, J., Iverson, P. L., and Wood, M. J. (2009) A fusion peptide directs enhanced systemic dystrophin exon skipping and functional restoration in dystrophin-deficient mdx mice, *Hum Mol Genet* **18**, 4405–4414.

PTD–DRBD siRNA Delivery

Caroline Palm-Apergi, Akiko Eguchi, and Steven F. Dowdy

Abstract

A major hurdle in drug delivery today is for the drug to reach inside the cell to exert its biological effect. Many drug candidates are hydrophilic and are therefore not able to cross the hydrophobic plasma membrane, which serves to protect the cell from foreign molecules and pathogens. One promising drug candidate is the hydrophilic and negatively charged short-interfering RNA (siRNA), known to degrade target mRNA 1,000-fold more efficiently than small molecule drugs. The delivery capacity of small cationic peptides called protein transduction domains or cell-penetrating peptides, suggested them to be suitable delivery vehicles for siRNA. However, it has proven troublesome to utilize the PTD–siRNA conjugates for mRNA degradation due to the characteristics of siRNA, often resulting in precipitation and aggregation. This chapter describes a recently reported delivery strategy, PTD–DRBD fusion protein siRNA delivery, where a double-stranded RNA-binding domain expressed as a fusion protein together with three TAT PTDs binds the siRNA, thus masking the negatively charged backbone and preventing aggregation. This new protocol results in noncytotoxic mRNA degradation even more effective than lipofection.

Key words: CPP, PTD, siRNA, RNAi, Double-stranded RNA binding domain

1. Introduction

One of the greatest hindrances in delivery of hydrophilic drugs is to cross the hydrophobic plasma membrane, in order to reach the cytoplasm or nucleus to exert their therapeutic effect. Several transporters in the plasma membrane are able to internalize smaller molecules but for larger macromolecules such as peptides, proteins, and oligonucleotides, a delivery vehicle is needed to transport the cargo to the cytoplasm or nucleus. Thus, there is a great need to design drug delivery vehicles able to cross the protective plasma membrane without inducing toxicity. Twenty years ago it was found that certain proteins alone were able internalize

cells (1). From these proteins, a new group of transporters named protein transduction domains (PTDs) or cell-penetrating peptides (CPPs) has evolved. These drug delivery vehicles have been shown to deliver different cargo into the cell such as drugs and oligonucleotides both in vivo and in vitro (2, 3). One of these PTDs belongs to the human immunodeficiency virus type 1 (HIV-1) and is derived from the *trans*-activator of transcription (TAT) protein (4).

Around a decade ago, it was found that short double-stranded RNAs can target and degrade mRNA in a process called RNA interference (RNAi) (5). During RNAi, a ribonuclease III (RNaseIII) enzyme named Dicer, cleaves endogenous long double-stranded RNA into 21–23 mer RNA duplexes, resulting in a 5'-phosphate group and 2-nucleotide 3' overhangs. After cleavage, the duplex is unwound and one of the strands, known as the antisense or guide strand, is loaded into the RNA-induced silencing complex (RISC). Concurrently, the other sense strand is cleaved by another protein named Argonaute 2 (Ago2). The RISC-antisense strand complex then directs an endonuclease to cleave complementary mRNAs repeatedly. Due to the sequence-specificity of this three-step process, a new field of therapeutic drug design has opened up.

In the diverse class of double-stranded RNA binding proteins (DRBP), there are certain domains that bind double-stranded RNA. These double-stranded RNA binding domains (DRBDs) are highly abundant and can be found in different organisms such as *Escherichia coli* and man. A consensus sequence of about 65–68 amino acid residues specific for binding dsRNA was identified in 1992 (6). The DRBPs have different functions but are similar in that they contain varying copies of DRBDs. A minimum number of 16 bp of siRNAs are required for binding, however, for longer RNAs only 11 bp are required (7). DRBDs are known to bind the compressed A-form of siRNA sequence independently and almost without changing the structure. The binding occurs between the sugar phosphate backbone and each 2'-OH group of every 11-mer is involved in the interaction. Consequently, DRBDs cannot bind dsDNA or even RNA/DNA hybrids, since dsDNA is predominantly found in the more open B-form (7). Three regions are responsible for binding the dsRNA where two of three bind the minor groove and one binds the major groove. By making a fusion protein of three TAT peptides and a DRBD (PTD-DRBD), the previous obstacles in siRNA delivery can be overcome (3). Thus, the PTD-DRBD fusion protein serves as an excellent vehicle for siRNA delivery. A detailed protocol of the design, construction, and purification of the PTD-DRBD is described below followed by several methods that can be utilized to assess the siRNA delivery and resulting knockdown.

2. Materials

A wide range of cell lines can be used in PTD-DRBD siRNA delivery (3). For simplicity, only one cell line will be described in the delivery protocols, namely, the dGFP-H1299 cell line expressing destabilized GFP. However, in the IFN- α and TNF- α analyses, human peripheral blood mononuclear cells (PMBCs) isolated from healthy donors are preferably used, and, in the immunohistochemistry section, a human embryonic stem cell line HUES 9 (H9 hES) is to be used.

2.1. PTD-DRBD Fusion Protein Design, Construction, and Purification

1. BL21 codon plus (DE3) *E. coli* (Stratagene) grown in Luria Bertani medium containing kanamycin.
2. PCR-cloned PKR DRBD-1-modified pTAT vector (8) resulting in TAT-TAT-HA tag-TAT-DRBD-6xHis.
3. Kanamycin-containing agar plates.
4. Ni-NTA column (Qiagen).
5. 400 μ M Isopropyl- β -D-thiogalactoside.
6. Imidazole.
7. Buffer A (20 mM HEPES [pH 7.5], 500 mM NaCl, 5 μ g/ml aprotinin, 1 μ g/ml leupeptin, 0.8 mM phenylmethylsulfonyl fluoride [PMSF]) plus 20 mM imidazole.
8. Buffer B (50 mM HEPES [pH 7.5], 20 mM NaCl, 5% glycerol).
9. Buffer C (Buffer B plus 1.5 M NaCl).
10. PD-10 column.
11. PBS with 10% glycerol.
12. EGFP-PEST (dGFP) or DsRed-PEST (dDsRed) lentiviruses produced by pCSC-SP-CW-EGFP-PEST or pCSC-SP-CW-DSRED (9) and pd2EGFP-N1- (destabilized GFP; BD Clontech) or pDsRed-Express-DR (destabilized DsRed; BD Clontech).
13. Mono-S AKAT FPLC.

2.2. PTD-DRBD siRNA Delivery into Cells

1. dGFP-H1299 cells cultured in Dulbecco's Modified Eagle's Media (DMEM) supplemented with 10% fetal bovine serum (FBS), 100 μ g/ml streptomycin, 100 U/ml penicillin.
2. 48-Well plates.
3. 10 μ l of 1–5 μ M (EGFP1 [Ambion predesigned siRNA], EGFP2 [Ambion Silencer GFP], Silencer Negative [control 1; Ambion], and/or luciferase [control 2; Dharmacon] siRNA) siRNA in water.

4. 10 μ l of 10–50 μ M PTD–DRBD in PBS with 10% glycerol.
5. Trypsin/EDTA.
6. Source 30Q resin (Amersham Bioscience).
7. Lipofectamine-2000 and Lipofectamine-RNAiMAX (Invitrogen).

2.3. Immunoblotting

1. dGFP-H1299 cells cultured in DMEM supplemented with 10% FBS, 100 μ g/ml streptomycin, 100 U/ml penicillin.
2. 48-Well plates.
3. Trypsin/EDTA.
4. RIPA buffer (1% TritonX-100, 1% sodium deoxycholate, 40 mM Tris–HCl, 150 mM NaCl, 0.2% SDS, 5 μ g/ml aprotinin, 1 μ g/ml leupeptin, 0.8 mM phenylmethylsulfonyl fluoride).
5. 10% SDS–PAGE.
6. Polyvinyl difluoride membranes.
7. 4% Skim milk.
8. PBS-T (0.05% PBS, Tween20).
9. OCT4 (Ambion predesigned), Silencer Negative (control 1; Ambion), and/or luciferase (control 2; Dharmacon) siRNA.
10. PTD–DRBD in PBS with 10% glycerol.
11. Anti-OCT4 (Santa Cruz), anti-GAPDH (Santa Cruz), and anti- α -tubulin (Sigma) antibodies.
12. HRP-conjugated anti-IgG (Santa Cruz) antibodies.
13. Electrochemical luminescence (Pierce).

2.4. RT-PCR and Microarrays

1. dGFP-H1299 cells cultured in DMEM supplemented with 10% FBS, 100 μ g/ml streptomycin, 100 U/ml penicillin.
2. 48-Well plates.
3. 400 nM GAPDH1 (Ambion), GAPDH2 (Ambion), Silencer Negative (control 1; Ambion), and/or luciferase (control 2; Dharmacon) siRNA.
4. PTD–DRBD in PBS with 10% glycerol.
5. RNeasy Mini Kit (QIAGEN).
6. Omniscript RT kit (QIAGEN) with Oligo-dT and RNase OUT.
7. 2 \times Universal Mastermix (Ambion) and TaqMan 20 \times probe.
8. 7300 Real-time PCR system (Applied Biosystems).
9. Whole genome microarray chip (Illumina).

2.5. Immunohistochemistry and Flow Cytometry Analysis

1. dGFP-H1299 cells cultured in DMEM supplemented with 10% FBS, 100 µg/ml streptomycin, 100 U/ml penicillin, and H9 hES cells cultured in 20% knockout serum-DMEM-F12 plus 55 µM β-mercaptoethanol, nonessential amino acids, Gluta-Max, 4 ng/ml bFGF, and antibiotics on murine fibroblast feeder layer.
2. 48-Well plates.
3. 4% Paraformaldehyde.
4. 0.1% TritonX-100 in PBS.
5. 3% Skim milk in PBS.
6. 0.1% BSA in PBS.
7. OCT4 (Ambion predesigned), Nanog (Ambion predesigned), Sox2 (Ambion predesigned), DsRed (Ambion predesigned), EGFP1 (Ambion predesigned siRNA), EGFP2 (Ambion Silencer GFP), Silencer Negative (control 1; Ambion), and/or luciferase (control 2; Dharmacon) siRNA.
8. PTD-DRBD in PBS with 10% glycerol.
9. Anti-OCT4 (Santa Cruz), anti-SSEA4 (Santa Cruz), and anti-GATA6 (Santa Cruz) antibodies.
10. Alexa488- or Alexa594-conjugated anti-IgG (Molecular Probes).
11. Hoechst 33342 (Molecular Probes).
12. Confocal microscope (Olympus Flouview).
13. FACScan (BD Biosciences).

2.6. IFN-α and TNF-α Analyses

1. PBMCs isolated from healthy donors.
2. Ficoll-Paque PLUSTM density medium (Amersham Biosciences).
3. 96-Well plates.
4. PBS.
5. 100 nM β-gal (Dharmacon) siRNA.
6. PTD-DRBD in PBS with 10% glycerol.
7. Lipofectamine 2000 (Invitrogen).
8. Imiquimid 10 µg/ml.
9. LPS 10 µg/ml.
10. ELISA (R&D systems).

3. Methods

Several studies have used PTDs to deliver siRNA to the cytoplasm both as covalently linked conjugates or electrostatically bound

complexes. However, the efficiency has not been satisfying because of the cationic properties of the PTDs together with the anionic characteristics of the siRNAs, leading to aggregation or precipitation. In this new strategy, the PTD–DRBD masks the negative charges of the siRNA. Thus, the positively charged side chains of the peptide can interact with the proteoglycans in the plasma membrane and induce internalization. The PTD–DRBD is expressed as a fusion protein containing three TAT sequences and a DRBD. When siRNA is bound to the PTD–DRBD fusion protein, efficient knockdown of target mRNA is accomplished in a noncytotoxic manner. Herein, a protocol for the DRBD–PTD siRNA design, construction, and purification is presented as well as delivery and knockdown analysis protocols.

3.1. PTD–DRBD Fusion Protein Design, Construction, and Purification

1. pPTD–DRBD is constructed by PCR cloning of PKR DRBD-1 into a modified pTAT vector (8) resulting in TAT–TAT–HA tag–TAT–DRBD–6xHis (see Notes 1 and 2).
2. For PTD–DRBD expression use BL21 codon plus (DE3) *E. coli* (Stratagene).
3. Transform a 50 μ l stock of BL21 codon plus (DE3) *E. coli* (Stratagene) cells with pPTD–DRBD.
4. Streak the cells onto a Kanamycin-containing plate and incubate for 12 h at 37°C.
5. Culture the cells in Luria Bertani broth containing kanamycin at 37°C until optimal bacterial density is reached.
6. Add isopropyl- β -D-thiogalactoside to a final concentration of 400 μ M and culture the cells at 25°C for 12 h.
7. Recover the cells by centrifugation for 5 min at 4,500 $\times g$.
8. Sonicate the cell pellet in Buffer A plus 20 mM imidazole on ice.
9. Isolate soluble protein by centrifugation for 15 min at 50,000 $\times g$.
10. Purify the PTD–DRBD containing supernatant on a column containing 5 ml of Ni–NTA resin (Qiagen) pre-equilibrated in Buffer A plus 20 mM imidazole.
11. Wash the column and elute the PTD–DRBD with Buffer A plus 100, 250, 500 mM, and 1 M imidazole.
12. Pool PTD–DRBD fractions and load onto a Mono-S column on an AKAT FPLC in Buffer B.
13. Use an exchange gradient from Buffer B to Buffer C and elute in Buffer C.
14. Pool PTD–DRBD fractions and desalt using PD-10 columns into PBS-10% glycerol.
15. Store at –80°C.

**3.2. PTD-DRBD siRNA
Delivery into Cells**

1. Seed 60,000 cells in 48-well plates 1 day before treatment.
2. Mix 10 μ l of 1–5 μ M siRNA in water, 10 μ l of 10–50 μ M PTD-DRBD in PBS containing 10% glycerol, and 5 μ l PBS containing 10% glycerol in an Eppendorf tube.
3. Pipette up and down quickly ~15 times.
4. Leave mixture on ice for 30 min.
5. Dilute mixture in serum-free medium 1:5.
6. Add mixture to cells and incubate 1–6 h at 37°C (see Notes 3 and 4).
7. Wash the cells with trypsin/EDTA for 10 min (see Note 5).
8. Add fresh medium containing 10% FBS to the cells.
9. Incubate the cells at 37°C for 6–48 h.
10. Analyze knockdown by FACScan.

3.3. Immunoblotting

1. Seed 60,000 cells in 48-well plates 1 day before treatment.
2. Treat cells as described in Subheading 3.2.
3. Recover the cells with trypsin/EDTA.
4. Lyse the cells in RIPA buffer for 30 min on ice, centrifuge, and resolve proteins by 10% SDS-PAGE.
5. Immunoblot on polyvinyl difluoride membranes blocked in 4% skim milk, PBS-T (0.05% PBS, Tween20) for 1 h at 21°C.
6. Incubate membranes with anti-OCT4 (Santa Cruz), anti-GAPDH (Santa Cruz), and anti- α -tubulin (Sigma) antibodies overnight at 4°C.
7. Wash and expose membranes to HRP-conjugated anti-IgG (Santa Cruz) antibodies and detect proteins by electrochemical luminescence (Pierce).

**3.4. RT-PCR
and Microarrays**

1. Seed 60,000 cells in 48-well plates 1 day before treatment.
2. Treat cells with 400 nM GAPDH, control Silencer Negative or control luciferase siRNA as described in Subheading 3.2.
3. Isolate total RNA after 6, 12, 24, 36, 72, and 96 h by RNeasy Mini Kit.
4. Make cDNA by Omniscript RT kit (QIAGEN) with Oligo-dT and RNase OUT.
5. Mix cDNA and TaqMan probe (Ambion) to detect GAPDH mRNA expression on a 7300 real-time PCR system (Applied Biosystems) (see Note 6).
6. For whole-genome microarray analysis, treat the cells as described above and use isolated RNA after 12 and 24 h to probe whole-genome microarrays (Illumina).

3.5. Immunohistochemistry and Flow Cytometry Analysis

1. Seed 60,000 cells in 48-well plates 1 day before treatment.
2. Treat cells as described in Subheading 3.2.
3. Fix the cells with 4% paraformaldehyde for 30 min at 21°C.
4. Permeabilize the cells in 0.1% TritonX-100–PBS for 15 min at 21°C.
5. Block in 3% skim milk–PBS for 30 min at 21°C.
6. Incubate with anti-OCT4 (Santa Cruz), anti-SSEA4 (Santa Cruz), and anti-GATA6 (Santa Cruz) antibodies in 0.1% BSA–PBS overnight at 4°C.
7. Wash the cells and incubate with either Alexa488- or Alexa594-conjugated anti-IgG (Molecular Probes) for 30 min at 21°C.
8. Counter stain DNA with Hoechst 33342 (Molecular Probes).
9. Analyze cells by confocal microscopy (Olympus Flouview).
10. For flow cytometry, analyze 1×10^4 dGFP- and/or dDsRed-positive cells on a FACScan (BD Biosciences).

3.6. IFN- α and TNF- α Analyses

1. Isolate PBMCs by standard density gradient centrifugation with Ficoll_Paque PLUS™ at $800 \times g$ for 20 min at 20°C.
2. Wash PBMCs 4 \times with PBS.
3. Centrifuge at $450 \times g$ for 8 min at 4°C (see Note 7).
4. Treat 800,000 freshly isolated PBMCs with 100 nM β -gal siRNA (10) together with PTD–DRBD or lipofectamine 2000. As a positive control, treat PBMCs with 10 μ g/ml imiquimod and 10 μ g/ml LPS (see Note 8).
5. Seed-treated cells into a 96-well plate and collect culture supernatants at 4 and 24 h.
6. Assay for IFN- α and TNF- α by ELISA (R&D systems).

4. Notes

1. The hemagglutinin (HA) epitope tag is used to follow the protein by immunoblot analysis.
2. The 6xHis tag is used for purification over the first column, Ni–NTA.
3. Final peptide concentration should be 100–500 nM.
4. For control siRNA lipofections, treat cells with a dose curve that yields the highest RNAi response with 100 nM siRNA in Lipofectamine-2000 (Invitrogen) or 10–50 nM siRNA in Lipofectamine-RNAiMAX (Invitrogen) per the manufacturer's instructions.

5. This is done to remove extracellular PTD-DRBD:siRNA.
6. Mean values are normalized to $\beta 2$ microglobulin and reported as percent of mock GAPDH control.
7. This is done to remove platelets.
8. Imiquimod and LPS is used to induce IFN- α and TNF- α , respectively.

Acknowledgments

C.P.-A. was funded by a Knut & Alice Wallenberg's Foundation Research Fellowship. A.E. was funded by a JSPS Research Fellowships for Young Scientists. This work was supported by the Leukemia and Lymphoma Society, the Pardee Foundation, California Institute of Regenerative Medicine, and Howard Hughes Medical Institute.

References

1. Frankel, A. D. and Pabo, C. O. (1988) Cellular uptake of the tat protein from human immunodeficiency virus. *Cell* **55**, 1189–1193.
2. Snyder, E. L. and Dowdy, S. F. (2004) Cell penetrating peptides in drug delivery. *Pharm Res* **21**, 389–393.
3. Eguchi, A., Meade, B. R., Chang, Y. C., Fredrickson, C. T., Willert, K., Puri, N., and Dowdy, S. F. (2009) Efficient siRNA delivery into primary cells by a peptide transduction domain-dsRNA binding domain fusion protein. *Nat Biotechnol* **27**, 567–571.
4. Vives, E., Brodin, P., and Lebleu, B. (1997) A truncated HIV-1 Tat protein basic domain rapidly translocates through the plasma membrane and accumulates in the cell nucleus. *J Biol Chem* **272**, 16010–16017.
5. Fire, A., Xu, S., Montgomery, M. K., Kostas, S. A., Driver, S. E., and Mello, C. C. (1998) Potent and specific genetic interference by doublestranded RNA in *Caenorhabditis elegans*. *Nature* **391**, 806–811.
6. St Johnston, D., Brown, N. H., Gall, J. G., and Jantsch, M. (1992) A conserved double-stranded RNA-binding domain. *Proc Natl Acad Sci U S A* **89**, 10979–10983.
7. Bevilacqua, P. C. and Cech, T. R. (1996) Minor-groove recognition of double-stranded RNA by the double-stranded RNA-binding domain from the RNA-activated protein kinase PKR. *Biochemistry* **35**, 9983–9984.
8. Wadia, J. S., Stan, R. V., and Dowdy, S. F. (2004) Transducible TAT-HA fusogenic peptide enhances escape of TAT-fusion proteins after lipid raft macropinocytosis. *Nat Med* **10**, 310–315.
9. Miyoshi, H., Blömer, U., Takahashi, M., Gage, F. H., and Verma, I. M. (1998) Development of a self-inactivating lentivirus vector. *J Virol* **72**, 8150–8157.
10. Judge, A. D., Bola, G., Lee, A. C., and MacLachlan, I. (2006) Design of noninflammatory synthetic siRNA mediating potent gene silencing in vivo. *Mol Ther* **13**, 494–505.

A Non-Covalent Peptide-Based Strategy for siRNA Delivery

Laurence Crombez and Gilles Divita

Abstract

The development of short-interfering RNA (siRNA) has provided great hope for therapeutic targeting of specific genes responsible for pathological disorders. However, the poor cellular uptake of siRNA together with the low permeability of the cell membrane to negatively charged molecules, remain major obstacles to clinical development. So far there is no universal method for siRNA delivery as they all present several limitations. Several non-viral strategies have been proposed to improve the delivery of synthetic siRNAs in both cultured cells and in vivo. Cell-penetrating peptides (CPPs) or protein transduction domains (PTD) constitute very promising tools for non-invasive cellular import of siRNA and non-covalent CPP/PTD-based strategies have been successfully applied for ex vivo and in vivo delivery of therapeutic siRNA molecules. We recently described a new peptide-based system, CADY, for efficient delivery of siRNA in both primary and suspension cell lines. CADY is a secondary amphiphatic peptide able to form stable non-covalent complexes with siRNA and to improve their cellular uptake independently of the endosomal pathway. This chapter describes easy to handle protocols for the use of the CADY-nanoparticle technology for the delivery of siRNA into both adherent and suspension cell lines. It will also highlight different critical points in the peptide/siRNA complex preparation and transfection protocols, in order to obtain siRNA-associated interfering response at low nanomolar concentration.

Key words: Cell-penetrating peptide, Peptide-based non-covalent strategy, Amphiphatic peptide, Non-endosomal pathway, siRNA delivery

1. Introduction

The discovery and development of siRNA has provided great hope for therapeutic targeting of specific genes responsible for pathological disorders (1). Nowadays short-interfering RNAs (siRNA) constitute powerful biomedical tools to specifically control protein activation and/or gene expression post-transcriptionally, with the aim of understanding their function and/or developing therapeutic strategies (2, 3). However, the major obstacle to clinical application of siRNA, like most antisense- or nucleic acid-based

strategies, remains their poor cellular uptake associated with the low permeability of the cell membrane to negatively charged molecules. Therefore, several viral and non-viral strategies have been proposed to improve the delivery of either siRNA-expressing vectors or synthetic siRNAs in both cultured cells and *in vivo*, including lipids, cationic polymers, antibody–protamines, RNA-aptamers, nanoparticles, and cell-penetrating peptides (CPP) (4–7).

Nowadays, CPP or protein transduction domain (PTD) constitute very promising tools for non-invasive cellular import of cargo and have been successfully applied for *ex vivo* and *in vivo* delivery of therapeutic molecules (8–10). PTD/CPP can be grouped into two major classes, the first requiring chemical linkage with the drug for cellular internalization and the second involving formation of stable, non-covalent complexes with drugs (9). However, delivery of charged oligonucleotides and siRNA is more challenging as multiple anionic charges of the nucleic acid interact with CPP moiety and inhibit uptakes by steric hindrance. Recently, CPPs have also been optimized for siRNA delivery (7, 11, 12). Although conjugation strategy with either Transportan (13), Penetratin (14), or Tat (15), certainly improve the delivery of siRNA into cultured cells, nevertheless, non-covalent strategies appear to be more appropriate for siRNA delivery and yield significant-associated biological response (7, 11, 12). The primary amphiphatic MPG peptide has been reported to improve siRNA delivery *ex vivo* into a large panel of cell lines (16–18) and *in vivo* of siRNA targeting either OCT-4 into mouse blastocytes (19) or Cyclin B1, an essential cell cycle protein, into tumour model mice (20). The non-covalent approach has been extended to other CPPs including polyarginine (21–23) and Penetratin (24)-derived peptides. Tat peptide associated with an RNA binding motif has been reported to block *in vivo* EGF factor (25), cholesterol-Arg9 has been shown to enhance siRNA delivery *in vivo* against vascular endothelial growth factors (21) and a small peptide derived from rabies virus glycoprotein (RVG) associated to poly-arginine R9 has been shown to deliver siRNA in the CNS (22).

We have recently described a new peptide-based strategy for siRNA delivery based on a secondary amphiphatic peptide: CADY (26). CADY is a short 20-residue peptide (Ac-GLWRALWRLLRSLWRLLWRA-cysteamide) derived from PPTG1, a variant of the JTS1 fusion peptide (27). In order to improve both interaction of the peptide with siRNA and its ability to interact with the lipid phase of the membrane, seven residues of PPTG1 were changed, Phe³, Leu⁷, Leu¹⁸ and Lys⁴, Lys⁸, Lys¹¹ being mutated into Trp and Arg, respectively. When associated to phospholipids or siRNA, CADY-carrier adopts a helical conformation, whilst exposing charged residues on one side, and Trp groups that favour cellular uptake on the other (26). We have demonstrated that

CADY-peptide forms stable complex with siRNA, through non-covalent interactions, thereby increasing their stability and improving their delivery into a wide variety of cell lines, including suspension and primary cell lines. CADY-mediated siRNA cellular uptake mechanism is independent of the major endocytosis pathways and controlled by both CADY structural versatility and its ability to interact with phospholipids (26, 28).

This chapter will describe easy to handle protocols for the use of the non-covalent CADY technology for the delivery of siRNA into mammalian adherent and “hard-to-transfect” suspension cell lines.

2. Materials

2.1. Cell Lines and Cell Cultures

Phosphate-buffered saline (PBS) (Cat No. 14190-169), Dulbecco's Modified Eagle's Medium (DMEM) (Cat No. 41965-062), glutamine, streptomycin/penicillin (Cat No. 15140-130) were from Invitrogen Life Technologies (Carlsbad-USA). Foetal bovine serum (FBS) is from PERBIO (Lot 3264EHJ, Cat No. CH30160-03). The HeLa, human osteosarcoma U₂OS, THP-1 monocytes, and Jurkat clone E6-1 (derived from human acute T-cell leukaemia) cell lines were obtained from the American Type Culture Collection (Manassas, VA, USA). U₂OS cells were maintained as monolayer cultures in DMEM supplemented with 10% foetal calf serum (FCS). THP-1 and Jurkat suspension cell lines were cultured in RPMI-1640 medium supplemented with 10% FCS and 0.05 mM 2-mercaptoethanol.

2.2. Oligonucleotides and siRNAs

The siRNAs targeting *gapdh* mRNA (5'-CAUCAUCCCUGCCUCUACUTT-3' for the sense strand) were obtained HPLC purified from Eurogentec (Belgium). The stock solution of siRNA was prepared at a concentration of 5 μM in 50 mM Tris-HCl pH 7.0, 0.5 mM EDTA buffer or in RNase-free water.

2.3. Peptide Carrier CADY

CADY (20-residues: Ac-GLWRALWRLRLSLWRLWRA-cya; MW: 2,653 Da) was synthesized by solid-phase peptide synthesis using AEDI-expensin resin with (fluorenylmethoxy)-carbonyl (Fmoc) continuous (Pioneer, Applied Biosystems, Foster city, CA) as described previously (26, 29). CADY was purified by semi-preparative reverse-phase high performance liquid chromatography (RP-HPLC; C18 column Interchrom UP5 WOD/25M Uptisphere 300 5 ODB, 250×21.2 mm) and identified by electrospray mass spectrometry and amino acid analysis (26). The peptide is acetylated at its N-terminus and carried a cysteamide group at its C-terminus, both of which are essential for CADY stability, cellular uptake, and formation of CADY/siRNA particles (26).

Peptide can be synthesized in house or obtained from commercial sources (Panomics/Affimetrix Inc., Cat No.: DX005). CADY is stable for at least 1 year when stored at -20°C in lyophilized form.

2.4. Other Reagents

PBS pH 7.4 (Gibco, REF: 1098-040), Ultra-Pure DNase–RNase-free Sterile Water (GIBCO/REF: 10977-035), dimethyl sulfoxide (DMSO) (Sigma: REF IS0467), Trypsine–EDTA (Sigma REF: G4876), Bradford Protein Assay (Pierce Inc.), QuantiGene® 2.0 Reagent System (Panomics/Affymetrix: Cat No.: QS0012), Monoclonal mouse primary antibodies anti-GAPDH (6C5) (Santa Cruz Biotechnology), Rabbit anti-actin antibody (Sigma), Sheep secondary anti-mouse HRP-linked whole antibody (GE Healthcare).

3. Methods

The protocol described below outline (1) the formation and storage of CADY/siRNA complexes and optimized protocols for siRNA transfection, (2) in mammalian adherent, and (3) suspension “hard-to-transfect” cell lines. The different procedures were performed using an siRNA targeting *gapdh* gene and modified according to ref. (26).

3.1. Preparation of CADY/siRNA Complexes

The procedure for complex formation constitutes a major factor in the success and efficiency of CADY technology and should be followed carefully (see Notes 1 and 2).

3.1.1. Stock Solutions of Vector-Peptide CADY and siRNA

1. Take the vial containing the peptide powder out of the freezer and equilibrate for 30 min at room temperature without opening the vial. Resuspend CADY at a final concentration of 2 mg/ml (774.5 μM) in ultra pure water RNase, DNase free (GIBCO/REF: 10977-035), and 2% DMSO. CADY powder should be first solubilized directly in DMSO, then add calculated volume of water to reach the 2 mg/ml final CADY concentration and 2% DMSO.
2. Mix gently by tapping the tube.
3. Sonicate the CADY solution for 10 min in the water bath sonicator. Sonication is essential to prevent aggregation and finalize the solubilization of CADY.
4. For siRNA transfection experiment, dilute the CADY solution at 100 μM in ultra pure water RNase, DNase free. Repeated freeze/thaw cycles can induce peptide aggregation, therefore, it is recommended to aliquot the CADY stock solution into tubes containing the amount you expect to use in a

typical experiment prior to freezing. The CADY stock solution is stable for about 4 months when stored at -20°C .

5. Prepare a stock solution of siRNA in water at $5\ \mu\text{M}$. Usually the concentration of commercially available solution of annealed siRNA is at $100\ \mu\text{M}$ should be diluted to $5\ \mu\text{M}$ in water or in buffer containing $50\ \text{nM}$ Tris-HCl pH 7.0 and $2\ \text{mM}$ EDTA.

3.1.2. CADY/siRNA Complexes for Transfection

1. If needed defrost on ice the CADY solution at $100\ \mu\text{M}$. At this stage, sonication of the peptide solution is recommended, to limit aggregation, for 5 min in a water bath sonicator. Alternatively a probe sonicator can also be used: place the tube in cold water and sonicate for 1 min at amplitude of 30%. If needed defrost siRNA solution at $5\ \mu\text{M}$. Vortex siRNA before use. Do not vortex CADY or CADY/siRNA complex. Although CADY/siRNA complexes are stable 2 weeks at 4°C , we suggested for a high efficiency to prepare them freshly for each experiment (see Notes 4 and 6).

2. Depending on the cell line, the biological response expected and the target gene, siRNA can be used at concentrations varying for 5–200 nM. From our experience, concentrations ranging from 20 to 50 nM of siRNA are sufficient for a gene expression knockdown greater than 80%. Accordingly, the protocols described are for 35 mm culture plate using a final concentration of 40 nM of siRNA complexed with 800 nM (adherent cell lines) or 1,600 nM (suspension cell lines) of CADY, corresponding to a peptide/siRNA molar ratio of 20/1 and 40/1, respectively.

For adherent cell line, dilute $5\ \mu\text{M}$ siRNA ($12.8\ \mu\text{l}$) in PBS ($87.2\ \mu\text{l}$) and $100\ \mu\text{M}$ CADY ($12.8\ \mu\text{l}$) in water ($87.2\ \mu\text{l}$) into two separate tubes.

For suspension cell lines, dilute $5\ \mu\text{M}$ siRNA ($12.8\ \mu\text{l}$) in PBS ($87.2\ \mu\text{l}$) and $100\ \mu\text{M}$ CADY ($25.6\ \mu\text{l}$) in water ($74.4\ \mu\text{l}$) into two separate tubes.

3. Add $100\ \mu\text{l}$ of diluted CADY peptide solution to $100\ \mu\text{l}$ siRNA solution. Mix gently by tapping the tube.
4. Incubate at 37°C for 20–30 min to allow the CADY/siRNA complexes to be formed, and then proceed immediately to the transfection experiments. For lower concentrations of siRNA, dilute the CADY/siRNA complex in PBS ($0.5\times$) using serial dilutions, to reach the needed concentration. For multiple assays, a mix of 6–12 transfection can be used at a molar ratio of 20/1. Do not exceed the volume required for 12 reactions and the 20/1 CADY/siRNA ratio, as this may induce aggregation.

3.2. Protocol for CADY-Mediated siRNA Transfection into Adherent Cell Lines

The protocol is described for HeLa and U₂OS cell lines cultured in six-well plates, using a siRNA targeting the *gapdh* gene (Fig. 1). The siRNA-associated silencing responses were followed at both the mRNA (Fig. 2a) and protein levels (Fig. 2b) using Quantigen technology and western blot analysis, respectively. The amount of siRNA, CADY, transfection volume, and number of cells should be adjusted accordingly to the size of the culture plate used (see Notes 1, 5, and 6).

1. Trypsinize and count the cells on the day before transfection, then split cells in six-well plates at a density of 1.3×10^4 cells per well with 2 ml of preheated complete growth medium. It is recommended to pass the cell the day before treatment for a better response following transfection. Incubate cells overnight at 37°C in a humidified atmosphere containing 5% CO₂ until the cells are 50–70% confluent. It is important (1) not to add antibiotics to the media during transfection, (2) to minimize trypsinization treatment, and (3) to use prewarmed trypsin solution (at least 15 min at room temperature) to limit cell cycle arrest or/and cell death.

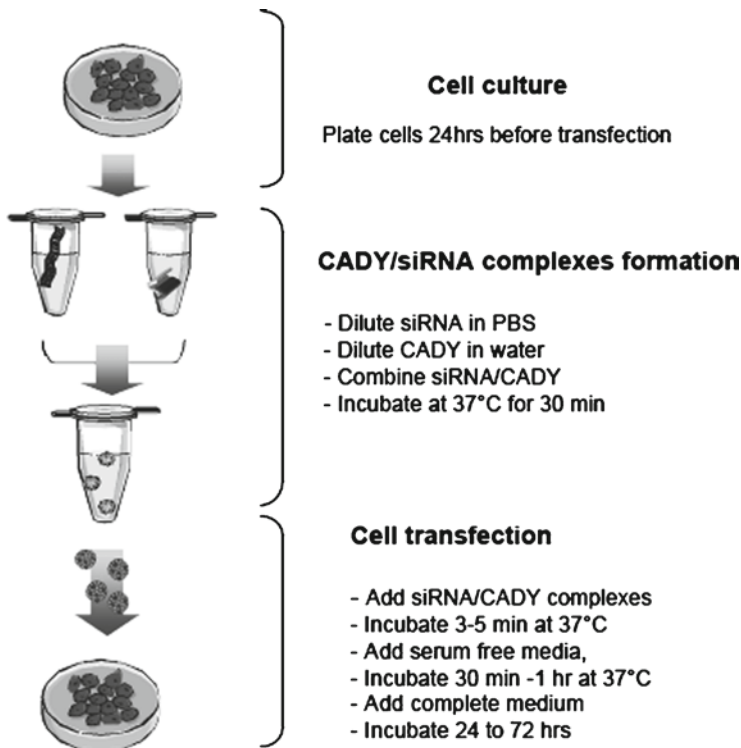


Fig. 1. Schematic diagram of the protocol for CADY-mediated siRNA delivery. The protocol involves the formation and handling of CADY/siRNA complexes, then siRNA transfection into either adherent or suspension “hard-to-transfect” cell lines.

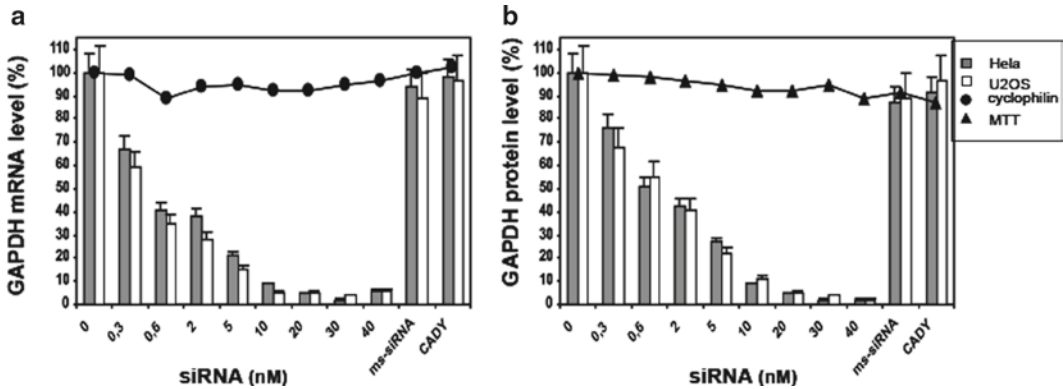


Fig. 2. CADCY-mediated siRNA delivery into adherent cell lines. Stock solutions of CADCY/siRNA (100 nM) particles were prepared at a molar ratio of 1/20, and lower concentrations (from 50 to 0.3 nM) were obtained by serial dilution of the stock solution in PBS. HeLa (in *grey*) and U2OS (*white*) cells were then transfected with varying concentrations (0.3–40 nM) of human GAPDH siRNA complexed with CADCY. Twenty-four hours post-transfection, cells were lysed and *gapdh* mRNA (a) and GAPDH protein (b) levels were quantified by Quantigen technology and western blotting, respectively. Mismatched siRNA associated with CADCY (50 nM) and empty CADCY particles (5 μ M) were used as a control. Changes in *gapdh* mRNA and GAPDH protein levels were normalized to cyclophilin B (*open circle*) gene expression and non-transfected cells, respectively.

2. Preheat growth medium (DMEM containing GlutaMAX and 10% FBS) at 37°C in a CO₂ incubator for at least 30 min before use.
3. Remove growth medium from the cells by aspiration and rinse the cells twice with PBS. It is important to remove the entire growth medium, as serum will lower the transfection efficiency of the CADCY/siRNA complex.
4. Add the 200 μ l of CADCY/siRNA complex directly onto the cells and incubated for 3–5 min at 37°C. Do not exceed 5 min to avoid the cells to dry.
5. Add 400 μ l of the appropriate medium without serum (DMEM or others) to achieve a final volume of 600 μ l for a 35 mm plate. At that stage, 5% serum can be added to the medium, for sensitive cell lines.
6. Incubate at 37°C in a humidified atmosphere containing 5% CO₂ for 30 min.
7. Add 1 ml of complete growth medium with 16% FBS to obtain a final concentration of 10% FBS. Do not remove the CADCY/siRNA complex.
8. Incubate at 37°C in a humidified atmosphere containing 5% CO₂ for 24–48 h, depending on the cellular response expected and on the analysis approaches (see Note 2). The siRNA is fully released in the cells after 1 h.
9. Process the cells for observation or detection assays. (Subheading 3.3, steps 1 and 2).

3.3. Protocol for CADY-Mediated siRNA Transfection into Suspension Cell Lines

The protocol of CADY-mediated siRNA delivery was optimized on Jurkat T and THP1 cell lines, using a siRNA targeting the *gapdh* gene. The siRNA-associated silencing responses were followed at the mRNA (Fig. 3a) and protein (Fig. 3b) levels by Quantigen technology and western blot, respectively.

1. The same number of cells recommended for seeding adherent cells is recommended for suspension cells (confluency between 50 and 70%). Cells are cultured in appropriate medium (RPMI 1640 supplemented with 10% FSC) in 35 mm dishes or six-well plates (see Notes 5 and 6).
2. The CADY/siRNA complexes at molar ratio are formed as described for adherent cells (Subheading 3.1.2, steps 1–4).
3. Collect the suspension cells by centrifugation at $400 \times g$ for 5 min. Remove the supernatant and wash the cells twice with PBS.
4. Centrifuge at $400 \times g$ for 5 min to pellet the cells. Remove the supernatant.
5. Solubilize the cell pellet in the CADY/siRNA complex solution (200 μ l). Add serum-free medium to achieve a final transduction volume of 600 μ l.
6. Incubate at 37°C in a humidified atmosphere containing 5% CO_2 for 30 min to 1 h depending on the cell lines.
7. Add complete growth medium to the cells and adjust serum levels according to culture requirements. Do not remove the CADY/siRNA complex. Continue to incubate at 37°C in a

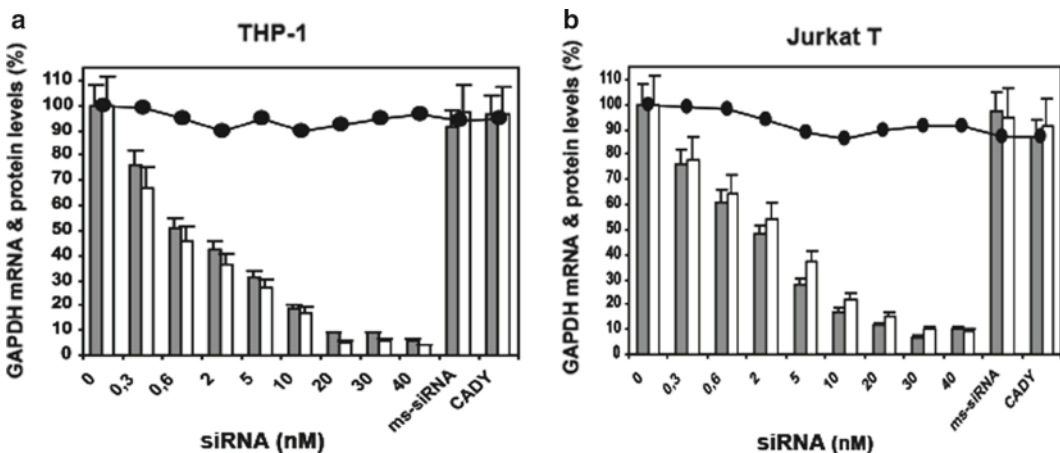


Fig. 3. CADY-mediated siRNA delivery into challenging cell lines. CADY was evaluated on two challenging cell lines THP1 (a) and primary Jurkat T (b). A stock solution of CADY/siRNA (100 nM) was prepared at a molar ratio of 1/40, and then lower concentrations of formulated siRNA (from 40 to 0.6 nM) were obtained by serial dilution of the stock solution in PBS. GAPDH mRNA (grey) and protein (white) levels were quantified 24 h post-transfection as described in Fig. 2. IC_{50} values of 0.7 ± 0.1 and 3.2 ± 0.5 nM were calculated for THP1 and Jurkat cells, respectively.

humidified atmosphere containing 5% CO₂ for 24–48 h depending on the expected cellular response. As described for adherent cells, siRNA are fully released into cells 1 h later.

8. Process the cells for observation or detection assays (Subheading 3.3, steps 1 and 2).

3.4. Analysis of CADY/ siRNA Complex Uptake and Associated Silencing Response

3.4.1. mRNA Quantification

GAPDH protein and mRNA levels were determined by western blot and Quantigen™, respectively.

mRNA quantification was performed using QuantiGene® 2.0 Reagent System (Affimetrix/Panomics Inc., CA, USA) directly on cell lysates without mRNA purification or amplification according to manufacturer's instructions.

1. Stock solution of lysis buffer contains 50 mM Tris-HCl pH 7.5, 150 mM NaCl, 2 mM EDTA, 0.1% NP-40, 0.1% deoxycholate. Proteases cocktail inhibitors including PMSF (phenylmethylsulphonyl fluoride, 1 mM final concentration), leupeptine (10 µg/ml final concentration), apoprotinin (10 µg/ml final concentration), pepstatin (10 µg/ml final concentration) are added just before used.
2. Add lysis buffer from QuantiGene® 2.0 Reagent System directly in transfection mixture-growth medium on cells.
3. Measure the mRNA level of the gene of interest (*gapdh*) normalized to the control housekeeping gene of cyclophilin-B, according to manufacturers' recommendations.

3.4.2. Western Blot Analysis of Protein Levels

1. Remove the transfection mixture and growth medium from the cells.
2. Wash cells twice with PBS.
3. Add 0.2 ml of trypsin on cells and incubate plate approximately for 5 min at room temperature (until cells begin detaching from plate). Stop reaction with 10% FBS medium.
4. Transfer cells to a tube. Centrifuge cells at 900 *g* for 5 min at 6–8°C.
5. Remove supernatant from the centrifuge tube.
6. Add 1 ml of PBS to rinse the pellet and then re-centrifuge at 1,200 rpm for 5 min at 6–8°C.
7. Remove the supernatant.
8. Lyse cells with 0.1 ml lysis buffer for 30 min on ice, vortexing samples every 5 min. Then centrifuge at 4°C for 15 min at 10,000 × *g*.
9. Supernatants were collected and protein concentrations were determined using the Bradford assay.

10. Thirty micrograms of cell extracts were separated by SDS–PAGE on a 12.5% SDS–polyacrylamide gel. After electrophoresis, samples were transferred onto nitrocellulose in a semi-dry transfer apparatus for 1 h at 1 mA/cm².
11. Analyse samples by western blot as reported before in ref. (26), using monoclonal mouse primary antibodies anti-GAPDH (6C5) from Santa Cruz Biotechnology and rabbit anti-actin antibody (as a loading control) from Sigma-Aldrich (France) and sheep secondary anti-mouse HRP-linked whole antibody from Amersham (France).

4. Notes

1. This technology is not dependent on the siRNA sequence and so is usable for targeting any gene without further optimization. A large variety of siRNA have been successfully applied using CADY technology for silencing activity in different cell lines (9, 11, 26) (see Note 3).
2. The incubation time of the CADY/siRNA complex onto transfected cells is an important point and is directly associated to the target protein half-life. Hence the RNA interfering effect must be long enough to allow already present protein to be degraded and so permits the knock-down effect detection.
3. The advantages of CADY technology are directly associated with lack of toxicity and the mechanism through which this carrier promotes delivery of siRNA into cells. The independence of CADY-mediated siRNA transfection on the endosomal pathway significantly limits degradation and preserves the biological activity of internalized cargoes for prolonged time periods.
4. It is essential to perform complex formation between CADY and the siRNA in the absence of serum to limit degradation of siRNA and interactions with serum proteins. However, the transfection process itself is not affected by the presence of serum, which is a considerable advantage for most biological applications (26).
5. Although this protocol was tested on several cells lines, conditions for efficient siRNA delivery should be optimized for every new cell line, including reagent concentration, cell number, and exposure time of cells to the CADY/siRNA complexes. A well-characterized siRNA should always be used as a positive control of transfection.
6. Low efficiency may be associated with several parameters: (a) *Cell confluency*: for adherent cells the optimal confluence is of

about 50–60%, higher confluence (90%) dramatically reduces the transduction efficiency. Cells must be in the exponential growth stage at the time of transfection; thus, confluency of 40–60% is recommended. (b) *Formation of CADY/siRNA complexes*: conditions for the formation of CADY/siRNA complexes are critical and should be respected. Special attention should be paid to the recommended volumes, incubation times for the formation of the complexes, and time of exposure of these complexes to cells.

Acknowledgments

This work was supported in part by the Centre National de la Recherche Scientifique (CNRS), by the Agence Nationale de la Recherche (ANR, ANR-06-BLAN-0071-Pepvec4Ther), and by a grant from Panomics Inc. L.C. was supported by a grant from the Ligue de Recherche contre le Cancer (LNCC). We thank M.C. Morris for critical reading of the manuscript and all members of the laboratory for fruitful discussions.

References

1. Fire, A., Xu, S., Montgomery, MK., Kostas, SA., Driver, SE., and Mello, CC. (1988) Potent and specific genetic interference by double-stranded RNA in *Caenorhabditis elegans*. *Nature*. **391**, 806–811.
2. Elbashir, SM., Harborth, J., Lendeckel, W., Yalcin, A., Weber, K., and Tuschl, T. (2001) Duplexes of 21-nucleotide RNAs mediate RNA interference in cultured mammalian cells. *Nature*. **411**, 494–498.
3. Hannon, GJ. (2002) RNA interference. *Nature*. **418**, 244–251.
4. De Fougerolles, A., Vornlocher, H-P., Maraganore, J., and Lieberman, J. (2007) Interfering with disease: a progress report on siRNA-based therapeutics. *Nat Rev Drug Discov*. **6**, 443–453.
5. Juliano, R., Alam, MR., Dixit, V., and Kang, H. (2008) Mechanisms and strategies for effective delivery of antisense and siRNA oligonucleotides. *Nucleic Acids Res*. **36**, 4158–4171.
6. Whitehead, KA., Langer, R., and Anderson, DG. (2009) Knocking down barriers: advances in siRNA delivery. *Nat Rev Drug Discov*. **8**, 129–138.
7. Eguchi, A., and Dowdy, SF. (2009) siRNA delivery using peptide transduction domains. *Trends Pharmacol Sci*. **30**, 341–345.
8. El-Andaloussi, S., Holm, T., and Langel, U. (2005) Cell-penetrating peptides: mechanisms and applications. *Curr Pharm Des*. **11**, 3597–3611.
9. Heitz, F., Morris, MC., and Divita, G. (2009) Twenty years of cell-penetrating peptides: from molecular mechanisms to therapeutics. *Br J Pharmacol*. **157**, 195–206.
10. Foerg, C., and Merkle, HP. (2008) On the biomedical promise of cell penetrating peptides: limits versus prospects. *J Pharm Sci*. **97**, 144–162.
11. Crombez, L., Morris, MC., Deshayes, S., and Divita G. (2008) Peptide-based nanoparticles for ex vivo and in vivo drug delivery. *Curr Pharm Des*. **14**, 3656–3665.
12. Meade, BR., and Dowdy, SF. (2007) Exogenous siRNA delivery using peptide transduction domains/cell penetrating peptides. *Adv Drug Deliv Rev*. **59**, 134–140.
13. Muratovska, A., and Eccles, MR. (2004) Conjugate for efficient delivery of short interfering RNA (siRNA) into mammalian cells. *FEBS Lett*. **558**, 63–75.
14. Davidson, TJ., Harel, S., Arboleda, VA., Prunell, GF., Shelanski, ML., Greene, LA., and Troy, CM. (2004) Highly efficient small interfering RNA delivery to primary mammalian

- neurons induces MicroRNA-like effects before mRNA degradation. *J Neurosci.* **10**, 10040–10046.
15. Moschos, SA., Jones, SW., Perry, MM., Williams, AE., Erjefalt, JS., Turner, JJ., Barnes, PJ., Sproat, BS., Gait, MJ., and Lindsay, MA. (2007) Lung delivery studies using siRNA conjugated to TAT(48-60) and penetratin reveal peptide induced reduction in gene expression and induction of innate immunity. *Bioconjug Chem.* **18**, 1450–1459.
 16. Simeoni, F., Morris, MC., Heitz, F., and Divita, G. (2003) Insight into the mechanism of the peptide-based gene delivery system MPG: implications for delivery of siRNA into mammalian cells. *Nucleic Acids Res.* **31**, 2717–2724.
 17. Veldhoen, S., Laufer, SD., Trampe, A., and Restle, T. (2006) Cellular delivery of small interfering RNA by a non-covalently attached cell-penetrating peptide: quantitative analysis of uptake and biological effect. *Nucleic Acids Res.* **34**, 6561–6573.
 18. Morris, KV., Chan, SW., Jacobsen, SE., and Looney, DJ. (2004) Small interfering RNA-induced transcriptional gene silencing in human cells. *Science.* **305**, 1289–1292.
 19. Zeineddine, D., Papadimou, E., Chebli, K., Gineste, M., Liu, J., Grey, C., Thurig, S., Behfar, A., Wallace, VA., Skerjanc, IS., and Puceat, M. (2006) Oct-3/4 dose dependently regulates specification of embryonic stem cells toward a cardiac lineage and early heart development. *Dev Cell.* **11**, 535–546.
 20. Crombez, L., Morris, MC., Dufort, S., Aldrian-Herrada, G., Nguyen, Q., Mc Master, G., Coll, JL., Heitz, F., and Divita, G. (2009) Targeting cyclin B1 through peptide-based delivery of siRNA prevents tumour growth. *Nucleic Acids Res.* **37**, 4559–4569.
 21. Kim, WJ., Christensen, LV., Jo, S., Yockman, JW., Jeong, JH., Kim, YH., and Kim, SW. (2006) Cholesteryl oligoarginine delivering vascular endothelial growth factor siRNA effectively inhibits tumor growth in colon adenocarcinoma. *Mol Ther.* **14**, 343–350.
 22. Kumar, P., Wu, H., McBride, JL., Jung, KE., Kim, MH., Davidson, BL., Lee, SK., Shankar, P., and Manjunath, N. (2007) Transvascular delivery of small interfering RNA to the central nervous system. *Nature.* **7149**, 39–43.
 23. Kumar, P., Ban, HS., Kim, SS., Wu, H., Pearson, T., Greiner, DL., Laouar, A., Yao, J., Haridas, V., Habiro, K., Yang, YG, Jeong, JH., Lee, KY., Kim, YH., Kim, SW., Peipp, M., Fey, GH., Manjunath, N., Shultz, LD., Lee, SK., and Shankar, P. (2008) T cell-specific siRNA delivery suppresses HIV-1 infection in humanized mice. *Cell.* **134**, 577–586.
 24. Lundberg, P., El-Andaloussi, S., Sutlu, T., Johansson, H., and Langel, U. (2007) Delivery of short interfering RNA using endosomolytic cell-penetrating peptides. *FASEB J.* **11**, 2664–2671.
 25. Eguchi, A., Meade, BR., Chang, YC., Fredrickson, CT., Willert, K., Puri, N., and Dowdy, SF. (2009) Efficient siRNA delivery into primary cells by a peptide transduction domain-dsRNA binding domain fusion protein. *Nat Biotechnol.* **27**, 567–571.
 26. Crombez, L., Aldrian-Herrada, G., Konate, K., Nguyen, Q-N., McMaster, G., Brasseur, R., Heitz F., and Divita, G. (2009) A new potent secondary amphipathic cell-penetrating peptide for siRNA delivery into mammalian cells. *Mol Ther.* **17**, 95–103.
 27. Rittner, K., Benavente, A., Bompard-Sorlet, A., Heitz, F., Divita, G., Brasseur, R., and Jacobs, E. (2002) New basic membrane-destabilizing peptides for plasmid-based gene delivery in vitro and in vivo. *Mol Ther.* **5**, 104–114.
 28. Deshayes, S., Konate, K., Aldrian, G., Heitz, F., and Divita, G. (2010) Interactions of amphipathic CPPs with model membranes. In: Ülo Langel (ed.) *Cell-Penetrating Peptides: Methods and Protocol (Methods Mol Biol, 683). Chapter 4*, Springer, New York.
 29. Morris, MC., Vidal, P., Chaloin, L., Heitz, F., and Divita, G. (1997) A new peptide vector for efficient delivery of oligonucleotides into mammalian cells. *Nucleic Acids Res.* **25**, 2730–2736.

Application of PepFect Peptides for the Delivery of Splice-Correcting Oligonucleotides

Samir EL Andaloussi, Taavi Lehto, Per Lundin, and Ülo Langel

Abstract

One oligonucleotide-based approach that appear very promising for the treatment of different genetic disorders are based on so-called splice-correcting oligonucleotides (SCOs) that are exploited to manipulate splicing patterns. In order to increase the bioavailability, cell-penetrating peptides (CPPs) have readily been covalently conjugated to SCOs to facilitate cellular internalization. While being a successful strategy for the delivery of uncharged oligonucleotides (ONs), it is extremely difficult to generate covalent conjugates between commonly used negatively charged ON analogs and cationic CPPs. Furthermore, high concentrations of ONs in the micromolar range are often needed to obtain biological responses, most likely as a result of endosomal entrapment of material. Therefore, exploring other vectorization methods using CPPs with endosomolytic properties are highly desired.

A method of using stearyl modified CPP (i.e., TP10) analogs, named PepFect3 and PepFect4, are being described for the transfection of antisense SCOs using a simple one-step co-incubation procedure. These peptides form complexes with SCOs and efficiently promote cellular uptake by facilitating endosomal escape. This chapter describes the methods of how to form and characterize these nanoparticles and the cellular assay used to address the delivery.

Key words: Cell-penetrating peptides, Co-incubation, Oligonucleotide delivery, PepFect, Splice correction, Transfection

1. Introduction

Over the last decades several different technologies based on oligonucleotides (ONs) have emerged for the selective manipulation of gene expression. One approach with great clinical potential is based on the concept of manipulating splicing patterns using so-called splice-correcting ONs (SCOs) or splice switching ONs (SSOs). It has been estimated that 20–30% of all disease-causing mutations affects pre-mRNA splicing (1), giving rise to

diseases such as β -thalassemia, cystic fibrosis, muscular dystrophies, neurodegenerative disorders, and different types of cancer (2–4). Mutant forms of the human β -globin transcript were among the first targets in which the splicing patterns were manipulated with SCOs. By targeting aberrant splice sites with SCOs, splicing has been restored with concomitant production of β -globin, both in vitro and in vivo (5, 6). SCOs have also been applied to promote exon-skipping in several models of Duchenne muscular dystrophy (DMD), targeting mutations in dystrophin pre-mRNA (7–9). To date, there are at least two ongoing clinical trials with promising preliminary results (10, 11). Thus, manipulating splicing patterns with SCOs represents an attractive therapeutic approach for treatment of numerous genetic disorders.

A major obstacle with all ON-based approaches is the inherent low bioavailability of the pharmacological agent, ensuing inter alia from poor chemical stability of unmodified RNAs, and the low cellular uptake. The field has seen extensive improvements in terms of new ON analogs displaying increased serum stability and increased avidity for target RNA. However, despite substantial efforts, there are only few nonviral delivery vectors available that efficiently transfect cells in a relatively nontoxic fashion. Generally, there appears to be a correlation between high delivery efficacy and high toxicity (12, 13).

Cell-penetrating peptides (CPPs) represent a group of nonviral delivery vectors with significant potential for delivery of ONs of various kinds. Numerous studies have shown that upon covalent conjugation to ON analogs, such as peptide nucleic acids (PNAs) or morpholinos (PMOs), CPPs efficiently promote effector molecule uptake, both in vitro (14, 15) and in vivo (8, 16, 17). However, relatively high concentrations of CPP–ON conjugates are usually needed in order to obtain significant biological responses in vitro, thus raising concerns for potential obstacles when progressing the technology toward the bedside. Over the last years it has been realized that CPPs predominantly utilize endocytosis for cellular internalization (18–20). Although endocytosis offers an effective means of reaching the vicinity of the nucleus, where, for instance, SCOs exert their biological activity, thereby bypassing a crowded cytoplasm, the lion's share of the internalized material will eventually be degraded in endosomes or lysosomes. Thus, entrapment of peptides in endosomal compartments could be a plausible explanation for the need of high conjugate concentrations.

Another strategy that has been exploited is to noncovalently complex cationic CPPs with anionic ONs. Using this methodology, significantly lower ON concentrations are generally needed. Although complexes are readily internalized to cells using this approach, they are in many cases unable to induce any biological response, as a result of endosomal entrapment (21). A successful strategy that has been employed to increase the bioavailability of noncovalent CPP/ON complexes is to modify CPPs with lipophilic

moieties, such as fatty acids. Stearylation of oligoarginine peptides has previously been reported to enhance both the delivery of plasmids (22) and siRNAs (23). We recently reported that stearylation of an amphipathic CPP, Transportan 10 (TP10), significantly increased SCO-mediated splice correction, reaching virtually the same levels of correction as when using the commercial transfection reagent Lipofectamine™ 2000 (21).

The present chapter describes formation, characterization, and efficacy assessment of noncovalent complexes between stearylated CPPs and phosphorothioate (PS) 2'-O-methyl RNA (2'OMe RNA) targeting an aberrant splice site in HeLa pLuc 705 cells, using a simple co-incubation protocol. The splice correction promoted by N-terminally stearylated TP10 (i.e., PepFect3) is compared to the effects mediated by TP10 stearylated on lysine in position 7 (i.e., PepFect4), as well as Lipofectamine™ 2000. Both peptides display superior delivery properties compared to other stearylated CPPs, including oligoarginine, and the effects are in parity with Lipofectamine™ 2000 or even greater, while reducing the transfection-associated toxicity significantly.

2. Materials

As the focus of the present chapter pertains to delivery of SCOs, we have evaluated our new PepFect peptides in the splice correction assay introduced by Kole and colleagues (24). The assay is based on the human cervical cancer cell line HeLa, that has been genetically modified, i.e., HeLa pLuc705 cells. These cells are stably transfected with a plasmid carrying a luciferase-encoding sequence interrupted by an insertion of intron 2 from β -globin pre-mRNA carrying an aberrant splice site. Unless the aberrant splice site is masked by an SCO, the pre-mRNA of luciferase will be improperly processed. Thus, increases in luciferase expression after SCO treatment reflects the amount of active SCO in the nucleus of cells. Other cells could naturally also be utilized to evaluate the delivery of SCOs using the PepFect peptides, using the same assay if they carry the same splicing construct. The PepFect protocol is also applicable for other types of antisense ONs acting in the nucleus of cells or for the delivery of large plasmids. However, PepFect3 and PepFect4 are not suitable vectors for cytoplasmic transport of siRNAs or anti-microRNAs.

2.1. Peptides, Oligonucleotides, and Complex Formation

1. The sequence of the 2'-O-methyl phosphorothioate RNA used to target the aberrant 705 splice site is CCUCUUA CCUCAGUUACA (e.g., RiboTask or Dharmacon). Store 20 μ M aliquots (dissolved in MQ water) at -20°C (see Note 1).

2. The sequence of TP 10 is AGYLLGKINLKALAALAALA-KKIL. When a stearyl group is attached to the N terminus of the peptide via a peptide bond, the peptide is called PepFect3 and when a stearyl moiety is orthogonally conjugated via the ϵ -amino group of Lys⁷ the peptide is called PepFect4. Peptides can be purchased from Novagen or synthesized in-house as described in (21). 20 μ l of 1 mM peptide solutions in MQ water are stored at -20°C .
3. MQ water (pH5).
4. Lipofectamine™ 2000 (Invitrogen).
5. OptiMEM cell culture media (Invitrogen).
6. 1.5-ml Eppendorf tubes.

2.2. Ethidium Bromide Exclusion Assay

1. Same reagents as stated above.
2. Ethidium bromide, 10 μ M stock solution dissolved in water (see Note 2).
3. Black 96-well plate (Corning).

2.3. Cell Culturing and Lysis of Cells

1. HeLa pLuc 705 cells maintained in Dulbecco's Modified Eagle's Medium (DMEM) with Glutamax, supplemented with 0.1 mM nonessential amino acids, 1.0 mM sodium pyruvate, 10% fetal bovine serum, 100 U/ml penicillin, and 100 mg/ml streptomycin. All reagents are purchased from Invitrogen, Sweden.
2. 10-cm Cell culture dishes.
3. Trypsin (0.25%) and ethylenediamine tetraacetic acid (EDTA) (1 mM) (Gibco/BRL).
4. 24-Well culture plates.
5. Phosphate-buffered saline (PBS): 137 mM NaCl, 10 mM Na_2HPO_4 , and 2.7 mM KCl, with a pH of 7.4.
6. 0.1% Triton X-100 in Hepes Krebs Ringer (HKR) buffer: 130 mM NaCl, 5 mM KCl, 1.2 mM MgSO_4 , 1.2 mM CaCl_2 , 20 mM Hepes, 1.2 mM Na_2HPO_4 , and 10 mM glucose (pH 7.4), for lysis of cells.

2.4. Luciferase Assay and Protein Determination

1. White 96-well plate (Corning).
2. Cell lysate.
3. Luciferase assay substrate mix (Promega): Mix substrate with buffer solution and store 1 ml aliquots at -20°C for a maximum of 1 month.
4. Transparent 96-well plates.
5. Lowry detergent compatible protein determination kit (BioRad).

3. Methods

When addressing the delivery efficacy of CPPs, functional assays are generally preferred over methods based on fluorescence assays that monitors uptake of fluorophore-labeled peptides, since cellular uptake does not, in many cases, correlate with bioactivity (as a result of endosomal entrapment, etc.). Therefore, in order to evaluate the performance of the PepFect peptides, we employ the previously described splice correction assay, which generates a positive biological read-out.

Over the past years, several groups have reported on successful application of CPPs for the delivery of SCOs, using predominantly disulfide bond-mediated covalent conjugation to ONs. This is a convenient strategy if working with uncharged ON analogs based on PNAs or morpholinos. However, due to charge interactions, it is very difficult to generate conjugates between cationic peptides and negatively charged ONs.

In order to vectorize negatively charged phosphorothioate 2'-O-methyl RNA with CPPs we therefore utilize the previously described noncovalent co-incubation strategy, initially introduced by Divita and colleagues (25). As seen in Fig. 1, none of the tested CPPs, which all have been reported to be active when covalently linked to ONs, are able to convey SCOs inside cells upon co-incubation. Intriguingly, when introducing a stearic acid moiety to the N terminus of TP10, i.e., generating a PepFect3 peptide, transfections are improved dramatically, whereas stearylation has no impact on any other peptide. The activity of the peptide can be further increased by modifying it orthogonally on Lys⁷ (i.e., PepFect4) and, in fact, this peptide is more active than Lipofectamine™ 2000, using only 200 nM SCO (Fig. 2).

We here describe how to form and characterize these PepFect/SCO complexes and their further use in the splice correction assay.

3.1. Complex Formation with CPPs

1. Thaw frozen stock solutions of PepFect and add 180 µl of MQ water to obtain a final concentration of 100 µM.
2. Thaw a frozen 20 µM SCO solution.
3. Prepare PepFect/SCO complexes at different molar ratios and different SCO concentrations (see Note 3). For both PepFect peptides, molar ratios of peptide over SCO (MRs) of 5, 7, and 10 should be tested. Furthermore, a dose-response assessment should always be carried out at each molar ratio (see Note 4). The protocol below describes formation of complexes at MR 5 in duplicates using different SCO concentrations.
4. Pipette 40 µl of SCO solution into a 1.5-ml Eppendorf tube.

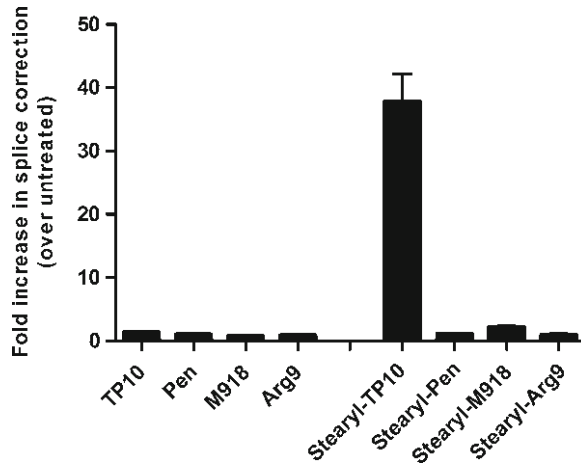


Fig. 1. Impact of stearylation on CPP-mediated SCO delivery and subsequent splice correction. Noncovalent complexes between various CPPs and SCO were formed in one-tenth of the final treatment volume using a fixed treatment concentration of 200 nM SCO and 2 μ M of peptide (i.e., molar ratio 10). First, 10 μ l of 20 μ M SCO was added to an Eppendorf tube and then 70 μ l of MQ water and finally 20 μ l of 100 μ M peptide solution was added to give a final volume of 100 μ l. While incubating at room temperature for 30 min, media was replaced in HeLa pLuc 705 cells (60,000 cells/well seeded 1 day prior experiment in 24-well plates) for 450 μ l serum-free DMEM. After incubation, 50 μ l of complex solution was added to wells in duplicate and incubated for 4 h at 37°C. Full media was then added to cells (1 ml) and cells were stored in the incubator for an additional 20 h. Media was then aspirated and cells washed two times with HKR before cell lysis using 100 μ l of 0.1% Triton X-100 in HKR at 4°C for 30 min. 20 μ l lysate was transferred to new wells in a white 96-well plate after which 80 μ l Luciferase substrate was added to each well and luminescence was recorded on a Spectra Max luminometer. The amount of protein was determined in each well using BioRad detergent compatible kit. Briefly, 5 μ l of cell lysate was transferred to new wells in a transparent 96-well plate after which 25 μ l of reagent A and subsequently 200 μ l of reagent B was added to the same wells. In parallel, known concentrations of internal standard BSA was added to other wells and treated the same way to obtain a standard curve. After 10-min incubation, absorbance was measured at 690 nm. Calculate protein concentrations in each well and normalize the relative luminescence (RLU) by dividing RLU values with protein content to obtain values in RLU per milligram. To facilitate comparison between different treatments it is advisable to translate the RLU per milligram of untreated cells to 1 and present the results of the treatments as fold-increase in luminescence compared to untreated cells. The results suggest that unmodified CPPs are unable to convey bioactive SCOs inside cells and that N-terminal stearylation improves the activity of TP10 drastically while having negligible effects on the other tested CPPs.

5. Add 120 μ l of MQ water into the same tube.
6. Add 40 μ l of PepFect to the same tube to obtain a final volume of 200 μ l.
7. Allow complexes to form by incubating the solution for 30 min at room temperature. Meanwhile, add 100 μ l of MQ water into three new Eppendorf tubes.

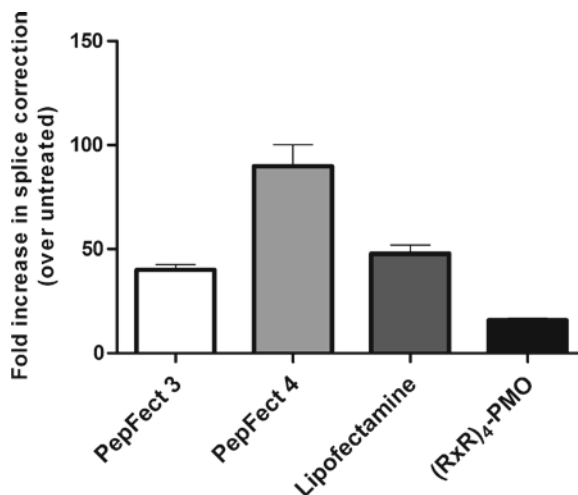


Fig. 2. Relative efficacy of PepFect 3 and PepFect 4 compared to the commercially available cationic lipid reagent Lipofectamine 2000 and the pre-clinically (RXR)₄-PMO conjugate for the delivery of SCOs. Complexes were formed and cells treated essentially as described in Fig. 2, with the exception that PepFect4 was complexed with SCO at molar ratio 7. Lipofectamine 2000/SCO complexes were formed by, in separate tubes, mixing 10 μ l of 20 μ M SCO with 90 μ l optiMEM and 2.8 μ l Lipofectamine 2000 with 97.2 μ l optiMEM, respectively. After 5 min, the two tubes were merged and incubated for 1 h at room temperature. Meanwhile, media was replaced in wells with cells for 400 μ l full growth media. After completing the incubation, 100 μ l Lipofectamine 2000/SCO complex was overlaid in wells in duplicate and incubated for 4 h. Thereafter, all wells were treated as previously described. Cells were treated the same way with (RXR)₄-PMO covalent conjugates in optiMEM using 5 μ M conjugate concentration. The results indicate that the splice correction efficiency of PepFect3 is in line with the commercially available transfection agent, Lipofectamine 2000, whereas, PepFect4 is significantly more efficient, reaching up to 100-fold increase in splice correction over untreated cells, at 200 nM SCO concentration. Both peptides complexed with SCOs are superior to (RXR)₄-PMO, using 25 times lower ON concentration.

8. After incubation, make a serial dilution by removing 100 μ l of complex solution from the first tube to the second tube, etc. In the end, there will be four tubes with 100 μ l of complex solution in each with concentrations ranging from 400 to 50 nM SCO. A dose-response example is shown in Fig. 3.
9. In parallel, prepare Lipofectamine™ 2000/SCO complexes according to the manufacturer's protocol (Invitrogen). For a final treatment concentration of 200 nM SCO in duplicates, particles are formed as described below.
10. 10 μ l of SCO is transferred to a 1.5-ml Eppendorf tube.
11. Add 90 μ l of optiMEM to the same tube and incubate for 5 min at room temperature.
12. In parallel, transfer 2.8 μ l of Lipofectamine 2000 to another Eppendorf tube (see Note 5).

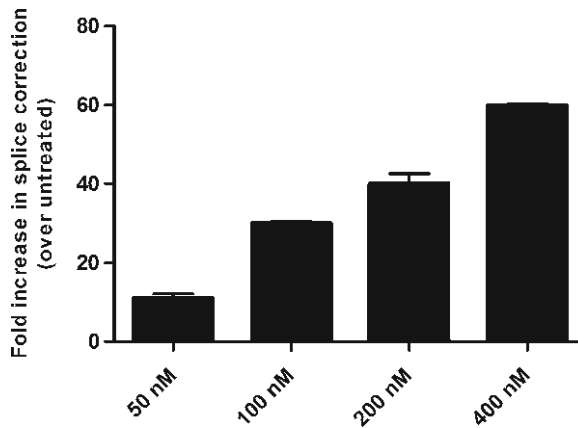


Fig. 3. Transfection of increasing amounts of SCOs using PepFect3. Cells were seeded and treated as described in Fig. 2. Complexes were formed at a molar ratio of 10 and the highest treatment concentration of SCO was 400 nM. 40 μ l of 20 μ M SCO solution was diluted with 80 μ l MQ water and finally 80 μ l of 100 μ M PepFect3 solution was added to an Eppendorf tube. While incubating for 30 min, three additional Eppendorf tubes comprising 100 μ l of MQ water were prepared. Complexes were then serially diluted to obtain final treatment concentrations of 400, 200, 100, and 50 nM SCO. A typical graph shows a dose-dependent increase in splice correction with increasing SCO concentration, resulting in up to 60-fold increase in splice correction over untreated cells at 400 nM SCO.

13. Add 97.2 μ l of optiMEM to the tube and incubate for 5 min at room temperature.
14. Merge the two tubes and incubate for 30 min at room temperature.

3.2. Determine the Efficacy of Complex Formation

1. Complexes should be formed essentially as described above (see Subheading 3.1), although omitting the serial dilution step and including more MRs ranging from 2 to 20. Also prepare a standard SCO solution without any peptide in the same manner.
2. Meanwhile, add 140 μ l of MQ water to required wells in a black 96-well plate (add 190 μ l of MQ water to the wells to get the background fluorescence).
3. Transfer 50 μ l of peptide/SCO complexes to each well.
4. Add 10 μ l of ethidium bromide (EtBr) solution (10 μ M) to each well to acquire an EtBr concentration of 400 nM and incubate for 10 min.
5. Measure fluorescence on a compatible fluorometer at $\lambda_{\text{ex}} = 518$ nm and $\lambda_{\text{em}} = 605$ nm.
6. Present results as relative fluorescence. Attribute a value of 100% to the fluorescence of naked SCO and utilize the fluorescence of EtBr in water as background (see Note 6). An example of results is shown in Fig. 4.

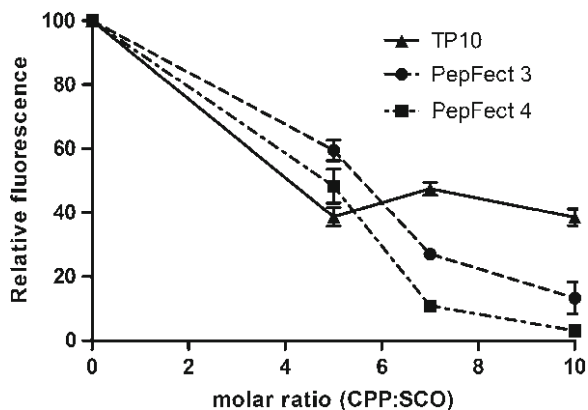


Fig. 4. Interaction between peptides and ONs decreases EtBr fluorescence. Complexes between CPPs and SCO were formed using a fixed SCO concentration and increasing peptide concentrations, generating molar ratios 5, 7, and 10 of peptide over SCO. For example, to obtain a molar ratio of 5, 10 μ l of 20 μ M SCO solution was added to a 1.5-ml Eppendorf tube, after which 80 μ l of MQ water was added and finally 10 μ l of 100 μ M peptide solution. Complexes were formed for 30 min at room temperature. Meanwhile, 140 μ l of water was added to a desired number of wells in a 96-well plate. 50 μ l of complex solution was then added in duplicate to wells and finally 10 μ l ethidium bromide (EtBr) solution (10 μ M) was transferred to each well, to obtain an EtBr concentration of 400 nM. Incubation was carried out for 10 min after which fluorescence was measured at $\lambda_{\text{ex}} = 518$ nm and $\lambda_{\text{em}} = 605$ nm. Results are presented as relative fluorescence. Attribute a value of 100% to the fluorescence of naked SCO and consider the fluorescence of EtBr in water as background. The results clearly illustrate that both PepFect peptides decrease EtBr RNA interaction more efficiently than TP10, and PepFect 4 is more efficient at condensing SCOs than PepFect 3.

3.3. Cell Culturing and Treatment of Cells

1. HeLa pLuc 705 cells are passaged when approaching full confluency with trypsin/EDTA. In general, cells are passaged every third day when using a 1:10 split.
2. The day before experiment, trypsinate cells and seed 60,000 cells/well in a 24-well plate in 500 μ l full media (see Note 7).
3. After 24 h, while complexes are formed (see Subheading 3.1), replace the media in each well for 450 μ l of serum-free DMEM. For wells that are treated with LipofectamineTM 2000, replace the media for 400 μ l full growth media in accordance with manufacturer's protocol (see Note 8).
4. Gently pipette up and down a couple of times in the tubes before adding 50 μ l of pre-formed complexes in duplicate to wells.
5. For treatment with the positive control LipofectamineTM 2000, add 100 μ l of complexes to each well.
6. Gently tilt the plate to allow complexes to distribute evenly in each well.
7. Incubate the cells at 37°C for 4 h and then add 1 ml of full growth media to each well.
8. Incubate the cells for an additional 20 h (see Note 9).

3.4. Splice Correction Assay

1. Aspirate the media from each well.
2. Wash each well twice with 1 ml HKR.
3. Aspirate the HKR and add 100 μ l of lysis buffer to each well.
4. Incubate the cells with lysis buffer at 4°C for 30 min.
5. Transfer 20 μ l of cell lysate to a corresponding well in a white 96-well plate.
6. Add 80 μ l of luciferase substrate into each well.
7. Measure luminescence in a luminometer.

3.5. Protein Determination

1. Transfer 5 μ l of cell lysate to a regular transparent 96-well plate.
2. Add 25 μ l of reagent A.
3. Add 200 μ l of reagent B and mix gently and incubate for 15 min.
4. Measure absorbance at 690 nm (see Note 10).
5. Calculate protein concentrations in each well and normalize the relative luminescence (RLU) by dividing RLU values with protein content expressed in milligram, obtaining values in RLU per milligram. To facilitate comparison between different treatments it is advisable to translate the RLU per milligram of untreated cells to 1 and present the results of the treatments as fold-increase in luminescence compared to untreated cells.

4. Notes

1. The protocol is not restricted to the use of 2'OMe RNA only but is also applicable to the delivery of other single-stranded negatively charged ON analogs, such as locked nucleic acids, etc. For the purpose of splice correction it is, however, important to use ONs that are not recruiting RNase H, which would otherwise degrade target pre-mRNAs. Another important notion is that for optimal use of the PepFect protocol, use desalted ONs since excess salt might interfere with the complex formation.
2. Be careful when handling the EtBr since it is highly carcinogenic. Store it well-protected and on a separate location in a fridge.
3. For optimal transfection results, MR10 and MR7 tend to give highest transfections when using PepFect3 and PepFect4,

respectively. Furthermore, it is advisable to form the complexes in MQ water (pH5) rather than in HKR. Excess salt might interfere with the ability of the peptide to form homogenous complexes.

4. It is highly important to always include a dose–response curve with each transfection reagent and each type of ON. For example, when utilizing Lipofectamine™ 2000, the splice correction activity decreases when exceeding 200 nM ON concentration, generating a bell-shaped dose–response curve. Similar dose–responses have been observed in other settings when targeting other pre-mRNAs with SCOs.
5. According to manufacturers protocol, 2.5 µl of Lipofectamine 2000 should be used for each microgram of ON, in HeLa cells. The molecular weight of our ON is approximately 6,000 Da and we use 200 nM in a final volume of 1 ml (for duplicate). Thus, this corresponds to 1.2 µg of ON and according to the protocol, 3 µl of Lipofectamine 2000 should be used. However, if using that amount of Lipofectamine 2000, significant toxicities have been observed wherefore we use 2.8 µl of the transfection reagent. Other transfection reagents could as well be used as positive control for SCO transfection. However, as Lipofectamine 2000 is the most commonly used reagent, it is utilized here.
6. The principle of the assay is based on the fact that when EtBr binds to RNA its fluorescent properties increases substantially. If PepFect binds to RNA and condenses it, less EtBr will bind, resulting in lower fluorescence. Thus, a decrease in fluorescence reflects the ability of the vector to condense RNA. It is advisable to complement this assay with methods that more precisely addresses the size and shape of formed complexes, such as dynamic light scattering or atomic force microscopy.
7. Seed cells in enough number of wells to include two wells with Lipofectamine 2000 transfections as positive control and two wells of untreated cells to obtain the background RLU values (a small fraction of the pre-mRNA will be properly spliced and hence give rise to a certain level of luminescence).
8. Transfections with Lipofectamine 2000 can be conducted in serum-free media; however, this increases the toxicity.
9. Always assess the toxicity of treatments initially, using for example the MTT assay described in Chapter 14.
10. Establish a protein concentration calibration curve using solutions with known protein concentrations. For example, use a known amount of BSA and make serial dilutions to obtain the standard curve.

Acknowledgments

The work presented in this article was supported by the Swedish Research Council (VR-NT); Center of Biomembrane research, Stockholm; and, Knut & Alice Wallenberg's Foundation; by the EU through the European Regional Development Fund through the Center of Excellence in Chemical Biology, Estonia; by the targeted financing SF0180027s08 from the Estonian Government; by the DoRa Program of the European Social Fund; and by Archimedes Foundation.

References

1. Faustino, N. A., and Cooper, T. A. (2003) Pre-mRNA splicing and human disease, *Genes Dev* **17**, 419–437.
2. Sazani, P., and Kole, R. (2003) Therapeutic potential of antisense oligonucleotides as modulators of alternative splicing, *J Clin Invest* **112**, 481–486.
3. Garcia-Blanco, M. A., Baraniak, A. P., and Lasda, E. L. (2004) Alternative splicing in disease and therapy, *Nat Biotechnol* **22**, 535–546.
4. Pajares, M. J., Ezponda, T., Catena, R., Calvo, A., Pio, R., and Montuenga, L. M. (2007) Alternative splicing: an emerging topic in molecular and clinical oncology, *Lancet Oncol* **8**, 349–357.
5. Sierakowska, H., Sambade, M. J., Agrawal, S., and Kole, R. (1996) Repair of thalassemic human beta-globin mRNA in mammalian cells by antisense oligonucleotides, *Proc Natl Acad Sci USA* **93**, 12840–12844.
6. Sazani, P., Gemignani, F., Kang, S. H., Maier, M. A., Manoharan, M., Persmark, M., Bortner, D., and Kole, R. (2002) Systemically delivered antisense oligomers upregulate gene expression in mouse tissues, *Nat Biotechnol* **20**, 1228–1233.
7. Lu, Q. L., Mann, C. J., Lou, F., Bou-Gharios, G., Morris, G. E., Xue, S. A., Fletcher, S., Partridge, T. A., and Wilton, S. D. (2003) Functional amounts of dystrophin produced by skipping the mutated exon in the mdx dystrophic mouse, *Nat Med* **9**, 1009–1014.
8. Ivanova, G. D., Arzumanov, A., Abes, R., Yin, H., Wood, M. J., Lebleu, B., and Gait, M. J. (2008) Improved cell-penetrating peptide-PNA conjugates for splicing redirection in HeLa cells and exon skipping in mdx mouse muscle, *Nucleic Acids Res* **36**, 6418–6428.
9. Fletcher, S., Honeyman, K., Fall, A. M., Harding, P. L., Johnsen, R. D., Steinhaus, J. P., Moulton, H. M., Iversen, P. L., and Wilton, S. D. (2007) Morpholino oligomer-mediated exon skipping averts the onset of dystrophic pathology in the mdx mouse, *Mol Ther* **15**, 1587–1592.
10. van Deutekom, J. C., Janson, A. A., Ginjaar, I. B., Frankhuizen, W. S., Aartsma-Rus, A., Bremmer-Bout, M., den Dunnen, J. T., Koop, K., van der Kooi, A. J., Goemans, N. M., de Kimpe, S. J., Ekhart, P. F., Venneker, E. H., Platenburg, G. J., Verschuuren, J. J., and van Ommen, G. J. (2007) Local dystrophin restoration with antisense oligonucleotide PRO051, *N Engl J Med* **357**, 2677–2686.
11. Aartsma-Rus, A., Fokkema, I., Verschuuren, J., Ginjaar, I., van Deutekom, J., van Ommen, G. J., and den Dunnen, J. T. (2009) Theoretic applicability of antisense-mediated exon skipping for Duchenne muscular dystrophy mutations, *Hum Mutat* **30**, 293–299.
12. Liu, D., Ren, T., and Gao, X. (2003) Cationic transfection lipids, *Curr Med Chem* **10**, 1307–1315.
13. Scheule, R. K., St George, J. A., Bagley, R. G., Marshall, J., Kaplan, J. M., Akita, G. Y., Wang, K. X., Lee, E. R., Harris, D. J., Jiang, C., Yew, N. S., Smith, A. E., and Cheng, S. H. (1997) Basis of pulmonary toxicity associated with cationic lipid-mediated gene transfer to the mammalian lung, *Hum Gene Ther* **8**, 689–707.
14. Abes, R., Moulton, H. M., Clair, P., Yang, S. T., Abes, S., Melikov, K., Prevot, P., Youngblood, D. S., Iversen, P. L., Chernomordik, L. V., and Lebleu, B. (2008) Delivery of steric block morpholino oligomers by (R-X-R)₄ peptides: structure-activity studies, *Nucleic Acids Res* **36**, 6343–6354.
15. El-Andaloussi, S., Johansson, H., Lundberg, P., and Langel, U. (2006) Induction of splice

- correction by cell-penetrating peptide nucleic acids, *J Gene Med* **8**, 1262–1273.
16. Jearawiriyapaisarn, N., Moulton, H. M., Buckley, B., Roberts, J., Sazani, P., Fucharoen, S., Iversen, P. L., and Kole, R. (2008) Sustained dystrophin expression induced by peptide-conjugated morpholino oligomers in the muscles of mdx mice, *Mol Ther* **16**, 1624–1629.
 17. Moulton, H. M., Fletcher, S., Neuman, B. W., McClorey, G., Stein, D. A., Abes, S., Wilton, S. D., Buchmeier, M. J., Lebleu, B., and Iversen, P. L. (2007) Cell-penetrating peptide-morpholino conjugates alter pre-mRNA splicing of DMD (Duchenne muscular dystrophy) and inhibit murine coronavirus replication in vivo, *Biochem Soc Trans* **35**, 826–828.
 18. Lundin, P., Johansson, H., Guterstam, P., Holm, T., Hansen, M., Langel, Ü., and El Andaloussi, S. (2008) Distinct uptake routes of cell-penetrating peptide conjugates, *Bioconjug Chem* **19**, 2535–2542.
 19. Duchardt, F., Fotin-Mleczek, M., Schwarz, H., Fischer, R., and Brock, R. (2007) A comprehensive model for the cellular uptake of cationic cell-penetrating peptides, *Traffic* **8**, 848–866.
 20. El Andaloussi, S., Guterstam, P., and Langel, Ü. (2007) Assessing the delivery efficacy and internalization route of cell-penetrating peptides, *Nat Protoc* **2**, 2043–2047.
 21. Mäe, M., El Andaloussi, S., Lundin, P., Oskolkov, N., Johansson, H. J., Guterstam, P., and Langel, Ü. (2009) A stearylated CPP for delivery of splice correcting oligonucleotides using a non-covalent co-incubation strategy, *J Control Release* **134**, 221–227.
 22. Futaki, S., Ohashi, W., Suzuki, T., Niwa, M., Tanaka, S., Ueda, K., Harashima, H., and Sugiura, Y. (2001) Stearylated arginine-rich peptides: a new class of transfection systems, *Bioconjug Chem* **12**, 1005–1011.
 23. Nakamura, Y., Kogure, K., Futaki, S., and Harashima, H. (2007) Octaarginine-modified multifunctional envelope-type nano device for siRNA, *J Control Release* **119**, 360–367.
 24. Kang, S. H., Cho, M. J., and Kole, R. (1998) Up-regulation of luciferase gene expression with antisense oligonucleotides: implications and applications in functional assay development, *Biochemistry* **37**, 6235–6239.
 25. Morris, M. C., Depollier, J., Mery, J., Heitz, F., and Divita, G. (2001) A peptide carrier for the delivery of biologically active proteins into mammalian cells, *Nat Biotechnol* **19**, 1173–1176.

Chapter 27

Internalization of Nucleoside Phosphates into Live Cells by Complex Formation with Different CPPs and JBS-Nucleoducin

Franziska Mussbach, Regina Pietrucha, Buerk Schaefer, and Siegmund Reissmann

Abstract

Nucleoside phosphates can bind to many functional proteins like G-proteins or other GTP-binding proteins in signal transduction or translation processes. Till now internalization of nucleoside phosphates into live cells remains a challenge. We study the internalization of a fluorescent-labelled deoxyuridine triphosphate into HeLa cells and other adhesion and suspension cells. We use different cell-penetrating peptides and a cocktail suitable for formation of non-covalent complexes with the nucleotide. Internalization is observed by fluorescence microscopy, and the uptake efficiency is quantitatively estimated by fluorescence spectroscopy. The applied concentrations of CPPs and the cocktail were checked on cell viability (MTT test) and membrane integrity (bioluminescence test with peptidyl-luciferin), indicating that the CPPs and the complexes with the nucleotide are cytotoxic above certain concentrations. These concentrations depend on CPP and cell type and are the limiting factors for the cargo uptake.

Key words: CPPs forming non-covalent complexes, Internalization of nucleoside phosphates, Cargo amount per cell, Optimization of internalization, Wash procedures, Highest non-toxic concentrations of CPPs and JBS-Nucleoducin, Adhesion and suspension cell lines, Viability, Membrane integrity

1. Introduction

Many intracellular proteins can bind nucleoside phosphates, e.g. nucleoside triphosphates (NTPs). Thus GTP binds on the one hand to initiations-, elongations-, and translocation-factors of

the translational machinery and on the other hand to guanine nucleotide-binding proteins of G-protein-coupled receptors (GPCR) or proteins from the Ras-family. Ras GTP/GDP levels are tightly controlled in cells which activates Ras by GTP uptake leading to a concerted downstream activation of a series of effector proteins.

But it is difficult to transport nucleoside phosphates into live cells. The commonly applied compound streptolysine damages the cell membrane strongly and limits measurements of intracellular processes to seconds or few minutes (1). To overcome these limitations we check some cell penetrating peptides for their transport efficiency for this cargo.

Manipulations on intracellular processes require in many cases a distinct intracellular concentration of the transported cargo. For this reason the transduction process is studied and improved. A fluorescent-labelled deoxyuridine triphosphate is used as cargo. The uptake of the labelled nucleotide is measured qualitatively by fluorescence microscopy and quantitatively by fluorescence spectroscopy. Uptake efficiencies of the used cell-penetrating peptides and the cocktail JBS-Nucleoducin are estimated. Because uptake is limited by the concentration-dependent cytotoxic effect of CPPs or cocktail, cell viability (2–4) and membrane integrity (5) are measured. The highest non-toxic concentrations for the used adherent and suspension cell lines are experimentally estimated. Calculating the cellular volume of HeLa cells from microscopic pictures the highest available intracellular concentration of NTP and its amount per cell is determined. The internalized amount of cargo can be falsified by cargo adhesion on the cell membranes. To measure only the real uptake and to avoid wrong results, different wash procedures are used and compared with each other.

Based on their different amino acid sequences the used CPPs differ in their stability in buffer solution and against extracellular and intracellular proteases. They are either very hydrophilic-like HIV-TAT, Penetratin, and MPG β or hydrophobic-like MPG α , and CAD-2. The latter is especially hydrophobic. These differences lead to preferences for different cargos and membrane structures and to different uptake processes. For scientific research are such relations between cell lines, membrane structures including membrane potentials, cargos, and uptake mechanisms of great interest. From practical point of view an optimized cocktail creates advantages. Thus the cocktail JBS-Nucleoducin allows a universal approach for cargo internalization through compatibility with numerous cell types, with various membrane structures, triggering different mechanisms of transduction. Furthermore the cocktail shows higher transduction efficiency compared to single CPPs.

2. Materials

2.1. Cell-Penetrating Peptides and Cocktail "JBS-Nucleoducin"

1. MPG α (6–9): AcGALFLAFLAAALSLMGLWSQPKKRKKV-NH-CH₂-CH₂-SH, five positive charges, MW 3,047 Da, Jena Bioscience GmbH.
2. MPG β (6–9): AcGALFLGFLGAAGSTMGAWSQPKKRKKV-NH-CH₂-CH₂-SH, five positive charges, MW 2,910 Da, Jena Bioscience GmbH.
3. CAD-2 (6–9): GLWRALWRLLRSLWRLWKA-NH-CH₂-CH₂-SH, six positive charges, MW 2,653 Da, Jena Bioscience GmbH.
4. Penetratin (6, 7, 10): RGIKWFGNRRMKWKK, eight positive charges, MW 2,247 Da.
5. HIV-Tat (47–57) (4, 11, 12): YGRKKRRQRR, nine positive charges, MW 1,560 Da.
6. CPPP-2 (BAX inhibitory peptide) (13): KLPVM, two positive charges, MW 605 Da, Jena Bioscience GmbH.
7. JBS-Nucleoducin, Jena Bioscience GmbH.

2.2. Cell Cultures

2.2.1. Adhesion Cells

1. HeLa (Human cervic carcinoma).
2. COS-7 (African green monkey kidney).
3. NIH 3T3 (Swiss mouse embryo).

2.2.2. Suspension Cells

1. Jurkat (Human T-cell leukaemia).
2. NB-4 (Human acute promyelocytic leukaemia).
3. Kasumi-1 (Human acute myeloid leukaemia).

2.3. Fluorescence-Labelled Nucleotide

Aminoallyl ATTO488-dUTP, Jena Bioscience GmbH.

2.4. Fluorescence Microscopy

Fluorescence microscope, Axiophot, Carl Zeiss, Oberkochen, Germany.

2.5. Fluorescence Spectroscopy

Fluorescence spectrometer LS50, Perkin Elmer, Waltham, USA.

2.6. Viability Assay

MTT Test, Jena Bioscience GmbH.

The assay is performed according to the instructions.

2.7. Membrane Integrity Assay

Cyto-Tox-Glo™ Cytotoxicity Assay, Promega, Madison, USA.

The assay is performed according to the instructions and adapted to 96-well plates.

2.8. Mycoplasma Test

Mycoplasma Detection Kit, Jena Bioscience GmbH.
The test is performed according to the instructions.

2.9. Cell Permeabilization with Streptolysine

Membrane permeabilization with streptolysine is achieved according to the procedure described by Rubio et al. (1).

2.10. Buffers

1. Tris, PUFFERAN[®], Carl Roth, Karlsruhe.
2. HEPES, PUFFERAN[®], Carl Roth, Karlsruhe.
3. Dulbecos PBS 1×, without Ca and Mg, pH 7.0–7.5.
4. Glycine buffer, pH 3, 200 mM.

Heparin sodium salt from porcine intestinal (Heparin).

3. Methods

3.1. Complex Formation

1. Prepare stock solutions of CPPs (see Note 1) or JBS-Nucleoducin (see Note 2). Dissolve 0.5 mg of CPP and the whole content of the JBS-Proteoducin tube according to the instructions in the calculated volume (1.25–1.50 ml) of sterile and oxygen-free water (bubble helium or argon through the water). To get by CPPP-2 (see Note 3) the required ten times higher molar ratio dissolve 1.2 mg in 1 ml. Vortex and repeat 3× freezing to –80°C and thawing. Sonicate 5 min. Use the stock solutions immediately or aliquote and store aliquots at –20°C.
2. Dissolve separately 1 µg of nucleotide (MW ca 500 Da, containing 3–4 negative charges) and 3–5 µl stock solution of CPPs or JBS-Nucleoducin each in 100 µl of phosphate buffer (e.g. Dulbecos PBS 1×). Mix both solutions thoroughly by repeated pipetting (6×). Incubate mixture for 30 min at 37°C to achieve complex formation. The molar ratio of cargo to nucleotide should be calculated to 1:10. When using CPPs you can also calculate a tenfold excess of positive charges from CPP (see Subheading 2). For internalization of higher amounts you can multiply both, the amount of nucleotide and of stock solution of CPP or cocktail, respectively. Multiply no more than up to five times. Before using higher amounts than 5 µg nucleotide the cytotoxicity of required amounts of CPPs/cocktail, nucleotide or complex should be tested.

3.2. Internalization

The transduction protocol is calculated for six-well/35-mm culture plates. For other vessels please adjust volumes of media accordingly.

Cultivate and transduce cells under the commonly used optimum conditions (see Note 4). Use cells only to low passage numbers (see Note 5), check the cells microscopically for their vital shape, the absence of bacteria, and additionally check for the absence of mycoplasma by PCR (see Note 6). Add a solution of penicillin and streptomycin to prevent growth of bacteria during incubation.

3.2.1. Adherent Cells

1. Aspirate medium from prepared cells thoroughly and wash three times with PBS at 37°C.
2. Add 200 µl of complex solution followed by 400 µl of serum-free medium.
3. Mix gently and incubate for 1 h at 37°C in a humidified atmosphere containing 5% CO₂.
4. Add 1 ml of complete growth medium and continue incubation at 37°C for approximately 20 h in a humidified atmosphere containing 5% CO₂.
5. Wash the cells 2× with PBS, 3× with glycine buffer (pH 3) and 2× with PBS (2 ml each).

3.2.2. Suspension Cells

1. Suspend the thoroughly washed cell pellet in 200 µl of complex solution followed by 400 µl of serum-free medium.
2. Mix gently and incubate for 1 h at 37°C in a humidified atmosphere containing 5% CO₂.
3. Add 1 ml of complete growth medium and continue incubation at 37°C for approximately 20 h in a humidified atmosphere containing 5% CO₂.
4. Wash/spin down cells twice with PBS, three times with glycine buffer (pH 3) and twice with PBS (2 ml each).

3.3. Qualitative Detection of Internalized Cargo by Fluorescence Microscopy

1. Growth cells on a cover slip (0.15 × 10⁶ cells per well). Use cover slips with modified surface (poly-lysine) for adhesion of suspension cells. Give the slip into a well before growing the adherent cells or before transferring transduced suspension cells.
2. After incubation place cover slip on a slide and observe fluorescence directly without fixation. Use a magnification of >100.
3. Use fluorescence microscopy to visualize cell shape (viability), to estimate transduction efficiency and to check intracellular distribution (vesicle, nucleus) (see Note 7).

3.4. Quantitative Detection of Internalized Cargo by Fluorescence Spectroscopy

1. Form complexes of ATTO488-dUTP with JBS-Nucleoducin as described above: 1 µg ATTO488-dUTP stock solution in 100 µl PBS with 6 µl stock solution of JBS-Nucleoducin in 100 µl PBS.

2. To study the internalization efficiency of different amounts of complexes use higher volumes of stock solutions from cargo and cocktail for complex formation: e.g. 0.5, 1, 5, and 10 μg ATTO488-dUTP with corresponding 3, 6, 30, and 60 μl JBS-Nucleoducin.
3. Cultivate and transduce HeLa cells as described above with the formed complexes. Final concentrations of complexes with ATTO488-dUTP enrich in the incubation medium (1.6 ml) 0.3, 0.6, 3.0, and 6.0 μM .
4. Wash the cells thoroughly: twice with PBS, three times with glycine buffer (pH 3), and twice with PBS.
5. Add 2 ml DMSO to each well and perform cell lyses by sonication.
6. Remove cell particles by centrifugation (15 min at $14,100\times g$).
7. Use untreated cells for estimation of zero fluorescence.
8. Measure concentration-dependent fluorescence of ATTO488-dUTP: excite at 500 nm and measure intensity at 534 nm.
9. Measure fluorescence of each probe and subtract zero value from non-transduced cells.

3.4.1. Comparison of Different Wash Procedures

1. Cultivate and transduce HeLa cells as described above and wash the cells thoroughly twice with PBS, three times either with PBS, either with glycine buffer (pH 3), or with glycine buffer containing 1% heparin. Wash all probes finally twice with PBS (see Note 8).
2. Compare the fluorescence spectra after cell lyses and centrifugation (Fig. 1).

3.4.2. Use of Auxiliary Compounds for High Yield Internalization

1. To enhance transduction efficiency bovine serum albumin (1%, see Note 9) and up to 10% DMSO (see Note 10) and protease inhibitors (aprotinin and/or *o*-phenanthroline, see Note 11) can be added to the serum-free incubation medium.
2. To release the cargo from intracellular vesicles destabilizers like chloroquine, wortmannin, and Ca-ions can be added after finishing the transduction process (see Note 12).
3. Application of auxiliaries requires checking their cytotoxicity (Fig. 2).

3.5. Viability Assay

The assay is performed according to the instructions as an MTT test. Six-well plates are used (see Note 13). Each value is estimated as a triplicate with a SD of ± 1.3 . Cells are transduced with CPPs and cocktail as described above and checked for their viability (Figs. 3 and 4).

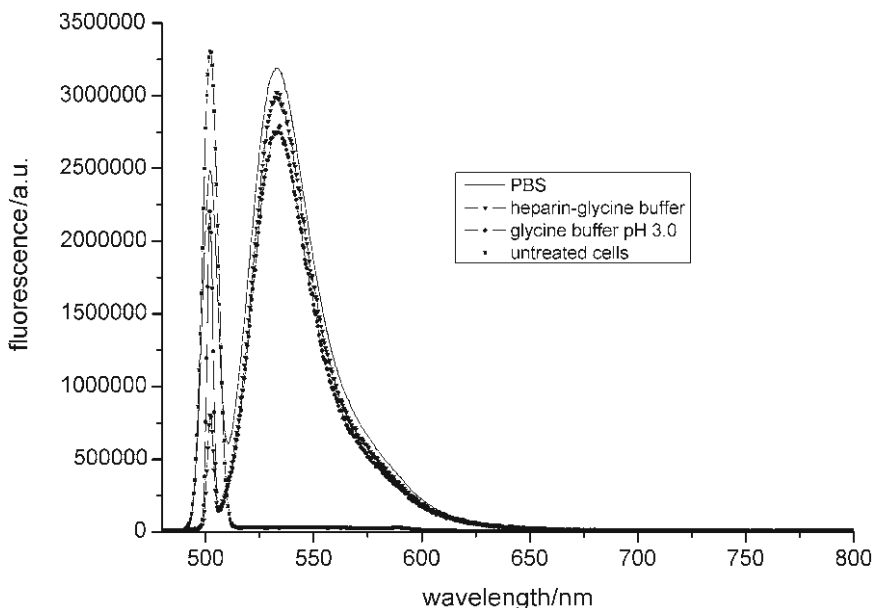


Fig. 1. Fluorescence spectra measured after uptake of ATTO488-dUTP using different washing procedures. Aminoallyl ATTO488-dUTP (1 μ g) is internalized (1 h serum-free, 20 h complete serum, 37°C) into HeLa cells after complex formation with JBS-Nucleoducin (3 μ l stock solution) at 37°C. Cells were washed three times with different buffers: PBS, glycine buffer (pH 3, 200 mM) and glycine buffer with 1% heparine, and finally twice with PBS. After cell lyses and centrifugation fluorescence spectra were measured at 540 nm. Comparison shows only marginal differences between the obtained curves, indicating equal amounts of internalization and only very small differences in the amount of adsorbed fluorescent nucleotide.

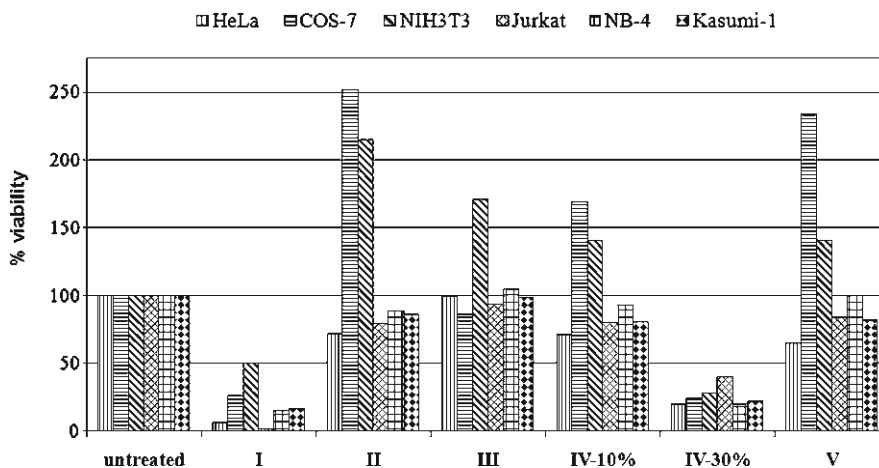


Fig. 2. Influence of auxiliary compounds on the viability of HeLa cells. Auxiliary compounds like permeability enhancers, protease inhibitors, and vesicle destabilizers can improve the transduction process. Their influence on cell viability depends on concentration and strongly on cell line. Millimolar concentrations of Ca^{++} reduce the viability of all six cell lines, whereas wortmannin and chloroquine can be used to destabilize vesicles. BSA can act as a co-substrate for proteases and influences the viability only marginally. 10% DMSO in serum-free transduction medium may enhance penetration without strong influence on viability. I: 6 mM Ca^{2+} ; II: 120 μ M Wortmannin; III: 0.5% BSA; IV-10%: 10% DMSO; IV-30%: 30% DMSO; V: 120 μ M Chloroquine.

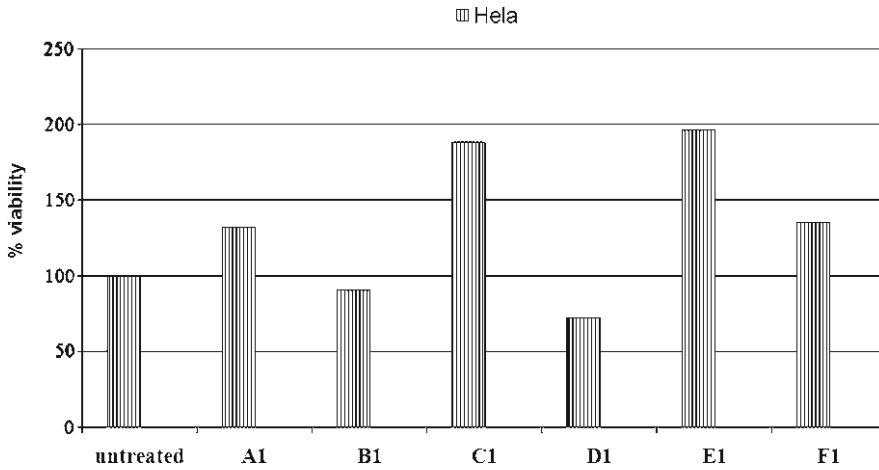


Fig. 3. Influence of different CPPs on the viability of HeLa cells. HeLa cells were cultivated under commonly used conditions and treated in serum-free medium for 1 h at 37°C with different CPPs. After removal of CPPs and repeated washings the viability of the cells was estimated by the MTT test. Untreated cells are defined as 100% viable. Since MPGβ and Penetratin reduces the viability, TAT, CAD-2, and CPPP-2 enhance the mitochondrial dehydrogenase activity, probably evoked by stabilization of the mitochondria or by cell proliferation A1: 8.2 μM MPGα; B1: 8.6 μM MPGβ; C1: 9.4 μM CAD-2; D1: 11.1 μM Penetratin; E1: 18.1 μM CPPP-2; F1: 16 μM TAT.

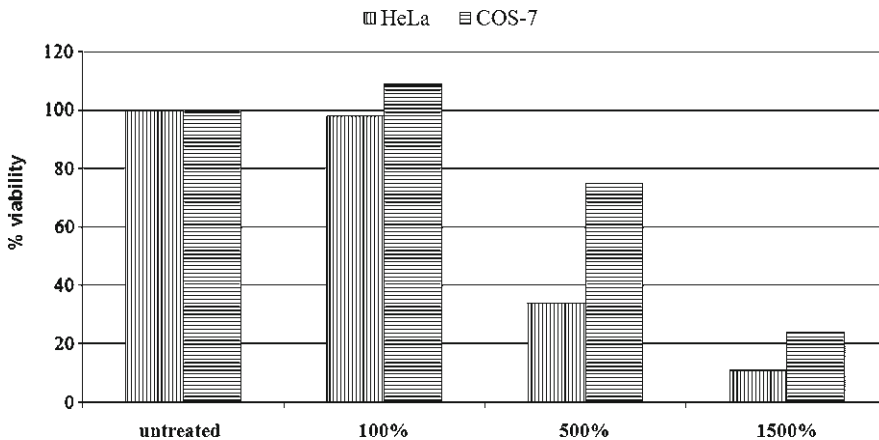


Fig. 4. Influence of JBS-Nucleoducin on the viability of HeLa- and COS-7 cells. HeLa- and COS-7 cells were cultivated and treated in serum-free medium for 1 h at 37°C with 3 μl (100%), 15 μl (500%), and 45 μl (1500%) stock solution of the cocktail JBS-Nucleoducin in 600 μl serum-free incubation medium. Viability was estimated by MTT test. Only an amount of 3 μl (100%) does not reduce the cell viability. Higher amounts reduce the viability strongly. Because the cocktail contains relatively high amounts of CPPs to form non-covalent complexes with nucleotides and plasmids, its amount should not exceed 6 μl of stock solution in 600 μl incubation medium.

3.6. Membrane Integrity Assay

Promega, Madison, USA.

The Cyto-Tox-Glo™ Cytotoxicity Assay is performed according to the instructions and adapted to 96-well plates (see Note 14).

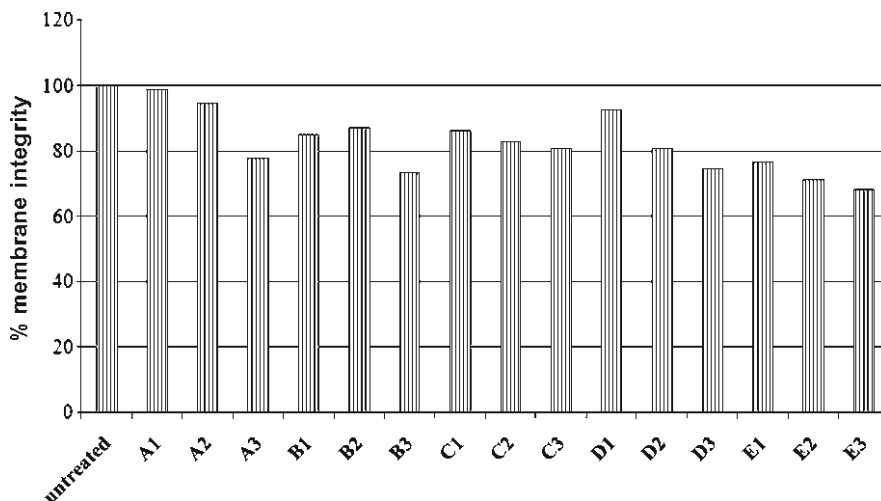


Fig. 5. Influence of different CPPs at increasing concentrations on the membrane integrity of HeLa cells. HeLa cells were cultivated under commonly used conditions and treated in serum-free medium for 1 h at 37°C with different CPPs. After removal of CPPs and repeated washings the membrane integrity of the cells was estimated by the bioluminescence test “Cyto-Tox-Glo™” measuring the release of a cytosolic protease. The CPPs were applied in higher concentrations than for the MTT test. Even in a more than tenfold higher concentration, compared to viability measurements the membrane integrity is only slightly reduced MPG α : A1 = 8.2 μ M, A2 = 41 μ M, A3 = 123 μ M; MPG β : B1 = 8.6 μ M, B2 = 43 μ M, B3 = 129 μ M; CAD-2: C1 = 9.4 μ M, C2 = 47 μ M, C3 = 141 μ M; Penetratin: D1 = 11.1 μ M, D2 = 55.5 μ M, D3 = 166.5 μ M; CPPP-2: E1 = 181 μ M, E2 = 543 μ M, E3 = 1629 μ M.

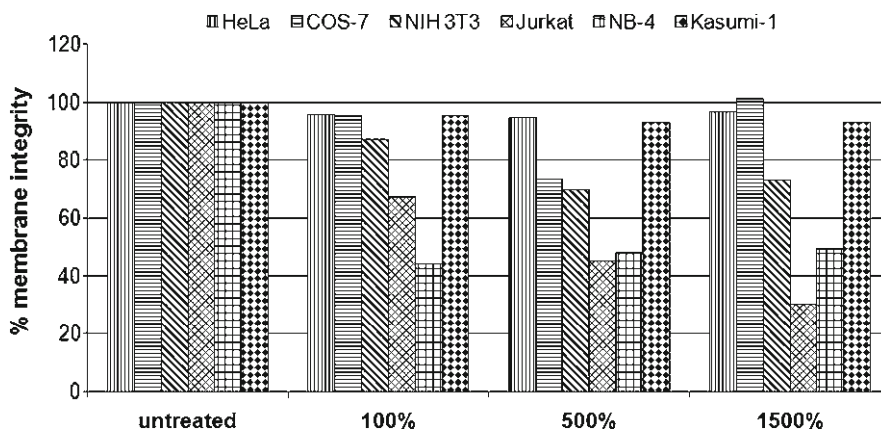


Fig. 6. Influence of JBS-Nucleoducin on the membrane integrity of different cells. The cell lines were cultivated and treated in serum-free medium for 1 h at 37°C with 3 μ l (100%), 15 μ l (500%), and 45 μ l (1,500%) stock solution of the cocktail JBS-Nucleoducin in 600 μ l serum-free incubation medium. Membrane integrity was estimated by the bioluminescence test “CytoTox-Glo™.” Some cell lines are even sensitive to the normal concentration of JBS-Nucleoducin, e.g. Jurkat and NB-4 cells. Other cell lines, including HeLa-, COS-7, and Kasumi-1, are able to tolerate high concentrations (1,500%). The result differs generally from that obtained with the MTT-test.

Each value is estimated as a triplicate with a SD of ± 1.2 . Cells are transduced with CPPs and cocktail as described above and checked for their membrane integrity (Figs. 5 and 6).

4. Notes

1. Formation of the complex is to perform in water or buffer, in an appropriate concentration, without medium, BSA, protease inhibitors, or other auxiliary substances. Use sonification to dissolve CPPs. Store the CPPs in solid state at -20°C in a dry atmosphere. Aliquoted stock solutions in sterile water should be stored in frozen state below -20°C .
2. The cocktail is checked at certain cell lines and is designed for a broad use. If the transduction efficiency is too low check other CPPs and optimize the conditions for the most efficient one.
3. CPPP-2 uses yet unidentified mechanisms for cell penetration including mechanisms not requiring interaction with proteoglycans. It is a cytoprotective peptide and can reduce the cytotoxicity of other CPPs. Since it is designed from BAX-inhibiting peptides it influences intracellular processes.
4. Some cells need to grow in special media, e.g. special calf sera. Use the optimized conditions. Let the cells grow up to a density of about 0.3×10^6 per 35 mm well. Higher densities of adherent cells reduce the uptake efficiency.

The internalization procedure can be optimized by changing the transduction temperature (4, 25, and 37°C), transduction time with serum-free medium (from 30 min to 6 h) and cultivation with complete medium (from 1 to 20 h).
5. Uptake efficiency and cytotoxic effects of CPPs depend on the passage number. But both effects differ by different cell lines.
6. Look for morphology of the cells and use the PCR-test to check for the absence of mycoplasma. Treat the cells to eliminate mycoplasma.

Check microscopically the cells for bacteria. If the cell culture is infected cultivate new cells from the stock, work under sterile conditions and add antibiotics.
7. The commonly used fluorescence labels have a different stability against bleaching by excitation. Avoid FITC-analogues, use Atto- and other more stable fluorescent labels.
8. Wash the cells after transduction thoroughly to remove adsorbed cargo. You can also use PBS containing 0.1% trypsin. But, avoid detachment of adherent cells.
9. BSA acts as a co-substrate for extra and intracellular proteases and enhances the cargo uptake in cancer cells.
10. DMSO enhances the permeability of cell membranes and influences in concentrations up to 10% (v/v) the viability only

marginally. For transduction use for six-well plates 10% DMSO in the final volume of 600 μl . Thus add the amount of DMSO after complex formation with the serum-free medium (400 μl containing 60 μl DMSO) to the transduction medium.

11. CPPs and cocktail can be degraded by secreted or membrane bound enzymes. To reduce this inactivation BSA, aprotinin, o-phenanthroline, and also other protease inhibitors can be added. But, avoid by the cocktail, MPG α , MPG β , and CAD-2 the addition of SH-reactive inhibitors.
12. Addition of 150 μM chloroquine, wortmannin, or 6 mM Ca⁺⁺ is recommended to destroy the vesicles. These compounds are given to the complete medium after transduction. Especially in the case of Ca⁺⁺ its toxicity to the used cell line should be tested before use. By the use of wortmannin keep in mind, that this inhibitor influences the PI3-kinase-mediated signal transduction.
13. Cells are seeded 1 day before treatment. Used cell densities are for adherent cells 0.3×10^6 /well and for suspension cells 1.0×10^6 /2-ml tube. After thoroughly washing with PBS (3 \times) the cells are incubated as described above with CPPs or the cocktail in interesting concentrations. After 1-h incubation at 37°C in a humidified atmosphere the serum-free medium is aspirated and replaced by complete growth medium, which contains MTT (0.5 mg/ml). After further incubation for 4 h at 37°C remove the medium to about 85% and replace it by acidic DMSO. After incubation for 10 min at 37°C remove pellets by centrifugation (5 min, $14 \times 10^3 \times g$) and measure the absorbance of the supernatant at 508 or 540 nm. Cell viability is estimated by correlation of obtained values to the mean value of untreated cells (=100%).
14. Trypsinated adherent and suspension cells are thoroughly washed and resuspended in serum-free medium, counted and diluted to 100,000 cells/ml. Each well in a 96-well plate is filled with 10,000 cells and incubated as above described with CPPs or cocktail in interesting concentrations for 1 h at 37°C. After cleavage of peptidyl-luciferin (15-min incubation) by released dead protease and addition of luciferase the bioluminescence is measured (L). Digitonin as reagent for cell lyses is given to all wells and after 15 min incubation at room temperature the luminescence is measured again to estimate the total content of dead protease ($L_{\text{total}} = 0\%$ membrane integrity). Untreated cells have 100% membrane integrity (L_0). Membrane integrity is calculated in percent by the following equation: $(L - L_0 / L_{\text{total}}) \times 100$.

5. Conclusions and Perspectives

Nucleoside phosphates are ligands or substrates for many intracellular proteins. Their transport into the cell evokes intracellular reactions and allows therefore studies on signal pathways. Till now the transport of these negatively charged compounds through cell membranes remains a challenge. For this purpose, the commonly used streptolysine damages the membrane dramatically, allows measurements for less than 5 min and transports very low amounts, not detectable with fluorescence spectroscopy. Only by radioactive labelling the internalized nucleotides can be measured. Because some functional proteins require sufficiently high concentrations of NTPs for binding and functionality we optimized their transport through cell membranes using cell penetrating peptides. Because of the absence of functional groups for formation of covalent conjugates with nucleotides the formation of non-covalent complexes between cargo and carrier is the only way for their internalization.

Till now the uptake was quantitatively evaluated by MALDI-TOF mass spectrometry (14) and by HPLC of fluorescent CPPs (15). The use of Atto488-dUTP as a fluorescent-labelled cargo allows qualitative as well as quantitative measurements of its uptake. Fluorescence microscopy provides a qualitative comparison. Atto488-dUTP (1 µg) is complexed with different CPPs and transported into HeLa cells. The uptake of fluorescent nucleotide is qualitatively estimated by fluorescence microscopy after thoroughly washing. Derived from the fluorescence intensities of the microscopic pictures the transduction efficiencies of the different cell-penetrating peptides are estimated. The following rank order is found for HeLa cells:

CAD-2 > MPGα = MPGβ > Penetratin » CPPP-2.

HIV-TAT (47-57) is unable to transport the NTP into the cell, whereas high concentrations of the BAX inhibitory peptide CPPP-2 transduce fluorescent NTP, but only in a low amount. Penetratin shows in contrast to the transport of peptides and proteins a sufficient efficiency in delivery. Addition of auxiliary compounds like BSA (0.5–1%), DMSO (10%), and protease inhibitors enhance the fluorescence of the microscopic picture slightly. Also prolongation of medium-free transduction time up to 4 h enhances the fluorescence.

Internalization is quantitatively measured at HeLa cells using fluorescence spectroscopy. After transduction and cell lyses the internalized amount is measured by fluorescence intensity of the ATTO-labelled compound. This quantitative method is used to measure internalized amounts per cell, intracellular concentrations and the attainable maximum of both. This method allows also estimation of

the influence of wash procedures on the internalized amount and allows the comparison to internalization with streptolysine.

One of the important problems by the quantitative determination of the transduced compounds is the complete removal of complexes from the outside of the plasma membrane. Used CPPs contain between two and nine positive charges and form positively charged complexes with the cargo, which bind to negatively charged structures (glycans) on the outside of the membrane. After finishing the internalization procedure the cells must be washed very thoroughly. We compared PBS to glycine buffer at pH 3 and to glycine buffer with heparin. The acidic glycine buffer is expected to remove the complexes by protonation of the lysine and arginine side chains better than PBS. Heparin has a structure similar to glycan structures at the outer membrane. Addition of heparin to the wash buffer should help to remove adsorbed complexes by competition. But, the fluorescence spectra of probes obtained after these three different wash procedures show only marginal differences.

This result (Fig. 1) indicates that probably the glycine buffer is able to remove the adsorbed complexes. Heparin shows no additional effect compared to glycine buffer alone. Thus we apply in our experiments a wash procedure with acidic glycine buffer.

The internalized amount of nucleotide is calculated from the fluorescence intensity of probes obtained with increasing extracellular concentrations of complexes with JBS-Nucleoducin. Internalized amounts are taken from a standard curve with ATTO488-dUTP, measured under the same conditions. JBS-Nucleoducin is able, in contrast to streptolysine, to transduce measurable amounts of the nucleotide. The percentage of uptake is higher at low extracellular concentrations. The intracellular amount can enrich 1.5 amole per cell. Taking the mean diameter of HeLa cells from fluorescence microscopic pictures their volume can also be calculated and used to estimate the intracellular concentration, which can enrich the low micromolar range.

The internalization process is limited by the concentration-dependent toxicity (3–5) of CPPs, cocktail, and cargo. With the aim to estimate the optimum concentration for cargo internalization into live cells the influence of CPPs and the cocktail is studied on viability and membrane integrity. Figures 2–6 show the cytotoxic effects of CPPs and JBS-Nucleoducin. The viability measured by the MTT test is reduced as well as by increasing concentrations of some single CPPs (Fig. 3) and of the cocktail, which in 15 times higher concentrations reduces the viability of HeLa cells even strongly (Fig. 4). In contrast to the viability the membrane integrity of HeLa cells is only slightly influenced by the most used CPPs, also at high concentrations (Fig. 5). The cytoprotective BAX inhibitory peptide CPPP-2 is applied in a ten times higher concentration than the other CPPs and shows no reduction of membrane integrity, too. The same picture is

obtained with JBS-Nucleoducin. Also the highest used concentration (1,500%= 15 times higher than recommended for 0.5 µg NTP) has no effect on the integrity of the HeLa cell membrane. Other cell lines, e.g. Kasumi and COS-7 are in the same manner insensitive as HeLa cells. Increasing concentrations of JBS-Nucleoducin reduce the membrane integrity of NIH 3T3 cells slightly and that of Jurkat cells even strongly (Fig. 6).

The strong differences found between the both cytotoxicity tests result from the different mechanisms, based on the oxidative activity of mitochondria (MTT test) on the one hand and on the integrity of the cell membrane on the other hand. Our FACS analysis with propidium iodide (not shown here) corresponds with the bioluminescence test for membrane integrity. To avoid wrong results due to working with damaged cells we recommend the use of low concentrations (1–5 times) of CPPs and no more as the recommended concentration of the cocktail. Each cell line has to be tested separately because the cells are differently sensitive to CPPs, to the cocktail, and to complexes formed with the cargo.

Acknowledgments

The authors would like to thank for helpful and kind support Prof. Hans Agricola for fluorescence microscopy, Dr. Eckhard Birckner for fluorescence spectroscopy, Prof. Thorsten Heinzl, Dr. Enrico Jandt, and Sigrid Reichardt for microscopical investigations and the bioluminescence test.

References

- Rubio, I., Pusch, R., and Wetzker, R. (2004) Quantification of absolute Ras-GDP/GTP levels by HPLC separation of Ras-bound [³²P]-labelled nucleotides. *J Biochem Biophys Methods* **58**, 111–117.
- Saar, K. and Langel, Ü. (2007) Toxicity Methods for Cell-Penetrating Peptides in *Handbook of Cell-Penetrating Peptides* (Ed. Ü. Langel), 2nd Edition, CRC-Press, Boca Raton, FL, pp. 553–565.
- Fenton, M., Bone, N., and Sinclair, A. J. (1998) The efficient and rapid import of a peptide into primary B and T lymphocytes and a lymphoblastoid cell line. *J Immunol Methods* **212**, 41–48.
- Wu, R. P., Youngblood, D. S., Hassinger, J. N., Lovejoy, C. E., Nelson, M. H., Iversen, P. L., and Moulton, H. M. (2007) Cell-penetrating peptides as transporters for morpholino oligomers: effects of amino acid composition on intracellular delivery and cytotoxicity. *Nucleic Acids Res* **35**, 5182–5191.
- Niles, A. L., Moravec R. A., Hesselberth, P. E., Scurria, M. A., Daily, W. J., and Riss, T. L. (2007) A homogeneous assay to measure live and dead cells in the same sample by detecting different protease markers. *Anal Biochem* **366**, 197–206.
- Gros, E., Deshayes, S., Morris, M. C., Aldrian-Herrada, G., Depollier, J., Heitz, F., and Divita, G. (2006) A non-covalent peptide-based strategy for protein and peptide nucleic acid transduction. *Biochim Biophys Acta* **1758**, 384–393.
- Morris, M. C., Deshayes, S., Heitz, F., and Divita, G. (2008) Cell-penetrating peptides: from molecular mechanisms to therapeutics. *Biol Cell* **100**, 201–217.
- Simeoni, F., Morris, M. C., Heitz, F., and Divita, G (2003) Insight into the mechanism

- of the peptide-based gene delivery system MPG: implication for delivery of siRNA into mammalian cells. *Nucleic Acids Res* **31**, 2717–2724.
9. Morris, M. C., Gros, E., Aldrian-Herrada, G., Choob, M., Archdeacon, J., Heitz, F., and Divita, G. (2007) A non-covalent peptide-based carrier for in vivo delivery of DNA mimics. *Nucleic Acids Res* **35**, e49.
 10. Derossi, D., Joliot, A. H., Chassaing, G., and Prochiantz, A. (1994) The third helix of the Antennapedia homeodomain translocates through biological membranes. *J Biol Chem* **269**, 10444–10450.
 11. Ignatovich, I. A., Dishe, E. B., Pavlotskaya, A. V., Akifiev, B. N., Burov, S. V., Orlov, S. V., and Perevozchikov, A. P. (2003) Complex of plasmid DNA with basic domain 47–57 of HIV-1 Tat protein are transferred to mammalian cells by endocytosis-mediated pathways. *J Biol Chem* **43**, 42625–42636.
 12. Jeang, K. T., Xiao, H., and Rich, E. A. (1999) Multifaced activities of the HIV-1 transactivator of transcription Tat. *J Biol Chem* **274**, 28837–28840.
 13. Gomez, J. A., Gama, V., Yoshida, T., Sun, W., Hayes, P., Leskov, K., Boothman, D., and Matsuyama, S. (2007) Bax-inhibiting peptides derived from Ku70 and cell-penetrating pentapeptides. *Biochem Soc Trans* **35**, 797–801.
 14. Aussedat, B., Sagan, S., Chassaing, G., Bolbach, G., and Burlina, F. (2006) Quantification of the efficiency of cargo delivery by peptidic and pseudo-peptidic Trojan carriers using MALDI-TOF mass spectrometry. *Biochim Biophys Acta* **1758**, 375–383.
 15. Palm, C., Netzereab, S., and Hällbrink, M. (2006) Quantitatively determined uptake of cell-penetrating peptides in non-mammalian cells with an evaluation of degradation and antimicrobial effects. *Peptides* **27**, 1710–1716.

Enhanced Cellular Delivery of Cell-Penetrating Peptide–Peptide Nucleic Acid Conjugates by Photochemical Internalization

Takehiko Shiraishi and Peter E. Nielsen

Abstract

Cell-penetrating peptides (CPPs) have been widely used for a cellular delivery of biologically relevant cargoes including antisense peptide nucleic acids (PNAs). Although chemical conjugation of PNA to a variety of CPPs significantly improves the cellular uptake of the PNAs, bioavailability (antisense activity) is still limited by endocytotic entrapment. We have shown that this low bioavailability can be greatly improved by combining CPP–PNA conjugate administration with a photochemical internalization technique using photosensitizers such as aluminum phthalocyanine (AlPcS_{2a}) or tetraphenylporphyrin tetrasulfonic acid (TPPS). Cellular uptake of the PNA conjugates were evaluated by using a sensitive cellular method with HeLa pLuc705 cells based on the splicing correction of luciferase gene by targeting antisense oligonucleotides to a cryptic splice site of the mutated luciferase gene. The cellular efficacy of CPP conjugates were evaluated by measuring luciferase activity as a result of splicing correction and was also confirmed by RT-PCR analysis of luciferase pre-mRNA.

Key words: Antisense, Cellular uptake, Cell-penetrating peptide, Peptide nucleic acid, Photochemical internalization

1. Introduction

In general, cellular delivery of larger, hydrophilic biomolecules such as oligonucleotides and in particular their charge neutral mimics can be significantly improved through conjugation to (or complexation with) cell-penetrating peptides [CPPs, or PTDs (protein transduction domains)] (1–4). However, it has become increasingly clear that cellular uptake of (most of) these peptides occurs through an endosomal internalization mechanism and consequently that endosomal escape is probably the greatest challenge to overcome in order to achieve sufficient cellular (and

eventually in vivo) bioavailability for drug discovery applications (5–7). Endosomal escape of CPP conjugates can be facilitated by a variety of auxiliary agents such chloroquine, Ca^{2+} , or certain light-activated photosensitizers (photochemical internalization, PCI) (8–11). In the present protocols, we describe the use of PCI exploiting the photosensitizers aluminum phthalocyanine (AlPcS_{2a}) or tetraphenylporphyrin tetrasulfonic acid (TPPS) for the cellular delivery of an antisense peptide nucleic acid (PNA)–Tat conjugate targeting the cryptic splice site in the globin-derived intron of the luciferase gene in the HeLa pLuc705 cell line (12). The experiment presented in Fig. 1 exemplify the very significant enhancing effects on PNA–Tat antisense activity of PCI using AlPcS_{2a} or TPPS assayed both by luciferase activity as well as mRNA splice correction by PCR (Fig. 2). The experiment presented in Fig. 3 shows the dependence of irradiation time as well as the importance of preincubation prior to irradiation to suppress toxicity.

2. Materials

2.1. Transfection of CPP–PNA Conjugates with PCI Method

1. Growth medium for cell culture: RPMI 1640 medium supplemented with 10% fetal bovine serum (FBS) and 1% Glutamax (Gibco).
2. Growth medium with a photosensitizer: RPMI1640 (10% FBS, 1% Glutamax) containing aluminum phthalocyanine

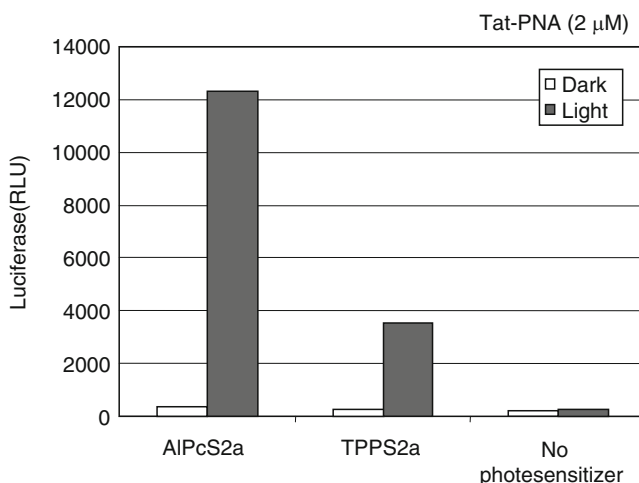


Fig. 1. Comparison of two photosensitizers [AlPcS_{2a} (5 $\mu\text{g}/\text{ml}$) or the TPPS (2 $\mu\text{g}/\text{ml}$)] for the PCI treatment effects on Tat–PNA (2 μM) transfection. HeLa pLuc705 cells, treated with one of the photosensitizer, were transfected with the Tat–PNA for 4 h and then irradiated with light (AlPcS_{2a} , 10 min with the *red light*. TPPS, 5 s with the *blue light*) after 4 h incubation in the complete growth medium. After 24 h incubation, the cells were subjected to the luciferase analysis.

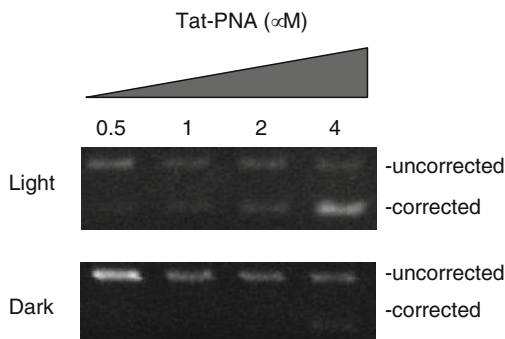


Fig. 2. Effect of PCI treatment on the splicing correction by Tat–PNA (2 μM). HeLa pLuc705 cells, treated with AIPcS_{2a} (5 $\mu\text{g}/\text{ml}$), were transfected with the Tat–PNA (0.5–4 μM for 4 h) and then irradiated with *red light* for 10 min. After 24 h incubation, the cells were subjected to the RT-PCR analysis.

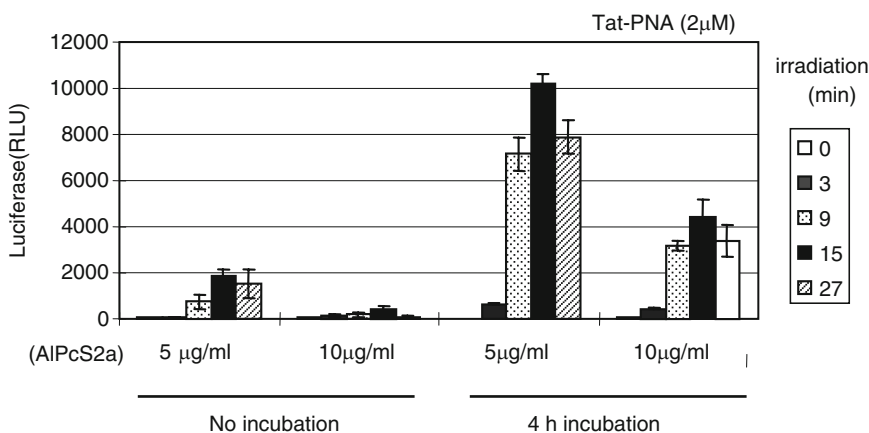


Fig. 3. Effect of PCI conditions (irradiation time, photosensitizer concentration) (4 h incubation before light irradiation) on the PCI-mediated Tat–PNA (H-GRKKRRRRPPQ-eg1-CCTCTTACCTCAGTTACA-NH₂) transfection into HeLa pLuc705 cells. The cells, treated with AIPcS_{2a} (5 or 10 $\mu\text{g}/\text{ml}$), were transfected with Tat–PNA (at 2 μM for 4 h) and then irradiated with *Red light* (0–27 min irradiation) after 0 or 4 h incubation in the complete growth medium. After 24 h incubation, the cells were subjected to the luciferase analysis.

(AIPcS_{2a}, Frontier Scientific) (5 $\mu\text{g}/\text{ml}$) or tetraphenylporphyrin tetrasulfonic acid (TPPS, Frontier Scientific) (2 $\mu\text{g}/\text{ml}$).

3. OPTI-MEM serum-free medium (Invitrogen).
4. CPP–PNA conjugates solution.
5. HeLa pLuc705 cells (Gene Tools).

Equipment (specially required)

- Light tubes: Red light irradiation (fluorescence tube; Arcadia, Cat. No. FO18) or blue light irradiation (40W/03 Phillips fluorescent light tube with maximum emission at 420 nm).

**2.2. Analysis
of the Splicing
Correction
by the Antisense
PNA with HeLa
pLuc705 Cells**

1. Phosphate-buffered saline (PBS).
2. Cell lysis buffer: Passive lysis buffer (Promega).
3. Luciferase Assay reagent (Promega).
4. Protein standards for calibration curve: 0–5 mg/ml of bovine serum albumin (BSA) solutions in the passive lysis buffer.
5. Protein assay kit: BCA Protein Assay kit (Pierce), make a working solution by mixing solution A and B at the ratio 50:1 just before measurement. Mix 5 μ l of the cell lysate (or the BSA standard) and 0.15 ml of the working solution and measure absorbance at 565 nm after 30 min incubation at 37°C.
6. Total RNA extraction kit: RNeasy Mini kit (Qiagen).
7. Luciferase primers (30 μ M each): Forward 5'-TTGATATGTGGATTTTCGAGTCGTC-3' and Reverse 5'-TGTC AATCAGAGTGCTTTTGGCG-3'.
8. RT-PCR master mix solution with OneStep RT-PCR Kit (Qiagen): Solutions for ten PCR samples (10 μ l each) 52.8 μ l of water, 22 μ l of 5 \times buffer, 4.4 μ l of dNTP mix (10 mM each), 4.4 μ l of enzyme solution, 2.2 μ l of the primers (both forward and reverse).

3. Methods

This method is designed for a 24-well plate format (although this can be applied for other formats depending on the required experimental setup by changing solution volume).

**3.1. Transfection
of CPP-PNA
Conjugates with PCI
Method**

1. Plate the HeLa pLuc705 cells (8×10^4 cells) in 24-well plates with 0.5 ml/well of growth medium (no antibiotics (see Note 1)) containing photosensitizer [5 μ g/ml of AlPcS_{2a} or 2 μ g/ml of TPPS (see Note 2)] and incubate at 37°C (5% humidified CO₂) the day before transfection.
2. Incubate the plate over night at 37°C (humidified 5% CO₂) (see Note 3).
3. Prepare the PNA solution by adding PNA stock solution to the OPI-MEM medium at the desired concentrations (see Note 4).
4. Remove entire growth medium and replace it with 0.3 ml/well of the PNA solution (from step 3) (see Note 5).
5. Incubate the plate for 4 h at 37°C (humidified 5% CO₂) (see Note 6).
6. Remove the PNA solution from the well and replace it with 0.5 ml/well of the growth medium.

7. Incubate the plate further for 4 h at 37°C (humidified 5% CO₂) (see Note 7).
8. Irradiate using light of the proper wavelength for photosensitizer excitation (For ALPcS_{2a}, 10 min with red light with maximum emission at 650–680 nm. For TPPS, 5 s with blue light tube with maximum emission at 420 nm.) (see Note 8).
9. Incubate the plate further for 1–3 days before the analysis.

**3.2. Analysis
of the Antisense PNA
Cellular Uptake by a
Splicing Correction
Assay Using HeLa
pLuc705 Cells**

This protocol is for the splicing correction analysis of antisense CPP–PNA conjugates using the HeLa pLuc705 cell line. The method is designed for analysis in a 24-well plate format, however it can be in different formats depending on the required experimental setup.

1. Take out the 24-well plate (from Subheading 3.1, step 9) and check the cells (see Note 9).
2. Remove the entire medium from the well.
3. Wash the cells with PBS (see Note 10).
4. Add 0.1 ml/well of the passive lysis buffer.
5. Incubate the plate on a plate shaker for at least 10 min (see Note 11).
6. Transfer the cell lysate to a 1.5 ml tube (see Note 12).
7. Analyze luciferase activity with 10 µl of cell lysate using 100 µl of luciferase assay reagent (10 s measurement) (see Note 13).
8. Quantify protein concentration of the cell lysates using the BCA protein assay kit based on a calibration curve from BSA protein standards.
9. Calculate the average of a number of samples and shown as relative light unit (luciferase activity as RLU) or calculate average RLU after normalize to the protein concentration (from step 8) and show as RLU/mg of protein.
10. Extract total RNA from 50 µl of the cell lysate (from step 6) using RNeasy kit (Qiagen) and adjust the RNA concentration to 1 ng/µl with RNase-free water (see Note 14).
11. Make an RT-PCR master mix solution and dispense 8 µl to a 0.2 ml PCR tube (see Note 15).
12. Add 2 µl of the RNA solution (1 ng/µl from step 10) to the PCR tube (from step 11) on ice (see Note 16).
13. Start a PCR machine with the following PCR program and set the PCR tubes when the sample block temperature reaches to 55°C. [(55°C, 35 min) × 1 cycle, (95°C, 15 min) × 1 cycle, (94°C, 0.5 min; 55°C, 0.5 min; 72°C, 0.5 min) × 26–28 cycles] (see Note 17).
14. Analyze samples by 2% agarose gel electrophoresis.

4. Notes

1. No antibiotics should be used in the growth medium since it will increase cellular toxicity.
2. The photosensitizer concentration must be optimized depending on the cell type and experimental setup [See Fig. 1 for comparison of two photosensitizers (AlPcS_{2a} and TPPS) and Fig. 3 illustrating the effect of photosensitizer concentration (AlPcS_{2a})].
3. The cells must be exponentially growing (A cell confluency of 40–60% at the transfection is recommended).
4. Use at least 0.3 ml/well of the PNA solution. Preheat OPTI-MEM in the 37°C incubator at least 30 min before start.
5. Try to remove the entire medium as serum inhibits a cellular uptake of CPP conjugates.
6. This incubation time must be optimized depending on the type of CPP conjugate and cell type.
7. This incubation step before irradiation (after PNA transfection) alleviates cellular toxicity by the PCI-treatment upon irradiation. Therefore, this incubation time should be optimized depending on the photosensitizer concentration and cell type (See Fig. 3 for the effect of postincubation (4 h) after PNA transfection).
8. These light intensities may be obtained by placing the plate at a distance of ca. 10 cm from the light tube. This irradiation time need to be optimized. Try 2–30 min irradiation for AlPcS_{2a} (See Fig. 3 for the effect of irradiation time for AlPcS_{2a}), and 1–60 s for TPPS.
9. Most of the cells must be viable (There should not be any significant cell death.).
10. Wash the cells gently to avoid detachment of the cells from the plate surface.
11. Ensure a complete cell lysis by microscope observation. Repeat freeze and thaw cycle(s) to help a complete cell lysis.
12. This cell lysate can be stored at –20°C for a few months.
13. Preheat all solutions (luciferase assay reagent and the cell lysate samples) to room temperature as the optimum temperature for the luciferase reaction is 25°C. This luciferase measurement can also be performed in a 96-well plate format by using a luciferase reagent with a longer signal half life such as the Bright-Glo assay reagent (Promega) designed for a high throughput measurement.
14. Use gloves to handle RNA samples in the following steps to avoid the RNase contamination.

15. Make this master mix solution on ice and keep the samples on ice during the following steps until you start RT-PCR.
16. Pipette 2 μ l of the RNA solution precisely and make sure to transfer all of it into an RT-PCR solution to obtain the comparable amplification for all samples. Optimize the amount of RNA for a reaction depending on the experimental set up.
17. PCR cycle number should be optimized depending on the RNA amount used for the RT-PCR. See Fig. 2 for the example of a splicing correction analysis of antisense Tat–PNA by RT-PCR.

References

1. Mäe, M., and Langel, Ü. (2006) Cell-penetrating peptides as vectors for peptide, protein and oligonucleotide delivery, *Curr Opin Pharmacol* **6**, 509–514.
2. Debart, F., Abes, S., Deglane, G., Moulton, H. M., Clair, P., Gait, M. J., Vasseur, J. J., and Lebleu, B. (2007) Chemical modifications to improve the cellular uptake of oligonucleotides, *Curr Top Med Chem* **7**, 727–737.
3. Gait, M. J. (2003) Peptide-mediated cellular delivery of antisense oligonucleotides and their analogues, *Cell Mol Life Sci* **60**, 844–853.
4. Zorko, M., and Langel, Ü. (2005) Cell-penetrating peptides: mechanism and kinetics of cargo delivery, *Adv Drug Deliv Rev* **57**, 529–545.
5. Fotin-Mleczek, M., Fischer, R., and Brock, R. (2005) Endocytosis and cationic cell-penetrating peptides – a merger of concepts and methods, *Curr Pharm Des* **11**, 3613–3628.
6. Nakase, I., Niwa, M., Takeuchi, T., Sonomura, K., Kawabata, N., Koike, Y., Takehashi, M., Tanaka, S., Ueda, K., Simpson, J. C., Jones, A. T., Sugiura, Y., and Futaki, S. (2004) Cellular uptake of arginine-rich peptides: roles for macropinocytosis and actin rearrangement, *Mol Ther* **10**, 1011–1022.
7. El-Andaloussi, S., Johansson, H. J., Lundberg, P., and Langel, Ü. (2006) Induction of splice correction by cell-penetrating peptide nucleic acids, *J Gene Med* **8**, 1262–1273.
8. Abes, S., Williams, D., Prevot, P., Thierry, A., Gait, M. J., and Lebleu, B. (2006) Endosome trapping limits the efficiency of splicing correction by PNA-oligolysine conjugates, *J Control Release* **110**, 595–604.
9. Shiraishi, T., Pankratova, S., and Nielsen, P. E. (2005) Calcium ions effectively enhance the effect of antisense Peptide nucleic acids conjugated to cationic tat and oligoarginine peptides, *Chem Biol* **12**, 923–929.
10. Turner, J. J., Ivanova, G. D., Verbeure, B., Williams, D., Arzumanov, A. A., Abes, S., Lebleu, B., and Gait, M. J. (2005) Cell-penetrating peptide conjugates of peptide nucleic acids (PNA) as inhibitors of HIV-1 Tat-dependent trans-activation in cells, *Nucleic Acids Res* **33**, 6837–6849.
11. Shiraishi, T., and Nielsen, P. E. (2006) Photochemically enhanced cellular delivery of cell penetrating peptide-PNA conjugates, *FEBS Lett* **580**, 1451–1456.
12. Kang, S. H., Cho, M. J., and Kole, R. (1998) Up-regulation of luciferase gene expression with antisense oligonucleotides: implications and applications in functional assay development, *Biochemistry* **37**, 6235–6239.

Part V

CPP In Vivo and as Future Drugs

Identification of Homing Peptides Using the In Vivo Phage Display Technology

Antti Rivinoja and Pirjo Laakkonen

Abstract

Each normal organ and pathological condition expresses a distinct set of molecules on their vasculature. These molecular signatures have been efficiently profiled using in vivo phage display technology. Using this technology, several peptides homing specifically to tumour blood vessels, lymphatic vessels, and/or tumour cells as well as to various normal organs have been isolated. Peptides homing to specific vascular addresses have revealed novel tissue-specific biomarkers of the normal and diseased vasculature. Tumour homing peptides have been successfully used to target therapies and imaging agents to tumours. In this review, we describe experimental setup for a combined ex vivo and in vivo screening procedure to select peptides homing to tumours.

Key words: Phage display, T7, Peptide, Tumour targeting, Vasculature, Nude mice, Ex vivo, In vivo

1. Introduction

During recent years, it has become clear that the vasculature in each individual normal organ as well as pathological condition expresses different set of molecules on its surface (1–3). Also other cell types within tumour tissue express tumour-specific molecules. In vivo phage display technology has been used to profile these distinct molecular signatures in normal (4–7) and tumour vasculature (8–11). Furthermore, arthritic blood vessels have been targeted using this technology (12). We have also profiled tumour stage-specific differences and shown that the vasculature of a pre-malignant lesion can be distinguished from that of a full-blown tumour and corresponding normal organ (13, 14). In addition to the blood vasculature, the lymphatic vasculature expresses both tumour-type and tumour stage-specific molecules

(reviewed in ref. (15)). Tumour homing peptides have been successfully used as delivery vehicles for targeted therapy and imaging purposes (reviewed in ref. (1, 16)). Recently, as an example of other pathological condition besides tumours, a muscle homing peptide was demonstrated to enhance the delivery of an anti-sense oligonucleotide. This resulted in exon skipping of dystrophin gene and functional restoration of dystrophin expression in dystrophin-deficient mdx mice (17).

2. Materials

2.1. Cell Culture (See Note 1)

1. Cancer cells.
2. Appropriate growth medium for the cells to be used supplemented with 10% FBS, glutamine and 100 µg penicillin streptomycin.
3. 1× PBS, pH 7.4.
4. Solution of 0.25% (w/v) trypsin and 1 mM ethylenediamine tetraacetic acid (EDTA) in serum-free medium or PBS.
5. Cell culture plates (Φ 10–20 cm).
6. Pipettes (e.g. 2, 5, 10, and 25 ml).
7. A haemocytometer.

2.2. Subcutaneous Injection of Cancer Cells

1. Sterile insulin syringes (e.g. BD Micro-Fine™ + insulin syringes, 0.30 mm (30 G) × 8 mm).
2. Matrigel (e.g. BD Matrigel™ Basement Membrane Matrix, Growth Factor Reduced, product code #354230, see Note 2).
3. Anaesthetics (e.g. Rompun® vet, 20 mg/ml and Ketaminol® vet, 50 mg/ml).
4. Trypsinized cells (5×10^5 – 5×10^6 cells/50–100 µl/injection).
5. Immunodeficient mice if non-murine cancer cells are used (see Note 3).

2.3. Phage Display Using the Lytic T7 Bacteriophage

2.3.1. Ex Vivo Selection

1. At least one mouse carrying a xenograft tumour.
2. One set of surgical instruments containing a haemostat, a pair of scissors, a razor blade (or a scalpel) and a pair of tweezers.
3. One insulin syringe per mouse.
4. Collagenase solution (50 ml of PBS, 0.5 g BSA, 50 µl of DNAase, 0.125 g collagenase IV, 0.125 g collagenase II).
5. One clean plate per mouse (e.g. empty bacterial culture plate).
6. One 50-ml Falcon tube per mouse.
7. Tared Eppendorf tubes.

8. Phage (T7 control phage and phage displayed peptide library or a solution of selected bacteriophage, see Note 10).

2.3.2. In Vivo Selection

1. Mice carrying xenograft tumours.
2. One set of surgical instruments per mouse (see Subheading 2.3.1).
3. Two insulin syringes per mouse (one for anaesthetic and the other for tail vein injection).
4. One 10-ml syringe and a needle (0.50 mm (25 G) × 16 mm) per mouse.
5. Sterile 1 × PBS, pH 7.4.
6. Collagenase solution (see Subheading 2.3.1).
7. One 50-ml Falcon tube per mouse.
8. One empty bacterial culture plate per mouse.
9. Tared Eppendorf tubes.
10. Phage.

2.3.3. Growth and Amplification of T7 Bacteriophage

1. BLT5403 or BLT5615 bacteria (Novagen).
2. M9TB growth medium (5 ml of 20 × M9 salts, 2 ml 20% glucose, 0.1 ml 1 M MgSO₄, 100 ml TB). 20 × M9 salts: 0.37 M NH₄Cl, 0.44 M KH₂PO₄, 0.45 M Na₂HPO₄.
3. Antibiotics (e.g. 25 mg/ml carbenicillin).
4. 0.6% top agar (per 100 ml: 1 g Bacto tryptone, 0.5 g yeast extract, 0.5 g NaCl, 0.6 g agarose, 100 ml deionized water).
5. Luria plates supplemented with antibiotics (e.g. 50 µg/ml carbenicillin).
6. Phage.

2.3.4. Identification of Individual Peptides

1. 1 × TBS, pH 7.8.
2. Primers to amplify the multi-cloning site containing the insert encoding displayed peptide.
3. Sequencing facility.

2.4. Validation of the Specificity of Displayed Peptides

1. Synthetic peptide conjugated to a fluorochrome or biotin. These are commercially available.
2. Tumour-bearing mice.
3. One set of surgical instruments per mouse (see Subheading 2.3.1).
4. Two insulin syringes per mouse (One for anaesthetic and the other for tail vein injection).
5. Two 10-ml syringes and needles (0.50 mm (25 G) × 16 mm) per mouse.

6. Sterile 1× PBS, pH 7.4.
7. 4% Paraformaldehyde (PFA) in PBS.
8. One 50-ml Falcon tube per mouse.
9. One empty bacterial culture plate per mouse.
10. Tared Eppendorf tubes.
11. O.C.T mounting compound (Tissue-Tek).
12. Cold 30% sucrose in PBS.
13. Cryostat.
14. Fluorescence microscope.

3. Methods

Targeting/homing peptides can be selected for any tumour type grown either subcutaneously or orthotopically. If tumour cells are not of murine origin immunodeficient mouse strains are necessary for tumour implantation. The number of cells to be implanted and the requirement of a supporting matrix (e.g. Matrigel) depend on the tumour model to be used. In the *in vivo* phage screen, also called biopanning, the phage library is injected into the tail vein of tumour-bearing mice and allowed to circulate for 15 min. Excision of the tumour tissue is followed by preparation of a tumour-derived cell suspension. Bound phage is rescued and amplified by the addition of the bacterial culture. The amplified phage pool is then used for the next round of selection. Typically, the phage pool preferentially homes to the target tissue after three to five rounds of panning.

There are two major phage systems that have been used for the *in vivo* phage display: the fd-tet-derived FUSE5 vector system based on the M13 bacteriophage (18) and the T7 phage system (T7Select® system, Novagen). The two phage differ in size, shape, and life cycle; M13 is a 900-nm long filamentous phage and has a temperate life cycle, while T7 is an icosahedral phage with the diameter of about 60 nm and has a lytic life cycle. M13 system displays peptides in five copies as an N-terminal fusion of the minor coat protein P3. This system has also been widely used to display antibody libraries (19). T7 vectors display 1–415 copies of the peptide as a C-terminal fusion of the phage capsid protein. In this review, we concentrate on the use of the T7 phage system in the *in vivo* phage display application. However, this technology can also be used for the identification of peptides that recognize different targets *in vitro*, i.e. recombinant proteins/glycans, cultured cells, etc. The M13 system has been recently reviewed by Hoffman et al. (20).

3.1. Propagation of Cancer Cells (See Note 4)

1. Harvest cells with trypsin–EDTA solution when 80–90% confluent. For a 10-cm cell culture dish, an appropriate amount of trypsin–EDTA solution is 1–2 ml. You may need multiple plates of cells to acquire enough of them for implantation.
2. Add 8 ml of serum containing growth medium to the cell after detachment to inactive the trypsin and split the suspension 1:2. Add medium to the final volume: 10 ml for 10-cm plates and 20 ml for 15-cm plates. Let the cells adhere and grow them overnight in a cell incubator.
3. Next day harvest the cells with trypsin–EDTA. After detachment of the cells collect them by centrifugation ($300\text{--}500\times g/2\text{--}5$ min). Remove the supernatant and resuspend the cells in $1\times$ PBS.
4. Count the cells using a haemocytometer. If you have several plates, combine the cell suspensions before counting. If you need to dilute the cell suspension for cell counting, take a small aliquot (e.g. 10 μl) and dilute it using growth medium or $1\times$ PBS.
5. Transfer cells to a Falcon tube for centrifugation ($300\text{--}500\times g/2\text{--}5$ min). Resuspend the cells in an appropriate volume of $1\times$ PBS so that the final solution contains $5\times 10^5\text{--}5\times 10^6$ cells/50–100 μl (see Note 5). Store the cells on ice. You are now ready for inoculation of the tumours.

3.2. Inoculation of Tumour Cells to Generate Xenograft Tumours

1. Anaesthetize mice using a mixture of Rombun and Ketalar according to the manufacturer's recommendations. Test the deepness of the anaesthesia by pressing the footpad of the hind limb.
2. Mix an aliquot of thawed Matrigel with 50–100 μl of cell suspension (1:1) and inject the mixture subcutaneously to the abdominal site of an anaesthetized mouse using an insulin syringe (see Note 6). Wait 30 s before removing the needle to allow the Matrigel to solidify properly. Otherwise the Matrigel/cell suspension mixture may leak out of the injection site. It is recommended to always inject on the same side of the abdomen since tumours may grow with different rate in different locations.
3. Monitor the tumour growth and use for the experiments when they reach the desired size.

3.3. Phage Display

To our experience the combination of an ex vivo/in vivo screen is more efficient in identifying homing peptides than an in vivo screen alone. We use the term ex vivo phage display to describe the addition of phage solutions to primary cell suspensions of organs and tissues. The screen is initiated with one to three ex

vivo selection rounds followed by three to five in vivo selection rounds. During the ex vivo selections, you select for peptide/phage that is able to bind to all tumour-derived cells, while during the in vivo selections, you select for the peptide/phage that is able to home and bind to the tumour tissue after systemic administration via the tail vein.

3.3.1. Ex Vivo Selection

1. Inoculate an overnight culture from a single BLT5403 or BLT5615 colony ($V=5$ ml, supplied with $10\ \mu\text{l}$ of $25\ \text{mg/ml}$ carbenicillin) 1 day prior the experiment.
2. Dilute overnight culture 1:100 and grow to $\text{OD}_{600} \sim 1.0$ (see Note 7). During the incubation you should accomplish steps 3–12.
3. Anaesthetize a mouse carrying a xenograft tumour (see Note 8).
4. To expose the heart for perfusion, use your scissors to make a wide cut in the abdomen directly under the rib cage. Then move the liver aside and puncture the diaphragm. Cut the diaphragm from side to side to reveal the lungs. Then cut both sides of the rib cage. Clasp the apex of xiphoid process (xiphisternum) with a haemostat and bend the rib cage back to expose the heart. Be careful not to puncture the heart.
5. Make a cut on the right atrium or the main vein (superior vena cava).
6. Perfuse the mouse with 10 ml of PBS to remove the blood. The needle should penetrate only the wall of the left ventricle (i.e. insert the needle 2–3 mm into the heart). Perfusion is successful when the skin and the liver of the mouse become pale.
7. Excise the tumour. Remove as much as possible of the surrounding mouse tissue.
8. Weight the tumour and mince it to small pieces using a razor blade or a scalpel.
9. Digest the tumour in the collagenase solution by incubating at $+37^\circ\text{C}$ for 30–45 min. Vortex few times during the incubation. The collagenase solution should become more turbid, while the digestion of the tumour proceeds. An appropriate volume of the collagenase solution is 10–15 ml/g of tumour.
10. Following the digestion add 15 ml of DMEM supplied with 5% FCS to inactivate the collagenases. Filter the suspension using a cell strainer (pore size $100\ \mu\text{m}$) and collect the cells by centrifugation ($250 \times g$, 10 min). Discard the supernatant and resuspend the cells in 5 ml of 1% BSA in DMEM. Collect the cells by centrifugation ($250 \times g$, 10 min). Discard the supernatant and weight the pellet. Resuspend the cells in 1 ml of 1% BSA in DMEM. Divide the suspension in aliquots. One

aliquot containing 0.05–0.10 g or $\sim 10^6$ of tumour cells is enough for an ex vivo experiment.

11. Add 100–500 μl of the phage library (see Note 9) or an amplified phage pool/individual phage (the titre should be 10^6 – 10^{10} pfu/ μl) to tumour cells and fill the total volume to 1 ml with 1% BSA in DMEM. Prepare an identical suspension using a control phage (see Note 10). Incubate the phage/tumour cell suspensions at $+4^\circ\text{C}$ in a rotator. The incubation time may require optimization, but it usually varies between 2 and 24 h.
12. In order to remove the unbound phage collect the tumour cells and phage bound to them by centrifugation ($600\times g$, 3 min, RT). Resuspend the pellet into 0.5 ml of 1% BSA in DMEM and transfer the suspension to a fresh tube (see Note 11). Repeat the wash step four times. After the final wash, transfer the suspension again to a fresh tube and collect the cells with centrifugation. Discard the supernatant and add 50 μl of sterile PBS on top of the pellet to prevent drying. Alternatively, the pellet can be lysed by adding 100 μl of 1% NP-40 in PBS.
13. Add 1.0 ml of BLT5403 or BLT5615 culture ($\text{OD}_{600} \sim 1.0$) (from step 2) to the tube containing tumour cell/phage mixture and suspend well. Incubate 10 min at RT to allow phage to infect the bacteria.
14. To define the number of bound phage (phage output, Fig. 1), add 0.1, 1, and 10 μl of the suspension from step 13 to 350 μl of BLT5403 or BLT5615 culture ($\text{OD}_{600} \sim 1.0$) and 3 ml of melted (45 – 50°C) top agar. Pour the top agar containing the phage and bacteria onto LB agar plates containing 50 $\mu\text{g}/\text{ml}$

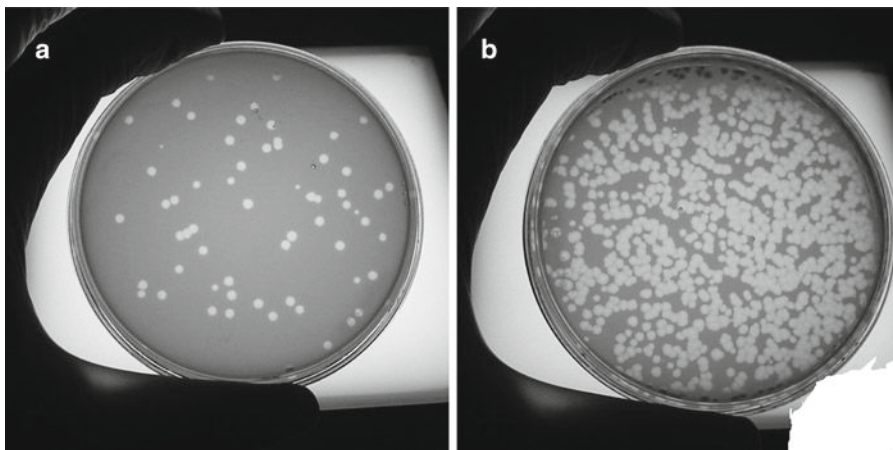


Fig. 1. Individual phage appear as holes (=plaques) in the bacterial plates. The figure shows titration of the binding of a control phage (a) and a homing phage (b) to the tumour tissue ex vivo.

carbenicillin. Incubate the plates 1.5–3 h at 37°C or overnight at room temperature.

Save the rest of the suspensions for amplification (see Subheading 3.3.5). They can be stored overnight at +4°C (see Note 12). Since the infection efficiency of the T7 phage solution may differ between different bacterial cultures, the most reliable results in defining the selection output are obtained by simultaneous determination of the output and input (=the number of phage particles added to the tumour cell suspension).

3.3.2. *In Vivo Selection*

1. Anaesthetize a mouse carrying a xenograft tumour.
2. Warm the mouse's tail in warm water to dilate the tail veins and facilitate the injection.
3. Inject slowly 150–200 μl of phage solution (the titre should be around 10^6 – 10^{10} pfu/ μl) into the tail vein. Too fast injection rate may cause failure in cardiac function and be fatal for the mouse. Usually a rate of 20 $\mu\text{l}/10$ s is appropriate.
4. Open the chest and expose the heart as described in Subheading 3.3.1.
5. Perfuse the mouse with 10 ml of PBS to remove the unbound phage.
6. Excise the tumour and separate it from the surrounding mouse tissue (e.g. skin) as well as possible.
7. Weight the tumour.
8. Digest the tumour with collagenase solution and prepare the cell suspension as described above steps 9–10 in Subheading 3.3.1.
9. Wash the cell suspension and add bacteria as described in steps 12–13 in Subheading 3.3.1.
10. For titration of the phage output, add 0.1, 1, and 10 μl of the suspension to 350 μl of BLT5403 or BLT5615 culture ($\text{OD}_{600} \sim 1.0$) and 3 ml of top agar. Save the rest of the suspensions for amplification (see Subheading 3.3.5). They can be stored overnight at +4°C (see Note 12). Prepare also titre plates to determine the phage input if not determined earlier.

3.3.3. *Analysis of Selection Output (Number of Bound Phage)*

1. Count the plaques from the titre plates (see Note 13). Define titre/ μl by multiplying plaque count with the dilution factor and dividing it by the volume of phage solution plated (see Note 14).
2. Calculate phage input by multiplying titre/ μl with volume of phage solution used for selection (see Note 14).
3. Phage output is calculated by multiplying titre/ μl with the total volume of suspension containing tumour cells, phage, and bacteria. Since the tumours vary in size, the tumour mass must also be taken into account for analysis of the *in vivo*

selection output. Divide the relative output value with the mass of the tumour cells to accomplish this (see Note 14).

4. Divide the output value with the input value and you will have a relative value that can be compared between different phage and screening rounds. Increase in this value by each round indicates *enrichment* and a successful selection of the homing phage. Decrease in this value, in turn, indicates that the homing capability of the phage pool to the tumour tissue is reduced (see Note 15).

3.3.4. Amplification of Phage After Ex Vivo or In Vivo Selection

1. Inoculate an overnight culture from a single BLT5403 or BLT5615 colony ($V = 5$ ml, supplied with $10 \mu\text{l}$ of 25 mg/ml carbenicillin).
2. Dilute the overnight culture 1:100, $V = 10$ ml and grow to $\text{OD}_{600} \sim 0.5$ (see Note 7).
3. (a) Amplification of a phage pool: Add phage and tumour cell mixture to an IPTG-induced BLT5403 or BLT5615 bacterial culture grown to $\text{OD}_{600} \sim 0.5$. (b) Amplification of a single phage: Pick a plaque from a phage plate to a tube containing $20 \mu\text{l}$ of $1\times$ TBS, pH 7.8 and add $5 \mu\text{l}$ of phage solution to an IPTG-induced culture grown to $\text{OD}_{600} \sim 0.5$.
4. Incubate the culture at 37°C for 3–5 h, or until the culture is clarified (phage lyses the bacteria). Sometimes, because of the tumour cell material, the clarification of the culture might not be complete and the lysis may appear only as reduced turbidity.
5. Remove the cell debris by centrifugation ($7,670\times g$, 10 min, at $+4^\circ\text{C}$). Carefully, transfer the supernatant by decanting or pipeting to a new sterile falcon tube.
6. Filter the supernatant through a $0.45\text{-}\mu\text{m}$ filter followed by filtration through a $0.2\text{-}\mu\text{m}$ filter (e.g. by using a syringe tipped with an appropriate filter). Now you have a phage solution ready to be used for the experiments.

3.3.5. Identification of Peptides Displayed by the Phage

1. Isolate individual phage from the bacterial plates by picking randomly selected plaques with a tip of a pipette or a sterile stick to tubes containing $20 \mu\text{l}$ of $1\times$ TBS, pH 7.8. Label the tubes clearly.
2. Amplify the cloning site by PCR. A PCR example is provided in Note 16. Presence of the leftover primers after PCR may disturb sequencing reaction and require an additional purification step.
3. Check PCR products in a 2% agarose gel.
4. Prepare sequencing samples (see Note 17).

3.3.6. Validation of the Specificity of Tumour Targeting

Once tumour-targeting phage is enriched, it is important to verify their specificity. This is performed as normal in vivo phage display (Subheading 3.3.2), but with a single phage instead of a

library or a phage pool. This step is necessary to validate how well any individual phage homes to the target tissue compared to the control phage and whether it also homes to other organs (see Note 18).

1. Anaesthetize a mouse carrying a xenograft tumour.
2. Place the mouse's tail in warm water to dilate the tail veins.
3. Inject 150–200 μ l of phage solution into the tail vein and allow it to circulate for 15 min.
4. Open the chest and expose the heart as described in Subheading 3.3.1.
5. Perfuse the mouse with 10 ml of PBS.
6. Excise tumour and other necessary control organs (e.g. liver, kidney, lungs, and brain). Selection of control organs will depend on your target organ.
7. Titre the phage from the organs as described in Subheading 3.3.3. The specificity of the phage can be estimated by comparing the output of the phage of interest to that of the control phage (see Note 14).

3.3.7. Validation of the Specificity of Displayed Peptides

To ensure that your selected peptide is responsible for the specific homing, you should test the homing efficiency and specificity of a synthetic peptide conjugated to a fluorochrome or biotin. We usually inject 100 μ l of 1 mM peptide solution into the tail vein of tumour-bearing mice and allow it to circulate for 15–120 min. In order to study the homing of the peptide, tumour and the control organs are excised and prepared for histological examination.

1. Inject the peptide into the tail vein of tumour-bearing mouse and let it circulate for 15–120 min.
2. Perfuse the mice through the heart with 10 ml of PBS followed by 10 ml of 4% PFA in PBS to remove the unbound peptide and fix the tissue.
3. Excise tumour and control organs.
4. Fix the tissues further by incubating them in 4% PFA for 2–4 h at 4°C.
5. Wash twice with PBS and add 30% sucrose to the tissues. Incubate overnight at 4%.
6. Dry the extra sucrose and mount in O.C.T compound (Tissue-Tek) mounting media.
7. Cut cryo-sections and prepare them for microscopy (see Note 19).

4. Notes

1. All equipment and solutions used in cell culture must be sterile. Cell culture should be performed in a special room designed and designated for that use. Room should be equipped with a table-top centrifuge, a microscope, a flow chamber suitable for cell cultivation, and a cell incubator that can be adjusted to 5.0% CO₂, +37°C.
2. Some cell lines do not form tumours unless inoculated together with Matrigel, which provides matrix to cells to attach to. Matrigel must be thawed slowly on an ice bath at +4°C overnight. Matrigel will remain liquid as long as kept cold – it will solidify rapidly when the temperature raises. Matrigel can be either growth factor rich or reduced depending on your tumour model.
3. If cancer cells are of non-murine origin immunodeficient mouse strain has to be used for the formation of tumours. In immunocompetent animals, the immune response prevents tumour growth or results in regression of tumours after initial growth. Take into account the gender of the mice when studying a cancer, which growth might be affected by hormonal levels, e.g. it is not rational to study prostate cancer in female mice.
4. Cells should be checked frequently for possible contaminations. It is extremely important that only clean cells are used for the inoculation of xenograft tumours. Cells should be in the exponential growth phase when implanted into mice.
5. The number of cells to be implanted depends on the cell type.
6. If cell line does not require Matrigel inject the cell suspension as such.
7. Some vector systems (T7Select1-1 and T7Select10-3 that display an average of 0.1–1 and 10 copies of peptides/phage particle, respectively) and the bacterial strains BLT5430 and BLT5615 require the induction of the expression of wild-type capsid protein in bacteria to allow the assembly of the phage. This is done by the addition of isopropyl thiogalactoside (IPTG) to the bacterial growth medium. Add IPTG to a final concentration of 10 μM 45–60 min after inoculation of the diluted culture. We often amplify also the T7Select415-1b vector in the BLT5615 bacterial strain in the presence of IPTG to prepare mosaic phage to facilitate the phage assembly.

8. One tumour can be divided into several aliquots after preparation of the cell suspension for the ex vivo experiments.
9. The volume of the library used for the first round of selection depends on the diversity and titre of the library. The first round should contain at least ten copies of each individual phage particles (i.e. ten times the diversity of the library).
10. As a control phage, we use a non-recombinant phage T7Select 415-1 (T7-negative control from Novagen), which displays the stuffer-encoded SSVD peptide.
11. Since phage is very sticky you will get rid of all the phage that has bound to the walls of the tubes by transferring the cell suspension with bound phage to a new tube.
12. The number of plaques should be 20–100/plate in order to accurately quantify the results. If the number of plaques is too low or too high the phage/tumour cell suspension can be retitrated the next day. Since the phage might slightly amplify during the overnight incubation even at 4°C prepare new titration for the all the phage simultaneously for comparable results.
13. T7 is a lytic phage, which means that following the infection phage lyses the infected bacterial cells that results in the release of new phage particles to the culture medium (about 200 phage particles/infected cell). Top agar is used to prevent the escape of the released phage. Therefore, the phage will stay next to the lysed bacteria and infect the bacterial cells next to the dead cell resulting in a hole=plaque in the bacterial culture.
14. Example of the calculation of the selection outputs.
Phage titre (number of infective phage particles in the solution):

Input		Plaque count				
Phage	Dilution	Plated (μl)	Plate #1	Plate #2	Average	Titre/ μl (in)
T7 control	1:10 ⁶	10	54	57	55.5	5.55 \times 10 ⁶
	1:10 ⁶	1	4	5	4.5	4.50 \times 10 ⁶
Phage of interest	1:10 ⁶	10	45	40	42.5	4.25 \times 10 ⁶
	1:10 ⁶	1	3	5	4.0	4.00 \times 10 ⁶

Phage input (number of infective phage particles added to the experiment).

The total input of the phage is calculated by multiplying titre/ μl with the volume of the phage solution added to the selection.

Phage	Titre/ μl (in) average	Input volume (μl)	Input
T7 control	5.03 \times 10 ⁶	200	1.01 \times 10 ⁹
Phage of interest	4.13 \times 10 ⁶	200	8.25 \times 10 ⁸

Phage output (number of infective phage particles bound to the target).

Titre/ μl is calculated by dividing average of the plaque count with the volumes of the diluted phage added to plates. Value for titre/ml is calculated by multiplying titre/ μl with 1,000.

Output		Plaque count					
Phage	Dilution	Plated (μl)	Plate #1	Plate #2	Average	Titre/ μl (out)	Titre/ml (out)
T7 control	1:100	10	13	15	14	140	1.40×10^5
Phage of interest	1:100	10	167	173	170.0	1700	1.70×10^6

Relative value for output is calculated by dividing the “titre/ml” of the output with the value of “phage input.” This relative value is comparable between different phage and different experiments.

Phage	Titre/ml (out)	Out/in	Versus control
T7 control	1.40×10^5	1.39×10^{-4}	1
Phage of interest	1.70×10^6	2.06×10^{-3}	14.79

In this example, the phage of interest binds almost 15-fold better to the tumour than the control phage

Phage output for the in vivo experiment: In an in vivo experiment, the mass of tumour cells must be taken into account. Titre/ml is divided by the weight of tumour cells to obtain value “output/g of tissue.” Then this value is divided by the input to obtain a relative value “output/(input*g) of tissue.” This value is a comparable selection output of different phage and can be used to compare different selection rounds with each other. In an ex vivo selection, this is not necessary, because the tumour cells used in the experiment are divided equally between different samples.

Phage	Titre/ml (out)	Weight (g)	Out/g of tissue	Out/(in*g) of tissue	Versus control
T7 control	1.40×10^5	0.109	1.28×10^6	1.28×10^{-3}	1
Phage of interest	1.70×10^6	0.097	1.75×10^7	2.12×10^{-2}	16.62

In this example, the phage of interest homes and binds almost 17-fold better to the tumour than the control phage.

- An individual phage can enrich in a phage pool due to selection or amplification. Enrichment by selection means that more phage will specifically home and bind to the tumour tissue each round due to the amplification of the phage that

resides in the tumour at the time of tumour excision. Enrichment by amplification means that empty phage or a phage displaying truncated peptide sequences amplifies more rapidly and takes over the phage pool. The enrichment of phage carrying truncated peptides may develop, for instance, from a random mutation in DNA encoding the displayed peptide.

16. An example of a PCR to amplify the DNA sequence encoding the displayed peptide from the phage genome performed using Dynazyme II polymerase (Finnzymes) and primers 5'-AGC GGA CCA GAT TAT CGC TA-3' (forward) and 5'-AAC CCC TCA AGA CCC GTT TA-3' (reverse).

Reagent	1 × Reaction (μl)
Phage solution	2.0
10× Buffer	2.5
dNTPs	0.5
Forward primer (10 μM)	0.3
Reverse primer (10 μM)	0.3
dH ₂ O	19.4
Dynazyme II	1.0

^a1× TBS containing a picked phage from point (b) of step 3, Subheading 3.3.4.

17. Procedure for preparing sequencing samples depends greatly on the equipment and services of your local sequencing facility. Therefore, no instructions are provided here. Sequencing can be performed, e.g. using the forward primer (see Note 16).
18. Phage binds unspecifically to any surface to certain extent and therefore it is necessary to always assess the background of the binding or homing in your system using a control phage. Please note that the more phage you put into your system the more phage you will get out (this implies also for the control phage). The background in different organs will vary and therefore you will need to compare the homing of your phage to that of the control phage in different organs.
19. If the peptide is conjugated to a fluorochrome, it might be visible in the tissue without further staining. If not enhance the staining using antibodies against the fluorochrome. Tissue can be stained with, e.g. markers for blood and lymphatic vasculature and tumour cells to localize the peptide within the tissue using the standard procedures. Please note that systemically administered peptide will be secreted through the kidneys to the urine. Therefore, the peptide should always be visible in the kidney tubules. This will also serve as a control organ for a successful injection.

Acknowledgments

This study was funded by the Finnish Cancer Organizations and the Academy of Finland as well as by research collaboration with the Marina Biotech.

References

1. Ruoslahti, E. (2002) Specialization of tumour vasculature. *Nat Rev Cancer* **2**, 83–90.
2. St Croix, B., Rago, C., Velculescu, V., Traverso, G., Romans, K.E., Montgomery, E., Lal, A., Riggins, G.J., Lengauer, C., Vogelstein, B., and Kinzler, K.W. (2000) Genes expressed in human tumor endothelium. *Science* **289**, 1197–1202.
3. Oh, P., Li, Y., Yu, J., Durr, E., Krasinska, K.M., Carver, L.A., Testa, J.E., and Schnitzer, J.E. (2004) Subtractive proteomic mapping of the endothelial surface in lung and solid tumours for tissue-specific therapy. *Nature* **429**, 629–35.
4. Zhang, L., Hoffman, J.A., and Ruoslahti, E. (2005) Molecular profiling of heart endothelial cells. *Circulation* **112**, 1601–11.
5. Arap, W., Haedicke, W., Bernasconi, M., Kain, R., Rajotte, D., Krajewski, S., Ellerby, H.M., Bredesen, D.E., Pasqualini, R., and Ruoslahti, E. (2002) Targeting the prostate for destruction through a vascular address. *Proc Natl Acad Sci USA* **99**, 1527–31.
6. Rajotte, D., Arap, W., Hagedorn, M., Koivunen, E., Pasqualini, R., and Ruoslahti, E. (1998) Molecular heterogeneity of the vascular endothelium revealed by in vivo phage display. *J Clin Invest* **102**, 430–37.
7. Pasqualini, R. and Ruoslahti, E. (1996) Organ targeting in vivo using phage display peptide libraries. *Nature* **380**, 364–66.
8. Porkka, K., Laakkonen, P., Hoffman, J.A., Bernasconi, M., and Ruoslahti, E. (2002) A fragment of the HMG2 protein homes to the nuclei of tumor cells and tumor endothelial cells in vivo. *Proc Natl Acad Sci USA* **99**, 7444–49.
9. Laakkonen, P., Porkka, K., Hoffman, J.A., and Ruoslahti, E. (2002) A tumor-homing peptide with a targeting specificity related to lymphatic vessels. *Nat Med* **8**, 751–55.
10. Pasqualini, R., Koivunen, E., and Ruoslahti, E. (1997) Alpha v integrins as receptors for tumor targeting by circulating ligands. *Nat Biotechnol* **15**, 542–46.
11. Burg, M.A., Pasqualini, R., Arap, W., Ruoslahti, E., and Stallcup, W.B. (1999) NG2 proteoglycan-binding peptides target tumor neovasculature. *Cancer Res* **59**, 2869–74.
12. Gerlag, D.M., Borges, E., Tak, P.P., Ellerby, H.M., Bredesen, D.E., Pasqualini, R., Ruoslahti, E., and Firestein, G.S. (2001) Suppression of murine collagen-induced arthritis by targeted apoptosis of synovial neovasculature. *Arthritis Res* **3**, 357–61.
13. Joyce, J.A., Laakkonen, P., Bernasconi, M., Bergers, G., Ruoslahti, E., and Hanahan, D. (2003) Stage-specific vascular markers revealed by phage display in a mouse model of pancreatic islet tumorigenesis. *Cancer Cell* **4**, 393–403.
14. Hoffman, J.A., Giraudo, E., Singh, M., Zhang, L., Inoue, M., Porkka, K., Hanahan, D., and Ruoslahti, E. (2003) Progressive vascular changes in a transgenic mouse model of squamous cell carcinoma. *Cancer Cell* **4**, 383–91.
15. Laakkonen, P., Zhang, L., and Ruoslahti, E. (2008) Peptide targeting of tumor lymph vessels. *Ann N Y Acad Sci* **1131**, 37–43.
16. Enback, J. and Laakkonen, P. (2007) Tumour-homing peptides: tools for targeting, imaging and destruction. *Biochem Soc Trans* **35**, 780–83.
17. Yin, H., Moulton, H.M., Betts, C., Seow, Y., Boutilier, J., Iverson, P.L., and Wood, M.J. (2009) A fusion peptide directs enhanced systemic dystrophin exon skipping and functional restoration in dystrophin-deficient mdx mice. *Hum Mol Genet* **18**, 4405–14.
18. Smith, G.P. and Scott, J.K. (1993) Libraries of peptides and proteins displayed on filamentous phage. *Methods Enzymol* **217**, 228–57.
19. Hoogenboom, H.R. (2002) Overview of antibody phage-display technology and its applications. *Methods Mol Biol* **178**, 1–37.
20. Hoffman, J.A., Laakkonen, P., Porkka, K., Bernasconi, M., and Ruoslahti, E. (2004) In vivo and ex vivo selections using phage-displayed libraries In: *Phage Display: A Practical Approach*, Clarkson, T. and Lowman, H. eds (Oxford University Press, Oxford), 171–92.

Measuring the Action of CPP–siRNA Conjugates in the Lung

Sterghios A. Moschos, Karen G. Spink, and Mark A. Lindsay

Abstract

Two of the most promising and complex areas in biologics development, either as research tools or potential therapeutics, are cell-penetrating peptides (CPPs) and RNA interference (RNAi) modulators. Consequently, the combined application of these technologies in pursuit of improved delivery profiles for RNAi cargoes presents its own unique challenges. Direct access to the targeted tissue is luxury not always available to the researcher; however, the example of lung presents an excellent opportunity for presenting methodologies relevant to understanding the local impact of CPP-conjugated RNAi modulators. This chapter therefore expands upon updated protocols established on the study of the function of endogenous RNAi and the utility of CPPs in the delivery of short interfering RNA (siRNA) to therapeutically relevant cells in the lung. Methods for sample collection, preservation, and processing are provided with a view to facilitate qualitative and quantitative analysis of delivery. In addition, a protocol for mapping siRNA delivery by in situ hybridisation is provided.

Key words: CPP, siRNA, Lung, RNA extraction, Protein extraction, In situ hybridisation, In vivo siRNA quantification

1. Introduction

Historically, cell-penetrating peptide (CPP) utility in the delivery of biological cargoes has been successful pre-clinically with a wide variety of protein and peptide cargoes conjugates (1). These modalities were understood to achieve cellular uptake through a variety of mechanisms that depend upon the CPP design and commonly involved a few CPPs per cargo molecule. In stark contrast, while some early claims of success in delivering antisense and short interfering RNA (siRNA) in vitro were reported, better appreciation of cargo physicochemical properties and purification procedures suggested that CPP conjugation onto oligonucleotides was insufficient for delivery in vitro and in vivo (2, 3).

Moreover, *in vivo* evidence indicated that the particular uptake mechanism accessed by a CPP might result in unforeseeable adverse effects such as immunostimulation. Crucially, these may not necessarily manifest when either a given CPP or the unconjugated cargo is independently administered, or when different CPPs are assessed for the same cargo, probably due to the different intracellular compartments accessed (4). These phenomena are believed to be driven through toll-like receptor (TLR) recognition of activating motifs on oligonucleotide cargoes, and directed by the presence of relevant TLRs in the internalisation compartments accessed by the given delivery system (5). Studies with siRNAs incorporating nucleoside analogues such as 2'-OMe have been shown to address parts of the known immunostimulatory mechanisms (e.g. TLR7/8) (6). Others, however, are less well understood (e.g. TLR3) (7–10). An alternative approach is to mask the physicochemical properties and activation motifs of siRNA by using defined protein scaffolds with dsRNA binding motifs, which are themselves tagged with CPPs (11). Alternatively, the use of amphipathic peptides that complex with oligonucleotides such as siRNA can mediate *in vitro* delivery and bioactivity (12). While promising, these advances may yet harbour risks of TLR and associated receptor activation pathways. Thus, *in vivo* studies of CPP–siRNA delivery should not only aim at measuring target RNA and protein (if relevant) knockdown, but also evaluate off-target effects including local and systemic immune stimulation. There is a plethora of techniques available for measuring the levels of RNA and proteins of interest. In this chapter, we have thus focused on describing protocols which have been found to reliably produce materials suitable for most analytical techniques. We also present considerations in the application of commonly used techniques for avoiding false-positive/-negative results. In the same context, a method for the qualitative analysis of siRNA uptake is described.

Tissue collection should be carried out according to experimental requirements (e.g. perfusion, bronchoalveolar lavage, etc.). Generally, it is advisable to remove all non-lung tissues that should not contribute to readout, e.g. blood, connective tissue, etc. One approach for achieving multiple readouts from the same animal lung is to tie off particular lobes and treat them independently, if possible. A caveat to this is that dose deposition is dependant on the administration method. There are conflicting reports in the literature with regard to access to the lower airways following intranasal administration of siRNA (e.g. (13–15)). Consequently, it is advisable to pursue intratracheal administration. This, however, requires considerable experience for successful implementation as it is easy for the inexperienced *in vivo* biologist to accidentally inject materials in the oesophagus or damage the trachea. In contrast to intranasal administration, repeated intratracheal administrations can cause inflammatory responses in the

airways (Belvisi, M. and Birrel, M., unpublished data). Typically, dosing is restricted to not more than twice daily and up to three administrations over 3 days. The simplest method, achieving concomitantly the most even deposition across lobes, is aerosol administration. However, this is at a considerable cost of materials due to >90% product loss during the aerosolisation process. This can be controlled to an extent using small, needle-type nebulisation devices (e.g. Penn-Century). These are suitable for relatively large volumes, which consequently makes them practical for rat or larger laboratory species.

The primary readout of any RNA interference (RNAi) experiment is target RNA knockdown by either absolute or relative quantification. As the bottleneck of RNAi is believed to be efficient delivery, quantification of the siRNA in the tissue of interest is also of scientific interest. In our experience, the most sensitive and highest throughput methodology available for these purposes is RT-qPCR. Adaptation of the miRNA qPCR method proposed by Raymond et al. is simple and suitable for siRNA quantification in tissue RNA extracts (16). There is a variety of commercially available solutions for transcript quantification which are outside the remit of this chapter; however, a number of important parameters in successful implementation and interpretation of any of these techniques will be discussed.

As strain-to-strain polymorphisms occasionally impact upon assay functionality, qPCR primer-probe sets should be either validated in-house using reference RNA material from the animal strain in question or the target itself should be sequenced to confirm conformity with published sequences. Equally, it is important to confirm by sequencing that the siRNA to be used can catalyse the restriction of the target in the specific strain; though very rare, target site polymorphisms between cell lines and animals leading to inactive siRNAs *in vivo* have been anecdotally reported. Careful consideration must also be applied on the choice of primer-probe set location. As the degradation rates of the 5' and 3' fragments generated by RISC slicer activity may differ, the co-ordinates of the qPCR assay should ideally span the restriction site to avoid under-estimation of knockdown efficacy. An often overlooked component is also baseline expression variability for the targeted transcript. Determination of this in more than ten subjects will permit power analysis and appropriate experimental design (experimental group *n* numbers), thus ensuring statistically significant observation of experimental knockdown efficacy. Of the various approaches in quantifying qPCR amplicon levels, we prefer the $2^{-\Delta\Delta C_t}$ method for endogenously expressed genes (17). The Raymond et al. siRNA RT-qPCR method relies on standard curves of siRNA cDNA material (16). This relies on 3'-end antisense strand hybridisation for reverse transcription (RT). In our experience, synthetic RNA templates harbouring RNase-resistant nucleosides exhibit different RT

efficiencies, and this is particularly true for high T_M -inducing modifications such as locked nucleic acid (LNA). Consequently, the user is advised to quantify siRNA delivery using synthetic template harbouring nucleoside modifications identical to the material administered *in vivo*. The presence of other RNA increases background levels and thus siRNA RT-qPCR assay sensitivity, and dynamic range must be established in isolation and in presence of fixed amounts of total RNA from tissue extracts.

Following confirmation of RNA knockdown, target protein levels, if relevant, are evaluated. This can be performed using standard methodologies with variable sensitivity such as western blotting, enzyme-linked immunosorbent assay (ELISA), or through quantitative immunohistochemistry. All these require careful preservation of samples to ensure minimal protein degradation. We thus have provided a suitable tissue preservation methodology, and provide standard RNA extraction protocol adaptations that result in either intact or denatured protein extraction.

siRNA off-target effects are currently believed to manifest in terms of non-specific target knockdown (mRNA level) and immune stimulation. The former is best characterised through genome-wide gene expression quantification approaches. A variety of custom and commercially available solutions are available to the researcher; however, the most informative is deep sequencing (for a review of the area see (18)). Global gene expression analysis should be followed by bioinformatic and, if necessary, proteomic validation of the potential impact of these changes. This is especially important if components within the pathway targeted are also observed to be affected at the transcriptomic level (rheostat hypothesis). Immune stimulation can be monitored locally (tissue of interest) or systemically (serum). There are currently no commonly accepted, highly sensitive markers and appropriate timepoints post-dosing for detecting immunostimulation. Data from multiple laboratories indicate that siRNA-induced inflammatory response nature and kinetics are driven by the delivery system (4–6, 19–21). Consequently, there is no single inflammation biomarker or timepoint that can reliably report such events. In our experience, monitoring of several markers [e.g. IL-6, IL-8 (KC in mouse), GM-CSF, TNF-alpha, IFN-alpha, IFN-beta, IFN-gamma, IL-12 p40] at regular intervals (at least every 6 h over a 48 h period) is required to ensure the lack of innate immunity activation.

The advent of molecular beacon technologies has prompted the use of small molecule fluorophores by us and others for the detection of siRNA delivery *in vivo* both in specific cells and across the entire animal (4, 22). It is now generally accepted that small lipophilic modifications such as cholesterol can mediate the delivery of siRNA *in vivo*, even on mucosal surfaces (23). This raises the question of the contribution of fluorophores, which can be of similar lipophilicity and MW as cholesterol, on delivery

mechanisms. Use of more hydrophilic fluorophores such as sulfonated Cy5 (GE Healthcare, UK) can in part address this; however, detailed studies are lacking on the matter. Consequently, the most reliable approach is the post-experimental validation of siRNA uptake by in situ hybridisation. Such protocols have been developed for microRNA expression analysis (24), and custom probes for siRNA detection using LNA bases are commercially available.

2. Materials

Numerous kits and compounds are also available commercially for total and small RNA, as well as protein extraction. The RNA extraction protocol in this chapter is a modified version of that provided by the supplier and has consistently yielded high-quality material from lung tissue [yield (\pm SD): 120 ± 40 μ g; purity (A_{260}/A_{280}): 1.9 ± 0.1]. Moreover, spiked siRNA recovery typically ranges in 97–99% so long as the biological sample is not overloaded with synthetic material, consequently exceeding the loading capacity of the spin column used.

2.1. Tissue Preservation for RNA or Protein Extraction

1. RNA^{later}[®] or RNA^{later}[®]-ICE (Ambion, UK).
2. 5 ml bijoux containers.
3. 70% EtOH.
4. Dissection scissors, blunt ended.
5. Forceps, serrated, blunt ended.
6. Sterile scalpel.
7. Dissection pins.

2.2. Total Tissue RNA Extraction and Purification Using a Modified Protocol of the mirVana™ (or mirVana PARIS™) Kit

1. Nuclease-free water (Promega, UK).
2. Ice.
3. Electronic rotor–stator homogeniser.
4. 100% ethanol, molecular biology grade.
5. mirVana™ or mirVana™ PARIS™ kits (Ambion, UK).
6. 1.5 and 2.0 ml microfuge tubes, certified nuclease free.
7. Barrier tips, certified nuclease free (see Note 1).

2.3. Total Tissue Protein Extraction

1. Protease inhibitor-supplemented 1 \times RIPA buffer [25 μ g/ml aprotinin (Sigma, UK), 10 μ g/ml leupeptin (Sigma), 10 μ g/ml pepstatin A (Sigma), 5 mM DTT (Sigma), 0.5 mM PMSF (Sigma), 2 mM Na orthovanadate (Sigma), 1.25 mM NaFl (Sigma), 1 mM Na pyrophosphate (Sigma), 25 mM Tris–HCl (Sigma), 75 mM NaCl (Sigma), 0.5% v/v Triton-X-100 (Sigma),

0.05% w/v SDS (Sigma), 0.25% Deoxycholic acid (Sigma), 5 mM EDTA (Sigma)] (see Note 2).

2. Autoclaved 2 ml microfuge tubes and/or 5 ml bijoux (for larger tissues).

**2.4. Histological
Assessment of siRNA
Delivery by In Situ
Hybridisation**

1. 70% EtOH.
2. Dissection scissors, blunt ended.
3. Forceps, serrated, blunt ended.
4. 2× small bent, serrated blunt-ended forceps.
5. Dissection pins.
6. Surgical thread.
7. Cannulas for mouse tracheas.
8. Microscissors.
9. 10% neutral-buffered formalin (Surgipath, UK).
10. 1 ml syringe.
11. Histological specimen containers filled 50–75 ml of neutral-buffered formalin (Surgipath).
12. 4% paraformaldehyde (Sigma, UK) in PBS.
13. Proteinase K buffer [10 µg/ml proteinase K (Sigma) in PBS].
14. Hybridisation buffer [50% formamide (Sigma), 5× SSC buffer (Sigma), 250 µg/ml yeast RNA (Ambion), 1× Denhardt's solution (Sigma) in DEPC-treated water (Sigma)].
15. Stringency buffer (50% formamide, 5× SSC buffer in DEPC-treated water).
16. Blocking buffer (10% sheep serum in PBS).
17. Custom, miRNA-16 (positive control) and scrambled (negative control) locked nucleic acid probes (LNA) for the siRNA used, dual digoxigenin (DIG)-labelled (Exiqon, Denmark).
18. Sheep anti-DIG fAb fragments, alkaline phosphatase (AP)-labelled (Roche Diagnostics, UK).
19. AP-substrate BCIP/NBT substrate kit (Vector Laboratories, UK).
20. Aqueous mounting media (DAKO, Denmark).

3. Methods

The protocols described herein were developed on BALB/c mouse lung experiments, and assume experience in standard necropsy procedures and basic histological techniques (formalin fixation

followed by paraffin embedding, sectioning and cryosectioning). Procedures and compounds are expected to perform equally efficiently in other mouse strains and across other species using standard allometric scaling methodologies (e.g. tenfold scaling between mouse and rat, etc.). The performance of commonly used analytical assays has been found to be comparable with substrates purified from different tissue types. Extraction procedures, however, may require a degree of optimisation for tissues with significant structural differences, e.g. fibrous tissues.

3.1. Tissue Preservation for RNA or Protein Extraction

1. Under terminal anaesthesia, pin down the animal through the footpads.
2. Wet the ventral surface of the mouse with 70% EtOH to sterilise.
3. Working carefully, expose to the thoracic cavity.
4. Using blunt forceps, raise the lung lobes and detach from the spine by carefully snipping away connective tissue.
5. Blot any blood from the lungs, and remove any non-lung tissue (e.g. trachea, heart, thymus, oesophagus, connective tissue, etc.).
6. Rinse the lungs in PBS, blot dry, and weigh out. Record the weight.
7. Using a sterile scalpel, dice the lungs into <math><1\text{ mm}^3</math> pieces.
8. Place the diced lungs into a large excess of *RNAlater*[®] in a 5 ml bijoux container (see Note 3).
9. Shake vigorously to mix tissue and ensure thorough access of the preserving solution. Ensure all tissue fragments are submerged following mixing.
10. Store overnight at 4°C, then transfer to –20°C or, preferably to –80°C (see Note 4).

3.2. Total Tissue RNA Extraction and Purification Using a Modified Protocol of the *mirVana*[™] (or *mirVana PARIS*[™]) Kit

1. Remove samples from storage and thaw on ice (see Note 5).
2. Once the solution is fully thawed, blot dry the tissue, weigh it, and transfer it into a 2 ml microfuge tube.
3. Add 1 ml lysis buffer per 100 mg tissue. The total volume is now 1.1× the lysis buffer used (volume A).
4. Working on ice, homogenise the tissue using a rotor–stator homogeniser (e.g. Ultraturrax) with an appropriate probe size (see Note 6).
5. Add miRNA homogenate additive at a volume equal to one-tenth of the total homogenate volume (volume A).
6. Mix by inversion.
7. Transfer the homogenate to wet ice and process the next tissue.

8. Upon completion of the tissue batch, incubate on ice for <30 min.
9. If the homogenate volume is >0.8 ml, then split it equally across two microfuge tubes.
10. Add acid/phenol chloroform at a volume equal to that of the total homogenate volume (volume A; if the sample has been split across two tubes, each tube should receive 0.5× volume A).
11. Vortex for 60 s (note: allowing for a significant air pocket in the tube improves vortexing. Tubes may need shaking to start mixing as the interphase may be quite stable. We have found that vortexing for at least 60 s ensures thorough mixing and good purification).
12. Allow to stand for 15 min to ensure complete dissociation of ribonucleoprotein complexes.
13. Centrifuge at 15,000×*g* for 15 min at 4°C (see Note 7).
14. Measuring the volume (volume B), carefully transfer the upper, aqueous phase into a fresh 2 ml microfuge tube. Do not disturb the interphase (see Note 8).
15. If the aqueous phase is >0.8 ml, then split it equally across two microfuge tubes.
16. Start heating your elution solution of choice to 95°C (see Note 9).
17. Add to the aqueous phase 1.25× volumes of 100% EtOH (volume B; if the sample has been split across two tubes, each tube should receive 0.625× volume B).
18. Mix by vortexing for 10 s.
19. Assemble a filter cartridge and collection tube per tissue. Process the aqueous phase-ethanol mixture in 0.7 ml batches by centrifugation at <9,900×*g* for 15 s at 4°C. Discard the flow-through.
20. Add 0.7 ml of wash solution 1 to the filter cartridges, centrifuge at 9,900×*g* for 15 s at 4°C, and discard the flow-through.
21. Repeat this wash twice more with 0.5 ml of wash solution 2.
22. Dry the cartridge by centrifugation at 9,900×*g* for 1 min at 4°C.
23. Place the cartridge into a fresh collection tube, and dispense 0.1 ml of pre-heated elution solution at the centre of the cartridge.
24. Centrifuge at 15,000×*g* for 30 s at 4°C.
25. Obtain spectrophotometric readings at 260 and 280 nm to assess yield and quality of the purified RNA (see Note 10).

3.3. Total Tissue Protein Extraction

1. Remove samples from storage and thaw on ice (see Note 5).
2. Once the solution is fully thawed, blot dry the tissue, weigh it, and transfer it into a 2 ml microfuge tube.
3. Add 1 ml of 1× RIPA buffer per 100 mg tissue (see Note 11).
4. Working on ice, homogenise the tissue using a rotor/stator homogeniser with an appropriate probe size.
5. Transfer the mixture to microfuge tubes if necessary and allow settling for <60 min on wet ice.
6. Centrifuge at $3,500 \times g$ for 20 min, 4°C.
7. Transfer the supernatant to fresh microfuge tubes and centrifuge at $21,000 \times g$ for 40 min at 4°C.
8. Transfer the supernatant to fresh microfuge tubes and quantify protein yield (e.g. Bradford assay, Biorad).

3.4. Histological Assessment of siRNA Delivery by In Situ Hybridisation

1. Follow standard formalin fixation and paraffin embedding (FFPE) procedures to prepare inflated lungs from animals treated with CPP-siRNA (see Note 12).
2. Cut 10 µm thick sections and fix in 4% paraformaldehyde (Sigma) in PBS for 10 min.
3. Wash three times in PBS for 2 min per wash.
4. Incubate the sections with 10 µg/ml proteinase K in PBS for 10 min at room temperature.
5. Fix again in 4% paraformaldehyde.
6. Wash three times in PBS for 10 min at room temperature.
7. Pre-hybridise in hybridisation buffer for 1 h at room temperature in a humidifying chamber.
8. Pre-incubate the LNA probes at 65°C for 5 min and immediately place on ice.
9. Decant the hybridisation buffer from the sections.
10. Prepare LNA probes at 2 µM in hybridisation buffer, cover the sections, and incubate in a humidifying chamber at 50°C for 18 h.
11. Wash the sections twice for 45 min in stringency buffer warmed to 50°C.
12. Wash the sections three times in PBS at room temperature.
13. Incubate in blocking buffer for 1 h at room temperature.
14. Prepare sheep anti-DIG fAb fragments (Roche Diagnostics) labelled with AP, diluted 1:5,000 in blocking buffer, and incubate for 2 h at room temperature.
15. Wash three times for 2 min in PBS.
16. Incubate with AP-substrate BCIP/NBT substrate for 12 h at room temperature in a humidifying chamber.

17. Wash twice in PBS and once in water.
18. Mount with aqueous mounting media.
19. Document the histological sections according to available equipment.

4. Notes

1. Use of barrier tips is required only after phase separation of RNA. It is however good practice to use nuclease-free disposables throughout the process.
2. Prepare stock protease inhibitor mix according to Table 1. 637.5 μ l of this can then be diluted to 10 ml of 1 \times RIPA buffer, by preparing 2 \times stock of RIPA buffer according to Table 2.
3. Volumes typically used are 1–1.5 ml per 100 mg of tissue.
4. We have not systematically tested RNA and protein stability at different temperatures and store at -80°C as a matter of course.

Table 1
Protease inhibitor mix stock (15.7 \times) preparation

Inhibitor	Stock concentration	Aliquot (μ l)	Dilution factor	Final concentration
Aprotinin	4 mg/ml	62.5	1:160	25 μ g/ml
Leupeptin	4 mg/ml	25	1:400	10 μ g/ml
Pepstatin A (methanol)	4 mg/ml	25	1:400	10 μ g/ml
DTT	1 M (154.25 mg/ ml)	50	1:200	5 mM
PMSF ^a	100 mM (17.42 mg/ml)	50	1:200	0.5 mM
Na orthovanadate	100 mM (18.39 mg/ml)	200	1:50	2 mM
Na fluoride	100 mM (4.2 mg/ml)	125	1:80	1.25 mM
Na pyrophosphate	100 mM (221.94 mg/ml)	100	1:100	1 mM
Total volume		637.5		

All individual components should be prepared in deionised water unless otherwise specified, aliquoted, and stored at -20°C or less^aPrepare in isopropanol

Table 2
Stock RIPA buffer (2×) recipe: protease inhibitor mix stock (15.7×) preparation

Stock	Volume used	Final concentration
Tris-HCl pH 6.8 (1 M)	5 ml	50 mM
NaCl (1 M)	15 ml	150 mM
Triton-X-100	1 ml	1%
10% SDS	1 ml	0.1%
Deoxycholic acid	500 mg	0.5%
EDTA (0.5 M)	2 ml	0.01 M
Deionised water	75 ml	
Total volume	100 ml	

The impact of accidental prolonged storage at room temperature or 4°C on RNA stability can be determined by either polyacrylamide or capillary gel electrophoresis. Alternatively, 18S levels determined by RT-PCR for a given amount of RNA per RT reaction can be a reliable indicator of RNA stability. We have observed significant impact on qPCR data quality and reliability when 18S measurement drop by >4 Ct.

5. RNAlater[®] does not always freeze at -20°C. This has not been found to compromise RNA or protein stability. If samples were flash frozen in liquid nitrogen and stored dry, transfer them to RNAlater[®]-ICE (1.0–1.5 ml per 100 mg tissue weight for known weights, 2 ml if tissue weight is unknown) and allow to thaw on ice.
6. Start at low speeds and progress to full speed. Ensure that all tissue fragments are thoroughly homogenised and use pointed forceps to dislodge any pieces in the probe. Thorough homogenisation can be assisted by moving the probe vertically.
7. Increase the speed to 20,000 × g or more if the resulting interphase is not compact. When processing multiple tissues, the interphase may loosen up. Repeat the centrifugation process if needed.
8. This can be recovered if required using standard protocols available for Tri Reagent (Sigma, UK). The lower, oily phase contains protein which can be recovered using standard Tri Reagent methodologies.
9. RNase-free water is recommended as this does not impact upon downstream reactions.

10. 1:50 dilutions in RNase-free water appropriate for plate-based UV readers. Typical purifications result in ~1 mg/ml RNA per 100 mg tissue and A_{260}/A_{280} ratios of ~1.9.
11. Alternatively, the oil phase from a phenol–chloroform extraction using a mirVana[®]/mirVana[®] PARIS kit or part of the initial tissue homogenate of a mirVana[®] PARIS kit can be used. The oil phase contains denatured protein, whereas the tissue homogenate contains no denaturing agents and importantly, no protease inhibitors. It is, therefore, essential to work this material on ice and supplement it with concentrated RIPA buffer (with protease inhibitors) to achieve a final 1× RIPA buffer concentration and minimise protein degradation. For best results, proceed with rotor–stator homogenisation.
12. It is essential to perform tissue inflation with the fixative to ensure lung structure is retained. Ensure the use of RNase-free solutions and equipment treated against RNase contamination with, e.g. 0.1% diethylpyrocarbonate or RNaseZAP[®] (Ambion, UK), and minimise the duration of processing at high temperatures, as this carries a risk of siRNA degradation. An alternative approach is inflation and/or perfusion (as appropriate) of the tissue with 50% O.C.T. compound (Tissue-Tek, UK) in PBS at 37°C, followed by embedding and freezing over liquid nitrogen gas. This is performed by placing the inflated/perfused tissue on a piece of cardboard, covering it with 50% O.C.T. compound, and holding ~0.5 in. above liquid nitrogen until the compound freezes, whereupon it can be safely dropped into liquid nitrogen without the tissue cracking. This cryopreservation method to date remains the most efficient at retaining tissue structure. Cryosectioning should be followed by dehydration in 95% EtOH for 10 min at room temperature and drying in a room temperature dessicator for 20 min. Further processing for ISH should continue from step 2 onwards.

References

1. Wagstaff, K.M., and Jans, D.A. (2006) Protein transduction: cell penetrating peptides and their therapeutic applications. *Curr Med Chem* **13**(12), 1371–87.
2. Morris, M.C., Deshayes, S., Heitz, F., and Divita, G. (2008) Cell-penetrating peptides: from molecular mechanisms to therapeutics. *Biol Cell* **100**(4), 201–17.
3. Moschos, S.A., Williams, A.E., and Lindsay, M.A. (2007) Cell-penetrating-peptide-mediated siRNA lung delivery. *Biochem Soc Trans* **35**(Pt 4), 807–10.
4. Moschos, S.A., Jones, S.W., Perry, M.M., Williams, A.E., Erjefalt, J.S., Turner, J.J., Barnes, P.J., Sproat, B.S., Gait, M.J., and Lindsay, M.A. (2007) Lung delivery studies using siRNA conjugated to TAT(48-60) and penetratin reveal peptide induced reduction in gene expression and induction of innate immunity. *Bioconjug Chem* **18**(5), 1450–9.
5. Richardt-Pargmann, D., and Vollmer, J. (2009) Stimulation of the immune system by therapeutic antisense oligodeoxynucleotides and small interfering RNAs via nucleic acid receptors. *Ann N Y Acad Sci* **1175**, 40–54.
6. Robbins, M., Judge, A., Liang, L., McClintock, K., Yaworski, E., and MacLachlan, I. (2007)

- 2-O-methyl-modified RNAs act as TLR7 antagonists. *Mol Ther* **15**(9), 1663–9.
7. Karikó, K., Bhuyan, P., Capodici, J., and Weissman, D. (2004) Small interfering RNAs mediate sequence-independent gene suppression and induce immune activation by signaling through toll-like receptor 3. *J Immunol* **172**(11), 6545–9.
 8. Matsukura, S., Kokubu, F., Kurokawa, M., Kawaguchi, M., Ieki, K., Kuga, H., Odaka, M., Suzuki, S., Watanabe, S., Takeuchi, H., Kasama, T., and Adachi, M. (2006) Synthetic double-stranded RNA induces multiple genes related to inflammation through Toll-like receptor 3 depending on NF-kappaB and/or IRF-3 in airway epithelial cells. *Clin Exp Allergy* **36**(8), 1049–62.
 9. Kleinman, M.E., Yamada, K., Takeda, A., Chandrasekaran, V., Nozaki, M., Baffi, J.Z., Albuquerque, R.J., Yamasaki, S., Itaya, M., Pan, Y., Appukkuttan, B., Gibbs, D., Yang, Z., Karikó, K., Ambati, B.K., Wilgus, T.A., DiPietro, L.A., Sakurai, E., Zhang, K., Smith, J.R., Taylor, E.W., and Ambati, J. (2008) *Nature* **452**(7187), 591–7.
 10. Fukuda, K., Watanabe, T., Tokisue, T., Tsujita, T., Nishikawa, S., Hasegawa, T., Seya, T., and Matsumoto, M. (2008) Modulation of double-stranded RNA recognition by the N-terminal histidine-rich region of the human toll-like receptor 3. *J Biol Chem* **283**(33), 22787–94.
 11. Eguchi, A., Meade, B.R., Chang, Y.C., Fredrickson, C.T., Willert, K., Puri, N., and Dowdy, S.F. (2009) Efficient siRNA delivery into primary cells by a peptide transduction domain-dsRNA binding domain fusion protein. *Nat Biotechnol* **27**(6), 567–71.
 12. Crombez, L., Aldrian-Herrada, G., Konate, K., Nguyen, Q.N., McMaster, G.K., Brasseur, R., Heitz, F., and Divita, G. (2009) A new potent secondary amphipathic cell-penetrating peptide for siRNA delivery into mammalian cells. *Mol Ther* **17**(1), 95–103.
 13. Howard, K.A., Rahbek, U.L., Liu, X., Damgaard, C.K., Glud, S.Z., Andersen, M.Ø., Hovgaard, M.B., Schmitz, A., Nyengaard, J.R., Besenbacher, F., and Kjems, J. (2006) RNA interference in vitro and in vivo using a novel chitosan/siRNA nanoparticle system. *Mol Ther* **14**(4), 476–84.
 14. Zhang, X., Shan, P., Jiang, D., Noble, P.W., Abraham, N.G., Kappas, A., and Lee, P.J. (2004) Small interfering RNA targeting heme oxygenase-1 enhances ischemia-reperfusion-induced lung apoptosis. *J Biol Chem* **279**(11), 10677–84.
 15. Alvarez, R., Elbashir, S., Borland, T., Toudjarska, I., Hadwiger, P., John, M., Roehl, I., Morskaya, S.S., Martinello, R., Kahn, J., Van Ranst, M., Tripp, R.A., DeVincenzo, J.P., Pandey, R., Maier, M., Nechev, L., Manoharan, M., Kotlianski, V., and Meyers R. (2009) RNA interference-mediated silencing of the respiratory syncytial virus nucleocapsid defines a potent antiviral strategy. *Antimicrob Agents Chemother* **53**(9), 3952–62.
 16. Raymond, C.K., Roberts, B.S., Garrett-Engele, P., Lim, L.P., and Johnson, J.M. (2005) Simple, quantitative primer-extension PCR assay for direct monitoring of microRNAs and short-interfering RNAs. *RNA* **11**(11), 1737–44.
 17. Livak, K.J., and Schmittgen, T.D. (2001) Analysis of relative gene expression data using real-time quantitative PCR and the $2^{-\Delta\Delta Ct}$ method. *Methods* **25**, 402–8.
 18. Wang, Z., Gerstein, M., and Snyder, M. (2009) RNA-Seq: a revolutionary tool for transcriptomics. *Nat Rev Genet* **10**(1), 57–63.
 19. Cubillos-Ruiz, J.R., Engle, X., Scarlett, U.K., Martinez, D., Barber, A., Elgueta, R., Wang, L., Nesbeth, Y., Durant, Y., Gewirtz, A.T., Sentman, C.L., Kedl, R., and Conejo-Garcia, J.R. (2009) Polyethylenimine-based siRNA nanocomplexes reprogram tumor-associated dendritic cells via TLR5 to elicit therapeutic antitumor immunity. *J Clin Invest* **119**(8), 2231–44.
 20. Forsbach, A., Nemorin, J.G., Montino, C., Müller, C., Samulowitz, U., Vicari, A.P., Jurk, M., Mutwiri, G.K., Krieg, A.M., Lipford, G.B., and Vollmer, J. (2008) Identification of RNA sequence motifs stimulating sequence-specific TLR8-dependent immune responses. *J Immunol* **180**(6), 3729–38.
 21. Judge, A.D., Sood, V., Shaw, J.R., Fang, D., McClintock, K., and MacLachlan, I. (2005) Sequence-dependent stimulation of the mammalian innate immune response by synthetic siRNA. *Nat Biotechnol* **23**(4), 457–62.
 22. Crombez, L., Morris, M.C., Dufort, S., Aldrian-Herrada, G., Nguyen, Q., McMaster, G., Coll, J.L., Heitz, F., and Divita, G. (2009) Targeting cyclin B1 through peptide-based delivery of siRNA prevents tumour growth. *Nucleic Acids Res* **37**(14), 4559–69.
 23. Wu, Y., Navarro, F., Lal, A., Basar, E., Pandey, R.K., Manoharan, M., Feng, Y., Lee, S.J., Lieberman, J., and Palliser, D. (2009) Durable protection from Herpes Simplex Virus-2 transmission following intravaginal application of siRNAs targeting both a viral and host gene. *Cell Host Microbe* **5**(1), 84–94.
 24. Williams, A.E., Moschos, S.A., Perry, M.M., Barnes, P.J., and Lindsay, M.A. (2007) Maternally imprinted microRNAs are differentially expressed during mouse and human lung development. *Dev Dyn* **236**(2), 572–80.

Chapter 31

Intracellular Delivery of Nanoparticles with CPPs

Rupa Sawant and Vladimir Torchilin

Abstract

Cell-penetrating peptides (CPPs), in particular TATp, have been widely used for intracellular delivery of various cargoes, both in vitro and in vivo. Modifications of nanoparticles with CPPs require either covalent or noncovalent approach. Here we describe various methods to attach CPP, such as TATp to surface of nanocarriers (such as liposomes and micelles), loading with drug or DNA and characterization of same for in vitro and in vivo applications. Due to nonselectivity of CPPs and wide distribution in nontarget areas, method for preparation of “smart” nanocarrier with hidden TATp function is also described.

Key words: CPP, Liposomes, Micelles, Nanoparticles, “Smart” Drug Delivery System, TATp, pH sensitive, DNA

1. Introduction

Efficient intracellular delivery of therapeutic molecules still remains a challenging task. In particular, very few attempts have been made to deliver drugs or drug-loaded nanocarriers directly into the cell cytoplasm bypassing the endocytic pathway. Successful intracellular delivery is especially important in the case of many peptide and protein-based agents and also for gene delivery to target certain cellular functions.

Over the last decade, cell-penetrating peptides (CPPs) have shown some potential for overcoming the cellular barrier for intracellular drug delivery (1). Such peptides usually contain domains of less than 20 amino acids that are highly rich in basic residues. These peptides include Antennapedia (Antp) (2), VP22 (3), transportan (4), model amphipathic peptide MAP (5), signal sequence-based peptides (6), and synthetic polyarginines (7), such as R₉ analog of TAT (R₉-TAT), HIV-1 Rev (34–50), flock house virus coat (35–49) peptide, and DNA-binding peptides

such as c-Fos (139–164), c-Jun (252–279), and yeast GCN4 (231–152). These peptides have been used for intracellular delivery of various cargoes with molecular weights significantly higher than their own (8). In early studies it was demonstrated that dextran-coated superparamagnetic iron oxide particles (CLIO) coupled with TATp (48–57) provided efficient labeling of cells, and thus could serve as a tool for magnetic resonance imaging (9). The uptake of TATp-CLIO nanoparticles by cells was about 100-fold higher than that of nonmodified iron oxide particles. CPPs have proven to be successful for delivery of protein (10–12), antibodies that are usually difficult to deliver into cells (13, 14) as well as for small molecule drugs (15, 16). CPPs are also useful as nonviral gene delivery systems and can be further modified to promote endosomal escape, thus preventing degradation and allowing nucleic acid to reach nuclear targets (17, 18). RNAi technology has also been improved with CPP-mediated delivery of siRNA (19, 20).

TATp, derived from the transcriptional activator protein encoded by human immunodeficiency virus type I (HIV-1), has received a great deal of attention (21). Both in vitro and in vivo studies have shown that by covalently linking TATp to nearly any drug class, including hydrophilic compounds and large protein molecules (MW > 150 kDa), it was able to transduce the attached cargoes into cells of all organ types including the brain (22, 23). Indeed, rapid and receptor-independent uptake of TAT-conjugated peptides has been demonstrated to occur in many cell types and animals (24, 25). TATp-mediated cytoplasmic uptake of polymers, plasmid DNA (26–29), nanoparticles (30–34), liposomes (35–37), and micelles (38, 39) has been reported. TATp-modified nanoparticles have also been investigated for their capability to deliver diagnostic and therapeutic agents across the blood–brain barrier. For in vivo bioimaging, TATp-FITC-doped silica nanoparticles (FSNPs) were administered intra-arterially to the brain of rats. TATp-conjugated FSNPs labeled the brain blood vessels, showing the potential for delivering agents to the brain without compromising the blood–brain barrier (40). TATp-functionalized boron carbide nanoparticles were translocated into murine EL4 lymphoma cells and B16F10 melanoma cells, which can be used for boron neutron capture therapy (41).

The most popular and well-investigated drug carriers are liposomes (mainly, for water-soluble drugs) and micelles (for poorly soluble drugs). Liposomes are artificial phospholipid vesicles with size varying from 50 to 1,000 nm and greater, which can be loaded with a variety of drugs and are considered as promising drug carriers (42, 43). Further, addition of polyethylene glycol (PEG) coating renders these liposomes long-circulating (the ability to stay in the blood for a prolonged period) (44) so as to allow accumulation in various pathological areas with compromised

(leaky) vasculature, such as tumors. It has been proven that (45) such long-circulating liposomes can be “targeted” with antibodies or other specific binding molecules attached to the water-exposed tips of PEG chains (46).

Micelles, including polymeric micelles, are widely gaining interest as pharmaceutical carriers due to their small size (10–100 nm), *in vivo* stability, ability to solubilize water-insoluble anticancer drugs, and prolonged blood circulation times (47, 48). The typical core shell structure of polymeric micelles is formed by self-assembly of amphiphilic block copolymers consisting of hydrophilic and hydrophobic monomer units in aqueous media (47). The use of special amphiphilic molecules as micelle building blocks can also introduce the property of micelle extended blood half-life upon intravenous administration. Such block copolymer micelles can also target their payload to specific tissues through either passive or active means. Passive targeting is due to their small micellar size which assists in spontaneous penetration into the interstitium into compartments with the leaky vasculature (tumors and infarcts) by the enhanced permeability and retention (EPR) effect (47–50). Active targeting can be achieved by attachment of target-specific molecules to their surface (47, 48). Micelles made of PEG-phosphatidylethanolamine (PEG-PE) are of special interest. Here, the use of lipid moieties as hydrophobic blocks capping hydrophilic polymer (such as PEG) chains can provide additional advantages for particle stability when compared with conventional amphiphilic polymer micelles due to the existence of two fatty acid acyls, which might contribute considerably to an increase in the hydrophobic interactions between the polymeric chains in the micelle core (51). PEG-PE micelles demonstrate good stability, longevity, and an ability to accumulate in areas with a damaged vasculature (EPR effect in leaky areas, such as infarcts and tumors) (51, 52). All versions of PEG-PE conjugates form micelles with a spherical shape, uniform size distribution (7–35 nm), and with very low critical micelle concentration values (in a high nanomolar to low micromolar range) because of the strong hydrophobic interactions between double acyl chains of phospholipid residues. These micelles are structured in such a way that the outer PEG corona, known to be highly water soluble and highly hydrated, serves as an efficient steric protector in biological media. On the other hand, the phospholipid residues, which represent the micelle core, are extremely hydrophobic and can solubilize various poorly soluble drugs including paclitaxel, camptothecin, porphyrine, tamoxifen, vitamin K₃, and others (53–55).

There are many examples in the literature using TATp-modified liposomes and micelles. TATp (47–57)-modified liposomes were delivered intracellularly in different cells, such as murine Lewis lung carcinoma (LLC), human breast tumor (BT20), and rat cardiac myocyte (H9C2) (35). The liposomes were

tagged with TATp via the spacer, *p*-nitrophenylcarbonyl-PEG-PE, at a density of a few hundreds of TATp per single liposome vesicle. The preparations of TATp-liposomes, which allowed for the direct contact of TATp residues with cells, displayed an enhanced cellular uptake. This suggested that the translocation of TATp-liposomes into cells required direct free interaction of TATp with the cell surface. It was found that the translocation of liposomes by TATp or penetratin was proportional to the number of peptide molecules attached to the liposomal surface. As few as five peptide number was sufficient to enhance the intracellular delivery of liposomes. The kinetics of the uptake was peptide- and cell-type dependent (56). Coupling of TATp to the outer surface of liposomes resulted in an enhanced binding and endocytosis of the liposomes in ovarian carcinoma cells (36). TATp liposomes prepared with the addition of a small quantity of cationic lipid (DOTAP) were used to form noncovalent complexes with DNA. Such TATp-liposome-DNA complexes when incubated with mouse fibroblast (NIH 3T3) and cardiac myocytes (H9C2) showed substantially higher transfection both in vitro and in vivo, with lower cytotoxicity than the commonly used Lipofectin® (57). We have also recently shown that TATp-lipoplexes exhibited enhanced delivery of pEGFP-N1 to U-87 MG tumor cells in vitro at lipid/DNA (+/-) charge ratios of 5 and 10. Such lipoplexes showed enhanced delivery of pEGFP-N1 selectively to tumor cells (58). Another example is gene delivery into immunocompetent cells to modulate immune response. Antigen-presenting cells (APC) are among the most important cells of the immune system since they link the innate and the adaptive immune responses, directing the type of immune response to be elicited. However, APC are very resistant to transfection. To increase the efficiency of APC transfection, we have used liposome-based lipoplexes additionally modified with cell-penetrating TATp for better intracellular delivery of a model plasmid encoding for the enhanced-green fluorescent protein (pEGFP). pEGFP-bearing lipoplexes made of a mixture of PC:Chol:DOTAP (60:30:10 molar ratio) with the addition of 2% mol of PEG-PE conjugate (plain-L) or TATp-PEG-PE (TATp-L) were shown to effectively protect the incorporated DNA from degradation. Uptake assays of rhodamine-labeled lipoplexes and transfections with the EGFP reporter gene were performed with APC derived from the mouse spleen. TATp-L-based lipoplexes allowed for significantly enhanced both, the uptake and transfection in APC (59).

Quantum dots trapped within PEG-PE micelles bearing TATp-PEG-PE linker were successfully applied for labeling mouse endothelial cells in vitro. For in vivo tracking, bone marrow-derived progenitor cells were labeled with TATp-bearing quantum dot-containing micelle ex vivo, and then injected in the mouse bearing tumor in a cranial window model. It was then pos-

sible to track the movement of the labeled progenitor cells to tumor endothelium, providing some understanding of the fine details of tumor neovascularization (60). Several examples related to the intracellular delivery of pharmaceutical nanocarriers by CPPs are presented in Table 1.

A variety of uptake mechanisms appear to be involved within different systems, and in some cases, the mechanism is cell-type or cargo-specific (73). A recent mechanism proposed for CPP-conjugated large cargoes (MW > 30,000 Da) is nonclathrin, non-caveolar endocytosis, called macropinocytosis (74). The important step in uptake appears to be via surface adsorption and the binding of the cationic TATp to the anionic heparan sulfate on the cell surface, because TATp-mediated cell translocation of the attached cargoes was completely inhibited in the presence of heparin, heparan, or dextran sulfate (75).

The main limitation in CPP-mediated delivery of biologically active molecules is the sequestration and entrapment of the majority of internalized material within endocytic vesicles. In certain cases it is necessary that these molecules reach their target which can be located in certain cellular organelles. A variety of tools to enhance the endosomal escape of CPP-attached cargoes are reported in the literature such as the use of fusogenic lipids (76–78), membrane disruptive peptides (79–83), polymers (69, 84), and lysomotropic agents (79, 85, 86). Stearylolation of CPPs has proven to be another successful methodology to increase the transfection efficiency of both plasmids (72, 87) and SiRNA (88) through a noncovalent approach resulting in the formation of nanoparticle complex.

The major drawback of TATp-mediated intracellular delivery is the lack of selectivity of TATp which has rendered this cellular drug delivery method unacceptable at present, due to concerns about drug-induced toxic effects on normal tissues. This has led to efforts to build “smart” nanocarriers (Fig. 1) in such a way that during the first phase of delivery the nonspecific cell-penetrating function (in our case TATp) is shielded by the function providing organ/tissue-specific delivery (with a sterically protecting polymer or targeting antibody). Upon accumulation in the target, the protecting polymer or antibody attached to the surface of the nanocarrier via stimuli-sensitive bond should detach under the action of local pathological conditions (abnormal pH or temperature) and expose the previously hidden second function and allow the subsequent delivery of the carrier and its cargo inside cells (89). All these approaches have important implications for successful intracellular delivery of a nanocarrier for a drug or a gene delivery system.

In this chapter we discuss various protocols for the incorporation of TATp on nanocarriers such as micelles and liposomes and their characterization both in vitro and in vivo.

Table 1
Examples of nanoparticles delivered into cells using CPPs

Particle, CPP used	Target cell, study purpose	References
Liposomes, TATp, Antennapedia, octaarginine	Airway cells. For intracellular drug delivery by inhalation	(61)
Liposomes, lipid-modified TATp	Various cells	(62)
Sterically stabilized liposomes, 200 nm, TATp coupled to the linker	Mouse LLC, human BT20, rat H9C2, LLC tumor in mice. To show the potential of TAT-liposome for intracellular delivery, and the intracellular gene delivery in vitro and in vivo	(56, 57)
Liposomes, polyarginine	For siRNA delivery into cells and gene silencing	(63)
Liposomes, TATp	To show improved transfection of spleen-derived antigen-presenting cells in culture	(59)
Low cationic liposomes–plasmid DNA complexes (lipoplexes) modified with TATp and/or with monoclonal anti-myosin monoclonal antibody 2G4 (mAb 2G4) specific toward cardiac myosin	Enhanced transfection of normoxic and hypoxic cardiomyocytes by using lipoplexes modified with TATp and/or mAb 2G4. Also increased accumulation in the ischemic myocardium and effective transfection of hypoxic cardiomyocytes in vivo	(64)
pEGFP-bearing lipoplexes, TATp	Improved transfection of antigen-presenting cells in culture	(59)
CLIO (MION) particles, 41 nm, TATp	Mouse lymphocytes, human natural killer, HeLa, human hematopoietic CD34+, mouse neural progenitor C17.2, human lymphocytes CD4+, T cells, B cells, macrophages, immune cells, stem cells. For intracellular labeling, MRI, magnetic separation of homed cells, cell imaging	(9, 31, 65)
Poly lactide nanoparticles, TATp	For drug delivery to brain	(34)
PEG-poly lactic acid micelles, 20–45 nm, TATp	For drug delivery to acidic tumors	(38)
PEG-PE micelles, TATp	Increased cell interaction in vitro	(66)
Paclitaxel-loaded PEG-PE micelles, TATp	Increased cytotoxicity in vitro and in vivo	(39)

(continued)

Table 1
(continued)

Particle, CPP used	Target cell, study purpose	References
pH-sensitive polymeric micelles, 20–45 nm, TATp	Various cells. For tumor-specific intracellular drug delivery	(38)
Gold particles, 20 nm, TATp	NIH3T3, HepG2, HeLa, human fibroblast HTERT-BJ1. For intracellular localization studies	(67, 68)
Quantum dot-loaded polymeric micelles, 20 nm, TATp coupled to a linker	Mouse endothelial cells, bone marrow derived progenitor cells. For studying tumor pathophysiology under dynamic conditions, useful for concurrent imaging and distinguishing tumor vessels from perivascular cells and matrix	(60)
Nanocomplexes of PEI and DNA, TATp	SH-SY5Y cells. For gene delivery to neurotypic cells	(69)
PEG-PEI conjugates, TATp	For DNA delivery to lung in mice	(70, 71)
Splice correcting oligonucleotides, stearylated CPP (TP10)	For noncovalent delivery of oligonucleotides	(72)
Boron carbide nanoparticles, TATp	Murine EL4 lymphoma cells, B16F10 melanoma cells. For boron neutron capture therapy	(41)
Dendrimers, various CPPs	For oligonucleotide delivery into various cells	(56)

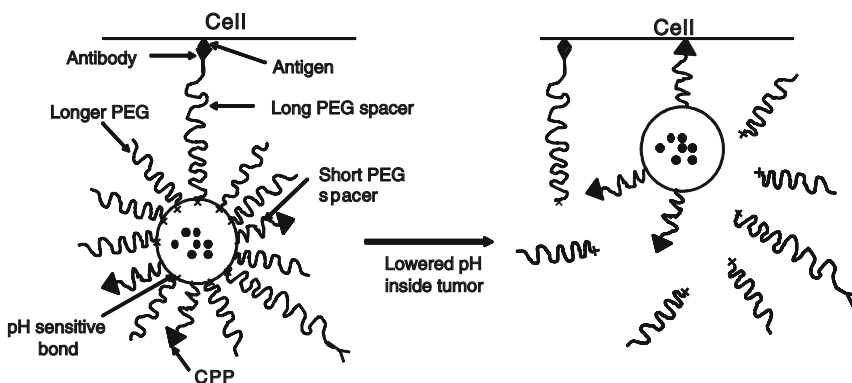


Fig. 1. Schematic of a “smart” nanocarrier with temporarily “hidden” function, for example CPP, and “shielding” polymeric coat (with or without targeting antibody attached to it) providing longevity in the blood and specific target (tumor) accumulation and preventing the hidden function from the premature interaction with target cells. Polymeric chains are attached to the carrier surface via low pH-degradable bonds. After the accumulation in the tumor due to PEG (longevity) and/or antibody (specific targeting), pH-dependent deshielding of the temporarily hidden cell-penetrating function allows for carrier penetration inside tumor cells.

2. Materials

2.1. Preparation of TATp-Modified Liposomes

1. Egg phosphatidylcholine (PC), cholesterol (Ch), and 1,2-dipalmitoyl-*sn*-glycero-3-phosphoethanolamine-*N*-(lissamine rhodamine B sulfonyl) (Rh-PE) (Avanti Polar Lipids, Alabaster, AL). Stored at -80°C .
2. *p*-Nitrophenylcarbonyl-PEG-dioleoyl phosphatidylethanolamine (pNP-PEG-PE) (46) synthesized in-house. Stored at -80°C .
3. Citrate-buffered saline (CBS): 5 mM Na-citrate, 141 mM NaCl. Adjust pH to 5.4 with 1 N HCl. Stored at room temperature.
4. FITC-dextran (4,400 Da) (Sigma, St. Louis, MO).
5. Borate buffer: 0.1 M sodium tetraborate, 150 mM NaCl. Adjust pH to 9.2 with 1 N HCl or 1 N NaOH. Stored at room temperature.
6. TAT-peptide (TATp-NH₂) (11-mer: TyrGlyArgLysLysArgArgGlnArgArgArg) and TAT-cysteine peptide (TATp-Cys) (12-mer: CysTyrGlyArgLys-LysArgArgGlnArgArgArg) (Tufts University Core Facility, Boston, MA).

2.2. Preparation of TATp Liposome Plasmid Complex

1. 1,2-Dioleoyl-3-trimethylammonium-propane (DOTAP) (Avanti Polar Lipids, Alabaster, AL). Stored at -80°C .
2. pEGFP-N1 plasmid designed for eukaryotic cell expression of green fluorescent protein (GFP) (Elim Biopharmaceuticals, Hayward, CA).
3. Lipofectin reagent (Invitrogen, Carlsbad, CA).

2.3. Preparation of TATp-Modified Micelles

1. Polyethyleneglycol-phosphatidylethanolamine (PEG₇₅₀-PE) (Avanti Polar Lipids Alabaster, AL). Stored at -80°C .
2. TATp-PEG₁₀₀₀-PE synthesized in-house (90, 91). Stored at -80°C .

2.4. Preparation of TATp-Modified pH-Sensitive or pH-Insensitive Micelles

1. Polyethyleneglycol-phosphatidylethanolamine (PEG₂₀₀₀-PE) (Avanti Polar Lipids Alabaster, AL). Stored at -80°C .
2. mPEG₂₀₀₀-HZ-PE (90, 91) synthesized in-house. Stored at -80°C .
3. Phosphate-buffered saline (PBS): 140 mM NaCl, 10 mM Na₂HPO₄, 1.8 mM KH₂PO₄, 2.7 mM KCl. Adjust pH to 7.4 with 1 N HCl or 1 N NaOH. Stored at room temperature.

2.5. Preparation of TATp-Modified Immunocarriers

1. Tris-buffered saline (TBS): 50 mM Tris (free base), 150 mM NaCl. Adjust pH to 8.7 with 1 N HCl. Stored at room temperature.

2. Monoclonal antibody (mAb) 2G4 produced and purified in our laboratory.

2.6. ELISA

1. Tris-buffered saline (TBS): 50 mM Tris (free base), 150 mM NaCl. Adjust pH to 7.4 with 1 N HCl. Stored at room temperature.
2. TBS containing 0.05 % w/v Tween-20 (TBST). Stored at 2–8°C.
3. TBS containing 0.05 % w/v Tween-20 and 2 mg/mL casein (TBST-Cas). Stored at 2–8°C.
4. Standard mAb 2G4 in TBST-Cas at 10 µg/mL. Stored at 2–8°C.
5. Goat anti-mouse IgG peroxidase conjugates (ICN Biomedical, Aurora, OH) in TBST-Cas 1:5,000 dilution, prepared fresh. Original stored at –20°C.
6. Enhanced Kblue® TMB peroxidase substrate (Neogen, Lexington, KY). Stored at 2–8°C.

2.7. Interaction with Cells In Vitro

1. Six-well culture plates.
2. Sterile PBS: 140 mM NaCl, 10 mM Na₂HPO₄, 1.8 mM KH₂PO₄, 2.7 mM KCl. Adjust pH to 7.4 with 1 N HCl or 1 NaOH. Stored at room temperature.
3. Cell lines from ATCC (Rockville, MD), cell culture media and fetal bovine serum from Cellgro (Kansas City, MO).

3. Methods

Two protocols have been used for preparing TATp-modified liposomes. In the first method, liposomes containing pNP-PEG-PE are prepared and TATp is then attached via pNP groups at the distal ends of the liposome containing pNP-PEG-PE (Fig. 2). In the second case liposomes are prepared using preconjugated TATp-PEG-PE. These liposomes can be used to prepare plasmid liposome complexes (see Note 1).

3.1. Preparation of TATp-Modified Liposomes

1. Prepare a mixture of lipid components of PC, Ch, and pNP-PEG-PE (7:3:0.05, molar ratio) in chloroform in a round-bottom flask (see Note 2).
2. Remove the solvents by rotary evaporation followed by freeze-drying on a Freezone 4.5 (Labconco, Kansas City, MO).
3. Rehydrate the film in 5 mM CBS (pH 5.4) (see Note 3).
4. Extrude the lipid dispersion 21 times through polycarbonate filters (pore size 200 nm) with a Micro extruder (Avanti).

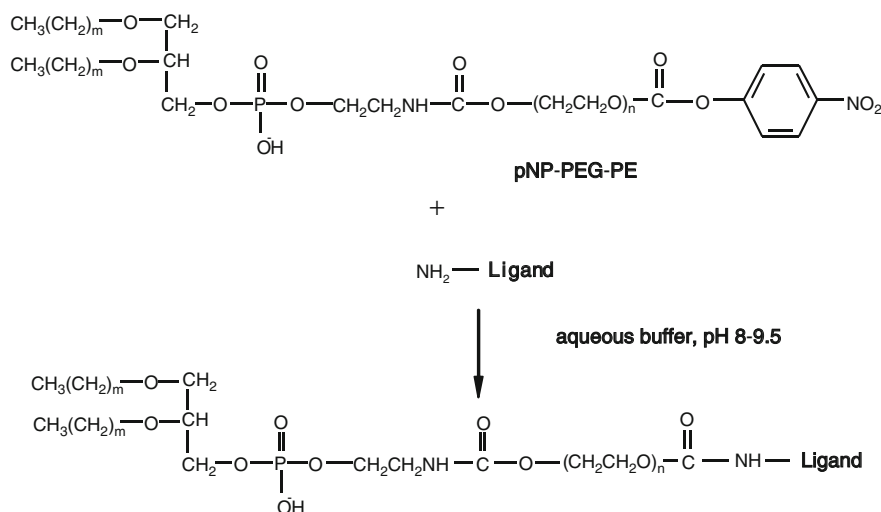


Fig. 2. Schematic of amino-group-containing ligand, such as peptide attachment using pNP-PEG-PE.

5. For visualization label the liposomes by adding 0.5 mol% of Rh-PE in step 1 or add FITC-dextran (45 mg/mL) to the CBS during hydration. Remove nonincorporated FITC-dextran on a Bio-Gel A-1.5 m (0.7 × 25 cm) column (Bio-Rad).
6. To attach TATp to liposomes, add 1 mg of peptide in borate buffer to 10 mg of pNP-PEG-PE containing liposomes in CBS (see Note 4) and incubate overnight at room temperature (see the scheme of peptide attachment in Fig. 2). Purify the TATp-liposomes from unbound TATp and released pNP by gel filtration on a BioGel A-1.5 m (0.7 × 25 cm) column (Bio-Rad).
7. Alternatively prepare TATp-PEG₃₄₀₀-PE by reacting TATp with pNP-PEG₃₄₀₀-PE and add to the lipid film instead of pNP-PEG-PE. In a typical case, incubate a solution of 5 mg of TATp-NH₂ in 1 mL chloroform supplemented with 10 μL of triethylamine with 12 mg of pNP-PEG₃₄₀₀-PE in 0.6 mL chloroform overnight with stirring at room temperature. Remove the organic solvents by rotary evaporation and freeze-drying. To the resultant film, add 1 mL of deionized water and vortex to remove the film from the flask. Purify the TATp-PEG₃₄₀₀-PE from unconjugated TATp-NH₂ and released pNP, by dialyzing the solution using cellulose ester dialysis membranes MWCO 2000 (Spectrum Medical Industries, Rancho Dominguez, CA) at room temperature against water.

3.2. Preparation of TATp Liposome-Plasmid Complex

Attempts have been made to use CPP for intracellular delivery of DNA. Though intracellular delivery of DNA can be enhanced, the method still requires the modification of DNA with CPPs.

Here we prepare noncovalent complexes of DNA with slightly positively charged TATp-bearing liposomes that can provide effective alternative transfection system.

1. Prepare liposomes from a mixture of PC, Ch, DOTAP, and pNP-PEG-PE at a molar ratio 7:3:1:0.05 as described above and incubate with pEGFP-N1 overnight at 4°C. In a typical case, incubate the liposome-plasmid complex containing a total of 2 mg of lipid and 200 µg of DNA and appropriate amount of TATp overnight at pH 8.5 in a borate buffer and then purify by gel filtration on a Bio-Gel A-1.5 m column (Bio-Rad).
2. To test for the presence and intactness of the plasmid within liposomes, subject the postcolumn fraction to agarose gel electrophoresis.
3. Determine the DNA content of the fractions after treating with Triton X-100 for 1 h at 37°C to release the plasmid from the complex and then subject to agarose gel electrophoresis. Prepare Lipofectin-pEGFP-N1 complex according to manufacturer instructions (Invitrogen) by using same quantities and ratios of lipid and DNA.

3.3. Preparation of TATp-Modified Micelles

Polymeric micelles are another promising drug carrier which can also be surface decorated with TATp. A very simple protocol can be used to insert TATp into PEG-PE micelles. Here we use the preconjugated TATp-PEG₁₀₀₀-PE for insertion into micelles.

1. Prepare a lipid film from a mixture of PEG₇₅₀-PE, TATp-PEG₁₀₀₀-PE, Rh-PE and at a molar ratio of 9.7:0.25:0.05 as described above.
2. Hydrate the dry lipid film with PBS, pH 7.4.

3.4. Preparation of TATp-Modified pH-Sensitive or pH-Insensitive Liposomes

The idea is to prepare liposomes containing TATp moieties shielded by the PEG chains. Here the PEG chain is incorporated into the liposome membrane via the PEG-attached PE residue with PEG and PE conjugated with the lowered pH-degradable hydrazone bond (PEG-Hz-PE). Under normal conditions, liposome-grafted PEG shields the TATp moieties attached to the shorter PEG spacer and protected by the longer PEG₂₀₀₀. Once accumulated in a specific target such as a tumor by the EPR effect, the liposomes lose their PEG coating due to the lowered pH inside cells and expose TATp moieties.

Liposomes

1. Prepare a lipid film from a mixture of PC:Ch (7:3), TATp-PEG₁₀₀₀-PE, Rh-PE and either mPEG₂₀₀₀-Hz-PE (pH sensitive) or mPEG₂₀₀₀-DSPE (pH insensitive) at a molar ratio of 10:0.25:0.1:15 as described above.

- Hydrate the dry lipid film with PBS, pH 7.4 and extrude the lipid dispersion 21 times through polycarbonate filters (pore size 200 nm) with a Micro extruder (Avanti).

Micelles

- Prepare a lipid film from a mixture of mPEG₇₅₀-PE, TATp-PE, Rh-PE, and either (pH sensitive) or mPEG₂₀₀₀-DSPE (pH insensitive) at a molar ratio of 4:0.5:0.1:5.4 as described above.
- Hydrate the dry lipid film with PBS, pH 7.4.

3.5. Preparation of TAT-Modified Immunocarriers

TATp-containing liposomes/micelles can be additionally modified with antibody to make them targeted. In this case the antibody is first conjugated to pNP-PEG₃₄₀₀-PE.

- Prepare a film of the pNP-PEG₃₄₀₀-PE and mPEG₇₅₀-PE as described above and hydrate the film with CBS, pH 5.0.
- Add antibody solution (prepared in 50 mM Tris-buffered saline, pH 8.7) and incubate with a tenfold molar excess of pNP-PEG₃₄₀₀-PE for 24 h at 4°C.
- Add the required amount of this solution to liposomes or micelles (with TATp) and incubate for 1 h.

3.6. Characterization

3.6.1. Size Distribution Analysis

The size (hydrodynamic diameter) is usually measured by dynamic light scattering (DLS) using a N4 Plus Submicron Particle System (Coulter Corporation, Miami, FL). Liposomes with and without TATp generally have a size distribution in the range of 150–200 nm and in 7–20 nm for micelles. The size can also be measured by freeze-fracture electron microscopy (Fig. 3).

3.6.2. Specific Activity of Micelle-Attached mAb 2G4

An ELISA assay (indirect, using an enzyme-tagged secondary Ab) can be performed to show the ability of the pH-sensitive immunocarriers to recognize the target antigen at different pH values (pH 8.0 and 5.0).

- Add to the microplate 50 µL/well of 10 µg/mL cardiac myosin solution and incubate overnight at 4°C.
- Wash the wells three times with 200 µL of TBST (TBS, pH 7.4 containing 0.05% w/v Tween-20).
- Incubate the wells with different concentrations of native mAb 2G4 (or nonspecific IgG) and mAb 2G4-modified micelles in TBST-casein (TBST with 2 mg/mL casein) for 1 h at room temperature.
- Discard the samples and wash the wells three times with 200 µL of TBST.
- Incubate with 50 µL/well of a 1:5,000 dilution of goat anti-mouse IgG peroxidase conjugate in TBST-Cas for 1 h at room temperature.

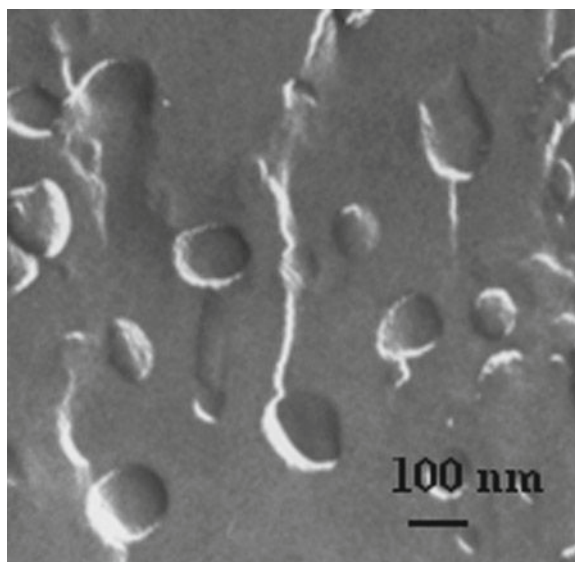


Fig. 3. Freeze-etching electron microscopy of TATp-liposomes. The TATp-liposomes are essentially spherical shape with a size of ~200 nm. It also shows convex and concave fracture planes typical of liposomal structure.

6. Discard the goat anti-mouse IgG peroxidase and wash the wells three times with 200 μ L of TBST.
7. Incubate with 100 μ L of enhanced Kblue[®] TMB peroxidase substrate for 15 min. Read the microplate at a dual wavelength of 620 nm with the reference filter at 492 nm using a Labsystems Multiscan MCC/340 microplate reader installed with GENESIS-LITE windows-based microplate software.

A result for ELISA of immunomicelles is shown in Fig. 4.

3.6.3. Interaction with Cells In Vitro

To study the interaction of TATp-bearing liposomes in vitro,

1. Grow the cells on coverslips in six-well tissue culture plates.
2. After the cells are 60–70% confluent, wash plates twice with sterile PBS, pH 7.4.
3. Add samples in serum-free medium (2 mL/well 20 and 100 μ g of total lipid per mL for liposomes and micelles, respectively. In the case of pH-sensitive formulations, preincubate samples at pH 5.0 for 20 min) (see Note 5).
4. After various incubation times, remove the medium and wash plates thrice with sterile PBS.
5. Mount the individual coverslip with cell side down onto a fresh glass slide with PBS (see Note 6). The cells are viewed with a Nikon Eclipse E400 microscope under bright light, or under epifluorescence with rhodamine/TRITC and fluorescein/FITC filters (Figs. 5 and 6).

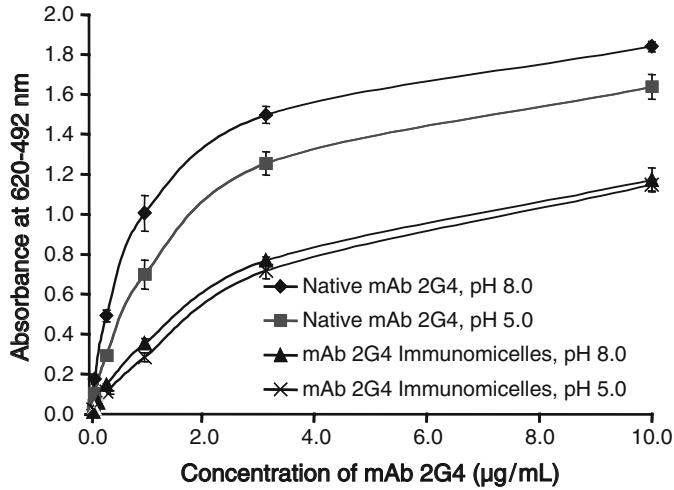


Fig. 4. Binding of antimyosin mAb 2G4-PEG₂₀₀₀-Hz-PE-immunomicelles to a monolayer of dog cardiac myosin in comparison to the native mAb 2G4 at corresponding pH values (mean \pm S.D.; $n=3$). Although there is an affinity decrease for the antibodies modified with the pNP-PEG-PE anchor and incorporated into the micelle structure, this decrease is more apparent than real, since not all nanocarrier-attached antibodies, even if they remain active, can interact with the substrate because of their steric orientation on the nanocarrier surface.

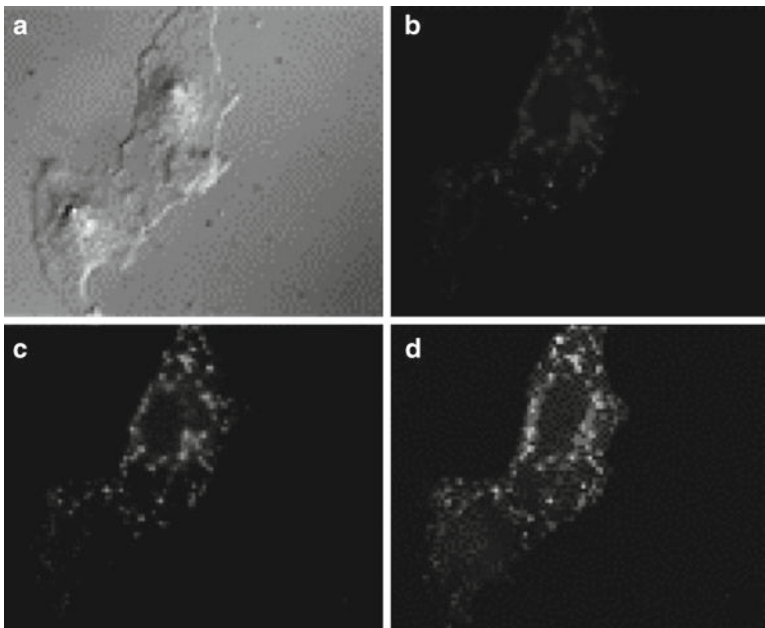


Fig. 5. Intracellular trafficking of Rh-PE-labeled and FITC-dextran-loaded TATp-liposomes within BT20 cells. Typical patterns of intracellular localization and integrity of TATp-liposome after 1 h. (a) DIC light; (b) DIC with an Rh filter; (c) DIC with an FITC filter; (d) DIC composite of (b, c) (magnification, $\times 400$). Rh-labeled TATp-liposomes loaded with FITC-dextran rapidly translocated into these cells. Intracellular liposomes apparently remained intact within this time period, because the fluorescence of the intraliposomal (FITC-dextran) and membrane (Rh-PE) labels coincided.

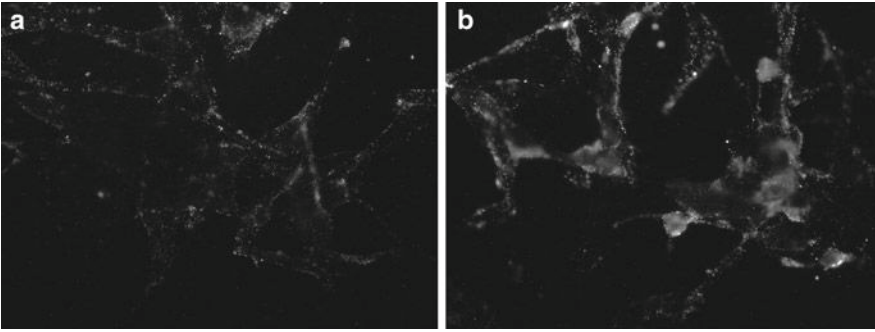


Fig. 6. Fluorescence microscopy showing internalization of Rh-PE-labeled-TATp containing liposomes by U-87 MG astrocytoma cells using: (a) 9 mol% pH-nonsensitive PEG-PE at pH 7.4; (b) 9 mol% pH-sensitive PEG-Hz-PE after incubation at pH 5.0 for 20 min (the pH of these formulations was raised back to pH 7.4 after their incubation at pH 5.0 and prior to incubation with cell). The TATp-containing liposomes kept at pH 7.4 show only marginal association with cells. The pH-sensitive liposomes preincubated for 20 min at pH 5.0 demonstrated a dramatically enhanced association with the cells (higher fluorescence), i.e., better accessibility of TATp moieties for cell interaction.

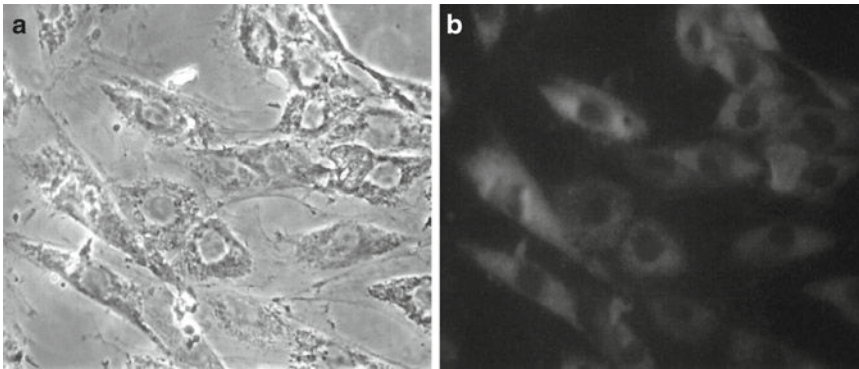


Fig. 7. Microscopy of H9C2 cardiomyocytes transfected with TATp-liposome/pEGFP-N1 complex with: (a) bright-field light microscopy; (b) epifluorescence microscopy with an FITC filter.

3.6.4. *In Vitro* Transfection

For transfection studies

1. Grow cells on coverslips as described above and add the liposome-plasmid complex with or without TATp (in the quantity required to deliver 5 μg of DNA per 200,000 cells at DNA concentration of 0.3 $\mu\text{g}/\mu\text{L}$ added to a liposomal suspension) for 4 h at 37°C under 6% CO_2 .
2. Add the same quantity of lipofectin-pEGFP-N1 complex with same lipid-to-DNA ratio as a control.
3. After incubation, remove the media and wash cells twice with sterile PBS and reincubate in complete media containing 10% FBS for 72 h. GFP expression can be visualized by light microscopy and epifluorescence microscopy with an FITC filter (Fig. 7).

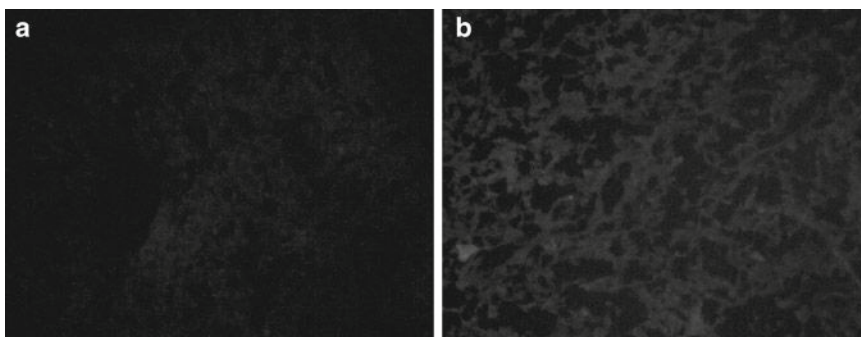


Fig. 8. Fluorescence microscopy of the LLC tumor sections from the murine tumors injected with: (a) pGFP-loaded TATp-modified PEG-liposomes with non-pH-sensitive PEG coat; (b) pH-sensitive PEG coat. The pGFP-TATp-liposomes with the low pH-sensitive PEG results in a highly efficient transfection since the removal of PEG under the action of the decreased intratumoral pH leads to the exposure of the liposome-attached TATp residues, enhanced penetration of the liposomes inside tumor cells, and a more effective intracellular delivery of the pGFP.

3.6.5. *In Vivo Study*

In vivo study of TATp formulations can be done in tumor-bearing mice for *in vivo* transfection or for increased intracellular delivery using “smart” nanocarriers. In a typical case, LLC tumors are grown in C57BL/6 mice by s.c. injection of 80,000 LLC cells per mouse into left flank. Tumors are directly injected at several spots with 100–150 μ L of TATp formulations in phosphate-buffered saline pH 7.4. Mice are killed by cervical dislocation at specific time interval. The excised tumors are cryofixed after hardening at -80°C in Tissue-Tek (Ted Pella Inc., Redding, CA) and cut into sections on a Microtome Pluse TBS (Triangular Biomedical Sciences Inc., Durham, NC). Sections are washed several times in phosphate-buffered saline, pH 7.4, and analyzed by fluorescence microscopy. The administration of pGFP-TATp-liposomes with the low pH-sensitive PEG results in a highly efficient transfection since the removal of PEG under the action of the decreased intratumoral pH leads to the exposure of the liposome-attached TATp residues, enhanced penetration of the liposomes inside tumor cells, and a more effective intracellular delivery of the pGFP (Fig. 8).

4. Notes

1. Here we describe two protocols for incorporation in liposomes or micelles. However, in both the protocols it is important to maintain the length of PEG to which TATp is attached above the surface of nanocarrier. Since the internalization process requires an initial direct contact between TATp and cell membrane, PEG-attached TATp moieties should be

located above the layer protecting PEG not buried inside this layer. If steric hindrances are created by the surrounding PEG grafts of the liposomal surface itself, no efficient transduction takes place.

2. The pNP-PEG-PE is capable of incorporation into both liposomes and micelles via its hydrophobic PE group and easily attaches any amino group containing ligand via the pNP group with the formation of stable carbamate bond. As little as 0.5 mol% of pNP-PEG-PE incorporated into the mixture of liposomal lipids provides sufficient number of reactive groups on the liposomal surface to bind approximately 500 TATp molecules per single 200 nm liposome as was estimated by following TATp-associated radioactivity.
3. It is important to hydrate the film in acidic buffer so as to prevent hydrolysis of pNP groups.
4. After the addition of borate buffer, the final pH of mixture should be around 8–8.5 for efficient conjugation of amino groups of peptide with pNP-PEG-PE.
5. After preincubating the pH-sensitive micelles/liposomes at low pH, the pH should be raised to pH 7.4 before adding to cells.
6. For microscopic visualizations, live cells should be used as fixation of cells will lead to artifacts.

References

1. Deshayes, S., Morris, M. C., Divita, G., and Heitz, F. (2005) Cell-penetrating peptides: tools for intracellular delivery of therapeutics. *Cell Mol Life Sci* **62**, 1839–1849.
2. Joliot, A., Pernelle, C., Deagostini-Bazin, H., and Prochiantz, A. (1991) Antennapedia homeobox peptide regulates neural morphogenesis. *Proc Natl Acad Sci U S A* **88**, 1864–1868.
3. Elliott, G., and O'Hare, P. (1997) Intercellular trafficking and protein delivery by a herpesvirus structural protein. *Cell* **88**, 223–233.
4. Pooga, M., Hallbrink, M., Zorko, M., and Langel, Ü. (1998) Cell penetration by transportan. *FASEB J* **12**, 67–77.
5. Oehlke, J., Scheller, A., Wiesner, B., Krause, E., Beyermann, M., Klauschenz, E., Melzig, M., and Bienert, M. (1998) Cellular uptake of an alpha-helical amphipathic model peptide with the potential to deliver polar compounds into the cell interior non-endocytically. *Biochim Biophys Acta* **1414**, 127–139.
6. Rojas, M., Donahue, J. P., Tan, Z., and Lin, Y. Z. (1998) Genetic engineering of proteins with cell membrane permeability. *Nat Biotechnol* **16**, 370–375.
7. Futaki, S., Suzuki, T., Ohashi, W., Yagami, T., Tanaka, S., Ueda, K., and Sugiura, Y. (2001) Arginine-rich peptides. An abundant source of membrane-permeable peptides having potential as carriers for intracellular protein delivery. *J Biol Chem* **276**, 5836–5840.
8. Gupta, B., Levchenko, T. S., and Torchilin, V. P. (2005) Intracellular delivery of large molecules and small particles by cell-penetrating proteins and peptides. *Adv Drug Deliv Rev* **57**, 637–651.
9. Josephson, L., Tung, C. H., Moore, A., and Weissleder, R. (1999) High-efficiency intracellular magnetic labeling with novel superparamagnetic-Tat peptide conjugates. *Bioconjug Chem* **10**, 186–191.
10. Rothbard, J. B., Jessop, T. C., and Wender, P. A. (2005) Adaptive translocation: the role of hydrogen bonding and membrane potential in the uptake of guanidinium-rich transporters into cells. *Adv Drug Deliv Rev* **57**, 495–504.

11. Fuchs, S. M., and Raines, R. T. (2004) Pathway for polyarginine entry into mammalian cells *Biochemistry* **43**, 2438–2444.
12. Fretz, M., Jin, J., Conibere, R., Penning, N. A., Al-Taei, S., Storm, G., Futaki, S., Takeuchi, T., Nakase, I., and Jones, A. T. (2006) Effects of Na⁺/H⁺ exchanger inhibitors on subcellular localisation of endocytic organelles and intracellular dynamics of protein transduction domains HIV-TAT peptide and octaarginine. *J Control Release* **116**, 247–254.
13. Snyder, E. L., and Dowdy, S. F. (2004) Cell penetrating peptides in drug delivery. *Pharm Res* **21**, 389–393.
14. Wadia, J. S., and Dowdy, S. F. (2005) Transmembrane delivery of protein and peptide drugs by TAT-mediated transduction in the treatment of cancer. *Adv Drug Deliv Rev* **57**, 579–596.
15. Rothbard, J. B., Garlington, S., Lin, Q., Kirschberg, T., Kreider, E., McGrane, P. L., Wender, P. A., and Khavari, P. A. (2000) Conjugation of arginine oligomers to cyclosporin A facilitates topical delivery and inhibition of inflammation. *Nat Med* **6**, 1253–1257.
16. Goun, E. A., Pillow, T. H., Jones, L. R., Rothbard, J. B., and Wender, P. A. (2006) Molecular transporters: synthesis of oligoguanidinium transporters and their application to drug delivery and real-time imaging *Chembiochem* **7**, 1497–1515.
17. Abes, S., Moulton, H. M., Clair, P., Prevot, P., Youngblood, D. S., Wu, R. P., Iversen, P. L., and Lebleu, B. (2006) Vectorization of morpholino oligomers by the (R-Ahx-R)₄ peptide allows efficient splicing correction in the absence of endosomolytic agents. *J Control Release* **116**, 304–313.
18. Abes, S., Turner, J. J., Ivanova, G. D., Owen, D., Williams, D., Arzumanov, A., Clair, P., Gait, M. J., and Lebleu, B. (2007) Efficient splicing correction by PNA conjugation to an R6-Penetratin delivery peptide. *Nucleic Acids Res* **35**, 4495–4502.
19. Meade, B. R., and Dowdy, S. F. (2007) Exogenous siRNA delivery using peptide transduction domains/cell penetrating peptides. *Adv Drug Deliv Rev* **59**, 134–140.
20. Meade, B. R., and Dowdy, S. F. (2008) Enhancing the cellular uptake of siRNA duplexes following noncovalent packaging with protein transduction domain peptides. *Adv Drug Deliv Rev* **60**, 530–536.
21. Jeang, K. T., Xiao, H., and Rich, E. A. (1999) Multifaceted activities of the HIV-1 transactivator of transcription, Tat. *J Biol Chem* **274**, 28837–28840.
22. Phelan, A., Elliott, G., and O'Hare, P. (1998) Intercellular delivery of functional p53 by the herpesvirus protein VP22. *Nat Biotechnol* **16**, 440–443.
23. Schwarze, S. R., Ho, A., Vocero-Akbani, A., and Dowdy, S. F. (1999) In vivo protein transduction: delivery of a biologically active protein into the mouse *Science* **285**, 1569–1572.
24. Cao, G., Pei, W., Ge, H., Liang, Q., Luo, Y., Sharp, F. R., Lu, A., Ran, R., Graham, S. H., and Chen, J. (2002) In vivo delivery of a Bcl-xL fusion protein containing the TAT protein transduction domain protects against ischemic brain injury and neuronal apoptosis. *J Neurosci* **22**, 5423–5431.
25. Denicourt, C., and Dowdy, S. F. (2003) Protein transduction technology offers novel therapeutic approach for brain ischemia. *Trends Pharmacol Sci* **24**, 216–218.
26. Astriab-Fisher, A., Sergueev, D., Fisher, M., Shaw, B. R., and Juliano, R. L. (2002) Conjugates of antisense oligonucleotides with the Tat and antennapedia cell-penetrating peptides: effects on cellular uptake, binding to target sequences, and biologic actions. *Pharm Res* **19**, 744–754.
27. Yang, S., Coles, D. J., Esposito, A., Mitchell, D. J., Toth, I., and Minchin, R. F. (2009) Cellular uptake of self-assembled cationic peptide-DNA complexes: multifunctional role of the enhancer chloroquine. *J Control Release* **135**, 159–165.
28. Trabulo, S., Mano, M., Faneca, H., Cardoso, A. L., Duarte, S., Henriques, A., Paiva, A., Gomes, P., Simoes, S., and de Lima, M. C. (2008) S4(13)-PV cell penetrating peptide and cationic liposomes act synergistically to mediate intracellular delivery of plasmid DNA. *J Gene Med* **10**, 1210–1222.
29. Fujita, T., Furuhashi, M., Hattori, Y., Kawakami, H., Toma, K., and Maitani, Y. (2008) High gene delivery in tumor by intratumoral injection of tetraarginine-PEG lipid-coated protamine/DNA. *J Control Release* **129**, 124–127.
30. Zhao, M., Kircher, M. F., Josephson, L., and Weissleder, R. (2002) Differential conjugation of tat peptide to superparamagnetic nanoparticles and its effect on cellular uptake. *Bioconjug Chem* **13**, 840–844.
31. Lewin, M., Carlesso, N., Tung, C. H., Tang, X. W., Cory, D., Scadden, D. T., and Weissleder, R. (2000) Tat peptide-derivatized magnetic nanoparticles allow in vivo tracking and recovery of progenitor cells. *Nat Biotechnol* **18**, 410–414.

32. Zhang, K., Fang, H., Chen, Z., Taylor, J. S., and Wooley, K. L. (2008) Shape effects of nanoparticles conjugated with cell-penetrating peptides (HIV Tat PTD) on CHO cell uptake. *Bioconjug Chem* **19**, 1880–1887.
33. Berry, C. C., de la Fuente, J. M., Mullin, M., Chu, S. W., and Curtis, A. S. (2007) Nuclear localization of HIV-1 tat functionalized gold nanoparticles. *IEEE Trans Nanobioscience* **6**, 262–269.
34. Rao, K. S., Reddy, M. K., Horning, J. L., and Labhasetwar, V. (2008) TAT-conjugated nanoparticles for the CNS delivery of anti-HIV drugs *Biomaterials* **29**, 4429–4438.
35. Torchilin, V. P., Rammohan, R., Weissig, V., and Levchenko, T. S. (2001) TAT peptide on the surface of liposomes affords their efficient intracellular delivery even at low temperature and in the presence of metabolic inhibitors. *Proc Natl Acad Sci U S A* **98**, 8786–8791.
36. Fretz, M. M., Koning, G. A., Mastrobattista, E., Jiskoot, W., and Storm, G. (2004) OVCAR-3 cells internalize TAT-peptide modified liposomes by endocytosis. *Biochim Biophys Acta* **1665**, 48–56.
37. Levchenko, T. S., Rammohan, R., Volodina, N., and Torchilin, V. P. (2003) Tat peptide-mediated intracellular delivery of liposomes. *Methods Enzymol* **372**, 339–349.
38. Sethuraman, V. A., and Bae, Y. H. (2007) TAT peptide-based micelle system for potential active targeting of anti-cancer agents to acidic solid tumors. *J Control Release* **118**, 216–224.
39. Sawant, R. R., and Torchilin, V. P. (2009) Enhanced cytotoxicity of TATp-bearing paclitaxel-loaded micelles in vitro and in vivo. *Int J Pharm* **374**, 114–118.
40. Santra, S., Yang, H., Dutta, D., Stanley, J. T., Holloway, P. H., Tan, W., Moudgil, B. M., and Mericle, R. A. (2004) TAT conjugated, FITC doped silica nanoparticles for bioimaging applications. *Chem Commun (Camb)* (24), 2810–2811.
41. Mortensen, M. W., Bjorkdahl, O., Sorensen, P. G., Hansen, T., Jensen, M. R., Gundersen, H. J., and Bjornholm, T. (2006) Functionalization and cellular uptake of boron carbide nanoparticles. The first step toward T cell-guided boron neutron capture therapy. *Bioconjug Chem* **17**, 284–290.
42. Lasic, D. D. (1993) *Liposomes: From Physics to Applications*, Elsevier, Amsterdam.
43. Torchilin, V. P. (2005) Recent advances with liposomes as pharmaceutical carriers. *Nat Rev Drug Discov* **4**, 145–160.
44. Lasic, D. D., and Martin, F. J. (1995) *Stealth Liposomes*, CRC Press, Boca Raton.
45. Torchilin, V. P., Narula, J., Halpern, E., and Khaw, B. A. (1996) Poly(ethylene glycol)-coated anti-cardiac myosin immunoliposomes: factors influencing targeted accumulation in the infarcted myocardium. *Biochim Biophys Acta* **1279**, 75–83.
46. Torchilin, V. P., Levchenko, T. S., Lukyanov, A. N., Khaw, B. A., Klibanov, A. L., Rammohan, R., Samokhin, G. P., and Whiteman, K. R. (2001) *p*-Nitrophenylcarbonyl-PEG-PE-liposomes: fast and simple attachment of specific ligands, including monoclonal antibodies, to distal ends of PEG chains via *p*-nitrophenylcarbonyl groups. *Biochim Biophys Acta* **1511**, 397–411.
47. Torchilin, V. P. (2001) Structure and design of polymeric surfactant-based drug delivery systems. *J Control Release* **73**, 137–172.
48. Torchilin, V. P. (2007) Micellar nanocarriers: pharmaceutical perspectives. *Pharm Res* **24**, 1–16.
49. Maeda, H., Wu, J., Sawa, T., Matsumura, Y., and Hori, K. (2000) Tumor vascular permeability and the EPR effect in macromolecular therapeutics: a review. *J Control Release* **65**, 271–284.
50. Maeda, H., Bharate, G. Y., and Daruwalla, J. (2009) Polymeric drugs for efficient tumor-targeted drug delivery based on EPR-effect. *Eur J Pharm Biopharm* **71**, 409–419.
51. Lukyanov, A. N., and Torchilin, V. P. (2004) Micelles from lipid derivatives of water-soluble polymers as delivery systems for poorly soluble drugs. *Adv Drug Deliv Rev* **56**, 1273–1289.
52. Lukyanov, A. N., Gao, Z., Mazzola, L., and Torchilin, V. P. (2002) Polyethylene glycol-diacyl lipid micelles demonstrate increased accumulation in subcutaneous tumors in mice. *Pharm Res* **19**, 1424–1429.
53. Eum, W. S., Kim, D. W., Hwang, I. K., Yoo, K. Y., Kang, T. C., Jang, S. H., Choi, H. S., Choi, S. H., Kim, Y. H., Kim, S. Y., Kwon, H. Y., Kang, J. H., Kwon, O. S., Cho, S. W., Lee, K. S., Park, J., Won, M. H., and Choi, S. Y. (2004) In vivo protein transduction: biologically active intact pep-1-superoxide dismutase fusion protein efficiently protects against ischemic insult. *Free Radic Biol Med* **37**, 1656–1669.
54. Torchilin, V. P., Lukyanov, A. N., Gao, Z., and Papahadjopoulos-Sternberg, B. (2003) Immunomicelles: targeted pharmaceutical carriers for poorly soluble drugs. *Proc Natl Acad Sci U S A* **100**, 6039–6044.

55. Li, M., Chrastina, A., Levchenko, T., and Torchilin, V. P. (2005) Micelles from poly(ethylene glycol)-phosphatidyl ethanolamine conjugates (PEG-PE) as pharmaceutical nanocarriers for poorly soluble drug camptothecin. *J Biomed Nanotechnol* **1**, 190–195.
56. Tseng, Y. L., Liu, J. J., and Hong, R. L. (2002) Translocation of liposomes into cancer cells by cell-penetrating peptides penetratin and tat: a kinetic and efficacy study. *Mol Pharmacol* **62**, 864–872.
57. Torchilin, V. P., Levchenko, T. S., Rammohan, R., Volodina, N., Papahadjopoulos-Sternberg, B., and D'Souza, G. G. (2003) Cell transfection in vitro and in vivo with nontoxic TAT peptide-liposome-DNA complexes. *Proc Natl Acad Sci U S A* **100**, 1972–1977.
58. Gupta, B., Levchenko, T. S., and Torchilin, V. P. (2007) TAT peptide-modified liposomes provide enhanced gene delivery to intracranial human brain tumor xenografts in nude mice. *Oncol Res* **16**, 351–359.
59. Pappalardo, J. S., Quattrocchi, V., Langellotti, C., Di Giacomo, S., Gnazzo, V., Olivera, V., Calamante, G., Zamorano, P. I., Levchenko, T. S., and Torchilin, V. P. (2009) Improved transfection of spleen-derived antigen-presenting cells in culture using TATp-liposomes. *J Control Release* **134**, 41–46.
60. Stroh, M., Zimmer, J. P., Duda, D. G., Levchenko, T. S., Cohen, K. S., Brown, E. B., Scadden, D. T., Torchilin, V. P., Bawendi, M. G., Fukumura, D., and Jain, R. K. (2005) Quantum dots spectrally distinguish multiple species within the tumor milieu in vivo. *Nat Med* **11**, 678–682.
61. Cryan, S. A., Devocelle, M., Moran, P. J., Hickey, A. J., and Kelly, J. G. (2006) Increased intracellular targeting to airway cells using octaarginine-coated liposomes: in vitro assessment of their suitability for inhalation. *Mol Pharm* **3**, 104–112.
62. Yagi, N., Yano, Y., Hatanaka, K., Yokoyama, Y., and Okuno, H. (2007) Synthesis and evaluation of a novel lipid-peptide conjugate for functionalized liposome. *Bioorg Med Chem Lett* **17**, 2590–2593.
63. Zhang, C., Tang, N., Liu, X., Liang, W., Xu, W., and Torchilin, V. P. (2006) siRNA-containing liposomes modified with polyarginine effectively silence the targeted gene. *J Control Release* **112**, 229–239.
64. Ko, Y. T., Hartner, W. C., Kale, A., and Torchilin, V. P. (2009) Gene delivery into ischemic myocardium by double-targeted lipoplexes with anti-myosin antibody and TAT peptide. *Gene Ther* **16**, 52–59.
65. Dodd, C. H., Hsu, H. C., Chu, W. J., Yang, P., Zhang, H. G., Mountz, J. D., Jr., Zinn, K., Forster, J., Josephson, L., Weissleder, R., Mountz, J. M., and Mountz, J. D. (2001) Normal T-cell response and in vivo magnetic resonance imaging of T cells loaded with HIV transactivator-peptide-derived superparamagnetic nanoparticles. *J Immunol Methods* **256**, 89–105.
66. Sawant, R. R., Sawant, R. M., Kale, A. A., and Torchilin, V. P. (2008) The architecture of ligand attachment to nanocarriers controls their specific interaction with target cells. *J Drug Target* **16**, 596–600.
67. Tkachenko, A. G., Xie, H., Liu, Y., Coleman, D., Ryan, J., Glomm, W. R., Shipton, M. K., Franzen, S., and Feldheim, D. L. (2004) Cellular trajectories of peptide-modified gold particle complexes: comparison of nuclear localization signals and peptide transduction domains. *Bioconjug Chem* **15**, 482–490.
68. de la Fuente, J. M., and Berry, C. C. (2005) Tat peptide as an efficient molecule to translocate gold nanoparticles into the cell nucleus. *Bioconjug Chem* **16**, 1176–1180.
69. Suk, J. S., Suh, J., Choy, K., Lai, S. K., Fu, J., and Hanes, J. (2006) Gene delivery to differentiated neurotypic cells with RGD and HIV Tat peptide functionalized polymeric nanoparticles. *Biomaterials* **27**, 5143–5150.
70. Kleemann, E., Neu, M., Jekel, N., Fink, L., Schmehl, T., Gessler, T., Seeger, W., and Kissel, T. (2005) Nano-carriers for DNA delivery to the lung based upon a TAT-derived peptide covalently coupled to PEG-PEI. *J Control Release* **109**, 299–316.
71. Nguyen, J., Xie, X., Neu, M., Dumitrascu, R., Reul, R., Sitterberg, J., Bakowsky, U., Schermuly, R., Fink, L., Schmehl, T., Gessler, T., Seeger, W., and Kissel, T. (2008) Effects of cell-penetrating peptides and pegylation on transfection efficiency of polyethylenimine in mouse lungs. *J Gene Med* **10**, 1236–1246.
72. Mae, M., El Andaloussi, S., Lundin, P., Oskolkov, N., Johansson, H. J., Guterstam, P., and Langel, U. (2009) A stearylated CPP for delivery of splice correcting oligonucleotides using a non-covalent co-incubation strategy. *J Control Release* **134**, 221–227.
73. Zorko, M., and Langel, U. (2005) Cell-penetrating peptides: mechanism and kinetics of cargo delivery. *Adv Drug Deliv Rev* **57**, 529–545.
74. Kaplan, I. M., Wadia, J. S., and Dowdy, S. F. (2005) Cationic TAT peptide transduction domain enters cells by macropinocytosis. *J Control Release* **102**, 247–253.

75. Derossi, D., Calvet, S., Trembleau, A., Brunissen, A., Chassaing, G., and Prochiantz, A. (1996) Cell internalization of the third helix of the Antennapedia homeodomain is receptor-independent. *J Biol Chem* **271**, 18188–18193.
76. Hyndman, L., Lemoine, J. L., Huang, L., Porteous, D. J., Boyd, A. C., and Nan, X. (2004) HIV-1 Tat protein transduction domain peptide facilitates gene transfer in combination with cationic liposomes. *J Control Release* **99**, 435–444.
77. Khalil, I. A., Kogure, K., Futaki, S., Hama, S., Akita, H., Ueno, M., Kishida, H., Kudoh, M., Mishina, Y., Kataoka, K., Yamada, M., and Harashima, H. (2007) Octaarginine-modified multifunctional envelope-type nanoparticles for gene delivery. *Gene Ther* **14**, 682–689.
78. Yamada, Y., Akita, H., Kamiya, H., Kogure, K., Yamamoto, T., Shinohara, Y., Yamashita, K., Kobayashi, H., Kikuchi, H., and Harashima, H. (2008) MITO-Porter: A liposome-based carrier system for delivery of macromolecules into mitochondria via membrane fusion. *Biochim Biophys Acta* **1778**, 423–432.
79. Wadia, J. S., Stan, R. V., and Dowdy, S. F. (2004) Transducible TAT-HA fusogenic peptide enhances escape of TAT-fusion proteins after lipid raft macropinocytosis. *Nat Med* **10**, 310–315.
80. El-Andaloussi, S., Johansson, H. J., Lundberg, P., and Langel, U. (2006) Induction of splice correction by cell-penetrating peptide nucleic acids. *J Gene Med* **8**, 1262–1273.
81. Plank, C., Oberhauser, B., Mechtler, K., Koch, C., and Wagner, E. (1994) The influence of endosome-disruptive peptides on gene transfer using synthetic virus-like gene transfer systems. *J Biol Chem* **269**, 12918–12924.
82. Sugita, T., Yoshikawa, T., Mukai, Y., Yamanada, N., Imai, S., Nagano, K., Yoshida, Y., Shibata, H., Yoshioka, Y., Nakagawa, S., Kamada, H., Tsunoda, S., and Tsutsumi, Y. (2007) Improved cytosolic translocation and tumor-killing activity of Tat-shepherdin conjugates mediated by co-treatment with Tat-fused endosome-disruptive HA2 peptide. *Biochem Biophys Res Commun* **363**, 1027–1032.
83. Moore, N. M., Sheppard, C. L., and Sakiyama-Elbert, S. E. (2009) Characterization of a multifunctional PEG-based gene delivery system containing nuclear localization signals and endosomal escape peptides. *Acta Biomater* **5**, 854–864.
84. Sirsi, S. R., Schray, R. C., Guan, X., Lykens, N. M., Williams, J. H., Erney, M. L., and Lutz, G. J. (2008) Functionalized PEG-PEI copolymers complexed to exon-skipping oligonucleotides improve dystrophin expression in mdx mice. *Hum Gene Ther* **19**, 795–806.
85. Shiraishi, T., Pankratova, S., and Nielsen, P. E. (2005) Calcium ions effectively enhance the effect of antisense peptide nucleic acids conjugated to cationic tat and oligoarginine peptides. *Chem Biol* **12**, 923–929.
86. Shiraishi, T., and Nielsen, P. E. (2006) Enhanced delivery of cell-penetrating peptide-peptide nucleic acid conjugates by endosomal disruption. *Nat Protoc* **1**, 633–636.
87. Futaki, S., Ohashi, W., Suzuki, T., Niwa, M., Tanaka, S., Ueda, K., Harashima, H., and Sugiura, Y. (2001) Stearylarginine-rich peptides: a new class of transfection systems. *Bioconjug Chem* **12**, 1005–1011.
88. Tonges, L., Lingor, P., Egle, R., Dietz, G. P., Fahr, A., and Bahr, M. (2006) Stearylarginine and artificial virus-like particles for transfection of siRNA into primary rat neurons. *RNA* **12**, 1431–1438.
89. Sawant, R. M., Hurley, J. P., Salmaso, S., Kale, A., Tolcheva, E., Levchenko, T. S., and Torchilin, V. P. (2006) “SMART” drug delivery systems: double-targeted pH-responsive pharmaceutical nanocarriers. *Bioconjug Chem* **17**, 943–949.
90. Kale, A. A., and Torchilin, V. P. (2007) Design, synthesis, and characterization of pH-sensitive PEG-PE conjugates for stimuli-sensitive pharmaceutical nanocarriers: the effect of substituents at the hydrazone linkage on the pH stability of PEG-PE conjugates. *Bioconjug Chem* **18**, 363–370.
91. Kale, A. A., and Torchilin, V. P. (2007) Enhanced transfection of tumor cells in vivo using “Smart” pH-sensitive TAT-modified pegylated liposomes. *J Drug Target* **15**, 538–545.

Multifunctional CPP Polymer System for Tumor-Targeted pDNA and siRNA Delivery

Christian Dohmen and Ernst Wagner

Abstract

Cell-penetrating peptides (CPPs) are a very interesting class of molecules to be introduced in gene and siRNA vectors. They can be used to overcome one of the biggest hurdles in gene and siRNA delivery in vitro and in vivo, the transfer across cell membranes. This chapter describes protocols for the synthesis and biological evaluation of a polylysine-based polymer. In this carrier system, melittin is used as CPP with a high activity to disrupt membranes. pH-Labile masking is applied to render the lytic activity specific for intracellular acidic endolysosomal organelles.

Key words: Endosomal release, Nonviral vector, Plasmid DNA, Polymer, Polyplex, RNA interference, siRNA

1. Introduction

Efficient pDNA gene transfer and siRNA delivery are very complex and difficult challenges with many different bottlenecks in vitro as well as in vivo. Many hurdles have to be overcome, especially when a pharmaceutical active compound should be able to find the target cell after intravenous injection. The single delivery steps and requirements are extracellular stabilization of the nucleic acid cargo, specific cell attachment, endosomal uptake, endosomal escape, release of the nucleic acid for the carrier, and, in case of gene delivery, nuclear uptake. The optimal functionality in every single step is crucial for an efficient delivery system.

Polycations may overcome many of the described hurdles (1). They are able to interact with negatively charged nucleic acids by ionic interactions, resulting in so-called polyplexes. The overall positive charge of these polyplexes enables them to interact with

the negatively charged cellular membrane resulting in uptake into endosomes. Alternatively, cell binding can be more specific use of targeting ligands, for example, for tumor targeting (2). In most cases, the endosomal escape is the major challenge. The polyplex has to escape from the endosome before degradation in the late endolysosomal compartment.

Biodegradable polycations such as polylysine or polyarginine have been used as carrier. The peptidic structures can be metabolized by the cellular system and therefore do not accumulate inside the cell. The main hurdle for these carriers is endosomal escape. An endosomolytic domain can be introduced into these molecules to overcome this hurdle, resulting in a functional carrier.

Cell-penetrating peptides (CPPs) which show a high potency to interact with biological membranes have been used as endosomolytic domain in several approaches (3). The protocols described in this chapter use melittin, a 26 amino acid long peptide. As main substance of bee venom, it shows a high potency to disrupt cellular membranes (4, 5). Therefore, it is an ideal candidate for an endosomolytic domain. A main disadvantage of this molecule is the lacking specificity for endosomes. Melittin with standard natural sequence is active at any physiological pH and disrupts all membranes without differing between endosomal and cellular membrane. Therefore, carriers including this peptide cause significantly higher toxicity. To overcome this problem, investigators masked the lytic activity of melittin under physiological conditions by the addition of 2,3-dimethylmaleic anhydride (DMMAAn) to ϵ -amino groups of the four lysine included in the peptide structure (6, 7). The masking is reversible and cleaved during acidification. This results in a nonlytic molecule under physiologically neutral conditions outside the cell, and a highly lytic molecule after acidification inside the endosome (7–9).

A molecule combining different properties in one functional polymer is poly-L-lysine (PLL) modified with polyethylene glycol (PEG) and DMMAAn-shielded melittin (PEG-PLL-DMMAAnMel; Fig. 1).

All single included substructures have a special functionality during the delivery process. PLL is the backbone of the multifunctional polymer. With its positive charge, it is able to bind the nucleic acid and build ionic polyplexes. PEG raises the solubility of polyplexes and reduces aggregation events, for example, during blood circulation. DMMAAnMel (2,3-dimethyl maleic anhydride-modified melittin) enables the endosomal escape of the polyplex.

The synthesis, in-process control, and biological evaluation of this carrier system are described in the following protocols. Optionally, the conjugate may contain further functional domains like targeting ligands that can easily be introduced into this system.

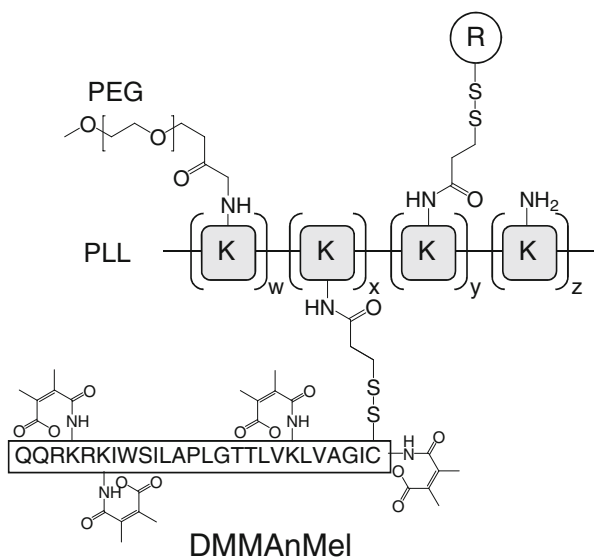


Fig. 1. Structure of PEG-PLL-DMMAnMel. The functional components PEG, PLL, DMMAn, and Mel are explained in the text. "R" presents an optional component which may be incorporated, for example, a targeting ligand or covalently attached siRNA.

siRNA can also be covalently attached, resulting in a conjugate stable in the extracellular environment which can release siRNA in the cytosol (9).

2. Materials

2.1. DTT Assay

1. HBS: 20 mM HEPES, 150 mM NaCl, pH 7.4.
2. 0.1 M DTT in HBS.

2.2. TNBS Assay

1. Borate buffer: 0.1 M sodium tetraborate in water. To dissolve in water, the buffer has to be heated up to 80°C and stirred for several hours.
2. PLL standard: 0.5 mg/mL PLL (Sigma-Aldrich) in borate buffer.
3. 96-Well plate, flat bottom (TPP).
4. TNBS reagent: 2, 4, 6-trinitrobenzenesulfonic acid solution (Fluka), 33 mM in HBS.

2.3. Polymer Synthesis

1. PLL (Sigma-Aldrich) (see Note 1).
2. Sample buffer: 20 mM HEPES, 0.5 M NaCl, pH 7.4.
3. mPEG-SPA (Rapp Polymere): PEG (5,000 Da) with an amino-reactive NHS ester.

4. DMSO (Sigma-Aldrich).
5. MacroPrep High S column 10/16.
6. Äkta™basic 10 (GE healthcare).
7. Buffer A: 20 mM HEPES, 600 mM NaCl, pH 7.4.
8. Buffer B: 20 mM HEPES, 3 M NaCl, pH 7.4.
9. Dialysis membrane (6,000–8,000 Da molecular weight cut-off).
10. SPDP: *N*-succinimidyl 3-(2-pyridyldithio)-propionate (Sigma-Aldrich).
11. Buffer C: 20 mM HEPES, 1 M NaCl, pH 7.4.
12. DMMAAn: 2,3-dimethylmaleic anhydride (Sigma-Aldrich).
13. Melittin peptide: Sequence: CIGA VLKV LTTG LPAL ISWI KRKR QQ (Biosynthan, Berlin).
14. Peptide buffer: 70% 250 mM HEPPS, pH 8.2, 30% acetonitrile (see Note 4).
15. Lysine (Fluka).
16. Buffer D: 20 mM HEPES, 500 mM NaCl, pH 8.2.

2.4. Erythrocyte Leakage Assay

1. Fresh citrate-treated murine blood (see Note 7).
2. PBS: 140 mM NaCl, 10 mM Na₂HPO₄, 2.7 mM KCl, 1.8 mM KH₂PO₄, pH 7.4.
3. V-bottom 96-well plates.
4. 150 mM NaCl solution.
5. HBS, pH 7.4 (see Subheading 2.1).
6. 1% (v/v) Triton-X-100 in HBS.
7. 96-Well plate, flat bottom (TPP).

2.5. Gel Shift Assay

1. Agarose.
2. TBE buffer: 89 mM Tris-HCl, 89 mM boric acid, 2 mM EDTA, pH 8.0.
3. GelRed (Biotrend).
4. Electrophoresis unit.
5. Loading buffer: 3 mM bromophenol blue, 60 mM EDTA, 60% (v/v) glycerol.
6. HBG: 20 mM HEPES, pH 7.4, 5% (w/v) glucose.

2.6. Cell Culture

1. Neuro2A/Neuro2A-Luc cells are cultured in Dulbecco's Modified Eagle's Medium (DMEM) 1 g glucose/L, 2 mM L-glutamine, 10% fetal bovine serum, 100 U/mL penicillin, and 100 mg/mL streptomycin. All reagents purchased from Invitrogen.

2. Trypsin/EDTA (Biochrom).
3. pDNA solution: pEGFPLuc (Clontech) 20 $\mu\text{g}/\text{mL}$ in water.
4. siRNA solution: Luc-/control-siRNA 50 $\mu\text{g}/\text{mL}$ in water.
5. Luc-siRNA (Dharmacon):
Sequence: 5'-CUUACGCUGAGUACUUCGAdTdT-3' (sense strand).
6. Control siRNA (Dharmacon):
Sequence: 5'-AUGUAUUGGCCUGUAUUAGUU-3' (sense strand).
7. Lysis buffer: cell culture lysis reagent 5 \times (Promega) tenfold diluted in water.
8. LAR reagent: 20 mM glycylglycine, 1 mM MgCl_2 , 0.5 mM EDTA, 3.3 mM DTT, 0.55 mM ATP, pH 8.5.
9. Luciferin in LAR: 0.5 mM luciferin (Promega) in LAR reagent.
10. MTT reagent: 3-(4,5-dimethylthiazol-2-yl)-2,5-diphenyltetrazolium bromide in water.
11. Luminometer (e.g., Lumat LB 9507, Berthold Technologies).
12. HBG (see Subheading 2.5).

3. Methods

3.1. Analytical Methods

3.1.1. DTT Assay

The DTT assay is one of the methods used to determine the composition of the polymer synthesized in the following steps. It is necessary to quantify the amount of functional PDP-linker available in the sample.

1. Take a sample of your conjugate solution containing ~ 10 nmol PDP-linker and dilute it in HBS to get 100 μL of a solution with a PDP concentration of 100 μM .
2. Measure the absorption at 343 nm and set it to zero.
3. Add 50 μL of a 0.1 M DTT solution to this sample to cleave all the PDP groups, resulting in free pyridine-2-thione.
4. Measure this free pyridine-2-thione at 343 nm.
5. The PDP concentration can be determined with the extinction coefficient of pyridine-2-thione of $\epsilon = 8,080 \text{ M}^{-1} \text{ cm}^{-1}$.

3.1.2. TNBS Assay

This assay detects primary amino groups and can thus be used to determine the PLL concentration in a solution.

1. Dilute your sample containing PLL and the PLL standard in borate buffer resulting in PLL concentrations of 15, 30, and 45 $\mu\text{g}/\text{mL}$.

2. Fill 100 μL of each sample in a cavity of a 96-well plate. Work in triplicates. As zero-control take 100 μL borate buffer.
3. Add 2.5 μL TNBS reagent to each well and incubate for 10 min at RT.
4. Measure the absorption at 405 nm.

3.1.3. Polymer Synthesis

3.1.3.1. Synthesis of PEG-PLL

1. Dissolve 1.25 μmol PLL (see Note 1) in 2 mL sample buffer and 1.6 μmol mPEG-SPA in 400 μL DMSO.
2. Mix both solutions and let the reaction take place for 2 h at RT under argon conditions.
3. Purify the resulting PEG-PLL from unreacted mPEG-SPA, by cation-exchange chromatography using a MacroPrep High S column on a HPLC system. Prior to use, the column should be cleaned by using the standard cleaning in place (CIP) protocol. Load the product on the column using a 2.5 mL loop, a flow of 1 mL/min, and detect the absorption at $A_{240\text{nm}}$. Wash away free PEG with 15 mL buffer A. The bound PEG-PLL is eluted with a gradient to 100% buffer B in 10 min. Collect the fractions of 1 mL volume (see Note 2, Fig. 2a).

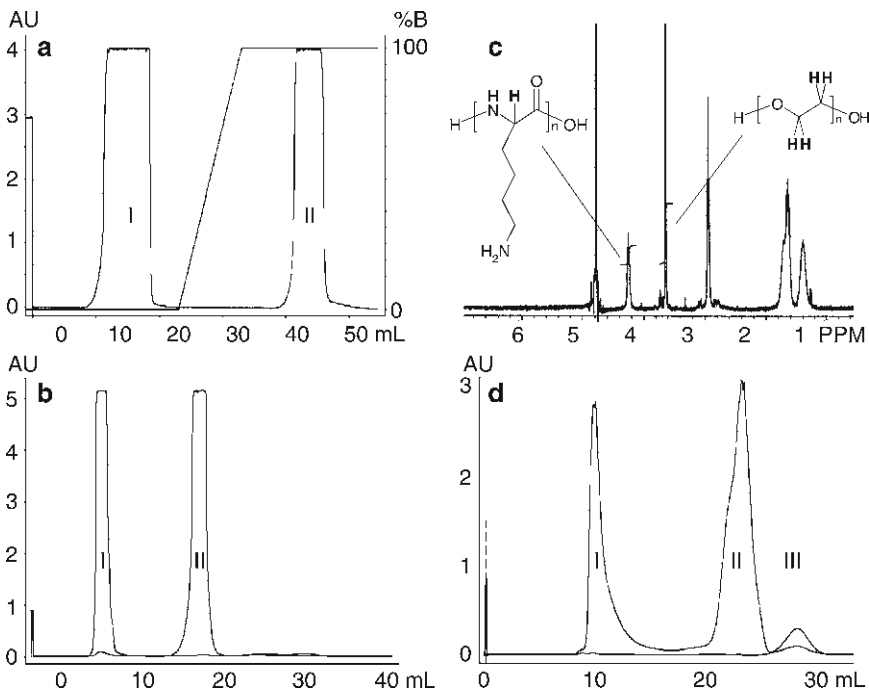


Fig. 2. Chromatograms and NMR spectrum generated during the described synthesis. (a) Chromatogram of the purification process of PEG-PLL; product peak: Peak II; (b) ^1H -NMR spectrum of purified PEG-PLL; (c) chromatogram of the purification process of PEG-PLL-PDP; product peak: Peak II; (d) chromatogram of the purification process of PEG-PLL-DMMAnMeI; product peak: Peak II.

4. Pool the collected fractions containing purified PEG–PLL, dialyze them against water (MWCO 6,000–8,000 Da), and freeze dry the sample.
5. Determine the resulting PEG/PLL-ratio by ¹H-NMR analysis in D₂O. The aim is a ratio of 1:1 (for analysis, see Note 2, Fig. 2b).

3.1.3.2. Synthesis of PEG–PLL–PDP

1. Dissolve 0.313 μmol PEG–PLL in 800 μL sample buffer and 3.8 μmol SPDP in 200 μL DMSO.
2. Mix both solutions and let the components react for 2 h at RT under argon conditions.
3. The product PEG–PLL–PDP is purified by size-exclusion chromatography using a Sephadex G25 superfine HR 10/30 column on a HPLC system. Equilibrate the column with 30 mL buffer C with a flow of 1 mL/min. Detection wavelengths are set to 280 and 343 nm (see Note 2, Fig. 2c). Pool the fractions containing the product.
4. The PEG–PLL/PDP-ratio is ascertained by the determination of PLL concentration by TNBS assay and PDP concentration by DTT assay. The desired ratio is PLL/PDP 1/8–10.

3.1.3.3. Modification of Melittin (see Notes 3–5)

Before the endosomolytic peptide melittin is attached covalently to the PEG–PLL–PDP, the lytic function is shielded reversibly by the modification of lysine side chains with 2,3-dimethylmaleic anhydride (DMMAAn).

1. Dissolve 1.38 μmol melittin in 400 μL peptide buffer and dissolve 15.8 μmol DMMAAn in 50 μL acetonitrile.
2. Mix both solutions and let the compounds react for 30 min at RT under argon conditions.
3. For quenching the excess of DMMAAn dissolve 79 μmol lysine in 100 μL peptide buffer and add them to the reaction. Reaction takes place after 30 min at RT under argon conditions.

3.1.3.4. Synthesis of PEG–PLL–DMMAAnMel

In this step, the DMMAAn-modified melittin is introduced into the polymer structure (see Note 6)

1. Add acetonitrile to the sample containing PEG–PLL–PDP (amount of 0.93 μmol PDP) resulting in a buffer containing 30% acetonitrile (see Note 4).
2. Add the entire amount of DMMAAn-modified melittin. Reaction takes place for 1 h at RT under argon conditions.
3. The product is purified by size-exclusion chromatography on a Superdex 75 HR 10/30 column equilibrated with buffer D (see Note 2, Fig. 2d).

- Analyze the product by TNBS assay and DTT assay. The amount of coupled DMMA_nMel is the difference of PDP groups per PLL detected before and after coupling.

3.1.4. Erythrocyte Leakage Assay

- Collect 1 mL fresh citrate-buffered murine blood. Wash the erythrocytes three times. For this purpose, dilute the blood in 9 mL PBS and mix gently. Centrifuge the mixture for sedimentation of containing erythrocytes at 800 g and 4°C for 10 min, and decant the supernatant. Repeat this washing step two times (see Note 7).
- Dilute the pellet tenfold in 150 mM NaCl and count the cells.
- The suspension is diluted to get an erythrocyte concentration of 1×10^7 cells/mL.
- Prepare conjugate samples containing 0.25–16 μM melittin or DMMA_n-melittin in HBS. Prepare a second batch of samples in the same concentration, with conjugate preincubated at pH 5.5. Fill 90 μL of each dilution in a cavity of a 96-well-V-bottom plate. Use a 1% Triton-X solution as 100% control. For 0% lysis, HBS is filled into the wells. Work in triplicates.
- Add 10 μL of the erythrocyte solution to each well and incubate the plate at 37°C for 30 min under constant shaking.
- Centrifuge the plate at 300g for 10 min to sediment the erythrocytes and transfer 60 μL supernatant of each well into a flat-bottom-96-well plate.
- Detect the released hemoglobin at 405 nm with a micro-plate reader.

3.1.5. Gel Shift Assay

The agarose gel shift assay is a method to determine the nucleic acid complexation ability of the polymer.

- Prepare a 1% agarose gel (2.5% for siRNA) by dissolving 0.4 g (1 g) agarose in 40 g TBE buffer and boiling the suspension at 100°C. After cooling down to about 50°C, add 40 μL GelRed to the suspension. The agarose gel is filled into the electrophoresis unit where it solidifies.
- Samples containing 200 ng pDNA or 500 ng siRNA are prepared under transfection conditions. Therefore, dilute the appropriate amount of pDNA/siRNA in 10 μL HBG. Serially dilute the polymer solution resulting in 10 μL HBG with 100–1,600 ng (250–4,000 ng) polymer. Mix nucleic acid and polymer, and incubate for 30 min at RT to get polyplexes with a weight/weight-ratio of 0.5–4.
- Add 4 μL loading buffer to each sample, mix and load the sample into the gel-pockets.
- Electrophoresis conditions: 80 V/40 min.

3.1.6. Cell Culture

All preliminary experiments show the functionality of the single compounds used in this complex system. The interaction between these single components can be shown by *in vitro* testing of the transfection ability of the system. Thus, a reporter gene is used that can either be introduced by pDNA delivery or knock-down by siRNA delivery. A further information given by the cell culture experiments is the toxicity of the carrier system.

3.1.6.1. pDNA Delivery (Luciferase Reporter Gene)

1. One day before transfection: harvest Neuro2A-cells with trypsin/EDTA when approaching confluence. Subsequently seed 80 μL medium containing 10,000 cells in each well of a 96-well plate and incubate for 24 h.
2. At the day of transfection: prepare the polyplexes in different weight/weight-ratios. Work in triplicates. Therefore, fill 30 μL of pDNA solution per w/w-ratio in a 1.5-mL Eppendorf tube. Serially dilute the polymer in HBG, resulting in 30 μL with a concentration of 10–80 $\mu\text{g}/\text{mL}$.
3. Mix the 30 μL polymer dilution with 30 μL pDNA by pipetting and let the polyplexes be formed for 30 min at RT.
4. Add 20 μL of the polyplex solution to each well of the 96-well plate. As control use 20 μL HBG.
5. After 4 h incubation at 37°C and 5% CO₂, carefully exchange the medium against 100 μL fresh medium. Let the cells grow for another 24 h.
6. Remove the medium from the cells and add 55 μL lysis buffer. Incubate for 30 min at RT.
7. Take 25 μL of the lysate and measure the bioluminescence in a luminometer automatically adding 100 μL luciferin solution.

3.1.6.2. siRNA Delivery (Luciferase Reporter Cell Line)

1. One day before transfection: harvest Neuro2A-Luc cells with Trypsin/EDTA when approaching confluence. Subsequently seed 100 μL medium containing 5,000 cells in each well of a 96-well plate and incubate for 24 h.
2. At the day of transfection: prepare the polyplexes in different weight/weight-ratios. Work in triplicates. Therefore, fill 30 μL of siRNA solution per w/w-ratio in a 1.5-mL Eppendorf tube. Serially dilute the polymer in HBG, resulting in 30 μL with a concentration of 25–200 $\mu\text{g}/\text{mL}$. As control, prepare the same polyplexes with control siRNA instead of Luc-siRNA.
3. Mix the 30 μL polymer dilution with 30 μL siRNA by pipetting and let the polyplexes be formed for 30 min at RT.
4. Meanwhile exchange the medium of the cells against 80 μL fresh medium.

5. Add 20 μL of the polyplex solution to each well of the 96-well plate and let it incubate for 48 h without medium exchange.
6. Remove the medium from the cells and add 55 μL lysis buffer. Incubate for 30 min at RT.
7. Take 25 μL of the lysate and measure the bioluminescence in a luminometer automatically adding 100 μL luciferin solution.

3.1.6.3. MTT Assay

This assay is used to evaluate cytotoxic effects of the polyplexes.

1. Harvest, seed, and transfect cells as explained above, to get the same conditions for the MTT- as for the luciferase assay.
2. Instead of removing the medium and lysing the cells at the final day of the experiment, 10 μL of MTT reagent is added to each cavity.
3. Incubate the cells at 37°C and 5% CO₂ for another 2 h.
4. Remove the medium from the cells and freeze them at -80°C for 2 h to break the cells.
5. Add 100 μL DMSO to each well and incubate for 2 h at RT to dissolve the formazan crystals.
6. Measure absorption at 590 nm [reference wavelength (630 nm)] on a micro-plate reader. Set HBG as 100% viability control.

4. Notes

1. PLL purchased from Sigma-Aldrich is a polydisperse product. The polymerization degree is batch-dependent.
2. Please refer to Fig. 2.
3. The melittin peptide bears a cysteine at the carboxy-terminus for coupling to the SPDP-linker. The thiol-group is prone to dimerize with a second thiol-group under aqueous conditions. Thus, it is important to have the reactions as short as possible and always use argon conditions.
4. Melittin is not well soluble in water. Thus, it is always necessary to work with buffers containing 30% acetonitrile during the treatment of melittin or DMMAAn-modified melittin. Never let the acetonitrile concentration drop below 30% until the peptide has reacted with PLL, otherwise it might agglomerate. After covalent attachment to the polycation, the construct is soluble even without acetonitrile.
5. The modification of melittin with 2,3-dimethylmaleic anhydride (DMMAAn) is reversible under acidic pH. Thus, it is very important to keep the pH above 8 during every reaction

step including DMMA. Always control and adjust the pH of all included buffers, before and after adding a new component and after the incubation/reaction time to be sure that the pH never gets too low. If the buffer containing DMMA_{mel} drops below pH 8, restart the synthesis.

6. For the optional covalent coupling of siRNA (see Fig. 1, R= siRNA), siRNA thiol-modified at the 5' end of the sense strand has to be attached before this step (for further information, see ref. 9).
7. Store erythrocytes at 4°C for no longer than 24 h to be sure to get reproducible and comparable results.

Acknowledgments

The described work was supported by DFG SFB486, Excellence Cluster “Nanosystems Initiative Munich (NIM)” and the EC project GIANT.

References

1. Schaffert, D. and Wagner, E. (2008) Gene therapy progress and prospects: synthetic polymer-based systems, *Gene Ther* **15**, 1131–1138.
2. Philipp, A., Meyer, M., and Wagner, E. (2008) Extracellular targeting of synthetic therapeutic nucleic acid formulations, *Curr Gene Ther* **8**, 324–334.
3. Plank, C., Zauner, W., and Wagner, E. (1998) Application of membrane-active peptides for drug and gene delivery across cellular membranes, *Adv Drug Deliv Rev* **34**, 21–35.
4. Ogris, M., Carlisle, R. C., Bettinger, T., and Seymour, L. W. (2001) Melittin enables efficient vesicular escape and enhanced nuclear access of nonviral gene delivery vectors, *J Biol Chem* **276**, 47550–47555.
5. Boeckle, S., Fahrmeir, J., Roedel, W., Ogris, M., and Wagner, E. (2006) Melittin analogs with high lytic activity at endosomal pH enhance transfection with purified targeted PEI polyplexes, *J Control Release* **112**, 240–248.
6. Rozema, D. B., Ekena, K., Lewis, D. L., Loomis, A. G., and Wolff, J. A. (2003) Endosomolysis by masking of a membrane-active agent (EMMA) for cytoplasmic release of macromolecules, *Bioconjug Chem* **14**, 51–57.
7. Meyer, M., Zintchenko, A., Ogris, M., and Wagner, E. (2007) A dimethylmaleic acid-melittin-polylysine conjugate with reduced toxicity, pH-triggered endosomolytic activity and enhanced gene transfer potential, *J Gene Med* **9**, 797–805.
8. Meyer, M., Philipp, A., Oskuec, R., Schmidt, C., and Wagner, E. (2008) Breathing life into polycations: functionalization with pH-responsive endosomolytic peptides and polyethylene glycol enables siRNA delivery, *J Am Chem Soc* **130**, 3272–3273.
9. Meyer, M., Dohmen, C., Philipp, A., Kiener, D., Maiwald, G., Scheu, C., Ogris, M., and Wagner, E. (2009) Synthesis and biological evaluation of a bioresponsive and endosomolytic siRNA-polymer conjugate, *Mol Pharm* **6**, 752–762.

Cell-Penetrating Penta-Peptides and Bax-Inhibiting Peptides: Protocol for Their Application

Jose Gomez and Shigemi Matsuyama

Abstract

The first series of cell-penetrating penta-peptides (CPP5s) were discovered as cytoprotective penta-peptides designed from the Bax-inhibiting domain of Ku70. Bax is an inducer of programmed cell death, and Ku70 is a multifunctional protein maintaining genomic stability and protecting cells from death by inhibiting the cytotoxic activity of Bax. Since these peptides bind and inhibit Bax, they are named Bax-inhibiting peptides (BIPs). The second series of CPP5s were developed by mutating BIP's amino acid sequences to abolish the Bax-binding activity. These peptides were used as negative control peptides to evaluate the Bax-inhibiting activity of BIPs. CPP5s are able to enter cells when they are added to the culture medium. The mechanism of cell entry of CPP5s is not yet understood. Numerous studies showed that BIP rescued cells from cytotoxic stresses both in cell culture and animal model, suggesting the therapeutic potential of BIP. Both BIPs and noncytoprotective CPP5s did not show significant toxicity even at 1.6 mM concentration in cell culture. Our recent study suggests that CPP5s has the protein transduction activity, though only green fluorescent protein (GFP) has been tested as a cargo protein. If CPP5s can deliver wide range of cargo molecules into the cell, CPP5s may be utilized as nontoxic drug delivery tool. In this article, we describe our laboratory's protocols of how to synthesize, store, and apply CPP5s for the examination of their activities of cell penetration and cytoprotection.

Key words: Cell-penetrating peptide, Cell-penetrating penta-peptide, Ku70, Bax, Protein transduction, Apoptosis, Programmed cell death

1. Introduction

The first series of cell-penetrating penta-peptides (CPP5s) were discovered as Bax-inhibiting peptides (BIPs) that were designed from the Bax-binding domain of Ku70 (1–3). Ku70 is a multifunctional protein involved in nonhomologous end joining DNA repair (4, 5) and apoptosis regulation (1, 2). Ku70 binds and inhibits the proapoptotic protein Bax in the cytosol, and thus Ku70 protects cells from Bax-mediated cell death (1, 2). We found

that the Bax-binding domain composed of five amino acids in the C-terminus of Ku70 (1, 3). Interestingly, synthetic pentapeptides of this domain showed cell-penetrating activity, and these peptides were able to rescue cells from death by simply adding them into the cell culture (1). These cytoprotective peptides were named BIPs. Various versions of BIPs were designed from the Bax-binding domain of Ku70 of different species including human (VPMLK), rat (VPALR), and mouse (VPTLK) (1, 3). In addition, the second series of CPP5s (e.g., IPMIK and KLPVM) were developed by mutating the BIP sequence. These noncytoprotective CPP5s were originally designed as negative control peptides to verify the Bax-inhibiting activity of Ku70-derived BIPs. In this article, we describe the experimental protocols of how to determine the activities of cell penetration and cytoprotection.

2. Methods

2.1. Peptides Synthesis

All the peptides examined in our laboratory were synthesized by companies (e.g., Biopeptide Co., Inc. San Diego, CA, USA) as order-made peptides. Since we often use CPP5s for the protection of cells from damage, we purchase HPLC-purified peptide (98% <purity). It is reported that the usage of D-type amino acids increases the stability of peptides in the cell since D-type peptides are resistant to protease-dependent degradation (6). We compared the cytoprotective activities of D-type and L-type VPTLK (BIP designed from mouse Ku70) in HeLa cells; however, we could not see a significant difference between these two versions (Gomez and Matsuyama, unpublished observation). Therefore, at least in the case of VPTLK, the usage of D-type amino acid is not effective to increase the biological activity. We have not examined D-type amino acids in other CPP5s. It is still possible that the utilization of D-type amino acids improves the biological activities in other CPP5s.

2.2. Storage of the Peptide

When we order CPP5 synthesis, we request companies to dispense peptide in tubes with known quantity, for example, 5 mg (dried powder) in each tube. Upon arrival, the peptides are stored in -80 or -20°C freezer. As long as peptides are stored as dried powder, we did not observe significant decrease of biological activities after 1 year or longer storage in the freezer.

For preparation of stock solution, we use dimethyl sulfoxide (DMSO) to dissolve peptides at 100 or 200 mM concentration in polypropylene tube (0.5-ml tube), and the solutions are stored at -20 or -80°C . The stock solution prepared by DMSO showed stable biological activities (cell penetration and cytoprotection) even after three times of freeze-thaw cycle. It is very important to use nonoxidized DMSO which has been stored by filling the con-

tainer with nonreactive gas (e.g., N₂ gas). It is not recommended to use old DMSO stored at room temperature without filling the bottle by nonreactive gas. Our laboratory uses DMSO dispensed in small ample tubes (5 ml for each ample) (Sigma-Aldrich, D2650). To be noted, it is not recommended to use glass tubes for the preparation of CPP5 stock solution if DMSO is used. Once we experienced that VPMLK lost its cytoprotective activity when the peptide was dissolved in DMSO and stored in a glass tube. After this experience, we are using polypropylene tube (0.5-ml or 1.5-ml centrifuge tube) for storage and preparation of stock solution.

Most of CPP5s are water soluble and it is possible to prepare stock solution in water, phosphate buffer saline (PBS), or other types of buffer. For example, stock solution in PBS may be suitable for *in vivo* experiment. We examined the effects of freeze–thaw cycle on cytoprotective activities of VPMLK and VPMLK dissolved in PBS. Two times of freeze–thaw cycle did not show significant decrease of the activity, but the decrease was observed after the third cycle. Therefore, it is recommended to avoid more than three times of freeze–thaw cycle when stock solution is prepared in water or buffer.

2.3. List of Materials Needed for Experiments

- 6-Well culture plate.
- 10% Fetal calf serum(FCS) containing Dulbecco's Modified Minimum Essential Medium (DMEM).
- FITC (or other appropriate florescent dye)-conjugated CPP5.
- BIP (fluorescent dye conjugation is not necessary to the inhibition of Bax activity).
- 0.25% Trypsin–EDTA.
- Hank's buffered saline solution (HBSS).
- Hoechst dye (33258 or the similar nuclear staining dye).

2.4. Addition of Peptides to the Cell Culture

In general, we add CPP5 into the culture medium at the concentration ranging from 10 to 400 μM. In most of the cell types, the cell entry of FITC-CPP5 can be detected by fluorescent microscope by culturing cells in the presence of 10 μM or above for more than 3 h. In the case of HeLa and DAMI cells (human megakaryotic cell line), the cell entry of FITC-VPTLK and -KLPVM was observed within 15 min of the incubation when FITC's fluorescence was measured by flow cytometry (1, 7). To protect cells from apoptosis by BIP, 10–400 μM BIP is required depending on cell type and strength of stress. For example, 200 μM is required to protect HEK293T cells from Bax overexpression (transient transfection of Bax-expressing plasmid).

CPP5 is stable in culture medium for more than 3 days, since BIP maintained its cytoprotective activity in cell culture for 3 days after the

addition of BIP to the media. In our laboratory, we usually re-add BIP every 3 days (by replacing old medium with fresh medium) if we need to inhibit Bax-mediated cell death for longer than 3 days.

2.5. Detection of Fluorescence Dye-Labeled CPP5 in the Cell

For the detection of FITC-labeled CPP5 in the cell, we usually incubate cells for 3 h in the presence of the peptide at the concentration of 10 μM or higher. The presence of serum in the medium does not interfere the cellular uptake of CPP5. Therefore, commonly used culture media containing 10% serum can be used for the examination of the cell entry and cytoprotection by CPP5.

Incubation time can be varied depends on cell type and CPP5 concentration. In the case of HeLa and DAMI cells, 15 min incubation was sufficient to detect the cell-penetrating activity of FITC-labeled CPP5 (100 μM concentration in the medium) by flow cytometric analysis (1, 7).

2.6. Cell Death Inhibition by BIP

As described earlier, BIPs were designed from Bax-inhibiting domain of Ku70 from several species (1, 3). VPMLK and PMLKE were designed from human Ku70, VPTLK was from mouse Ku70, and VPALR was from rat Ku70 (3). All these BIPs were able to bind human Bax, and they can rescue human cells from Bax-mediated cell death. In our laboratory, VPTLK is mainly used since this BIP showed the best stability for cytoprotection after the long storage for more than 1 year. We experienced a significant decrease of Bax-inhibiting activity of VPMLK and PMLKE after several freeze–thaw cycles. At present, we do not know the exact reason of the loss of activity, but we suspect that oxidation of methionine (M) during the long storage might be the cause of the problem. On the other hand, VPTLK showed very constant cytoprotective activity. If there is no special reason to use VPMLK or PLMKE, it is recommended to use VPTLK for the protection of cells from Bax-mediated cell death.

In general, we use 50–400 μM BIP to protect cells from stresses that activate Bax (1–3). The concentration of effective BIP should be determined by dose-dependent analysis. For example, 200 μM BIP is effective to protect HeLa cells, human epithelial kidney (HEK) 293T and HEK293 cells, DAMI cells (human megakaryocytic cell line), human umbilical cord endothelial cells (HUVEC), and mouse embryonic fibroblasts (MEFs) from several stresses including anti-cancer drugs (etoposide, doxorubicin, taxol, etc.), and other chemicals inducing Bax-mediated apoptosis (e.g., staurosporin) (1–3). There are numerous reports showing the protection of various cell types from cytotoxic stresses. For example, VPMLK and VPTLK protected retinal cells from oxidative stress and glutamate-induced cell death (8, 9), and stresses inducing macular degeneration (10). BIP also protected neuron from tropic factor deprivation (11) and polyglutamate overexpression (2). It was also shown that BIP increased the survival of transplanted liver cells in mouse model by the preincubation of liver

cells in BIP-containing medium (12). To be noted, VPMLK was able to protect the protozoan parasite (*Giardia lamblia*) from death caused by ectopic expression of mammalian Bax protein (13).

2.7. Addition of Peptides to Animal Model

There are some reports examining the effects of BIP in mouse model (11, 12, 14), and these reports indicate that BIP has a therapeutic potential to rescue damaged cells from Bax-mediated cell demise program. For example, BIP was able to rescue retinal cells from apoptosis induced by optic nerve injury in mouse (14). In this case, 4 μ l of BIP solution (46.9 μ g/ μ l in PBS) was intravitreally injected to the eye for every 3 days and for 6 days.

In our laboratory, we examined the toxicity of KLPVM and VPTLK in mouse by injecting these peptides by i.v., i.p., and s.c. We examined maximum dose of 275 mg/kg, but we did not observe any toxicity, and the mice were able to show normal reproductive activity after the injection of the peptides (Gomez and Matsuyama, unpublished observation).

2.8. Examination of Protein Transduction Activity

In addition to cell-penetrating activity, there is a possibility that CPP5 has protein transduction activity. Among several CPP5s, we tested KLPVM and VPTLK whether these CPP5s can deliver green fluorescence protein (GFP) into cultured cells (1, 7). CPP5 sequence was fused to the C-terminus of GFP and the recombinant proteins of GFP-CPP5 were prepared. HeLa cells were cultured with 1 μ M of GFP-VPTLK, GFP-KLPVM, or GFP (no CPP5 tag) for 24 h in 10% FCS containing DMEM. After the extensive wash of the cells by culture medium, cells were observed under the fluorescent microscope. As reported in our previous publication (1, 7), green fluorescence was observed from cells incubated with GFP-VPTLK and GFP-KLPVM, but not by GFP. This result suggests that CPP5 has a potential to deliver cargo molecule across the plasma membrane. At present, we are performing further experiments to determine whether CPP5 has protein transduction as TAT peptide does (15).

3. Protocol Examples

3.1. Experiment 1

Examination of cell penetration activity of FITC-labeled CPP5 in HeLa cells.

1. Start cell culture in 6-well plate (1×10^5 cells/2 ml/well). Use 10% FCS containing DMEM. Incubate cells for overnight (see Note 1).
2. Prepare FITC-CPP5 containing medium. For example, if you use 100 mM stock solution prepared in DMSO, add 10 μ l of this stock solution into 10 ml DMEM containing 10% FCS to prepare 100 μ M FITC-CPP5 containing medium.

3. Aspirate the medium from each well and add FITC-CPP5 containing medium.
4. Incubate 3 h.
5. Wash cells by HBSS at least two times.
6. Re-add DMEM containing 10% FCS, and observe cells under fluorescent microscope. If flow cytometric analysis is performed, collect cells by trypsinization (use 0.25% trypsin-EDTA) and wash cells by HBSS at least one time by centrifugation. Then, resuspend cells in HBSS.

3.2. Experiment 2

Protection of HeLa cells by BIP from cytotoxic stresses.

1. Start cell culture in 6-well dish (1×10^5 cells/2 ml/well). See Subheading 4.
2. Prepare BIP-containing medium. For example, if you use 100 mM stock solution prepared in DMSO, add 20 μ l of this stock solution into 10 ml DMEM containing 10% FCS to prepare 200 μ M BIP-containing medium.
3. Change the medium with BIP-containing medium, and preincubate cells for 3 h or overnight.
4. Treat cells with apoptotic stresses. For example, add staurosporin (final concentration 100 nM), etoposide (1–10 μ M), or doxorubicine (1 μ M). If medium change is necessary, do not forget to re-add BIP into the fresh medium.
5. Incubate cells with apoptosis-inducing reagent for the necessary period such as 12, 24, and 48 h.
6. Add Hoechst dye to the medium at the final concentration of 4 μ g/ml. Incubate cells at least for 10 min.
7. Observe cells under the fluorescent microscope and detect apoptosis by the change of nuclear morphology (nuclear condensation and nuclear fragmentation).

4. Notes

1. *Cell density is an important factor.* The efficiency of cell penetration by CPP5s can be significantly influenced by culture condition, especially by cell density (cell number per dish). In “100% confluent” condition, the efficiency of cell entry of CPP5s becomes less than that in lower cell density condition. Important issue is that cell density must be accurately controlled in each experiment to obtain constant result. In this protocol, HeLa cells are plated at the density of 1×10^5 cells/well (6-well plate) that results in 30–40% confluent condition. In this condition, CPP5s show very fast cell penetration activity (cell entry can be detected within 15 min of incubation).

Acknowledgment

This work was supported in part by National Institute of Health (NIH) grants RO1AG031903 (to Shigemi Matsuyama) and PC0CA1037 (Pilot Grant from Case Comprehensive Cancer center), and an American heart Association fellowship 0615139B (to Jose Gomez). The Study was also supported in part by the Flow Cytometry and Confocal Microscopy core facilities of the Comprehensive Cancer Center of Case western Reserve University and University Hospital P30CA43703.

References

- Gomez, J. A., Gama, V., Yoshida, T., Sun, W., Hayes, P., Leskov, K., Boothman, D., and Matsuyama, S. (2007) Bax-inhibiting peptides derived from Ku70 and cell-penetrating pentapeptides, *Biochem Soc Trans* 35, 797–801.
- Li, Y., Yokota, T., Gama, V., Yoshida, T., Gomez, J. A., Ishikawa, K., Sasaguri, H., Cohen, H. Y., Sinclair, D. A., Mizusawa, H., and Matsuyama, S. (2007) Bax-inhibiting peptide protects cells from polyglutamine toxicity caused by Ku70 acetylation, *Cell Death Differ* 14, 2058–2067.
- Yoshida, T., Tomioka, I., Nagahara, T., Holyst, T., Sawada, M., Hayes, P., Gama, V., Okuno, M., Chen, Y., Abe, Y., Kanouchi, T., Sasada, H., Wang, D., Yokota, T., Sato, E., and Matsuyama, S. (2004) Bax-inhibiting peptide derived from mouse and rat Ku70, *Biochem Biophys Res Commun* 321, 961–966.
- Doherty, A. J. and Jackson, S. P. (2001) DNA repair: how Ku makes ends meet, *Curr Biol* 11, R920–R924.
- Downs, J. A. and Jackson, S. P. (2004) A means to a DNA end: the many roles of Ku, *Nat Rev Mol Cell Biol* 5, 367–378.
- Pujals, S., Fernandez-Carneado, J., Ludevid, M. D., and Giralt, E. (2008) D-SAP: a new, noncytotoxic, and fully protease resistant cell-penetrating peptide, *Chem Med Chem* 3, 296–301.
- Gomez, J. A., Gama, V., and Matsuyama, S. (2006) Cell-permeable penta-peptides derived from Bax-inhibiting peptide, *Cell Penetrating Peptide* (Ed. Langel, U.), 2nd edition, pp. 469–481. CRC, Boca Raton.
- Chen, Y. N., Yamada, H., Mao, W., Matsuyama, S., Aihara, M., and Araie, M. (2007) Hypoxia-induced retinal ganglion cell death and the neuroprotective effects of beta-adrenergic antagonists, *Brain Res* 1148, 28–37.
- Iriyama, T., Kamei, Y., Kozuma, S., and Taketani, Y. (2009) Bax-inhibiting peptide protects glutamate-induced cerebellar granule cell death by blocking Bax translocation, *Neurosci Lett* 451, 11–15.
- Maeda, A., Maeda, T., Golczak, M., Chou, S., Desai, A., Hoppel, C. L., Matsuyama, S., and Palczewski, K. (2009) Involvement of all-trans-retinal in acute light-induced retinopathy of mice, *J Biol Chem* 284, 15173–15183.
- Yu, L. Y., Jokitalo, E., Sun, Y. F., Mehlen, P., Lindholm, D., Saarma, M., and Arumae, U. (2003) GDNF-deprived sympathetic neurons die via a novel nonmitochondrial pathway, *J Cell Biol* 163, 987–997.
- Tanaka, K., Kobayashi, N., Gutierrez, A. S., Rivas-Carrillo, J. D., Navarro-Alvarez, N., Chen, Y., Narushima, M., Miki, A., Okitsu, T., Noguchi, H., and Tanaka, N. (2006) Prolonged survival of mice with acute liver failure with transplantation of monkey hepatocytes cultured with an antiapoptotic pentapeptide V5, *Transplantation* 81, 427–437.
- Hehl, A. B., Regos, A., Schraner, E., and Schneider, A. (2007) Bax function in the absence of mitochondria in the primitive protozoan *Giardia lamblia*, *PLoS One* 2, e488.
- Qin, Q., Patil, K., and Sharma, S. C. (2004) The role of Bax-inhibiting peptide in retinal ganglion cell apoptosis after optic nerve transection, *Neurosci Lett* 372, 17–21.
- Wadia, J. S., Stan, R. V., and Dowdy, S. F. (2004) Transducible TAT-HA fusogenic peptide enhances escape of TAT-fusion proteins after lipid raft macropinocytosis, *Nat Med* 10, 310–315.

PAIR Technology: Exon-Specific RNA-Binding Protein Isolation in Live Cells

Thomas J. Bell, Emelía Eiríksdóttir, Ülo Langel, and James Eberwine

Abstract

RNA-binding proteins (RBPs) are fundamental regulatory proteins for all forms of transcriptional and posttranscriptional control of gene expression. However, isolating RBPs is technically challenging for investigators. Currently, the most widely used techniques to isolate RBPs are in vitro biochemical approaches. Although these approaches have been useful, they have several limitations. One key limitation to using in vitro biochemical approaches is that RBP–RNA interactions are isolated under nonbiological conditions. Here we review a novel experimental approach to identify RBPs called peptide nucleic acid (PNA)-assisted identification of RBPs (PAIR) technology (Zielinski et al., Proc Natl Acad Sci USA 103:1557–1562, 2006). This technology has two significant advantages over traditional approaches. (1) It overcomes the in vitro limitation of biochemical approaches by allowing investigators to isolate RBP–RNA interactions under in vivo conditions. (2) This technology is highly mRNA specific; it isolates RBPs in an exon-specific manner. By selectively targeting alternatively spliced exons with PAIR technology, investigators can isolate splice variant-specific and mRNA region-specific (5-UTR and 3-UTR) RBP complexes for any mRNA of interest.

Key words: RNA-binding proteins, Cell-penetrating peptide, Post-transcriptional regulation, Alternative splicing

1. Introduction

All modes of post-transcriptional control of gene expression require specific RNA-binding protein (RBP) interactions with key regulatory sequences in their target mRNA. Although these interactions control multiple post-transcriptional events, only a relatively small number of RBPs and their respective target mRNA-binding sequences have been identified. Furthermore, reports usually only describe half of the story, the key RNA sequences. For example, the key regulatory pre-mRNA sequences that control activity-dependent splicing of the *KCNMA1* STREX

splice variant have been identified (2, 3), but the RBPs that direct this splicing event have yet to be identified. Neuronal RBPs and their functional roles have remained particularly elusive to neuroscience investigators. For example, in synaptic plasticity studies only a small number of RBPs have been identified, such as Fragile X mental retardation protein (FMRP) (4, 5), cytoplasmic polyadenylation element (CPE) protein (6–8), and neuro-oncological ventral antigen (NOVA) (9). The clinical importance of neuronal RBPs has been highlighted in studies on Fragile X syndrome. This well-studied neurological disease is caused by mutations in the RBPs called FMRPs. In particular it is thought that a mutated FMRP cannot “appropriately target” its RNA cargoes thereby giving rise to alterations in the biology associated with its RNA cargoes.

**1.1. PAIR Technology
Isolates RBP
Complexes in an
Exon-Specific Manner**

Mammalian cells contain 4,000–12,000 mRNAs in their intracellular compartments (10). This diverse mixture of cellular mRNAs requires RBP complexes to associate with the mRNAs and direct their post-transcriptional processing. Perhaps even more important than transcriptional regulation, RBP complexes control a very diverse range of post-transcriptional events that ultimately yield mRNA-specific splicing patterns (exon utilization), subcellular localization patterns, and RNA stabilities. To accomplish these critical events, a large number of different RBPs complexes coat the entire topography of an mRNA. Each RBP complex along the mRNA can directly regulate or contribute to the regulation of different post-transcriptional events. Therefore, identifying RBPs in select gene regions (5-UTR or 3-UTR) or exons (alternatively spliced or constitutive) can offer a more direct experimental approach to study different post-transcriptional events.

The PAIR technology delivers the advantage of allowing investigator to identify RBP complexes in selected gene regions or exons in live cells. Analogous to designing PCR primers, investigators will directly target exons in their mRNA of interest. Instead of using nucleic acid probes, this technology relies on peptide nucleic acid (PNA) analogs. PNAs are composed of peptide backbone and nucleotide bases and are, therefore, not recognized by proteases or nucleases. This unique composition of PNAs gives them extraordinary stability over nucleic acids in the cytoplasm of live cells. The PNA probe design strategy is relatively straightforward. The PNA probe sequences need to be complementary for their target mRNA sequence and ~12–18 nucleotides in length to be gene-specific. To optimize hybridization conditions in the cytoplasm of live cells, the GC content should be limited to ~50% and the PNA sequence should not have three consecutive purine nucleotides. NIH BLAST search should be used to verify that each PNA probe is specific for their respective target sequences. Lastly, to improve the stringency of the RBP screen, a minimum of two PNA probes should be

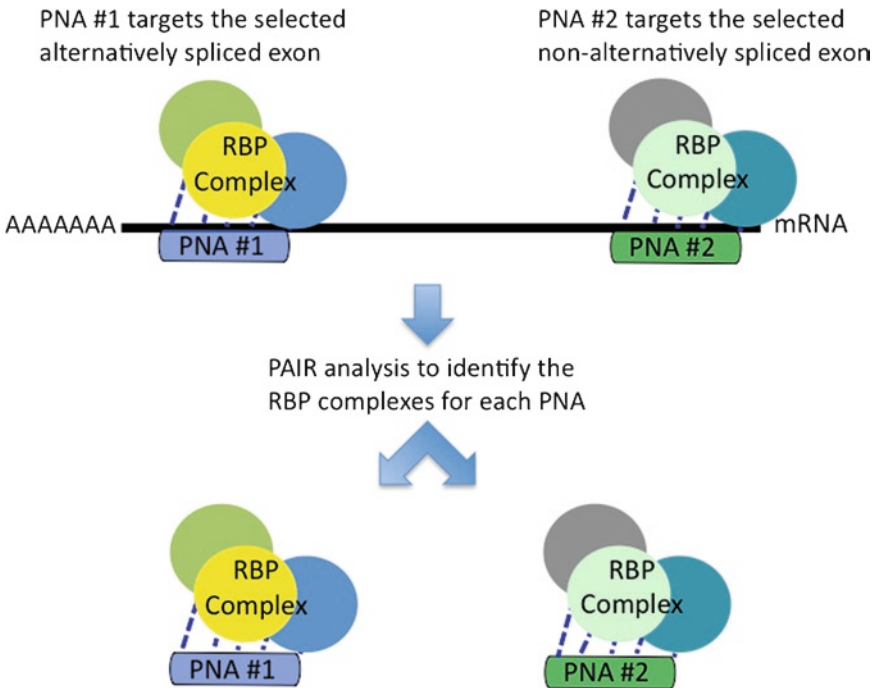


Fig. 1. **PAIR procedure can isolate different RBP complexes from same mRNA.** This cartoon shows how PAIR procedure can be used to identify the RBP complexes that regulate different exons of a selected mRNA. PNA#1 is designed to identify the RBP complexes that regulate the expression of one alternatively spliced exon. PNA#2 is designed to identify a different set of RBP complexes. This set regulates the expression of a nonalternatively spliced exon.

designed for each target exon. Currently, we are taking advantage of the experimental flexibility in PAIR technology to isolate a variety of RBP complexes for BKCa channel mRNAs (Fig. 1). Our PNA probes are designed to isolate RBP complexes that regulate two different forms of post-transcriptional processing in BKCa channel mRNAs: intron retention (11) and activity-dependent alternative splicing (3).

1.2. A General PAIR Overview

A schematic of the PAIR procedure is provided in Fig. 2. This technology was developed to isolate RBPs in the cytoplasm of live cells (1). In the current iteration of the PAIR technology, the PNAs are linked with two other molecules: (1) a cell-penetrating peptide (CPP) via a reducible disulfide bridge and (2) a photo-activatable compound *p*-benzoylphenylalanine (Bpa) via a peptide bond. The cell-penetrating peptides are used to get the CPP–PNA–Bpa complexes efficiently into the cellular cytoplasm. Once the CPP–PNA–Bpa complexes are taken up into the cellular cytoplasm, the CPP component of the complex is reduced due to cytosolic glutathione, thereby removing the CPP from the complex. The remaining molecules in the complex, PNA–Bpa, anneals to their target mRNA sequences in the cytoplasm of live cells.

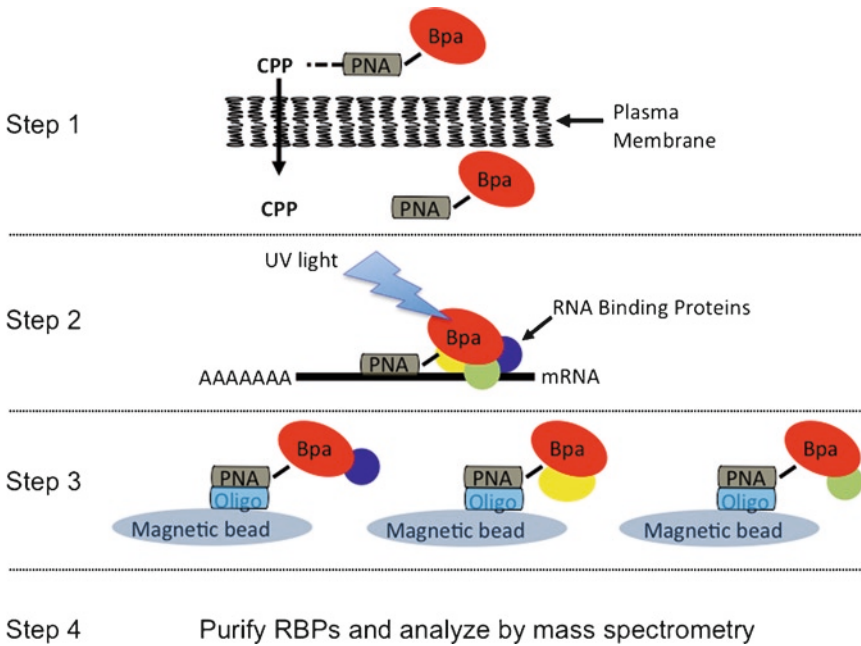


Fig. 2. **A schematic of the PAIR procedure.** **Step 1**, a cell-penetrating peptide (CPP) gets the PNA-Bpa complexes across the plasma membrane. **Step 2**, the PNAs hybridize to their target mRNAs in live neurons. Next, UV light stimulation activates *p*-benzoylphenylalanine (Bpa) and cross-links the PNA-Bpa-RBP complexes. **Step 3**, the neurons are collected and magnetic beads are used to isolate the PNA-Bpa-RBP complexes. **Step 4**, RNA-RBPs complexes are eluted from the beads and purified by chloroform-methanol precipitation. SDS-PAGE and silver staining is used to visualize the isolated RBPs. The protein bands of interest will be excised and subjected to mass spectrometry analysis.

After the PNA-Bpa complex anneals to the target mRNA, the photo-activatable moiety, *p*-benzoylphenylalanine (Bpa), is used to physically link the PNA-Bpa complexes to nearby RBP complexes. To accomplish this step, live cells are simply exposed to UV irradiation. This step activates the Bpa and cross-links the mRNA-PNA-Bpa complexes to all the nearby RBP complexes.

After cross-linking the PNA-Bpa complexes to the RBPs, the cells are treated with Triton-100 lysis buffer to disrupt the cellular membranes. The cellular lysates are next subjected to RNase A treatment to release the mRNA-PNA-Bpa complexes. Magnetic beads coupled to oligonucleotide primers that are complementary to the PNA probes are used to isolate the PNA-RBP complexes from cellular lysates. RNA-RBPs complexes are eluted from the beads and the RBPs are purified by chloroform-methanol precipitation. SDS-PAGE and silver staining is used to visualize the isolated RBPs. Protein bands or gel regions of interest are simply excised and analyzed by mass spectrometry.

1.3. Summary

RBPs are fundamental regulatory proteins in all neurons. In fact, one of the most well-studied neurological diseases, Fragile X

syndrome, is caused by mutations in the RBP called FMRP. To date only a few functionally significant RBPs have been identified in neurons. To understand the biological roles of these neuronally localized RBPs, further advancements in isolating, characterizing, and understanding how the RBPs work is required. Innovation is one of the best ways to stimulate progress in a particular field, so here we highlight a novel experimental approach to in vivo identify neuronal RBPs that bind to particular RNAs. The PAIR procedure gives investigators a major advantage over other techniques because it permits the isolation of splice variant-specific and mRNA region-specific (5-UTR and 3-UTR) RBP complexes for any mRNA of interest under in vivo conditions.

2. Materials

2.1. Buffers

1. HEPES-buffered saline (HBS), pH 7.4: 25 mM HEPES, 0.75 mM Na₂HPO₄, 70 mM NaCl₂. Filter sterilize. Store at -20°C.
2. TX-100 lysis buffer, pH 8.0: 25 mM HEPES, 0.1% Triton X-100, 300 mM NaCl₂, 20 mM glycerophosphate, 1.5 mM MgCl₂, 1 mM DTT, 2 mM EDTA. Filter sterilize. Store at 4°C.
 Add fresh protease inhibitors to the TX-100 lysis buffer immediately before each experiment. As per the manufacturer's recommendation, 10 µl Protease Inhibitor Cocktail for each 1-ml cell extracts. The final concentration of PMSF should be 1 mM.
3. Salt-free lysis buffer, pH 8.0: 25 mM HEPES, 0.1% Triton X-100, 20 mM glycerophosphate, 1.5 mM MgCl₂, 1 mM DTT, 2 mM EDTA. Filter sterilize. Store at 4°C.
 Add fresh protease inhibitors to the Salt-free lysis buffer immediately before each experiment. As per the manufacturer's recommendation, 10 µl Protease Inhibitor Cocktail for each 1-ml cell extracts. The final concentration of PMSF should be 1 mM.
4. Ammonium bicarbonate buffer, pH 8.0: 25 mM NH₄HCO₃. Filter sterilize. Store at -80°C.
5. Streptavidin magnetic bead storage buffer: Dulbecco's phosphate-buffered saline (D-PBS) (1×), 0.1% bovine serum albumin (BSA), 0.2% NaN₃. Store at -20°C.
6. Blocking nonspecific buffer for streptavidin magnetic bead: D-PBS (1×), 0.1% BSA. Store at 4°C.
7. D-PBS (1×), pH 7.4. Store at 4°C.
8. GnHCl buffer for dissolving protein pellets: 3 M GnHCl. Filter sterilize. Store at 4°C.

2.2. Protease Inhibitors

1. Protease inhibitor cocktail, Sigma, No: P8340. Store at -20°C .
2. Phenylmethanesulfonyl fluoride solution (PMSF), Fluka, No: 93482. Store at 4°C .

2.3. Chemicals for Buffers

1. Sodium hydroxide (NaOH), Fisher, Product No: BP359-500.
2. Sodium phosphate dibasic dihydrate ($\text{Na}_2\text{HPO}_4 \cdot 2\text{H}_2\text{O}$), Fisher, Product No: S381-500.
3. Ethylene diamine tetra-acetic acid disodium salt dihydrate, Fisher, Product No: BP120-500.
4. Ammonium bicarbonate (NH_4HCO_3), Fisher, Product No: BP2413-500.
5. UltraPure 1 M Tris-HCl pH 8.0, Invitrogen, Cat. No. 15568-025.
6. Sodium chloride (NaCl), Sigma, Product No: S7653.
7. Triton X-100, Sigma, Product No: T8787.
8. Glycerol 2-phosphate disodium salt hydrate ($\text{C}_3\text{H}_7\text{O}_6\text{Na}_2 \cdot x\text{H}_2\text{O}$), Sigma, Product No: G9891-25G.
9. Magnesium chloride hexahydrate ($\text{MgCl}_2 \cdot 6\text{H}_2\text{O}$), Sigma, Product name or No: M-9272.
10. Calcium chloride dihydrate ($\text{CaCl}_2 \cdot 2\text{H}_2\text{O}$), Fisher, Product No: C79-500.
11. Potassium chloride (KCl), Sigma, Product No: P9541.
12. Potassium dihydrogen phosphate (KH_2PO_4), Sigma, Product No: P5379-500G.
13. Sodium azide (NaN_3), Sigma, Product No: S-8032.
14. Purified BSA, New England BioLabs, Product No: B9001S.

2.4. Chemicals for Protein Precipitation

1. Methanol (MeOH), Fisher, Product No: A412.
2. Chloroform (CHCl_3), Sigma, Product No: C2432.
3. Guanidine hydrochloride (GnHCl), Life Technologies, Inc., Cat. No. 5502UA.

2.5. Protein Gel Reagents

1. NuPAGE 10% Bis-Tris gel 1.0 mm X 12 well, Invitrogen, Cat. No. NP0302.
2. NuPAGE Sample Reducing Agent (Dithiothreitol), Invitrogen, Cat. No. NP0004.
3. NuPAGE LDS Sample Buffer (Lauryl alcohol sulfate, lithium salt), Invitrogen, Cat. No. NP0007.
4. NuPAGE Antioxidant (*N,N*-dimethylformamide and sodium bisulfite (NaHSO_3)), Invitrogen, Cat. No. NP0005.
5. SilverQuest Silver staining kit, Invitrogen.

2.6. Other Reagents

1. RNase A, Roche.
2. Dynabeads M-270 streptavidin magnetic beads, Invitrogen, Cat. No. 653.05.
3. Biotinylated sense (complementary to the PNA sequence) oligonucleotide primer.
4. Nuclease-free water.
5. Cell scrapers.
6. 15-ml capped tubes.
7. Eppendorf tubes.
8. Microcentrifuge.
9. Centrifuge for 15-ml tubes.

2.7. Cultured Cells

The procedure can be performed in any cell culture system. We typically use rat cortical neurons plated in 35-mm dishes in ~12 ml of media at 400,000 cells/ml ($\sim 4.8 \times 10^6$ cells in each plate). For each PNA, we use minimum of 1.4×10^7 cells per experiment. However, the number of cells required for PAIR analysis depends on the abundance of the target mRNA. Lower abundant mRNAs may require increasing the number of cells.

3. Methods**3.1. Forming of PNA-RNA-Binding Protein Complexes in Live Cells**

Materials:

Cultured cells

TX-100 lysis buffer

HBS

RNase A

Protease inhibitors

Dry ice

UV light source

Cell scrapers

15-ml tubes

PNA solutions: 15 μ M of PNA in HBS. Different concentrations of each PNA can be tested.

A representative PAIR experiment:

Sample name	Treatment
PNA #1 low concentration	20 μ l of PNA #1
PNA #1 high concentration	40 μ l of PNA #1
PNA #2 low concentration	20 μ l of PNA #2
PNA #2 high concentration	40 μ l of PNA #2
Negative control low concentration	20 μ l of HBS
Negative control high concentration	40 μ l of HBS

1. Collect 4 ml of media from each plate into a 15-ml tube. Aspirate the rest of the medium from the plate.
2. Add the 4-ml back to the plate.
3. Directly add 20 or 40 μ l of each treatment (see chart above) to a plate.
4. Mix by slowly moving the plates in circles for ~20 s.
5. Incubate for 90 min at 37°C in tissue culture incubator.
6. Rinse the cells 2 \times with 4-ml HBS (at room temperature).
7. UV cross-link for 2.5 min with UV light source.
8. Replace the HBS with 4-ml ice-cold TX-100 lysis buffer (with freshly added protease inhibitors: PI and PMSF).
9. Scrape the cells and collect the cell lysate in a 15-ml tube.
10. Remove 30 μ l of each sample and save this aliquot (labeled as Total Cell Lysate) for protein gel analysis. Store at -80°C.
11. Place the cell lysates in the 15-ml tubes on dry ice for 60 min. Either proceed to the next step or store the samples at -80°C.

(Potential Stopping point)

3.2. Releasing the PNA-RNA-Binding Protein Complexes from the Cellular mRNAs

Materials:

Cell lysates
RNase A
Dry ice
37°C incubator with rotator
Room temperature water bath

1. Thaw the cell lysates in room temperature water bath.
2. Add 12 μ l of RNase A (1 mg/ml) to the cell lysates. Rotate the tubes at 37°C for 20 min.
3. Place the cell lysates on dry ice for 60 min. Store the samples at -80°C.

(Potential Stopping point)

3.3. Coupling of Biotinylated Sense Oligonucleotide Primer to Streptavidin Magnetic Beads

Materials:

Blocking nonspecific buffer for streptavidin magnetic bead
Biotinylated sense oligonucleotide primer
Magnetic stand
Dynabeads M-270 streptavidin magnetic beads
1 \times D-PBS
Room temperature rotator

1. Put 1 ml (=10 mg) of streptavidin magnetic beads into an Eppendorf tube.
2. Place the tube in the magnetic stand for 10 min, then remove the buffer.
3. Add 1 ml of D-PBS and rotate for 10 min at room temperature.

4. Place the tube in the magnetic stand for 10 min, then remove the buffer.
5. Wash the beads again with 1-ml D-PBS (repeat steps 2 and 3).
6. Dissolve the oligonucleotide (1 mg/ml in Tris-EDTA buffer).
7. Add 50 μ l (=50 μ g) of each oligonucleotide solution to 950 μ l of 1 \times D-PBS.
8. Remove the buffer from the beads and resuspend them in 1 ml 1 \times D-PBS containing 50 μ g of the biotinylated sense oligonucleotide (step 7).
9. Rotate the solution at room temperature for 1 h.
10. Magnetically separate the beads from the solution.
11. Wash the beads five times with 1 ml 1 \times D-PBS (see steps 2 and 3).
12. After completing the last wash, resuspend the beads in 1 ml D-PBS containing 0.2% BSA to block nonspecific binding to the beads.
13. Rotate the tubes at RT for 1 h.
14. Place the tube in the magnetic stand for 10 min, then remove the buffer.
15. Briefly, wash the magnetic bead-streptavidin-biotin-oligo complex with D-PBS. For this wash, add 1 ml of D-PBS and vortex for 10 s at room temperature.
16. Place the tube in the magnetic stand for 10 min, then remove the buffer.
17. Wash again (repeat steps 14-16).
18. Resuspend the bead complex in 1 ml (final concentration of 10 mg/ml) in storage buffer and store at 4°C.

**3.4. Washing the
Magnetic Bead-
Streptavidin-Biotin-
Oligo Complexes**

Materials:

Magnetic beads coupled to oligonucleotide primers
 Magnetic stand
 TX-100 lysis buffer
 Protease inhibitors
 Room temperature rotator
 Eppendorf tubes
 Microcentrifuge

1. Place 30 μ l of the magnetic bead-streptavidin-biotin-oligo complexes (prepared in Subheading 3.4) in an Eppendorf tube.
2. Place the tube in the magnetic stand for 10 min, then remove the buffer.

3. Add 1 ml TX-100 lysis buffer containing freshly added protease inhibitors.
4. Rotate for 10 min at RT.
5. Centrifuge briefly.
6. Magnetically separate for 10 min on magnetic stand, then remove the buffer.
7. Wash the magnetic bead–streptavidin–biotin–oligo complexes again (repeat steps 3–7).
8. After the last wash, remove the buffer and resuspend the magnetic bead–streptavidin–biotin–oligo complexes in 30 μ l of the TX-100 lysis buffer containing freshly added protease inhibitor.

Note: The beads can be prepared in advance. The washed beads can be stored at 4°C for a week.

3.5. Isolating PNA–RNA-Binding Protein Complexes from the Cell Lysate

Materials:

Cell lysates
 Washed magnetic bead–streptavidin–biotin–oligo complexes
 Magnetic stand
 TX-100 lysis buffer
 Protease inhibitors
 Room temperature rotator
 37°C incubator with rotator
 Microcentrifuge
 Room temperature water bath

1. Thaw the cell lysate in a room temperature water bath.
2. Add 30 μ l of the washed magnetic bead–streptavidin–biotin–oligo complexes to the cell lysates.
3. Rotate the tubes at 37°C for 30 min and at RT for 30 min. The magnetic bead–streptavidin–biotin–oligo complexes should now be annealed to the PNAs cross-linked to RBPs.
4. Centrifuge the samples at 2300 *g*-force for 1 min.
5. Save a 30- μ l aliquot (labeled as FT for flow-through) of the supernatant of each PNA sample for protein gel analysis. Store at –80°C.
6. Without disturbing the pelleted beads, remove the supernatant until 500 μ l of the lysate remains.
7. Transfer the PNA-coupled beads to an Eppendorf tube.
8. Magnetically separate the beads from the lysate for 10 min and aspirate the supernatant.
9. While magnetized, rinse the beads 2 \times with 1 ml TX-100 lysis buffer containing freshly added protease inhibitors to remove any uncoupled lysate proteins.
10. Rotate for 20 min at RT, centrifuge briefly, magnetically separate for 10 min and remove the buffer.

3.6. Eluting the RBP Complexes for the Magnetic Beads

Materials:

Cell lysates
Salt-free TX-100 lysis buffer
Protease inhibitors
50°C water bath
Microcentrifuge

1. Resuspend the beads in 100 µl of salt-free TX-100 lysis buffer (with freshly added protease inhibitors) pre-warmed to 50°C to elute the PNA–RBP complex.
2. Incubate the beads at 50°C in a benchtop water bath flicking the tube periodically for 20 min.
3. Centrifuge the beads for 1 min at RT at maximum speed (16100 *g*-force) in a benchtop centrifuge.
4. Transfer the eluate to a new Eppendorf. The eluate now contains the RBPs bound to the specific PNA.

3.7. RBP Complex Precipitation

Materials:

Cell lysates
Methanol
Ammonium bicarbonate buffer
Nuclease-free water
Chloroform
Microcentrifuge

1. Add 400 µl of methanol to each Eppendorf containing the eluate. Vortex for 10 s and centrifuge at 9300 *g*-force for 10 s.
2. Add 100 µl chloroform, vortex for 10 s and centrifuge at 10,000 rpm for 10 s.
3. Add 300 µl nuclease-free water, vortex for 10 s and centrifuge at 10,000 rpm for 3 min at 4°C.
4. The interphase now contains the proteins. Aspirate and discard the upper phase and leave ≤20 µl of the upper phase in the tube.
5. Add 300 µl methanol, vortex for 10 s and centrifuge at 13,200 rpm for 10 min at 4°C.
6. Decant the supernatant and air dry the pellet for ~5 min.
7. Add 50 µl of 25 mM ammonium bicarbonate buffer.
8. Store at –80°C for Protein Gel analysis. Alternatively, the entire RBP precipitation can be used for mass spectrometry analysis.

(Potential Stopping point)

3.8. SDS-PAGE and Silver Staining Analysis of the Isolated RBP Complexes

Materials:

- Samples (three samples per PNA)
 - Total cell lysates (TCL; from Subheading 3.1, step 10)
 - Flow-through (FT; from Subheading 3.5, step 5)

- Isolated RBP complexes (from Subheading 3.7, step 8)
 - NuPAGE 10% Bis-Tris gel 1.0 mm × 12 well
 - NuPAGE sample reducing agent
 - NuPAGE LDS sample buffer
 - NuPAGE antioxidant
 - SilverQuest silver staining kit
1. Run SDS-PAGE gels to analyze the PAIR results for each PNA. Load three samples for each PNA: (1) the total cell lysate, (2) flow-through, and (3) RBP complex precipitation.
 2. Stain the gel with silver staining kit.
 3. Excised protein bands of interest are analyzed by mass spectrometry.

4. Notes

1. *Keratin or other contaminants in the mass spec analysis.* The source of keratin contamination is most likely from human skin. Investigators should eliminate any direct exposure to their skin by wearing gloves and lab coats. Next, restricting the opening of the tissue culture dishes to well-ventilated tissue culture hoods will prevent the introduction of other contaminants. Lastly, BSA and trypsin are used during the PAIR procedure, so it is highly likely that they will be detected in mass spectrometry analysis.
2. *No RBPs isolated or low yields.* Some PNAs may not isolate a sufficient quantity of RBP complexes to allow the mass spectrometry analysis. Therefore, multiple PNAs (at least two) should be designed for each exon of interest. One can further optimize their yields by performing the PAIR procedure with a few different concentrations of each PNA (see Subheading 3.1).
3. *Verifying the PAIR results.* For any experimental result, using multiple experimental methodologies to verify initial findings is always a prudent approach. Therefore, before pursuing PAIR-identified mRNA–RBP complexes in more complex experimental systems (transgenic animals) or functional studies (physiology or imaging experiments), investigators should consider confirming their results with other RBP isolation methodologies, such as immuno-precipitation. However, the in vitro biochemical approaches may not replicate the PAIR results, because they do not replicate the in vitro

PAIR conditions. Also, other methods depend on antibodies to the target RBP to perform the experiments; this could be a limiting factor in using antibody-based methods. Investigators should be aware that it may not be possible to verify all PAIR results by traditional biochemical approaches and some PAIR results may not be reproduced by these approaches.

4. *Predicted PAIR results.* The limited number of known neuronal RBPs makes it somewhat difficult to predict the potential identities of the proteins that will be identified with PAIR analysis. However, investigators should be open to pursuing a wide range of candidate proteins (traditional and nontraditional RBPs) for their exons of interest. PAIR analysis could yield novel RNA-binding proteins, signaling proteins that regulate RBP complexes associated with their exon, or known RNA-binding proteins (such as FRMP).
5. *Determining the functional roles of the PAIR-isolated RBPs.* The PAIR procedure isolates RBP complexes that associate with select mRNA regions and exons. The next challenge for investigators is to identify the functional impacts of their PAIR-identified RBP complexes. Most molecular, imaging, and electrophysiological techniques are compatible with cell culture-based model systems. This allows investigators to perform their functional screens and RBP isolations in identical model systems and rapid transition from PAIR analysis to functional studies. One approach that we frequently use to determine the functional impacts of PAIR-identified RBP complexes is RNA interference in conjunction with functional screens. (a) *Do the PAIR-identified RBPs regulate subcellular distribution patterns of the exon of interest?* The combination of RNA interference and in situ hybridization (ISH) can be used to determine whether PAIR-identified RBP complexes regulate the localization patterns of the exon of interest. The levels of PAIR-identified RBP can be selectively reduced by RNA interference and ISH can be used to screen for changes in the localization patterns of the exon of interest. (b) *Do the PAIR-identified RBPs regulate subcellular distribution patterns of exon of the interest protein products?* The combination of RNA interference and immunostaining can be used to determine whether PAIR-identified RBP play a role in regulating the subcellular distribution patterns of the exon of interest protein products. The levels of PAIR-identified RBP can be selectively reduced by RNA interference and immunostaining can be used to screen for changes in the subcellular distribution patterns of the exon of interest protein products. (c) *Do the PAIR-identified RBPs regulate the excitability of neurons?* The combination of RNA interference and

current clamp analysis can be used to determine if PAIR-identified RBP play a role in regulating the membrane properties of neurons. Again, the levels of PAIR-identified RBP can be selectively reduced by RNA interference and current clamp analysis to screen for changes in neuronal membrane properties.

6. *Screening for activity-dependent changes in RBP complexes.* One advantage of using a cell culture-based model experimental systems is that the cells are easily manipulated by pharmacological treatments. Therefore, investigators can combine the PAIR procedure with pharmacological manipulations such as KCl or glutamate treatments to screen for activity-dependent changes in their exon-specific RBP complexes.

Acknowledgments

We would like to acknowledge our colleagues who have helped to refine the cell biology of the PAIR technology including Jennifer Zielinski, Tiina Peritz, and Drs. Fanyi Zeng, Peter Buckley, and Kalle Kilk. Also we appreciate funding from the the NIH Institutes on Aging and Mental Health as well as the Swedish Science Foundation and a European Community Grant.

References

1. Zielinski J, Kilk K, Peritz T, Kannanayakal T, Miyashiro KY, Eiriksdottir E, Jochems J, Langel U, & Eberwine J (2006) *Proc Natl Acad Sci USA* **103**, 1557–1562.
2. Xie J & Black DL (2001) *Nature* **410**, 936–939.
3. Xie J, Jan C, Stoilov P, Park J, & Black DL (2005) *RNA* **11**, 1825–1834.
4. Huber KM, Gallagher SM, Warren ST, & Bear MF (2002) *Proc Natl Acad Sci USA* **99**, 7746–7750.
5. Koekkoek SK, Yamaguchi K, Milojkovic BA, Dortmund BR, Ruigrok TJ, Maex R, De Graaf W, Smit AE, VanderWerf F, Bakker CE, *et al.* (2005) *Neuron* **47**, 339–352.
6. Si K, Giustetto M, Etkin A, Hsu R, Janisiewicz AM, Miniaci MC, Kim JH, Zhu H, & Kandel ER (2003) *Cell* **115**, 893–904.
7. Alarcon JM, Hodgman R, Theis M, Huang YS, Kandel ER, & Richter JD (2004) *Learn Mem* **11**, 318–327.
8. Wells DG, Dong X, Quinlan EM, Huang YS, Bear MF, Richter JD, & Fallon JR (2001) *J Neurosci* **21**, 9541–9548.
9. Huang CS, Shi SH, Ule J, Ruggiu M, Barker LA, Darnell RB, Jan YN, & Jan LY (2005) *Cell* **123**, 105–118.
10. Eberwine J, Belt B, Kacharina JE, & Miyashiro K (2002) *Neurochem Res* **27**, 1065–1077.
11. Bell TJ, Miyashiro KY, Sul JY, McCullough R, Buckley PT, Jochems J, Meaney DF, Haydon P, Cantor C, Parsons TD, *et al.* (2008) *Proc Natl Acad Sci USA* **105**, 1901–1906.

Quantitation of Cellular and Topical Uptake of Luciferin–Oligoarginine Conjugates

Jonathan B. Rothbard and Lisa R. Jones

Abstract

A major challenge confronting the further advancement of using molecular transporters conjugated to small molecular weight therapeutics in the clinic is the development of linkers that would allow for the controllable release of a free drug/probe only after cell entry. Development of assays that would allow for the rapid real-time quantification of transporter conjugate uptake and cargo release in cells and animals would greatly help in their development. In this chapter, we describe a imaging method that quantitatively measures transporter conjugate uptake and cargo release in real-time in both cell culture and animal models.

Key words: Topical drug delivery, Drug conjugates, Luciferin, Bioluminescence

1. Introduction

Many promising therapeutic leads fail to advance clinically due to problems with formulation and/or bioavailability. Conversion of the lead to a more polar prodrug often minimizes problems with aqueous formulation, but at the same time increases problems with passive diffusion across the relatively non-polar membrane of cells. We previously have shown that conjugation of small molecules, peptides, proteins, nucleic acids, or imaging agents to an octaarginine or oligoguanidine transporter produces conjugates that are water soluble and readily enter cells and tissue (1–7).

A major challenge confronting the further advancement of this field is the development of linkers that would allow for the controllable release of a free drug/probe only after cell entry. Realization of this goal is coupled directly to the development of assays that would allow for the rapid real-time quantification of transporter conjugate uptake and cargo release in cells and animals. Transporters covalently conjugated to fluorescent dyes can be

used to measure uptake *in vitro*, but they cannot be used to measure cargo release in a cell or applied to real time, *in vivo* analyses. Radiolabeled conjugates can be used for *in vivo* studies, but they neither establish whether the labeled conjugate is intra- or extracellular, nor whether they are intact or have released their cargo. We have shown that intracellular cargo release is possible and measurable when an oligoarginine transporter is attached through a cysteine disulfide bond to an otherwise cell-impermeable peptide cargo (4). The resultant conjugate enters cells and is then cleaved to the free bioactive peptide as determined in a functional assay for ischemic damage. This assay, however, does not lend itself to rapidly evaluating new transporters, linkers, or release systems, as it is labor intensive, time consuming, difficult to quantify, and only indirectly measures release of the active cargo. To address these problems we have developed a releasable luciferin conjugate as a representative (reporter) cargo, which allows measurement of conjugate uptake and cargo release in real time in luciferase-transfected cells and in transgenic animals through the emission of light, collectively emulating drug uptake, and intracellular release.

2. Materials

2.1. Synthesis of Conjugates

3-Mercapto-1-ethanol (Aldrich, St. Louis, MO).
3-Mercapto-1-propanol (Aldrich, St. Louis, MO).
3-Mercapto-1-butanol (Aldrich, St. Louis, MO).
2,2'-Dithiodipyridine (Aldrich, St. Louis, MO).
Methanol (Aldrich, St. Louis, MO).
Phosgene, toluene, pyridine (Aldrich, St. Louis, MO).
Potassium salt of D-luciferin (Xenogen, Alameda, CA).
Sodium hydroxide (Aldrich, St. Louis, MO).
Water.
Acylated D-cysteine D-octaarginine (peptide synthesis) (see Note 1).
Acylated D-cysteine D-tetraarginine (peptide synthesis).
Acylated D-cysteine D-tetralysine (peptide synthesis).

2.2. *In Vitro* Release of Luciferin from the Conjugates

Analytical HPLC Varian ProStar 210/215 HPLC using a preparative column (Alltec Alltima C18, 250×22 mm) or on an Agilent 1100 analytical HPLC with an analytical column (Vydak C18, 150×4.6 mm). The products were eluted utilizing a solvent gradient (solvent A=0.1% TFA/H₂O; solvent B=0.1% TFA/CH₃CN).

1-Naphthalenemethanol as an internal standard.
Potassium salt of luciferin (Xenogen Corp., Alameda, CA).
5 mM Magnesium sulfate.

HEPES-buffered saline (HBS; 150 mM NaCl, 20 mM HEPES) w/1 mM EDTA pH 7.4.

Firefly luciferase (Promega, Madison, WI).

DTT (Sigma, St. Louis, MO).

ATP (Sigma, St. Louis, MO).

Luminometer (Berthold detection systems, model: Sirius).

2.3. Cellular Uptake

PC3M-luc cells; an adherent prostate cancer cell line that stably expresses luciferase.

RPMI media with 10% fetal calf serum, glutamine, penicillin, and streptomycin (all available from Gibco, Grand Island, MI).

Polypropylene 96-well plates (Becton Dickinson, Franklin Lakes, NJ).

HBS pH 7.4 (20 mM HEPES, 150 mM NaCl).

High potassium HEPES solution pH 7.4 (20 mM HEPES, 150 mM KCl)

Luciferin conjugated to an D-arginine tetramer (r4).

Luciferin conjugated to an D-arginine octamer (r8).

Luciferin conjugated to an D-lysine tetramer (k4)

CCD camera with dark chamber, computer, and software (Living Image, Xenogen, Alameda, CA) for collecting bioluminescence from small animals (IVIS100; Xenogen, Alameda, CA) (see Note 2).

2.4. Topical Application

Transgenic reporter mice, FVB-luc+, where the transgene is comprised of a strong constitutive promoter (synthetic β -actin) and the coding sequence from firefly luciferase such that all cells of this animal express the luciferase reporter gene.

Nair.

Sodium acetate buffer pH 6.0 (Sigma, St. Louis, MO).

PEG 400 (Sigma, St. Louis, MO).

Isoflurane (Halocarbon, River Edge, NJ).

CCD camera with dark chamber, computer, and software (Living Image, Xenogen, Alameda, CA) for collecting bioluminescence from small animals (IVIS100; Xenogen, Alameda, CA).

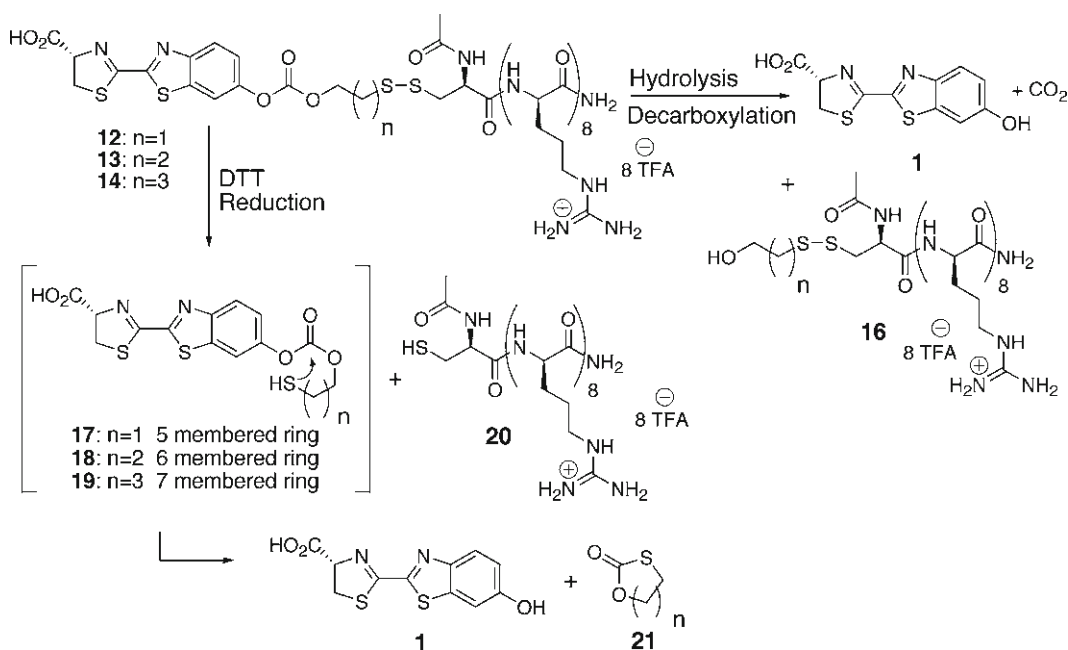
3. Methods

A major obstacle in implementing our strategy proved to be the synthetic difficulty of making luciferin conjugates. While luciferin itself has figured prominently as a research tool for decades, little is known about its modification and no information is available on its

1. In this route, the varying lengthed hydroxy thiols (3–5) are transformed with 2,2'-dithiopyridine to activated disulfides 2 (6–8).
2. Chloroformates are then formed by reaction of disulfide 6–8 in CH_2Cl_2 with a solution of phosgene in toluene (20%). Due to the limited solubility of D-luciferin (1) in organic solvents, and to avoid protecting groups, the organic solvent is removed in vacuo and the potassium salt of luciferin is added with aqueous base to the chloroformate to form, upon acidic workup, the carbonate 9–11.
3. This carbonate serves as a reagent for conjugation to a variety of transporters. The thiopyridyl moiety of 9–11 was displaced with acylated D-cysteine D-octaarginine ($\text{AcNHCr}_8\text{CONH}_2$) to give the transporter–linker conjugate 12–14. A tetraarginine (15) and a tetralysine conjugate also were synthesized in this manner. The avoidance of protecting groups in this sequence provides a flexible and step economical route to these densely functionalized transporter conjugates, which bodes well for the use of this system for the synthesis and study of other transporter–linker conjugates.

3.2. Assays Measuring the Release of Luciferin from the Oligoarginine Conjugates

Luciferin can be generated from the conjugates either by hydrolysis or reduction of the disulfide bond and subsequent cyclization (Scheme 3). To help interpret the intracellular mechanisms, the rates of the two processes were studied in vitro.



Scheme 3. Decomposition pathways of the luciferin conjugates.

3.2.1. Rate of the Hydrolysis and Decarboxylation of the Conjugates

1. Each of the conjugates (0.2 mg) were dissolved in 250 μ L HBS pH 7.4 in 1.5 mL microfuge tubes and incubated at 37°C containing 10 μ L of a solution of 10 mg of 1-naphthalenemethanol in 24 mL of methanol, which served as an internal standard.
2. At appropriate time points 20 μ L of the solutions were removed and analyzed by reverse phase HPLC.
3. The percent decomposition was calculated from the integrated peak areas of the conjugate, the internal standard, and the various decomposition products.

The half-lives of the conjugates differed significantly, ranging from 3 h for conjugate 12, to 11 h for conjugate 13, to 33 h for conjugate 14. The decomposition products were luciferin, alcohol 16, and CO₂ as expected from slow hydrolysis of the carbonate. The pattern of increasing stability correlates with the increasing distance between the carbonyl group and the proximate sulfur atom, suggesting a role for the latter in the hydrolysis step.

3.2.2. Release of Luciferin by Reduction and Cyclization of the Conjugates

1. Add varying concentrations (from 20 to 2,000 nM) of the potassium salt of luciferin (Xenogen Corp., Alameda, CA) in 50 mL of 5 mM MgSO₄, 200 mM NaCl, 20 mM HEPES, 1 mM EDTA pH 7.4 to 100 ng of firefly luciferase (Promega, Madison, WI) in 50 mL of the same buffer containing 1 mM DTT, 2 mM ATP to generate standard curves of luminescence.
2. Read the resulting luminescence as a function of time using a luminometer (Berthold Detection Systems, model: Sirius).
3. Add 50 mL of a 50-mM solution of conjugate 12 and 13 separately in 5 mM MgSO₄, 200 mM NaCl, 20 mM HEPES, 1 mM EDTA pH 7.4 to 100 ng of firefly luciferase in 50 mL of the same buffer containing 1 mM DTT, 2 mM ATP.
4. Measure the resultant luminescence as a function of time.

The luminescent signals observed when varying amounts of luciferin were added correlated with the relative amounts of substrate added (Fig. 1). The area under the luminescent curve was proportional to the amount of luciferin added. In contrast, there was a significant difference in light produced when the conjugates were analyzed (Fig. 2). Conjugate 13 generating only approximately 12% of the light generated by conjugate 12 (Fig. 2a). The difference was shown to be due to varying rates of release of luciferin because equivalent molar amounts of luciferin were released from each conjugate if they were preincubated with 1 mM DTT for 20 min prior to the addition of the enzyme. Under these conditions, the profile of luminescence was similar to that seen with purified luciferin (Fig. 1) and equivalent amounts of light was observed for both conjugates (Fig. 2b).

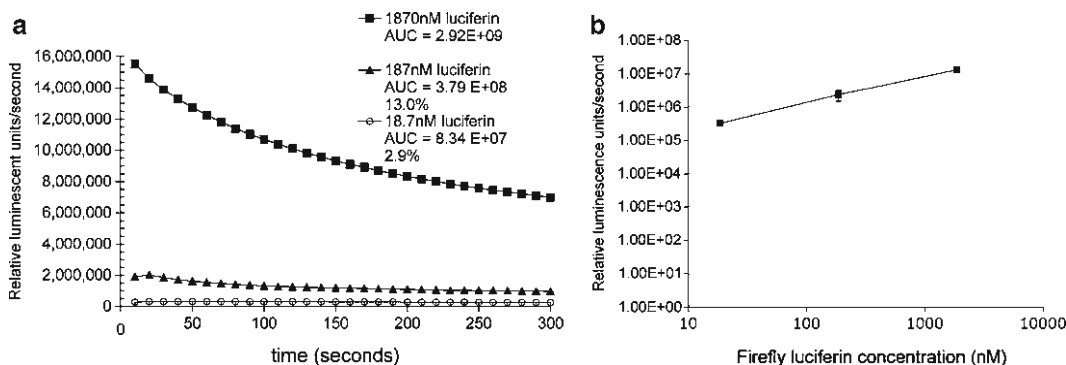


Fig. 1. Standard curves of luminescence resulting from the addition of known amount of luciferin to 100 ng of firefly luciferase in 5 mM MgSO_4 , 200 mM NaCl, 20 mM HEPES, 1 mM EDTA, 1 mM DTT, 2 mM ATP pH 7.4 (*left panel*); units for the integrated area under the curves (AUC) are photons. The percentiles represent normalized amounts of light to the highest dose of luciferin (*right panel*); a linear relationship was observed when the log of the concentration was plotted as a function of the log of the concentration of luciferin.

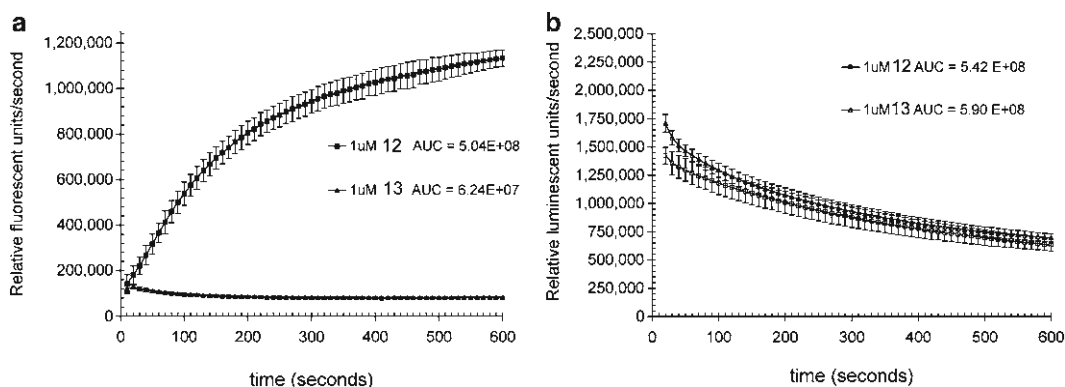


Fig. 2. Differential luminescence produced when r8 conjugates **12** and **13** were mixed with luciferase. Resultant luminescence when 1 mM solutions of r8 conjugates **12** and **13** were mixed with 100 ng of firefly luciferase in 5 mM MgSO_4 , 200 mM NaCl, 20 mM HEPES, 1 mM EDTA, 1 mM DTT, 2 mM ATP pH 7.4 (*panel a*). Units for the integrated area under the curves (AUC) are photons. If the two conjugates were reduced with 1 mM DTT for 20 min prior to exposure to firefly luciferase a profile of luminescence similar to that seen for luciferin was observed. Importantly, equivalent amount of light was produced for both conjugates (*panel b*).

3.3. Quantitative Analysis of Cellular Uptake of Luciferin Conjugate

The firefly luciferin/luciferase system is known to be extremely efficient and has been used in many assays to date (8). There are exquisitely sensitive cameras available that can measure the amount of light produced in both cell and animal assays (9). The concept for utilizing the luciferin/luciferase system to probe release is shown in Fig. 3.

Cellular studies were performed on PC3M-luc cells; an adherent prostate cancer cell line that stably expresses luciferase. Luciferin is capable of crossing cellular membranes, though it does so poorly. Consequently the cellular studies required a negative control to show definitively that the light observed is due to

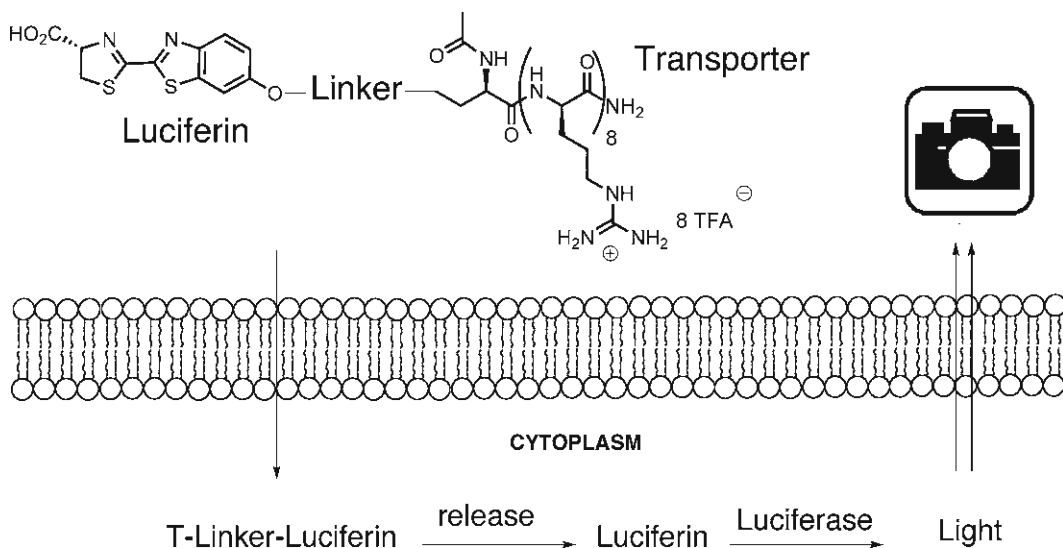


Fig. 3. Luciferin conjugate to probe the real-time release of cargo from a transporter.

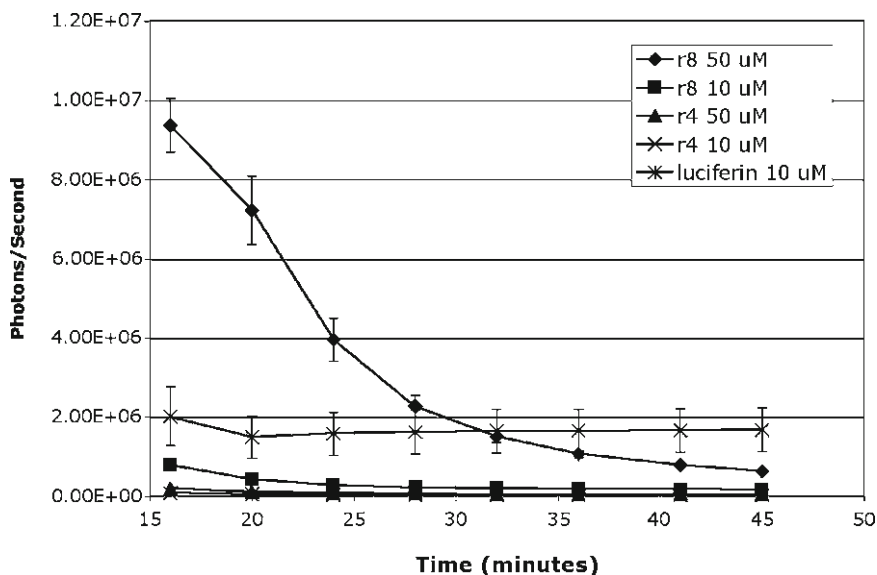


Fig. 4. Pulsed assay in PC3M-luc cells treated with r8 carbonate (12), the negative control, the r4 conjugate with the same linker (15), and luciferin (1). Cells were treated with 50 and 10 μM of the conjugates for 15 min in HBS, pH 7.4 then cells were washed and bioluminescence measured.

transport across the cellular membrane and intracellular release of luciferin and not extracellular decomposition. A tetramer of D-arginine, r4, known not to be able to cross biological membranes was used as a suitable negative control (Fig. 4). Though stability studies suggest that the compounds will be stable within the time period of the assays, a negative control provided additional support. We found that the best experimental system was

to pulse the cells with the conjugate for a short period of time and watch the appearance and disappearance of the bioluminescent signal. The amount of released luciferin was calculated by integrating the area under the curve.

3.3.1. Measurement of Bioluminescence After Pulsing Cells with Drug Conjugates

1. A prostate tumor cell line, stably transfected with luciferase, PC3M-luc, was plated at 60,000 cells per well in 96-well, flat bottomed plates 12 h prior to the assay.
2. The cells were incubated with varying concentrations of either the potassium salt of luciferin (Xenogen Corp., Alameda, CA) or conjugates 12 and 15, in triplicate, for 1 min, in HBS pH 7.4.
3. The cells were washed, resuspended with HBS, and the resultant luminescence was measured using a charged coupled device camera and analyzed using Living Image software (IVIS200, Xenogen, Corp., Alameda, CA) for a period of 45 min.

The r8 conjugate 12 exhibited very different behavior from the other compounds tested. Light levels were much higher and lasted longer, which could be due to the fact that the r8 transporter 12 more effectively enters cells than luciferin. If the bioluminescence of the r4 negative control 15 was subtracted from the r8 data, the resultant graph is shown in Fig. 5.

The data was fit to an exponential decay with an $R^2=0.97$ based on this the half-life was determined to be 6.9 min.

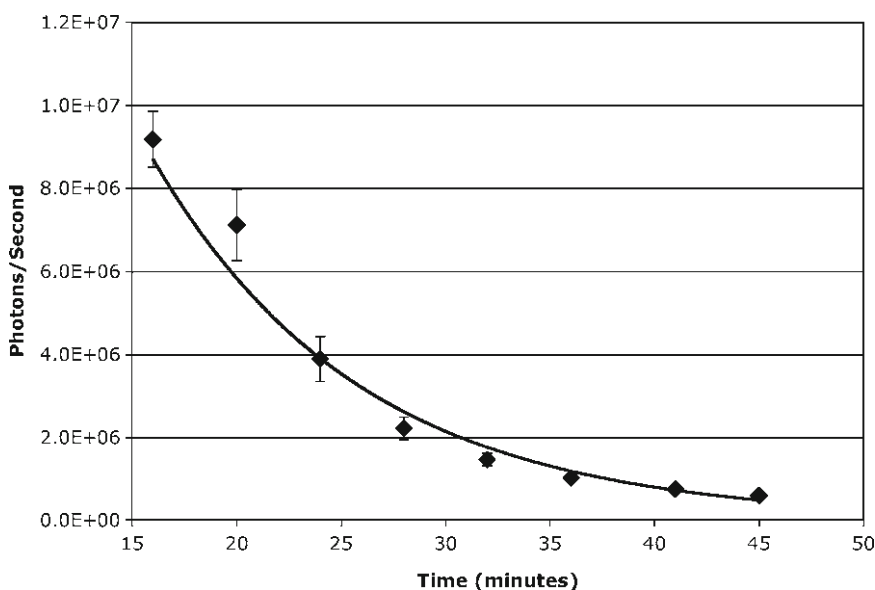


Fig. 5. The resultant curve when the light from cells treated with the r4 conjugate, 15, was subtracted from light generated from cells treated with the r8 conjugate 12.

3.3.2. Role of Membrane Potential in Cellular Uptake of Conjugates

Previous studies have established that the membrane potential of cells is an important factor in translocation of peptides containing oligoarginine across biological membranes (10, 11). A simple method to lower the membrane potential from cells is to increase the extracellular concentration of potassium. Using this method the role of the membrane potential in this system can be tested.

1. Prepare 1 L of “High potassium-buffered HEPES” by replacing the 0.15 M sodium chloride in HBS, with equimolar amount of the potassium chloride. Adjust pH to 7.4.
2. Plate PC3M-luc cells at 60,000 cells per well in 96-well, flat-bottomed plates 12 h prior to the assay.
3. Add conjugates 13 and 14 at 15 μM , and luciferin (1) at 25 μM , dissolved in either HBS or K⁺ HBS, pH 7.4.
4. Allow conjugates and luciferin to incubate with cells for 1 min, after which the plates were spun at 1,000 cpm for 2 min, the supernatants were removed by aspiration, 100 μL of fresh RPMI was added, and the resultant bioluminescence was measured over time with the IVIS camera and analyzed using Living Image software (see Note 2).

The luminescent signal from cells pulsed with conjugate 13, which is a measure of the intracellular release of free luciferin and its turnover by intracellular luciferase, increased slightly in the first few seconds and gradually decayed, reaching background after approximately 1,000 s (Fig. 6a). Cells treated with conjugate 14 at the same concentration generated a different curve with less initial light, a slower rate of decay, and only two-thirds of the total photons were produced when compared to that seen for conjugate 13 (Fig. 6a). The observed luminescence was shown to be due to intracellular release of luciferin and its reaction with luciferase and not extracellular hydrolysis of the conjugate and luciferin uptake by the fact that when the experiment was repeated in K⁺ HBS very little bioluminescence was observed. The total number of photons observed and therefore the total amount of luciferin delivered can be calculated by integrating the area under the curve for each compound (Fig. 6b). Under high potassium conditions, luminescence from the conjugate (and therefore uptake and release) was reduced by >>90% whereas luminescence from luciferin itself increased slightly. Consequently, the vast majority of the light arises from conjugate uptake into the cells and subsequent release of luciferin.

3.4. Quantitative Measurement of Uptake and Release of Luciferin Conjugates After Topical Application to Transgenic Mice

The quantification of the uptake of a transporter–linker–luciferin conjugate and release of luciferin, *in vivo*, was accomplished in transgenic reporter mice, FVB-luc+, where the expression of the coding sequence from firefly luciferase is controlled by the strong constitutive actin promoter. Consequently, all cells of this animal express the luciferase reporter gene (12).

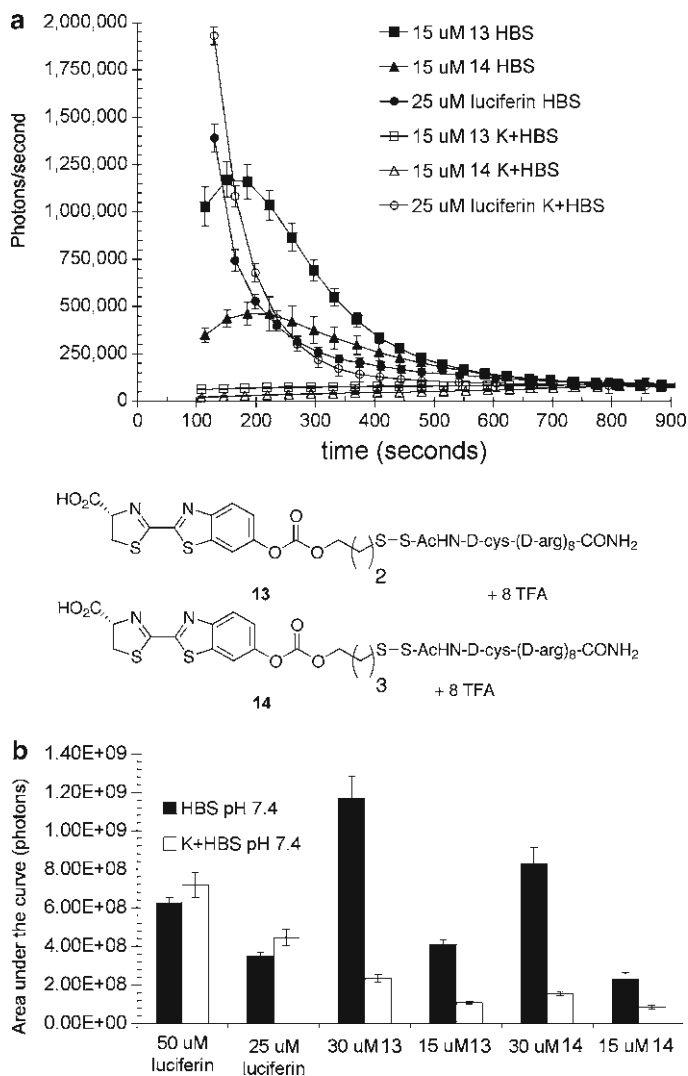


Fig. 6. Pulsed assay in PC3M-luc cells treated with compounds **13**, **14**, and luciferin (**1**) with, and without, high potassium buffer. (a) Observed bioluminescence as a function of time. (b) The integrated area under each of the curves, which represents total number of photons emitted in 900 s.

3.4.1. Calibration with Intradermal Injection of Luciferin

The initial experiment is designed to establish the amount of free luciferin needed for signal detection from the skin of FVB-luc+ mice and whether, or not, the signal was dose dependent.

1. Anesthetize the mice with isoflurane.
2. Shave the animals with hair clippers, and then apply the depilatory Nair™ to the flank of the animal for 3 min, after which the fur is wiped off using a damp paper towel (see Note 3).
3. Allow the animals to recover a minimum of 5 days, which allows reformation of the stratum corneum (see Note 4).

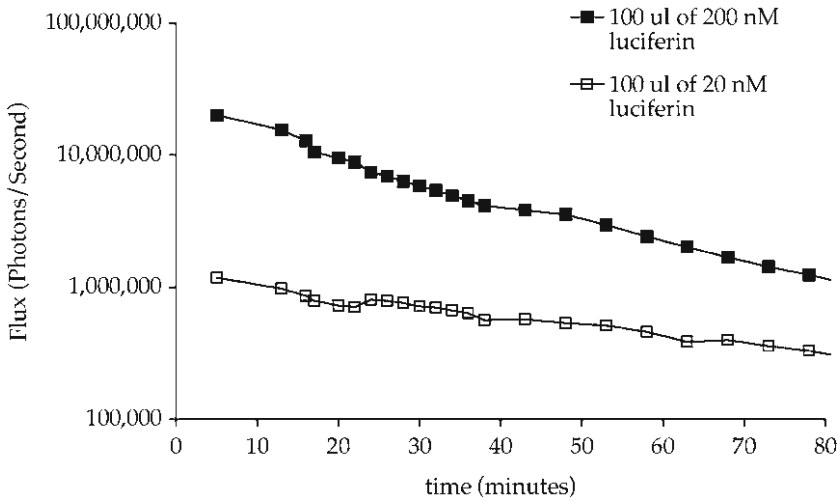


Fig. 7. Intradermal injection of luciferin. Resultant bioluminescence after intradermal injection of 20 and 200 nM luciferin (1) in HBS pH 7.4 (100 μ L) into transgenic (FVB-luc+) mice.

4. Inject 100 μ L of 20 and 200 nM luciferin solutions in HBS, intradermally into the flanks of mice using a 1-mL syringe and 25-gauge needle.
5. Place the animals in the cavity of the IVAX instrument and measure the resulting bioluminescence signal (photons/unit time) from the region of interest (ROI) was measured (Fig. 7).
6. Inject a second set of animals with 200 μ L of a 200-nM solution of r8 conjugate 13.
7. Place the animals in the cavity of the IVAX instrument and measure the resulting bioluminescence signal (photons/unit time) from the ROI was measured (Fig. 8).

The pattern of luminescence as a function of time was reproducible and similar for both doses, with a steady post-injection decrease in light emission over the duration of measurement. The total number of photons emitted was calculated by integrating the area under the curve. For the 200 nM dose the area under the curve was found to be 3.02×10^{10} photons, while for 20 nM was 3.11×10^9 photons. The tenfold higher dose was almost exactly ten times that of the lower dose, indicating at these concentrations a linear reproducible response to dose. Based on the known amount of luciferin injected and the observed luminescence, one photon of light is detected by the camera for every 400 molecules of luciferin injected. The difference between the amount of luciferin injected and of photons detected is in part a reflection of the amount of injected luciferin that has access to the intracellular enzyme, the uniformity of luciferase expression in different cell types, the number of luciferin molecules turned over by luciferase,

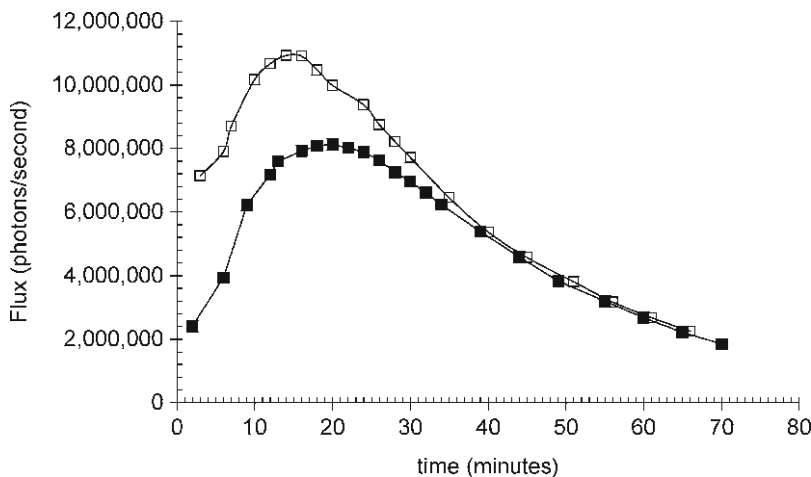


Fig. 8. Resultant bioluminescence after intradermal injection of 100 μ L of 200 nM r8-luciferin carbonate, **13** pH 7.4 into luciferase transgenic (FVB-luc+) mice. Experimental variation is shown for two different animals.

the quantum efficiency of the enzyme, and the absorption and scattering of the signal by mammalian tissues. The photon flux thus represents a minimum but reproducibly quantifiable measure of uptake and release.

For topical applications, the conjugate would pass from the administration vehicle across the stratum corneum of the skin and the plasma membrane of cells, at which point it would be cleaved and the released luciferin converted by luciferase to oxyluciferin and light. To determine the number of photons produced from a known amount of the conjugate independent of transporter-mediated skin entry, the luciferin conjugate **13** was injected intradermally as described above for free luciferin (Fig. 8).

As expected from the effect of the transporter and the requirement for intracellular release, intradermal injection of conjugate **13** generated a distinctly different temporal pattern of bioluminescence relative to that observed for free luciferin. As seen in cellular assays, significant signal is apparent immediately after injection, increases for the next 20 min and then slowly decays over the next 50 min. The profile is consistent with the time-dependent generation and depletion of luciferin upon cellular uptake and linker cleavage. Approximately 80% of the theoretical amount of luciferin in the injected sample of conjugate **13** was accounted for when the total number of photons emitted in 60 min (the area under the curve) was multiplied by the previously calculated number of 400 molecules of luciferin per photon detected.

3.4.2. Topical Application

1. Anesthetize the mice with isofluorane.
2. Shave the animals with hair clippers, and then apply the depilatory Nair™ to the flank of the animal for 3 min, after which the fur is wiped off using a damp paper towel.

3. Allow the animals to recover a minimum of 5 days, which allows reformation of the stratum corneum.
4. Place 15 μL of a 5.5-mM solution of r8 conjugates, 13 and 14 in 25% 200 mM NaOAc pH 6.0, 75% PEG 400 on the naked flank of the transgenic mice. Buffering of the solution is critical because a 5-mM solution of the trifluoroacetate salts of octa-D-arginine luciferin conjugates has a pH close to 2.0. Acidification of the tissue greatly inhibits the appearance of the bioluminescence.
5. Place the animals in the cavity of the IVAX instrument and measure the resulting bioluminescence signal (photons/unit time) from the ROI was measured (Fig. 9).
6. Titrate uptake by placing 15 μL of r8 conjugate 13 (0.5, 2.0, 3.0, 4.0, and 4.5 mM) in 75% PEG 400/25% 200 mM NaOAc pH=6.0 on the naked flank of the transgenic mice.

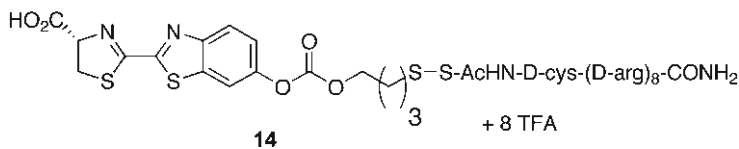
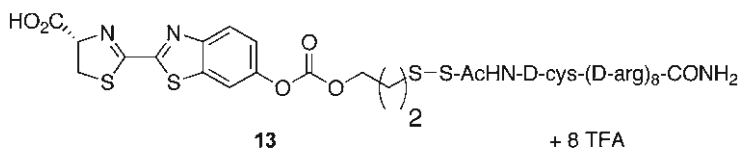
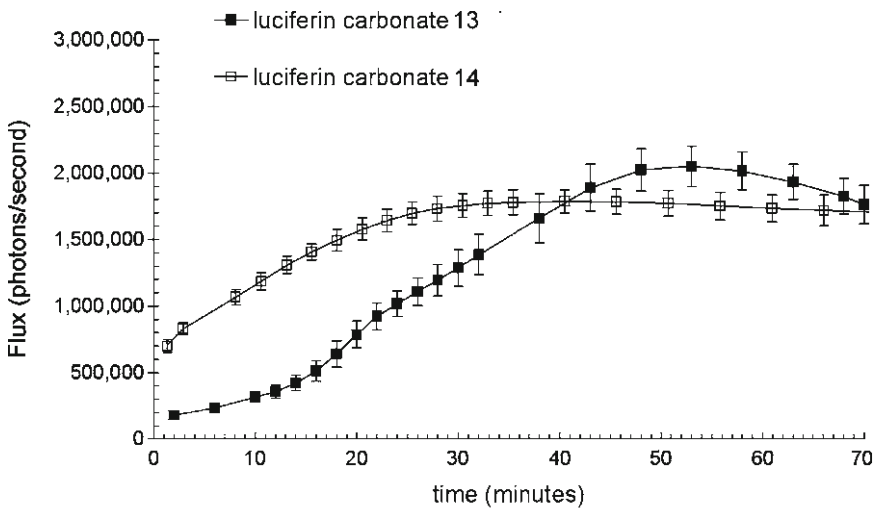


Fig. 9. Topical application of conjugates **13** and **14**. Observed bioluminescence from luciferase transgenic mice as a function of time after topical application of 15 μL of 5 mM conjugates in 75% PEG 400/25% 200 mM NaOAc, pH 6.0.

7. Establish that the observed bioluminescence was solely from luciferin released within the tissue by placing 15 μL of a 5.5-mM solution of D-tetralysine conjugate, 22, in 25% 200 mM NaOAc pH 6.0, 75% PEG 400 on the naked flank of the transgenic mice.

As is shown in Fig. 9, both conjugates generated a strong and reproducible luminescence signal. The difference between this signal and the amount of conjugate entering skin would collectively represent the non-productive fates of the conjugate (e.g., incomplete uptake, incomplete cleavage, clearance from the skin, metabolism). As determined by the intradermal injection of free luciferin, every 400 molecules of luciferin results in one detectable photon. Therefore, the total amount of luciferin released in 1 h can be determined by multiplying the area under the curve by 400 molecules/detected photon. Dividing by Avogadro's number indicates that the amount of luciferin released is 3.62×10^{-12} mol for conjugate 13 and 2.0×10^{-11} mol for conjugate 14. From the area of application and the thickness of mouse skin (0.69 mm), the cumulative local concentrations resulting from skin exposure followed by measurement over 1 h are 47 and 62 nM, respectively. The amount of light generated is in linear proportion with the amount of conjugate applied within the range of 0.5–4.5 mM as shown in Fig. 10, and a concentration as high as 299 nM was obtained.

To determine whether release of luciferin might occur during administration and contact with the skin surface it was necessary to show that the light observed was solely due to transport and intracellular release vs. decomposition and release of extracellular luciferin. Toward this end, after each exposure period the material remaining on the skin was removed from the mouse by washing

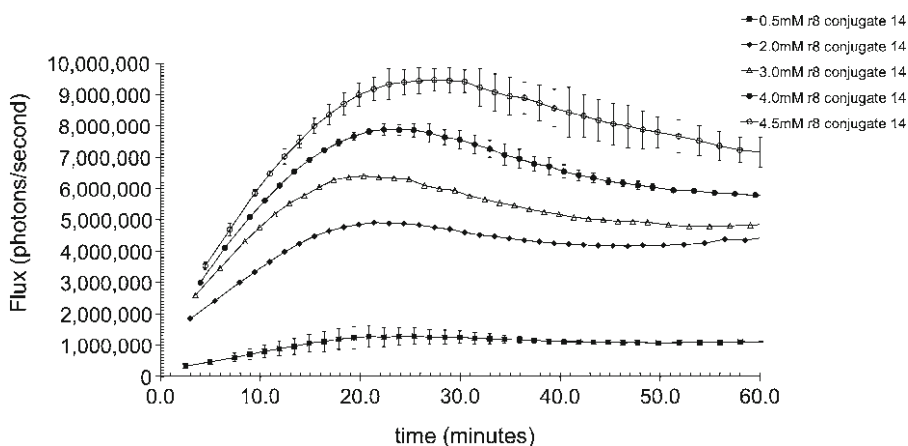


Fig. 10. Dose–response of topical application of varying concentrations of r8 conjugate 14. Total number of photons observed from luciferase transgenic mice as a function of time after topical application of 15 μL of the r8 conjugate 14 (0.5, 2.0, 3.0, 4.0, and 4.5 mM) in 75% PEG 400/25% 200 mM NaOAc, pH 6.0.

and analyzed by analytical HPLC to detect any free luciferin in the wash. In each assay shown there was no free luciferin observed as would be expected from our stability assays. Another control was to test a conjugate that is composed of an inefficient transporter with the exact same releasable linker and luciferin cargo. Lysine tetramers are known to be poor transporters for skin entry. Therefore a luciferin conjugate of a lysine tetramer **22** was synthesized and tested. When this less effective transporter conjugate **22** is compared to the corresponding r8 conjugate **14** as is shown in Fig. 11 there is much less light, thus establishing that luminescence results primarily from the intracellular release and not external hydrolysis of the prodrug.

As the field of transporter-mediated drug and probe delivery moves forward, quantification of the comparative performance of existing and new transporters will have increasing importance in the selection of preferred systems for therapeutic, diagnostic, or imaging purposes. Methods that allow for quantification of transporter uptake into both cells and animals and especially temporal tissue distribution are needed. In addition, for many conjugates, release of free cargo is required and thus real-time release must also be evaluated in intact animals.

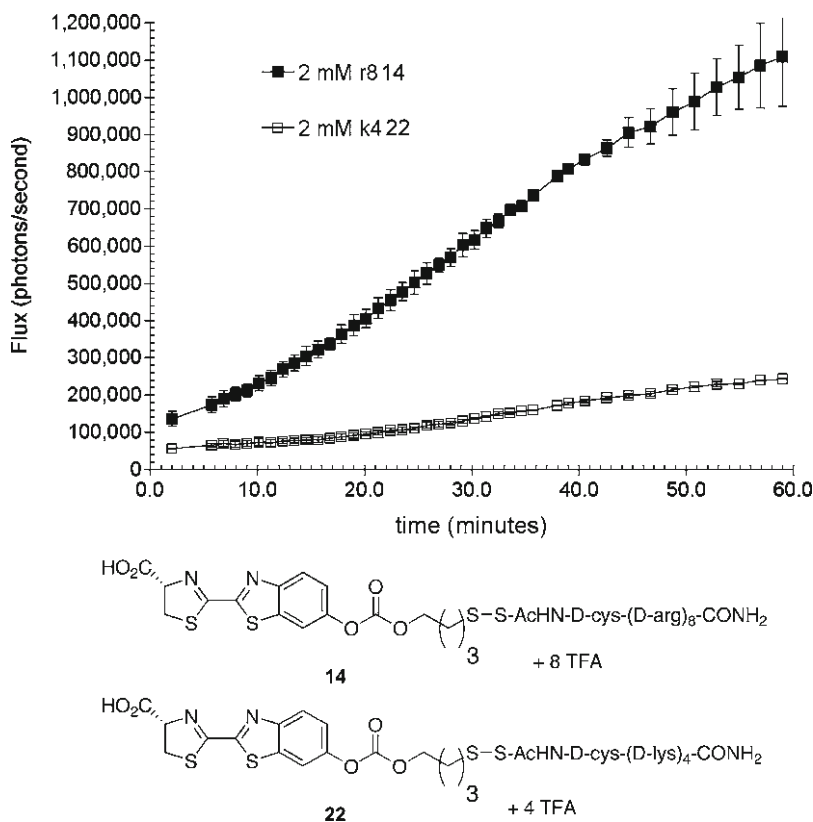


Fig. 11. Observed bioluminescence from luciferase transgenic mice as a function of time after topical application of 15 μ L of 2 mM solutions of the r8 conjugate **14** and the k4 conjugate **22** in 75% PEG 400/25% 200 mM NaOAc, pH 6.0.

4. Notes

1. The octaarginine peptides are hygroscopic and should be stored in a desiccator.
2. For more information on the CCD camera system, please go to the following link: <http://www.caliperls.com/products/optical-imaging/>
3. The hair clippers were purchased from a barber supply company. Animals were shaved carefully on both flanks and stomach. Nair was applied as per the directions on the product and left for no more than 3 min. If hair remained, reapply Nair and rewipe area. Care must be taken to remove all the Nair to minimize inflammation.
4. We measured uptake of luciferin on the skin each day for 5 days. As the stratum corneum barrier reformed, the uptake of the free drug was diminished.

Acknowledgments

This work was done in collaboration with Drs. Paul Wender, Christopher Contag, Rajeshe Shinde, Thomas Pillow, and Elena Goun in the Departments of Chemistry, Chemical Systems Biology, and Pediatrics at Stanford University, Stanford California.

References

1. Rothbard, J., Garlington, S., Lin, Q., Kirschberg, T., Kreider, E., McGrane, P., Wender, P., Khavari, P. (2000) Conjugation of arginine oligomers to cyclosporin A facilitates topical delivery and inhibition of inflammation. *Nat. Med.*, **6**, 1253–1257.
2. Kirschberg, T., VanDeusen, C., Rothbard, J., Yang, M., Wender, P. (2003) Arginine-based molecular transporters: the synthesis and chemical evaluation of releasable taxol-transporter conjugates. *Org. Lett.*, **5**, 3459–3462.
3. Samuel, B., Hearn, B., Mack, D., Wender, P., Rothbard, J., Kirisits, M., Mui, E., Wernimont, S., Roberts, C., Muench, S., Rice, D., Prigge, S., Law, A., McLeod, R. (2003) Delivery of antimicrobials into parasites. *Proc. Natl. Acad. Sci. USA*, **100**, 14281–14286.
4. Chen, L., Wright, L., Chen, C., Oliver, S., Wender, P., Mochly-Rosen, D. (2001) Molecular transporters for peptides: delivery of a cardioprotective epsilon PKC agonist peptide into cells and intact ischemic heart using a transport system, R(7). *Chem. Biol.*, **8**, 1123–1129.
5. Kim, D., Mitchell, D., Brockstedt, D., Fong, L., Nolan, G., Fathman, C., Engleman, E., Rothbard, J. (1997) Introduction of soluble proteins into the MHC class I pathway by conjugation to an HIV tat peptide. *J. Immunol.*, **159**, 1666–1668.
6. Robbins, P., Oliver, S., Sheu, S., Goodnough, J., Wender, P., Khavari, P. (2002) Peptide delivery to tissues via reversibly linked protein transduction sequences. *Biotechniques*, **33**, 190–192.
7. Siphraashvili, Z., Scholl, F., Oliver, S., Adams, A., Contag, C., Wender, P., Khavari, P. (2003) Gene transfer via reversible plasmid condensation with cysteine-flanked, internally spaced

- arginine-rich peptides. *Hum. Gene Ther.*, **14**, 1225–1233.
8. Greer, L., Szalay, A. (2002) Imaging of light emission from the expression of luciferases in living cells and organisms: a review. *Luminescence*, **17**, 43–74.
 9. Contag, C.H., Bachmann, M.H. (2002) Advances in in vivo bioluminescence imaging of gene expression. *Annu. Rev. Biomed. Eng.*, **4**, 235–260.
 10. Rothbard, J.B., Jessop, T.C., Lewis, R.S., Murray, B.A., Wender, P.A. (2004) Role of membrane potential and hydrogen bonding in the mechanism of translocation of guanidinium-rich peptides into cells. *J. Am. Chem. Soc.*, **126**, 9506–9507.
 11. Rothbard, J.B., Jessop, T.C., Wender, P.A. (2005) Adaptive translocation: the role of hydrogen bonding and membrane potential in the uptake of guanidinium-rich transporters into cells. *Adv. Drug Deliv. Rev.*, **57**, 495–504.
 12. Cao, Y.A., Wagers, A.J., Beilhack, A., Dusich, J., Bachmann, M., Negrin, R., Weismann, I., Contag, C. (2004) Shifting foci of hematopoiesis during reconstitution from single stem cells. *Proc. Natl. Acad. Sci., USA* **101**, 221–226.

Industrial-Scale Manufacturing of a Possible Oligonucleotide Cargo CPP-Based Drug

Ulf Tedebark, Anthony Scozzari, Oleg Werbitzky, Daniel Capaldi, and Lars Holmberg

Abstract

This chapter describes the manufacturing process to a certain level for a possible oligonucleotide cargo and a peptide API in a multi-kilogram scale from a manufacture's point of view. In the concluding remarks, possible conjugation methods will be discussed from an industrial-scale perspective.

Key words: Industrial scale, Oligonucleotide, siRNA, Phosphorothioate, Peptide, CPP, Conjugate, Manufacturing, Solid-phase peptide synthesis (SPPS), Fmoc/tBu strategy, HPLC peptide and oligonucleotide purification, Peptide and oligonucleotide isolation

1. Introduction

1.1. CPP and Oligonucleotide Conjugation: An Overview

Development of an efficient delivery system including targeting is one of the major obstacles to turn a therapeutically interesting oligonucleotide into a clinically acceptable drug.

Using oligonucleotides (aptamers) rather than small molecules or protein drugs to target proteins is more advantageous due to higher specificity and broader therapeutic potential.

Free oligonucleotides are rapidly degraded in the blood by serum nucleases if injected intravenously (1). Modifications of oligonucleotides to first-, second- and/or third generation (2, 3) improve the susceptibility to nuclease degradation leaving size and negative charge as an obstacle to readily enter cells. Various modifications like first- to third generation together with compacting and protecting the oligonucleotide using a viral or a non-viral vector are possible routes for oligonucleotide delivery (4).

Viral vectors as, for example, retro- and adenoviruses were initially researched as they possess high DNA and RNA delivery efficiency to several cell lines (5). Non-viral vectors exhibiting lower toxicity and/or immunogenicity than viral, and the possibility to be scaled-up, has therefore gained increased attention even though non-viral delivery shows lower transfection efficiency of oligonucleotides.

Antisense oligonucleotides or short-interfering RNA, siRNA, are possible components for conjugate formation together with a cell-penetrating peptide (CPP) or other types of non-viral or viral carriers (6). The conjugating component's main purpose is firstly to compact and protect the oligonucleotide towards degradation and secondly to facilitate transport into the interior of the cell/tissue. As one of several possible cargoes to CPP, various oligonucleotides have successfully been evaluated for targeted cell or tissue delivery, both *in vitro* and *in vivo* (5). The peptide and oligonucleotide conjugate could either be linked covalently reversible e.g. disulfide or irreversible i.e. thioether, or by electrostatic interactions, taking advantage of the positively charged CPP and the negatively charged phosphate backbone of the oligonucleotide. Oligonucleotides can also be complexed with various non-peptidic cationic compounds, discussed elsewhere (7). The main purpose of the selected cationic compound is to provide charge neutralisation, compaction of the oligonucleotide, and to provide cell-penetrating properties, preferably and if possible, cell or tissue specificity. Increased specific cellular uptake by targeted delivery can be accomplished by including a cell receptor membrane or tissue-specific ligand like homing peptides, aptamers, antibodies, or surface carbohydrates.

Developing an oligonucleotide CPP-based drug will require a facility designed for GMP production of peptides and oligonucleotides in a multi-kilogram scale.

In the following sections, processes for manufacturing an oligonucleotide and a peptide in larger scales will be described by two of the major companies in their respective field, Isis Pharmaceuticals and Lonza AG.

1.2. Oligonucleotide Manufacturing Methods

All current large-scale oligonucleotide synthesis methods efforts utilise the basic four-step solid-phase phosphoramidite approach that was first described 25 years ago by Beaucage and Caruthers (8). The fact that the core chemistry remains essentially unchanged for greater than two decades is evident of the inherent simplicity, efficiency, and ruggedness of the approach. While no significant route improvement has occurred, advances in reagent, solid support, synthesiser design, purification, and isolation technologies have transformed the field so that the manufacture of several hundred kilogram quantities of modified DNA and RNA at reasonable cost is now a reality.

1.3. Industrial Chemical Synthesis of Peptides via Solid Phase in Fmoc/tBu Strategy

Solid-phase peptide synthesis is the sequential construction of a peptide chain linked to a solid support (resin). From today's perspective the easiest, most generic, and scalable approach for the synthesis of a 10–40 amino acid long peptide is the chemical solid-phase synthesis in Fmoc/tBu strategy (see Note 1). During the last decade the great potential of this technology has been successfully demonstrated in numerous large and industrial-scale applications (9–11). The elongation of the desired peptide chain starts with the covalent attachment of the α -N and side-chain protected C-terminal amino acids to the solid support (initial loading), then each of the following amino acids are attached to the growing chain one after the other, applying a sequence of two reactions: (1) cleavage of the α -N protecting group from the product on the solid support; (2) coupling the next protected amino acid to the product on the solid support. Depending on the type of linker on the SPPS resin, the process can either lead to peptides with a carboxyl group at the C-terminus (e.g. with a 2-CTC resin), or to peptide amides, if a resin with a peptide amide linker is utilised (e.g. Sieber linker resin). Characterised by milder reaction conditions in general, SPPS in Fmoc/tBu strategy provides a number of further advantages (see Note 2).

After the finalisation of the SPPS elongation, the peptide is cleaved from the solid support. Depending on the cleavage conditions, this step could either lead to the corresponding protected peptide, bearing the side-chain protecting groups, or to the fully deprotected crude peptide. The protected peptide can be used as an intermediate for additional chemical modifications or directly undergo a cleavage of the side-chain protecting groups to lead to the crude peptide.

The quality of the crude peptides in terms of overall purity and number and amounts of single impurities is mostly not sufficient, making an additional purification necessary. For this important step, preparative HPLC chromatography is presently the method of choice. It is easily scalable and allows to consistently obtain the desired product in high quality (e.g. >98% purity) and good yields.

In order to finally obtain the purified peptide as a solid, the product must generally be isolated out of a solution in organic solvent (e.g. acetonitrile) and aqueous buffers. The standard procedure here is the following: (1) Removal of the organic solvent (e.g. via distillation); (2) Lyophilisation of the residual aqueous product solution (see Note 3).

The term peptide is used here to describe a broad class of compounds, which can be very different not only in length and complexity, but also in their chemical and physical properties. Hence, it can be expected that a single generic process will never be optimal for each of these compounds. However, the process outlined below should be a good starting point for a potential industrial process and generally deliver initial amounts of the desired product in acceptable quality and yield. Considering the number of chemical

reactions and unit operations, it is obvious, that the development of an optimal SPPS process for a specific peptide could require substantial additional efforts and the need to deeply investigate different parts of the process and in particular the chemistry.

2. Materials

2.1. Oligonucleotide Chemical Synthesis

Nucleoside phosphoramidites [0.2 M in anhydrous acetonitrile (MeCN) under Ar].

4,5-Dicyanoimidazole (DCI, 1.0 M in anhydrous MeCN) (12).

Phenylacetyl disulfide [PADS, 0.2 M in anhydrous MeCN and 3-picoline (1:1 v/v)] (13).

Dichloroacetic acid (10% v/v solution in toluene) (14).

Capping A solution [acetic anhydride, pyridine, and MeCN (1:1:3 v/v/v)].

Capping B solution [*N*-methylimidazole and MeCN: (1:4 v/v)].

UnyLinker-loaded solid support (e.g. GE Primer Support™ 200) (15).

Triethylamine (TEA).

Anhydrous MeCN (water content <50 ppm).

Toluene.

3-Picoline.

2.1.1. Reverse Phase Purification

Methanol.

Purified water.

Sodium acetate.

2.1.2. Final Deprotection and Isolation

Ethanol.

Acetic acid.

Sodium hydroxide.

2.2. Solid-Phase Peptide Synthesis

2.2.1. Solid Supports

A solid support for SPPS consists of a polymeric particle bearing a reactive linker moiety for the attachment of the growing peptide chain to the solid support. Most of the large-scale solid supports used today are based on micro-porous (cross-linked with 1% divinylbenzene) polystyrene beads. These matrixes are relatively inexpensive to produce and easy to functionalise with the desired linker. The beads swell well in the solvents used for peptide synthesis, and should therefore preferably be used in batchwise reactors. A number of different solid supports for peptide synthesis in Fmoc/tBu strategy are commercially available; the following two types of supports belong to the group of super acid-labile SPPS resins and are broadly utilised for laboratory and large-scale synthesis:

1. 2-Chlorotriyl chloride resins (2-CTC resin) (CBL Patras, Greece), this resin is used for the preparation of peptides with an unmodified carboxy terminus. The support is commercial available as pre-loaded resin with different amino acids and at different loadings (see Note 4).
2. Fmoc Sieber linker resin (PL-Sieber resin, Polymer Laboratories, UK, now part of Varian), this resin bearing a xanthenyl-based linker may also be cleaved with low concentrations of TFA (1–5%). It leads to products with a peptide amide functionality at the C-terminal end. This resin does not need to be loaded with the first amino acid in a separate step, it can directly be used, starting the elongation with a Fmoc-deprotection step.

An important parameter to consider during the selection of a resin is the initial loading (level of functionality). In principle, a higher loading has the advantage to increase the volumetric yield of the process. However, for each peptide, due to its specific steric hindrance, and therefore also depending on its length, there is a maximal loading, at which an SPPS process still running smoothly and consistently delivers a product of good quality. As a rule of thumb, for peptides of 15–20 amino acids, a loading in the range of 0.4 mmol/g generally works well. For shorter peptides of ten amino acids, a higher loading of 0.7–0.9 mmol/g can be used. For peptides >20 amino acids, a convergent strategy should be contemplated.

2.2.2. Solvents

1. *Peptide elongation*: Polar solvents or solvent mixtures are used. Typical solvents for the coupling step are *N*-methylpyrrolidone (NMP), *N,N*-dimethyl formamide (DMF) or mixtures of NMP or DMF with dichloromethane (DCM). For the Fmoc-deprotection step a solution of piperidine in either neat NMP or DMF is used (see Note 5). All these solvents are available from different laboratory chemicals suppliers (e.g. Sigma-Aldrich) (see Note 6).
2. *Cleavage and deprotection*: These reactions are typically performed by acidic mixtures in DCM. Methyl *t*-butyl ether (MTBE) is available from different laboratory chemicals suppliers (e.g. Sigma-Aldrich).
3. *Chromatography* is commonly performed using gradients of acetonitrile (ACN) with aqueous buffers. HPLC grade ACN should be used (e.g. from Romil, UK) (see Note 7). For the preparation of the chromatography buffers purified water quality is recommended.

2.2.3. Reagents

1. *Fmoc-protected amino acids*: Today all natural amino acids are available in Fmoc-protected form at laboratory (e.g. Novabiochem, Switzerland, Iris Biotech, Germany) and industrial scale (e.g. CBL Patras, Greece; Genzyme

Switzerland; Flamma, Italy). Standard side-chain protecting groups are tBu (Asp, Glu, Ser, Thr, Tyr); Boc (Lys, Trp); Trt (Asn, Gln, His, Cys); and Pbf (Arg) (see Note 8). The quality of these building blocks has a direct impact on the quality of the synthesis, in particular a high optical purity (e.g. an ee >99%) is essential; however, single impurities can also be important.

2. Elongation:

- a. *Coupling reagents*: a large number of coupling reagents, including HOBt (a less explosive alternative is Oxyma (16)), HBTU, DIPCDI are available from different laboratory chemical suppliers (e.g. Iris Biotech, Germany; Novabiochem, Switzerland).
 - b. DIEA (Hünigs base) is available from laboratory chemical suppliers (e.g. Sigma-Aldrich).
3. *Fmoc-deprotection*: Piperidine is available from laboratory chemical suppliers (e.g. Sigma-Aldrich). Generally for Fmoc-deprotection a 20% (v/v) mixture of piperidine in either DMF or NMP is used.
 4. *Cleavage, side-chain deprotection*: Trifluoroacetic acid (TFA), pyridine, and scavengers, like triisopropylsilane (TIS) and others are available from laboratory chemical suppliers (e.g. Sigma-Aldrich).
 5. *Colour tests*: Ninhydrin, chloranil, KCN, acetone, phenol, and ethanol can all be obtained from laboratory chemical suppliers (e.g. Sigma-Aldrich). For the ninhydrin test, it is recommended to use freshly distilled pyridine.

2.2.4. HPLC Resin and Columns

To achieve a high purity (e.g. >95%) of the target peptide, HPLC chromatography is generally necessary. Depending on the size and hydrophobicity of the desired peptide, a silica-based C18 or C8 or C4 packing (e.g. Kromasil C18, EKA Chemicals, Sweden) is generally suitable (see Note 9). Pre-packed preparative columns in different sizes can be ordered directly from the resin manufacturers or from chromatography materials suppliers.

2.2.5. Reactor for SPPS

Today a number of automated peptide synthesisers for lab-scale synthesis are commercialised on the market. Most of these instruments can be efficiently used for the preparation of samples using generic synthesis conditions. However, these instruments have a low flexibility with regards to the variation of the synthesis scale and reaction conditions (temperature control, modes of addition of reagents). Quite often, the mixing intensity in these instruments is also not optimal. A good alternative are simple systems for manual or semi-automatic synthesis built on the basis of cylindrical fritted reaction vessels, comprising an outlet valve at the

bottom of the reactor. To ensure practical filtration times and a good mixing, a 250 ml laboratory reactor could have a diameter of 6–7 cm, and a sintered glass filter frit with a G3 porosity. Such a reactor can be easily equipped with a cooling/heating jacket, an adequate mechanical stirrer – to ensure mild, but efficient mixing – and a corresponding number of necks or ports, for the addition of solid and liquid reagents and nitrogen gas. For the acceleration of the filtration steps, vacuum can be applied to the outlet on the bottom of the reactor. SPPS processes in reactors of this type have been successfully scaled-up to >1 L scale in glass reactors in the lab, or even >1,000 L scale using stainless steel reactors in plants.

2.2.6. Other Reactors and Devices

1. *Cleavage of the protected peptide from the resin* can be performed in the SPPS reactor.
2. *Reactors for global side-chain deprotection, isolation of the protected, and the crude peptide, concentration of crude peptide fractions.* All these reactions and work-up steps can be performed in standard laboratory glassware for organic chemistry: magnetically or mechanically stirred flasks for reaction and precipitation steps. Rotavap for concentration, glass filter frits for isolation, vacuum oven for drying.
3. *HPLC unit for purification:* A standard preparative laboratory HPLC skid with UV detector and fraction collector can be used (e.g. ÄKTA Explorer, GE Healthcare).
4. *Lyophiliser:* A standard laboratory flask lyophiliser (e.g. Christ, Germany) can be used.

3. Methods

3.1. Overview of Oligonucleotide Synthetic Process

The manufacture of phosphorothioate oligonucleotides is a multi-step process consisting of reagent preparation, solid-phase synthesis using a computer-controlled synthesiser, cleavage, and deprotection steps. The process is outlined in Fig. 1

The flow chart describes the process of making a batch of drug substance from a single synthesis run. Sometimes, however, a single batch of drug substance is composed of the products of more than one solid-phase synthesis.

3.1.1. Oligonucleotide Chemical Synthesis

During the chemical synthesis, phosphoramidite monomers are sequentially coupled to an elongating oligonucleotide that is covalently bound to a solid support. Each elongation cycle consists of the following four steps:

1. Detritylation (removal of a 5'-hydroxyl protecting group with dichloroacetic acid).

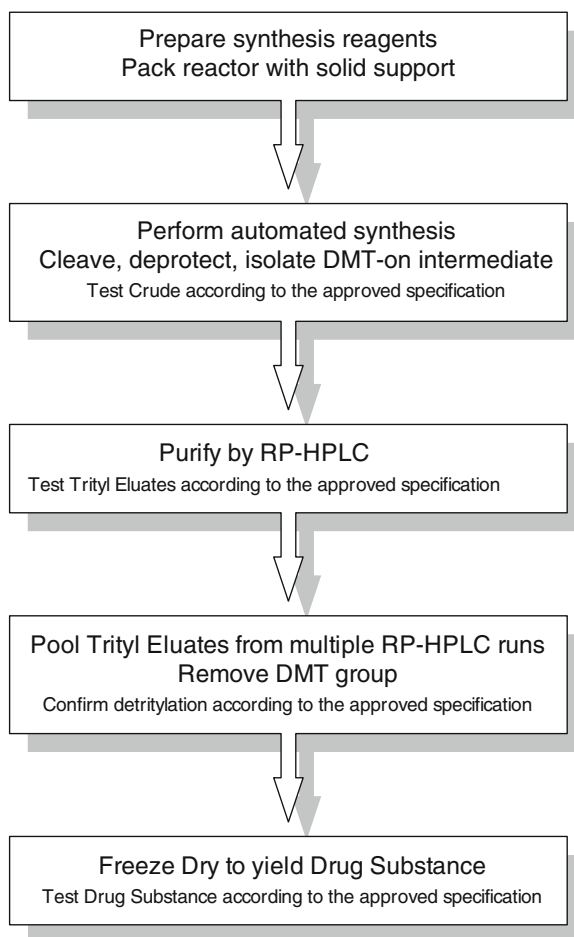


Fig. 1. Drug substance manufacturing process.

2. Coupling (attachment of an activated phosphoramidite to the support-bound oligonucleotide).
3. Sulphurisation [conversion of the newly formed phosphite triester to its phosphorothioate triester using phenylacetyl disulfide (PADS)].
4. Capping (acetylation of unreacted 5'-hydroxyls).

The chemical synthesis is summarised in Fig. 2.

After the final elongation cycle, the solid support-bound oligonucleotide is treated with a solution of triethylamine (TEA) in MeCN to remove the phosphorothioate triester protecting group (reaction 5) (17).

Synthesis begins by transferring a suitable amount of Unylinker™-loaded solid support into a steel column. Gram-scale syntheses are conducted using a GE Healthcare ÄKTA™ oligopilot™ oligonucleotide synthesiser; kilogram-scale syntheses are

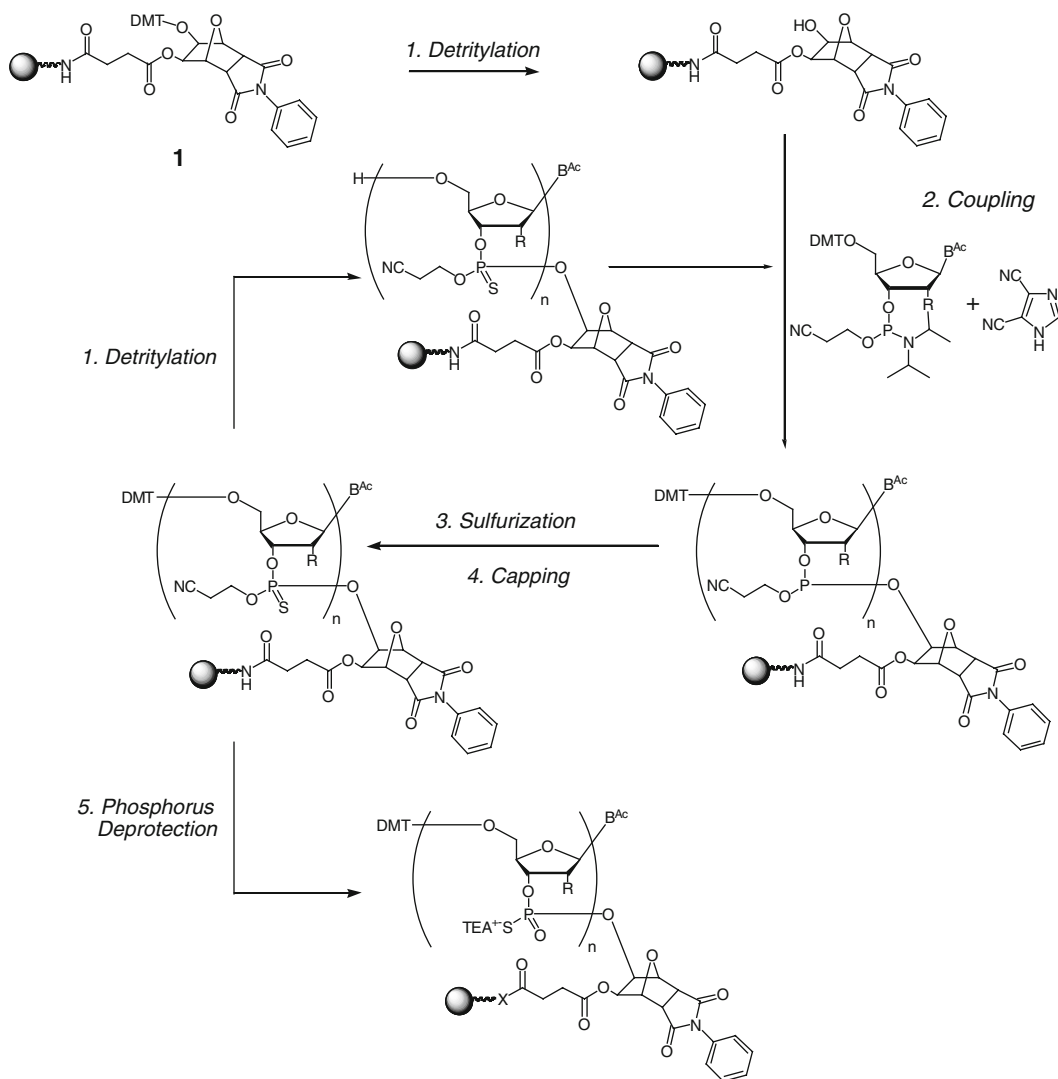


Fig. 2. Chemical synthesis of a phosphorothioate oligonucleotide.

conducted using a GE Healthcare OligoProcess™ oligonucleotide synthesiser. The following synthesis cycle parameters are used (Table 1).

The synthesis is conducted in DMT-on mode. After completion of the synthesis, the partially deprotected oligonucleotide, which is still bound to the solid support is removed from the reactor and treated with ammonium hydroxide at elevated temperature. This step simultaneously liberates the oligonucleotide from the solid support and cleaves the protecting groups from the exocyclic amino groups of the nucleobases. The crude oligonucleotide solution is separated from the solid support by filtration and then concentrated under vacuum to remove ammonia. The resulting crude solution is tested for identity and purity.

Table 1
Synthesis parameters

Step	Solvent/reagent	Flow rate (CV/min)	Delivery time	Equivalents of reagent
Column wash	Toluene	1	3	NA
Unylinker detritylation	10% DCA in toluene	1	3.5	98
Detritylation wash	MeCN	1	3	NA
Pipe wash	MeCN	NA	NA	NA
Coupling	0.2 M Phosphoramidite/1.0 M DCI in MeCN	0.38	0.76	1.75/5
Coupling push	Acetonitrile	0.38	0.7	NA
Sulphurisation	0.2 M PADS in MeCN/picoline (1:1 v/v)	0.44	1.4	6.5
Sulphurisation push	MeCN	0.44	0.7	NA
Capping unylinker	Cap A/Cap B (1:1 v/v)	0.47	3.5	86 ^a
Capping (standard)	Cap A/Cap B (1:1 v/v)	0.47	0.7	17.5 ^a
End wash	Toluene	1	3	NA
Detritylation	10% DCA in toluene	1	2.5	70
Phosphorous deprotection	50% TEA in MeCN	0.12	120	60
Column wash	MeCN	1	3	NA

^aEquivalents of acetic anhydride assuming no coupling

3.1.2. Reverse-Phase Purification

The products of synthesis contain the desired oligonucleotide and closely related process-related impurities which are DMT protected, along with a variety of DMT-off shorter oligonucleotides. The simplest process to purify synthetically prepared oligonucleotides is to separate and isolate the materials from synthesis which contain a DMT group from those which do not. Crude, DMT-protected product is purified by preparative reversed-phase (RP) HPLC. The product is eluted from the column with a multi-step gradient of methanol in 200 mM aqueous sodium acetate. The exact purification conditions vary from sequence to sequence, but typically, crude material is loaded onto C18 polymeric resin in 20% aqueous methanol. The elution profile is monitored by continuous UV absorption spectroscopy. The loading conditions are held until the cleaved protecting groups, i.e. benzamide, acetamide, and isobutyramide, elute from the column. The methanol content

is then increased to 40%, which is sufficient to elute all DMT-off failure sequences. The methanol content is then increased a second time to approximately 75% to elute the DMT-on product, which is collected as a single fraction. Finally, the column is washed with methanol then re-equilibrated in preparation for any additional purification runs. The time needed to execute the purification gradient, end wash, and re-equilibrate in preparation for an additional purification run is merely 2 h. The combination of the short preparative run time and high loading on polymeric supports allows a relatively small purification unit to purify a large amount of crude oligonucleotide efficiently. The HPLC–UV chromatogram of a typical purification run is shown in Fig. 3.

The purity of the material obtained from each purification run is checked by HPLC and the products from all successful runs combined.

3.1.3. Final Deprotection and Isolation

The purified oligonucleotide still has the DMT group attached and must be deprotected to deliver the final API. The DMT group is acid label and post-purification this deprotection occurs in an aqueous environment with acetic acid. The purified 5'-*o*-DMT-on product is fully deprotected by a three-step process. The oligonucleotide is first precipitated from the HPLC buffer by adding the product containing elute volume to a separate container which holds approximately three volumes of ethanol. A conical bottomed container can aide in easy removal of the supernatant, or alternatively the product can be centrifuged. The precipitated product, which separates from the supernatant under gravity, is re-dissolved in water and acetic acid added. Detritylation rates are pH, temperature,

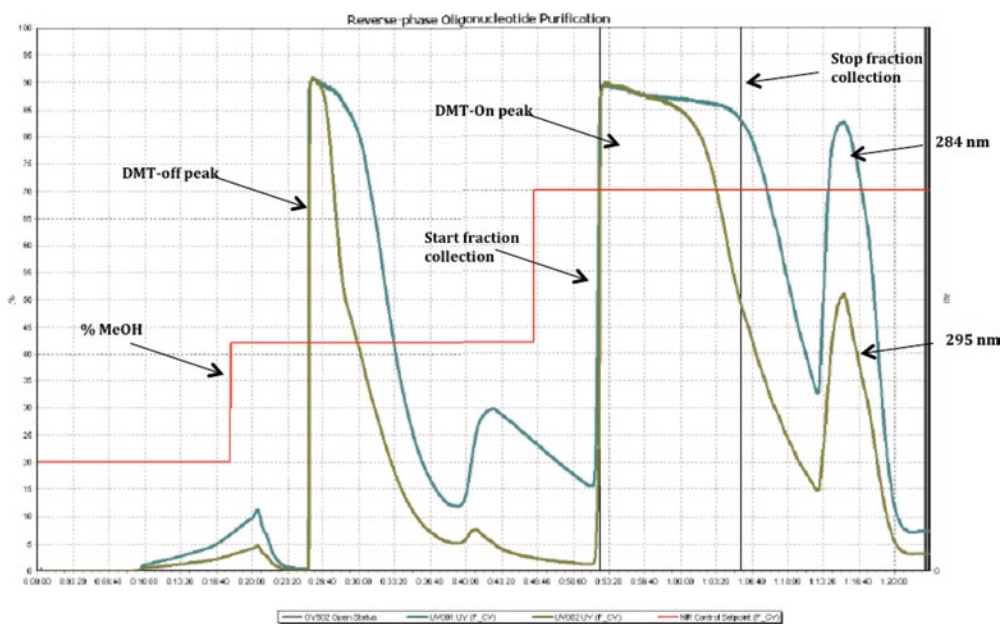


Fig. 3. HPLC UV chromatogram of a 20-mer phosphorothioate oligonucleotide purification.

and sequence dependent (18). Therefore, prior to large-scale detritylation, the half-lifetime ($t_{1/2}$) of the reaction is established empirically, at pilot scale. The same reaction conditions are then used to detritylate the remaining bulk. Typically, the reaction is allowed to proceed for approximately 15 half-lifetimes before the mixture is neutralised by addition of aqueous sodium hydroxide. The detritylated oligonucleotide is then precipitated by adding the acidified solution to three volumes of ethanol and the supernatant decanted. The product is re-dissolved in purified water and the extent of the detritylation reaction checked by HPLC. Provided the detritylation has gone to completion, a final desalting precipitation is performed by adding to ethanol again. The resulting solid is dissolved in purified water, and the solution filtered, and lyophilised to yield the oligonucleotide API.

3.1.4. Yield and Purity

Using the methods described above, yields of between 3.2 and 3.7 g/mmol of as-is 20-mer phosphorothioate oligonucleotide are typically observed. For a 600 mmol synthesis, this translates into an as-is weight of between 1.9 and 2.2 kg. The as-is weight includes between 3 and 5% residual moisture, between 0.5 and 1% ethanol, and up to 0.3% NaOAc. The purity of the isolated drug substance is determined by a selective and sensitive ion-pair HPLC method that utilises both UV and mass spectrometry detectors (19). A typical 20-mer phosphorothioate oligonucleotide has a purity of 90–92% when analysed by this methodology.

3.1.5. Reagent and Solvent Consumption

The manufacture of any molecule using solid-phase synthesis is a highly solvent consumptive process. Using the methods described above, approximately 4,000 kg of solvents, reagents, and water are needed to produce 1 kg of 20-mer phosphorothioate oligonucleotide API (Table 2).

Table 2
Materials consumed to produce 1 kg of 20-mer phosphorothioate oligonucleotide API

Material	Amount (kg)
Reagents and starting materials	137
Toluene	525
MeCN	1,000
3-Picoline	120
Purified water	1,200
Methanol	400
Ethanol	325

Because the process is so solvent consumptive, it is likely that solvent recovery will become important at very large scale. Alternatively, because much of it possesses a significant BTU value, schemes in which the waste stream is burned to provide power to operate the facility are also interesting.

3.2. Solid-Phase Peptide Synthesis Methods

3.2.1. Preparation of the Synthesis Support, Swelling of the Resin (see Note 10)

1. Charge the dry synthesis support (100–200mesh) into the SPPS reactor, (e.g. 10 g of resin into a 250 ml SPPS reactor) (see Note 11).
2. Add ten volumes of solvent (e.g. DCM, DMF, or NMP) to the resin (see Note 12).
3. Stir the suspension gently for 30 min.
4. Wash the swollen resin five additional times with ten volumes of solvents. For washing, it is recommended to use the solvent or solvent mix, which will be used in the following reaction step.
5. Filter the excess of solvent.

3.2.2. Elongation of the Peptide (see Note 13)

3.2.2.1. Fmoc-Deprotection

1. Add three volumes of deprotection reagent [e.g. 20% (v/v) solution of piperidine in DMF] to the swollen resin in the SPPS reactor.
2. Stir gently for 30 min at room temperature.
3. Filter resin and repeat the cleavage step 2 additional times.
4. Wash the resin with solvent (e.g. 5 × 5–8 volumes) until the chloranil test shows no residual piperidine in the filtrate.

3.2.2.2. Coupling (see Note 14)

1. Dissolve the Fmoc amino acid (e.g. 3.0 equivalents relative to resin loading) and HOBT (19) (e.g. 3.0 equivalents relative to resin loading; see Note 15) in ca. four volumes DMF/DCM (1:1) in a separated flask.
2. Add dropwise equimolar amount of DIPCDI (e.g. 3.0 equivalents relative to resin loading) (see Note 16).
3. Stir the mixture for 15 min at room temperature.
4. Add the solution to the filtered resin in the SPPS reactor, previously washed with solvent mix used for coupling.
5. Add additional four volumes of solvent (DCM/DMF 1:1).
6. Stir the mixture for 4 h at room temperature.
7. Take resin samples for in process control (IPC) (Ninhydrin/chloranil test; or IPC via HPLC) after each hour. If the coupling is not completed after 4 h, filter the resin, and repeat coupling step.

8. After completion of the coupling reaction (IPC indicates completion), filter resin from reaction mixture.
9. Wash resin five times with 5–8 volumes each of the solvent used for Fmoc-deprotection step (e.g. DMF or NMP).

3.2.3. IPC Elongation

3.2.3.1. Chloranil Test for Residual Piperidine After Fmoc-Deprotection

1. Prepare a saturated solution of chloranil in acetone.
2. Transfer 1 ml of acetone in a small glass tube.
3. Add one drop of the chloranil solution.
4. Add one drop of the sample.
5. Results: colourless or slightly yellow colour of the solution indicate the absence of piperidine, a blue colour indicates the presence of residual piperidine.

3.2.3.2. Kaiser Test for Completion of Coupling

1. Prepare following three solutions: (1) 5% ninhydrin in ethanol; (2) 80% phenol in ethanol; (3) 2% aqueous KCN (1 mM), in pyridine.
2. Sample a few resin beads (ca. 5 mg) in a glass tube and wash thoroughly first with elongation solvent, then with methanol by decanting the beads and discarding the supernatant.
3. Add three drops of each of the solutions above to the beads in the glass tube.
4. Mix well and heat to 80–90°C for ca. 5 min.
5. The presence of resin-bound free amine is indicated by blue resin beads (see Note 17).

3.2.3.3. HPLC for IPC During Elongation

1. Sample a few resin beads (ca. 5 mg) in a glass tube and wash thoroughly first with elongation solvent, then with DCM by decanting the beads and discarding the supernatant.
2. Add 200 µl of DCM and 5 µl of TFA to the beads.
3. React for 5 min at room temperature.
4. Add 1 ml acetonitrile, mix, and decant.
5. Analyse supernatant solution with HPLC, injection as is (see Note 18).

3.2.4. Cleavage of the Protected Peptide

1. Wash the elongated peptide resin in the SPPS with ten volumes of DCM.
2. Repeat the washing step 4 additional times.
3. Prepare a solution of 1%TFA in DCM (cleavage cocktail) in separate flask (see Note 19).
4. Add ten volumes of the cleavage cocktail to the resin in the SPPS.

5. Stir the suspension for 10 min at room temperature.
6. Filter the cleavage solution from the resin.
7. Neutralise the filtrate by addition of 1 vol% of pyridine.
8. Repeat the cleavage (as described in steps 3–7) five additional times.
9. Combine the cleavage solutions.
10. Concentrate the product solution by removing the excess of DCM via distillation under reduced pressure to about 30% of the initial volume.
11. Precipitate the protected peptide by stirring and slowly adding ethanol and then water to this solution (see Note 20).
12. Filter the protected peptide, wash with water, and dry in vacuum oven.

3.2.5. Global Side-Chain Deprotection

1. Charge 1 g of the protected peptide to a round bottom flask.
2. Add 10 ml of a deprotection cocktail composed of 95% TFA, 2.5% water, 2.5% TIS.
3. Stir the reaction at room temperature for the required time (see Note 21).
4. Cool the mixture to 0–5°C.
5. Add slowly 30 ml of MTBE to the stirred reaction mixture, at a rate such that the temperature does not exceed 10°C (be cautious: the reaction is very exothermic!).
6. Collect the precipitated solids by vacuum filtration.
7. Wash with MTBE and dry in vacuum oven.

3.2.6. HPLC Purification

1. Prepare *Eluent A* (0.1%TFA in purified water, with 10% ACN), and *Eluent B* (0.1%TFA in purified water, with 90% ACN).
2. Dissolve crude peptide at a concentration of 0.2 g (or more) in 10 ml of *Eluent A*.
3. Filter the crude peptide solution through a 10 µm polypropylene filter (e.g. from Pall, USA).
4. Inject 10 ml of the filtered crude peptide solution on a 250 × 10 mm diameter preparative HPLC column (e.g. 100-10-C18 Kromasil).
5. Start the chromatography pumping 4 ml/min of *Eluent A*.
6. Elute the product in separate fractions of 5 or 10 ml running an elution gradient of *Eluent B* from 0 to 50% in 50 min (see Note 22).
7. Analyse the single fractions of the chromatography.

8. Pool the fractions of the chromatography containing the product in the desired quality in a round bottom flask (OK-Pool).

3.2.7. Isolation of the Peptide

1. Recombine the OK-Pool fractions from different injections in a round bottom flask.
2. Remove the excess of acetonitrile from the pooled fractions by distillation under reduced pressure on a Rotavap (e.g. 50 mBar, 40°C).
3. Freeze the remaining aqueous peptide solution using a dry ice/isopropanol mix.
4. Lyophilise the frozen product solution at room temperature until a constant weight is reached (e.g. 48 h). (Note product hygroscopic!).

**3.3. Concluding Remarks:
Oligonucleotide/CPP
Conjugation**

As shown in the two previous sections, large-scale manufacturing processes are available for both oligonucleotides and peptides. Both the oligonucleotide and the peptide can optionally be modified at either 3' or 5'; N- or C-terminally, or orthogonally to facilitate, especially, covalent conjugate formation. There are several methods available to make oligonucleotide peptide conjugates both by non-covalent or covalent formation. The preferred conjugation method will depend on the properties to a certain degree of the target cell or tissue, and possible modifications of the peptide and the oligonucleotide. The conjugation method needs to be specific, preferably without protecting group requirements, reproducible, and generate homogenous material in a high yield. A targeted, effective, safe, and non-toxic systemic delivery strategy is the main barrier to the use of oligonucleotides clinically as therapeutics.

4. Notes

1. A number of other strategies for the synthesis and manufacturing of peptides are also known (e.g. synthesis in liquid phase, solid-phase synthesis in Boc strategy, recombinant synthesis) (20). Each of these methods has its own strength and drawbacks, and can be the method of choice for certain targets, depending on their structure and complexity, and on the required quantities.
2. Through the availability of super acid-labile linkers (e.g. 2-CTC or Sieber resin), peptides with protected side-chain functionalities have become accessible via SPPS. These intermediates can be used for the synthesis of longer peptides via convergent synthesis routes, in which the desired longer

peptide is made out of several protected shorter fragments, each of them synthesised separately by SPPS. Such a convergent process typically leads to crude peptides of higher quality and with a higher overall yield. Peptides with protected side chains also offer the possibility to perform side-chain modification reactions in a selective way.

3. Sometimes the HPLC purification process does not immediately provide the desired salt of the target peptide. In these cases an additional desalting step is needed. A possible process for such a salt exchange could consist of following steps: (1) recombine the HPLC fractions containing the purified peptide; (2) dilute with the same amount of water; (3) load the solution back to the column; (4) wash the product on the column with a none eluting mixture of an organic solvent and a buffer containing the desired counter ion, until the initial counter ion is fully displaced (generally 3–5 column volumes); (5) elute the desired salt of the product from the HPLC column by increasing the concentration of the organic solvent in the elution buffer.
4. Some of the loaded 2-CTC resins are sold without Fmoc protecting group on the α -amine due to stability issues of the corresponding protected derivatives.
5. Be cautious: piperidine and DCM can react with each other in an exothermic reaction. Therefore, mixing of these components in the process or in the waste streams should be avoided.
6. Depending on the properties of the target peptide, the choice of the solvent can have a significant impact on the quality of the elongation. The best solvent for the synthesis of a specific peptide has to be found experimentally. However, in order to avoid side reaction, it is important to carefully check the quality of the solvents: e.g. for DMF, peptide synthesis grade should be used (with lowest contents in formic acid and dimethylamine); while DCM should be free of HCl, otherwise premature cleavage of the peptide from the resin may occur.
7. Alternative organic solvents (instead of ACN) for similar aqueous gradients are methanol or isopropanol. Potential issues here could be esterification side reactions and a higher counter pressure during the chromatography.
8. For some amino acids several different side-chain protecting groups are commercially available.
9. As an alternative, polymer (e.g. polystyrene)-based reverse phase resins can also be used (e.g. Amberchrome HPR 20, Rohm and Hass, USA). The advantage of polymer-based materials is their stability towards basic conditions during the chromatography and also during the sanitisation of the

- chromatography column, which might be needed on industrial scale prior to the purification of clinical or commercial material.
10. When running chemistry on the solid-phase supports, it is important to make sure that the resin is fully swollen before use.
 11. Always keep the peptide synthesis reactions free of moisture (e.g. by using a Nitrogen blanket in the reactors).
 12. All the volumes indicated in the protocol, refer to the initial volume of the dry resin.
 13. An elongation cycle always consists of a coupling reaction and a Fmoc-deprotection reaction. For resins bearing an Fmoc-protected building block (e.g. Sieber linker resin or resin with an Fmoc-protected amino acid), the elongation cycle has to be started with the Fmoc-deprotection. In case of resins loaded with an amino acid *without* Fmoc-protection, the elongation cycle is started with the coupling reaction.
 14. The coupling reaction is the key reaction of the peptide synthesis process. It has the highest impact on the product quality: on one hand, it is important to drive the conversion of each of the coupling steps to completion (e.g. conversion of >99.5% or higher), on the other hand, it is also important to keep the level of side reactions as low as possible. The most important side reaction is the integration of the wrong enantiomer of the amino acid into the growing peptide chain. The primary source for wrong isomers is the racemisation of the activated amino acid in the coupling mixtures. Therefore, it is important to perform the coupling reaction under conditions, where the desired reaction (coupling of the activated right amino acid) will be significantly faster than the undesired one (combination of racemisation and coupling of the wrong isomer). In general terms, this is a very complex chemical problem, which in practice is resolved by identifying the best coupling conditions experimentally (e.g. screening of coupling reagents, solvents, temperature, pre-activation vs. in situ coupling, addition of base, type, and amount of added base, etc.). Although, in principle, each of the coupling reactions in the synthesis of a specific peptide can be optimised, not all of them turn out to be critical to the same extent: most couplings perform well under generic conditions. It should also be noted here, that racemisation is not the only important side reaction, and that a number of other side reactions also can lead to the formation of critical side products (21).
 15. The excesses of reagents required for successful coupling are dependent on a number of different factors: e.g. (1) quality of reagents and solvents, in particular with regards to

- contaminants, which can interfere with the desired reaction (water, primary amines, acids etc.); (2) design of the reactor (efficient mixing); (3) reaction time (influencing the racemisation level); (4) sequence and structure of the target peptide (e.g. in case of difficult couplings). Three equivalents should be sufficient for most of the cases. In an optimised process significantly lower excesses are typically achieved (<2 equivalents).
16. A number of other coupling systems for SPPS in Fmoc/tBu strategy are known in the literature (22): (1) use of additives (e.g. PyBop or HBTU + base); (2) use in situ activation with, e.g. PyBop, HBTU, or HCTU; (3) use other solvent mixtures (e.g. lower proportion of DCM as DMF/DCM 2:1; or use NMP instead of DMF). Some of these alternative coupling systems are stronger but have to be handled carefully, as they can also lead to an increase of side reactions.
 17. The ninhydrin test is a simple and rapid test for the detection of primary amino groups. Proline bearing a secondary amine does not yield a positive reaction, in addition some other amino acids do not show the same dark blue colour (serine, asparagine, aspartic acid). In all these case an IPC via HPLC analysis is recommended.
 18. Possible method for the HPLC analysis during peptide synthesis: Column: Waters X-Terra MS C18 3.5 μm , 4.6 \times 150 mm; *Eluent A*: 0.085%TFA in ACN; *Eluent B*: 0.1%TFA in water; column temperature 35°C; flow 1 ml/min; gradient: *Eluent A* from 10 to 97% in 20 min; injection volume: 1–2.5 μl ; UV detection 220 nm. Please note, that the UV absorption of specific absorption of Fmoc-protected peptides is significantly higher compared to peptides without Fmoc group, this just considered for quantification.
 19. In case of Sieber linker resin, a higher concentration of TFA in the cleavage (5%, in some cases even up to 10%) might be required.
 20. The precipitation conditions are strongly dependent on the nature of the peptide, and needs to be optimised for each target. The parameters to investigate are as follows: (1) relative amounts of the solvents (residual DCM, ethanol, water); (2) addition rates; (3) precipitation temperature.
 21. Depending on the number and type of side-chain protecting groups, the reaction can require 2–18 h. From the protecting groups proposed in this protocol, Arg(Pbf) is the slowest to cleave.
 22. The chromatography can be monitored by UV at 210–220 nm, or if the peptide contains aromatic side chain at 240–280 nm.

Acknowledgments

The authors thank Isaiah Cedillo and Kent VanSooy of Isis Pharmaceuticals, Inc. for their assistance.

References

- Niven, R., Pearlman, R., Wedeking, T., Mackeigan, J., Noker, P., Simpson-Herren, L., Smith, J. G. (1998) Biodistribution of radiolabeled lipid-DNA complexes and DNA in mice. *J Pharm Sci.* 87, 1292–1299.
- Behlke, M. A. (2008) Chemical modification of siRNA for *in vivo* use. *Oligonucleotides.* 18, 305–320.
- Juliano, R., Bauman, J., Kang, H., Ming, X. (2009) Biological barriers to therapy with antisense and siRNA oligonucleotides. *Mol Pharm.* 6 (3), 686–695.
- Castanotto, D. and Rossi, J. J. (2009) The promises and pitfalls of RNA-interference-based therapeutics. *Nature.* 457, 426–33.
- Anderson, W. F. (1998) Human gene therapy. *Nature.* 392, 25–30.
- Jeong, J. H., Mok, H., Oh, Y-K., Park, T. G. (2009) siRNA conjugate delivery systems. *Bioconjugate Chem.* 20, 5–14.
- Mintzer, M. A., Simanek, E. E. (2009) Non-viral vectors for gene delivery. *Chem Rev.* 109, 259–302.
- Beaucage, S. L. and Caruthers, M. H. (1981) Deoxynucleoside phosphoramidites – a new class of key intermediates for deoxypolynucleotide synthesis. *Tetrahedron Lett.* 22, 1859.
- Bray, B. L. (2003) Large-scale manufacturing of peptide therapeutics by chemical synthesis. *Nat Rev Drug Discov.* 2, 587–593.
- Verlander, M. (2007) Industrial applications of solid-phase peptide synthesis – a status report. *Int J Pept ResTher.* 13 (1–2), 75–82.
- Zompra, A. A., Galanis, A. S., Werbitzky, O., Albercio, F. (2009) Manufacturing peptides as active pharmaceutical ingredients. *Future Med Chem.* 1 (2), 361–377.
- Vargeese, C. et al. (1998) Efficient activation of nucleoside phosphoramidites with 4,5-dicyanoimidazole during oligonucleotide synthesis. *Nucleic Acids Res.* 26, 1046.
- Cheruvallath, Z. S. et al. (2000) Synthesis of antisense oligonucleotides: Replacement of 3*H*-1, 2-benzodithiole-3-one 1, 1-dioxide (Beaucage reagent) with phenylacetyl disulfide (PADS) as efficient sulfurization reagent: From bench to bulk manufacture of active pharmaceutical ingredient. *Org. Process. Res. Dev.* 4, 199.
- Krotz, A. H., Cole, D. L., and Ravikumar, V. T. (1999) Synthesis of an antisense oligonucleotide targeted against C-raf kinase: Efficient oligonucleotide synthesis without chlorinated solvents. *Bioorg Med Chem.* 7, 435.
- Kumar, R. K. et al. (2006) Efficient synthesis of antisense phosphorothioate oligonucleotides using a universal solid support. *Tetrahedron,* 62, 4528.
- Subirós-Funosas, R., Prohens, R., Barbas, R., El-Faham, A., Albericio, F. (2009) Oxyma: An efficient additive for peptide synthesis to replace the benzotriazole-based HOBt and HOAt with a lower risk of explosion. *Chem Eur J.* 15, 9394–9403.
- Capaldi, D. C. et al. (2003) Synthesis of high-quality antisense drugs. Addition of acrylonitrile to phosphorothioate oligonucleotides: Adduct characterization and avoidance. *Org Process Res Dev.* 7, 832.
- Krotz, A. H. et al. (2003) Controlled detritylation of antisense oligonucleotides. *Org Process Res Dev.* 7, 47.
- Capaldi, D. C. and Scozzari, A. N. (2006) Manufacturing and analytical processes for 2'-*O*-(2-methoxyethyl)-modified oligonucleotides. In: Croke, S. T., ed. *Antisense drug technology: Principals, strategies and applications*, 2nd Edition. Boca Raton, CRC Press, 401–434.
- Goodmann, M. edited by (2002) *Methods of organic chemistry, (Houben-Weyl), synthesis of peptides and peptidomimetics, Volumes E22a and E22b.* Georg Thieme Verlag, Stuttgart, New York.
- Benoiton, N. L. (2006) *Chemistry of peptide synthesis.* Taylor & Francis Group, Boca Raton, FL, USA.
- Chan, W. C. and White, P. D. edited by (2000) *Fmoc solid phase peptide synthesis – a practical approach.* Oxford University Press, UK.

Application of a Fusiogenic Peptide GALA for Intracellular Delivery

Ikuhiko Nakase, Kentaro Kogure, Hideyoshi Harashima, and Shiroh Futaki

Abstract

To enhance the cytosolic delivery of therapeutic drugs and genes, pH-sensitive and membrane fusiogenic peptides have been employed as additives for facilitating their endosomal escape. GALA is such a peptide composed of repeating sequences of Glu-Ala-Leu-Ala, which are designed to mimic the function of viral fusion protein sequences that mediate escape of virus genes from acidic endosomes to the cytosol. Recently, the peptide has been applied not only for improving the transfection efficiency of plasmid DNAs using cationic liposomes, but also as functional molecules of multifunctional envelope-type nano-device (MEND). The advantage of employing this peptide was also exemplified by the cytosolic delivery of proteins via efficient endosomal escape of the GALA–cargo conjugates in the presence of cationic lipid complexes. This chapter provides protocols for the efficient cytosolic delivery of cargo molecules using the GALA peptide.

Key words: Cytosolic delivery, GALA, Membrane fusiogenic peptide, Cationic liposome, Endosomal escape

1. Introduction

Plasma membranes have numerous critical functions for maintaining cellular survival. However, the membranes are also one of the major impediments for the delivery of therapeutic agents (especially macromolecular drugs such as genes and bioactive proteins) into cells. For improving the penetration of macromolecules through the membranes, membrane fusiogenic peptides such as the GALA peptide have been applied to allow leakage of the therapeutic agents into the cytosol.

The GALA peptide, a 30-residue amphiphilic peptide with the repeat sequence of Glu-Ala-Leu-Ala, was designed to mimic

the function of viral fusion protein sequences, which mediate escape of virus genes from acidic endosomes to the cytosol following endocytotic uptake of the virus (1, 2). The GALA peptide has a feature that converts its structure from random to helical, when the pH is reduced from 7.0 to 5.0, leading to destabilizing the lipid membranes (1, 2).

Using this unique peculiarity, the GALA peptide has contributed to stimulating the efficient endosomal escape of liposomes complexed with plasmid DNAs as a method to improve the transfection efficiency (3–5). Recently, a novel packaging method to encapsulate condensed plasmid DNAs into the PEGylated and transferrin (Tf)-modified liposomes (multifunctional envelope-type nanodevice, MEND) was developed to form a core-shell-type nanoparticle (6). By simultaneously incorporating the cholesteryl-GALA (Chol-GALA) into the membrane of MEND and GALA at the tips of the PEG chains, a condensed core was released into the cytosol, and this led to a significant increase in the transfection efficiency (6). Additionally, the cytosolic targeting of proteins using the GALA peptide in combination with cationic lipids was reported (7). Cationic lipids, complexed with a negatively charged GALA conjugated with cargo molecules, internalize into cells by endocytosis, and the cargo can escape from the endosomes with the help of GALA (Fig. 1) (7). This chapter presents protocols for the efficient cytosolic delivery of cargo molecules using the GALA peptide.

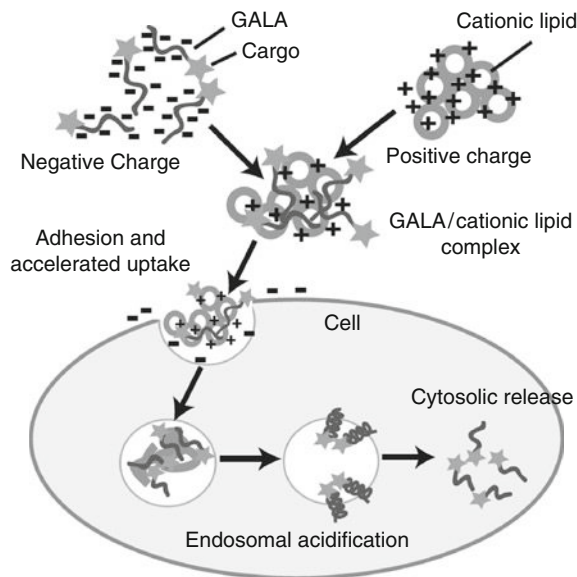


Fig. 1. Concept of cytosolic targeting using GALA as an addressing vehicle in combination with cationic liposomes.

2. Materials

2.1. Transfection of Plasmid DNA Using Cationic Lipids in Combination with GALA

1. COS-7 cells (a simian kidney cell line transformed with SV40) maintained in Dulbecco's Modified Eagle's Medium (DMEM) (Nissui Pharmaceutical, Tokyo, Japan) containing 10% heat-inactivated fetal bovine serum (FBS) (Biological Industries, Kibbutz Beit Haemek, Israel).
2. Glass-bottomed dish (35 mm) (Iwaki, Tokyo, Japan).
3. Cationic lipid (Lipofectin) (Invitrogen, Carlsbad, CA).
4. Plasmid DNA [enhanced green fluorescent protein (EGFP) gene (pEGFP-N1) (BD Biosciences Clontech, Palo Alto, CA)].
5. Synthetic peptide of GALA (amino acid sequence: WEAALAEALAEALAEHLAEALAEALEALAA-amide) (see Note 1).

2.2. Transfection of Plasmid DNAs Using MEND

1. Dioleoyl phosphatidylethanolamine (DOPE), lissamine rhodamine B-DOPE (Rho-DOPE), cholesterol (Chol), distearyl phosphatidyl ethanolamine-polyethyleneglycol 2000 (DSPE-PEG2000), maleimidic DSPE-PEG2000 (Avanti Polar Lipids Inc., Alabaster, AL). Dicetylphosphate (DCP), n-octyl β -D-glucopyranoside (OGP) (Sigma-Aldrich, St. Louis, MO).
2. Plasmid DNA (pDNA) pCAcc-luc+ (6,566 bp) encoding luciferase prepared using the EndFree Plasmid Mega Kit (Qiagen, Hilden, Germany).
3. Poly-L-lysine (PLL, M.W. 27,400) (Sigma-Aldrich, St. Louis, MO).
4. Human holo-transferrin (Tf) and 3-(2-pyridyldithio)propionic acid N-hydroxysuccinimide ester (SPDP) (Sigma-Aldrich, St. Louis, MO).
5. Label IT labeling kit (MIRUS, Madison, WI).
6. XAD porous beads (ORGANO, Tokyo, Japan).
7. Synthetic peptide of GALA-SH (amino acid sequence: WEAALAEALAEALAEHLAEALAEALEALAAAC-amide), and GALA modified with cholesterol at N-terminal of the peptide (Chol-GALA) (amino acid sequence: Chol-WEAALAEALAEALAEHLAEALAEALEALAA-amide) (see Notes 1 and 2).
8. Luciferase assay reagent and reporter lysis buffer (Promega, Madison, WI).
9. BCA protein assay kit (Pierce, Rockford, IL).
10. K562 cells (human chronic myelogenous leukemia cells) maintained in RPMI1640 (Invitrogen, Carlsbad, CA) containing 10% heat-inactivated FBS.

2.3. Intracellular Delivery of FITC–GALA or FITC–Avidin/Biotin–GALA Complex in Combination with Cationic Lipid

1. Synthetic peptide of GALA conjugated with biotinamidocaproate *N*-hydroxysuccinimide ester at N-terminal of the peptide (biotin–GALA) [amino acid sequence: biotinamidocaproyl-NH-(CH₂)₃-CO-WEAALAEALAEALAEHLAEALAEALEALAA-amide], and GALA conjugated with fluorescein-5-isothiocyanate (FITC) at N-terminal of the peptide (FITC–GALA) [amino acid sequence: FITC-NH-(CH₂)₃-CO-WEAALAEALAEALAEHLAEALAEALEALAA-amide] (see Notes 1 and 3).
2. FITC–avidin (Sigma-Aldrich, St. Louis, MO).
3. HeLa cells (human cervical cancer-derived cells) maintained in α -minimum essential medium (α -MEM) (Invitrogen, Carlsbad, CA) containing 10% heat-inactivated bovine serum (BS) (Invitrogen, Carlsbad, CA).
4. Cationic lipid (Lipofectamine 2000, LF2000) (Invitrogen, Carlsbad, CA).

3. Methods

To efficiently deliver the GALA conjugated with various cargo molecules in the presence of cationic lipids into cells and to maximally induce the biological function by the endosomal escape into the cytosol, it is important to consider the ratio of GALA, cationic lipids, and cargo molecules in forming their complexes. For example, because the GALA has seven Glu residues in its sequence and is negatively charged at neutral pH, the ratio effects on the positive-to-negative alteration in the total charge of the complexes, leading to a change in the internalization efficiency into the cells. Additionally, the amount of the GALA internalized into the cells by cationic lipids may influence the efficiency of the membrane disruption in the endosomes. Therefore, optimization of the ratio in forming complexes is significantly important.

3.1. Transfection of Plasmid DNA Using Cationic Lipids in Combination with GALA

1. Plate COS-7 cells (2×10^5 cells/well) in glass-bottomed dishes, and maintain in 1 mL of DMEM containing 10% FCS under 5% CO₂ at 37°C for 24 h.
2. Mix cationic lipids (Lipofectin) (10 μ L) in serum-free DMEM (90 μ L) with plasmid DNA (pEGFP-N1) (1 μ g) in serum-free DMEM (100 μ L), and store for 10 min at room temperature (see Note 4).
3. Mix GALA peptide in phosphate-buffered saline (PBS) (6 μ g/mL, 50 μ L) with the cationic lipids/plasmid DNA solution, and store at room temperature for 10 min. The mixture is then diluted with 750 μ L of serum-free DMEM (see Note 4).

4. Wash the cells with serum-free DMEM, followed by the addition of the above solution (cationic lipids/plasmid DNA) to the cells, and then incubate the cells for 5 h under 5% CO₂ at 37°C.
5. Replace the plasmid-containing medium with 2 mL of DMEM containing 10% FCS, and incubate the cells for another 24 h.
6. Analyze the expression of EGFP by confocal laser scanning microscopy.

3.2. Transfection of Plasmid DNAs by MEND

1. Dissolve DNA and PLL in 5 mM HEPES buffer (pH 7.4). The labeling of pDNA with rhodamine is performed using a Label IT labeling kit. To condense the pDNA, add the DNA solution (0.1 mg/mL) containing the rhodamine-labeled DNA (20% of total DNA) to a PLL or protamine solution (0.1 mg/mL) with vortexing at room temperature. The final DNA concentration of the DNA/polycation complex (DPC), prepared at a nitrogen/phosphate (N/P) ratio of 2.4, is 0.05 mg/mL.
2. Add a diluted DPC suspension (0.25 mg/mL) to a mixture of the lipid [DOPE/NBD (or rhodamine)-labeled DOPE/DCP/DSPE-PEG-2000 = 77:5:8:10 (molar ratio)] and detergent OGP containing 5 mM HEPES buffer (pH 7.4). The final concentrations of the DNA, lipid and detergent are 0.023 mg/mL, 0.49 μM and 18 mM, respectively.
3. Under these conditions, detergent-rich small unilamellar vesicles (SUV*) are formed and then bind to the surface of the DPC.
4. To remove the detergent, add Amberlite XAD porous beads to the SUV*/DPC suspension.
5. To isolate the MEND from the empty liposomes and uncoated DPC, layer the sample on a discontinuous sucrose density gradient (0–40%) and centrifuge at 160,000 × *g* for 2 h at 20°C.
6. Collect 1 mL aliquots starting from the top and measure the fluorescence intensities. The collected fraction containing the MEND is dialyzed three times against 1 L volumes of 5 mM HEPES buffer (pH 7.4) for >3 h to remove the sucrose.
7. To modify liposomes with Chol-GALA, add an *N,N*-dimethylformamide (DMF) solution of Chol-GALA to the suspensions of MEND so that the final concentration is 1 mol% before the Tf modification. The mixture is then incubated for 1 h at 37°C. Separate the unencapsulated Chol-GALA on a Bio-Gel A-1.5m column (100–200 mesh) equilibrated with PBS buffer.
8. Treat Tf (final concentration of 62.5 μM) with SPDP (final concentration of 66 μM) for 30 min at room temperature.

The resulting 3-(2-pyridyldithio)propionyl (PDP)-Tf is separated from the unreacted SPDP by gel filtration on a Sephadex G-25 column equilibrated with PBS. The PDP-Tf is then reduced with 50 mM dithiothreitol in H₂O for 30 min at room temperature to yield 3-mercaptopropyl-Tf, which is purified on a Sephadex G-25 column.

9. Treat the 3-mercaptopropyl-Tf with MEND containing 1 mol% maleimidic DSPE-PEG-2000 at a 1:20 lipid molar ratio at 4°C overnight for disulfide cross-linking between the Tf and liposomes.
10. To remove the unreacted Tf from MEND, centrifuge the reaction mixture (160,000×g) for 2 h at 4°C and remove the supernatant. The MEND is equilibrated with 50 mM Fe₂(SO₄)₃-EDTA (pH 7.4, final Fe³⁺ concentration of 100 μM) for the Tf resaturation with Fe³⁺.
11. To conjugate GALA-SH at the PEG terminal, add a DMSO solution of GALA-SH to suspensions of MEND containing 2 mol% maleimidic PEG lipid in order that the final concentration of GALA-SH is 1 mol% 30 min after the addition of the Tf, and incubate at 4°C overnight. The unreacted GALA-SH in the MEND suspensions is removed by gel filtration.
12. MEND containing 1 μg of DNA, determined by measuring the fluorescence of the rhodamine-labeled plasmid DNA, and suspended in 0.25 mL of RPMI1640 without serum and antibiotics are added to K562 cells (5×10⁴ cells) and incubated for 3 h at 37°C.
13. Add RPMI1640 containing 10% fetal calf serum (1 mL) to the cells, followed by a further incubation for 45 h. Then collect the cells from the dishes, wash, and solubilize with reporter lysis buffer.
14. Initiate the luciferase reaction by the addition of 50 μL of luciferase assay reagent into 20 μL of the cell lysate, and measure the activity using a luminometer.
15. Determine the amount of protein in the cell lysate using a BCA protein assay kit.

3.3. Intracellular Delivery of FITC-GALA or FITC-Avidin/Biotin-GALA Complex in Combination with Cationic Lipid

1. Plate HeLa cells (3.0×10⁵ cells/well) into 35-mm glass-bottomed dishes and culture for 24 h.
2. To prepare FITC-GALA and LF2000 complex, add LF2000 (2 μL) diluted with serum-free cell culture medium (18 μL) to a solution of FITC-GALA (10 μM) in serum-free cell culture medium (20 μL), and incubate the mixture for 15 min at room temperature. Add 13% BS-containing α-MEM (160 μL) to the solution of the FITC-GALA/FL2000 complex.
3. To prepare the FITC-avidin/biotin-GALA and LF2000 complex, mix biotin-GALA (10 μM) in serum-free α-MEM

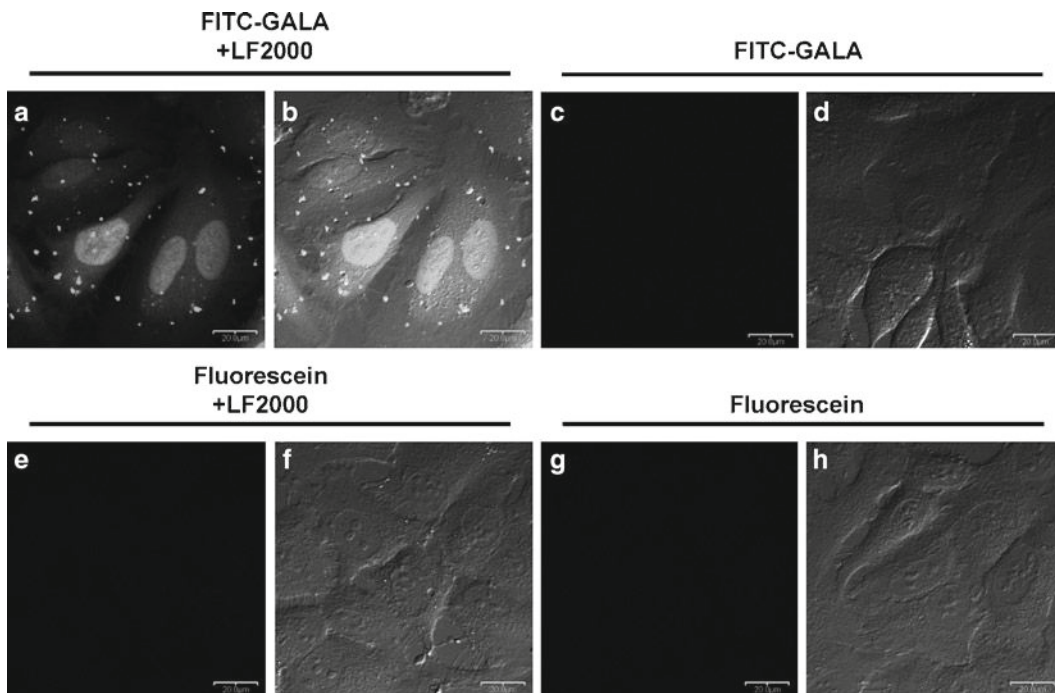


Fig. 2. Confocal microscopic observation of HeLa cells treated with FITC–GALA (1 μ M)/FL2000 [1% (v/v)] complex (a, b), FITC–GALA (1 μ M) (c, d), fluorescein (1 μ M)/FL2000 [1% (v/v)] complex (e, f), fluorescein (1 μ M) (g, h) for 4 h. Fluorescence imaging (a, c, e, g) and merge of fluorescence and DIC (b, d, f, h) are shown. Scale bars, 20 μ m.

(20 μ L) with the cationic lipid (LF2000) (2 μ L) in serum-free α -MEM (18 μ L), and incubate for 15 min at room temperature prior to adjustment of the total volume of the mixture to 200 μ L with a solution of FITC–avidin in 13% BS-containing α -MEM to yield a solution of the FITC–avidin/biotin–GALA complex (FITC–avidin 0.25 μ M; biotin–GALA 1 μ M) (see Note 5).

4. Incubate the cells with each mixture (200 μ L) at 37°C under 5% CO₂ for ~6 h.
5. Wash the cells with PBS and add 10% BS-containing α -MEM to the cells.
6. Analyze by confocal laser scanning microscopy. An example of the results is shown in Fig. 2.

4. Notes

1. The peptides are prepared by Fmoc-solid-phase peptide synthesis (Fmoc=9-fluorenylmethyloxycarbonyl) on a Rink amide resin using the standard peptide synthesizer protocol

- (8). A combination of benzotriazole-1-yloxytrispyrrolidino-phosphonium hexafluorophosphate (PyBOP), 1-hydroxybenzotriazole (HOBt), and 4-methylmorpholine (NMM) is employed as a coupling system. Fmoc-Trp-OH, Fmoc-Glu(OtBu)-OH, Fmoc-Ala-OH, Fmoc-Leu-OH, Fmoc-His(Trt)-OH, Fmoc-Gly-OH, and Fmoc-Cys(Trt)-OH are employed as amino acid derivatives. Treatment of the peptide resin with trifluoroacetic acid (TFA)-ethanedithiol (EDT) (95:5) at room temperature for 3 h is conducted for the cleavage of the peptide from the resin and deprotection of the peptides, followed by reverse-phase high-performance liquid chromatography purification. The structures of the synthesized peptides are confirmed by matrix-assisted laser desorption ionization time-of-flight mass spectrometry.
2. To prepare the Chol-GALA, treatment of the peptide resin with cholesteryl chloroformate and triethylamine (1.5 eq. each to the peptide resin) in DMF at room temperature for 2 h produces the cholesteryloxycarbonyl-peptide resin. The peptide resin is treated with TFA-EDT (95:5), purified, and the product is identified as already stated.
 3. To prepare the fluorescently labeled peptides, attach a gamma-aminobutyryl (GABA) residue to the N-terminus of the peptide resin as a spacer for connecting with a fluorescence label, and then treat the N-terminus of the resin with fluorescein-5-isothiocyanate and N-ethyl-diisopropylamine (DIEA) (3 eq. each to the peptide resin) in DMF at room temperature for 3 h. The fluorescein-labeled peptide resin is treated with TFA-EDT (95:5), purified, and the product is identified as already stated (7).
 4. Optimization of concentrations of cationic lipids and GALA should be needed (3).
 5. Expressed protein ligation is also useful for the preparation of the GALA-protein conjugation (7).

Acknowledgment

This work was supported in part by Grants-in-Aid for Scientific Research from the Ministry of Education, Culture, Sports, Science and Technology of Japan.

References

1. Subbarao, N. K., Parente, R. A., Szoka, F. C. Jr., Nadasdi, L., Pongracz, K. (1987) pH-dependent bilayer destabilization by an amphipathic peptide. *Biochemistry* **26**, 2964–2972.
2. Li, W., Nicol, F., Szoka, F. C. Jr. (2004) GALA: a designed synthetic pH-responsive amphipathic peptide with applications in drug and gene delivery. *Adv. Drug Deliv. Rev.* **56**, 967–985.

3. Futaki, S., Masui, Y., Nakase, I., Sugiura, Y., Nakamura, T., Kogure, K., Harashima, H. (2005) Unique features of a pH-sensitive fusogenic peptide that improves the transfection efficiency of cationic liposomes. *J. Gene Med.* **7**, 1450–1458.
4. Simões, S., Slepishkin, V., Gaspar, R., de Lima, M. C., Düzgüneş, N. (1998) Gene delivery by negatively charged ternary complexes of DNA, cationic liposomes and transferrin or fusigenic peptides. *Gene Ther.* **5**, 955–964.
5. Simões, S., Slepishkin, V., Pretzer, E., Dazin, P., Gaspar, R., Pedroso de Lima M. C., Düzgüneş, N. (1999) Transfection of human macrophages by lipoplexes via the combined use of transferrin and pH-sensitive peptides. *J. Leukoc. Biol.* **65**, 270–279.
6. Sasaki, K., Kogure, K., Chaki, S., Nakamura, Y., Moriguchi, R., Hamada, H., Danev, R., Nagayama, K., Futaki, S., Harashima, H. (2008) An artificial virus-like nano carrier system: enhanced endosomal escape of nanoparticles via synergistic action of pH-sensitive fusogenic peptide derivatives. *Anal. Bioanal. Chem.* **391**, 2717–2727.
7. Kobayashi, S., Nakase, I., Kawabata, N., Yu, H. H., Pujals, S., Imanishi, M., Giralt, E., Futaki, S. (2009) Cytosolic targeting of macromolecules using a pH-dependent fusogenic peptide in combination with cationic liposomes. *Bioconjug. Chem.* **20**, 953–959.
8. Futaki, S., Niwa, M., Nakase, I., Tadokoro, A., Zhang, Y., Nagaoka, M., Wakako, N., Sugiura, Y. (2004) Arginine carrier peptide bearing Ni(II) chelator to promote cellular uptake of histidine-tagged proteins. *Bioconjug. Chem.* **15**, 475–481.

Therapeutic Applications of Cell-Penetrating Peptides

Randolph M. Johnson, Stephen D. Harrison, and Derek Maclean

Abstract

Since the discovery over 15 years ago of a protein transcription factor that possessed the ability to cross the plasma membrane, cell-penetrating peptides (CPPs) have been evaluated for the ability to transport diverse cargoes into cells, tissues, and organs. Certain CPPs have been used for the intracellular delivery of information-rich molecules to modulate protein–protein interactions and thereby inhibit key cellular mechanisms of disease. The ability to introduce drugs into cells allows the conventional biodistribution of drugs to be altered in order to favorably impact toxicity, patient compliance, and other treatment factors.

In this monograph, we present the current status and future prospects for the application of CPPs to the development of human therapeutics. We discuss some of the advantages and disadvantages of using CPPs in the *in vivo* setting, and review the current status of a number of preclinical and human clinical studies of CPP-mediated delivery of therapeutics. These include CPP-conjugated moieties directed against a growing variety of targets and disease areas, including cancer, cardiology, pain, and stroke. Our discussion focuses on those therapeutics that have been tested in humans, including a CPP conjugate for the treatment of acute myocardial infarction. The promising results obtained in a number of these studies indicate that CPPs may have an important role in the development of novel therapeutics.

Key words: Cell-penetrating peptides, TAT, Protein kinase C isozymes, PKC, Drug discovery, Drug development, Pain, Cardioprotection, Neuroprotection

1. Introduction

Unlike small molecular weight drugs, most peptides do not efficiently penetrate tissues or enter cells. Cell-penetrating peptides (CPPs) are an exception to this rule. CPPs can be assigned to one of two broad classes: (a) those that possess a particular constrained tertiary structure that facilitates their passage through the membrane (e.g., cyclotides (1) and stapled peptides (2)) and (b) those peptides that are capable of entering the cell as a linear sequence. In some cases, members of this latter class of CPPs may act as

“carriers,” transporting conjugated “cargo” moieties into the cell. When present, this capability may allow the “carriers” to be used in a way that facilitates the uptake of otherwise noncell-penetrant drugs. It is these “carrier” peptides, and their uses, that we will be discussing in this chapter.

Over 15 years of research on CPPs has revealed a significant amount of information about the features of such molecules that enable them to penetrate cells, the cellular mechanisms of transport across membranes, and the molecular cargoes that they may potentially carry into cells (3–7).

Inhibition of intracellular protein–protein interactions (PPI) is a major opportunity for therapeutic development which has opened up, in part, due to the advent of CPPs. The inhibition of PPI-driven intracellular processes, such as signal transduction, has proven difficult with small molecule therapeutics, due to issues of nonselectivity (and resulting toxicity) and low potency. These factors have limited the use of many of these small molecule drugs. Large biomolecules provide specificity in targeting extracellular PPIs but typically do not penetrate the cell membrane. By harnessing the ability of CPPs to cross cell membranes, the therapeutic scope of such proteins and peptide drugs may be broadened to include the intracellular milieu.

A second area of opportunity for CPPs is in potentially altering the biodistribution of therapeutic molecules. Certain CPPs may be used to deliver molecules by routes which are not otherwise achievable (e.g., skin penetration) or into compartments or tissues which minimize potential toxicities (e.g., by avoiding exposure of certain tissues to the molecules) (4).

In this chapter, we will briefly discuss the chemistry of a number of CPPs, the putative mechanisms of cell penetration, potential advantages and disadvantages of using CPPs for drug delivery, and some preclinical studies with CPP-conjugated compounds that demonstrate their promise as therapeutic agents. We will then describe some recent clinical trial results with CPP-conjugated compounds and discuss future therapeutic applications.

2. Chemistry of CPPs and Mechanisms of Cell Penetration

The first reported CPPs emerged from research on protein transcription factors that possessed the ability to transit the plasma membrane and other membranes of cells (8, 9). One of these, the transactivator of transcription (TAT) from HIV-1 virus, was investigated to determine whether it could function as a carrier. In an early study, peptides derived from the TAT protein were chemically cross-linked to a variety of “cargo” molecules. The conjugates were reported to penetrate the plasma membranes of cells

in vitro and cells organized into tissues in vivo (10). Further studies revealed that the ability to penetrate plasma membranes was associated with certain domains of the TAT peptide (and other cell-penetrating proteins), and these domains were called protein transduction domains (PTD) (11, 12). Of these, an arginine-rich 11 amino acid sequence of the TAT peptide (TAT₄₇₋₅₇) has perhaps received the most attention. In one study, a fusion protein of TAT₄₇₋₅₇ and the large β -galactosidase molecule (β -Gal) was intraperitoneally injected into mice. Tissue samples from the liver, kidney, heart muscle, lung, and spleen obtained after injection showed β -Gal activity (13).

Certain arginine-rich peptides have been reported to be effective as CPPs (14). Indeed, a number of polyarginine peptides appear to have high levels of cellular uptake (15, 16). The guanidinium groups on the arginine residues of TAT₄₇₋₅₇ are believed to be involved in transduction (7, 17). In fact, nonpeptidic guanidinium moieties attached to other types of molecules can in some cases transport cargo across cell membranes more efficiently than TAT₄₉₋₅₇ (a TAT-derived PTD) or certain polyarginine peptides. It has been proposed that bidentate hydrogen bonds, characteristic of guanidinium groups, may bind to counteranions, such as proteoglycans associated with the plasma membrane, and this binding may be the first step in transduction. However, guanidinium-mediated cellular association is clearly not the only mechanism for initiating cellular uptake. For example, the cell-penetrating peptide Transportan (GWTLNSAGYLLGKINLKALAALAKKIL) contains no arginine residues, but it is as efficiently transported into cells as polyarginine (R₁₁) (15).

The mechanism or mechanisms of transport of various CPPs, and/or their cargoes, across membranes have been extensively investigated. There is evidence for all three major types of endocytosis (i.e., clathrin-mediated, caveolin-mediated, and macropinocytosis) (3, 18–22). In addition, there is evidence for nonendosomal mechanisms of transport (7, 23). Endosomal and nonendosomal pathways may not be mutually exclusive, although this topic is controversial and there is reason to believe that at least some reports of nonendosomal transport may be artifacts of methodology (3, 18). There is considerable evidence that the mechanisms of CPP transport may be dependent on the CPP at issue and the presence of certain cell-surface proteoglycans (21–25). If different CPPs bind to different glycosaminoglycan species, it may allow targeting specific cell types based on their expression patterns of glycosaminoglycans (21, 25). For the transport of CPPs and/or their cargoes by an endosomal pathway, it is important to understand how the molecules are released from endosomes into the cell cytoplasm as the efficiency of this mechanism may constitute the greatest impediment to intracellular bioavailability (3). Endosomal escape is reported to be facilitated by decreased endosomal pH,

and inhibited when the pH is buffered (19, 26). Other means of facilitating escape have been reported (3, 7), and it is also likely that different CPPs have different potentials for endocytic release. Modulation of the efficiency of endosomal release may provide additional control over cargo delivery and thus, if uptake is primarily endosomal, the nature of the endosomes and their intracellular trafficking become important to consider when assessing intracellular targets for cargo molecule binding (26).

After endosomal escape, the intracellular targeting of the cargo may be influenced by the presence (or absence) of the carrier. For example, if both the carrier and the cargo enter the cell and remain attached, the high positive charge on carriers, such as TAT₄₇₋₅₇ and Octa-Arg, may direct the CPP-conjugate to the nucleus, where the positively charged carrier may interact with negatively charged DNA. To avoid this possibility, some CPP conjugates have been designed so that the cargo may be released from the CPP once the conjugate reaches the cytosol. This has been investigated, among other ways, by using reducible disulfide linkages between the CPP and the cargo (7). The operative combination of carrier, cargo, and linkage typically cannot be determined a priori. In some instances, it appears that a releasable linker may be advantageous, as noncleavable linkers can inactivate the carrier–cargo conjugate (15). However, the ideal carrier–linker–cargo combination is not obvious a priori, as in many cases a noncleavable linker shows good activity (27–29).

3. CPPs for Drug Delivery

There are a significant number of variables that must be considered in the selection of an optimal CPP construct for drug delivery. Different CPPs will present varying modes of uptake, and this may be further affected by the properties of the attached cargo and on the nature of the linker used to conjugate these two components. Other factors to take into account include the efficiency of cellular penetration, the spectrum of cells targeted, and the intracellular targeting of the CPP, including release from endosomes. These latter two properties will be expected to be particularly influenced by whether the cargo–carrier linkage is cleavable or not.

Many of the properties of CPP delivery have been shown to display significant concentration dependence. While this is a variable that can readily be controlled in *in vitro* experiments, *in vivo* concentration effects can only be controlled indirectly through the administration regimen, and may largely depend on the intrinsic pharmacokinetic (PK) properties of a given drug. Consideration of administration route, dose, and frequency are

essential to provide the desired efficacy while ensuring safety and tolerability. Several routes of administration have been reported for CPP drug candidates. Intravascular administration has been shown to be feasible and efficacious in both preclinical and clinical studies (30–33). Other clinically relevant routes of administration that have been demonstrated are subcutaneous (34, 35), and topical, as for dermatological applications (36). Although much remains to be learned about the safety profiles of CPPs, preclinical studies with CPP-conjugated molecules and safety data from clinical trials have been encouraging (32, 37, 38) (Table 1).

In conjunction (although outside the scope of this chapter), bioanalytical methods that are capable of quantifying relevant levels of compounds from *ex vivo* samples are often critical to develop PK relationships in support of dose optimization. Due to the unique stability and analytical challenges posed by proteins and peptides, and due to the rapid cellular uptake of CPPs, innovative approaches need to be adopted to develop the bioanalytical assays for PK modeling.

An attractive feature of the use of CPPs is that this strategy can remove the constraint of finding molecules that are intrinsically capable of cellular uptake and which also happen to have the ability to modulate the activity of relevant intracellular target molecules. Lipophilic/amphiphilic small molecules can be engineered that penetrate cells; however, their small surface area is typically insufficient to modulate PPI. In contrast, small peptides of ~1–3 kDa can achieve PPI modulation and can be engineered to recapitulate small molecule-like cell penetration. This falls within the first class of CPPs mentioned in the introduction and examples of this include cyclosporine, cyclotides, “stapled” alpha-helical peptides (1, 2), and lipidated peptides (“pepducins”) (39). Peptides of these classes embody PPI modulation and cell penetration in a single entity. While attractive in principle (the latter two discoveries have each led to the founding of platform companies focusing on these approaches to targeting intracellular PPI), this may be less flexible than the more predictable, modular approach offered by CPP conjugation, as the properties of cell penetration and biological activity have to be balanced within a single, compact molecule. This first class of CPPs may be considered to have very limited “carrying capacity” in comparison to the better characterized CPPs that are the primary focus of this chapter.

The use of CPPs as carriers to transport peptides and other molecules into cells has been a facilitating strategy in a growing number of drug discovery programs (Table 38.1). CPP-conjugated molecules have been used to characterize signal transduction pathways in animal models of several human diseases (4, 40–43), and provide data supporting the targeting of these pathways for drug development. In vivo demonstration of

Table 1
Clinical development status of CPP-conjugated compounds

Company	Compound	Target/Action	CPP	Indication	Status
Capstone Therapeutics	AZX100	HSP20	PTD4	Keloid scarring	Phase 2
KAI Pharmaceuticals	KAI-9803	Protein kinase C δ inhibitor	TAT PTD	Myocardial infarction	Phase 2b
	KAI-1678	Protein kinase C ϵ inhibitor	TAT PTD	Pain	Phase 2a
	KAI-1455	Protein kinase C ϵ activator	TAT PTD	Cytoprotection/ischemia	Phase 1
Xigen	XG-102	c-Jun-N-terminal kinases	TAT PTD	Hearing loss	Phase 2
				Stroke	Phase 1
Revance Therapeutics	RT001	Transdermal delivery of Botulinum toxin type A	TAT PTD	Wrinkles	Phase 2b
				Excessive sweating	Phase 1
Diatos SA	DTS-108	Nuclear delivery of cytotoxicin	Anti-DNA antibody	Cancer	Preclinical
CellGate	PsorBan	Transdermal delivery of cyclosporin A	R8	Psoriasis	Phase 2 discontinued

the intracellular bioavailability of cargo molecules conjugated to CPPs has been achieved in a wide variety of cells and tissues in preclinical studies (10, 13, 40–43), providing proof-of-principle for the application of these conjugates as drug candidates in their own right.

4. Preclinical Studies with CPP-Conjugated Compounds

Therapeutic areas that have been the focus of preclinical studies with CPP-conjugated therapeutics represent some of the major unmet clinical needs. In neurology, cardiology, and oncology, for example, CPPs, properly developed, offer the prospect of delivering highly specific and low toxicity (peptidic) drugs to critical tissues (e.g., CNS, heart, and tumors) by relatively noninvasive administration. A very large number of studies have been directed to investigating therapeutic applications of CPPs. In a broad review of this topic, over 200 studies were reported as early as 2004 (44), almost 60 of which report in vivo data in various animal models. Some of the preclinical studies particularly relevant to clinical applications are described below. Additional areas of interest are described in other reviews, such as applications of CPPs to antimicrobial agents (45).

4.1. Neuroprotection/ Stroke

Among neurological indications, stroke represents a major unmet medical need in which CPPs have been used as a facilitating strategy for the delivery of novel therapeutic agents. The MCAO model (middle cerebral artery occlusion) is a commonly used animal model in such studies. Blockage of the artery causes oxygen deprivation (ischemia, hypoxia) in brain tissue. Transient and permanent occlusions in this model represent the effects of temporary or long-lived blockage in the disease state. Relief of transient occlusion often causes additional cell death due to the induction of apoptotic pathways upon reperfusion.

The selective δ -PKC inhibitor KAI-9803 has been shown to significantly decrease the infarct size following cerebral ischemic injury in the transient rat MCAO model when administered either by intra-arterial or intraperitoneal injection (43) or by intravenous bolus injection (31). This compound comprises a fragment of the δ -PKC C2 domain (δ V1-1) conjugated by disulfide bond to TAT_{47–57} and illustrates the application of a general design strategy to modulators of PKC isozymes (46, 47). The inhibitory conjugate was shown to reduce apoptotic cell death when administered after ischemia in this setting, which is consistent with what is known of the role of δ -PKC in reperfusion injury. KAI-9803 was found to reduce cellular injury as measured by density of neurons and astrocytes, as well as reduced

macrophage and neutrophil infiltration in the penumbra (brain tissue surrounding the ischemic core) and to protect against capillary damage due to reperfusion injury in the penumbra and ischemic core. In addition, astrocyte proliferation was significantly higher in the KAI-9803-treated group in the penumbra. These effects were maintained for at least 7 days after brief intravenous administration (31).

Using the antiapoptotic protein Bcl-xL conjugated to TAT₄₇₋₅₇ in a linear peptide structure, another group reported neuroprotection in a murine MCAO study. The compound, known as PTD-HA-Bcl-xL, was delivered by intraperitoneal injection up to 45 min after the start of reperfusion (42). The infarct size was significantly reduced in a dose-dependent manner when measured 3 days after the start of reperfusion. Furthermore, PTD-HA-Bcl-xL decreased ischemia-induced caspase-3 activation in ischemic neurons, indicating that the effect was mediated, at least in part, by a reduction in the cellular apoptosis response following ischemia.

Another group of investigators constructed a Bcl-xL mutant protein (three amino acid substitutions, called FNK) that has even greater antiapoptotic activity than Bcl-xL as demonstrated in cultured cells (48). Using a gerbil model of transient global ischemia (5 min of occlusion of the common carotid arteries bilaterally), FNK conjugated to TAT₄₇₋₅₇ (referred to as PTD-FNK) delivered by intraperitoneal injection 3 h prior to ischemia was reported to significantly increase neuron cell density in the hippocampus when measured 7 days after reperfusion (41).

Finally, D-JNKII, a peptide inhibitor of c-Jun-N-terminal kinase conjugated to TAT₄₈₋₅₇ (now in clinical development as XG-102 by Xigen), protected against apoptotic cell death in *in vitro* and *in vivo* models of cerebral ischemia (27).

These studies suggest that CPP-conjugated antiapoptotic peptides or proteins can cross the blood–brain barrier and penetrate into brain parenchyma sufficiently to demonstrate efficacy in reducing ischemic injury in several animal models of stroke.

4.2. Cardioprotection

Similar to the stroke setting described above, ischemia–reperfusion injury is believed to play a significant role in the etiology of cardiovascular disease. Due to the commonality of mechanism, the δ -PKC inhibitor KAI-9803 has been extensively tested in cardiac models.

In *ex vivo* studies, KAI-9803 inhibited global cardiac injury following ischemia and reperfusion in rat hearts (49) as well as in excised human cardiac tissue (50). Atrial tissue was harvested from patients undergoing cardiac bypass surgery and suspended in an organ bath. When KAI-9803 was administered at the beginning of the reperfusion period, recovery of contractile function following ischemia was significantly greater than that observed with the TAT₄₇₋₅₇ CPP control group.

KAI-9803 has also been tested in a number of *in vivo* cardiac models. In one study, the conjugate was found to decrease infarct size when administered directly to the ischemic pig heart in an *in vivo* model of ischemia–reperfusion injury (occlusion of the left anterior descending coronary artery (LAD)) (30). In another study, KAI-9803 was administered intravenously to rats in the transient LAD occlusion model of acute myocardial infarction (AMI) (51). When infused over a 30-min period, KAI-9803 significantly reduced the infarct size, protected against microvascular damage and microthrombi, and attenuated the acute inflammatory response following reperfusion. A second PKC-modulating peptide consisting of an ϵ -PKC activator peptide/TAT_{47–57} conjugate (40, 49) also significantly improved recovery of contractile function compared to CPP controls when administered at the beginning of the reperfusion period.

Using a quite distinct approach, cardiac fibroblasts stably transfected with the GATA4 transcription factor protein fused to the HSV-derived CPP VP22 were delivered to rats 1 month after LAD ligation (52). The transplanted cells secreted the GATA4 protein which was taken up by neighboring cells due to the presence of the CPP sequence. This treatment resulted in enhanced growth of cardiac myocytes and increased cardiac function 10 weeks after the original LAD occlusion.

4.3. Analgesia

Effective pain management remains a significant unmet need for a variety of acute and chronic pain syndromes (53). Neuropathic pain results from nerve injury as seen in diabetic neuropathy, trauma-associated neuropathy, and other conditions (54), and is a form of pain notoriously difficult to treat. CPP-conjugated therapeutics have been investigated for their ability to alleviate inflammatory and neuropathic pain.

A peptide inhibitor of ϵ -PKC (ϵ VI-2) has been widely tested in various models of pain. This inhibitor has been conjugated to TAT_{47–57} in a number of different constructs and administered by a number of routes. Intrathecal administration of ϵ VI-2 has been reported to reduce formalin pain (55) and ethanol withdrawal neuropathy (56). Delivery of ϵ VI-2 into the brain reverses the tolerance developed by chronic morphine administration (57), as well as pain associated with opioid withdrawal (58).

KAI-1678 comprises TAT_{47–57} conjugated to ϵ VI-2 and has been extensively investigated in a wide variety of additional rodent models of different classes of pain (29).

This fusion peptide was found to be effective in three rodent models of neuropathic pain: L5 spinal nerve transection, spared nerve injury, and chronic constriction injury (28). In the L5 spinal nerve transection model, KAI-1678, delivered as an acute subcutaneous bolus or chronic subcutaneous mini osmotic pump infusion, dose-dependently reversed mechanical allodynia (pain

responses to normally non-noxious touch stimuli) and thermal hyperalgesia (larger pain response to heat than before injury). In the spared nerve injury model, a subcutaneous bolus caused dose-dependent reversal of allodynia and hyperalgesia. Finally, in the chronic constriction model, mechanical allodynia was rapidly blocked in a dose-dependent fashion by bolus or chronic infusion.

KAI-1678 was also tested in several rodent models of acute pain (29). In the capsaicin injection model of acute nociceptive pain, a subcutaneous bolus of KAI-1678 attenuated mechanical allodynia and dose-dependently reduced neuronal activation in the dorsal horn of the spinal cord. In the incision model of post-surgical pain, infusion of KAI-1678 attenuated secondary allodynia. Finally, both subcutaneous bolus and infusion of KAI-1678 dose-dependently reversed existing mechanical hyperalgesia in the carrageenan injection model of acute inflammatory pain.

In another approach, a peptide inhibitor of binding between the Src tyrosine kinase and the *N*-methyl-D-aspartyl receptor (NMDAR) was conjugated to TAT₄₇₋₅₇ and tested in rodent models of inflammatory and neuropathic pain (33). Intravenous or intrathecal administration of this compound, Src40-49Tat, was reported to dose-dependently decrease evoked pain behavior in the formalin model. Src40-49Tat also reversed established thermal and mechanical hyperalgesia resulting from CFA-induced inflammation by intravenous administration. Finally, this compound administered either intravenously or intrathecally significantly decreased mechanical and cold hyperalgesia caused by peripheral nerve injury. Importantly, Src40-49Tat did not appear to interfere with NMDAR-dependent learning and memory. These data suggest that targeting a modulator of NMDARs with a specific peptide inhibitor conjugated to TAT₄₇₋₅₇ significantly decreased hyperalgesia in rodent models of inflammatory and neuropathic pain.

These preclinical studies with TAT-conjugated peptides illustrate the potential of CPPs, together with knowledge of intracellular signal transduction mechanisms to effectively target clinically significant forms of pain that are often not well treated by existing therapeutic agents.

4.4. Anti-inflammatory Indications: Cyclosporine A Conjugate

Cyclosporine A (CsA) is an immune suppressant and anti-inflammatory agent used in a number of indications. However, CsA cannot readily penetrate the epidermis, which presents a significant lipidic barrier. This prevents the drug being used for topical applications, although this route could be desirable for dermatological applications, such as psoriasis, to reduce side-effects of systemic administration. CsA, conjugated to a polyarginine CPP by a pH-sensitive linker (7-mer, called R7-CsA), was shown to penetrate into the dermis of mouse skin and human skin grafted onto

mice (36). Furthermore, the conjugate was taken up by dermal T lymphocytes wherein it reduced the secretion of the proinflammatory cytokine, interleukin-2, and significantly reduced cutaneous inflammation in a mouse model of contact dermatitis. It is noteworthy that in this case the CPP linkage strategy was set up to render the conjugate inactive until released inside cells, thus presenting a twofold approach to minimizing toxicity through the use of CPPs.

4.5. Oncology

CPPs have been used to facilitate a number of novel approaches to oncology applications utilizing both peptide and small molecule cargoes.

In one such example, a polyarginine CPP was conjugated to p53, a tumor suppressor protein that is often nonfunctional in cancer cells. This construct was reported to powerfully inhibit the proliferation of human glioma cells *in vitro* when the p53 protein was mutated to be ubiquitination resistant (59). Another group conjugated the TAT PTD to a peptide that activates p53 in cancer cells but not normal cells. Treatment with this molecule increased lifespan and resulted in disease-free animals in two animal models of terminal human malignancy (60).

Beyond the applications in neurology and cardiology described above, the PKC enzyme family offers opportunities for cancer therapy. The β -PKC isozyme has been shown to be involved in angiogenesis, an important process in tumor growth (61). A selective inhibitor of β -PKC (known as β II-V5-3) was conjugated to the TAT₄₇₋₅₇ PTD via a disulfide bond and tested in tumor xenograft models (62). Mice bearing PC-3 prostate cancer xenografts were treated with β II-V5-3/TAT conjugate infused through an in-dwelling osmotic pump. Tumor growth and cell proliferation were effectively reduced in a compound-dependent manner, and relevant intracellular markers of biochemical efficacy were shown to be affected by the conjugate molecules. In addition to cancer, pathological angiogenesis has been implicated in other diseases, such as diabetic neuropathy and age-related macular degeneration.

The conjugation of CPPs to small molecule cytotoxic agents has been explored with the goal of modifying the *in vivo* distribution and improving the efficacy profile of the parent molecule. The anthracycline cytotoxic doxorubicin was attached through a noncleavable linker to several CPPs derived from heparin-binding proteins or anti-DNA antibodies (termed “Vectocell” peptides) (63). At least one of the resulting conjugates (DTS-101) showed increased antitumor efficacy and reduced systemic toxicity compared to the parent cytotoxin. In a second example from the same group, a conjugate of Vectocell to an active metabolite of irinotecan was evaluated (64). The conjugated molecule had desirable properties over the parent cytotoxin, displaying greater efficacy

and higher plasma levels than irinotecan without associated toxicity.

5. Clinical Trials with CPP-Conjugated Compounds

5.1. KAI-9803 DELTA-MI Study

As discussed above, KAI-9803, a selective δ -PKC inhibitor conjugated to TAT₄₇₋₅₇, has been shown to reduce injury associated with ischemia and reperfusion in animal models of AMI, and recently this result has been confirmed in a phase 2 clinical trial in human patients. Despite reperfusion therapy, myocardial and microvascular damage often result following acute ST-segment elevation myocardial infarction (STEMI) (65). In the DELTA-MI clinical study (32), KAI-9803 or saline placebo was injected into the coronary artery after reestablishment of perfusion.

To assess efficacy of drug treatment, several biomarker endpoints were measured and compared to saline placebos. Myocardial enzymes (CK-MB), a biomarker for myocardial cell death, were lower with KAI-9803 than saline placebo. Recovery of the ST-segment elevation toward baseline (what one would see in a normal ECG) was also faster and more extensive with KAI-9803 than saline placebo and the overall effect was statistically significantly better than the placebo control. Finally, left ventricle infarct size was estimated using single photon emission computed tomographic imaging with ^{99m}technetium sestamibi. The infarct size was lower with KAI-9803 compared to saline placebo for the three lowest dose cohorts, but not for the cohort with the highest dose.

This clinical study demonstrated that intracoronary injection of KAI-9803, as an adjunct to percutaneous coronary intervention (PCI), decreased myocardial infarct size compared to placebo (i.e., PCI alone) as assessed with three biomarker endpoints, and did so without increasing risk as assessed by several safety endpoints. The results encourage further, larger clinical trials with KAI-9803 as an adjunct therapy to PCI and indicate that TAT₄₇₋₅₇ can be safely administered to humans.

5.2. Other CPPs in Clinical Development

XG-102 is a 20 amino acid peptide inhibitor of all three c-Jun N-terminal kinases covalently linked to TAT₄₈₋₅₇ that is currently in clinical development by Xigen. These kinases play a role in apoptotic cell death, which is an important feature of the cellular pathology in both cerebral ischemia (stroke) (27) and acoustic trauma-induced auditory hair cell loss (66). XG-102 has completed a phase 1/2 clinical trial for the treatment of acute acoustic trauma and is currently in a phase 1 clinical trial for the treatment of stroke (Xigenpharma.com).

Revence Therapeutics is developing a compound, RT001, which permits topical application (instead of needle injection) of botulinum toxin type A for lateral canthal lines (“crow’s feet”) and primary focal hyperhidrosis (excessive sweating) (Revence.com). Their Macromolecule Transport System (MTS) is composed of a positively charged, lysine-rich central peptide domain sandwiched between two identical TAT₄₉₋₅₇ PTD domains to form a peptide with 35 amino acid residues. The lysine-rich region forms noncovalent, electrostatic bonds with anionic portions of their proprietary botulinum toxin type A molecule (called RTT150). The entire molecular complex is referred to as RT001. RT001 is able to penetrate the epidermis and dermis in the case of treatment for lateral canthal lines to permit botulinum toxin type A to temporarily block neuromuscular synaptic transmission and paralyze facial muscles lateral to the eye. In the case of hyperhidrosis, RT001 penetrates into the dermis to permit botulinum toxin type A to temporarily block synaptic activation of sweat glands by the autonomic (sympathetic) nervous system (67). RT001 recently demonstrated safety and efficacy in a phase 2B study for the treatment of lateral canthal lines, and has completed a phase 1 (safety) study for the treatment of hyperhidrosis (Revence.com).

Capstone Therapeutics has demonstrated that CPPs other than those derived from TAT may have therapeutic benefit. This company has been using a CPP-conjugated peptide to disrupt connective tissue growth expression and thus minimize fibrosis and scarring. AZX100 contains a phosphorylated peptide analog of HSP20 (WLRRAS(phospho)APLPGLK) attached to the CPP known as PTD4 CPP (YARAAARQARA). AZX100 has been shown to reduce stress fiber formation, alter the morphology of human dermal keloid fibroblasts, and reduce scarring in vivo (68), and is consequently being tested in the clinic for its ability to reduce keloid scarring. AZX100 has completed two phase 2 studies (Capstonethx.com).

These clinical trials demonstrate the potential of CPPs as therapeutics in the treatment of human disease.

6. Conclusions

In principle, a broad range of therapeutic targets can be envisioned for CPP-conjugated molecules limited only by our knowledge of specific molecular interactions within target cells and the consequences of those interactions for cell function. In practice, progress in the use of CPPs in drug delivery would be further helped by a greater understanding of the mechanisms of entry of CPPs into cells, which could lead to the ability to target specific

cell and tissue types, and further elucidation of the intracellular trafficking of CPPs and their cargoes, including endosomal escape and the fate of cargoes inside cells. Characterization of the dependence of such trafficking on the chemical nature of individual CPPs will allow tailoring of specific CPPs to particular intracellular targets and optimization of potency. As with any drug candidate, bioavailability with different routes of administration, possible toxicity and mechanisms of toxicity, pharmacokinetics, pharmacodynamics are also important considerations, and are likely to depend on the nature of the CPP, the linker design, and the specific cargo. Judicious CPP-conjugate design will be essential to the development of safe and effective therapeutics. Regardless of these caveats, progress in the development of CPP-conjugated therapeutics, as discussed above, has been encouraging and the prospects of significant advances in the treatment of stroke, heart disease, intractable pain, cancer, and other diseases are exciting.

References

- Daly, N.L., Rosengren, K.J., and Craik, D.J. (2009) Discovery, structure and biological activities of cyclotides. *Adv. Drug Deliv. Rev.* **61**(11), 918–930.
- Walensky, L.D., Kung, A.L., Escher, I., Malia, T.J., Barbuto, S., Wright, R.D., Wagner, G., Verdine, G.L., and Korsmeyer, S.J. (2004) Activation of apoptosis in vivo by a hydrocarbon-stapled BH3 helix. *Science* **305**, 1466–1470.
- Gump, J.M., and Dowdy, S.F. (2007) TAT transduction: the molecular mechanism and therapeutic prospects. *Trends Mol. Med.* **13**, 443–448.
- Chen, L., and Harrison, S.D. (2007) Cell-penetrating peptides in drug development: enabling intracellular targets. *Biochem. Soc. Trans.* **35**, 821–825.
- Prochiantz, A. (2008) Protein and peptide transduction, twenty years later a happy birthday. *Adv. Drug Deliv. Rev.* **60**, 448–451.
- Torchilin, V.P. (2008) Tat peptide-mediated intracellular delivery of pharmaceutical nanocarriers. *Adv. Drug Deliv. Rev.* **60**, 548–558.
- Wender, P.A., Galliher, W.C., Goun, E.A., Jones, L.R., and Pillow, T.H. (2008) The design of guanidinium-rich transporters and their internalization mechanisms. *Adv. Drug Deliv. Rev.* **60**, 452–472.
- Frankel, A.D., Brecht, D.S., and Pabo, C.O. (1988) Tat protein from human immunodeficiency virus forms a metal-linked dimer. *Science* **240**, 70–73.
- Joliot, A., Pernelle, C., Deagostini-Bazin, H., and Prochiantz, A. (1991) Antennapedia homeobox peptide regulates neural morphogenesis. *Proc. Natl. Acad. Sci. U.S.A.* **88**, 1864–1868.
- Fawell, S., Seery, J., Daikh, Y., Moore, C., Chen, L.L., Pepinsky, B., and Barsoum, J. (1994) Tat-mediated delivery of heterologous proteins into cells. *Proc. Natl. Acad. Sci. U.S.A.* **91**, 664–668.
- Derossi, D., Joliot, A.H., Chassaing, G., and Prochiantz, A. (1994) The third helix of the antennapedia homeodomain translocates through biological membranes. *J. Biol. Chem.* **269**, 10444–10450.
- Vives, E., Brodin, P., and Lebleu, B. (1997) A truncated HIV-1 Tat protein basic domain rapidly translocates through the plasma membrane and accumulates in the cell nucleus. *J. Biol. Chem.* **272**, 16010–16017.
- Schwarze, S.R., Ho, A., Vocero-Akbani, A., and Dowdy, S.F. (1999) In vivo protein transduction: delivery of a biologically active protein into the mouse. *Science* **285**, 1569–1572.
- Futaki, S., Suzuki, T., Ohashi, W., Yagami, T., Tanaka, S., Ueda, K., and Sugitara, Y. (2001) Arginine-rich peptides: an abundant source of membrane-permeable peptides having potential as carriers for intracellular protein delivery. *J. Biol. Chem.* **276**, 5836–5840.
- Jones, S.W., Christison, R., Bundell, K., Voyce, C.J., Brockbank, S.M.V., Newham, P.,

- and Lindsay, M.A. (2005) Characterisation of cell-penetrating peptide-mediated peptide delivery. *Br. J. Pharmacol.* **145**, 1093–1102.
16. Chen, L., Wright, L.R., Chen, C.-H., Oliver, S.F., Wender, P.A., Mochly-Rosen, D. (2001) Molecular transporters for peptides: delivery of a cardioprotective ϵ PKC agonist peptide into cells and intact ischemic heart using a transport system, R. *Chem. Biol.* **8**, 1123–1129.
 17. Wender, P.A., Mitchell, D.J., Pattabiraman, K., Pelkey, E.T., Steinman, L., and Rothbard, J.B. (2000) The design, synthesis, and evaluation of molecules that enable or enhance cellular uptake: peptoid molecular transporters. *Proc. Natl. Acad. Sci. U.S.A.* **97**, 13003–13008.
 18. Richard, J.P., Melikov, K., Brooks, H., Prevot, P., Lebleu, B., and Chernomordik, L.V. (2005) Cellular uptake of unconjugated TAT peptide involves clathrin-dependent endocytosis and heparin sulfate receptors. *J. Biol. Chem.* **280**, 15300–15306.
 19. Potocky, T.B., Menon, A.K., and Gellman, S.H. (2003) Cytoplasmic and nuclear delivery of a TAT-derived peptide and a b-peptide after endocytic uptake into HeLa cells. *J. Biol. Chem.* **278**, 50188–50194.
 20. Fittipaldi, A., Ferrari, A., Zoppe, M., Arcangeli, C., Pellegrini, V., Beltram, F., and Giacca, M. (2003) Cell membrane lipid rafts mediate caveolar endocytosis of HIV-1 Tat fusion proteins. *J. Biol. Chem.* **278**, 34141–34149.
 21. Console, S., Marty, C., Garcia-Echeverria, C., Schwendener, R., and Ballmer-Hofer, K. (2003) Antennapedia and HIV transactivator of transcription (TAT) “protein transduction domains” promote endocytosis of high molecular weight cargo upon binding to cell surface glycosaminoglycans. *J. Biol. Chem.* **278**, 35109–35114.
 22. Richard, J.P., Melikov, K., Brooks, H., Prevot, P., Lebleu, B., and Chernomordik, L.V. (2005) Cellular uptake of unconjugated TAT peptide involves clathrin-dependent endocytosis and heparin sulfate receptors. *J. Biol. Chem.* **280**, 15300–15306.
 23. Mai, J.C., Shen, H., Watkins, S.C., Cheng, T., and Robbins, P.D. (2002) Efficiency of protein transduction is cell type-dependent and is enhanced by dextran sulfate. *J. Biol. Chem.* **277**, 30208–30218.
 24. Tyagi, M., Rusnati, M., Presta, M., and Giacca, M. (2001) Internalization of HIV-1 Tat requires cell surface heparan sulfate proteoglycans. *J. Biol. Chem.* **276**, 3254–3261.
 25. Sandgren, S., Cheng, F., and Belting, M. (2002) Nuclear targeting of macromolecular polyanions by an HIV-Tat derived peptide: role for cell-surface proteoglycans. *J. Biol. Chem.* **277**, 38877–38883.
 26. Fischer, R., Kohler, K., Fotin-Mleccek, M., and Brock, R. (2004) A stepwise dissection of the intracellular fate of cationic cell-penetrating peptides. *J. Biol. Chem.* **279**, 12625–12635.
 27. Hirt, L., Badaut, J., Thevenet, J., Granziera, C., Regli, L., Maurer, F., Bonny, C., and Bogousslavsky, J. (2004) D-JNK11, A cell-penetrating c-jun-N-terminal kinase inhibitor, protects against cell death in severe cerebral ischemia. *Stroke* **35**, 1738–1743.
 28. Miao, F. J.-P., Mohammad, H.K., Velazquez, K.T., Harrison, S.D., and Sweitzer, S.M. (2008) KAI-1678, a novel inhibitor of protein kinase C epsilon, attenuates hyperalgesia and allodynia in three neuropathic pain models in rodents. *Soc. Neurosci. (Abs.)* **774.10**.
 29. Velazquez, K.T., Miao, F.J.P., Mohammad, H.K., Ogden, C.J., Harrison, S.D., and Sweitzer, S.M. (2008) KAI-1678, a novel inhibitor of protein kinase C epsilon, attenuates mechanical hyperalgesia in rodent models of acute nociceptive, inflammatory and post-surgical pain. *Soc. Neurosci. (Abs.)* **468.16**.
 30. Inagaki, K., Chen, L., Ikeno, F., Lee, F.H., Imahashi, K., Bouley, D.M., Rezaee, M., Yock, P.G., Murphy, E., Mochly-Rosen, D. (2003) Inhibition of δ -protein kinase C protects against reperfusion injury of the ischemic heart in vivo. *Circulation* **108**, 2304–2307.
 31. Sho, E., Dong, J., Jin, Z., Begley, R., Chen, L., Harrison, S.D., and Mendel, D.B. (2008) Protein kinase C- δ inhibitor protects against ischemic stroke by inhibiting cellular injury and inflammation and promoting astrocyte proliferation. *Int. Stroke Conf. Abstr.* **39**, P422, 671–672.
 32. Direct inhibition of δ -protein kinase C enzyme to limit total infarct size in acute myocardial infarction (DELTA MI) investigators. (2008) Intracoronary KAI-9803 as an adjunct to primary percutaneous coronary intervention for acute ST-segment elevation myocardial infarction. *Circulation* **117**, 886–896.
 33. Liu, X. J., Gingrich, J.R., Vargas-Caballero, M., Dong, Y.N., Sengar, A., Beggs, S., Wang, S.-H., Ding, H.K., Frankland, P.W., and Salter, M.W. (2008) Treatment of inflammatory and neuropathic pain by uncoupling Src from the NMDA receptor complex. *Nat. Med.* **14**, 1325–1332.
 34. Sweitzer, S.M., Mohammad, H.K., Velazquez, K.T., and Harrison, S.D. (2007) Inhibition of

- protein kinase C epsilon translocation reduces allodynia and hyperalgesia in a rodent model of neuropathic pain. *Soc. Neurosci. (Abs.)* **185.2**.
35. Velazquez, K.T., Mohammad, H.K., Harrison, S.D., and Sweitzer, S.M. (2007) A small peptide inhibitor of γ PKC translocation attenuates allodynia and hyperalgesia in a rodent model of neuropathic pain. *Soc. Neurosci. (Abs.)* **185.4**.
 36. Rothbard, J.B., Garlington, S., Lin, Q., Kirschberg, T., Kreider, E., McGrane, P.L., Wender, P.A., and Khavari, P.A. (2000) Conjugation of arginine oligomers to cyclosporine A facilitates topical delivery and inhibition of inflammation. *Nat. Med.* **6**, 1253–1257.
 37. Begley, R., Liron, T., Baryza, J., and Mochly-Rosen, D. (2004) Biodistribution of intracellularly-acting peptides conjugated reversibly to Tat. *Biochem. Biophys. Res. Commun.* **318**, 949–954.
 38. Toro, A., and Grunebaum, E. (2006) TAT-mediated intracellular delivery of purine nucleoside phosphorylase corrects its deficiency in mice. *J. Clin. Invest.* **116**, 2717–2726.
 39. Covic, L., Gresser, A.L., Talavera, J., Swift, S., and Kuliopulos, A. (2002) Activation and inhibition of G protein-coupled receptors by cell-penetrating membrane-tethered peptides. *Proc. Natl. Acad. Sci. U.S.A.* **99**, 643–648.
 40. Chen, L., Hahn, H., Wu, G., Chen, C.-H., Liron, T., Schechtman, D., Cavallaro, G., Banci, L., Guo, Y., Bolli, R., Dorn II, G.W., and Mochly-Rosen, D. (2001) Opposing cardioprotective actions and parallel hypertrophic effects of δ PKC and ϵ PKC. *Proc. Natl. Acad. Sci. U.S.A.* **98**, 11114–11119.
 41. Asoh, S., Ohsawa, I., Mori, T., Katsura, K., Hiraide, T., Katayama, Y., Kimura, M., Ozaki, D., Yamagata, K., and Ohta, S. (2002) Protection against ischemic brain injury by protein therapeutics. *Proc. Natl. Acad. Sci. U.S.A.* **99**, 17107–17112.
 42. Cao, G., Pei, W., Ge, H., Liang, Q., Luo, Y., Sharp, F.R., Lu, A., Ran, R., Graham, S.H., and Chen, J. (2002) In vivo delivery of a Bcl-xL fusion protein containing TAT protein transduction domain protects against ischemic brain injury and neuronal apoptosis. *J. Neurosci.* **22**, 5423–5431.
 43. Bright, R., Raval, A.P., Dembner, J.M., Perez-Pinzon, M.A., Steinberg, G.K., Yenari, M.A., and Mochly-Rosen, D. (2004) Protein kinase C δ mediates cerebral reperfusion injury in vivo. *J. Neurosci.* **24**, 6880–6888.
 44. Dietz, G.P.H., and Bohr, M. (2004) Delivery of bioactive molecules into the cell: the Trojan horse approach. *Mol. Cell. Neurosci.* **27**(2), 85–131.
 45. Foerg, C., and Merkle, HP. (2008) On the biomedical promise of cell penetrating peptides: limits versus prospects. *J. Pharm. Sci.* **97**, 144–162
 46. Mochly-Rosen, D. (1995) Localization of protein kinases by anchoring proteins: a theme in signal transduction. *Science* **268**, 247–251.
 47. Mochly-Rosen, D., and Gordon, A.S. (1998) Anchoring proteins for protein kinase C: a means for isozyme selectivity. *FASEB J.* **12**, 35–42.
 48. Asoh, S., Ohtsu, T., Ohta, S. (2000) The super anti-apoptotic factor Bcl-xFNK constructed by disturbing intramolecular polar interactions in rat Bcl-x_L. *J. Biol. Chem.* **275**, 37240–37245.
 49. Inagaki, K., Hahn, H.S., Dorn II, G.W., and Mochly-Rosen, D. (2003) Additive protection of the ischemic heart *ex vivo* by combined treatment with δ -protein kinase C inhibitor and ϵ -protein kinase C activator. *Circulation* **108**, 869–875.
 50. Sivaraman, V., Hausenloy, D.J., Kolvekar, S., Hayward, M., Lawrence, D., Yap, J., Di Salvo, C., and Yellon, D.M. (2009) The divergent roles of protein kinase C epsilon and delta in simulated ischaemia-reperfusion injury in human myocardium. *J. Mol. Cell. Cardiol.* **46**, 758–764.
 51. Sho, E., Dong, J., Jin, Z., Lee, Y.S., Harrison, S., and Mendel, D. (2008) Protein kinase C- δ inhibitor protects against acute myocardial infarction by intravenous administration in different periods of cardiac ischemia-reperfusion. *J. Am. Coll. Cardiol. Suppl. A* **51**(10), 1003–1086, A188
 52. Bian, J., Popovic, Z.B., Benejam, C., Kiedrowski, M., Rodriguez, L.L., and Penn, M.S. (2007) Effect of cell-based intracellular delivery of transcription factor GATA4 on ischemic cardiomyopathy. *Circ. Res.* **100**, 1626–1633.
 53. Basbaum, A.I., and Julius, D. (2006) Toward better pain control. *Sci. Am.* **294**(6), 61–67.
 54. Woolf, C.J., and Mannion, R.J. (1999) Neuropathic pain: aetiology, symptoms, mechanisms, and management. *Lancet* **353**, 1959–1964.
 55. Sweitzer, S. M., Wong, S.M.E., Peters, M.C., Mochly-Rosen, D., Yeomans, D.C., and Kendig, J.J. (2004) Protein kinase C ϵ and γ : involvement in formalin-induced nociception in neonatal rats. *J. Pharmacol. Exp. Ther.* **309**, 616–625.

56. Shumilla, J.A., Liron, T., Mochly-Rosen, D., Kendig, J.J., and Sweitzer, S. M. (2005) Ethanol withdrawal-associated allodynia and hyperalgesia: age-dependent regulation by protein kinase C ϵ and γ isozymes. *J. Pain* **6**, 535–549.
57. Smith, F.L., Gabra, B.H., Smith, P.A., Redwood, M.C., and Dewey, W.L. (2007) Determination of the role of conventional, novel and atypical PKC isoforms in the expression of morphine tolerance in mice. *Pain* **127**, 129–139.
58. Sweitzer, S.M., Wong, S.M.E., Tjolsen, A., Allen, C.P., Mochly-Rosen, D., and Kendig, J.J. (2004) Exaggerated nociceptive responses on morphine withdrawal: roles of protein kinase C ϵ and γ . *Pain* **110**, 281–289.
59. Michiue, H., Tomizawa, K., Matsushita, M., Tamiya, T., Lu, Y.F., Ichikawa, T., Date, I., and Matsui, H. (2005) Ubiquitination-resistant p53 protein transduction therapy facilitates anti-cancer effect on the growth of human malignant glioma cells. *FEBS Lett.* **579**, 3965–3969.
60. Snyder, E.L., Meade, B.R., Saenz, C.C., and Dowdy, S.F. (2004) Treatment of terminal peritoneal carcinomatosis by a transducible p53-activating peptide. *PLoS Biol.* **2**, 186–193.
61. Yoshiji, H., Kuriyama, S., Ways, D.K., Yoshii, J., Miyamoto, Y., Kawata, M., Ikenaka, Y., Tsujinoue, H., Nakatani, T., Shibuya, M., and Fukui, H. (1999) Protein kinase C lies on the signaling pathway for vascular endothelial growth factor-mediated tumor development and angiogenesis. *Cancer Res.* **59**, 4413–4418.
62. Kim, J., Choi, Y.-L., Vallentin, A., Hunrichs, B.S., Hellerstein, M.K., Peehl, D.M., and Mochly-Rosen, D. (2008) Centrosomal PKC β II and pericentrin are critical for human prostate cancer growth and angiogenesis. *Cancer Res.* **68**(16), 6831–6839.
63. Meyer-Losic, F., Quinonero, J., Dubois, V., Alluis, B., Dechambre, M., Michel, M., Callier, F., Fernandez, A.-M., Trouet, A., and Kearsy, J. (2006) Improved therapeutic efficacy of doxorubicin through conjugation with a novel peptide drug delivery technology (Vectocell). *J. Med. Chem.* **49**(23), 6908–6916.
64. Meyer-Losic, F., Nicolazzi, C., Quinonero, J., Ribes, F., Michel, M., Dubois, V., de Coupade, C., Boukaissi, M., Chene, A.-S., Tranchant, I., Arranz, V., Zoubaa, I., Fruchart, J.-S., Ravel, D., and Kearsy, J. (2008) DTS-108, a novel peptidic prodrug of SN38: in vivo efficacy and toxicokinetic studies. *Clin. Cancer Res.* **14**(7), 2145–2153.
65. Roe, M.T., Ohman, E.M., Maas, A.C.P., Christenson, R.H., Mahaffey, K.W., Granger, C.B., Harrington, R.A., Califf, R.M., and Krucoff, M.W. (2001) Shifting the open artery hypothesis downstream: the quest for optimal reperfusion. *J. Am. Coll. Cardiol.* **37**, 9–18.
66. Wang, J., Van De Water, T.R., Bonny, C., de Ribaupierre, F., Puel, J.L., and Zine, A. (2003) A peptide inhibitor of c-jun N-terminal kinase protects against both aminoglycoside and acoustic trauma-induced auditory hair cell death and hearing loss. *J. Neurosci.* **23**, 8596–8607.
67. Glogau, R.G. (2007) Topically applied botulinum toxin type A for the treatment of primary axillary hyperhidrosis: results of a randomized, blinded vehicle-controlled study. *Dermatol. Surg.* **33**, S76–S80.
68. Lopes, L.B., Furnish, E.J., Komalavilas, P., Flynn, C.R., Ashby, P., Hansen, A., Ly, D.P., Yang, G.P., Longaker, M.T., Panitch, A., and Brophy, C.M. (2009) Cell permeant peptide analogues of the small heat shock protein, HSP20, reduce TGF- β 1-induced CTGF expression in keloid fibroblasts. *J. Invest. Dermatol.* **129**, 590–598.

Chapter 39

Nonclinical and Clinical Experiences with CPP-Based Self-Assembling Peptide Systems in Topical Drug Development

Jacob M. Waugh, Jane Lee, Michael D. Dake, and Dan Browne

Abstract

Considerations in rational designs of CPP-based transcutaneous delivery systems are described. Impact of design considerations of nonclinical and clinical results are presented in detail.

Key words: Botulinum toxin, Lateral canthal lines, Hyperhidrosis, TAT, Ionic

1. Introduction

As will be apparent upon reading the other chapters in this book, there are a number of laboratories exploring basic aspects of cell-penetrating peptides (CPPs). More is being elucidated about this powerful family of agents and their potential applications each day. In order to complement this work, our group has primarily focused on translational applications for CPPs. Specifically, we have focused on attributes of CPPs useful for dermatology and in particular for transcutaneous local delivery of macromolecules.

Given this approach, our group typically employs a noncovalent means of initially screening CPPs with potential therapeutic payloads. This has allowed exploration of various CPPs alone and in combination without issues relating to activity, altered pharmacologic properties, or safety issues related to generation of new chemical entities (NCE). The focus of this chapter is on the rational design of a self-assembling ionic system to deliver a macromolecule transcutaneously. More specifically, considerations in development of a CPP-enabled topical form of botulinum toxin for facial wrinkles and hyperhidrosis is explored. Although our

laboratories typically employ marker studies and *in vitro* work as an initial step, here we focus on transcutaneous flux studies, *in vivo* nonclinical biologic effects, and clinical outcomes primarily to illustrate the design principles in practice.

1.1. Clinical Use and Characteristics of Botulinum Toxin

Revance Therapeutics, Inc. (Revance) is developing a topical product, RT001 (Botulinum Toxin Type A Topical Gel), an investigational drug containing the 150 kDa portion of Botulinum Toxin Type A (BoNTA) as the active moiety, for the treatment of moderate to severe lateral canthal lines (crow's feet wrinkles) and severe primary axillary hyperhidrosis. Injectable BoNTA has been successfully used in a range of medical disorders including strabismus, blepharospasm, focal dystonias, spasticity associated with juvenile cerebral palsy and adult stroke, and various cosmetic treatments (1–5). Thus, the safety and effectiveness of BoNTA for treating these conditions has been well established for over 20 years now.

Aesthetic medicine has been inundated with treatments for facial rhytids. BoNTA is the only Food and Drug Administration (FDA)-approved treatment to temporarily relax the underlying facial muscle that pleats the skin resulting in hyperfunctional rhytids. Since 1992, botulinum toxin has been used to treat a variety of cosmetic conditions and medical indications. Following Carruthers' first description of treatment of glabellar rhytids ("frown line" wrinkles), botulinum toxin has revolutionized the practice of noninvasive aesthetic medicine (6). In 2002, the United States (US) FDA approved the use of BOTOX® Cosmetic (Botulinum Toxin Type A Purified Toxin Complex; Allergan) for the treatment of moderate-to-severe glabellar rhytids, associated with corrugator and/or procerus muscle activity in adult patients 65 years of age and younger. Patient satisfaction is above 80%, and BoNTA is considered to be effective and safe (7). By 2005, BOTOX® Cosmetic injections were the most common noninvasive physician-administered cosmetic procedure, with more than 3.2 million injections administered (8). In addition, botulinum toxin was initially shown to be effective in reducing sweat production in healthy volunteers (9, 10) and subsequently for the treatment of primary axillary hyperhidrosis, excessive underarm sweating (11–13).

Lateral canthal lines (LCLs), commonly termed crow's feet, result from muscle activity in combination with photoaging. Even though treatment of crow's feet has not been approved in the US, injectable 900 kDa BoNTA is used extensively off-label to treat LCLs. Typically, the initial dose chosen is 8–16 U per side in women and 12–16 U in men, with generally 3–4 U per injection and three injections per site. The duration of paralysis appears to be shorter with lower doses of toxin. The incidence of AEs in published studies was generally low. In the studies by Lowe et al.

(14, 15), bruising was the most commonly reported event, occurring at similar rates on active and placebo-treated sides. No serious or severe AEs, dose-related effects, or events of blepharoptosis, diplopia, lip ptosis, or muscle weakness were reported. However, Matarasso and Matarasso (16) felt that the paralytic effect of injected BoNTA can span up to 3 cm from the site of injection and even further when dilute concentrations and large volumes of BoNTA are used.

Limitations of injections, including those with BoNTA, include pain, erythema, swelling, needle marks, tenderness, and potential infection from needle use. The patient's medical regimen is potentially impacted by being advised to avoid aspirin, nonsteroidal anti-inflammatory drugs, and vitamin E prior to injection, to reduce the risk of bleeding and bruising. Bruising is of particular concern in the crow's feet/lateral canthus/orbicularis oculi region, where the blood vessels are superficial and the skin is thin. Treatments for primary axillary hyperhidrosis typically require 10–15 injections per treatment area (17), thus injection site pain is a major concern for treatment of this condition.

There are seven antigenically distinct serotypes of botulinum toxin (A, B, C1, D, E, F, and G), produced by a strain of the anaerobic bacterium *Clostridium botulinum*. Currently, types A and B are approved for physician use in the US and internationally. All types of botulinum toxin block cholinergic neurotransmission by preventing acetylcholine (ACh) release at peripheral neuromuscular junctions (4). Botulinum toxin type A is produced by *Clostridium botulinum* (serotype A-Hall strain) as a single inactive polypeptide chain of 150 kDa, which subsequently undergoes proteolytic cleavage by proteases present in the fermentation culture to yield the fully active di-chain molecule comprised of a 100 kDa heavy chain and a 50 kDa light chain linked via both noncovalent interactions and a disulfide bond (18). The heavy chain plays a role in cell binding, internalization, and translocation of botulinum toxin into nerve cells, while the light chain acts as a site-specific metalloprotease. Botulinum toxin acts on cholinergic nerve terminals of eccrine gland secretion and involuntary smooth muscle as well as striated muscle, but does not appear to act on cardiac muscle. The ACh vesicles in target neurons are associated with a protein aggregate called the SNARE complex (soluble N-ethylmaleimide-sensitive fusion attachment protein receptor). In order to affect signal transmission across the neuromuscular junction, vesicles of ACh in the presynaptic neural bouton must be released into the synaptic cleft. In the case of striated muscle, the neurotransmitter binds to specific receptors on the muscle plate that trigger opening of sodium ion channels, resulting in depolarization and contraction in the adjacent striated muscle. This ACh release requires the participation of the SNARE proteins that mediate the fusion of synaptic vesicles with the

neuronal plasma membrane (19). It is generally accepted that the SNARE proteins form the core of the machinery for the intracellular membrane fusion necessary for ACh exocytosis. The SNARE complex consists of at least five proteins that play differing roles in the exocytosis process. For example, VAMP (vesicle-associated membrane protein), also known as synaptobrevin, is associated with the synaptic vesicles, whereas SNAP-25 becomes associated with the synaptic membrane. Under the influence of an action potential in the neuron, calcium channels open and calcium binds to the SNARE proteins. This causes them to spontaneously assemble into a soluble ternary complex that moves to the neuronal plasma membrane where the SNARE complex enables the ACh vesicle to fuse with the cell membrane (20). The fewer the number of vesicles released into the synaptic cleft, the lower the probability that an action potential will propagate and result in muscle fiber contraction. It is important to note that inhibition of ACh exocytosis by botulinum toxin is temporary and that neurotransmission is eventually restored.

The RTT150 form of purified toxin (150 kDa) is different from the form of the toxin complex which is currently marketed as BOTOX® and BOTOX® Cosmetic (consisting of a 900 kDa complex comprised of the 150 kDa toxin with several bacterially derived accessory proteins). Unlike either marketed product (17), the RTT150 DP is not formulated in human serum albumin, hemagglutinin, or other pooled human or animal derived components. The structure of RTT150 is important in development of a CPP-based therapeutic, since any interference with selectivity, binding, or steps to generate a functional domain may render the product unusable. As a result, an ionic, rather than covalent, approach was taken. Essentially, a nonnative complex is self-assembled using a PTD-containing peptide and the RTT150 core. A similar approach can be taken using the larger 900 kDa complex as a core or variations thereupon, though the larger size and other physical characteristics render the self-assembled nonnative particle quite different in pharmacokinetics and pharmacodynamics.

2. RT001

The active pharmaceutical ingredient in RT001 is a purified 150 kDa BoNTA, derived from the Hall strain *Clostridium botulinum* supplied as lyophilized drug product referred to as RTT150. RT001 is composed of purified RTT150, formulated in a poloxamer gel containing a CPP-based permeation-enhancing peptide excipient, RTP004. The peptide excipient in this product ionically self-assembles and enables the transcutaneous delivery of the

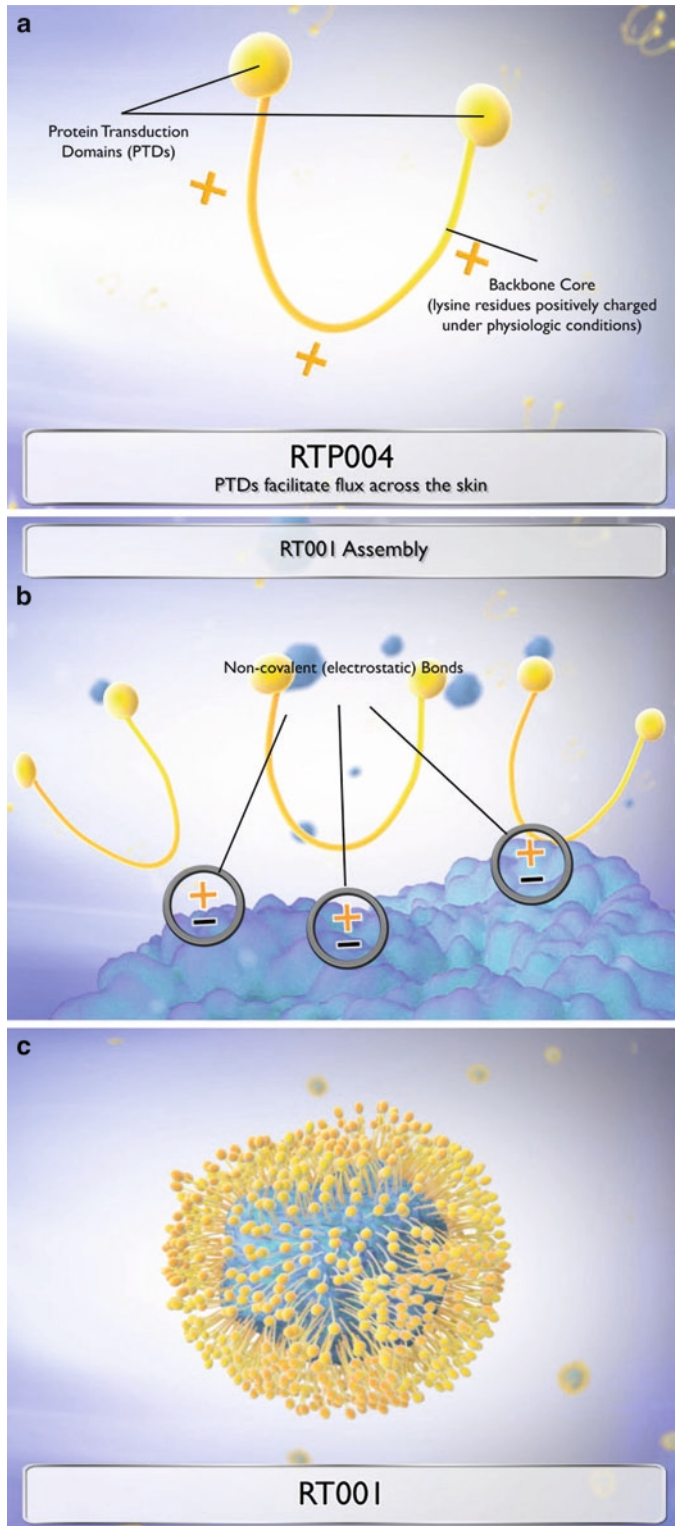


Fig. 1. RT001, an investigational drug. The positively charged core of RTP004 forms a noncovalent bond to associated CPPs with the RTT150 molecule to form RT001.

were constructed. After screening several combinations of these in marker experiments, a functional model of in vivo toxin function was employed after topical delivery. Polycations of varying lengths were conjugated to PTDs covalently (e.g., R9) and compared to controls of either polycation without PTD or toxin alone. For this experiment, a commercially available 900 kDa botulinum toxin complex (BOTOX®, Allergan, Inc., Irvine, CA) was employed as the active payload. BOTOX® was reconstituted according to the manufacturer's instructions. In each case, an excess of polycation was employed to assemble a final complex that has an excess of positive charge. Optimal ratios were selected based on pilot experiments (data not presented). BOTOX® dose was standardized across all groups as was total volume and final pH of the composition to be applied topically. Samples were prepared as detailed in Table 1.

All animal use was performed under IRB-approved protocols in compliance with all applicable laws and usage standards including NIH and institutional guidelines (Covance, Inc., Berkeley, CA). As with all our laboratory work, all observers were blinded to treatment group identities. Animals were anesthetized via inhalation of isoflurane during application of treatments. After being anesthetized, C57 black 6 mice ($N=4$ per group) underwent topical application of metered 400 μ L dose of the appropriate treatment applied uniformly from the toes to the mid-thigh. Both limbs were treated, and treatments were randomized to either side. Animals did not undergo depilation. At 30 min after the initial treatment, mice were evaluated for digital abduction capability according to published digital abduction scores for foot mobility after BOTOX® administration (22). Mouse mobility was also subjectively assessed. Digital abduction scores (DAS) were tabulated independently by two blinded observers. Mean and standard error were subsequently determined for each group with analysis of significance at 95% confidence in one way ANOVA repeated measures using StatView® software (Abacus Concepts, Inc., Berkeley, CA). Mean digital abduction scores after single-time topical administration are presented in Table 2 and illustrated in the representative photograph of Fig. 2 below. The Revance

Table 1
Description of the prepared samples

Group	PTD	MW polycation	Toxin dose
K125PTD	Yes	125,000	2 U
K30PTD	Yes	30,000	2 U
K125	None	125,000	2 U
Control	None	None	2 U

Table 2
Digital abduction scores 30 min after single-time topical application of BOTOX® with the poly-L-lysine of MW 125,000 or 30,000 conjugated to a PTD (K125R or K30R respectively), BOTOX® with a control polycation K (K125) or Controls (BOTOX® alone and untreated)

Group	Mean	Std. error
K125R	3.333	0.333
K30R	0.500	0.100
K125	0.333	0.333
Control	0.397	0.150

P=0.0351 (significant at 95%)

Transdermal Efficiency of Wipe-On Botulinum Therapeutics

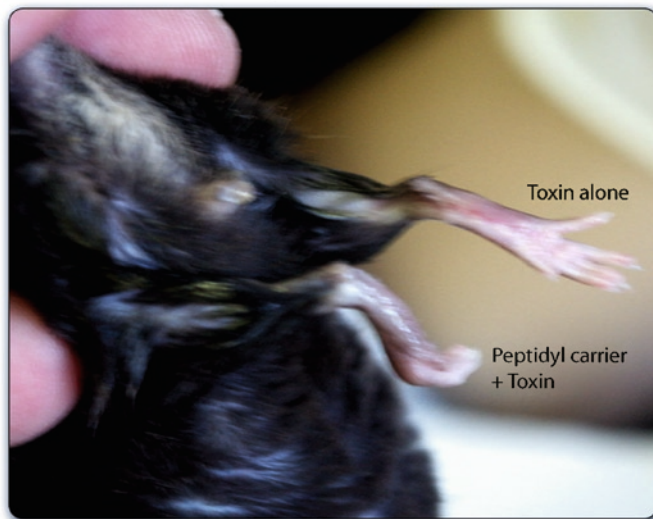


Fig. 2. Transdermal Efficiency of Wipe-On Botulinum Therapeutics. Limbs treated with BOTOX® plus the control polycation polylysine or BOTOX® without polycation (“Toxin alone”) can mobilize digits (as a defense mechanism when picked up), but the limbs treated with BOTOX® plus the Revance peptidyl carrier KNR (“Peptidyl Carrier + Toxin”) cannot be moved.

peptidyl carrier KNR affords statistically significant functional delivery of BOTOX® across skin relative to both controls, which were comparable to one another. Additional independent repetitions (total of three independent experiments all with identical conclusions in statistically significant paralysis from topical BOTOX®

with KNR but not controls) of the present experiment confirmed the present findings and revealed no significant differences between topical BOTOX® with or without K (i.e., both controls). Interestingly, mice consistently ambulate toward a paralyzed limb.

Since the relative targets presented by cosmetic applications and hyperhidrosis are quite superficial, the refinement of the cationic core in design of RTP004 was biased toward more superficial delivery. Shorter cationic cores were thus chosen over the long ones employed by our group in other applications. Given the elective, non-life-threatening nature of these conditions, a superficial and hence safer delivery system was essentially required for viability.

The primary design bias was thus for safety above efficiency for the intended clinical applications of RT001. As a result, a degradable sequence was required. L amino acids were thus employed for the sequence. Consistent with the density of dibasic L-amino acid sequences in the core, it was expected that the sequence would be trypsin- and serum-degradable. These effects were confirmed both in gel electrophoresis and HPLC with both time course and dosing studies. Results showing complete degradation by trypsin are presented as Fig. 3. Thus, a sequence that can be safely degraded by tissue trypsin activity or serum was selected for RTP004.

**2.2. Design
Considerations
Relating to the PTD**

With a given payload as the active, varying the CPP varies the delivery characteristics of the combined product independent of the length of the cationic portion of the molecule. In order to confirm the impact of PTD identity on transcutaneous delivery of

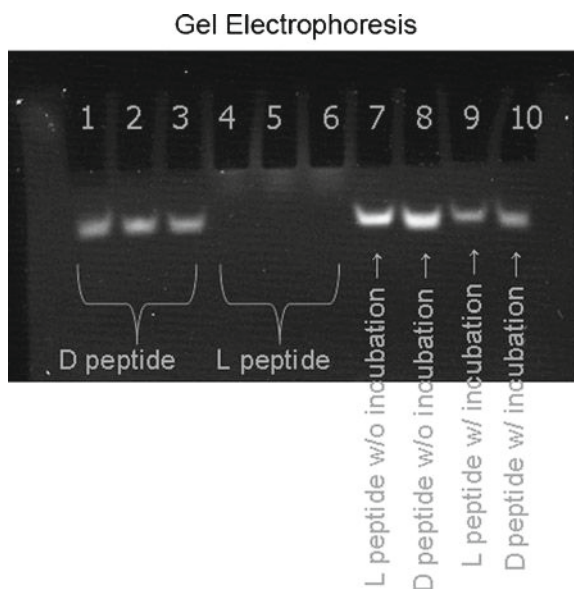


Fig. 3. Gel electrophoresis demonstrating that RTP004 can be degraded by trypsin.

botulinum toxin, several peptidyl carriers were constructed. After screening several combinations of these in marker experiments, a functional model of in vivo toxin function was employed after topical delivery. For this experiment, a MW 21,000 poly-L-lysine was conjugated to PTD that were either TAT minimal PTDs or 9-mers of arginine (R9). Controls for this study employed saline in place of the peptide. As a payload, a commercially available 900 kDa Botulinum Toxin Type A product (Dysport®, Ipsen, UK) was employed. C57 black 6, female mice (Charles River Laboratories International, Inc., Wilmington, MA) weighing 19–20 g were used. Animals were anesthetized using isoflurane, and topical application of treatment solutions (Table 3) was performed on mouse hind limbs. After recovery, hind-limb muscle weakening was scored using DAS values.

The Dysport® reconstituting solution of sterile 0.9% sodium chloride (Abbott Laboratories, North Chicago, IL) was prepared. Peptidyl carriers were prepared at 1 mg/mL concentration with 0.9% sodium chloride. 500 U of Dysport® (Ipsen) was reconstituted with 2.5 mL of reconstituting solution using sterile 3 mL latex free syringe with 18G11/2 (Becton Dickinson & Co., Franklin Lakes, NJ). The reconstituted Dysport® was carefully mixed by inversion. The treatment solution was prepared with 30 U of Dysport® and peptidyl carrier (i.e., 150 mcL of Dysport® was added to 75 mcL of Peptidyl-A, Peptidyl-P or Peptidyl-R) in a microcentrifuge tube and was left at room temperature for 5 min for the complexes to form. All animal use was performed under IRB-approved protocols in compliance with all applicable laws and usage standards including NIH and institutional guidelines (Covance, Inc., Berkeley, CA). Animals were anesthetized using 1.5% isoflurane mixed with oxygen and then injected with 0.05 mL rodent anesthetic cocktail (3.75 mL of 100 mg/mL ketamine, 3.00 mL of 20 mg/mL xylazine, and 23.25 mL of saline) intraperitoneally. After being anesthetized, C57 black 6 female mice ($N=3$ per group) were randomly divided and prepared for treatment. The treatment solution was applied to the

Table 3
Description of test
compounds and peptidyl
transdermal carriers

Group	Test compound
TAT	30 U Dysport
R9	30 U Dysport
Control	Saline

Table 4
Foot mobility score-DAS values. Mean and standard errors for each group are presented after 30 min posttreatment

Group	Mean	Std. error
TAT	2.500	0.267
R9	1.000	0.189
Control	0.333	0.333

$P=0.0001$ (significant at 95%)

hind limb using a pipette and massaged into the skin, wearing nitrile gloves. Animals were recovered in a controlled heat environment to prevent hypothermia. Baseline and posttreatment photographs, video of the animals' recovery, and DAS values were recorded. Statistical analysis was subsequently determined for each group using StatView® software and expressed as mean and standard error. Statistical significance for all comparison was determined using one-factor ANOVA repeated measures and Fisher PLSD post hoc testing at 95% confidence. Foot Mobility Scores were tabulated using DAS values where score of 0 indicates normal digit abduction (no muscle weakening), and a score of 4 indicates maximal reduction in digit abduction (maximal muscle weakening) (22).

Statistical analyses were determined by three different comparisons, and the results are presented in Tables 2–4. Mean DAS values showed statistically significant muscle weakening/paralysis between treatment groups versus control after single-time topical administration of treatment solution. Table 4 shows the statistically significant paralysis from topical Dysport® ($P=0.0001$) versus control. After recovery, animals were observed to walk in circles toward the paralyzed limbs.

Empirically, a TAT-based PTD was thus selected as having the distribution, kinetics, and tropism desired for delivery of botulinum toxin for the desired indications.

3. Confirmation of Intended Characteristics When RTP004 CPP-Containing Peptide Excipient Is Combined with Botulinum Toxin

RTP004 can be tuned to carry payloads to different depths of penetration based on the length of the peptide; the longer the peptide, the deeper the penetration. In the case of RT001, the RTP004 peptide is specifically formulated to deliver the toxin to a relatively superficial target in the mid-dermis as is necessary to treat lateral canthal lines or hyperhidrosis. The bias in development of

this peptide was safety over efficiency. Pharmacology studies have focused on the transcutaneous flux of RTT150 mediated by the RTP004 peptide in vitro (using labeled RTT150) and in vivo using the murine DAS assay, as well as by murine muscle force testing. Additional studies underway include the effort to characterize the kinetics and degree of denervation and renervation upon repeat dosing of animals with RT001. It is intended that these studies will aid in the design and dosing frequency of longer term toxicity studies.

3.1. Transdermal Flux of Biotinylated-RTT150 with and Without RTP004 (RT001-RD004)

The purpose of this study was to examine transcutaneous flux patterns of RTT150 alone or mixed with RTP004 using a Franz Chamber. RTT150 (0.05 mcg/in-line cell) was biotinylated and evaluated against biotinylated RTT150 (0.05 mcg/in-line cell) mixed with RTP004 (0.055 mcg). Freshly dermatomed living porcine skin was loaded into in-line cells, and 200 mL of the test article mixtures was added to each cell ($N=4$). The Franz Chamber was run for 4 h, with a shuttle change once per hour. Enzyme-linked immunosorbent assay (ELISA) analysis was performed on the resulting flow-through samples. Toxin delivery was measured by percentage of applied load appearing in the flow-through. The combination of RTT150 with RTP004 exhibited a statistically significant increase in the amount of fluxed RTT150 in the flow-through as compared to RTT150 alone as shown in Fig. 4, suggesting that approximately 8–9% of the dose applied to skin is able to cross into cell receptor fluid. Some toxin flux was noted in the absence of RTP004; however, this is attributed to the background signal of the assay.

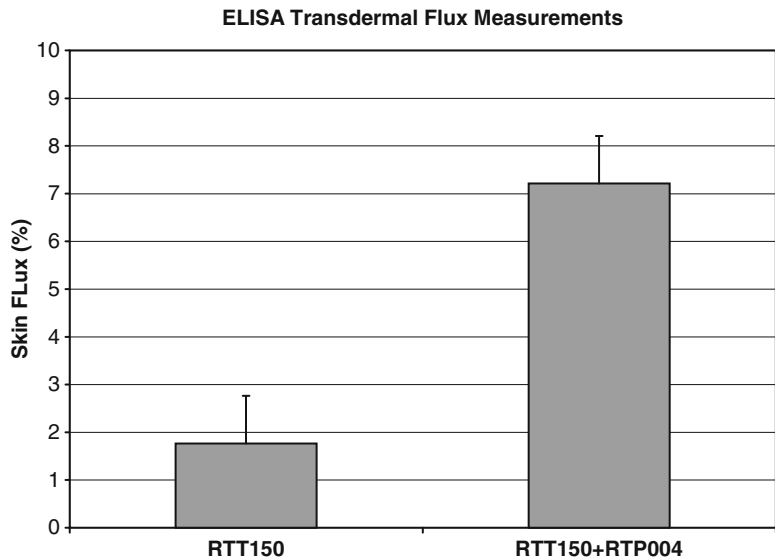


Fig. 4. ELISA transdermal flux measurements. Toxin delivery was measured by percentage of applied biotin-tag appearing in the flow-through.

3.2. Transdermal Flux of RT001

The purpose of this study was to examine transcutaneous flux patterns of RT001 using a Franz Chamber. Prior experiments (Subheading 3.1) relied on using biotin-tagged BoNTA; this type of experiment allows for facile detection but can lead to higher background levels and overestimation of degree of flux. As a result, a method for measuring untagged BoNTA directly was developed. Freshly dermatomed living porcine skin was loaded into in-line cells, and 190 mL of the test article mixtures was added to each cell ($N=10$ cells per test article). RT001 was applied to in-line cells at a dose of 711 U (approximately 4 ng). In-line cells with RTD006 reconstituted in RTD800 served as controls. The Franz Chamber was run for 6 h, with a shuttle change once per hour.

Alpha-LISA using antibodies to BoNTA was performed on the resulting flow-through samples to quantitate the amount of toxin present. Toxin flux was expressed as a percentage of applied load appearing in the flow-through. Results obtained in repeat experiments with independent analysts yielded transcutaneous flux measurements of approximately 3–6% of the applied dose during the 6 h time period as depicted in Fig. 5 for one such experiment.

Partial paralysis in a murine DAS model was confirmed (data not presented) as was preferentially superficial distribution in the mouse gastrocnemius muscle in quantitative nonclinical testing of muscle force with both single twitch and tetanus stimulation prior to initiation of clinical studies (data not presented).

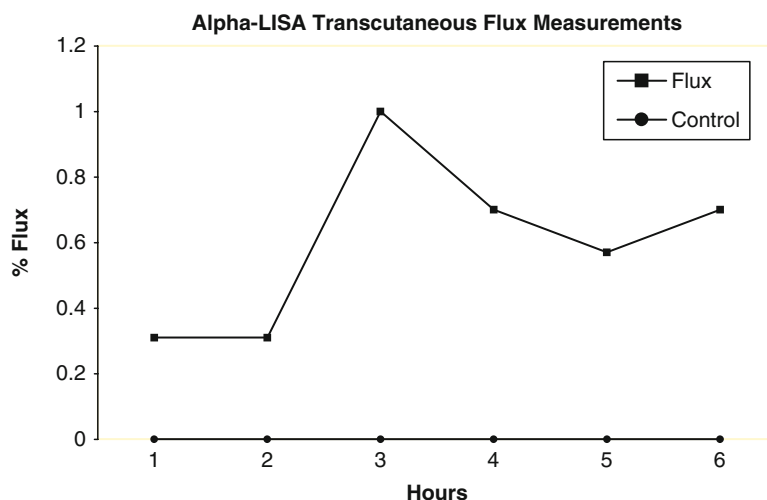


Fig. 5. Alpha-LISA transcutaneous flux measurements. Toxin flux was expressed as a percentage of applied RTT150 load appearing in the flow-through. Control is not detectable at any time point.

4. Clinical Experience

Revance is developing a topical drug product, RT001 (Botulinum Toxin Type A Topical Gel) for the treatment of moderate to severe LCLs and severe primary axillary hyperhidrosis. The anticipated clinical benefits are the temporary improvement in the appearance of LCLs and a temporary reduction in sweating.

The safety and efficacy of RT001 have been assessed in six clinical studies to date (five studies in LCLs and a single study in hyperhidrosis). Doses of 100, 300, 500, 750, and 1,000 U per lateral canthal area (LCA) have been studied with no significant safety issues. Topical administration of 900 kDa BoNTA with the Revance peptide excipient has been studied in two Phase I studies for the treatment of LCLs: in Mexico (Protocol RTI-002-CF-001) using commercially available BOTOX® Cosmetic and in Korea using commercially available Neuronox®. In primary axillary hyperhidrosis, an investigator-initiated pilot study was conducted using commercially available BOTOX® and a Revance proprietary peptide excipient.

4.1. RT001 for the Treatment of Lateral Canthal Lines: US Phase 1 Safety and Tolerability Study (RT001-CL004CF)

The objectives of the study were to evaluate the potential for irritation and sensitization, the topical and systemic safety of RT001, and the systemic immunogenicity of RT001. Each subject received both test articles, RT001 300 U (study drug) and RTD800 (placebo diluent) on the forearms; subjects were randomized as to which forearm received RT001 and which received RTD800. The study was conducted in three phases. During the Induction Phase (Days 0–28), treatments were applied to defined areas of the forearms on Days 0, 14, and 28. During the Rest Phase (Days 29–41), no treatments were applied. During the Challenge Phase (Days 42–56), the fourth and final treatment was applied on Day 42. Skin sensitization evaluations were performed on Days 2, 16, 30, 44, 45 (if required), and 56 (End of Study). All treatments were applied for 30 min with Tegaderm occlusion. Safety evaluations included skin irritation and sensitization evaluations, Clinical Signs/Symptoms Descriptors, AEs, clinical laboratory tests, ECG, serum BoNTA antibodies, and muscle grip strength. In addition to the per-protocol laboratory tests, serum RTP004 antibodies were measured.

Overall, no study pause criteria were met, and no SAEs were reported. There were only two transient, definitely related adverse events (papular rash and pruritus) experienced by one subject that were moderate in severity and resolved within 24 h, and two possibly related episodes of mild joint pain (occurring 2 weeks apart), each resolving within 24 h. There was no evidence to suggest any trend for skin sensitivity and neither test article caused cumulative irritation. In addition, there were no test article effects on muscle

grip strength, prothrombin time, or ECG results. Finally, there were no systemic or local clinically significant abnormalities or findings, and no subject had positive BoNTA antibody results at any time or developed antibodies reacting with RTP004.

This Phase I study helped establish that a novel and potent CPP-containing peptide like RTP004 can be used safely and with low irritancy and sensitization potential. This study thus represents an early validation of design considerations at least in application to less sensitive skin and coarser musculature.

**4.2. Phase 2 Study
of RT001 with Various
Concentrations
of RTP004 for Lateral
Canthal Lines
(RT001-CL003CF)**

The objective of this study was to evaluate the need for the CPP-containing peptide for transcutaneous delivery and evaluate safety of RT001 on sensitive target areas. A total of 77 subjects with moderate to severe LCLs were enrolled in two cohorts and randomized to receive RT001 300 U combined with RTD005 diluent concentrations of 0.5, 2.0, or 4.5 mcg/0.5 mL, or RTD800 placebo control (Cohort 1) and RT001 300 U combined with RTD005 diluent concentrations of 6.0, 7.5, or 10.5 mcg/0.5 mL, or RTD800 placebo control (Cohort 2). Treatments were applied for 30 min to each LCA with Tegaderm occlusion. Assessments included the Investigator Assessment Rating of Crow's Feet Facial Line Severity at maximum smile and at rest. Success was defined as a 1-point or greater improvement from Baseline. Safety assessments included AEs, skin irritation and sensitization, eye irritation, clinical laboratory tests, and evaluation of cranial nerves II–VII.

A total of 49 subjects (63.6%) had one or more AEs considered related to study treatment (Cohort 1, 73.0%, Cohort 2, 55.0%). All related AEs were mild or moderate in severity. The most common related AEs were: nervous system disorders (32.5%; mostly involuntary muscle contraction); general disorders and administration site conditions (26.0%; mostly erythema [23.3%]); skin and tissue disorders (16.2%; erythema, pain, and burning sensation); and eye disorders (13.0%; typically eye irritation, eye pain, or foreign body sensation). The most common systemic reaction was headache (2.6%). Most events of skin erythema were minimal. There were no notable changes in clinical laboratory variables, and no subject had any abnormality in the Regional House-Brackmann System for cranial nerve VII. All changes were unrelated to test article.

For the active treatment groups, a 1-point or 2-point improvement was observed for a majority of LCAs at rest, and a 1-point improvement was observed for a majority of LCAs at maximum smile. Compared to the placebo group, the response rate was significantly higher in the RT001 7.5 mcg/0.5 mL group for 2-point improvement at rest and 1-point improvement at maximum smile, and in the RT001 6.0 mcg/0.5 mL group for 1-point improvement at maximum smile. As illustrated in Fig. 6, this study

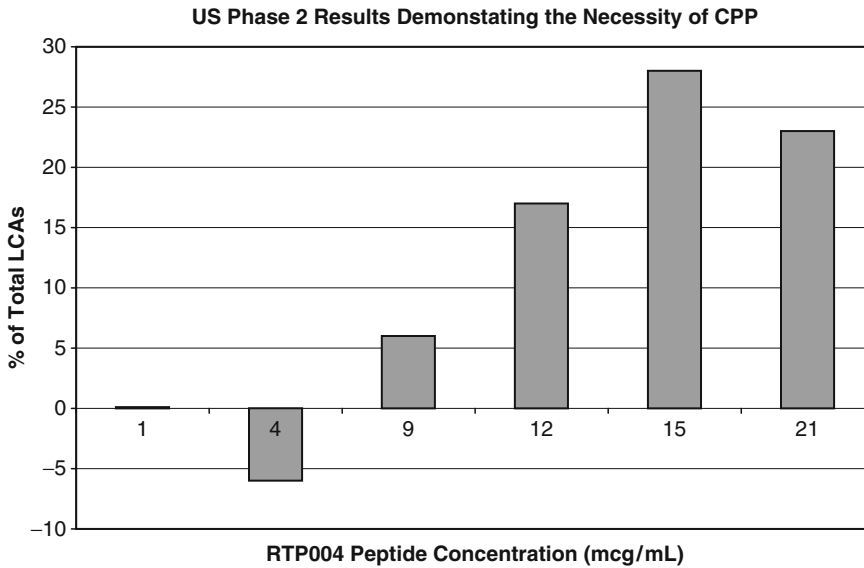


Fig. 6. US Phase 2 RT001-CL003CF results. RTP004 must be present at a threshold level or above in order to deliver functional toxin across skin.

established that not only was RTP004 required for function but it must also be present in a target concentration threshold to achieve a desired effect with a given dose of a payload. This finding is consistent with the nonclinical data to date, and external reality-macromolecules do not readily cross skin. A CPP-containing peptide can enable topical delivery of a therapeutic amount of a macromolecule, however, as shown here. That a threshold concentration of RTP004 appears necessary marks an interesting finding in this work as well. Here, as in the Phase 1 study on less-sensitive target areas, RT001 demonstrates a remarkable safety profile, particularly considering the powerful CPP employed in conjunction with the most potent toxin known to man. These results represent a validation of the previously discussed safety-biased design considerations for RTP004 even in application to fine musculature and sensitive skin around the eye.

4.3. Overview of the Safety Profile of RT001 Topical Gel

A total of 257 subjects have participated in the four LCL studies for which complete audited safety data is currently available. A total of 227 subjects received RT001 at doses of 100–2,000 U per treatment area; 11 subjects received peptide diluent (RTD006) as control, and 19 subjects (all of which also received active in RT001-CL004CF) received placebo diluent (RTD800). Overall, 90 subjects (35.0%) had one or more treatment-related AEs: 75 (33.0%) RT0001-treated subjects, 3 (27.3%) RTD006 vehicle control subjects, and 12 (63.2%) subjects who received RTD800

placebo diluent. The most common AEs were administration site conditions (15.6% of all subjects), nervous system disorders (14.0%), and eye disorders (7.7%). There were no notable differences in the incidence of any treatment-related AEs between the RT001 and placebo groups. Most subjects had events that were mild or moderate in severity. Three subjects had severe AEs. The moderate events were mostly involuntary muscle contraction (20 subjects) and application-site erythema (six subjects). The severe events were application-site erythema and back pain in Study RT001-CL001CF, and epistaxis in Study RT001-CL003CF, all of which were unrelated to study treatment. No serious AEs have been reported, and no subject discontinued a study due to an AE. There have been no clinically significant safety concerns in these studies for clinical laboratory results, ECGs, or cranial nerve evaluations. Skin or ocular irritation events were few and were usually transient, local, and mild in severity.

4.4. Investigator-Initiated Study of Botulinum Toxin Type A with Revance Diluent for Primary Axillary Hyperhidrosis

An Investigator-initiated pilot study in primary axillary hyperhidrosis was conducted at a single center in the US using commercially available BOTOX® and the Revance peptide diluent (23). Twelve adult subjects with a gravimetric measurement of sweat production of at least 50 mg over 5 min were enrolled. Each subject served as his or her own control with blinded, randomized assignment of each axilla to a treatment group. Study treatments were mixed with Cetaphil® cream, applied to the axillae, and remained in place for 60 min. Subjects returned for a follow-up evaluation at 4 weeks after treatment.

The mean reduction in sweat production at 4 weeks post-treatment was 65.3% for BOTOX®-treated axillae compared with a 25.3% for the control axillae ($P < 0.05$). The ratio of mean sweat production for the BOTOX®-treated axillae relative to the control axillae was 1.3 at baseline and 0.8 at 4 weeks posttreatment. The results from the Minor's iodine starch test to visualize sweating were consistent with the gravimetric results. No systemic AEs were reported. Four local AEs were reported, all of which occurred in the control axillae. The AEs were folliculitis, tenderness, erythema, and eczema (2 cm inferior to the axilla on the lateral trunk). The results of this study indicate that topically applied BoNTA appears to be safe and may prove to be effective for the treatment of axillary hyperhidrosis.

Perhaps more importantly from a CPP perspective, safety and efficacy of this CPP-based peptide are not specific to facial skin and apply to skin with high density of hair follicles and sweat glands. Delivery in this environment is particularly noteworthy given high levels of skin hydration and the physical barriers presented by hyperhidrosis.

4.5. US Phase 2 Studies of RT001 with Escalating Doses of RT001 for Lateral Canthal Lines (RT001-CL006LCL, RT001-CL010LCL and RT001-CL015LCL)

The objective of these studies was to evaluate the safety and efficacy of escalating toxin doses in RT001 in management of LCLs. Across three separate Phase 2 studies, 306 adult subjects with moderate to severe LCLs were randomized to receive control diluent (N=104) or RT001 at the following doses of toxin (U) with 9.0 mcg/mL RTP004: 300 U (N=26) 500 U (N=22); 1,000 U (N=72) or 2,000 U (N=82). The studies were conducted at multiple sites in the US. Subjects received a single 30-min treatment of 0.5 mL with Saran Wrap occlusion to each LCA. Follow-up evaluations were conducted at Days 14 and 28 for all subjects and 7, 21, 60, and 90 in some studies. These evaluations included AEs, clinical laboratory tests, ECG, skin and ocular irritation evaluations, evaluation of cranial nerves II–VII, and Investigator Global Assessment (IGA)-LCL-Rest and IGA-LCL-Smile Severity Scales. Adverse events were typically mild, transient, and local. The more common related events were administration site conditions and nervous system events. The nervous system events were burning sensation, facial paresis (two subjects in control), and headache. All events of skin or ocular irritation were mild. There were no clinically significant laboratory or ECG results. Complete detailed analysis of the AEs in this study is not currently available.

The primary efficacy endpoint for each of these studies was a 2-point improvement at rest in the IGA-LCL-Rest Scale. Preliminary results by dose group are presented in Fig. 7. Not only was statistically significant efficacy achieved, but also a dose response allowing dosage selection was observed. Duration data (not presented) demonstrates comparability to toxin results when

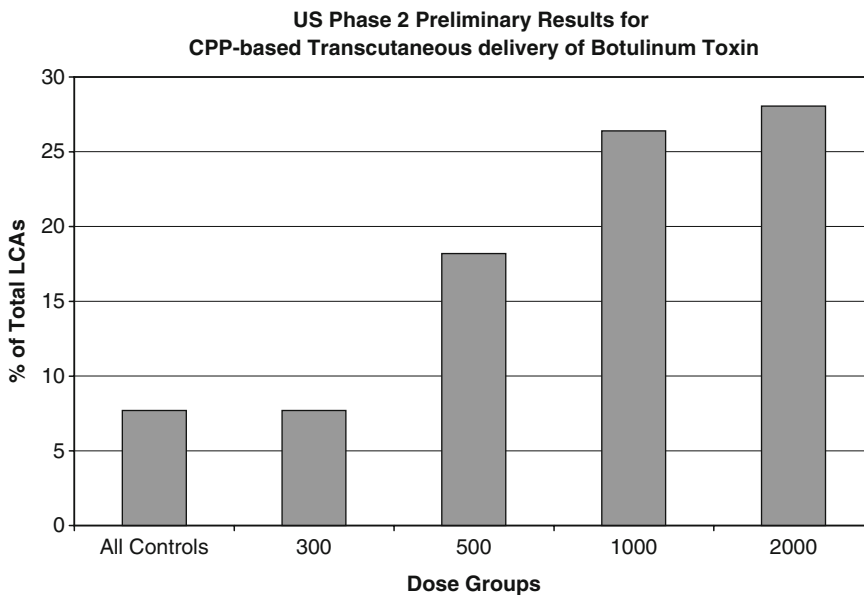


Fig. 7. US Phase 2 RT001-CL006LCL, RT001-CL010LCL, and RT001-CL015LCL preliminary results by dose group. Efficacy was defined as a 2-point improvement in the IGA-LCL-Rest Scale 28 days after single-time administration.

injected and further supports dosage selection. Here, as in prior phase 1 and 2 studies, RT001 demonstrates a remarkable safety profile, particularly considering the powerful CPP employed in conjunction with escalating dose of the most potent toxin known to man. Thus, the design considerations for the CPP-based peptide excipient have been validated with escalation of active dose to therapeutic effect in application to fine musculature and sensitive skin around the eye. Clinical validation of noncovalent PTD-based delivery of an active therapeutic across skin for a therapeutic benefit has thus been demonstrated here.

References

1. Scott, A.B. (1981) Botulinum toxin injection of eye muscles to correct strabismus *Trans Am Ophthalmol Soc* **79**, 734–770.
2. Hallett, M. (1999) One man's poison-clinical applications of botulinum toxin *N Engl J Med* **341**, 118–120.
3. Spencer, J.M. (2002) Botulinum Toxin B. The new option in cosmetic injection *J Drugs Dermatol* **1**, 17–22.
4. Carruthers, A. and Carruthers, J. (2005) Botulinum toxin type A *J Am Acad Dermatol* **53**, 284–290.
5. Carruthers, J. and Carruthers, A. (2007) The evolution of botulinum toxin type A for cosmetic applications *J Cosmet Laser Ther* **9**, 186–192.
6. Carruthers, J. and Carruthers, A. (1992) Treatment of glabellar frown lines with *C. botulinum-A* exotoxin *J Dermatol Surg Oncol* **18**, 17–21.
7. Carruthers, J., Fagien, S., Matarasso, S.L., and BOTOX Consensus Group. (2004) Consensus recommendations on the use of botulinum toxin type A in facial aesthetics *Plast Reconstr Surg* **114**:1S–22S.
8. The American Society for Aesthetic Plastic Surgery, Cosmetic Surgery National Data Bank. 2006 statistics. www.surgery.org/download/2006stats.pdf. Accessed 30 March 2007.
9. Bushara, K.O., Park, D.M., Jones, J.C., and Schutta, H.S. (1996) Botulinum toxin—a possible new treatment for axillary hyperhidrosis *Clin Exp Dermatol* **21**, 276–278.
10. Schnider, P., Binder, M., Berger, T., and Auff, E. (1996) Botulinum A toxin injection in focal hyperhidrosis *Br J Dermatol* **134**, 1160–1161.
11. Naumann, M., Hofmann, U., Bergmann, I., Hamm, H., Tiyka, K.V., and Reiners, K. (1998) Focal hyperhidrosis: effective treatment with intracutaneous botulinum toxin *Arch Dermatol* **134**, 301–304.
12. Heckmann, M., Ceballos-Baumann, A.O., and Plewig, G. (2001) Botulinum toxin A for axillary hyperhidrosis (excessive sweating) *N Engl J Med* **344**, 488–493.
13. Naumann, M. and Lowe, N.J. (2001) Botulinum toxin type A in treatment of bilateral primary axillary hyperhidrosis: randomised, parallel group, double blind, placebo controlled trial *BMJ* **323**, 596–599.
14. Lowe, N.J., Lask, G., Yamauchi, P., and Moore, D. (2002) Bilateral, double-blind, randomized comparison of 3 doses of botulinum toxin type A and placebo in patients with crow's feet *J Am Acad Dermatol* **47**, 834–840.
15. Lowe, N.J., Ascher, B., Heckmann, M., Kumar, C., Fraczek, S., and Eadie, N. (2005) BOTOX Facial Aesthetics Study Team. Double-blind, randomized, placebo-controlled, dose-response study of the safety and efficacy of botulinum toxin type A in subjects with crow's feet *Dermatol Surg* **31**, 257–262.
16. Matarasso, S.L. and Matarasso, A. (2001) Treatment guidelines for botulinum toxin type A for the periocular region and a report on partial upper lip ptosis following injections to the lateral canthal rhytids *Plast Reconstr Surg* **108**, 208–214.
17. Allergan, Inc. (2006) BOTOX Cosmetic (Botulinum Toxin Type A) Prescribing Information. Allergan, Inc., Irvine, CA
18. Aoki, K.R. and Guyer, B. (2001) Botulinum toxin type A and other botulinum toxin serotypes: a comparative review of biochemical and pharmacological actions *Eur J Neurol* **8**, 21–29.
19. Grumelli, C., Verderio, C., Pozzi, D., Rossetto, O., Montecucco, C., and Matteoli, M. (2005) Internalization and mechanism of

- action for clostridial toxins in neurons
Neurotoxicology **26**, 761–767.
20. Dutton, J.J. and Fowler, A.M. (2007) Botulinum toxin in ophthalmology *Surv Ophthalmol* **52**, 13–31.
 21. Ford, K.G., Souberbielle, B.E., Darling, D., and Farzaneh, F. (2001) Protein transduction: an alternative to genetic intervention? *Gene Ther* **8**, 1–4.
 22. Aoki, K.R. (2001) A comparison of the safety margins of botulinum toxin serotypes A, B, and F in mice *Toxicon* **39**, 1815–1820.
 23. Glogau, R.G. (2007) Topically applied botulinum toxin type A for the treatment of primary axillary hyperhidrosis: results of a randomized, blinded, vehicle-controlled study *Dermatol Surg* **33**, S76–S80.

INDEX

A

- A260/A280 ratio 36 421, 428
 Acetonitrile..... 183, 189–191, 224, 228, 310,
 312–315, 318, 456, 459, 462, 507–509,
 512, 518, 520
 Acrylamide324, 328, 330
 Actin cytoskeleton167, 170, 174–175
 Acylated WR₉.....129, 141, 148–149
 Administration
 aerosol..... 419
 intramuscular 322
 intranasal 418
 intratracheal..... 418
 intravenous 269, 323, 433, 542, 544
 nebulisation 419
 Agarose gel317, 324, 328, 395, 409, 441, 460
 Aggregation.....24, 25, 45, 55, 139, 144, 146,
 160, 168, 234, 235, 261–262, 267–269,
 339, 344, 352, 353, 454
 Äkta™ basic 10 456
 Alkaline phosphatase (AP) 422
 Allosteric 236
 Alternative splicing.....307–308, 473, 475
 Aminobenzoic acid, (Abz)..... 118–119
 Amphipathic peptides7, 43, 46, 48
 Amphipathicity25, 46, 47
 Amplicon..... 419
 Amplification of phage.....283, 285, 409, 413
 β -Amyloid 12, 26, 236
 Angiogenesis 239, 259, 260, 269–272, 545
 Anion exchange chromatography 101, 140
 Annexin V 139, 242, 291, 293, 294, 298, 299
 Antennapedia 4, 5, 21, 22, 235, 240, 241, 431, 436
 Anti-cancer therapy..... 278
 Anti-DS antibody3G10, 101, 103, 108–110
 Anti-inflammatory544–545, 555
 Antibody treatment
 LAMP-2 158
 phosphatidylinositol-3-phosphate (PI3P)..... 100
 Rab5, 168, 169, 173–174
 TGN..... 169, 173
 Antigen presenting cells (APC) 434, 436
 Antimicrobial peptides9, 11, 34, 46
 Antisense.....220,
 Antisense oligonucleotide..... 220, 223, 340, 349,
 392, 394, 395, 397, 417, 419,
 ANTS..... 131, 132, 141, 142, 149, 311, 317
 AP-1..... 242
 Apoptin 238
 Apoptogenic CPP292, 293, 295, 296, 298–300, 302
 Apoptosis
 detection294, 296–297
 inhibition242, 288, 467
 Apparent membrane partitioning constant, K_{app} 145
 Aptamer505, 506
 Arg9 350
 AT1AR..... 241
 ATTO-dUTP 377, 379–381, 386, 387
 Auxiliary compounds.....380, 381, 386
 Avidin.....168, 171, 172, 174, 176, 334, 336, 528, 530, 531

B

- Basic helix-loop-helix 236
 Basket cells 254
 Bax.....240–241, 465–469
 Bax inhibiting peptide 240, 377, 386, 387, 465–470
 Bcl-xL 236, 238, 239, 542
 Becker muscular dystrophy (BMD)..... 322
p-Benzoylphenylalanine (Bpa) 475–476
 B-hexosaminidase efflux assay..... 159, 162
 Bicelles 24, 34, 35, 58–65
 Binding thermodynamics 81
 Biodegradable 454
 Biodistribution13, 259–272, 536
 Bioinformatics 420
 Biological evaluation..... 454
 Biological response 3.53, 181, 213–214, 238,
 239, 241, 350, 362
 Bioluminescence assay120, 121, 124–125
 Biomarkers 420, 546
 Biomembranes..... 14
 Biopanning.....278–279, 404

- Bioportide..... 241
BIP. *See* Bax inhibiting peptide
Blastula..... 251
Blotting325, 328, 331, 332, 355, 420
Boc-strategy 520
Borate buffer.....438, 440, 441, 447, 455, 457–458
Botulinum toxin 540, 547, 553–557, 559,
562, 563–565, 570
Boundaries..... 250–252
Bovine blood.....200, 203, 240
Bradford assay335, 357, 425
- C**
- CAD-2 376, 382, 385, 386
CADY, nanoparticle technology 349
Calcein fluorescence36, 38–39, 143
Calcein leakage..... 36, 38–39, 142–144, 148–149
Calcineurin 238, 239
CaN..... 239
Cancer
 breast 7, 11–12, 199, 269, 270
 hepatocellular carcinoma 272
 melanoma 269
Capping..... 433, 508, 512, 514
Capsules185, 188
Carboxyfluorescein 72, 119, 141, 142, 149, 288
Cardiomyoblast cell line, H9C2278, 279, 282
Cardioprotection 542–543
Caspase..... 238, 240, 292, 293, 295, 298–300, 302, 542
Cationic, liposome 436, 526
Caveolae 9
Caveolin166, 169, 170, 173, 175, 537
CD. *See* Circular dichroism
CDB3..... 241
CDKN2A..... 241
Cell attachment..... 453
Cell interaction 436, 445
Cell lines
 COS-7..... 382, 383, 388, 527, 528
 HeLa 167, 392
 Jurkat 72, 76, 77–78, 356, 388
 Kasumi-1 377, 383
 NB-4 377, 383
 NIH 3T3..... 167, 170, 174, 377, 388, 434
 U373MG..... 293, 295, 297, 299–301
Cell lysis 113, 201, 213, 224, 366, 394, 396
Cell monolayer 296
Cell viability72, 177, 196, 201, 240, 293–296,
302, 376, 381, 382, 385
Cell-penetrating peptide (CPP)
 Arg9 350
 CAD-2 376, 377, 382, 385, 386
 CPPP-2..... 377, 378, 382, 384, 386–387
 HIV-Tat..... 100, 376, 377, 386
 M918..... 4, 243
 MPG α 376, 377, 385, 386
 MPG β 376, 377, 385, 386
 Penetratin 4, 5, 8, 9, 13, 60, 82, 87, 95, 96,
131, 149, 182, 196, 221–223, 227, 238, 323,
350, 376, 377, 382, 386
 (RxR)4..... 323
 Stearyl-Arg9..... 366
 Stearyl-M918 366
 Stearyl-Pen 366
 Stearyl-TP10363, 365–366, 437
 TP10..... 4, 6, 9, 363, 365–366, 437
Cell-penetrating peptide-PNA conjugate224–228, 242
Cellular delivery 26, 209, 214, 220, 391–397
Cellular uptake 13, 42, 189, 201, 209, 210, 212, 219,
221–223, 225, 227, 310, 315, 350–351, 362,
365, 391, 395, 396, 434, 468, 489, 493–496,
499, 506, 537, 539
Ceramide-Bodipy-TR-C5..... 169, 172
Chariot14, 44
Chemiluminescent HRP Substrate 325
Chemotherapy.....11, 214, 308
Chimeric peptides 12, 323
Chloroquine126, 221, 222, 224, 225, 287,
288, 380, 381, 385, 392
Chlorpromazine 221, 222, 224, 225
CHO-K1 cells100, 158–161, 163
Cholera toxin B subunit169, 171–172
Cholesterol 9, 13, 350, 420, 438, 527
Chondroitinase ABC 102, 103, 106–109, 254
Chromatography
 gel filtration 183, 186, 189, 191
 reversed phase..... 183, 186, 189, 191
Circular dichroism (CD) spectroscopy43, 49–52,
59, 81
CK2..... 239
Clathrin- and caveolin-independent 166, 169
Clathrin-dependent pathway.....9, 157, 166
Cleavage from resin 511, 518, 519, 521, 532
Clinical development..... 1, 540, 542, 546–547
Clinical trials 14, 308, 322, 326, 362,
539, 546–547
Clostridium botulinum.....555, 556
Co-incubation238, 363, 365
Co-localization..... 111, 166, 167, 171, 176, 210
Collagen 261, 267, 268–269
Colour tests 510
Complex formation constant, K 146
Confocal laser scanning microscopy, (CLSM)118, 119,
171, 172, 174–176, 529, 531
Confocal microscopy 23, 69, 76, 109, 209–212,
297, 298, 346
Conformation..... 24, 43, 53, 96, 350
Conjugated peptides432, 544, 547

- Conjugation
 covalent.....362, 365, 520
 non-covalent..... 520
Conjugation to oligonucleotide362, 365, 417,
 505–506, 520
COS cells..... 167, 169, 171, 172
COSY.....60, 62, 64
Coupling.....190, 214, 223, 434, 460, 462,
 463, 480–481, 507, 509, 510, 512, 514,
 517–518, 522–523, 532
Covalent conjugation..... 362, 365
CPP. *See* Cell-penetrating peptide
CPP uptake kinetics 117
 bioluminescence assay.....120, 124–125
 proximity quenching assay..... 118–119
 quenched fluorescence assay 118–119, 121–123, 143
 quenched time-lapse uptake assay 119–120
CPP-cargo construct 70
CPP-induced leakage 34
CPP-nanogold (CPP-NG) conjugates.....184, 186, 191
CPP-PMO conjugates 312–315, 319, 323
CPP-PNA conjugates223–228, 242
CPP-protein complexes.....166, 168, 171–175, 177
CPPP-2.....377, 378, 382, 384, 386, 387
Cre-*loxP* system.....21
Critical periods253
Cross-relaxation..... 61
Cryopreservation428
Cryosectioning 423, 428
CTC 507, 509, 520, 521
CXCR1260, 262, 264
CXCR2262, 264
CXCR4264–265, 269
Cyclin B1..... 350
Cyclin-dependent kinase inhibitor239
Cysteamide.....4, 43–44, 350, 351
Cytochalasin D.....221, 222, 224, 225
Cytochrome C.....240, 241, 288, 292
Cytoprotection466, 468, 540
Cytosol70, 130, 131, 182, 238, 455,
 465, 525–526, 528, 538
Cytosolic delivery 130, 526
Cytotoxic26, 195, 200, 239, 319, 376, 384,
 387, 462, 468, 470, 545
Cytotoxicity..... 13, 196, 200, 201, 204, 219, 221, 228,
 319, 377, 378, 380, 382, 384, 388, 434, 436
- D**
2D60, 62, 63
2-DDCt method 419
Delivery..... 3–5, 7, 8, 10–13, 21, 26, 42, 70,
 99–113, 118, 120, 130, 165, 166, 181, 182, 195,
 200, 209, 212–215, 219–228, 235–240,
 260–263, 277, 288, 291, 292, 308, 318, 322,
 323, 327, 339–347, 349–359, 361–371, 386,
 391–397, 402, 417–420, 422, 431–447,
 453–463, 502, 505, 506, 514, 520, 525–532,
 536, 538–541, 543, 547, 553, 556, 557,
 559–564, 567–571
Deoxyglucose (2-deoxy-D-[1-³H]-glucose) 199, 201
Deoxyglucose leakage assay 197, 199, 200–202
Deoxynucleotides
Deprotection508, 509, 511, 515, 517, 519, 532
Dermatology.....553
Desalting 103, 516, 521
Detritylation511, 514–516
dGFP-H1299 cells..... 341–33
DHPC. *See* Dihexanoyl-sn-glycero-3-phosphocholine
DIEA510, 532
Digoxigenin (DIG) 422, 425
Dihexanoyl-sn-glycero-3-phosphocholine 61
2-3-Dimethylmaleic anhydride
 (DMMAAn) 454–456, 459, 462–463
3-(4,5-Dimethylthiazol-2-yl)-2,5-diphenyltetrazolium
 bromide. *See* MTT
Dimyristoylphosphocholine 35, 39, 58–59, 62–64
Dimyristoylphosphoglycerol.....58–59, 62, 63, 65
1,2-Dimyristoyl-sn-glycero-3-
 [phospho-rac-(1-glycerol)] 59, 62
1,2-Dimyristoyl-sn-glycero-3-phosphocholine 59, 62
Dinitrophenyl 118–119
1,2-Dioleoyl-3-trimethylammonium-propane
 (DOTAP)434, 438, 441
DIPCDI/HOBT..... 510
Direct penetration8, 9, 157
Disseminated intravascular coagulation
 (DIC).....264–266, 300, 444, 531
DLS. *See* Dynamic light scattering
DMD gene..... 321–322
DMD mouse model 308
DMEM. *See* Dulbecco's Modified Eagle's Medium
DMMAAn. *See* 2-3-Dimethylmaleic anhydride
DMT removal512, 513, 515
DNA 3, 5, 12, 22, 23, 25, 44, 71, 99,
 130, 196, 197, 201, 214, 240, 284, 294,
 296–297, 300–302, 311, 324, 328, 340, 346,
 414, 431–434, 436, 437, 440, 441, 445, 465,
 506, 527–530, 538, 540, 545
DNA fragmentation. *See* TUNEL assay
DNP. *See* Dinitrophenol
DOTAP. *See* 1,2-Dioleoyl-3-trimethylammonium-propane
Double-stranded RNA binding domains (DRBDs)..... 340
Drug development. *See* Clinical development
Drug discovery 392, 539
DTT assay.....455, 457, 459–460
Duchenne Muscular Dystrophy (DMD)
 gene 321–322
 mouse model (mdx)..... 308

Dulbecco's Modified Eagle's Medium (DMEM)..... 102–104, 110, 111, 158–160, 199, 201–203, 224–226, 279, 281, 285, 293–295, 300, 309, 312, 315, 316, 341–343, 351, 355, 364, 366, 369, 406, 407, 456, 467, 469, 470, 527–529

Dynamic light scattering (DLS).....37, 137–139, 143, 371, 442

Dystrophin
cardiac dystrophin protein 323
Dystrophin Associated Protein Complex (DAPC).....326, 333, 334
protein 322, 325, 327, 329, 334

E

EDTA. *See* Ethylenediamine tetraacetic acid

E2F1.....236, 242

Electron microscopy 163, 181–192, 209, 212, 442–443

Electrophoresis
capillary 427
polyacrylamide.....324–325, 427

Electrostatic interactions 24, 57, 139, 145, 148, 308, 506, 557

ELISA. *See* Enzyme linked immunosorbent assay

Elongation
of oligonucleotide 511–512
of peptide.....507, 509, 517–520

Embedding
capsules 185, 188
flat-embedding 183, 188
resin 183, 185

Endocytic vesicles
non-acidic..... 166
recycling..... 166

Endocytosis
caveolin-dependent..... 166
clathrin-dependent 157, 166
flotillin-dependent..... 166

Endocytosis inhibitors 122, 126, 208, 212, 220, 221, 225, 319

Endo-lysosomal pathway.....166, 167, 169, 172

Endosomal
entrapment130, 362, 365
escape.....33, 391–392, 432, 435, 453–454, 526, 528, 537, 548

Endosome.....10, 130, 454

Endosomolytic domain..... 454

Engrailed..... 236, 237, 250, 252–255

Enhanced delivery by photochemical
internalization..... 391–397

Enhanced-green fluorescent protein (pEGFP)104, 434, 436, 438, 441, 445, 527, 528

Enzyme-linked Immunosorbent Assay (ELISA).....310, 311, 316, 343, 346, 420, 439, 442, 443, 564

Ephrins..... 252

Erb2 240

Erythrocyte leakage assay 456, 460

Escherichia coli..... 70, 340

Ethidium bromide 311, 324, 364, 368, 369

Ethylenediamine tetraacetic acid (EDTA) 72, 73, 102, 103, 121–123, 126, 199, 201, 203, 224, 279, 281, 282, 293–295, 309, 312, 315, 316, 324, 342, 345, 351–353, 357, 364, 369, 402, 405, 422, 427, 456, 457, 461, 467, 470, 477, 481, 489, 492, 493, 530

Ethylisopropylamiloride (EIPA)..... 25

Ex vivo selection 402–403, 406–408, 413

Exchange 14, 46, 61–64, 101, 104, 112, 344, 458, 461–462, 521

Exon 308, 473–486

Exon skipping.....321–337, 362, 402

Expression variability..... 419

Extracellular matrix 100, 121, 166, 191, 327

Extracellular stabilization 453

Extraction..... 310, 323–324, 327–328, 394, 420–425, 428

F

FACS. *See* Fluorescence activated cell sorting

FAM. *See* Carboxyfluorescein

Fast-tumbling bicelles, preparation of 62, 63

Fatty acid modification..... 362–363

FCS. *See* Fluorescence correlation spectroscopy

FFPE. *See* paraffin embedding

Fixation
formalin 422, 425
methanol..... 168
paraformaldehyde 168
PLP-fixative 168

Fixed cells 169–175, 210

Flat-embedding 183, 188, 192

Flow cytometry..... 69, 112, 119, 121, 260, 294, 298, 343, 346, 467

Fluorescein isothiocyanate-dextran (FITC-dextran)438, 440, 444

Fluorescence34, 36–39, 60, 69, 70, 77, 79, 118–123, 126, 132, 139, 142–144, 148–149, 158, 160, 161, 163, 175, 182, 208, 210–215, 219, 225–227, 261, 297, 298, 300, 315, 318, 334, 365, 368–369, 371, 376, 377, 379, 380–381, 384, 386, 387, 393, 444–446, 467, 469, 529, 530–532

Fluorescence activated cell sorting (FACS).....119, 203, 208, 211, 242, 294, 298, 310, 315, 319, 388

Fluorescence correlation spectroscopy, (FCS)..... 70–734 75–79

Fluorescence microscopy 111, 112, 158,
163, 166, 171, 182, 210, 376, 377,
379, 386, 445, 446
Fluorescence spectroscopy 60, 377, 379–380
Fluorescent fusion protein 166
Fluorescent probes 171–172
Fluorescent resonance energy transfer
(FRET) 60, 211, 261
Fluorescently-labeled 69, 70, 111, 112, 117,
119, 130, 168, 202, 212, 219–221, 225, 298,
301, 315, 532
Fluorophore labeled peptides 210, 213, 220, 365
Fluorophores
 hydrophilic 421
 molecular beacons 420
Fmoc-AA-OH 532
Fmoc deprotection 509, 510, 517, 518, 522
Fmoc/tBu strategy 507, 508, 523
Formalin 422, 425, 543, 544
Formalin fixation paraffin embedding (FFPE) 425
Fourier transformed-infrared (FT-IR) 49, 51, 53, 55
FRET. *See* Fluorescence resonance energy transfer
Functional splice correction assay 70, 220, 221,
242, 363, 365, 370
FURA-2 159–162
Fusogenic peptide 130

G

GABAergic interneurons 254
 β -Galactosidase 237, 238, 288, 537
GALA peptide 525–526, 528
Gbx2. *See* homeoproteins
GDNF 238
Gel filtration chromatography 189, 191
Gel shift assay 456, 460
Gene delivery 12, 181, 432, 434–437, 453
Gene expression
 analysis 420
 bioinformatics 420
 deep sequencing 420
 global 420
 transcriptomics 420
Gene silencing 436
Gene vector 12
Giant unilamellar vesicles (GUV) 35, 135
Gibbs free energy 83, 85–92
Global side-chain deprotection 511, 519
 β -Globin 214, 220, 222, 307, 308, 362, 363
GLP-1R 241
Glutaraldehyde 184, 186
Glycosaminoglycans (GAG) 25, 100, 101,
104–106, 113, 537
Glypican 100, 104, 108

GM-CSF. *See* Granulocyte macrophage colony stimulating
 factor
GMP 506
Gold nanoparticles 182
Golgi ring 167, 172–174
Gouy-Chapman theory 145
gp41 4, 6, 42
G protein coupled receptor (GPCR) 259–272, 376
Granulocyte macrophage colony stimulating factor 420
Green fluorescent protein (GFP) 104, 109, 111,
113, 166, 237, 238, 270, 271, 341, 343,
434, 438, 445, 469
Growth cone 252–253

H

^3H 101, 204
HBTU 510, 523
Heart 262, 263, 266, 269, 278–279, 281,
285, 286, 288, 323, 327, 329, 406, 408, 410,
423, 537, 541, 543, 548
HeLa cells 70, 71, 73–76, 102–108, 110–112,
121, 122, 124–126, 159, 161, 162, 172, 175,
183, 186, 199–203, 228, 371, 376, 380–383,
386–388, 466, 468–470, 528, 530, 531
HeLa pLuc705 222, 309, 315, 316, 319, 363, 392–395
 α -Helix 49, 53, 82, 85, 91, 234
Hemolysis assay 196, 200, 203–204
Hemostasis 260, 262, 268
Heparan sulfate 8, 9, 99, 149, 221, 222, 435
Heparan sulfate proteoglycans 99, 166
Heparin 72, 73, 78, 101, 221, 281, 285,
286, 378, 380, 387, 435, 545
Heparinase III 102, 103, 107–109, 221, 222, 224–226
Hepatocellular carcinoma 272
Hepes Krebs Ringer (HKR) buffer 121, 159–163,
199–203, 224, 226, 227, 364, 366, 370, 371
High performance liquid chromatography
(HPLC) 140, 158, 160, 163, 209,
211, 224, 225, 228, 310, 312, 313, 315, 351,
386, 458, 459, 466, 488, 492, 502, 507,
509–511, 514–521, 523, 532, 561
Histidine(dinitrophenol) 118–119
HIV-TAT 22, 100, 376, 377, 386
HKR. *See* Hepes Krebs Ringer buffer
Homeodomain 5, 22–23, 26
Homeogene 254
Homeogenetic expansion 251
Homeoproteins 4–6, 21, 22, 236, 237, 250–252, 255
Homogenisation 427, 428
Homogeniser 421, 423, 425
HoxB4 236, 237
HPLC. *See* High performance liquid chromatography
Hsp70 238
Hsp90 238

Human breast carcinoma (BT20)..... 199, 433, 436, 444
Hydrophobic partitioning..... 145
Hyperhidrosis.....547, 553–555, 561, 563, 566, 569

I

IAPs. *See* Inhibitor of apoptosis proteins
Identification of individual phage.....407, 409–410, 412, 413
IFN. *See* Interferon
IFN- α and TNF- α analyses..... 341, 343, 346, 347
IgG.....237, 325, 326, 334, 342, 343, 345, 346, 439, 442, 443
IL. *See* Interleukin
Immune stimulation..... 418, 420
Immunoblotting..... 342, 345
Immunocarriers.....438–439, 442
Immunohistochemical staining
 blocking solution..... 334
 Vector Biotin/Avidin Blocking Solution..... 334
 Vector MOM Immunodetection Kit..... 334
Immunohistochemistry..... 159–160, 162–163, 326, 332, 334, 341, 343, 346, 420
In situ hybridization (ISH)..... 421, 425, 428, 442, 485
 alkaline phosphatase..... 442
 blocking buffer..... 442
 hybridization buffer..... 422, 425
 LNA probes.....425
 miRNA.....422
 mRNA.....421
 siRNA..... 421, 425
 stringency buffer..... 422, 425
In vitro..... 3, 11, 165, 195, 204, 270, 278, 288, 340, 362, 404, 417, 418, 432, 434–436, 439, 443, 445, 453, 461, 484, 488, 491, 506, 537, 538, 542, 545, 554, 557, 564
In vivo..... 11–12, 14, 26, 149, 165, 195, 204, 212, 252, 253, 268, 270, 272, 278, 279, 284–288, 292, 340, 350, 362, 392, 401–414, 417–420, 432–436, 446, 453, 467, 473, 477, 488, 496, 506, 537–539, 541–543, 545, 547, 554, 557, 559, 562
In vivo selection.....403, 406, 408, 409
In-process controls (IPC).....454, 517, 518, 523
Industrial scale..... 505–523
Inflammation
 activation..... 420
 kinetics..... 420
 markers..... 420
 time-points..... 420
Infrared spectroscopy.....59
Inhibitor of apoptosis proteins (IAPs)..... 238
INK4a/ARF..... 241
Inner filter effect..... 132, 142

Inoculation of xenograft tumours..... 411
Interactions with phospholipid membranes..... 25, 351
Interfacial hydrophobicity scale.....82, 85, 86
Interferon (IFN)..... 341, 343, 346, 347, 420
Interleukin (IL)..... 545
Internalized protein..... 176, 250
Intracellular calcium measurement..... 158, 159, 161–162
Intracellular delivery..... 3, 10, 99, 112, 291, 431–447, 525–532
Intracellular localization.....209, 210, 437, 444
Intracellular trafficking..... 43, 166, 167, 182, 444, 538, 548
Intramuscular..... 322
Intranasal..... 418
Intratracheal..... 418
Intravenous.....204, 262, 263, 269, 271, 285, 288, 323, 329, 433, 453, 541, 542, 544
Inverted micelles..... 133, 149
Ionic interactions..... 453, 557
Ionic strength..... 141, 142
ISH. *See* In situ hybridisation
Isolation..... 104, 420, 473–486, 506, 508, 511, 515, 520
Isothermal titration calorimetry.....81, 134, 145

J

JBS-Nucleoducin..... 375–388
JIP-1..... 239
Jurkat..... 70, 72, 76–78, 351, 356, 377, 383, 388

K

Kaiser test..... 518
Kasumi-1.....377, 383
KCNMA..... 473
Kidney..... 13, 167, 262, 263, 278, 279, 286, 288, 377, 410, 414, 468, 527, 537
Kinetics..... 117–127, 137, 147, 318, 420, 434, 563, 564
Knockdown.....208, 340, 344, 345, 353, 418–420
KRX-725..... 270
Ku70..... 240, 241, 465–466, 468

L

Lactate dehydrogenase (LDH) leakage assay..... 158–161
Laemmli SDS sample buffer..... 325, 328
LAMP-2.....158, 159, 161–163, 166, 169, 173
LAR. *See* Luciferase-assay reagent
Large multilamellar vesicles (LMV).....34, 37, 38
Large unilamellar vesicles (LUV).....34–37, 135, 215
Lateral canthal lines (LCL)..... 547, 554, 563, 566, 567–568, 570
Lead citrate..... 185, 188
Leiden muscular dystrophy database..... 322
Lewis lung carcinoma (LLC)..... 433, 436

- Ligand 13, 100, 146–148, 240, 260, 266,
270, 447, 455, 506
- Lipids
binding 135
phase transition 137
quantification (phosphate assay) 139–140
spin-labelled 62–64
vesicle preparation 36, 134–135
- Lipofectamine/Lipofectamine™ 2000 363–365,
367, 369, 371
- Lipofection 10, 110, 113
- Lipoplexes 434, 436
- Liposomes
cationic 436, 526
cell interaction 436, 445
leakage assay 311, 317, 318
loading with FITC-dextran 444
luciferase assay 224, 227, 310, 311,
315–316, 364, 394–396, 462, 527, 530
modification with TATp 433
peptide-PNA conjugation 318
pH-sensitive 445
size distribution 442
- Live cell fluorescent probes 167
- Live cell imaging
ceramide-Bodipy-TR-C5 169, 172
cholera toxin B subunit 169, 171–172
live cell fluorescent probes 167, 171, 172
LysoSensor DND189 169, 172
transferrin 166, 169, 171
- Loading buffer 328, 456, 460
- Locked nucleic acid (LNA) 220, 221, 420–422
- Luciferase
activity 220, 221, 224, 226, 227, 310,
311, 316, 392, 395
pre-mRNA 220, 223, 363
- Lung 13, 270, 271, 417–447, 537
- LUV. *See* Unilamellar phospholipid vesicles
- Lyophilization 38
- Lyophilizer 36, 62
- Lyp-1 241
- LysoSensor DND189 169, 172
- Lysosomal associated membrane protein CD107b
(LAMP-2) 158, 159, 161–163, 166, 169, 173
- Lysosomal protease inhibitors 70–71, 73–76
- Lysosome 161
- Lytic activity 454
- M**
- M13 278, 280, 282, 285, 287, 404
- M511 241
- M918 4, 125, 243
- mAb 2G4 436, 439, 442–444
- Macropinocytosis 9, 33, 157, 166, 221–223,
435, 537
- Manufacturing 505–523
- Mass spectrometry 70, 209, 212, 213,
312, 313, 315, 318, 351, 386, 476, 483, 484,
516, 532
- Mastoparan 4, 6, 7, 292
- Max 239, 343, 366
- MCa 241
- MCF7 241
- MDA MB231 242
- MDM2 234, 241
mdx mouse.308 *See also* DMD mouse model
- Mechanisms of CPP uptake 9, 118, 221
- Melanoma 269
- Melittin 7, 85, 454, 456, 459, 460, 462
- Membrane 5, 21, 33, 42, 57, 82, 100, 119,
130, 157, 166, 196, 207, 219, 234, 250, 259,
289, 292, 308, 322, 339, 250, 376, 402, 435,
454, 469, 476, 487, 525, 556
- Membranolysis 119, 121, 123
- Mesencephalic dopaminergic neurons 254, 255
- Messenger RNA (mRNA)
endogenous 419
expression 345
genome-wide 420
variability 419
in situ hybridisation 421
knockdown, non-specific 420
polymorphisms 419
probes, LNA 421
purification 340
quantification 357
RT-qPCR 419
sequencing 20
- mGluR1 239
- Micelles 9, 35, 46, 58, 59, 62, 63, 414,
432–438, 441–443, 447
- Microarrays 342, 345
- Microscopy 23, 34, 69, 76, 77, 102, 106,
109, 111–113, 118, 130, 158, 163, 165–192,
297, 298, 346, 371, 376, 377, 379, 386, 410,
442, 443, 445, 446, 529, 531
- Mimic 235, 236, 238–240,
242, 525
- Mimicry of proteins by short peptides 234
- miRNA. *See* microRNA
- Mitoparan 292
- Mixed bilayered micelles 62, 63
- Model amphipathic peptide (MAP) 3, 4, 7, 202, 431
- Model membranes
modification of micelles 440
- Modification of

- 3' or 5'419, 463, 520
N- or C-terminal..... 520
Molecular beacons..... 420
Monoclonal antibody (mAb)..... 159, 162, 436, 439,
442, 444
Monomaleimido
nanogold.....183, 185, 190
undecaGold 183
Morphogens 249, 251
Morpholino phosphoramidate oligomer
(PMO)..... 306, 308, 310, 312–314, 318,
319, 323, 327, 333, 362, 367
Mounting media.....410, 422, 426
MPG 4, 8, 12, 41–44, 46, 47, 49–53, 350
MPG α 377.....385, 386
MPG β 377382, 385, 386
mRNA. *See* messenger RNA
MTT assay195–197, 201, 202, 291, 293, 371, 462
Multifunctional envelope-type nanodevice,
(MEND)525–527, 529, 530
Multilamellar vesicles (MLVs) 34, 37, 133–136,
138, 144
Multiple injections..... 323
Myc 104, 239, 242
Myocardial ischemia..... 266
- N**
- Nanocarrier.....435, 437, 444, 446
Nanocomplexes 42, 437
Nanogold (NG)
nanogold-labeled CPP..... 181
nanogold tag..... 182, 183
Nanoparticles.....12, 26, 182, 200, 277, 350, 431–447
NB-4377, 383
Nebulisation 419
Necrosis.....158, 293, 294, 298, 299, 301
Nested PCR 324, 335
Neuro2A cells..... 461
NeuroD/BETA2 236, 237
Neuroprotection 236, 238, 239, 541–542
Neutrophil chemotaxis 264
NFAT. *See* Nuclear factor of activated T cells
NF-kB.....6, 239, 288
NG. *See* Nanogold
NIH 3T3.....167, 170, 174, 377, 388, 434
Nitrotyrosine 118
NLS. *See* Nuclear localistaion signal
NMR. *See* Nuclear magnetic resonance
NOESY.....60–62, 64, 65
Nona-arginine71, 72, 76
Non-covalent 350, 351, 382, 520
Non-covalent approach 350
Non endosomal pathway 349
Non-viral delivery..... 506
NR2B9c..... 239
Nuclear factor of activated T cells (NFAT) 238, 239
Nuclear localistaion signal (NLS)..... 4, 6, 42
Nuclear magnetic resonance (NMR).....24, 34, 36–38,
58–65, 133, 136, 138, 144, 145, 149, 458
Nuclear magnetic resonance spectroscopy 59
Nuclear uptake 453
Nuclease317, 421, 426, 479, 483, 505
Nuclease degradation..... 505
Nucleic acid.....3, 12, 21, 42, 43, 219, 220, 242,
277, 308, 349, 350, 362, 370, 392, 420, 422,
432, 474, 487
Nucleic acid cargo 453
Nucleobase protecting group removal..... 387
Nucleoside analogues..... 418
- O**
- Occlusion time 267–269
Octanol hydrophobicity scale 82, 86–88
OCT compound..... 342, 350
Off-target effects
immune..... 420
inflammatory 420
transcriptomic..... 420
Oligofectamine.....170, 175, 177
Oligonucleotide delivery.....26, 219–228, 437, 505
Oligonucleotides
antisense 223, 321, 326, 506
aptamer..... 505
conjugation to
non-viral vectors 506
viral-vectors505, 506
DNA..... 12
first, second and third generation 505
GMP 506
industrial scale 505–523
isolation (*see* Manufacturing)
manufacturing
characterization, ion-pair LC-MS..... 516
elongation 510
capping508, 512
coupling..... 433, 508, 512, 514
detritylation 511, 513, 514, 516
isolation
lyophilization..... 38
precipitation..... 478
phosphoramidite approach 506
sulfurization 513
reagents
capping 433, 508, 512, 514
cleavage.....507–508
coupling510, 522
deprotection 517
DMT removal 512

- final DMT removal 512
nucleobase protecting group removal..... 513
phosphorothioate protecting group removal 512
oxidation 137, 139, 190, 468
reverse-phase (RP) HPLC columns 351
solid-support 506
solvents 509
synthesizers 531
nuclease degradation 505
phosphorothioate 512
purification (*see* Manufacturing)
RNA 340
siRNA 505
solid-support (*see* Manufacturing)
synthesis parameters 514
2'-O-Methyl Phosphorothioate 363
2'-O-Methyl RNA 220, 363, 365
Oncology 541, 545
Ortholog 235
Osmication 188
Osmium tetroxide 184, 189
Otx2, a homeoprotein. *See* Homeoproteins
Out of frame 308
Ovarian cancer 270
Oxyrna 510
- P**
- p16 239, 241
p53 234, 238, 241, 242, 291, 478, 545
p73 236, 238
PAGE. *See* Polyacrylamide gel electrophoresis
Pain 266, 540, 543, 544, 555,
566–569
PAIR technology 473–486
PAK1 239
pAntp(43–58) 241
Paraffin embedding 423, 425
Paraformaldehyde... 130, 159, 162, 168, 173, 174, 294, 296,
301, 343, 404, 422, 425
Paralog 235
Paramagnetic probe 61, 64
p14ARF 4, 235, 239, 241, 242
p19ARF 241
Parvalbumine 253, 254
Pathophysiological changes 322
Pax4 236, 237
Pax6 237, 251, 252
PBS. *See* Phosphate buffered saline
PCI. *See* Photochemical internalization
PCNA interacting protein (PIP) 240
PCR. *See* Polymerase chain reaction
pEGFP. *See* Enhanced-green fluorescent protein
PEG-Hz-PE. *See* Polyethyleneglycol-hydrazone-
phosphatidylethanolamine
- PEG-PE. *See* Polyethyleneglycol
phosphatidylethanolamine
PEGylated lipids 136, 139
Pen 239, 279, 332, 334
Penetratin 4, 5, 9, 13, 23–25, 141,
148, 149, 196, 223, 227, 238, 323, 350, 376,
382, 386, 434
Penetratin mutant p2AL 131, 132, 148
Pep-1 4, 8, 13, 42–44, 46, 48–53, 237, 238
Pepducin
biodistribution 263
delivery 260–263
fluorescently-labeled 219, 225
pharmacodynamics 262, 548, 556
pharmacokinetics 262, 264, 548, 556
radioactively-labeled 262
specificity 261
PepFect 361–372
PepFect 3 363, 365, 367, 368–370
PepFect 4 363, 365, 367, 369, 370
Peptide-based non covalent strategy 349–359
Peptide nucleic acid (PNA) 3, 242, 391–397, 474
cell-penetrating peptide conjugate 11
delivery by photochemical internalization 391–397
HeLa pLuc705 cells 222, 309, 315,
316, 393–395
M13 phage 285, 287
peptide phage display library 278, 280, 284,
285, 287
- Peptides
Boc-strategy 520
cell-penetrating 3–14, 33–53, 57–63, 81–97,
117–149, 165–178, 181–192, 219–228,
233–243, 277–288, 321–347, 431–447,
531–548, 553–571
cleavage from resin (*see* Manufacturing)
conjugation to, oligonucleotide 505
degradation 209, 211, 213
deprotection (*see* Manufacturing)
Fmoc/tBu strategy 507–508, 523
GMP 506
industrial scale 505–523
isolation (*see* Manufacturing)
manufacturing
HPLC 507
lyophilizer 36, 62
reactors, solid-support (*see* Resin)
reagents
colour tests 510
coupling reagents 510, 522
Fmoc-AIA-OH 532
solvents
cleavage and deprotection 507
peptide elongation 509

- Peptides (*continued*)
- vacuum oven 511, 519
 - cleavage 511, 519
 - clongation 517
 - coupling 510
 - Fmoc deprotection 509, 510, 518, 522
 - global side-chain deprotection 511, 519
 - HPLC purification 224
 - in-process controls (IPC) 454
 - isolation, precipitation 478
 - Kaiser test 518
 - purification (*see* Manufacturing)
 - quantification 141
 - resin
 - CTC 507, 509, 520, 521
 - Sieber 507, 509, 520, 522, 523
 - swelling of 517
 - solid-phase peptide synthesis (SPPS) 141, 351, 507–509, 517
 - solid-support (*see* Resin)
 - super-acid labile resins (*see* Resin)
 - synthesis 141, 351, 488, 508–509, 517, 522
- Permeabilization 168, 170, 173, 294, 308, 315, 319, 378
- Phage display
- amplification of phage 283, 285, 287
 - analysis of selection output 408–409
 - ex vivo selection 402–403, 406–408, 413
 - identification of individual phage 407, 409, 412
 - in vivo selection 403, 406, 408, 409
 - validation of the specificity 403–404, 409–410, 420, 568
- Phalloidin 170, 175, 177, 178
- Pharmacodynamics 262, 548, 556
- Pharmacokinetics 262, 264, 556
- Phenol chloroform 424, 428
- pH-labile masking 453
- Phosphate buffered saline (PBS) 102, 121, 128, 168, 169, 198, 199, 281, 294, 296, 309, 325, 329, 351, 364, 394, 438, 446, 528
- Phosphatidyl-inositol-3-Phosphate (PI3P) 173
- Phospholipid 9, 24, 34–36, 43–45, 48–50, 53, 54, 58, 60, 64, 133, 135, 139, 143, 261, 298, 311, 317, 318, 350, 351, 432, 433
- Phosphorodiamidate morpholino oligomers (PMO) ... 308, 310, 312, 313, 318, 319, 323, 329, 367
- Phosphorothioate 220, 363, 511–513, 515, 516
- Phosphorothioate protecting group removal 512
- Phosphorous-31 NMR 144
- Photochemical internalization (PCI)
- incubation 394
 - irradiation 393
 - peptide nucleic acid conjugate 391–397
 - photosensitizer 392–394
 - toxicity 392
- pH-sensitive 437, 438, 441–443, 445, 446, 544
- PEG-Hydrazone (Hz)-PE 441, 445
 - preparation of liposomes 438, 441, 445
 - preparation of micelles 438, 441
- pH sensitive peptide 544
- PI. *See* Propidium iodide
- p16INK4a 241
- PIP. *See* PCNA interacting protein
- PI3P. *See* Phosphatidyl-inositol-3-Phosphate
- Piperidine (Fmoc removal) 518
- PKC isozymes. *See* Protein kinase C
- Plasmodesmata 250
- Platelet 234, 260–262, 264, 268, 269, 347
- Platelet aggregation 235, 262, 267–269
- PLL. *See* Polylysine
- PLP-fixative 168, 173
- PMO-peptide conjugates 323
- Polyacrylamide gel electrophoresis (PAGE) 324–325
- Polyarginine 196, 350, 436, 454, 537, 544, 545
- Polyethyleneglycol-hydrazone-phosphatidylethanolamine (PEG-Hz-PE) 441, 445
- Polyethyleneglycol phosphatidylethanolamine (PEG-PE) 433, 438, 537
- Polyethylene glycol 132, 280, 432, 438, 454
- Poly -L -lysine 99, 130, 454, 560, 562
- Polylysine. *See* Poly -L -lysine
- Polymerase chain reaction (PCR) 317, 319, 328, 335, 348, 395, 409, 414
- amplicon 419
 - 2-DDCt method 419
 - dynamic range 420
 - endogenous control 419
 - primers, LNA 220, 420, 422, 425
 - probes 343
 - sensitivity 51, 65, 127, 139, 149, 420, 566
 - standard curve 140, 226, 227, 366, 371, 387
 - validation 126, 270, 420, 421, 567, 568, 571
- Polymeric micelles 441
- Polymorphisms 419
- Polyplex 453, 454, 460–462
- Pore 8, 9, 34, 37, 87, 130, 137, 196, 292
- Pore formation 9
- Post-transcriptional regulation 473
- P1pal-7 267, 269–271
- P1pal-12 261, 265–269, 272
- P1pal-13 265, 266
- P1pal-19 267, 269
- P4pal-10 262, 263, 265–269
- P4pal-i1 267, 268
- P1pal-12S 265, 266–269
- PPI. *See* Protein-protein interactions
- pPTD-DRBD 344
- Precipitation ... 144, 190, 191, 319, 476, 483, 484, 511, 523
- Pre-clinical studies 536, 541, 544

- Prediction 3–14, 87, 292
- pre-mRNA
- preparation of immunocarriers 438–439, 442
 - preparation of lipoplexes 434, 436
 - preparation of liposomes 439–441
 - preparation of micelles 441
- Preservation 420, 421, 423
- Primers 284, 310, 317, 409, 474, 476, 481
- Prochiantz, Alain 5, 21–26, 249–256
- Proliferation 186, 200, 202, 203, 209, 214, 238–240, 242, 272, 542
- Propidium iodide (PI) 119–121, 160, 163, 196, 199, 201–203, 293, 294, 298, 299, 310, 388
- Protease activated receptor 260
- Protease inhibitor 70, 71, 73, 381, 386, 426–428, 477, 480, 482, 483
- Protein
- blotting 325, 328, 342, 355
 - electrophoresis 101, 105, 311, 317, 324, 328, 395, 441, 456, 460, 561
 - extraction 420, 421, 423, 425
 - globular 142
 - interaction 233–237, 536
 - interface 234
 - mimicry 237–240
 - non-transducible 236
 - protease inhibitor 70, 71, 73–76, 103, 324, 381, 386, 426–428, 477, 478, 480, 482, 483
 - restoration 323, 402
 - transducible 236
- Proteinase K buffer 422
- Protein interaction
- hot spots 13–14, 234
 - linear motif 234
 - modulators 234–236, 291–302
 - peptides 235
- Protein kinase C (PKC) 540
- Protein kinase C isozymes 541
- Protein kinase C (PKC) isozymes 541
- Protein-protein interactions 233, 234–237, 536
- Protein restoration 329, 333, 402
- Protein transduction 3, 157, 165–178, 277, 340, 350, 469, 537, 557
- Protein transduction domains (PTD) 157, 207, 277–289, 340, 391, 537
- Proteoglycan 33, 99–113, 166, 221, 344, 537
- Proteolytic stability 70
- Proteomics 420
- Proteomimetic 297
- Proximity quenching assay 118–119
- pTAT vector 341, 344
- PTD. *See* Protein transduction domains
- PTD-DRBD
- construction
 - dGFP-H1299 cells 341–343
 - Escherichia coli* 70, 340
 - medium 341, 507 - pPTD-DRBD 344
 - pTAT vector 341, 344
- IFN- α and TNF- α analyses 341, 343, 346, 347
- immunoblotting 343, 345
- immunohistochemistry and flow cytometry analysis 420
- purification
- buffer A 224
 - buffer B 341
 - buffer C 341
 - mono-S column 344
 - Ni-NTA resin 344
 - PD-10 column 341
 - storage 466–467
- RNA interference (RNAi) 13, 340, 419, 485, 486
- RT-PCR and microarrays 342
- siRNA delivery into cells 341–342
- Purification 44, 100–102, 104–106, 140, 183, 186, 191, 224, 240, 317, 340, 341, 344, 409, 428, 458, 506, 508, 515, 519–522
- PVDF 109, 325, 331, 336
- pVEC 4, 12
- Pyramidal glutamatergic neurons 254
- Q**
- qPCR. *See* Polymerase chain reaction
- Quantitative uptake
- cellular imaging 187
 - dermis 544, 547
 - epidermis 544, 547
 - epithelia 265, 266, 278, 468
 - live animal imaging 335
 - prodrugs 487, 502
- Quenched fluorescence assay 118–119, 121–123
- Quenched time-lapse uptake assay 123–124
- Quencher 60, 118, 119, 126, 132, 142, 311, 317
- Quenching
- proximity quenching 118–119
- R**
- Rab5 174
- Radioactively-labeled 262, 263
- Raf-1 239
- Ras 242, 376
- RBP. *See* RNA binding protein
- Reactors 510–511, 517, 523
- Reading frame 241, 322

- Release, repair response, MRR 158
Resin..... 141, 183, 185, 188, 190, 344,
507, 509, 510, 514, 517–519, 521, 522, 531, 532
Reticuloendothelial system 278
Reversed phase chromatography 186, 189, 191
Reverse-phase (RP) HPLC columns..... 351, 514–515, 532
Reverse transcription 319, 419
Revertant fibres 322
Rheostat hypothesis..... 420
Ribonucleoprotein (RNP) 236, 237, 424
RIPA buffer..... 342, 345, 421, 425, 426–428
RISC. *See* RNA induced silencing complex
RNA
endogenous control..... 22, 111, 334, 340, 419
extraction
mirVana kit 421, 428
RNase contamination 396
small fraction 371
total..... 425
tri reagent 310, 316, 427
preservation 421, 423
purification 421, 423, 425
purity 516
quantification..... 141
RNase contamination 396
18S..... 427
spiking controls..... 421
stability 427
storage temperature 423, 427
yeast..... 422
yield..... 485, 516
RNA binding protein (RBP)..... 340, 473–486
RNA induced silencing complex (RISC) 340
RNA interference (RNAi)..... 13, 340, 419, 485, 486
RNAlater[®]..... 421, 423, 427
RNase..... 308, 340, 342, 345, 351, 352, 370,
395, 396, 419, 427, 428, 476, 479, 480
Rotor-stator homogeniser 421, 423, 425
R6-Penetratin motif..... 323
RT-PCR..... 310, 311, 316, 323, 324,
327–329, 335, 345, 393–395, 397, 427
RT-qPCR. *See* polymerase chain reaction
RTT150 547, 556, 557, 564, 565
(R_xR)₄..... 333, 367
S
Saponin 168, 169, 173, 308, 316, 319
Saponin permeabilized cells..... 316
SCO 314, 363, 365–369, 371
Screening method..... 211
SDS micelle..... 58, 59
Second mitochondria-derived activator
of caspases (SMAC) 234, 239
Sepsis..... 259, 264–266
Sequencing 280, 284, 409, 414
Shepherdin
Short interfering RNA (siRNA)
degradation 428
delivery 13, 339–351, 355,
356, 358, 461
detection 421
extraction 420
in situ hybridisation 421, 422, 425
modifications 421
quantification..... 141
treatment 166, 170, 175
vector 453
Sieber..... 507, 509
520, 523
Signal transducer and activator of transcription 3
(STAT3) 240
Signal transduction..... 242, 259,
291–302
Silver enhancement 184, 186
Simian virus 40, SV40 4, 6, 42
siRNA. *See* short interfering RNA
SIRS. *See* Systemic inflammatory response syndrome
SMAC. *See* Second mitochondria-derived activator
of caspases
SMAD 234
Small unilamellar vesicles (SUVs) 34, 36–37, 45,
59, 135, 529
Smart nanocarrier 435, 437, 446
SMO-i2-12 272
Sodium cacodylate buffer 184
Solid-phase peptide synthesis (SPPS) 141, 359,
507, 508, 517
Solid-support..... 506, 512, 513
S1P3..... 259, 260, 262, 269, 270
Spectrofluorometry..... 209, 211–212
Spectroscopy
circular dichroism 43, 49, 53, 81
fluorescence 36–38, 171,
210, 211, 379–380, 386, 445, 468
infrared 49, 51
nuclear magnetic resonance 50
Spin-labelled lipids
Splice correcting oligonucleotides 213, 361–372
Splice correction 14, 70, 221, 242, 321, 363,
366, 368, 370, 392
Splice switching oligonucleotides 308
Splicing..... 214, 220, 307, 308, 310–311,
315, 361–363, 473–475
Splicing redirection..... 308–310, 319
SPPS. *See* Solid-phase peptide synthesis
18S RNA..... 427
[35S]-sulfate..... 101–109, 112
Stable isotopes 70, 213

- STAT3. *See* Signal transducer and activator of transcription 3
STAT6-IP 239
Statistical analysis 119
Staurosporine 200
Stearylation 10, 363, 366, 435
Stimuli-sensitive 435
Stringency buffer 422, 425
Stroke 540, 546, 550
Substantia nigra 254
Sulfurization 513
Super-acid labile resins. *See* Resin
Superparamagnetic iron oxide 432
Surface partition constant, K_p 145
Survivin 238
SUVs. *See* Small unilamellar vesicles
Syndecan 100, 103, 104, 109, 111, 113
Synthesis parameters 514
Synthesizers 531
Systemic inflammatory response syndrome (SIRS) 264, 265
- T**
- Target cell 260, 288, 436, 437, 453, 520, 547
Targeted delivery 14, 502
Targeting ligand 13, 240, 454, 455
Tat 3, 21, 51, 82, 130, 196, 235, 249, 392, 431, 536
TAT peptide (TATp)
 liposomes 433–435
 modification of liposomes 433
 modification of micelles 432
 nanoparticles 182
 preparation of immunocarriers 438, 442
Tectum 252, 253
N,N,N,N'-Tetramethyl-ethylenediamine (TEMED) 325, 330, 335
TFLLRN 269
TGN 173
Thalamo-cortical projections 253
 β -Thalassemia 307, 309, 362
Thermodynamics 9
Thiol group 183, 190, 462
Third helix 5, 22, 23, 250
Three-dimensional structure 57–66
Threshold cycle 176
Thrombin 261, 262, 267, 268
Thrombosis 260, 268
Tissue
 collection 418
 cryopreservation 428
 cryosectioning 423, 428
 fixation 168
 homogenisation 428
 inflation 418
 perfusion 406, 418, 546
 preservation 420
 protein extraction 420, 421, 425
 RNA extraction 310, 323, 327–328, 420, 421, 423
 storage 138
Tissue-specific protein transduction domains 350, 557
TNBS. *See* 2, 4, 6-Trinitrobenzenesulfonic acid
TNBS-assay 455, 457, 460
TNF-alpha 420
TOCSY 60, 62, 64
Toll-like receptor 418
Topical uptake 487–503
Toxicity 7, 12, 131, 190, 195–204, 224, 385, 484, 547, 563
Toxicity methods 195–204
TP10 4, 6, 9, 363, 366, 437
Trafficking 166, 444
Transactivator of transcription 536
Transcriptomics 420
Transcutaneous delivery 556, 557, 561, 567, 570
Transducible 220, 236
Transfection
 cardiomyocytes (H9C2) 436
 in vitro 445–446
 in vivo 446
 lewis lung carcinoma (LLC) 433
 pEGFP 104, 434, 438, 441, 445, 527, 528
 with pH-sensitive liposomes 445
Transfer buffer 325, 331, 335
Transferrin, translocating sequences, MTS 547
Translocation 5–10, 23, 25, 33, 158, 161–163, 182, 214, 226, 236, 240, 292, 433
Transmission electron microscopy (TEM) 182
Transportan 3, 4, 6, 12, 87, 196, 362, 363, 431, 537
Transportan10 363
Trifluoroacetic acid 510, 511, 519
Trifluoroacetic acid (TFA) side chain
 deprotection 510, 511, 519
2, 4, 6-Trinitrobenzenesulfonic acid (TNBS) 455, 457–460
TRI REAGENTO 310, 316, 427
Triton X-100 71, 102, 103, 133, 143, 173, 175, 203, 204, 224, 226, 342, 345, 441, 477, 478
TRIZOL® reagent 324
Trojan peptides v
Trypan blue (TP) 120, 121
Trypsin 72, 73, 199, 201, 203, 212, 213, 279, 282, 293, 295, 593
Tumor
 digestion 285
 model mice 350
 selective targeting 240
 targeting 240
 vasculature 278
TUNEL assay DNA fragmentation *in situ*
 detection 294, 296

U

Ubiquitin C-terminal hydroxylase L1 (Uch-1) 238
 Undecagold..... 183
 Unilamellar phospholipid vesicles (LUV) 33–38,
 132, 136, 138, 143, 317
 Uptake measurements
 qualitative 210, 222
 quantitative 219, 224
 Uranyl acetate 185

V

Validation of the specificity 403–404
 Vascular injury 268
 Ventral tegmental area 254
 Versatility..... 351
 Vesicles34, 36, 37, 59, 182, 555
 Viability..... 72, 177, 196, 200,
 240, 293, 294, 377, 380–382,
 384, 387

VIVIT237, 239
 VP22 4, 6, 9, 208, 431, 543

W

Western blotting..... 325
 Wimley-White hydrophobicity scales 82
 Wortmannin 221, 222, 224, 225, 381, 385

X

X1/2LCA-i1.....264, 265
 X1/2pal-i3264, 265
 X4pal-i1.....264, 265
 X4pal-i2..... 264

Y

YTA.....7, 11

Z

ZipTip® 212